BEILSTEIN JOURNAL OF ORGANIC CHEMISTRY

Organic free radical chemistry

Edited by Corey R. J. Stephenson

Imprint

Beilstein Journal of Organic Chemistry
www.bjoc.org
ISSN 1860-5397
Email: journals-support@beilstein-institut.de

The *Beilstein Journal of Organic Chemistry* is published by the Beilstein-Institut zur Förderung der Chemischen Wissenschaften.

Beilstein-Institut zur Förderung der Chemischen Wissenschaften
Trakehner Straße 7–9
60487 Frankfurt am Main
Germany
www.beilstein-institut.de

Beilstein Journal of Organic Chemistry

The renaissance of organic radical chemistry – deja vu all over again

Corey R. J. Stephenson[*1], Armido Studer[*2] and Dennis P. Curran[*3]

Editorial

Open Access

Address:
[1]Department of Chemistry, University of Michigan, Ann Arbor, MI 48109, USA, [2]Institute of Organic Chemistry, Westfälische Wilhelms-University Münster, 48149 Münster, Germany and [3]Department of Chemistry, University of Pittsburgh, Pittsburgh, PA, 15208, USA

Email:
Corey R. J. Stephenson[*] - crjsteph@umich.edu; Armido Studer[*] - studer@uni-muenster.de; Dennis P. Curran[*] - curran@pitt.edu

* Corresponding author

Keywords:
free radical

Beilstein J. Org. Chem. **2013,** *9,* 2778–2780.
doi:10.3762/bjoc.9.312

Received: 18 November 2013
Accepted: 26 November 2013
Published: 04 December 2013

This article is part of the Thematic Series "Organic free radical chemistry".

Guest Editor: C. Stephenson

Long-thriving movements often have a habit of continually reinventing themselves in a process called renaissance. The word itself is an English reinvention (some would say theft) of the French word for "rebirth". Renaissances often occur in waves with each new wave typically building on the prior one. The European Renaissance is a perfect example, occurring in waves over about three centuries. Quoting from Yogi Berra, after a few of these waves that bear certain resemblances, it starts to feel like "deja vu all over again" [1].

The discipline of organic radical chemistry dates back over 110 years, and it has been thriving for decades because it continuously reinvents itself. Often this happens when groups of researchers with different interests and expertise immigrate to the field.

About 30 years ago there began a flourishing period in the field of organic radical chemistry that delivered groundbreaking results, especially in organic synthesis. By the 1990's, radical reactions (especially cyclizations) were broadly recognized as powerful tools to make molecules. This Renaissance I in organic radical chemistry was built on prior renaissances in polymer and physical (especially physical organic) chemistry of radicals. In turn, the knowledge gained during Renaissance I was diverted to spark new waves of developments in neighboring disciplines such as biology and materials science. A comprehensive overview of the various aspects of modern radical chemistry addressing all these major fields can be found in the recently published four-volume "Encyclopedia of Radicals in Chemistry, Biology and Materials" [2].

Over the past few years, the process has again come full circle as research in organic radical chemistry, especially synthetic radical chemistry, has been reignited. This renaissance, Renaissance II if you will, is documented by the many exciting contributions recently published in high impact journals. This Thematic Series on radical chemistry in the Beilstein Journal of Organic Chemistry brings together papers from top research groups and representing many of the most significant themes in the current field of radical chemistry.

A partial list of topics that have seen new developments in the past few years follows. Many of these themes are represented once or multiple times in papers of the Thematic Series:

a) Base mediated homolytic aromatic substitution (BHAS) [3],

b) photoredox catalysis [4-8],

c) redox chemistry using Bu_4NI in combination with *t*-BuOOH [9],

d) transition metal catalyzed processes where radicals are suggested to interact directly with copper, nickel, zinc, palladium, gold and so on [10-16],

e) radical trifluoromethylation [17] and radical fluorination [18-20],

f) natural product synthesis [21],

g) new main group radical chemistry involving elements like boron [22], phosphorous [23] and selenium [24], tellurium [25], among others,

h) synthesis or functionalization of all sorts of heterocyclic ring systems, especially heteroaromatic systems [26,27],

i) radical chemistry with water or in water [28],

k) sequential transformations with both reductants and oxidants,

l) radical chemistry in materials science [29,30], and

m) high level computations of radicals and their reactions [31].

Just as in Renaissance I, the field of radical chemistry is currently being joined by all sorts of researchers whose primary interests have until recently been elsewhere. In the 1980's there were immigrants from natural products chemistry and synthetic methodology. Today, many of the new immigrants again come from a background of synthesis, often with a focus on catalysis. They bring along new ideas and different perspectives. As both new and established researchers have dared to try radical reactions in challenging new areas, their results have lit up the field.

Successful explorers of all ages have always taken the best existing maps on their voyages of discovery. These maps were invaluable, even though they inevitably were incomplete and even inconsistent. Little by little, the inconsistencies got fixed and the empty spaces got filled in. The reviews in the Encyclopedia of Radical Chemistry and other sources serve as maps to drive organic radical research in new directions. Like old maps of the earth, these maps are also inevitably incomplete and at times inconsistent. But they are powerful aids to help you understand both where you are and where you are going. Or, you can forget the maps and wander out on your own. But to again quote Yogi, "if you don't understand where you are going, you might end up someplace else [1]." To all those new folks joining the field, we welcome you to the world of organic radical chemistry. Get yourself a good set of maps and start exploring.

There is one final parallel to draw between Renaissance I and Renaissance II in organic radical chemistry. In 1985, a thematic special issue on organic radical chemistry in Tetrahedron organized by Bernd Giese [32] brought many of the advances of radical chemistry to a wider audience. Similarly, this Thematic Series edited by Corey Stephenson advances the same goal.

Take some time to read a few of the papers in this Thematic Series. Think of the papers as evolving maps of regions of radical chemistry under exploration. Allow yourself to be drawn into the exciting world that is modern organic radical chemistry.

References

1. Dale (Yogi) Berra is perhaps the most famous living American baseball player, known as much for his exploits in language as on the baseball field. Several of his other quotes have relevance to chemistry. For example, his description of the relationship between theory and practice goes "in theory, there is no difference between theory and practice. In practice, there is". See http://www.yogiberra.com/yogi-isms.html Accessed November 26, 2013, and http://www.brainyquote.com/quotes/authors/y/yogi_berra.html Accessed November 26, 2013.
2. Chatgilialoglu, C.; Studer, A., Eds. *Encyclopedia of Radicals in Chemistry, Biology and Materials;* Wiley-Interscience, 2012. doi:10.1002/9781119953678
3. Studer, A.; Curran, D. P. *Angew. Chem., Int. Ed.* **2011,** *50,* 5018–5022. doi:10.1002/anie.201101597
4. Prier, C. K.; Rankic, D. A.; MacMillan, D. W. C. *Chem. Rev.* **2013,** *113,* 5322–5363. doi:10.1021/cr300503r
5. Hu, J.; Wang, J.; Nguyen, T. H.; Zheng, N. *Beilstein J. Org. Chem.* **2013,** *9,* 1977–2001. doi:10.3762/bjoc.9.234
6. Pirnot, M. T.; Rankic, D. A.; Martin, D. B. C.; MacMillan, D. W. C. *Science* **2013,** *339,* 1593–1596. doi:10.1126/science.1232993
7. Ruiz Espelt, L.; Wiensch, E. M.; Yoon, T. P. *J. Org. Chem.* **2013,** *78,* 4107–4114. doi:10.1021/jo400428m
8. Nguyen, J. D.; D'Amato, E. M.; Narayanam, J. M. R.; Stephenson, C. R. J. *Nat. Chem.* **2012,** *4,* 854–859. doi:10.1038/nchem.1452
9. Finkbeiner, P.; Nachtsheim, B. J. *Synthesis* **2013,** 979–999. doi:10.1055/s-0032-1318330
10. Too, P. C.; Tnay, Y. L.; Chiba, S. *Beilstein J. Org. Chem.* **2013,** *9,* 1217–1225. doi:10.3762/bjoc.9.138

11. Neufeldt, S. R.; Sanford, M. S. *Adv. Synth. Catal.* **2012,** *354,* 3517–3522. doi:10.1002/adsc.201200738
12. Xiao, B.; Liu, Z.-J.; Liu, L.; Fu, Y. *J. Am. Chem. Soc.* **2013,** *135,* 616–619. doi:10.1021/ja3113752
13. Zultanski, S. L.; Fu, G. C. *J. Am. Chem. Soc.* **2013,** *135,* 624–627. doi:10.1021/ja311669p
14. Li, D.; Wang, M.; Liu, J.; Zhao, Q.; Wang, L. *Chem. Commun.* **2013,** *49,* 3640–3642. doi:10.1039/c3cc41188e
15. Sahoo, B.; Hopkinson, M. N.; Glorius, F. *J. Am. Chem. Soc.* **2013,** *135,* 5505–5508. doi:10.1021/ja400311h
16. Wu, Z.; Pi, C.; Cui, X.; Bai, J.; Wu, Y. *Adv. Synth. Catal.* **2013,** *355,* 1971–1976. doi:10.1002/adsc.201300111
17. Studer, A. *Angew. Chem., Int. Ed.* **2012,** *51,* 8950–8958. doi:10.1002/anie.201202624
18. Li, Z.; Song, L.; Li, C. *J. Am. Chem. Soc.* **2013,** *135,* 4640–4643. doi:10.1021/ja400124t
19. Sibi, M. P.; Landais, Y. *Angew. Chem., Int. Ed.* **2013,** *52,* 3570–3572. doi:10.1002/anie.201209583
20. Rueda-Becerril, M.; Chatalova Sazepin, C.; Leung, J. C. T.; Okbinoglu, T.; Kennepohl, P.; Paquin, J.-F.; Sammis, G. M. *J. Am. Chem. Soc.* **2012,** *134,* 4026–4029. doi:10.1021/ja211679v
21. Shigeoka, D.; Kamon, T.; Yoshimitsu, T. *Beilstein J. Org. Chem.* **2013,** *9,* 860–865. doi:10.3762/bjoc.9.99
22. Curran, D. P.; Solovyev, A.; Brahmi, M. M.; Fensterbank, L.; Malacria, M.; Lacôte, L. *Angew. Chem., Int. Ed.* **2011,** *50,* 10294–10317. doi:10.1002/anie.201102717
23. Yorimitsu, H. *Beilstein J. Org. Chem.* **2013,** *9,* 1269–1277. doi:10.3762/bjoc.9.143
24. Kobiki, Y.; Kawaguchi, S.-i.; Ohe, T.; Ogawa, A. *Beilstein J. Org. Chem.* **2013,** *9,* 1141–1147. doi:10.3762/bjoc.9.127
25. Nakamura, Y.; Yamago, S. *Beilstein J. Org. Chem.* **2013,** *9,* 1607–1612. doi:10.3762/bjoc.9.183
26. Miyabe, H.; Asada, R.; Takemoto, Y. *Beilstein J. Org. Chem.* **2013,** *9,* 1148–1155. doi:10.3762/bjoc.9.128
27. McBurney, R. T.; Walton, J. C. *Beilstein J. Org. Chem.* **2013,** *9,* 1083–1092. doi:10.3762/bjoc.9.120
28. Hirose, D.; Taniguchi, T. *Beilstein J. Org. Chem.* **2013,** *9,* 1713–1717. doi:10.3762/bjoc.9.196
29. Moraes, J.; Ohno, K.; Gody, G.; Maschmeyer, T.; Perrier, S. *Beilstein J. Org. Chem.* **2013,** *9,* 1226–1234. doi:10.3762/bjoc.9.139
30. Telitel, S.; Dumur, F.; Faury, T.; Graff, B.; Tehfe, M.-A.; Gigmes, D.; Fouassier, J.-P.; Lalevée, J. *Beilstein J. Org. Chem.* **2013,** *9,* 877–890. doi:10.3762/bjoc.9.101
31. Gansäuer, A.; Seddiqzai, M.; Dahmen, T.; Sure, R.; Grimme, S. *Beilstein J. Org. Chem.* **2013,** *9,* 1620–1629. doi:10.3762/bjoc.9.185
32. Giese, B., Ed. Selectivity and synthetic applications of radical reactions. *Tetrahedron* **1985,** *41,* 3887–4364.

License and Terms

Beilstein Journal of Organic Chemistry

Formal synthesis of (−)-agelastatin A: an iron(II)-mediated cyclization strategy

Daisuke Shigeoka, Takuma Kamon and Takehiko Yoshimitsu*

Full Research Paper

Open Access

Address:
Graduate School of Pharmaceutical Sciences, Osaka University, 1-6 Yamadaoka, Suita, Osaka 565-0871, Japan

Email:
Takehiko Yoshimitsu* - yoshimit@phs.osaka-u.ac.jp

* Corresponding author

Keywords:
agelastatin; aminohalogenation; iron(II); free radical; natural product synthesis

Beilstein J. Org. Chem. **2013,** *9,* 860–865.
doi:10.3762/bjoc.9.99

Received: 23 February 2013
Accepted: 10 April 2013
Published: 03 May 2013

This article is part of the Thematic Series "Organic free radical chemistry".

Guest Editor: C. Stephenson

Abstract

An iron(II)-mediated aminohalogenation of a cyclopentenyl *N*-tosyloxycarbamate provided new access to the key intermediate for the synthesis of (−)-agelastatin A (AA, **1**), a potent antiproliferative alkaloid. The present synthetic endeavour offered an insight into the mechanism underlying the iron(II)-mediated aminohalogenation of *N*-tosyloxycarbamate, in which the radical properties of the N–iron intermediates in the redox states were operative.

Introduction

Marine organisms often produce bioactive substances that potentially serve as attractive resources for drug discovery. (−)-Agelastatin A (AA, **1**), a cytotoxic alkaloid isolated from marine sponges *Agelas dendromorpha* and *Cymbastela* sp., is one such substance, which has drawn considerable attention due to its potential applicability in the development of anticancer agents [1-5]. The intriguing biological activity of **1** has stimulated interest in developing various chemical accesses to the natural product [6-25]. Our previous synthetic endeavours have established two approaches to **1**, in which cyclopentenyl azidoformates **2** and **3** were utilized as the pivotal intermediates (Scheme 1).

The first-generation strategy employed a stereoselective thermal aziridination of azidoformate **2** and a subsequent aziridine-opening reaction to establish the vicinal *trans* nitrogen motif **4** [26]. The second-generation strategy involved the radical aminobromination of azidoformate **3** followed by lactamization of the resultant bromide **5a** to furnish a tetracyclic compound (structure not shown), which was transformed into the natural product [27]. In the present study, we disclose a new approach to the key intermediate for AA synthesis in which *N*-tosyloxycarbamate **8**, a nonhazardous azidoformate surrogate, is transformed into aminohalogenated compounds **5a** and **5b** by $FeBr_2$/Bu_4NBr [28,29], $FeCl_2$/Bu_4NCl, or $FeCl_2$/TMSCl [30-35]

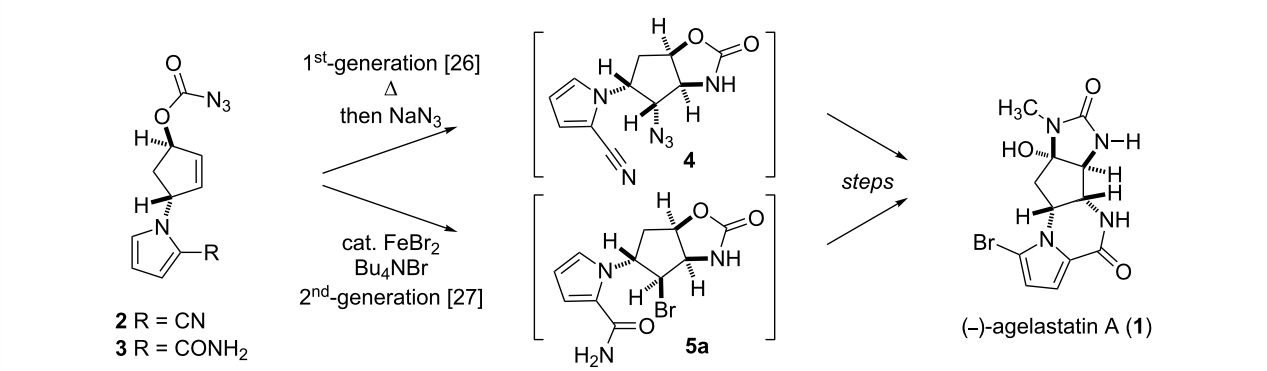

Scheme 1: Our first- [26] and second-generation [27] approaches to (−)-agelastatin A (**1**).

(Scheme 2). Moreover, a plausible mechanism of the present iron(II)-mediated aminohalogenation, which is inferred from the unique reactivity of *N*-tosyloxycarbamate **8** with the reagents, is discussed.

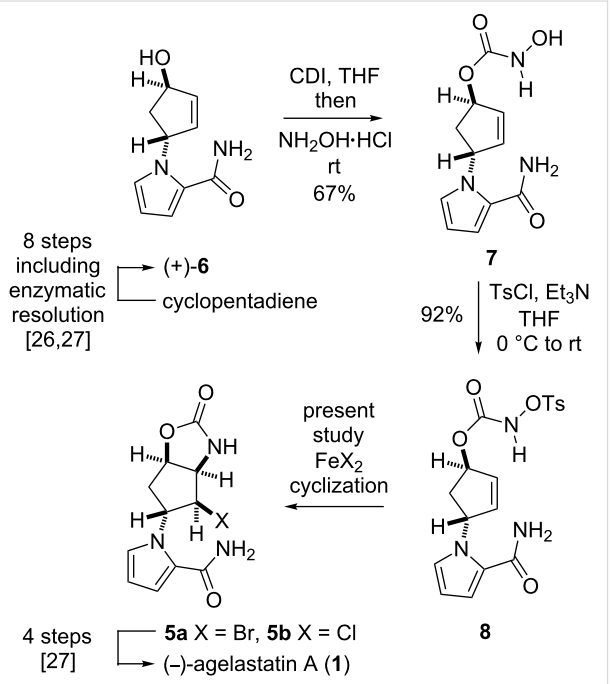

Scheme 2: The present iron(II)-mediated aminohalogenation of *N*-tosyloxycarbamate **8** providing key intermediates **5a**/**5b** for (−)-agelastatin A synthesis.

Results and Discussion

N-Tosyloxycarbamate **8** was prepared from alcohol **6**, which was obtained by a previously reported protocol (Scheme 2) [26,27]. Alcohol **6** was first treated with CDI (*N*,*N*'-carbonyldiimidazole) and then with hydroxylamine hydrochloric acid salt to afford *N*-hydroxycarbamate **7** in 67% yield [36]. Thereafter, *N*-hydroxycarbamate **7** was reacted with TsCl and triethylamine in THF to furnish *N*-tosyloxycarbamate **8** in 92% yield. With this carbamate **8**, we examined the iron(II)-mediated cyclization under various conditions (Table 1).

The application of $FeBr_2$ (0.5 equiv)/Bu_4NBr (1.5 equiv) in EtOH effected cyclization, but the yield of **5a** was poor due to the concomitant formation of carbamate **9** (39%) and enone **10** (30%) (Table 1, entry 1). This was in marked contrast to the observation that the same reagent system, i.e., $FeBr_2$ (0.5 equiv)/Bu_4NBr (1.2 equiv), allowed the efficient conversion of azidoformate **3** (2 g scale) in EtOH to afford **5a** in 70% yield (Scheme 3). The distinct yields of the cyclized materials obtained from *N*-tosyloxycarbamate **8** and azidoformate **3** suggested the unique reactivity of each substrate towards the iron(II) halide (see below). An aminochlorination reagent system, i.e., $FeCl_2$ (0.5 equiv)/Bu_4NCl (1.2 equiv) in EtOH, in turn, furnished the corresponding chloride **5b** in 39% yield as the major product (Table 1, entry 2). Our recent studies on the iron(II)-mediated aminobromination reactions of structurally simple *N*-tosyloxycarbamates with $FeBr_2$/Bu_4NBr revealed significant solvent effects on the product yields [28]. This was also the case in the present study: $FeBr_2$ (0.5 equiv)/Bu_4NBr (1.2 equiv) in *t*-BuOH successfully improved the yield of **5a** relative to the reaction in EtOH (Table 1, entry 3). $FeCl_2$ (0.5 equiv)/Bu_4NCl (1.2 equiv) in *t*-BuOH culminated in the highest yield of **5b** among the examined conditions (Table 1, entry 4) However, a reduction of FeX_2 loading even in *t*-BuOH led to erosion of the yields of halides **5a** and **5b** with recovery of the substrate (Table 1, entries 5 and 6). With the $FeCl_2$/TMSCl reagent system [30-35], chloride **5b** was accessible from *N*-tosyloxycarbamate **8** in 29% yield, along with **9** in 12% yield (Table 1, entry 7). In this particular case, cyclopentanone derivative **11** (16%) and diethyl ketal **12** (14%) were produced as well (Figure 1). An additional experiment to elucidate the origin of their formation provided evidence that these byproducts were generated by the intramolecular cyclization of enone **10** with TMSCl in EtOH, suggesting that the $FeCl_2$/TMSCl system also gave enone **10** in ca. 30% yield [37].

Table 1: Aminohalogenation of *N*-tosyloxycarbamate **8** by iron(II) catalysis.

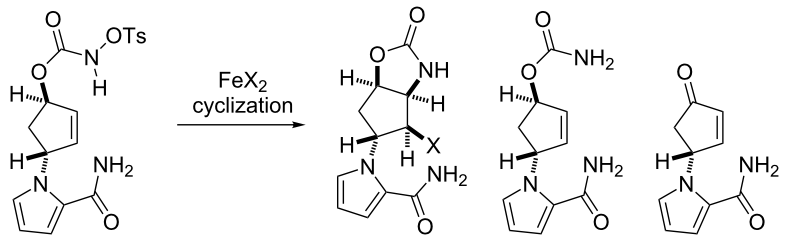

8 **5a** R = Br, **5b** R = Cl **9** **10**

entry	conditions[a]	products (%)
1	$FeBr_2$ (0.5 equiv), Bu_4NBr (1.5 equiv), EtOH, rt, 1.75 h	**5a** (13), **9** (39), **10** (30)
2	$FeCl_2$ (0.5 equiv), Bu_4NCl (1.2 equiv), EtOH, rt, 0.75 h	**5b** (39), **9** (20), **10** (19)
3	$FeBr_2$ (0.5 equiv), Bu_4NBr (1.2 equiv), *t*-BuOH, rt, 0.5 h	**5a** (38), **9** (22), **10** (19)
4	$FeCl_2$ (0.5 equiv), Bu_4NCl (1.2 equiv), *t*-BuOH, rt, 2.5 h	**5b** (48), **9** (9), **10** (9)
5	$FeBr_2$ (0.2 equiv), Bu_4NBr (1.2 equiv), *t*-BuOH, rt, 3.3 h	**5a** (25)[b], **9** (16), **10** (5)
6	$FeCl_2$ (0.2 equiv), Bu_4NCl (1.2 equiv), *t*-BuOH, rt, 3.3 h	**5b** (31)[c], **9** (9), **10** (14)
7	$FeCl_2$ (0.5 equiv), TMSCl (1.5 equiv), EtOH, 0 °C to rt, 16 h	**5b** (29), **9** (12)[d]

[a]All reactions were conducted using 20 mg of substrate **8**. [b]22% of **8** was recovered. [c]35% of **8** was recovered. [d]Compounds **11** (16%) and **12** (14%) were obtained.

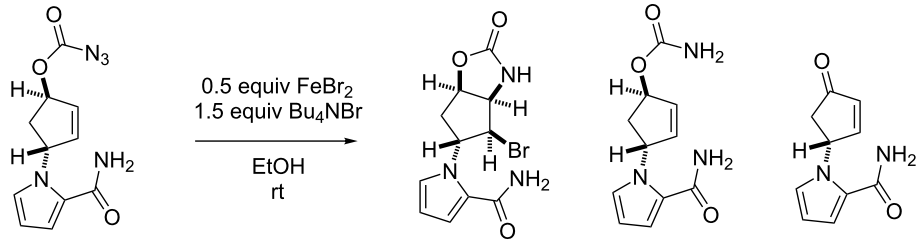

3 **5a** 70% **9** 16% **10** 3%

Scheme 3: Aminohalogenation of azidoformate **3** (2 g scale) under $FeBr_2$/Bu_4NBr conditions.

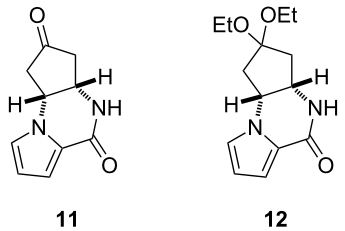

11 **12**

Figure 1: Byproducts formed by aminohalogenation of *N*-tosyloxycarbamate **8** with $FeCl_2$/TMSCl in EtOH (see Table 1; entry 7).

The present study on the aminohalogenation reaction of carbamate **8** has inspired mechanistic insights that deserve discussion (Scheme 4). We hypothesize that cyclized material **5a**/**5b**, reduced material **9**, and enone **10** are generated from an N–iron complex (**i**) that has free-radical character, as previously proposed in the catalytic cyclization of azidoformates [30,38-40]. The contrasting yields obtained from *N*-tosyloxycarbamate **8** and azidoformate **3** under $FeBr_2$/Bu_4NBr in EtOH conditions (see Table 1, entry 1 versus Scheme 3) likely originate from the distinct chemical property of the N–iron species (**i**) generated from each substrate. The possible coordination of tosylate anion to the N–iron after the N–O bond cleavage with FeX_2 may have affected the electronic and steric characters of intermediate (**i**), leading to retardation of the subsequent cyclization. Because of the low cyclization rate, the production of reduced carbamate **9** and enone **10** became pronounced. This is consistent with the observation that the relatively efficient production of cyclized material **5a** was observed for azidoformate **3**, where N–iron intermediate (**i**) was free from such interactions. One of the

other characteristics found in the present transformations was the incomplete consumption of substrate **8** by lowering $FeBr_2$/Bu_4NBr loading (e.g., Table 1, entry 5), which, in turn, enabled the efficient conversion of structurally simple *N*-tosyloxycarbamates into the corresponding cyclic aminobromides [28]. This poor conversion under conditions of less FeX_2/Bu_4NX loading may be attributable to the decrease of the concentration of reactive FeX_2 through capture with the polar amide functionality of **8**.

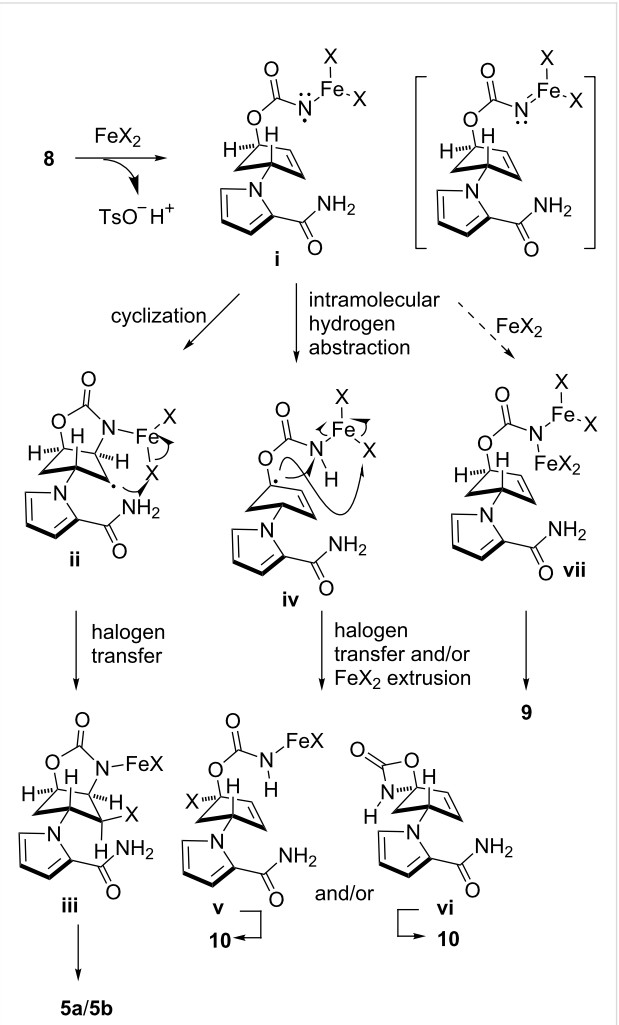

Scheme 4: Plausible reaction pathways in the aminohalogenation of *N*-tosyloxycarbamate **8** with FeX_2/Bu_4NX.

It is speculated that product **9** may be produced by trapping N–iron complex (**i**) with another FeX_2 (**i**→**vii**→**9**), whereas enone **10** is likely to be generated via intramolecular allylic hydrogen abstraction followed by halogen transfer to regenerate iron(II) species (**i**→**iv**→**v**→**10**) and/or by directly releasing FeX_2 (**i**→**iv**→**vi**→**10**) [41]. However, it is worth discussing the process for yielding **9**, which theoretically generates two equivalents of iron(III) species per one equivalent of **vii**. Given the observation that $FeCl_3$/Bu_4NCl gave none of the products shown in Table 1, an iron(III) species possibly generated via the halogen exchange of **vii** with Bu_4NX, if any, no longer has catalytic activity and thus the catalytic cycle is terminated. Therefore, active FeX_2 species should somehow be regenerated to maintain the catalysis. One possible pathway that may account for the production of carbamate **9** through the regeneration of FeX_2 species is the intermolecular hydrogen abstraction from substrate **8** by N–iron species (**i**) (Scheme 5). The intermediacy of the intermolecular hydrogen abstraction of N–iron species (**i**) is supported by the fact that the production of **9** was more pronounced in EtOH having a C–H bond α to the oxygen, which likely served as a hydrogen donor (Table 1, entries 1 and 2). It should be mentioned that reduced material **9** may also be produced by Bu_4NBr alone as observed in our previous study [28]. To elucidate the contribution of this pathway, compound **8** was treated with Bu_4NX in *t*-BuOH. However, no reduced material was obtained within the reaction times depicted in Table 1 [for instance, 0.5 h stirring for Bu_4NBr (Table 1, entry 3) and 2.5 h stirring for Bu_4NCl (Table 1, entry 4)], indicating that the non-iron-mediated process is not significant [42]. Various yields of **9** obtained by loading consistent amounts (1.2–1.5 equiv) of Bu_4NX salts also indicated the poor contribution of the pathway. Chan and co-workers demonstrated that an iron–imido complex generated from $FeCl_2$/PhI=NTs underwent radical hydrogen abstraction from a formyl group, and combined the resultant radicals (hydrogen atom abstraction/radical rebound pathway) to provide amides [43,44]. The involvement of such an iron complex (shown in brackets in Scheme 4) that features radical/metal–nitrenoid properties can be considered in our reactions. A recent study by Betley and co-workers on high-spin iron–imido complexes generated by the reactions of alkyl azides with $FeCl_2$ bearing dipyrromethene ligands revealed the radical character of the complex [39,40], harmonizing well with our result, which implies the intermediacy of the nitrogen radical species.

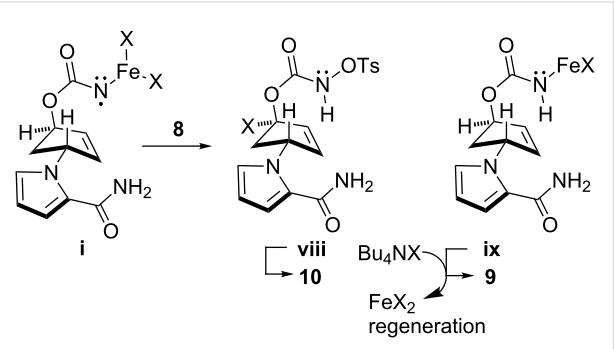

Scheme 5: Plausible reaction pathway to produce compounds **9** and **10**.

Conclusion

We have developed a new approach to key compounds **5a**/**5b** for (−)-agelastatin A (**1**) synthesis, which features the iron(II)-mediated radical cyclization of *N*-tosyloxycarbamate, a safe azidoformate surrogate. Although somewhat moderate chemical yields of the compounds were obtained in this study, the elimination of hazardous synthetic processes enables the establishment of more robust strategies to access **1**. Furthermore, the present study has allowed us to obtain mechanistic insights suggesting that N–iron species (**i**) has a metal-radical character. Much work is currently being undertaken to comprehend fully the unique properties of the present reactions.

Supporting Information

Supporting Information File 1

Experimental procedures, characterization data of new compounds, and $^{1}H/^{13}C$ NMR spectra.
[http://www.beilstein-journals.org/bjoc/content/supplementary/1860-5397-9-99-S1.pdf]

Acknowledgements

The authors are deeply indebted to Professor Tetsuaki Tanaka for his encouragement. This work was supported by a Special Grant generously provided by the Hoansha Foundation and a Grant-in-Aid for Scientific Research on Innovative Areas [No. 22136006] from the Ministry of Education, Culture, Sports, Science and Technology of Japan (MEXT).

References

1. D'Ambrosio, M.; Guerriero, A.; Debitus, C.; Ribes, O.; Pusset, J.; Leroy, S.; Pietra, F. *J. Chem. Soc., Chem. Commun.* **1993,** 1305. doi:10.1039/C39930001305
2. Hong, T. W.; Jímenez, D. R.; Molinski, T. F. *J. Nat. Prod.* **1998,** *61,* 158. doi:10.1021/np9703813
3. Tilvi, S.; Moriou, C.; Martin, M.-T.; Gallard, J.-F.; Sorres, J.; Patel, K.; Petek, S.; Debitus, C.; Ermolenko, L.; Al-Mourabit, A. *J. Nat. Prod.* **2010,** *73,* 720. doi:10.1021/np900539j
4. Pettit, G. R.; Ducki, S.; Herald, D. L.; Doubek, D. L.; Schmidt, J. M.; Chapuis, J.-C. *Oncol. Res.* **2005,** *15,* 11.
5. Mason, C. K.; McFarlane, S.; Johnston, P. G.; Crowe, P.; Erwin, P. J.; Domostoj, M. M.; Campbell, F. C.; Manaviazar, S.; Hale, K. J.; El-Tanani, M. *Mol. Cancer Ther.* **2008,** *7,* 548. doi:10.1158/1535-7163.MCT-07-2251
6. Stien, D.; Anderson, G. T.; Chase, C. E.; Koh, Y.-H.; Weinreb, S. M. *J. Am. Chem. Soc.* **1999,** *121,* 9574. doi:10.1021/ja992487l
7. Feldman, K. S.; Saunders, J. C. *J. Am. Chem. Soc.* **2002,** *124,* 9060. doi:10.1021/ja027121e
8. Hale, K. J.; Domostoj, M. M.; Tocher, D. A.; Irving, E.; Scheinmann, F. *Org. Lett.* **2003,** *5,* 2927. doi:10.1021/ol035036l
9. Domostoj, M. M.; Irving, E.; Scheinmann, F.; Hale, K. J. *Org. Lett.* **2004,** *6,* 2615. doi:10.1021/ol0490476
10. Davis, F. A.; Deng, J. *Org. Lett.* **2005,** *7,* 621. doi:10.1021/ol047634l
11. Trost, B. M.; Dong, G. *J. Am. Chem. Soc.* **2006,** *128,* 6054. doi:10.1021/ja061105q
12. Ichikawa, Y.; Yamaoka, T.; Nakano, K.; Kotsuki, H. *Org. Lett.* **2007,** *9,* 2989. doi:10.1021/ol0709735
13. Dickson, D. P.; Wardrop, D. J. *Org. Lett.* **2009,** *11,* 1341. doi:10.1021/ol900133v
14. Wehn, P. M.; Du Bois, J. *Angew. Chem., Int. Ed.* **2009,** *48,* 3802. doi:10.1002/anie.200806292
15. Hama, N.; Matsuda, T.; Sato, T.; Chida, N. *Org. Lett.* **2009,** *11,* 2687. doi:10.1021/ol900799e
16. Movassaghi, M.; Siegel, D. S.; Han, S. *Chem. Sci.* **2010,** *1,* 561. doi:10.1039/c0sc00351d
17. Menjo, Y.; Hamajima, A.; Sasaki, N.; Hamada, Y. *Org. Lett.* **2011,** *13,* 5744. doi:10.1021/ol2023054
18. Reyes, J. C. P.; Romo, D. *Angew. Chem., Int. Ed.* **2012,** *51,* 6870. doi:10.1002/anie.201200959
19. Kano, T.; Sakamoto, R.; Akakura, M.; Maruoka, K. *J. Am. Chem. Soc.* **2012,** *134,* 7516. doi:10.1021/ja301120z
20. Hale, K. J.; Domostoj, M. M.; El-Tanani, M.; Campbell, F. C.; Mason, C. K. In *Strategies and Tactics in Organic Synthesis;* Harmata, M., Ed.; Academic Press: London, 2005; Vol. 6, p 352. doi:10.1016/S1874-6004(05)80034-6
See for selected reviews of agelastatins and related compounds.
21. Weinreb, S. M. *Nat. Prod. Rep.* **2007,** *24,* 931. doi:10.1039/b700206h
22. Dong, G. *Pure Appl. Chem.* **2010,** *82,* 2231. doi:10.1351/PAC-CON-10-08-04
23. Young, I. S.; Thornton, P. D.; Thompson, A. *Nat. Prod. Rep.* **2010,** *27,* 1801. doi:10.1039/c0np00014k
24. Al-Mourabit, A.; Zancanella, M. A.; Tilvi, S.; Romo, D. *Nat. Prod. Rep.* **2011,** *28,* 1229. doi:10.1039/c0np00013b
25. Yamaoka, T.; Ichikawa, Y.; Kotsuki, H. *J. Synth. Org. Chem., Jpn.* **2012,** *70,* 615. doi:10.5059/yukigoseikyokaishi.70.615
26. Yoshimitsu, T.; Ino, T.; Tanaka, T. *Org. Lett.* **2008,** *10,* 5457. doi:10.1021/ol802225g
27. Yoshimitsu, T.; Ino, T.; Futamura, N.; Kamon, T.; Tanaka, T. *Org. Lett.* **2009,** *11,* 3402. doi:10.1021/ol9012684
28. Kamon, T.; Shigeoka, D.; Tanaka, T.; Yoshimitsu, T. *Org. Biomol. Chem.* **2012,** *10,* 2363. doi:10.1039/c2ob07190h
29. Nguyen, Q.; Nguyen, T.; Driver, T. G. *J. Am. Chem. Soc.* **2013,** *135,* 620. doi:10.1021/ja3113565
See for a recent application of catalytic $FeBr_2$ to C–H amination.
30. Bach, T.; Schlummer, B.; Harms, K. *Chem. Commun.* **2000,** 287. doi:10.1039/a909009f
31. Bach, T.; Schlummer, B.; Harms, K. *Synlett* **2000,** 1330. doi:10.1055/s-2000-7129
32. Bach, T.; Schlummer, B.; Harms, K. *Chem.–Eur. J.* **2001,** *7,* 2581. doi:10.1002/1521-3765(20010618)7:12<2581::AID-CHEM25810>3.0.CO;2-O
33. Churchill, D. G.; Rojas, C. M. *Tetrahedron Lett.* **2002,** *43,* 7225. doi:10.1016/S0040-4039(02)01658-1
34. Bacci, J. P.; Greenman, K. L.; Van Vranken, D. L. *J. Org. Chem.* **2003,** *68,* 4955. doi:10.1021/jo0340410
35. Danielec, H.; Klügge, J.; Schlummer, B.; Bach, T. *Synthesis* **2004,** 551. doi:10.1055/s-2005-918500
36. Lebel, H.; Huard, K.; Lectard, S. *J. Am. Chem. Soc.* **2005,** *127,* 14198. doi:10.1021/ja0552850

37. When enone **10** was treated with TMSCl in EtOH at room temperature, diethylketal **12** (19%) and ketone **11** (10%) were generated. The TLC analysis of the reaction mixture clearly showed that diethylketal **12** was an initial product, which gradually underwent decomposition to give ketone **11**.
38. Protonated cation radical **x** is considered to be produced immediately after N–O cleavage and may be responsible for the distinct reactivities. However, because of its high acidity, the proton on the carbamoyl nitrogen atom of **x** likely dissociates to provide intermediate **i**.

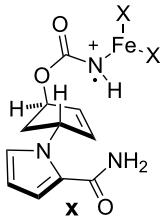

39. King, E. R.; Hennessy, E. T.; Betley, T. A. *J. Am. Chem. Soc.* **2011,** *133,* 4917. doi:10.1021/ja110066j
See for recent studies on C–H cleavage by N–iron complex showing radical character.
40. Paradine, S. M.; White, M. C. *J. Am. Chem. Soc.* **2012,** *134,* 2036. doi:10.1021/ja211600g
And references cited therein.
41. It can also be assumed that enone **10** is generated from intermediate **iv** via direct fragmentation of an isocyanate and iron(II) halide. We thank one of the referees for suggesting such a possibility.
42. Treatment of substrate **8** with Bu_4NBr for 2.5 h gave a small amount of **9** (9%) along with unreacted **8** (74%), whose chemical yields were estimated by ^1H NMR analysis of the crude mixture. In contrast, no reduced product **9** was generated at all with Bu_4NCl after 2.5 h. In this case, after 5.5 h, carbamate **9** was formed in 3% yield accompanying the recovery of **8** (85%).
43. Ton, T. M. U.; Tejo, C.; Tania, S.; Chang, J. W. W.; Chan, P. W. H. *J. Org. Chem.* **2011,** *76,* 4894. doi:10.1021/jo200284a
44. Maestre, L.; Sameera, W. M. C.; Mar Díaz-Requejo, M.; Maseras, F.; Pérez, P. J. *J. Am. Chem. Soc.* **2013,** *135,* 1338. doi:10.1021/ja307229e
See for a recent discussion on the mechanisms of metal–nitrenide catalysis.

License and Terms

Beilstein Journal of Organic Chemistry

New core-pyrene π structure organophotocatalysts usable as highly efficient photoinitiators

Sofia Telitel[1], Frédéric Dumur[2], Thomas Faury[2], Bernadette Graff[1], Mohamad-Ali Tehfe[1], Didier Gigmes[*2], Jean-Pierre Fouassier[3] and Jacques Lalevée[*1]

Full Research Paper

Open Access

Address:
[1]Institut de Science des Matériaux de Mulhouse IS2M – UMR 7361 – UHA; 15, rue Jean Starcky, F-68057 Mulhouse Cedex, France, [2]Aix-Marseille Université, CNRS, Institut de Chimie Radicalaire, UMR 7273, F-13397 Marseille, France and [3]ENSCMu-UHA, 3 rue Alfred Werner, F-68093 Mulhouse Cedex, France

Email:
Didier Gigmes[*] - didier.gigmes@univ-amu.fr; Jacques Lalevée[*] - jacques.lalevee@uha.fr

* Corresponding author

Keywords:
cationic photopolymerization; free-radical-promoted cationic photopolymerization; photocatalysts; photoinitiators; radical photopolymerization

Beilstein J. Org. Chem. **2013,** *9,* 877–890.
doi:10.3762/bjoc.9.101

Received: 02 March 2013
Accepted: 12 April 2013
Published: 07 May 2013

This article is part of the Thematic Series "Organic free radical chemistry".

Guest Editor: C. Stephenson

Abstract

Eleven di- and trifunctional compounds based on a core-pyrene π structure (Co_Py) were synthesized and investigated for the formation of free radicals. The application of two- and three-component photoinitiating systems (different Co_Pys with the addition of iodonium or sulfonium salts, alkyl halide or amine) was investigated in detail for cationic and radical photopolymerization reactions under near-UV–vis light. The proposed compounds can behave as new photocatalysts. Successful results in terms of rates of polymerization and final conversions were obtained. The strong MO coupling between the six different cores and the pyrene moiety was studied by DFT calculations. The different chemical intermediates are characterized by ESR and laser flash photolysis experiments. The mechanisms involved in the initiation step are discussed, and relationships between the core structure, the Co_Py absorption property, and the polymerization ability are tentatively proposed.

Introduction

Free radical sources are encountered in various areas such as organic chemistry, biochemistry and polymer chemistry. In the field of polymer photochemistry applied to photopolymerization reactions, they are referred to as photoinitiators (PI) [1]. These PIs are usable in two scenarios, both of which are light induced. Firstly, they are usable in free radical polymerization (FRP), where the PIs work as either cleavable type I PIs or uncleavable type II PIs in dependence of couples formed by the PI and hydrogen or electron donors (r1 in Scheme 1). Secondly, PIs may be used in free-radical-promoted cationic polymerization (FRPCP), in which the produced radical $R^{\bullet}$ is oxidized by an onium salt, e.g., Ar_2I^+, to form $Ar_2I^{\bullet}$ and a cation R^+ suit-

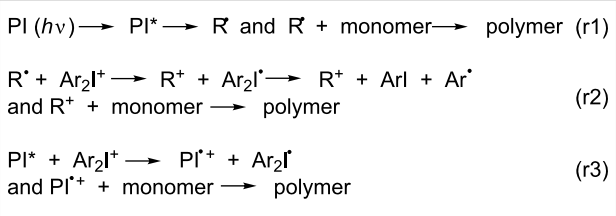

Scheme 1: Typical reactions for photoinitiated cationic polymerization.

able for the ROP reaction. The $Ar_2I^•$ species is readily decomposed into ArI and Ar• (r2 in Scheme 1). There is also an usual cationic polymerization (CP; r3 in Scheme 1) [1,2]. When the PIs exhibit a catalytic behavior analogous to a photocatalyst (PC) in organic chemistry, they are designed as photoinitiator catalysts (PIC). PIs as well as PICs are based on pure organic, that is, metal free, or organometallic compounds. In the presence of additives, they constitute a photoinitiating system (PIS).

Among others, two points of interest in the photopolymerization area are (i) the reactivity and efficiency of the PIs and PICs and (ii) the irradiation conditions. Indeed, the absorption properties (wavelengths λ, molar extinction coefficients ε), the excited-state processes, the reactivity of the produced radicals, and the characteristics of the light sources (emission spectra, available luminous power density) govern the polymerization efficiency (rate of polymerization, final monomer conversion). The photopolymerization reactions in radiation curing technologies are often carried out under high-intensity light sources (>1000 mW cm^{-2}). Applications in this area and in other fields may require to avoid the use of UV rays delivered by Hg lamps or to irradiate with visible light (400–700 nm) and low photon fluxes (~2–10 mW cm^{-2}). Recent works have aimed at working under soft irradiation conditions (near-UV–vis light, low light intensity), which allows the use of Xe lamps, laser diodes, solar radiation, household halogen lamps, fluorescent bulbs and blue, green and white LEDs (see a recent review in [1]).

New high-performance PIs and PICs are continuously being developed [1-10] through the design of novel structures (e.g., novel chromophores, novel cleavable bonds) and the modification ofexisting structures by using the classical introduction of electron-donating or -withdrawing substituents, conjugated groups or moieties, and more complex changes on the skeleton (see typical recent examples in [11-41]). To meet the challenge of designing efficient PIs and PICs under soft irradiation, we have recently started the search for suitable multifunctional arrangements exhibiting a strong coupling of the molecular orbitals MOs [42,43]. Improved absorption properties (red-shifted λ, higher ε) while keeping a high reactivity have been already achieved. Examples of these investigated architectures (Scheme 2) [42-44] are linked PI–PI units (e.g., PI = pyrene) or PI-PI' (e.g., PI = pyrene and PI' = 2,2'-dimethoxy-2-phenylace-

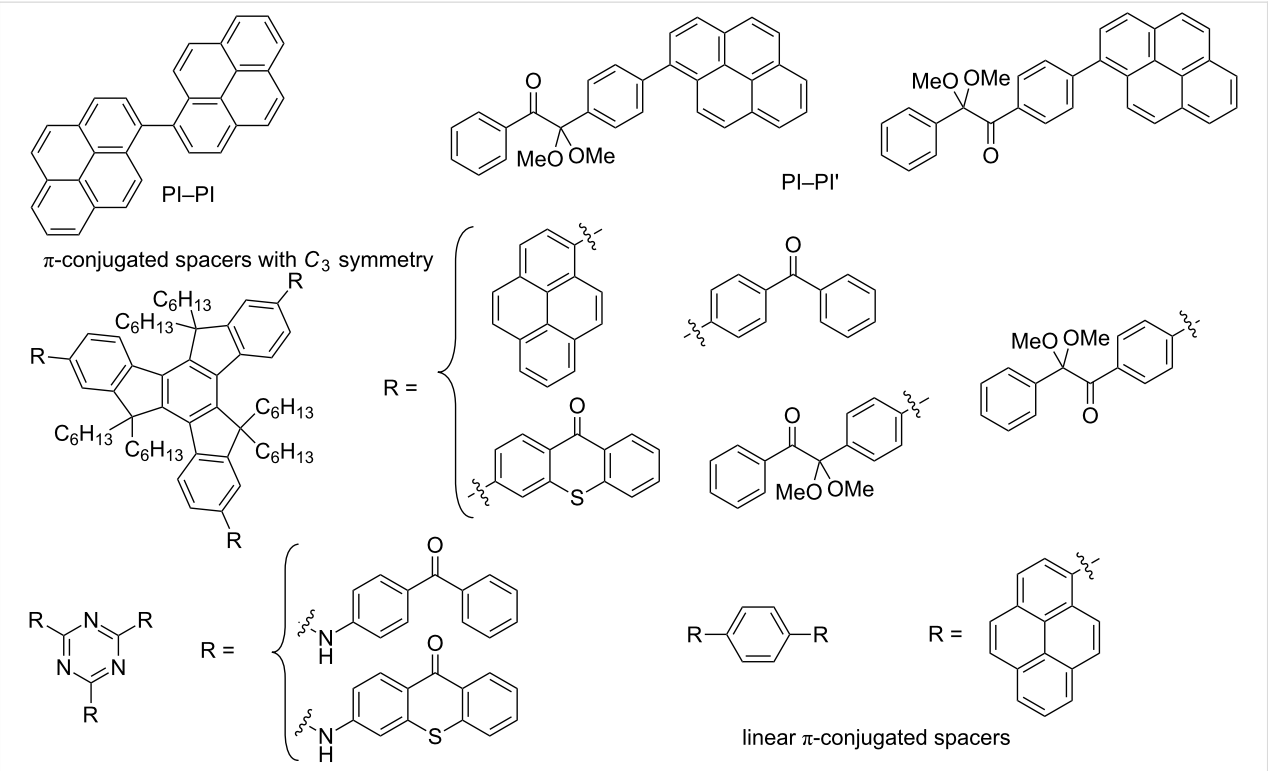

Scheme 2: Examples of previously investigated architectures.

tophenone) and PI moieties (e.g., PI = benzophenone, thioxanthone, 2,2'-dimethoxy-2-phenylacetophenone, pyrene) linked to a trifunctional core (truxene, triazine, benzene); the same could be expected by using a difunctional core.

In the present paper, we consider a series of eleven di- and trifunctional core-pyrene π compounds Co_Py, where the pyrene moiety is used as a PI. The cores include a functionalized truxene (**Py_5**), several substituted phenyl rings (**Py_2**, **Py_3**, **Py_4**, **Py_9**, **Py_10**) two functionalized triazines (**Py_7**, **Py_12**), a triphenylamine (**Py_6**), a carbazole (**Py_11**) and a benzothiadiazole (**Py_8**) (Scheme 3). The idea is to get a high absorption around 380–410 nm where Xe–Hg lamps, Xe lamps, LED, laser diodes and even household halogen lamps are usable. The large choice of Co_Pys should allow for studying the effect of the core on the MO coupling and the resulting

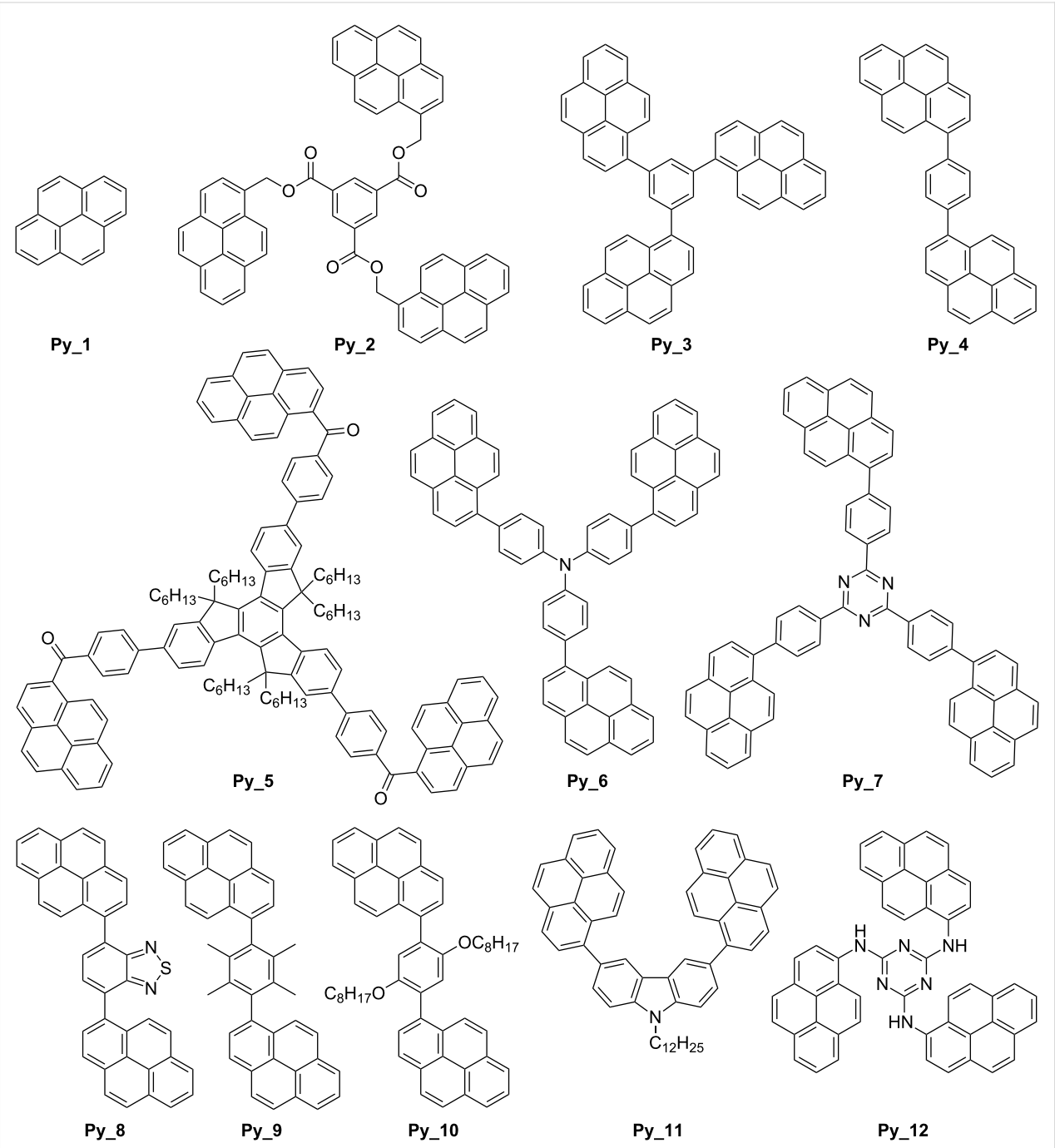

Scheme 3: Investigated **Co_Pys**.

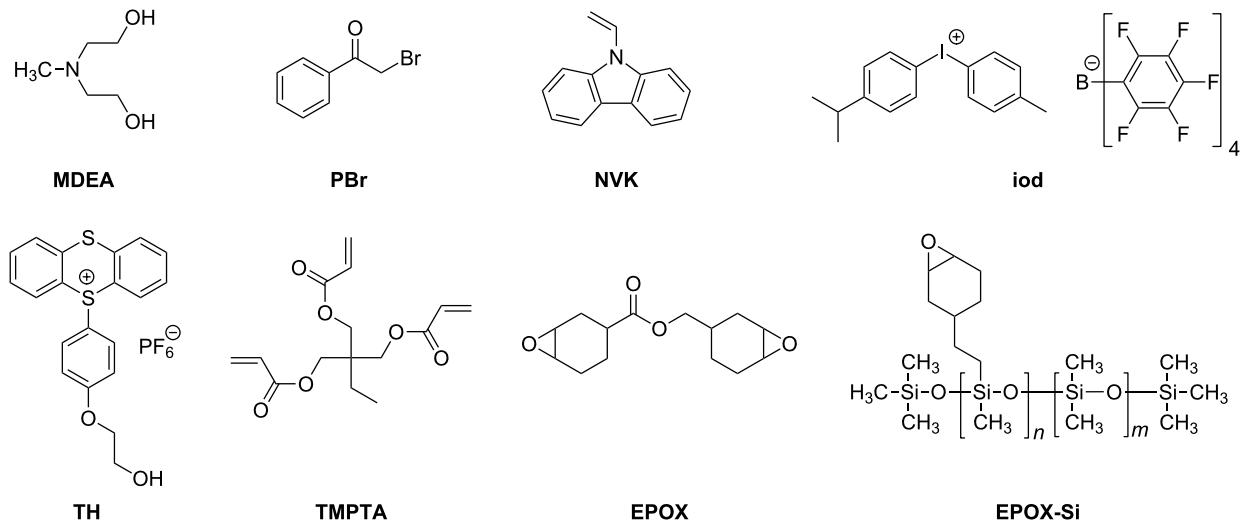

Scheme 4: Other chemical compounds.

absorption properties. The activity of these Co_Py compounds in the FRP of acrylates and the FRPCP (and eventually the cationic polymerization CP) of epoxides through a ring-opening polymerization (ROP) under exposure to the near-UV–vis light delivered by a Hg–Xe lamp (~30 mW cm^{-2}) and the visible light of a halogen lamp (soft irradiation conditions; ~10 mW cm^{-2}) is investigated. The Co_Pys are used in combination with additives: iodonium or sulfonium salts for ROP and amine or/and alkyl halide for FRP. The monomers investigated are given in Scheme 4. The mechanisms are analyzed by electron spin resonance (ESR), steady-state photolysis, fluorescence and laser flash photolysis (LFP). The ability of Co_Pys to behave as new organophotocatalysts is also discussed.

Results and Discussion

Light absorption, redox properties and MO calculations

The UV absorption spectra of the different pyrene derivatives are depicted in Figure 1. The solvents were selected for good solubility of the Co_Pys. Absorption maxima are located at ~350 nm for **Py_2**, **Py_3**, **Py_4**, **Py_5**, **Py_12**, **Py_8**, **Py_9**, **Py_10**, **Py_11**, ~370 nm for **Py_6**, **Py_7**, and 330 nm for **Py_1** (Table 1). This corresponds to a red shift of the absorption for

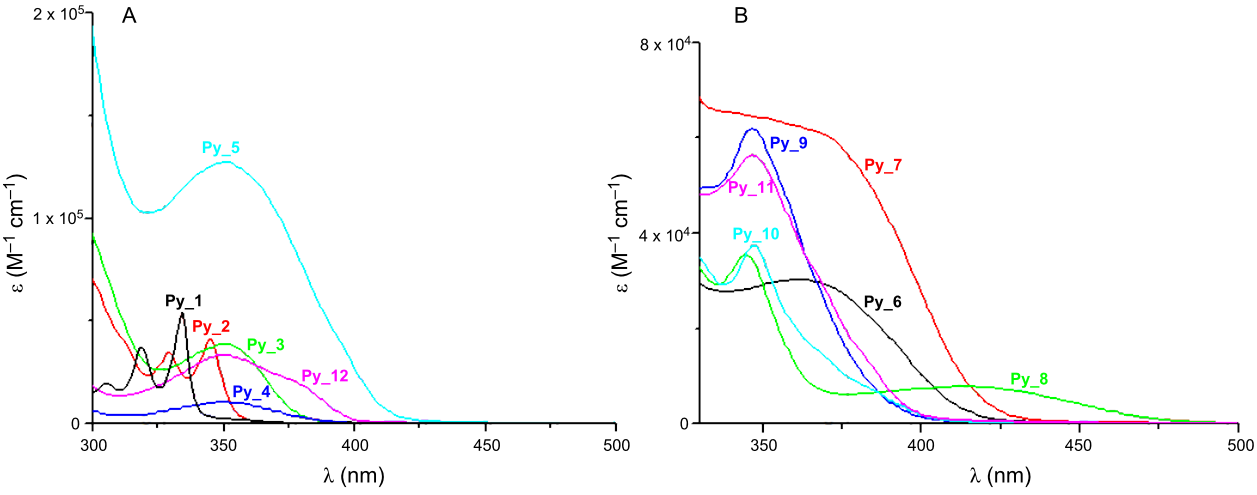

Figure 1: UV–vis absorption spectra of the investigated compounds: (A) In acetonitrile for **Py_1** and acetonitrile/toluene (50/50) for the other molecules, (B) in toluene.

Table 1: Properties of the pyrene derivatives in acetonitrile (*) and toluene. Light absorption and emission properties (experimental $\lambda_{max,abs,exp}$ and calculated $\lambda_{max,abs,calc}$ maximum absorption wavelengths, emission wavelengths $\lambda_{max,em}$), excited-state energy levels (E_S), oxidation potentials (E_{ox}) and free-energy changes ΔG (see text) [1].

	$\lambda_{max,abs,exp}$ (nm)	$\lambda_{max,abs,calc}$[a] (nm)	$\lambda_{max,em}$ (nm)	E_{ox} (V/SCE)	E_S (eV)	ΔG_{PBr} (eV)	ΔG_{Iod} (eV)
Py_1*	334	327 (f = 0.27)	393	1.33	3.44	−1.33	−1.9
Py_2	344	334 (f = 0.41)	380	0.8	3.45	−1.87	−2.45
Py_3	351	356 (f = 0.50)	393	0.9	3.36	−1.68	−2.26
Py_4	351	373 (f = 0.3)	423	0.6	3.21	−1.83	−2.41
Py_5	353	387 (f = 1.16)	404	0.7	3.24	−1.76	−2.34
Py_6	365	344 (f = 0.52); 403 (f = 0.74)	441	0.9	3.04	−1.36	−1.94
Py_7	367	344 (f = 0.68)	440	–	3.02	–	–
Py_8	344	365 (f = 0.39)	530	0.7	2.6	−1.12	−1.7
Py_9	346	336 (f = 0.44)	428	0.8	3.2	−1.62	−2.2
Py_10	347	376 (f = 0.51)	425	0.9	3.2	−1.52	−2.1
Py_11	346	370 (f = 0.4)	409	−	3.22	–	–
Py_12	346	377 (f = 1.00)	397	0.6	3.22	−1.84	−2.42

[a]Molecular orbital MO calculations (using the time-dependent density functional theory at B3LYP/6-31G* level on the relaxed geometries calculated at UB3LYP/6-31G* level); f = oscillator strength.

Py_2 to **Py_12** compared to the reference compound **Py_1**. At 365 nm, the maximum emission wavelength of the Hg–Xe lamp, the molar extinction coefficients ε_{max} of the different Co_Pys follow the order **Py_5** > **Py_7** > **Py_11** > **Py_9** > **Py_6** > **Py_12** > **Py_3** > **Py_10** > **Py_8** > **Py_4** > **Py_1** = **Py_2**. The highest ε_{max} is obtained for **Py_5** ($\varepsilon_{353} = 13 \times 10^4$ M^{-1} cm^{-1}, $\varepsilon_{346} = 6 \times 10^4$ M^{-1} cm^{-1} versus $\varepsilon_{334} = 6 \times 10^4$ M^{-1} cm^{-1} for **Py_5**, **Py_9** and **Py_1**, respectively). **Py_4** exhibits low ε values, and thus a low efficiency can be expected for this compound.

The oxidation potentials of the Co_Pys (Table 1) range from 1.33 V (**Py_1**) to 0.6 V (**Py_4**, **Py_12**). The singlet-state energy is also affected by the core of the structure, i.e., 2.6 eV for **Py_8** versus 3.44 eV for the reference **Py_1**. The free-energy change ΔG of the Co_Py/phenacyl bromide PBr (or the iodonium salt, Iod) interaction is very favorable ($\Delta G << 0$). **Py_2** exhibits the most favorable ΔGs: −2.45 eV (Iod) and −1.87 eV (PBr).

MO calculations show that the calculated and experimental values (Table 1) are approximately the same, e.g., a difference of 5 to 10 nm is observed for **Py_2** and **Py_3**. The oscillator strengths (noted f in Table 1) are higher for the new proposed structures than for **Py_1** in agreement with their better light absorption properties (Figure 1). A strong coupling of the π MOs of the core with those of the pyrene substituents is shown supporting a clear ππ* character of the HOMO–LUMO transition, as evidenced in Figure 2 for the investigated derivatives. For the various π-core/pyrene substituent combinations, different coupling strengths can be observed (Figure 2). Strong couplings of the MOs lead to red-shifted transitions compared to **Py_1** and enhanced absorption coefficients (Figure 1), e.g., for **Py_3**, **Py_5**, **Py_6**, **Py_8**, **Py_11** and **Py_12**. A strong delocalization of the HOMOs and LUMOs is observed in line with their better absorption properties. For **Py_2**, the coupling is weak and the absorption properties are moderately affected compared to **Py_1**.

Photochemical reactivity

Fluorescence experiments

A strong quenching of the Co_Py singlet states by PBr, amine (MDEA), Iod and the sulfonium salt TH is found. **Py_3** is selected for this mechanistic study (Figure 3) because of the high reactivity of this compound in photopolymerization experiments (see below). The rate constants in that case are 1.5×10^{10}, 9×10^9, 1×10^{10} and 3.7×10^9 M^{-1} s^{-1}, respectively. The ^{1}**Py_3**/PBr, ^{1}**Py_3**/Iod and ^{1}**Py_3**/TH interactions are diffusion-controlled in full agreement with the highly favorable ΔGs (Table 1; the reduction potential for TH is −1.3 V [1]; the calculated ΔG is −1.16 eV). They correspond to an efficient electron transfer followed by the usual fast generation of radicals from the radical anion species (r5–r7 in Scheme 5) or an electron/proton transfer with the amine (r8 in Scheme 5).

ESR spin trapping experiments

In ESR spin trapping experiments upon UV light exposure, the interaction of the Co_Pys with the iodonium salt Iod (Figure 4A) or the sulfonium salt TH (Figure 1 in Supporting Information File 1) leads to an aryl radical $Ar^•$ (e.g., hyperfine coupling constants *hfcs* of the PBN adduct: a_N = 14.2 G and a_H

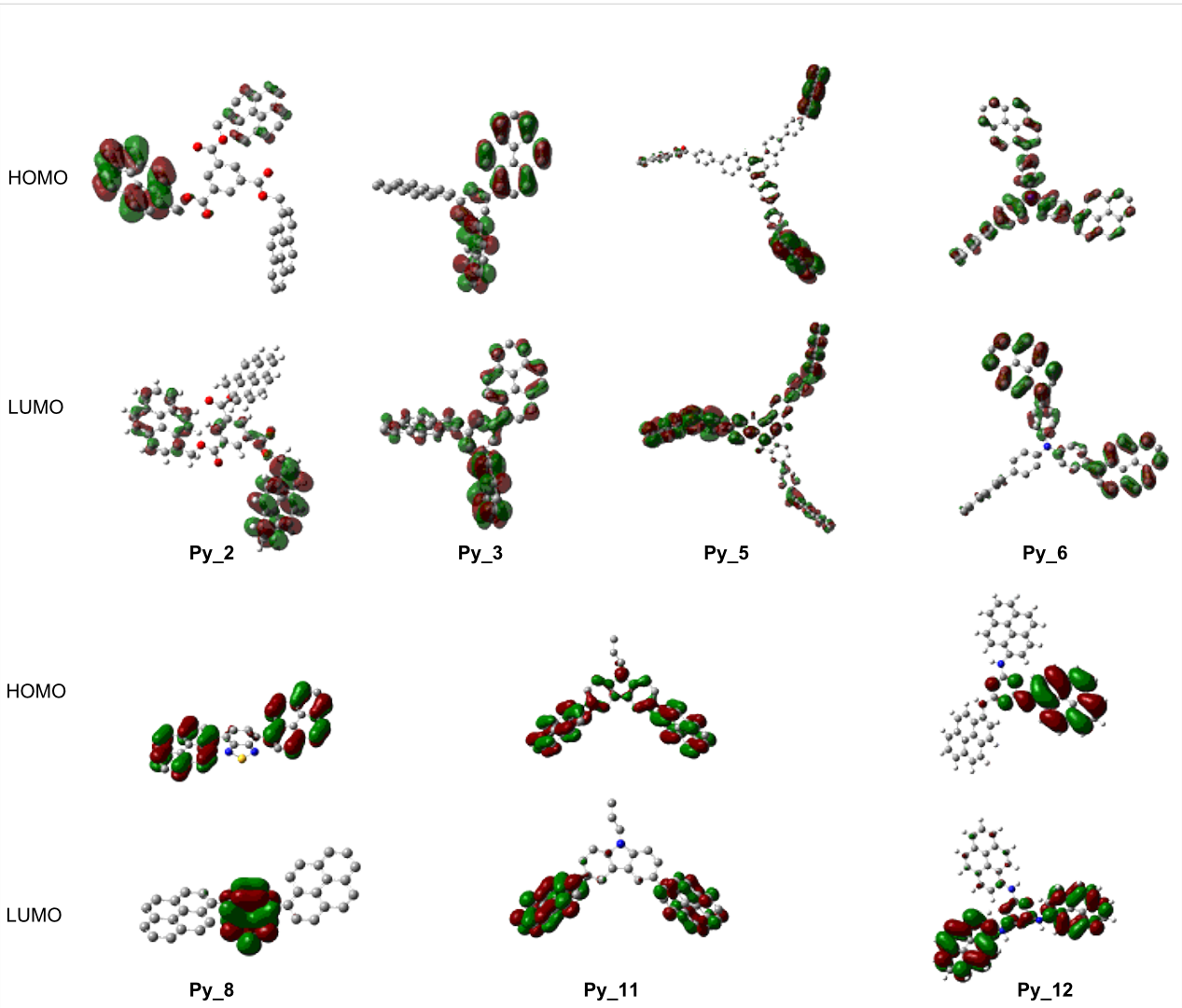

Figure 2: HOMO–LUMO orbitals for **Py_2**, **Py_3**, **Py_5**, **Py_6**, **Py_8**, **Py_11** and **Py_12** involved in the π–π* transition (calculated at UB3LYP/6-31G* level; for **Py_5** and **Py_11**, the alkyl chains have been simplified to reduce the computational cost).

$$\mathbf{Py\_3} \longrightarrow {}^1\mathbf{Py\_3}\ (h\nu) \quad \text{(r4)}$$

$${}^1\mathbf{Py\_3} + \text{Iod}\ (Ar_2I^+) \longrightarrow {}^1\mathbf{Py\_3}^{\bullet+} + \text{ArI} + Ar^{\bullet} \quad \text{(r5)}$$

$${}^1\mathbf{Py\_3} + \text{TH}\ (R_2S^+Ar') \longrightarrow \text{Py\_3}^{\bullet+} + R_2S + Ar^{\bullet} \quad \text{(r6)}$$

$${}^1\mathbf{Py\_3} + \text{PBr}\ (PhC(=O)CH_2Br) \longrightarrow \text{Py\_3}^{\bullet+} + (PhC(O)CH_2Br)^{\bullet-}$$
$$\longrightarrow \text{Py\_3}^{\bullet+} + PhC(=O)CH_2^{\bullet} + Br^- \quad \text{(r7)}$$

$${}^1\mathbf{Py\_3} + \text{MDEA} \longrightarrow \text{Py\_3}^{\bullet-} + \text{MDEA}^{\bullet+} \longrightarrow (\mathbf{Py\_3})\text{–H}^{\bullet} + \text{MDEA}^{\bullet}\,(\text{–H}) \quad \text{(r8)}$$

$$Ar^{\bullet} + \text{NVK} \longrightarrow \text{Ar–NVK}^{\bullet} \quad \text{(r9)}$$

$$\text{Ar–NVK}^{\bullet} + Ar_2I^+ \longrightarrow \text{Ar–NVK}^+ + \text{ArI} + Ar^{\bullet} \quad \text{(r10)}$$

$$\mathbf{Py\_9} + Ar_2I^+\ (\Delta) \longrightarrow \mathbf{Py\_9}^{\bullet+} + \text{ArI} + Ar^{\bullet} \quad \text{(r11)}$$

$$\text{Ar–NVK}^{\bullet} + \mathbf{Py\_11}^{\bullet+} \longrightarrow \mathbf{Py\_11} + \text{Ar–NVK}^+ \quad \text{(r12)}$$

Scheme 5: Photochemical processes for the different Co_Pys.

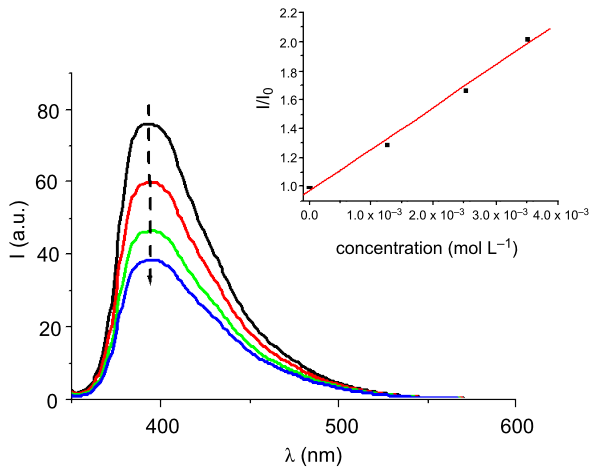

Figure 3: Fluorescence quenching of ^{1}**Py_3** by the phenacylbromide (PBr) in acetonitrile/toluene (50/50). Insert: Stern–Volmer plot (the concentrations used are given in this plot).

= 2.2 G in agreement with known data [22-25,45]) in line with (r5). In the same way, phenacyl radicals and α-aminoalkyl radicals (r7 and r8 in Scheme 5) are observed in ^{1}**Py_3**/PBr and ^{1}**Py_3**/EDB (a_N = 14.6 G, a_H = 4.5 G and a_N = 14.3 G, a_H = 2.5 G, respectively; Figure 4B and Figure 4C; ethyldimethylaminobenzoate (EDB) instead of MDEA is used to avoid a high polarity of the sample preventing an ESR investigation). The **Py_3**/Iod or the **Py_3**/TH couple generates a cation radical (**Py_3**$^{\bullet+}$) that can initiate a cationic polymerization whereas the phenacyl and aminoalkyl radicals formed in **Py_3**/PBr or **Py_3**/MDEA are susceptible to radical polymerization.

Laser flash photolysis

Upon laser excitation of **Py_3** at 355 nm, a triplet state T_1 characterized by a maximum absorption at ~420 nm and a rather long lifetime is formed (t > 4 µs) (Figure S2 in Supporting Information File 1). This T_1 state is similar to that of **Py_1** [31]. The short S_1 lifetime (e.g., ~55 ns under N_2 for **Py_3**) and the diffusion controlled interactions of S_1 with Iod, PBr or MDEA (see above) prevent a significant production of T_1 in Co_Py/Iod (PBr or MDEA). Therefore, a triplet-state pathway can be neglected in the investigated systems.

Thermal processes

For some Co_Py/Iod couples, a slow thermal redox process can also occur. Indeed, in ESR–ST experiments, aryl radicals are generated without irradiation within 24 h (no free radical was observed in **Py_9** or Iod alone). For example, in **Py_9**/Iod, the same radicals as in r5 are produced (Figure 5; *hfccs*: a_N = 14.2 G and a_H = 2.2 G for the PBN radical adduct). Peroxyl radicals are also observed, as aryls easily add to O_2 (a_N = 13.3 G and a_H = 1.6 G for the PBN radical adduct, in agreement with [45]). As in r5 in Scheme 5, a cation radical **Py_9**$^{\bullet+}$ is concomitantly formed. This thermal process is slow as E_{ox}(**Py_9**) > E_{red}(Iod) (Table 1). The formation of radical cations can be worthwhile to initiate cationic polymerization at room temperature (see below).

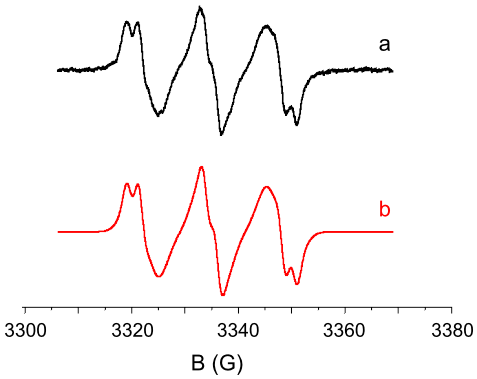

Figure 5: ESR-spin trapping spectra of **Py_9**/Iod in *tert*-butylbenzene (storage at rt for 24 h); (a) experimental and (b) simulated spectra.

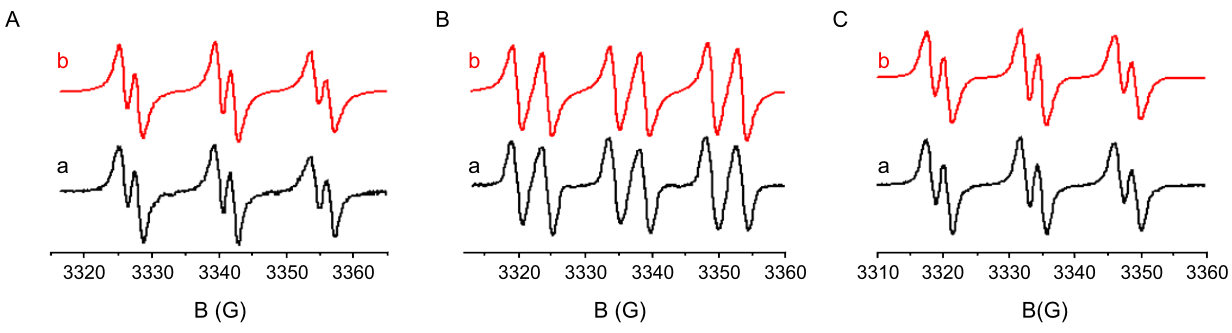

Figure 4: ESR spectra obtained upon irradiation of (A) **Py_3**/Iod, (B) **Py_3**/PBr and (C) **Py_3**/EDB in *tert*-butylbenzene. Phenyl-*N*-*tert*-butylnitrone (PBN) is used as a spin trap; (a) experimental and (b) simulated ESR spectra.

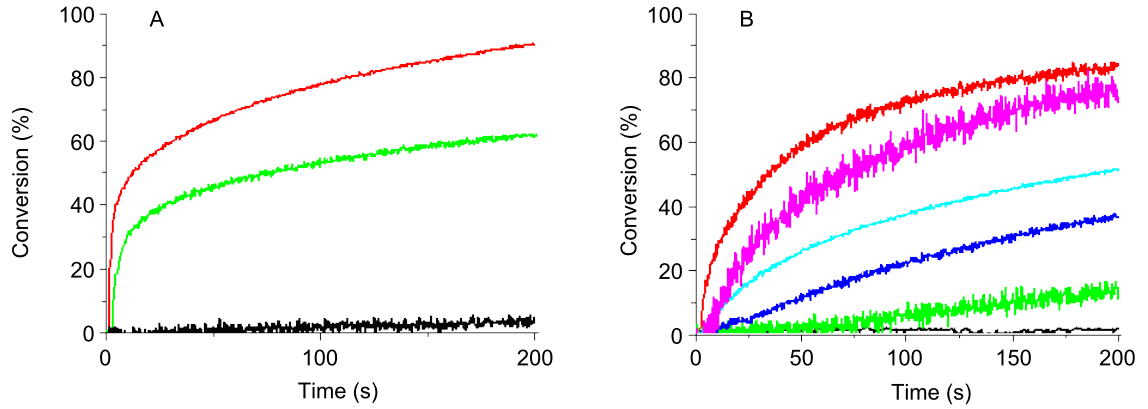

Figure 6: Photopolymerization profiles of EPOX upon Xe–Hg lamp irradiation (λ > 340 nm) under air for different photoinitiating systems: (A) (a) Iod (2% w/w); (b) **Py_3**/Iod (1%/2% w/w); (c) **Py_1**/Iod (1%/2% w/w); (B) (a) TH (2% w/w); (b) **Py_3**/TH (0.2%/2% w/w); (c) **Py_8**/TH (0.2%/2% w/w); (d) **Py_9**/TH (0.2%/2% w/w); (e) **Py_10**/TH (0.2%/2% w/w); (f) **Py_11**/TH (0.2%/2% w/w).

Ability of the different pyrene structures in photopolymerization reactions

Cationic photopolymerization (CP)

The ring-opening polymerization profiles of EPOX upon exposure to the Xe–Hg lamp under air using two-component PISs are shown in Figure 6, Figure 7 and Figure 8. A comparison of the photopolymerization profiles using the **Py_1** (to **Py_12**)/Iod couples (Figures 6–8) shows that the fastest polymerization rates (Rp) and the highest final conversion (conv) are obtained with **Py_11**/Iod and **Py_3**/Iod. No polymerization is observed in the presence of Iod alone Figure 6A and Figure 8A, curves a.) **Py_3**/Iod leads to a conv ~90% (Figure 6A, curve b) compared to **Py_1**/Iod (conv ~50%; Figure 6A, curve c). Almost all the new proposed structures are better than the starting structure **Py_1** (Figure 7, curve b). This highlights the interest of the present approach associated with the modification of the Py chromophore. CP can also be initiated in the presence of the sulfonium salt TH, e.g., with **Py_3**, **Py_8**, **Py_9**, **Py_10** and **Py_11** (Figure 6B). The conversions reach 80% and 75% with **Py_3**/TH and **Py_11**/TH, respectively (after 200 s light exposure). EPOX-Si can also be easily polymerized (Figure 8). **Py_3**/Iod (Figure 8A) is still efficient (conv ~50%).

In these systems, the Co_Py$^{\bullet+}$ generated in r5,r6 (Scheme 5) can initiate the CP process. The relative efficiency of these Co_Py/Iod (or TH) combinations will be affected by different parameters: (i) their relative light absorption properties, (ii) the quantum yields of radical or radical cation formation in the singlet state (the singlet state is predominant, see above), (iii) the rate constants for reactions r5 and r6 and (iv) the ability of Co_Py$^{\bullet+}$ to initiate a ring-opening polymerization process. Structure–reactivity relationships for the different derivatives can hardly be extracted. This is probably ascribed to a strong interplay between (i) to (iv).

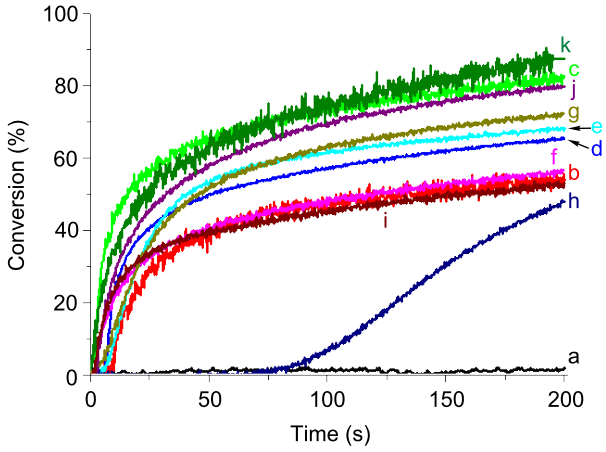

Figure 7: Photopolymerization profiles of EPOX upon a Xe–Hg lamp irradiation (λ > 340 nm) under air for different photoinitiating systems: (a) Iod (2% w/w); (b) **Py_1**/Iod (0.2%/2% w/w); (c) **Py_3**/Iod (0.2%/2% w/w); (d) **Py_4**/Iod (0.2%/2% w/w); (e) **Py_5**/Iod (0.2%/2% w/w); (f) **Py_6**/Iod (0.2%/2% w/w); (g) **Py_7**/Iod (0.2%/2% w/w); (h) **Py_8**/Iod (0.2%/2% w/w); (i) **Py_9**/Iod (0.2%/2% w/w); (j) **Py_10**/Iod (0.2%/2% w/w) ; (k) **Py_11**/Iod (0.2%/2% w/w).

A cationic photopolymerization profile of EPOX under very soft irradiation (halogen lamp exposure) is represented in Figure 8B. In the presence of Iod, several Co_Pys exhibiting an acceptable absorption at λ > 380 nm lead to efficient polymerization reactions. For example, conv = 40 and 55% within 200 s with the **Py_7**/Iod and **Py_11**/Iod couples.

The three-component PIS (**Py_11**/Iod/NVK) (Figure 8B, curve 5) allows an increase of the EPOX conversion up to 75%. A consumption of the NVK double bond is observed (Figure S3 in Supporting Information File 1). As known in other systems, this is accounted for by the addition of Ar$^{\bullet}$ to the NVK double bond

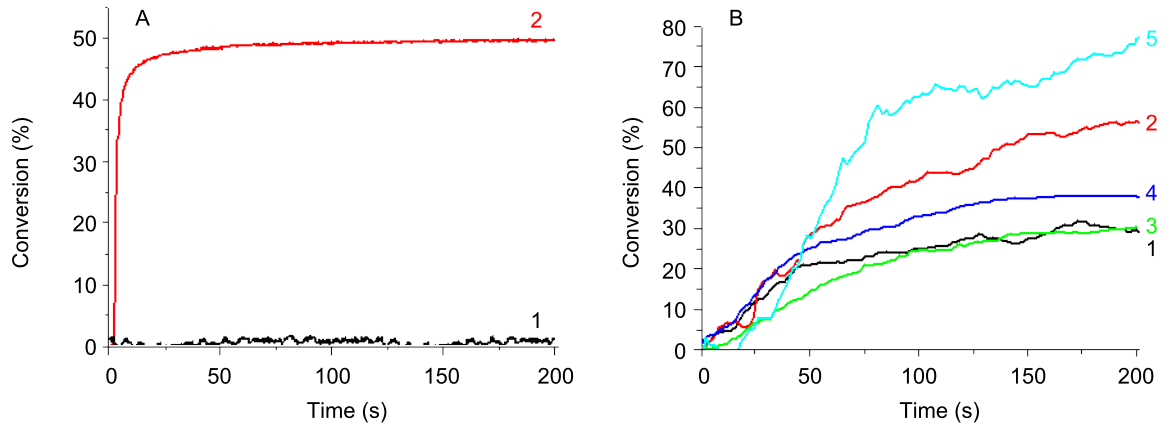

Figure 8: (A) Photopolymerization profiles of EPOX-Si upon a Xe–Hg lamp irradiation (λ > 340 nm) under air for different photoinitiating systems: (A) (1) Iod (2% w/w); (2) **Py_3**/Iod (1%/2% w/w); (B) Photopolymerization profiles of EPOX under air upon halogen-lamp irradiation in the presence of (1) **Py_6**/Iod (0.2%/2% w/w); (2) **Py_7**/Iod (0.2%/2% w/w); (3) **Py_10**/Iod (0.2%/2% w/w); (4) **Py_11**/Iod (0.2%/2% w/w); (5) **Py_11**/Iod/NVK (0.2%/2%/2% w/w).

(formation of an Ar–NVK$^{\bullet}$ radical) (r9 in Scheme 5). This electron rich radical is easily oxidized (r10 in Scheme 5) by Iod, the resulting cation Ar–NVK^{+} being able to initiate the cationic polymerization.

Thermal polymerization at room temperature

Remarkably, the thermal polymerization of EPOX can also be initiated by different Co_Py/Iod (1%/2% w/w) systems. This reaction proceeds smoothly at rt but is completed after 24 h, e.g., with **Py_9**, **Py_6**, **Py_10** or **Py_11**/Iod, the final conversion is >55%. As supported by the ESR experiments (see above), the presence of, e.g., **Py_9**$^{\bullet+}$ explains the thermal initiation of the cationic polymerization of the epoxide (r11 in Scheme 5). For the other Co_Py, a good thermal stability is found. This dual behavior of some Co_Pys, which are able to initiate both a thermal and a photochemical cationic polymerization, can be very useful to initiate the polymerization in the shadow areas.

Free radical photopolymerization (FRP)

Typical free radical polymerization profiles of TMPTA upon the Xe–Hg lamp exposure in laminate by using the Co_Py/MDEA (or PBr) two-component PISs are represented in Figure 9. In the presence of Co_Py alone, FRP occurs but the inhibition time is high and the final conversion is low (50 s; 35% with **Py_3**). The addition of PBr (Figure 9A) or MDEA

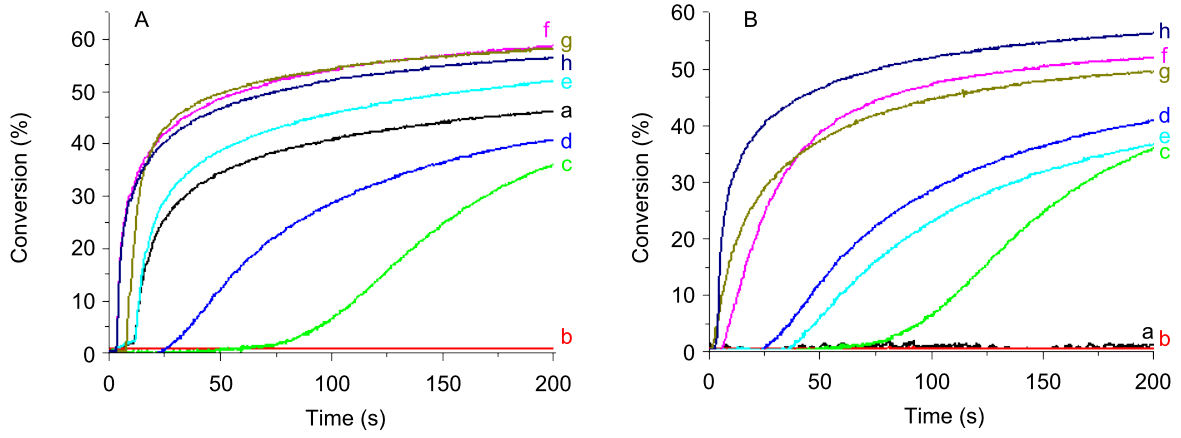

Figure 9: Photopolymerization profiles of TMPTA upon Xe–Hg lamp irradiation (λ > 340 nm) in laminate for different photoinitiating systems: (A) (a) PBr (2% w/w); (b) **Py_2** (0.2% w/w); (c) **Py_3** (0.2% w/w); (d) **Py_5** (0.2% w/w); (e) **Py_2**/PBr (0.2%/2% w/w); (f) **Py_3**/PBr (0.2%/2% w/w); (g) **Py_5**/PBr (0.2%/2% w/w); (h) **Py_3**/MDEA/PBr (0.2%/2%/2% w/w); (B) (a) MDEA (2% w/w); (b) **Py_2** (0.2% w/w); (c) **Py_3** (0.2% w/w); (d) **Py_5** (0.2% w/w); (e) **Py_2**/MDEA (0.2%/2% w/w); (f) **Py_3**/MDEA (0.2%/2% w/w); (g) **Py_5**/MDEA (0.2%/2% w/w); (h) **Py_3**/MDEA/PBr (0.2%/2%/2% w/w).

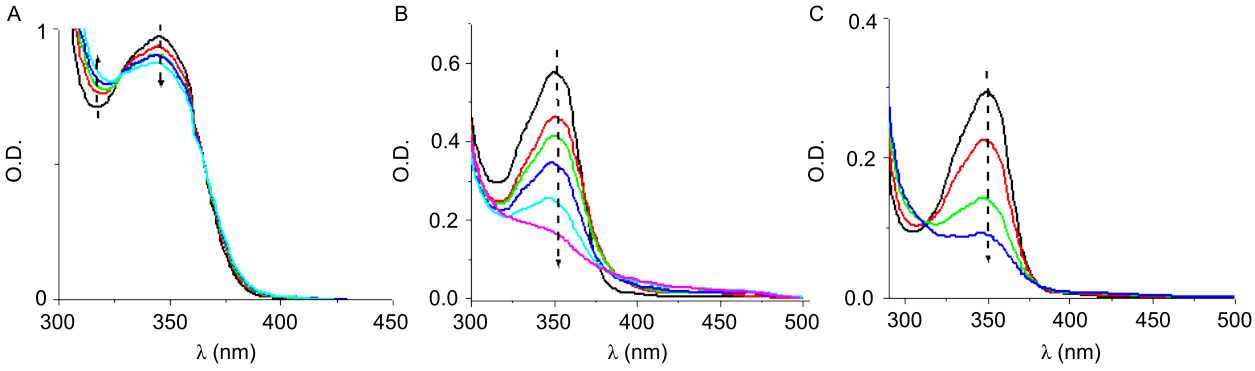

Figure 10: Photolysis of (A) the **Py_3**/PBr couple, (B) the **Py_3**/Iod couple, and (C) the **Py_3**/MDEA couple; Xe–Hg lamp irradiation. In acetonitrile/toluene (50/50); from *t* = 0 to 5 min.

(Figure 9B) shortens the inhibition time and increases the final conversion to ~55%. For the Co_Py/amine or Co_Py/PBr two-component systems, the radicals generated in r7 and r8 in Scheme 5 can initiate the FRP process. Due to its absorption in the UV, PBr alone initiates the acrylate photopolymerization (conv = 45%; Figure 9A, curve a). No striking improvement of the final conversion is observed when using the **Py_3**/MDEA/PBr three-component PIS instead of **Py_3**/PBr (~55%; Figure 9A, curve f versus h), but both Rp and conv are better when comparing to **Py_3**/MDEA.

Photocatalyst behavior of the Co_Pys

The photocatalytic behavior of the Co_Pys is investigated in the most interesting compounds reported above for the photopolymerization reactions. The steady-state photolysis of **Py_3**/PBr, **Py_3**/Iod, **Py_3**/MDEA couples highlights the consumption of the pyrene moiety under light exposure (Figure 10). In **Py_3**/PBr and **Py_3**/MDEA, isosbestic points are present at 330 nm (Figure 10A) and 315 nm (Figure 10B), respectively, suggesting stoichiometric reactions and no other side reactions.

The addition of NVK to **Py_11**/Iod shows that the photolysis is faster with **Py_11**/Iod than with **Py_11**/Iod/NVK couples (Figure 11A versus Figure 11B). This difference highlights that in the presence of NVK, **Py_11** is regenerated according to an oxidation cycle (Scheme 6). Therefore, **Py_11** behaves as a new photocatalyst in agreement with (r12 in Scheme 5).

In the Co_Py/PBr/MDEA three-component system, reactions (r7, r8) are probably competitive (e.g., k[MDEA] ~ k[PBr]

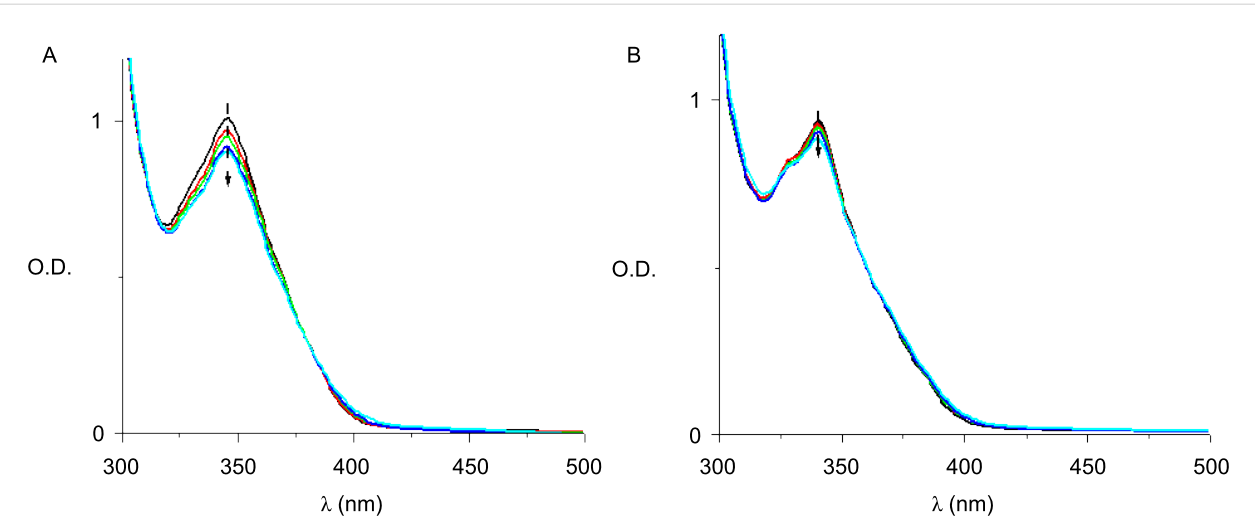

Figure 11: Photolysis of (A) the **Py_11**/Iod and (B) the **Py_11**/Iod/NVK couple. Halogen lamp irradiation. In acetonitrile/toluene (50/50); from *t* = 0 to 5 min.

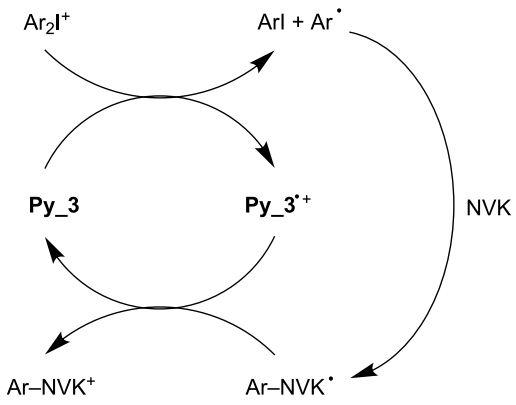

Scheme 6: The oxidative cycle.

using **Py_3**). As a consequence, both a reduction and an oxidation cycle could simultaneously proceed (Scheme 7). However, the ESR and polymerization results (see above) (i) suggest that the contribution of the reduction cycle should be weak and (ii) confirm that the regeneration in the oxidation cycle has a low efficiency. This might be due to a $MDEA^{\bullet+} \rightarrow MDEA\_H^{\bullet}$ process (in r8 in Scheme 5) less efficient than $PBr^{\bullet-} \rightarrow$ phenacyl radical (in r7 in Scheme 5). Nevertheless, such an oxidation cycle that can contribute here to some extent appears as one of the rare examples observed in photocatalyst (PC)/PBr/amine systems, because most of them work according to a reduction cycle [30,46] (see other examples in [47]; in a related system, still unpublished, based on another PC, we have demonstrated the true occurrence of a unique oxidation cycle).

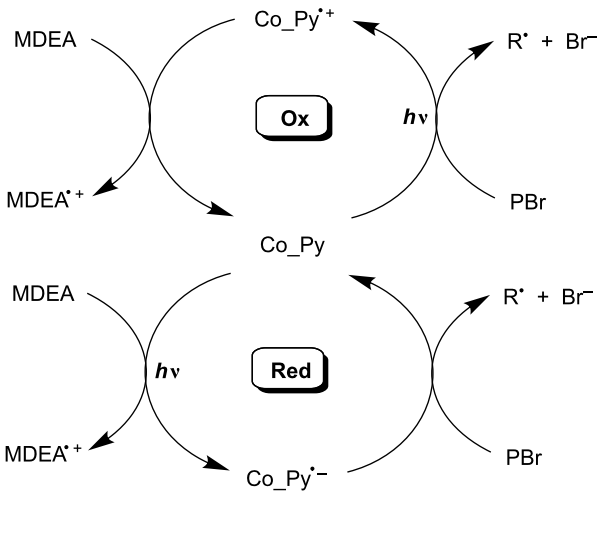

Scheme 7: Oxidation versus reduction cycles.

Conclusion

In this paper, the core-pyrene π structures Co_Pys appear as interesting photoinitiators. Successful cationic and radical photopolymerization reactions were carried out under near-UV–vis irradiation. A photocatalytic behavior is noted, that is, an oxidation cycle for Co_Py/Iod/NVK and a partial oxidation cycle for Co_Py/MDEA/PBr. These experimentally and theoretically investigated di- and trifunctional compounds outline the interest in a suitable strong MO coupling. This could open the way to an a priori choice of absorption spectra driven by the theoretical design of chemical compounds. Other proposals will be provided in the future.

Experimental

Co_Pys

The synthesized compounds are presented in Scheme 3. The procedures are presented in detail in Supporting Information File 1. ^{1}H and ^{13}C NMR spectra and HRMS mass spectral analysis are also given. **Py_1** was purchased from Aldrich. 1,4-Di(pyren-1-yl)benzene (**Py_4**) was prepared by adapting a literature procedure [48]. **Py_12** was synthesized as previously reported [49]. The syntheses of **Py_2** [50], **Py_3** [51], **Py_6** [52] and **Py_7** [53] were already reported under reaction conditions different to the ones reported in this article and in lower yields. The results obtained in our work agree with the previously reported characterization of these products.

Other chemical compounds

The [methyl-4-phenyl (methyl-1-ethyl)-4-phenyl] iodonium tetrakis(pentafluorophenyl)borate [54,55] (Iod; PI 2074 from Bluestar Silicones - France) was used as the iodonium salt (Scheme 4). Phenacyl bromide (PBr), *N*-methyldiethanolamine (MDEA) and *N*-vinylcarbazole (NVK) were obtained from Aldrich and (4-hydroxyethoxyphenyl) thianthrenium hexafluorophosphate (TH; recrystallized form of Esacure 1187) from Lamberti Spa. The (epoxycyclohexylethyl)methylsiloxane-dimethylsiloxane copolymer (EPOX-Si) was obtained from Bluestar Silicones-France (Silcolease UV POLY 200); trimethylolpropane triacrylate TMPTA and (3,4-epoxycyclohexane)methyl 3,4-epoxycyclohexylcarboxylate (EPOX or UVACURE 1500) were provided by Cytec.

Photopolymerization procedures

TMPTA was irradiated at room temperature under lamination conditions: the formulation (25 μm thick) is sandwiched between two polypropylene films. The weight percentages for the photoinitiators are given in the figure captions. The evolution of the acrylate content was continuously followed by real-time FTIR spectroscopy (FTIR NEXUS 870) at ~1620 cm^{-1}. The formulations (25 μm thick) based on the cationic monomers (EPOX, EPOX-Si) deposited on a BaF_2 pellet were irradiated

under air inside the IR spectrometer cavity at room temperature [56,57]. The evolution of the epoxy content was also continuously followed by real-time FTIR spectroscopy (FTIR NEXUS 870). A Xe–Hg lamp (Hamamatsu, L8252, 150 W, filtered light at $\lambda > 340$ nm; intensity ~ 30 mW/cm²) and a halogen lamp (intensity ~10 mW/cm²; the emission spectrum is given in [43]) were used as the irradiation sources.

ESR experiments

ESR spin-trapping (ESR-ST) experiments were carried out by using a X-Band ESR spectrometer (EMX-plus from Bruker Biospin or MS400 from Magnettech). The radicals were produced at RT under Xe–Hg lamp exposure and trapped by phenyl-*N*-*tert*-butylnitrone (PBN) according to a procedure described in detail in [58,59].

Redox potentials

The redox potentials were measured in acetonitrile by cyclic voltammetry with tetrabutylammonium hexafluorophosphate (98%) as a supporting electrolyte (0.1 M) (Voltalab 6 Radiometer; the working electrode was a platinum disk and the reference a saturated calomel electrode-SCE). Ferrocene was used as a standard and the potentials were determined from half-peak potentials. The free energy change ΔG_{et} for an electron-transfer reaction is calculated from the classical Rehm–Weller equation (Equation 1) [60] where E_{ox}, E_{red}, E_S and C are the oxidation potential of the donor, the reduction potential of the acceptor, the excited state energy and the coulombic term for the initially formed ion pair, respectively. C is neglected as usually done in polar solvents.

$$\Delta G_{et} = E_{ox} - E_{red} - E_s + C \quad (1)$$

Fluorescence experiments

The fluorescence properties of the different Co_Pys were studied by using a JASCO FP-750 spectrometer.

Computational procedure

Molecular orbital calculations were done with the Gaussian 03 suite of programs [61,62]. The electronic absorption spectra for the different compounds were calculated with the time-dependent density functional theory at B3LYP/6-31G* level on the relaxed geometries calculated at UB3LYP/6-31G* level.

Laser flash photolysis

Nanosecond laser flash photolysis (LFP) experiments were carried out [26-35] by using a Qswitched nanosecond Nd/YAG laser (λ_{exc} = 355 nm, 9 ns pulses; energy reduced down to 10 mJ) from Continuum (Minilite) and an analyzing system consisting of a ceramic Xenon lamp, a monochromator, a fast photomultiplier, and a transient digitizer (Luzchem LFP 212).

Supporting Information

Supporting Information File 1

Experimental procedures, characterization data, and additional spectra.
[http://www.beilstein-journals.org/bjoc/content/supplementary/1860-5397-9-101-S1.pdf]

Acknowledgements

This work was partly supported by the "Agence Nationale de la Recherche" grant ANR 2010-BLAN-0802. JL thanks the Institut Universitaire de France for the financial support.

References

1. Fouassier, J.-P.; Lalevée, J. *Photoinitiators for Polymer Synthesis: Scope, Reactivity and Efficiency;* Wiley-VCH: Weinheim, Germany, 2012. doi:10.1002/9783527648245
2. Fouassier, J.-P. *Photoinitiation, Photopolymerization, Photocuring;* Hanser: Münen, Germany, 1995.
3. Fouassier, J.-P.; Rabek, F. J., Eds. *Radiation Curing in Polymer Science and Technology;* Chapman & Hall: London, U.K., 1993.
4. Crivello, J. V.; Dietliker, K. In *Photoinitiators for Free Radical, Cationic and Anionic Photopolymerization;* Bradley, G., Ed.; Surface Coatings Technology, Vol. III; Wiley/SITA, 1999.
5. Dietliker, K. A. *Compilation of Photoinitiators Commercially Available for UV Today;* Sita Technology Ltd: London, U.K., 2002.
6. Belfied, K. D.; Crivello, J. V., Eds. *Photoinitiated Polymerization;* ACS Symposium Series, Vol. 847; American Chemical Society: Washington DC, U.S.A., 2003. doi:10.1021/bk-2003-0847
7. Allen, N. S., Ed. *Photochemistry and Photophysics of Polymer Materials;* Wiley: Hoboken, 2010.
8. Scranton, A. B.; Bowman, A.; Peiffer, R. W., Eds. *Photopolymerization: Fundamentals and Applications;* ACS Symposium Series, Vol. 673; American Chemical Society: Washington DC, U.S.A., 1997. doi:10.1021/bk-1997-0673
9. Green, W. A. *Industrial Photoinitiators;* CRC Press: Boca Raton, 2010. doi:10.1201/9781439827468
10. Mishra, M. K.; Yagci, Y., Eds. *Handbook of Vinyl Polymers;* CRC Press, 2008.
11. Wang, K.; Jiang, S.; Liu, J.; Nie, J.; Yu, Q. *Prog. Org. Coat.* **2011,** *72,* 517–521. doi:10.1016/j.porgcoat.2011.06.011
12. Temel, G.; Enginol, B.; Aydin, M.; Karaca Balta, D.; Arsu, N. *J. Photochem. Photobiol., A: Chem.* **2011,** *219,* 26–31. doi:10.1016/j.jphotochem.2011.01.012
13. Wei, J.; Wang, B. *Macromol. Chem. Phys.* **2011,** *212,* 88–95. doi:10.1002/macp.201000535
14. Asvos, X.; Siskos, M. G.; Zarkadis, A. K.; Hermann, R.; Brede, O. *J. Photochem. Photobiol., A: Chem.* **2011,** *219,* 255–264. doi:10.1016/j.jphotochem.2011.02.028
15. Kabatc, J.; Jurek, K. *Polymer* **2012,** *53,* 1973–1980. doi:10.1016/j.polymer.2012.03.027
16. Rosspeintner, A.; Griesser, M.; Pucher, N.; Iskra, K.; Liska, R.; Gescheidt, G. *Macromolecules* **2009,** *42,* 8034–8038. doi:10.1021/ma901570h
17. Karaka-Balta, D.; Temel, G.; Goksu, G.; Okal, N.; Arsu, N. *Macromolecules* **2012,** *45,* 119–125. doi:10.1021/ma202168m

18. Yilmaz, G.; Acik, G.; Yagci, Y. *Macromolecules* **2012,** *45,* 2219–2224. doi:10.1021/ma3000169
19. Kumbaraci, V.; Aydogan, B.; Talinli, N.; Yagci, Y. *J. Polym. Sci., Part A: Polym. Chem.* **2012,** *50,* 2612–2618. doi:10.1002/pola.26034
20. Tunc, D.; Yagci, Y. *Polym. Chem.* **2011,** *2,* 2557–2563. doi:10.1039/c1py00269d
21. Kreutzer, J.; Dogan Demir, K.; Yagci, Y. *Polym. J.* **2011,** *47,* 792–799.
22. Lalevée, J.; Blanchard, N.; Tehfe, M. A.; Morlet-Savary, F.; Fouassier, J. P. *Macromolecules* **2010,** *43,* 10191–10195. doi:10.1021/ma1023318
23. Zhang, G.; Song, I. Y.; Ahn, K. H.; Park, T.; Choi, W. *Macromolecules* **2011,** *44,* 7594–7599. doi:10.1021/ma201546c
24. Lalevée, J.; Peter, M.; Dumur, F.; Gigmes, D.; Blanchard, N.; Tehfe, M.-A.; Morlet-Savary, F.; Fouassier, J. P. *Chem.–Eur. J.* **2011,** *17,* 15027–15031. doi:10.1002/chem.201101445
25. Tehfe, M.-A.; Ma, L.; Graff, B.; Morlet-Savary, F.; Fouassier, J.-P.; Zhao, J.; Lalevée, J. *Macromol. Chem. Phys.* **2012,** *213,* 2282–2286. doi:10.1002/macp.201200489
26. Lalevée, J.; Blanchard, N.; Fries, C.; Tehfe, M. A.; Morlet-Savary, F.; Fouassier, J. P. *Polym. Chem.* **2011,** *2,* 1077–1084. doi:10.1039/c0py00392a
27. Tehfe, M.-A.; Zein-Fakih, A.; Lalevée, J.; Dumur, F.; Gigmes, D.; Graff, B.; Morlet-Savary, F.; Hamieh, T.; Fouassier, J. P. *Eur. Polym. J.* **2013,** *49,* 567–574. doi:10.1016/j.eurpolymj.2012.10.010
28. Telitel, S.; Lalevée, J.; Blanchard, N.; Kavalli, T.; Tehfe, M.-A.; Schweizer, S.; Morlet-Savary, F.; Graff, B.; Fouassier, J. P. *Macromolecules* **2012,** *45,* 6864–6868. doi:10.1021/ma301293m
29. Tehfe, M.-A.; Lalevée, J.; Morlet-Savary, F.; Graff, B.; Blanchard, N.; Fouassier, J. P. *ACS Macro Lett.* **2012,** *1,* 198–203. doi:10.1021/mz200140y
30. Tehfe, M.-A.; Lalevée, J.; Morlet-Savary, F.; Graff, B.; Blanchard, N.; Fouassier, J. P. *Macromolecules* **2012,** *45,* 1746–1752. doi:10.1021/ma300050n
31. Tehfe, M.-A.; Dumur, F.; Contal, E.; Graff, B.; Morlet-Savary, F.; Gigmes, D.; Fouassier, J. P.; Lalevée, J. *Polym. Chem.* **2013,** *4,* 1625–1634. doi:10.1039/c2py20950k
32. Tehfe, M.-A.; Lalevée, J.; Morlet-Savary, F.; Graff, B.; Fouassier, J.-P. *Macromolecules* **2012,** *45,* 356–361. doi:10.1021/ma202307x
33. Lalevée, J.; Dumur, F.; Tehfe, M.-A.; Zein-Fakih, A.; Gigmes, D.; Morlet-Savary, F.; Fouassier, J. P. *Polymer* **2012,** *53,* 4947–4954. doi:10.1016/j.polymer.2012.08.067
34. Lalevée, J.; Tehfe, M.-A.; Dumur, F.; Gigmes, D.; Blanchard, N.; Morlet-Savary, F.; Graff, B.; Fouassier, J. P. *ACS Macro Lett.* **2012,** *1,* 286–290. doi:10.1021/mz2001753
35. Tehfe, M.-A.; Lalevée, J.; Telitel, S.; Sun, J.; Zhao, J.; Graff, B.; Morlet-Savary, F.; Fouassier, J.-P. *Polymer* **2012,** *53,* 2803–2808. doi:10.1016/j.polymer.2012.05.009
36. Aydogan, B.; Yagci, Y.; Toppare, L.; Jockusch, S.; Turro, N. J. *Macromolecules* **2012,** *45,* 7829–7834. doi:10.1021/ma301546d
37. Aydogan, B.; Durmaz, Y. Y.; Kahveci, M. U.; Uygun, M.; Tasdelen, M. A.; Yagci, Y. *Macromol. Symp.* **2011,** *308,* 25–34. doi:10.1002/masy.201151005
38. Aydogan, B.; Gunbas, G. E.; Durmus, A.; Toppare, L.; Yagci, Y. *Macromolecules* **2010,** *43,* 101–106. doi:10.1021/ma901858p
39. Bulut, U.; Gunbas, G. E.; Toppare, L. *J. Polym. Sci., Part A: Polym. Chem.* **2010,** *48,* 209–213. doi:10.1002/pola.23779
40. Bulut, U.; Balan, A.; Caliskan, C. *J. Polym. Sci., Part A: Polym. Chem.* **2011,** *49,* 729–733. doi:10.1002/pola.24485
41. Yagci, Y.; Jockusch, S.; Turro, N. J. *Macromolecules* **2007,** *40,* 4481–4485. doi:10.1021/ma070586a
42. Lalevée, J.; Tehfe, M. A.; Dumur, F.; Gigmes, D.; Graff, B.; Morlet-Savary, F.; Fouassier, J. P. *Macromol. Rapid Commun.* **2013,** *34,* 239–245. doi:10.1002/marc.201200578
43. Tehfe, M.-A.; Dumur, F.; Graff, B.; Clément, J.-L.; Gigmes, D.; Morlet-Savary, F.; Fouassier, J. P.; Lalevée, J. *Macromolecules* **2013,** *46,* 736–746. doi:10.1021/ma3024359
44. Tehfe, M.-A.; Lalevée, J.; Telitel, S.; Contal, E.; Dumur, F.; Gigmes, D.; Bertin, D.; Nechab, M.; Graff, B.; Morlet-Savary, F.; Fouassier, J. P. *Macromolecules* **2012,** *45,* 4454–4460. doi:10.1021/ma300760c
45. Magnetic Properties of Free Radicals, Nitroxide Radicals and Nitroxide Based High-Spin Systems. In *Landolt-Börnstein - Group II, Molecules and Radicals;* Fisher, H., Ed.; Springer Verlag: Berlin, Germany, 2005; Vol. 26d.
46. Narayanam, J. M. R.; Stephenson, C. R. J. *Chem. Soc. Rev.* **2011,** *40,* 102–113. doi:10.1039/b913880n
47. Nguyen, J. D.; Tucker, J. W.; Konieczynska, M. D.; Stephenson, C. R. J. *J. Am. Chem. Soc.* **2011,** *133,* 4160–4163. doi:10.1021/ja108560e
48. Yang, C.-H.; Guo, T.-F.; Sun, I.-W. *J. Lumin.* **2007,** *124,* 93–98. doi:10.1016/j.jlumin.2006.02.003
49. Tehfe, M.-A.; Dumur, F.; Graff, B.; Morlet-Savary, F.; Fouassier, J.-P.; Gigmes, D.; Lalevée, J. *Macromolecules* **2012,** *45,* 8639–8647. doi:10.1021/ma301931p
50. Rajakumar, P.; Visalakshi, K.; Ganesan, S.; Maruthamuthu, P.; Suthanthiraraj, S. A. *Bull. Chem. Soc. Jpn.* **2012,** *85,* 902–911. doi:10.1246/bcsj.20110280
51. Lee, D.-H.; Jin, M.-J. *Org. Lett.* **2011,** *13,* 252–255. doi:10.1021/ol102677r
52. Kim, M. K.; Kwon, J.; Hong, J. P.; Lee, S.; Hong, J. I. *Bull. Korean Chem. Soc.* **2011,** *32,* 2899–2905. doi:10.5012/bkcs.2011.32.8.2899
53. Ishi-i, T.; Yaguma, K.; Thiemann, T.; Yashima, M.; Ueno, K.; Mataka, S. *Chem. Lett.* **2004,** *33,* 1244–1245. doi:10.1246/cl.2004.1244
54. Castellanos, F.; Fouassier, J. P.; Priou, D.; Cavezzan, A. Onium borates/borates of organometallic complexes and cationic initiation of polymerization therewith. U.S. Patent 5,668,192, Sept 16, 1997.
55. Castellanos, F.; Fouassier, J. P.; Priou, C.; Cavezzan, J. *J. Appl. Polym. Sci.* **1996,** *60,* 705–713. doi:10.1002/(SICI)1097-4628(19960502)60:5<705::AID-APP7>3.0.CO;2-U
56. Tehfe, M.-A.; Lalevée, J.; Gigmes, D.; Fouassier, J. P. *Macromolecules* **2010,** *43,* 1364–1370. doi:10.1021/ma9025702
57. Tehfe, M.-A.; Lalevée, J.; Gigmes, D.; Fouassier, J. P. *J. Polym. Sci., Part A: Polym. Chem.* **2010,** *48,* 1830–1837. doi:10.1002/pola.23956
58. Tordo, P. Spin-trapping: recent developments and applications. In *Electron Pragmagnetic Resonance;* Gilbert, B. C.; Atherton, N. M.; Davies, M. J., Eds.; The Royal Society of Chemistry: Cambridge, U. K., 1998; Vol. 16.
59. Lalevée, J.; Dumur, F.; Mayer, C. R.; Gigmes, D.; Nasr, G.; Tehfe, M.-A.; Telitel, S.; Morlet-Savary, F.; Graff, B.; Fouassier, J. P. *Macromolecules* **2012,** *45,* 4134–4141. doi:10.1021/ma3005229
60. Rehm, D.; Weller, A. *Isr. J. Chem.* **1970,** *8,* 259–271.
61. *Gaussian 03,* Revision B2; Gaussian, Inc.: Wallingford, CT, 2003.
62. Foresman, J. B.; Frisch, A. *Exploring Chemistry with Electronic Structure Methods,* 2nd ed.; Gaussian, Inc.: Wallingford, CT, 1996.

Beilstein Journal of Organic Chemistry

Interplay of ortho- with spiro-cyclisation during iminyl radical closures onto arenes and heteroarenes

Roy T. McBurney* and John C. Walton*

Full Research Paper

Open Access

Address:
EaStCHEM School of Chemistry, University of St. Andrews, St. Andrews, Fife, KY16 9ST, UK

Email:
Roy T. McBurney* - roy.mcburney@glasgow.ac.uk; John C. Walton* - jcw@st-and.ac.uk

* Corresponding author

Keywords:
cyclisation; EPR spectroscopy; free radicals; heterocycles; oxime carbonates

Beilstein J. Org. Chem. **2013,** *9,* 1083–1092.
doi:10.3762/bjoc.9.120

Received: 01 April 2013
Accepted: 09 May 2013
Published: 04 June 2013

This article is part of the Thematic Series "Organic free radical chemistry".

Guest Editor: C. Stephenson

Abstract

Sensitised photolyses of ethoxycarbonyl oximes of aromatic and heteroaromatic ketones yielded iminyl radicals, which were characterised by EPR spectroscopy. Iminyls with suitably placed arene or heteroarene acceptors underwent cyclisations yielding phenanthridine-type products from ortho-additions. For benzofuran and benzothiophene acceptors, spiro-cyclisation predominated at low temperatures, but thermodynamic control ensured ortho-products, benzofuro- or benzothieno-isoquinolines, formed at higher temperatures. Estimates by steady-state kinetic EPR established that iminyl radical cyclisations onto aromatics took place about an order of magnitude more slowly than prototypical C-centred radicals. The cyclisation energetics were investigated by DFT computations, which gave insights into factors influencing the two cyclisation modes.

Introduction

Radical cyclisations onto aromatic acceptors take place readily, even though disruption of the 6π-electron system necessarily occurs. The most commonly encountered type is C-centred radical addition (often an aryl radical) to an aromatic or heteroaromatic ring ortho to the point of attachment of the tether. In Pschorr and related processes re-aromatisation follows with production of phenanthrene-type derivatives [1,2]. Spiro-cyclisations in which tethered radicals add to the ipso-C-atoms of the rings are less common, although minor spiro-products not infrequently accompany the main ortho-ones in Pschorr syntheses [3-5]. Cyclisations onto arenes by N-centred radicals are rarer, but iminyl radical ArC(R)=N$^{\bullet}$ closures are well documented. Forrester and co-workers were probably the first to utilise iminyl radicals synthetically. They obtained iminyls by persulfate oxidation of imino-oxyacetic acids in aqueous solvents and prepared azines [6], *N*-heterocycles [7,8], and other derivatives [9]. This research initiated spiralling interest by synthetic chemists in iminyl radical-mediated preparations. Recently iminyls have been generated from quite a variety of precursors [10-15], and their cyclisations onto arenes [16-21] and heteroarenes [22-24] have attracted attention. Iminyl cyclisations have also been utilised in natural-product syntheses

[10,16,25,26]. Iminyl radical spiro-cyclisations onto aromatics have been reported in a few cases, and spiro-intermediates have occasionally been proposed in mechanistic explanations [15,18,27-29].

Although a moderate amount of information about iminyl radical structure and reactivity exists, few conceptual tools to help predict their cyclisation selectivity are available. EPR spectroscopic and other evidence established that iminyl radicals behave as σ-type species with their unpaired electrons in orbitals in the nodal plane of their C=N π-systems [30-32]. This precludes substantial delocalization of the unpaired electron into the ring π-system of aryliminyls. Consequently, strong effects from ring substituents of aryliminyls are not expected to come into play. Small to moderate size iminyl radicals terminate rapidly at diffusion-controlled rates by N–N coupling to give azines [32]. β-Scission reactions yielding nitriles do occur, but are not important at $T < \sim 420$ K for aryliminyls or for iminyls with primary alkyl substituents [32]. The rate constants for H-abstraction by iminyls yielding imines are more than an order of magnitude slower than for C-centred analogues [33]. Iminyls undergo 5-*exo*-ring closures onto alkenes about a factor of 25 more slowly than C-centred analogues [34]. Since ring closure is often in competition with H-abstraction, the comparatively slow H-abstraction by iminyls is important for the success of many heterocycle syntheses.

Spiro-cyclisations of iminyls lead to formation of strained quaternary C-atoms, and the spiro-intermediates have no straightforward reaction channel for return to aromaticity. The process might be reversible, depending on the architecture of the chain and the extent of strain in the spiro-radical. On the other hand ortho-cyclisations can easily be followed by return to aromaticity of the cyclohexadienyl radicals, either by transfer out of the labile H-atom, or by transfer of an electron to a suitable sink with generation of the corresponding carbocation, followed by proton loss. Kinetic or other data to help predict which mode would be favoured for a novel iminyl radical is essentially nonexistent.

We discovered recently that oxime carbonates ArC(R)=N–OC(O)OR' are clean and convenient precursors for iminyl as well as O-centred radicals [26,35]. Their weak N–O bonds selectively cleave on UV photolysis, particularly when sensitised with 4-methoxyacetophenone (MAP), thus facilitating investigations of the behaviour of both iminyl and alkoxycarbonyloxyl radicals R'OC(O)O$^{\bullet}$. A distinct advantage of these precursors is that they enable the iminyl radical intermediates to be directly monitored by EPR spectroscopy. We have now prepared a representative set of oxime carbonates with the aim of studying competition between ortho- and spiro-ring closures of the released iminyl radicals. Precursors **1a–f**, **2a**,**b**, **3** and **4**, consist of *O*-ethoxycarbonyl derivatives of oximes with various aromatic and heteroaromatic architectures (Figure 1). Compounds **1a–f** contain comparatively rigid arms and their aromatic acceptors range from electron-withdrawing to electron-releasing in character. In compounds **2a**,**b** and **3** heteroarenes replace the benzene rings and in **4** the arm is much more flexible.

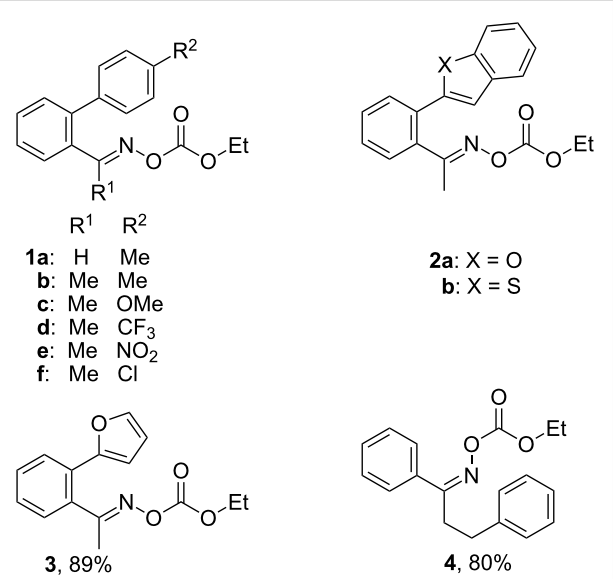

Figure 1: *O*-Ethoxycarbonyl oximes prepared.

This paper reports our study of the chemistry of these compounds by means of product analyses, solution EPR spectroscopy and DFT computations. We encountered an intriguing interplay between spiro-cyclisation and ortho-cyclisation of the iminyl intermediates and factors affecting this are weighed up.

Results and Discussion

The arene and heteroarene-based oxime carbonates **1** and **2** were prepared as described previously by reaction of the corresponding aromatic ethanone oximes with ethyl chloroformate [26]. Precursors **3** and **4** were made in a similar way from the oximes of 2-furanylphenylethanone and 1,3-diphenylpropan-1-one.

Ring closures of aryl-iminyl radicals

Individual members of the set of substituted biphenyl *O*-ethoxycarbonyl oximes **1a–f** were UV irradiated for 3 h at ambient temperature in deoxygenated benzotrifluoride solutions with 1 equiv wt/wt of MAP as a photosensitizer. As communicated previously, 3-substituted phenanthridines **10a–f** were isolated in good to quantitative yields (52–99%, Scheme 1) irrespective of the nature of the 4-substituent [26]. No spiro-products were

detected even by GC–MS analyses of reaction mixtures. Byproducts included traces of imines ArC(R^2)=NH (ImH) and the ketones ArC(R^2)=O from imine hydrolyses. Photolysis of the more flexible precursor **4** gave a complex mixture of products. The MS and NMR data indicated that the main components were probably the corresponding imine ImH and ketone together with the iminyl radical dimer (Im_2). Neither spiro- nor ortho-cyclised products had formed. Therefore, for **4** in $PhCF_3$ solvent, iminyl radical ring closures were too slow to compete with H-atom abstractions and terminations.

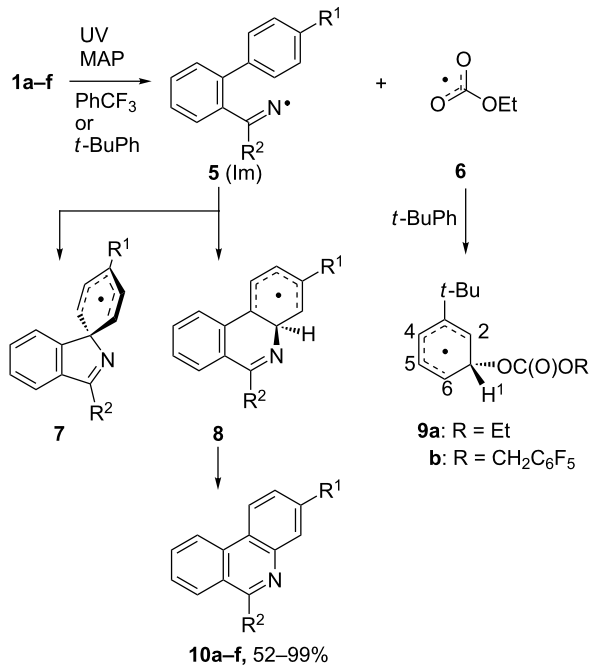

Scheme 1: Photochemical reactions of biphenyl oxime carbonates.

The photolytic reactions of oxime carbonates **1a–f** and **4** were next investigated by 9 GHz EPR spectroscopy. Deaerated samples of each oxime carbonate, plus 1 equiv of MAP, in *t*-BuPh or cyclopropane solvent, were irradiated with a 500 W unfiltered Hg lamp directly in the spectrometer resonant cavity. The spectrum obtained from precursor **1f** (Figure 2) shows a central 1:1:1 triplet from iminyl radical **5f** together with a second species. Similar spectra were obtained, in the temperature range 210 to 270 K, from all the other members of the set, including **4**, showing the corresponding iminyl radicals plus the same second radical. The EPR parameters of all the iminyls were very similar [g = 2.0030, a(N) = 10.0 G] and closely in line with literature data for ArCMe=N• type radicals [36,37].

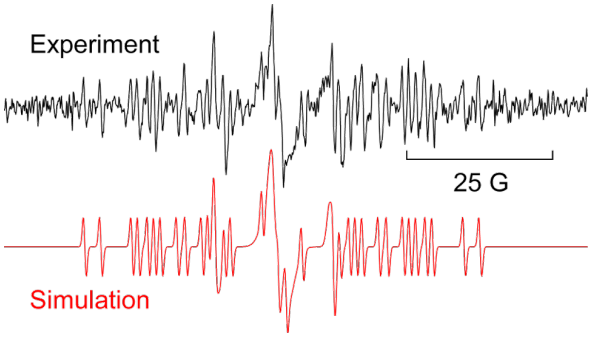

Figure 2: EPR spectrum during photolysis of **1f** in *t*-BuPh at 240 K. Top (black): experimental spectrum. Bottom (red): computer simulation.

Simulation of the second species indicated one large and four smaller doublet hyperfine splittings (hfs) characteristic of a cyclohexadienyl type radical (Table 1). This spectrum was evidently due to the intermediate from addition of some radical meta to the *tert*-butyl substituent of the solvent. It is known that ArCMe=N• type radicals do not add to *t*-BuPh under EPR conditions [19,37] neither do EtO• radicals (from dissociation of **6**), and hence, we assign this spectrum to the ethoxycarbonyloxyl adduct **9a**. This identification was supported by a DFT computation [38] that gave hfs in close agreement with experiment (Table 1). This was a surprising result because previously the only radicals of type **9** that had been spectroscopically detected had resulted from additions of phenyl [34] or bridge-

Table 1: EPR parameters of cyclohexadienyl radicals **9** from meta-additions to *t*-BuPh[a].

Radical	T/K or method	*g*-factor	$a(H^1)$	$a(H^2)$	$a(H^4)$	$a(H^5)$	$a(H^6)$
9a	240	2.0025	34.6	8.1	13.1	2.8	9.2
9a	DFT[b]	–	35.0	−8.3	−12.8	3.5	−9.8
9b[c]	210	2.0026	33.5	8.1	13.1	2.7	9.3
9(Ph)[d]	220	2.0030	35.5	8.1	13.3	2.7	9.1
9(222)[e]	220	2.0030	42.6	8.1	13.1	2.8	9.0

[a]At 9.4 GHz in *t*-BuPh solution; hfs in Gauss. Note that the signs of hfs cannot be obtained from isotropic EPR spectra. [b]UB3LYP/6-311+G(2d,p); hfs computed with the epr-iii basis set [42] designed for EPR hfs, were virtually identical. [c]R. T. McBurney and J. C. Walton unpublished. [d]As **9** but with Ph in place of OC(O)OEt [34]. [e]As **9** but with bicyclo[2.2.2]oct-1-yl in place of OC(O)OEt [39].

head radicals (bicyclo[2.2.2]oct-1-yl and adamantyl) [39]. These are localized σ-type radicals with bent or pyramidal centres and significant s-character. Ethoxycarbonyloxyl (**6**) is planar with a SOMO delocalized over the whole OC(O)O unit. The observation of **9a** at temperatures below 273 K is dramatic evidence of the exceptionally high reactivity of alkoxycarbonyloxyl radicals. An interesting feature was that addition was selective for meta to the *t*-Bu group; as was previously observed with the σ-radicals. Product studies with bridgehead radicals at higher temperatures (80 °C) had also revealed this preference for meta-attack [40,41]. The selectivity for meta-addition may result from the electron-releasing character of the *t*-Bu substituent. The SOMO in **9a** has a node at C(3) so electron–electron repulsion is smaller than in the SOMOs for para- or ortho-attack. This will lower the activation energy for meta-addition relative to para- or ortho-addition.

For all precursors **1a–f** the EPR spectra revealed uncyclised iminyls (**5a–f**) together with **9** up to T ~270 K. Above this temperature the EPR spectra became too weak for radical identification. No cyclohexadienyl type radicals from either spiro or ortho ring closure (**7** or **8**) were detected. It can be concluded that the iminyl cyclisations are comparatively slow and, based on the previous product analyses, the ortho- (Ar_1-6) mode predominates at room temperature and above.

Spiro-cyclisations with benzofuran and benzothiophene acceptors

EPR spectra from oxime carbonate **2a**, containing a benzofuran acceptor, gave well resolved spectra only at 230–235 K (Figure 3). The corresponding benzofuranyl-iminyl was not detectable at 230 K or above.

The EPR hfs obtained from simulation of the spectrum (Table 2) show this to be a benzyl type radical and we assign it structure **12a** (Scheme 2). A DFT computation for **12a** at the UB3LYP/6-311+G(2d,p) level of theory gave hfs in close agreement with experiment (Table 2). The EPR hfs are certainly not consistent with structure **13**, which was not spectroscopically detected. It is evident therefore that iminyl radical **11a** rapidly and selectively undergoes spiro-cyclisation with the benzofuran acceptor.

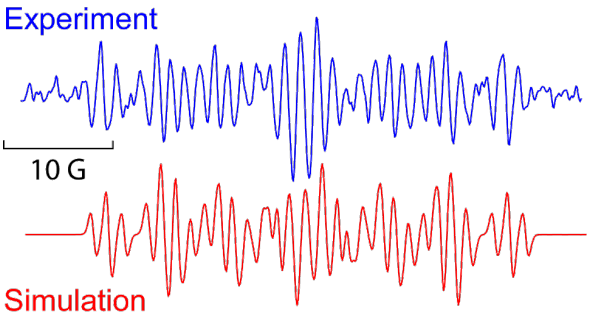

Figure 3: EPR spectrum during photolysis of **2a** in *t*-BuPh at 230 K. Top (blue): experiment; bottom (red): simulation.

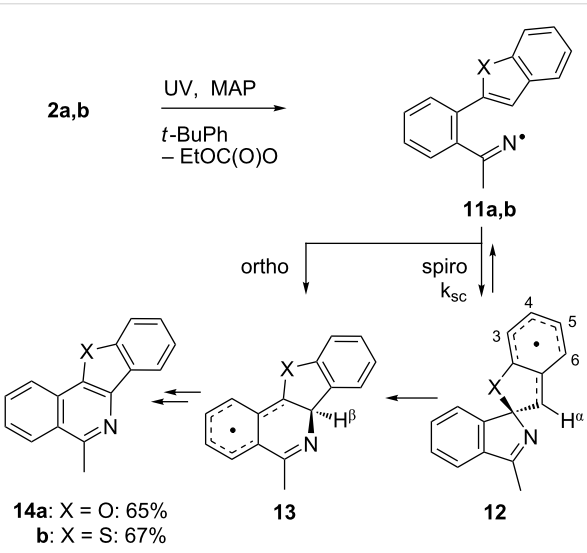

Scheme 2: Ring closure of iminyl radicals derived from **2a**,**b**.

Table 2: EPR parameters of spiro-benzyl radicals **12** derived from **2a**,**b**[a].

Radical	T/K or DFT method	*g*-factor	$a(H^{\alpha})$	$a(H^{3})$	$a(H^{4})$	$a(H^{5})$	$a(H^{6})$	$a(N)$
12a (X = O)	230	2.0025	14.9	1.4	6.3	1.4	5.0	5.4
12a (X = O)	UB3LYP/6-311+G(2d,p)	–	−14.2	1.6	−5.9	1.6	−5.0	5.2
12b (X = S)	230	–	13.0	1.5	6.0	1.5	5.3	4.1
12b (X = S)	UB3LYP/6-311+G(2d,p)		−13.9	2.0	−5.9	2.0	−5.1	5.8

[a]At 9.4 GHz in *t*-BuPh solution; hfs in Gauss.

Rate constants of ring-closure reactions can be determined for sterically unhindered radicals by measurements of the concentrations of the ring-open and cyclised radicals under EPR conditions [43-45]. Steady-state concentrations of **12a** were determined in the usual way from the spectra [46].

We estimated that the concentration ratio [**12a**]/[**11a**] > 4 at 230 K, and hence k_{sc}(230 K) > 55 s^{-1} (see Supporting Information File 1 for details). Most radical cyclisations have Arrhenius log(A_c) ≈ 10.5 s^{-1} [47,48] and, by assuming that this holds for **12a**, an activation energy E_{sc} < 9 kcal mol^{-1} and k_{sc}(300 K) > 5 × 10^3 s^{-1} are obtained (see Supporting Information File 1). The rate constant for *5-exo*-cyclisation of the phenylpentenyliminyl radical **15** was reported [34] to be k_c(300 K) = 8.8 × 10^3 s^{-1} with E_c = 8.3 kcal mol^{-1} and therefore, particularly in view of the large resonance stabilisation of spiro-cyclised radical **12a**, these rate parameters seem to be very reasonable estimates (Table 3).

Curiously, analysis of the products from a photolysis of **2a** carried out at higher temperature (rt) in benzotrifluoride solvent, showed benzofuro[3,2-*c*]isoquinoline derivative **14a** to be the main product (65%) [26]. This implied ortho-radicals **13** as intermediates and appeared to conflict with the EPR result. The most likely explanation is that, at the temperature of the preparative experiments (~100 K higher than the EPR study) the spiro-cyclisation is reversible whereas the 6-ortho-process is not. The ortho-product then accumulates because of thermodynamic control. Alternatively, spiro-radical **12a** might rearrange via a tetracyclic aziridinyl intermediate (or transition state) at higher temperatures. DFT computations (see below) undermined this possibility however.

EPR experiments with the benzothiophene-containing precursor **2b** showed a complex spectrum from at least two radicals. A reasonable simulation (see Supporting Information File 1) was obtained as a combination of the spiro-radical **12b** (hfs in Table 2) and the solvent-derived adduct **9a**. Most likely therefore spiro-cyclisation predominates at low temperature but again thermodynamic control takes over at higher temperatures because **14b** was isolated as the main product.

EPR spectra from the furan-containing precursor **3**, and from the more flexible aromatic precursor **4**, revealed only the corresponding ring-open iminyl radicals and neither spiro- nor ortho-radicals in the temperature range 230–260 K. It can be concluded that the rates of their iminyl ring closures are significantly slower. This accords with expectation, because the cyclised radical from **3**, without the benzo-ring of **12**, would be less thermodynamically stabilised. The iminyl radical from **4** has a more flexible chain and this probably accounts for its slower ring closure.

Table 3: Rate data for spiro- and other cyclisations of C- and N-centred radicals.

Entry	Radical	Structure	Mode	log(A_c/s^{-1})[a]	E_c/kcal mol^{-1}	k_c(300 K)/s^{-1}	Ref.
1	**16**		*5-exo*	10.4	6.85	2.3 × 10^5	[49]
2	**15**	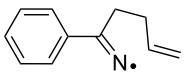	*5-exo*	[10.0]	8.3	8.3 × 10^3	[34]
3		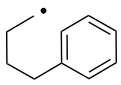	spiro			<5 × 10^4 (323 K)	[50]
4		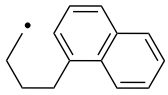	spiro			<10^4 (353 K)	[51]
5	**5b**	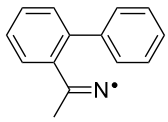	ortho			<5 × 10^3	this work
6	**12a**	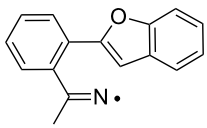	spiro	[10.5]	< 9	>5 × 10^3	this work

[a]Values in parenthesis assumed.

Kinetic data for iminyl radical ring closures is compared with analogous data for model C-centred radicals in Table 3. As mentioned above, biphenyl-iminyl radicals **5** were spectroscopically detectable at 270 K; well above the temperature at which **12a** underwent spiro-cyclisation. It follows that k_c(300 K) for **5b** must be < k_c for **12a** and this information is included in Table 3.

The rate constant for *5-exo*-cyclisation the archetype iminyl **15** (Table 3, entry 2) is more than an order of magnitude smaller than the rate constant for hex-5-enyl (**16**, Table 3, entry 1) [49]. Our rates for ortho- (Table 3, entry 5) and spiro- (Table 3, entry 6) cyclisations of iminyls onto aromatics were also slower than for C-centred radicals (Table 3, entries 3 and 4) [50,51]. The pattern of slower cyclisations for iminyls compared with alkyls seems established for both alkene- and arene-type acceptors.

QM Computations

To shed further light on the spiro versus ortho alternatives we computed the activation parameters [$\Delta E^{\ddagger}_{298}$] and reaction enthalpies [ΔH_{298}], corrected to 298 K for thermal effects, for the spiro- and ortho-cyclisation modes of a representative set of aryliminyl radicals (Table 4). It was known that the DFT UB3LYP/6-31+G(d) and UB3LYP/6-311+G(2d,p) methods gave results in reasonable harmony with experiment for related iminyl radicals [34] and therefore these methods were adopted. For each process the two basis sets gave results in reasonable agreement (Table 4). The cyclisations of the flexible iminyl radicals **4Im** (Tabel 4, entries 1 and 2) were predicted to have the highest activation energies in either mode and to be strongly endothermic. This accords well with the absence of cyclised species in the EPR spectra and with the lack of cyclised products.

For the parent biphenyliminyl radical **5a** the ortho-ring closure (Table 4, entry 5) was computed to have a lower activation energy than spiro-cyclisation (Table 4, entry 4) and to be exothermic in comparison with the endothermic spiro-mode. This was in good accordance with the observed exclusive formation of phenanthridines derived from radicals **5a–f** for these

Table 4: DFT computed activation energies ($\Delta E^{\ddagger}_{298}$) and reaction enthalpies (ΔH_{298}) in kcal mol^{-1} for aromatic iminyl radicals.

Entry	Iminyl	Product	Method[a]	$\Delta E^{\ddagger}_{298}$	ΔH_{298}
1	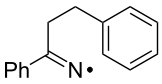 **4Im**	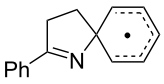 **4sp**	A B	16.6 16.9	6.6 7.3
2	**4Im**	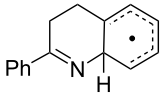 **4or**	B	19.9	8.0
3	**4Im**	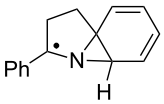 **4az**	B		32.9
4	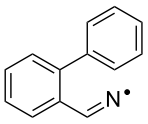 **5a**	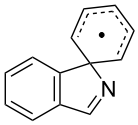 **7a**	A B	14.7 15.0	7.0 7.6
5	**5a**	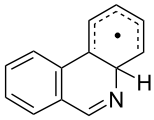 **8a**	A B	11.3 11.6	−2.8 −2.1
6	**5a**	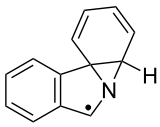 **5az**	B		29.5

Table 4: DFT computed activation energies ($\Delta E^{\ddagger}_{298}$) and reaction enthalpies (ΔH_{298}) in kcal mol^{-1} for aromatic iminyl radicals. (continued)

7	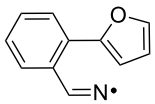 **3Im**	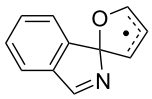 **3sp**	A B	11.6 12.1	−1.1 −0.5
8	**3Im**	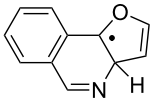 **3en**	A B	14.2 14.7	−2.3 −1.8
9	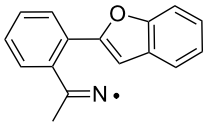 **11a**	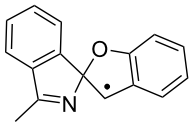 **12a**	A B	8.9 9.3	−7.8 −6.9
10	**11a**	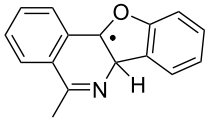 **13a**	A B	12.6 13.1	−8.6 −8.1
11	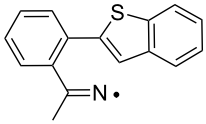 **11b**	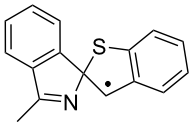 **12b**	B	9.5	−6.2
12	**11b**	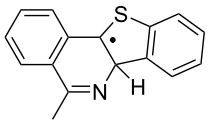 **13b**	B	10.5	−11.3

[a]A = UB3LYP/6-31+G(d), B = UB3LYP/6-311+G(2d,p).

compounds. The possibility of the rearrangement of spiro- to ortho-species via aziridinyl intermediates (or transition states) (**az**) which contain benzyl stabilization was examined. However, the computations for **4az** (Table 4, entry 3) and **5az** (Table 4, entry 6) found these processes to be strongly endothermic, so they can probably be ruled out of consideration. Predicted activation energies and reaction enthalpies for spiro- (Table 4, entry 7) and ortho-ring closure (Table 4, entry 8) of the furanyl-iminyl **3Im**, suggested spiro-closure would be favoured. However, the magnitude of $\Delta E^{\ddagger}_{298}$ is close to that for ortho-closure of the biphenyl analogue **5a**. Thus cyclised products might be obtainable from photolyses of **3** at higher temperatures.

For the benzofuranyl- and benzothiophenyl-iminyl radicals **11a** and **11b** (Table 4, entries 9–12) the computations predicted a reversal in the preferred mode of ring closure: $\Delta E^{\ddagger}_{298}$ values for spiro-cyclisation were significantly lower than for ortho-cyclisation and lower than for **5a.** This agreed well with the EPR detection of the spiro-intermediates **12a** and **12b**. From the EPR experiments the E_{sc} of < 9 kcal mol^{-1} for spiro-cyclisation of **11a** (see above Table 3) was close to the computed $\Delta E^{\ddagger}_{298}$ values of 8.9 and 9.3 kcal mol^{-1} (Table 4, entry 9). For both **11a** and **11b**, although the computed $\Delta E^{\ddagger}_{298}$ values for ortho-ring closure are significantly higher than for spiro-ring closure, the ortho-processes are computed to be more exothermic. Thus, theory supports the idea, derived from the isolation of products from ortho-closure of **14a**,**b**, that thermodynamic control supervenes at higher temperatures.

Some clues as to why the biphenyl-iminyls **5** prefer the ortho mode whereas the benzofuranyl- and benzothiophenyl-iminyls **11** prefer the spiro mode can be obtained by consideration of the structures of the transition states (TS, Figure 4). The top line shows the computed spin density (ρ) maps for the reactant iminyls. In agreement with the EPR spectra, the spin density is largely concentrated in orbitals in the plane of the iminyl units. The middle line of Figure 4 shows the TS structures and

SOMOs for spiro-cyclisations of **5a** and **11a**. For both radicals the iminyl units approach the acceptor rings from vertically above; the angle between the ArC(R)=N unit and the plane of the acceptor ring is ~90° for both TSs. This ensures that overlap between the incoming iminyl orbital and the acceptor ring orbitals is optimum. The bottom line shows the TS structures and SOMOs for the ortho-cyclisations of **5a** and **11a**. For both radicals the architectures oblige the iminyl units to approach the acceptor rings at much more oblique angles. Thus, overlap of the in-plane iminyl orbital with the acceptor ring orbitals is poorer than for spiro-cyclisation. However, this is offset by the greater resonance delocalisation in the TS frontier orbitals for ortho-cyclisation (see Figure 4). There is a trade-off between these two factors and the default is that the resonance delocalisation factor in ortho-cyclisation prevails. Evidently **11a**,**b**, are exceptional in that the iminyl/acceptor overlap factor outweighs the resonance delocalisation factor.

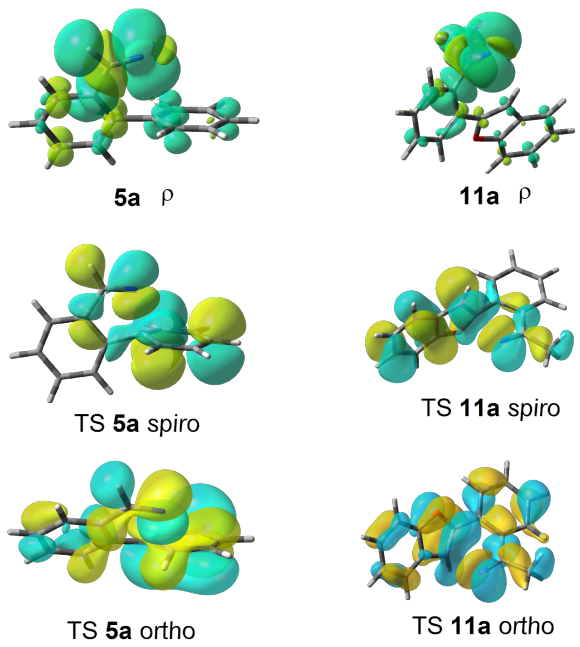

Figure 4: DFT computed structures for **5a**, **11a** and their cyclisation transition states (TS). Top line: spin density distribution maps for iminyls **5a** and **11a**. Middle line: spiro TSs, r(N···C) for **5a** = 1.928 and for **11a** = 2.064 Å. Bottom line: ortho TSs, r(N···C) for **5a** = 1.954 and for **11a** = 2.027 Å.

Conclusion

Ethoxycarbonyl oximes of aromatic and heteroaromatic ketones are easily made and handled and have long shelf lives. We have found them to be outstanding precursors for the photochemical generation of aromatic iminyl radicals. Product analyses, EPR spectroscopic observations and DFT computations all converged in indicating that the "default" ring closure mode for iminyl radicals is ortho-cyclisation onto suitably situated aromatic rings. The exception to this rule was spiro-cyclisation onto benzofuran and benzothiophene rings at low temperatures. Even for these acceptors, however, thermodynamic control ensured that the only isolable products were from ortho-closures. Rate parameters for the spiro-cyclisation of **11a**, estimated by the steady-state kinetic EPR method, showed the process to be about an order of magnitude slower than for archetype C-centred radicals. This was in harmony with the generally slower reaction rates of iminyl radicals compared with alkyl radicals. DFT-computed energetics were in good agreement with experiment and supported the idea of thermodynamic control for the cyclisation of **11a**,**b**.

Experimental

EPR spectra were obtained at X-Band on Bruker EMX 10/12 spectrometers at St. Andrews and Manchester. Oxime carbonates (2 to 15 mg) and MAP (1 equiv wt/wt) in *t*-BuPh or benzene (0.5 mL) were prepared in quartz tubes and deaerated by bubbling with nitrogen for 15 min. Photolysis in the resonant cavity was by unfiltered light from a 500 W super-pressure mercury arc lamp or, in the Manchester experiments, from a Luxtel CL300BUV lamp. EPR signals were digitally filtered and double integrated by using the Bruker WinEPR software, and radical concentrations were calculated by reference to the double integral of the signal from a known concentration of the stable radical DPPH run under identical conditions. The majority of EPR spectra were recorded with 2.0 mW power, 0.8 G_{pp} modulation intensity and gain of 10^6.

QM calculations were carried out by using the Gaussian 09 program package. Geometries were fully optimised for all model compounds. Optimised structures were characterised as minima or saddle points by frequency calculations. The experimental kinetic and spectroscopic data was all obtained in the nonpolar hydrocarbon solvents *t*-BuPh or cyclopropane. Solvent effects, particularly differences in solvation between the neutral reactants and neutral transition states, were therefore expected to be minimal. In view of this, no attempt was made to model the effect of the solvent computationally.

Supporting Information

Supporting Information File 1

General procedures. Preparation and characterization data of oxime carbonates. Sample EPR spectra and kinetic data. ^{1}H and ^{13}C NMR spectra for novel compounds.
[http://www.beilstein-journals.org/bjoc/content/supplementary/1860-5397-9-120-S1.pdf]

Acknowledgements

We thank the EPSRC (grant EP/I003479/1) & EaStCHEM for funding, the EPSRC UK National Electron Paramagnetic Resonance Service at the University of Manchester and the EPSRC National Mass Spectrometry Service, Swansea.

References

1. Pratsch, G.; Heinrich, M. R. Modern Development in Aryl Radical Chemistry. *Radicals in Synthesis III;* Topics in Currrent Chemistry, Vol. 320; Springer Verlag: Berlin, Germany, 2012; pp 33–59. doi:10.1007/128_2011_127
2. Laali, K. K.; Shokouhimehr, M. *Curr. Org. Synth.* **2009,** *6,* 193–202. doi:10.2174/157017909788167275
3. Crich, D.; Hwang, J.-T. *J. Org. Chem.* **1998,** *63,* 2765–2770. doi:10.1021/jo972197s
4. Maggio, B.; Daidone, G.; Raffa, D.; Plescia, S.; Bombieri, G.; Meneghetti, F. *Helv. Chim. Acta* **2005,** *88,* 2272–2281. doi:10.1002/hlca.200590161
5. Moorthy, J. N.; Samanta, S. *J. Org. Chem.* **2007,** *72,* 9786–9789. doi:10.1021/jo7017872
6. Forrester, A. R.; Gill, M.; Meyer, C. J.; Sadd, J. S.; Thomson, R. H. *J. Chem. Soc., Perkin Trans. 1* **1979,** 606–611. doi:10.1039/P19790000606
7. Forrester, A. R.; Gill, M.; Sadd, J. S.; Thomson, R. H. *J. Chem. Soc., Perkin Trans. 1* **1979,** 612–615. doi:10.1039/P19790000612
8. Forrester, A. R.; Gill, M.; Thomson, R. H. *J. Chem. Soc., Perkin Trans. 1* **1979,** 616–620. doi:10.1039/P19790000616
9. Forrester, A. R.; Napier, R. J.; Thomson, R. H. *J. Chem. Soc., Perkin Trans. 1* **1981,** 984–987. doi:10.1039/P19810000984
10. Zard, S. Z. *Synlett* **1996,** 1148–1154. doi:10.1055/s-1996-5698
11. Gagosz, F.; Zard, S. Z. *Synlett* **1999,** 1978–1980. doi:10.1055/s-1999-2971
12. Bowman, W. R.; Bridge, C. F.; Brookes, P. *Tetrahedron Lett.* **2000,** *41,* 8989–8994. doi:10.1016/S0040-4039(00)01596-3
13. McCarroll, A. J.; Walton, J. C. *Chem. Commun.* **2000,** 351–352. doi:10.1039/a910346p
14. Bencivenni, G.; Lanza, T.; Leardini, R.; Minozzi, M.; Nanni, D.; Spagnolo, P.; Zanardi, G. *J. Org. Chem.* **2008,** *73,* 4721–4724. doi:10.1021/jo800453z
15. Lanza, T.; Leardini, R.; Minozzi, M.; Nanni, D.; Spagnolo, P.; Zanardi, G. *Angew. Chem., Int. Ed.* **2008,** *47,* 9439–9442. doi:10.1002/anie.200804333
16. Bowman, W. R.; Bridge, C. F.; Cloonan, M. O.; Leach, D. C. *Synlett* **2001,** 765–768. doi:10.1055/s-2001-14592
17. Blake, J. A.; Pratt, D. A.; Lin, S.; Walton, J. C.; Mulder, P.; Ingold, K. U. *J. Org. Chem.* **2004,** *69,* 3112–3120. doi:10.1021/jo049927y
18. Bowman, W. R.; Cloonan, M. O.; Fletcher, A. J.; Stein, T. *Org. Biomol. Chem.* **2005,** *3,* 1460–1467. doi:10.1039/b501509j
19. Portela-Cubillo, F.; Scott, J. S.; Walton, J. C. *Chem. Commun.* **2008,** 2935–2937. doi:10.1039/b803630f
20. Alonso, R.; Campos, P. J.; García, B.; Rodríguez, M. A. *Org. Lett.* **2006,** *8,* 3521–3523. doi:10.1021/ol061258i
21. Portela-Cubillo, F.; Lymer, J.; Scanlan, E. M.; Scott, J. S.; Walton, J. C. *Tetrahedron* **2008,** *64,* 11908–11916. doi:10.1016/j.tet.2008.08.112
22. Beaume, A.; Courillon, C.; Derat, E.; Malacria, M. *Chem.–Eur. J.* **2008,** *14,* 1238–1252. doi:10.1002/chem.200700884
23. Portela-Cubillo, F.; Scott, J. S.; Walton, J. C. *J. Org. Chem.* **2008,** *73,* 5558–5565. doi:10.1021/jo800847h
24. Alonso, R.; Caballero, A.; Campos, P. J.; Rodríguez, M. A. *Tetrahedron* **2010,** *66,* 8828–8831. doi:10.1016/j.tet.2010.09.078
25. Portela-Cubillo, F.; Scott, J. S.; Walton, J. C. *J. Org. Chem.* **2009,** *74,* 4934–4942. doi:10.1021/jo900629g
26. McBurney, R. T.; Slawin, A. M. Z.; Smart, L. A.; Yu, Y.; Walton, J. C. *Chem. Commun.* **2011,** *47,* 7974–7976. doi:10.1039/c1cc12720a
27. Sridar, V.; Babu, G. *Synth. Commun.* **1997,** *27,* 323–330. doi:10.1080/00397919708005035
28. Calestani, G.; Leardini, R.; McNab, H.; Nanni, D.; Zanardi, G. *J. Chem. Soc., Perkin Trans. 1* **1998,** 1813–1824. doi:10.1039/A800868J
29. Bowman, W. R.; Bridge, C. F.; Brookes, P.; Cloonan, M. O.; Leach, D. C. *J. Chem. Soc., Perkin Trans. 1* **2002,** 58–68. doi:10.1039/B108323F
30. Neta, P.; Fessenden, R. W. *J. Phys. Chem.* **1970,** *74,* 3362–3365. doi:10.1021/j100712a009
31. Hudson, R. F.; Lawson, A. J.; Lucken, E. A. C. *J. Chem. Soc. D* **1971,** 807–808. doi:10.1039/C29710000807
32. Griller, D.; Mendenhall, G. D.; Van Hoof, W.; Ingold, K. U. *J. Am. Chem. Soc.* **1974,** *96,* 6068–6070. doi:10.1021/ja00826a018
33. Le Tadic-Biadatti, M.-H.; Callier-Dublanchet, A.-C.; Horner, J. H.; Quiclet-Sire, B.; Zard, S. Z.; Newcomb, M. *J. Org. Chem.* **1997,** *62,* 559–563. doi:10.1021/jo961530+
34. Portela-Cubillo, F.; Alonso-Ruiz, R.; Sampedro, D.; Walton, J. C. *J. Phys. Chem. A* **2009,** *113,* 10005–10012. doi:10.1021/jp9047902
35. McBurney, R. T.; Harper, A. D.; Slawin, A. M. Z.; Walton, J. C. *Chem. Sci.* **2012,** *3,* 3436–3444. doi:10.1039/c2sc21298f
36. Hudson, R. F.; Record, K. A. F. *J. Chem. Soc., Chem. Commun.* **1976,** 831–832. doi:10.1039/C39760000831
37. McCarroll, A. J.; Walton, J. C. *J. Chem. Soc., Perkin Trans. 2* **2000,** 2399–2409. doi:10.1039/b007212p
38. *Gaussian 09,* Revision A.02; Gaussian, Inc.: Wallingford, CT, 2009.
39. Binmore, G. T.; Walton, J. C.; Adcock, W.; Clark, C. I.; Kristic, A. R. *Magn. Reson. Chem.* **1995,** *33,* S53–S59. doi:10.1002/mrc.1260331310
40. Mangini, A.; Spagnolo, P.; Tassi, D.; Tiecco, M.; Zanirato, P. *Tetrahedron* **1972,** *28,* 3485–3488. doi:10.1016/0040-4020(72)88109-2
41. Tiecco, M. *Pure Appl. Chem.* **1981,** *53,* 239–258. doi:10.1351/pac198153010239
42. Barone, V. Structure, Magnetic Properties and Reactivities of Open-Shell Species From Density Functional and Self-Consistent Hybrid Methods. In *Recent Advances in Density Functional Methods;* Chong, D. P., Ed.; Recent Advances in Computational Chemistry, Vol. 1; World Scientific: Singapore, 1995; pp 287–334. doi:10.1142/9789812830586_0008
43. Griller, D.; Ingold, K. U. *Acc. Chem. Res.* **1980,** *13,* 193–200. doi:10.1021/ar50151a001
44. Griller, D.; Ingold, K. U. *Acc. Chem. Res.* **1980,** *13,* 317–323. doi:10.1021/ar50153a004
45. Walton, J. C. *J. Chem. Soc., Perkin Trans. 2* **1987,** 231–235. doi:10.1039/p29870000231
46. Walton, J. C. In *Encyclopedia of Radicals in Chemistry, Biology and Materials;* Chatgilialoglu, C.; Studer, A., Eds.; John Wiley & Sons: Chichester, UK, 2012; pp 147–174.

47. Beckwith, A. L. J.; Brumby, S. In *Landolt-Börnstein, Radical Reaction Rates in Liquids;* Fischer, H., Ed.; Springer Verlag: Berlin, 1994; Vol. II18a, pp 171–254.
48. Beckwith, A. L. J. In *Landolt-Börnstein, Radical Reaction Rates in Liquids;* Fischer, H., Ed.; Springer Verlag: Berlin, 1984; Vol. II13a, pp 252–315.
49. Chatgilialoglu, C.; Ingold, K. U.; Scaiano, J. C. *J. Am. Chem. Soc.* **1981,** *103,* 7739–7742. doi:10.1021/ja00416a008
50. Julia, M. *Pure Appl. Chem.* **1974,** *40,* 553–567. doi:10.1351/pac197440040553
51. Kochi, J. K.; Gilliom, R. D. *J. Am. Chem. Soc.* **1964,** *86,* 5251–5256. doi:10.1021/ja01077a042

Beilstein Journal of Organic Chemistry

Photoinduced synthesis of unsymmetrical diaryl selenides from triarylbismuthines and diaryl diselenides

Yohsuke Kobiki, Shin-ichi Kawaguchi, Takashi Ohe and Akiya Ogawa*

Letter

Open Access

Address:
Department of Applied Chemistry, Graduate School of Engineering, Osaka Prefecture University, 1-1 Gakuen-cho, Nakaku, Sakai, Osaka 599-8531, Japan

Email:
Akiya Ogawa* - ogawa@chem.osakafu-u.ac.jp

* Corresponding author

Keywords:
arylation; unsymmetrical diaryl selenide; free radical; organobismuth; photoinduced reaction

Beilstein J. Org. Chem. **2013,** *9,* 1141–1147.
doi:10.3762/bjoc.9.127

Received: 16 April 2013
Accepted: 22 May 2013
Published: 13 June 2013

This article is part of the Thematic Series "Organic free radical chemistry".

Guest Editor: C. Stephenson

Abstract

A novel method of photoinduced synthesis of unsymmetrical diaryl selenides from triarylbismuthines and diaryl diselenides has been developed. Although the arylation reactions with triarylbismuthines are usually catalyzed by transition-metal complexes, the present arylation of diaryl diselenides with triarylbismuthines proceeds upon photoirradiation in the absence of transition-metal catalysts. A variety of unsymmetrical diaryl selenides can be conveniently prepared by using this arylation method.

Introduction

A number of organoselenium compounds are known to be biologically active [1-4]. In particular, diaryl selenides are known to have antioxidative effects [5]. Therefore, many studies on the synthetic methods for unsymmetrical diaryl selenides have recently been reported [6-32]. Most of these methods use coupling reactions catalyzed by transition-metal complexes. To avoid the contamination of product selenides with transition-metals, the development of synthetic methods for unsymmetrical diaryl selenides in the absence of transition-metal catalysts is desirable. On the other hand, triarylbismuthines are gaining interest as useful arylation reagents, because organobismuth compounds are nontoxic and have excellent reactivity, which has led to several applications in organic synthesis [33]. Therefore, numerous transition-metal-catalyzed coupling reactions with organobismuth compounds have been reported [34-53]. Although triphenylbismuthine can generate a phenyl radical [33,54] in the absence of a radical initiator simply by photoirradiation, few arylation reactions using this mechanism have been reported [55,56]. We presume that a phenyl radical generated from triphenylbismuthine can be captured by organic diselenides, which have a high carbon-radical-capturing ability [57-64] and as a result, diaryl selenide will be generated (Scheme 1). In 1999, Barton and co-workers reported that diaryl selenide was obtained by the reaction of triarylbismuthine with

diphenyl diselenide under heating at high temperature (140 °C) [65], but the photoinduced reaction was not investigated. In this letter, we will report the radical reaction of diaryl diselenides with triarylbismuthines from the viewpoint of a photoinduced reaction in the synthesis of unsymmetrical diaryl selenides.

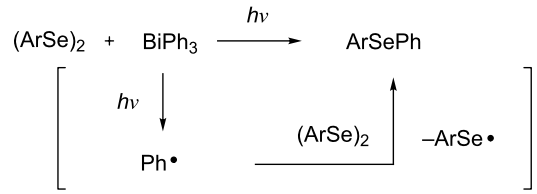

Scheme 1: Photoinduced radical reaction of diaryl diselenide with triphenylbismuthine.

Results and Discussion

First, we investigated the photoinduced reaction of diphenyl diselenide with triphenylbismuthine. Diphenyl diselenide (**1a**, 0.1 mmol) and triphenylbismuthine (**2a**, 0.5 mmol) were placed in a Pyrex test tube (∅ = 9 mm) with $CHCl_3$ (4 mL), and the mixture was irradiated by a xenon lamp for 5 h at room temperature. As a result, 0.042 mmol (21% yield based on the amount of selenium atoms) of diphenyl selenide (**3aa**) was obtained after the isolation by silica gel chromatography (the yield was determined by HPLC). Next, optimization of the reaction conditions was investigated as shown in Table 1. Irradiation by a tungsten lamp instead of a xenon lamp did not induce the desired arylation reaction (Table 1, entry 2), and in the dark, the reaction did not proceed at all (Table 1, entry 3). When 2,2′-azobis(isobutyronitrile) (AIBN) was used as a radical initiator, the desired reaction proceeded ineffectively (Table 1, entry 4). Among several solvents, such as benzene, DMSO and CH_3CN, the use of CH_3CN improved the yield of **3aa** (Table 1, entries 5–7). Although the solubility of **2a** is different depending on the solvent, the yield of **3aa** is not correlated with the solubility of **2a**. It may be more important to choose a solvent that does not react with the generated aryl radical. Moreover, a lower amount of solvent and the utilization of a quartz test tube (∅ = 9 mm) contributed to the increase in the yield of **3aa** (Table 1, entries 8 and 9).

Next, we investigated the scope of the synthesis of unsymmetrical diaryl selenides by using different diaryl diselenides and triarylbismuthines (Table 2). The employed diaryl diselenides were diphenyl diselenide (**1a**), bis(4-fluorophenyl) diselenide (**1b**), bis(4-(trifluoromethyl)phenyl) diselenide (**1c**), bis(1-naphthyl) diselenide (**1d**), and bis(2-naphthyl) diselenide (**1e**). The used triarylbismuthines were triphenylbismuthine (**2a**), tris(4-methylphenyl)bismuthine (**2b**), tris(4-chlorophenyl)bismuthine (**2c**), and tris(4-fluorophenyl)bismuthine (**2d**). A number of combinations of **1** and **2** were examined and as a result, unsymmetrical diaryl selenides **3** were obtained in moderate to high yields (45–86%) in every case (Table 2, entries 1–10) after the isolation by preparative TLC on silica gel. The chemical shifts of ^{77}Se NMR spectra of diaryl selenides **3** are also shown in

Table 1: Reaction of diphenyl diselenide with triphenylbismuthine under different conditions.

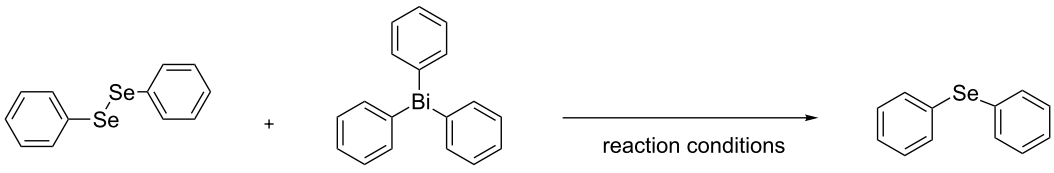

1a 0.1 mmol

2a 0.5 mmol

3aa

entry	reaction conditions	yield of **3aa**[a]
1	$CHCl_3$ (4 mL), xenon lamp, Pyrex test tube, 5 h	0.042 mmol, 21%
2	$CHCl_3$ (4 mL), tungsten lamp, Pyrex test tube, 5 h	0.004 mmol, 2%
3	$CHCl_3$ (4 mL), dark, 24 h	0%
4	C_6H_6 (5 mL), AIBN (1.5 mmol), 80 °C, two-necked flask, 8 h	0.012 mmol, 6%
5	C_6H_6 (4 mL), xenon lamp, Pyrex test tube, 5 h	0.102 mmol, 51%
6	DMSO (4 mL), xenon lamp, Pyrex test tube, 5 h	0.034 mmol, 17%
7	CH_3CN (4 mL), xenon lamp, Pyrex test tube, 5 h	0.114 mmol, 57%
8	CH_3CN (2 mL), xenon lamp, Pyrex test tube, 5 h	0.126 mmol, 63%
9	CH_3CN (2 mL), xenon lamp, quartz test tube, 5 h	0.138 mmol, 69%

[a]The yields were determined by HPLC.

Table 2: Syntheses of unsymmetrical diaryl selenides.

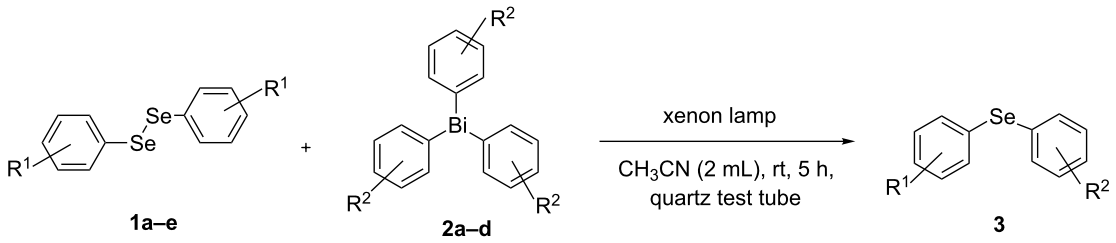

1a–e 0.1 mmol + **2a–d** 0.3 mmol or 0.5 mmol → **3**

entry	$(ArSe)_2$ **1**	Ar'_3Bi **2**	product **3** (ArSeAr')	^{77}Se NMR, δ ppm	yield[a]
1[b]	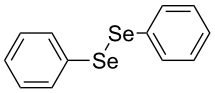 **1a**	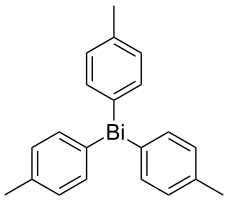 **2b**	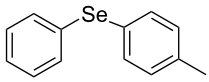 **3ab**	407	65%
2[b]	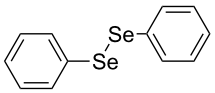 **1a**	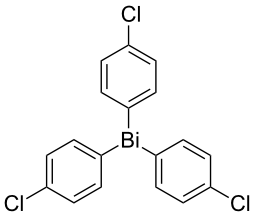 **2c**	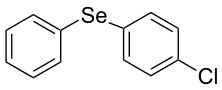 **3ac**	416	45%
3[c]	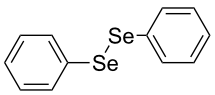 **1a**	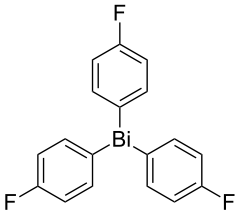 **2d**	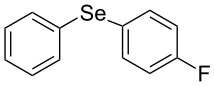 **3ad**	411	66%
4[b]	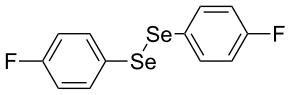 **1b**	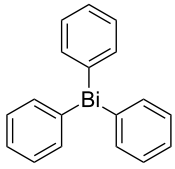 **2a**	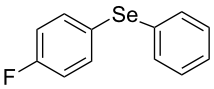 **3ba**	411	57%
5[b]	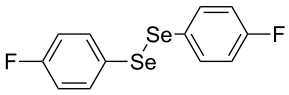 **1b**	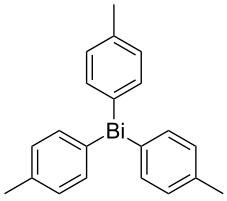 **2b**	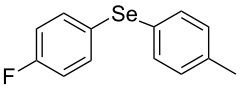 **3bb**	404	86%

Table 2: Syntheses of unsymmetrical diaryl selenides. (continued)

6[b]	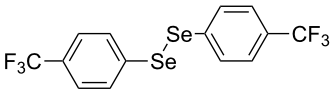 **1c**	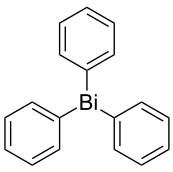 **2a**	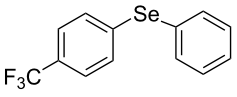 **3ca**	427	67%
7[b]	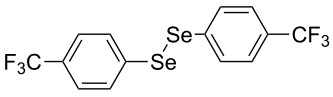 **1c**	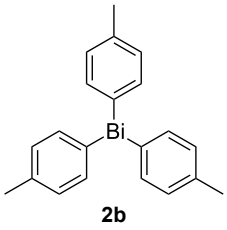 **2b**	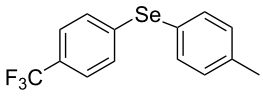 **3cb**	418	51%
8[c]	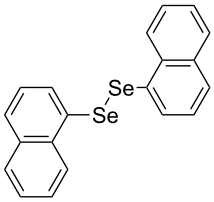 **1d**	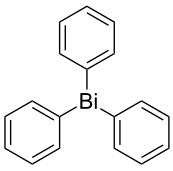 **2a**	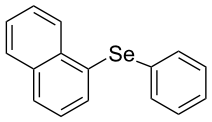 **3da**	355	51%
9[c]	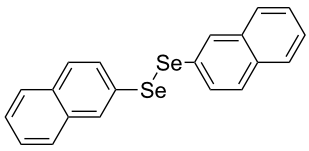 **1e**	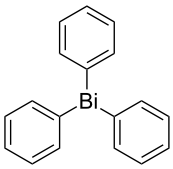 **2a**	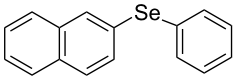 **3ea**	418	71%
10[c]	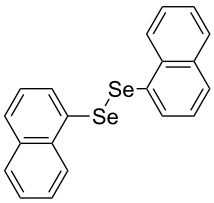 **1d**	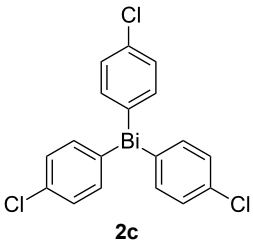 **2c**	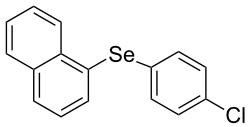 **3dc**	354	57%

[a]The yields were determined after isolation. [b]0.5 mmol of triarylbismuthine was used. [c]0.3 mmol of triarylbismuthine was used.

Table 2, because ^{77}Se NMR is a tool well suited to identify diorganyl monoselenides.

To get information about the reaction pathway of this arylation, we first investigated the arylation of diphenyl diselenide by varying the **1a**/**2a** molar ratio (Table 3). When excess amounts of either starting substrate were employed, the yields of **3aa** increased (Table 3, entries 1, 2 and 5).

In the case of the reaction of triphenylbismuthine with diphenyl disulfide (**4**) instead of diphenyl diselenide, diphenyl sulfide **5** was obtained in lower yield with unidentified byproducts, unlike in the case of diphenyl selenide **3aa** (Scheme 2).

Additionally, air is entrained in the reaction system, since a test tube with a septum was used in which a needle was inserted. When the reaction of diaryl diselenide with triarylbismuthine was conducted with a strictly sealed tube in Ar atmosphere, a bismuth mirror was observed and the yield of **3aa** decreased. We assume that the reaction proceeds with bismuth residue getting oxidized.

A plausible reaction pathway for the photoinduced reaction of diaryl diselenide with triarylbismuthine is shown in Scheme 3. First, an aryl radical is generated from triarylbismuthine by near-UV light irradiation [33,54,55]. The generated aryl radical is captured by diaryl diselenide to produce diaryl selenide and a

Table 3: The yield of diphenyl selenide **3aa** upon changing the ratio **1a**/**2a**.

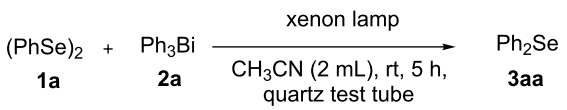

entry	amount of **1a**	amount of **2a**	yield of **3aa**[a]
1	0.1 mmol	0.5 mmol	69% 0.138 mmol
2	0.1 mmol	0.3 mmol	69% 0.138 mmol
3	0.1 mmol	0.1 mmol	59% 0.118 mmol
4	0.1 mmol	0.067 mmol (2/3 equiv)	57% 0.118 mmol
5	0.2 mmol	0.1 mmol	88%[b] 0.263 mmol

[a]The yields were determined by HPLC based on the amount of **1a**. [b]The yield was calculated based on the amount of **2a**.

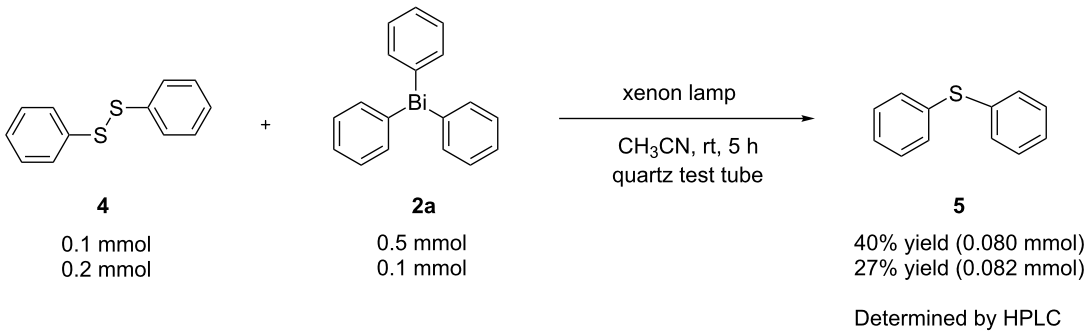

Scheme 2: Photoinduced reaction of diphenyl disulfide with triphenylbismuthine.

seleno radical. The seleno radical may dimerize to re-form diselenide. Diphenyl diselenide has its absorption maximum (λ_{max}) at 340 nm ($\varepsilon = 10^3$) [66] and accordingly, the seleno radical could be produced by the irradiation with a tungsten lamp. However, the irradiation by a tungsten lamp instead of a xenon lamp did not result in the desired reaction (Table 1, entry 3). This fact strongly suggests that the formation of a phenylseleno radical is not important for the formation of diphenyl selenide. Conceivably, when the reaction proceeds, a phenyl radical may be formed directly from triphenylbismuthine upon photoirradiation. Moreover, the use of an excess amount of **1**, which has a relatively high carbon-radical-capturing ability, increased the yield of **3**, and the use of diphenyl disulfide (**4**), which has a lower carbon-radical-capturing ability than diselenide, decreased the yield of **5**. (The exact capturing abilities of diselenide and disulfide toward the phenyl radical are not known, but they have been reported toward vinyl radicals, where diselenide has a higher capturing ability than disulfide: $k_{Se}/k_S = 160$ [57-59].) These facts also support that the reaction starts from the generation of an aryl radical. On the other hand, a pale yellow solid, insoluble in organic solvents, was obtained as a byproduct after the reaction. We assume that this solid is a bismuth residue, which can consist of bismuth oxides and/or bismuth selenides. Moreover, it may form biaryls (Ar–Ar) as byproducts, but no biaryl was observed after the reaction.

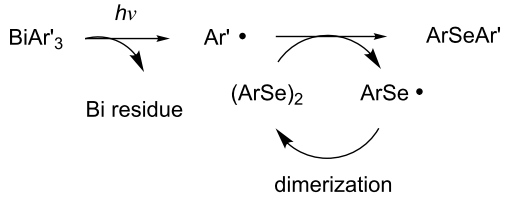

Scheme 3: A plausible reaction pathway for the photoinduced reaction of diaryl diselenide with triarylbismuthine.

Conclusion

We have found that the photoinduced reaction of diaryl diselenides with triarylbismuthines affords unsymmetrical diaryl selenides in good yields. This method is efficient, because two arylseleno groups from diaryl selenides can be used as a selenium source, and its advantage is that the reaction proceeds in the absence of transition-metal catalysts.

Experimental

General comments

Compounds **1a**, **2a**, **3aa**, **4**, and **5** were obtained from commercially available materials. Diaryl diselenides **1b**–**e** [67] and triarylbismuthines **2b**–**d** [68] were synthesized according to the literature procedures.

General procedure for the photoinduced synthesis of unsymmetrical diaryl selenides from diaryl diselenide and triarylbismuthine

$(Ar^1Se)_2$ (0.1 mmol), and $Ar^2{}_3Bi$ (0.3 mmol) were dispersed in CH_3CN (2 mL) with a stirring bar in a quartz test tube (∅ = 9 mm) with a septum in which a needle was inserted. The mixture was stirred and irradiated by a xenon lamp for 5 h at room temperature. The reaction mixture was filtered through a bed of celite (Celite 535). The crude product was purified by preparative TLC on silica gel (eluent: hexane/EtOAc). Details about compounds **3ab** [30], **3ac** [14], **3ad** [17], **3ba** [17], **3bb** [31], **3ca** [17], **3da** [32], **3ea** [28] and **3dc** [30] were reported in the corresponding articles.

Supporting Information

Supporting Information File 1

Spectral and analytical data of the new compound **3cb**.
[http://www.beilstein-journals.org/bjoc/content/supplementary/1860-5397-9-127-S1.pdf]

Acknowledgements

This work is supported by a Grant-in-Aid for Scientific Research (C, 23550057) from the Ministry of Education, Culture, Sports, Science and Technology.

References

1. Klayman, D. L.; Günther, W. H. H. *Organic Selenium Compounds: Their Chemistry and Biology;* John Wiley & Sons: New York, 1973.
2. Wirth, T., Ed. *Organoselenium Chemistry;* Topics in Current Chemistry, Vol. 208; Springer: Berlin, 2000. doi:10.1007/3-540-48171-0
3. Ogawa, A. Selenium and Tellurium in Organic Synthesis. In *Main Group Metals in Organic Synthesis;* Yamamoto, H.; Oshima, K., Eds.; Wiley-VCH: Weinheim, Germany, 2004; Vol. 2, pp 813–866.
4. Nogueira, C. W.; Rocha, J. B. *Arch. Toxicol.* **2011,** *85,* 1313–1359. doi:10.1007/s00204-011-0720-3
5. Andersson, C.-M.; Hallberg, A.; Linden, M.; Brattsand, R.; Moldéus, P.; Cotgreave, I. *Free Radical Biol. Med.* **1994,** *16,* 17–28. doi:10.1016/0891-5849(94)90238-0
6. Campbell, T. W.; Walker, H. G.; Coppinger, G. M. *Chem. Rev.* **1952,** *50,* 279–349. doi:10.1021/cr60156a003
7. Greenberg, B.; Gould, E. S.; Burlant, W. *J. Am. Chem. Soc.* **1956,** *78,* 4028–4029. doi:10.1021/ja01597a043
8. Cristau, H. J.; Chabaud, B.; Labaudiniere, R.; Christol, H. *Organometallics* **1985,** *4,* 657–661. doi:10.1021/om00123a007
9. Beletskaya, I. P.; Sigeev, A. S.; Peregudov, A. S.; Petrovskii, P. V. *J. Organomet. Chem.* **2000,** *605,* 96–101. doi:10.1016/S0022-328X(00)00265-5
10. Gujadhur, R. K.; Venkataraman, D. *Tetrahedron Lett.* **2003,** *44,* 81–84. doi:10.1016/S0040-4039(02)02480-2
11. Taniguchi, N.; Onami, T. *J. Org. Chem.* **2004,** *69,* 915–920. doi:10.1021/jo030300+
12. Kumar, S.; Engman, L. *J. Org. Chem.* **2006,** *71,* 5400–5403. doi:10.1021/jo060690a
13. Varala, R.; Ramu, E.; Adapa, S. R. *Bull. Chem. Soc. Jpn.* **2006,** *79,* 140–141. doi:10.1246/bcsj.79.140
14. Taniguchi, N. *J. Org. Chem.* **2007,** *72,* 1241–1245. doi:10.1021/jo062131+
15. Alves, D.; Santos, C. G.; Paixão, M. W.; Soares, L. C.; Souza, D. D.; Rodrigues, O. E. D.; Braga, A. L. *Tetrahedron Lett.* **2009,** *50,* 6635–6638. doi:10.1016/j.tetlet.2009.09.052
16. Murthy, S. N.; Madhav, B.; Reddy, V. P.; Nageswar, Y. V. D. *Eur. J. Org. Chem.* **2009,** 5902–5905. doi:10.1002/ejoc.200900989
17. Reddy, V. P.; Kumar, A. V.; Swapna, K.; Rao, K. R. *Org. Lett.* **2009,** *11,* 951–953. doi:10.1021/ol802734f
18. Singh, D.; Alberto, E. E.; Rodrigues, O. E. D.; Braga, A. L. *Green Chem.* **2009,** *11,* 1521–1524. doi:10.1039/b916266f
19. Bhadra, S.; Saha, A.; Ranu, B. C. *J. Org. Chem.* **2010,** *75,* 4864–4867. doi:10.1021/jo100755g
20. Li, Y.; Wang, H.; Li, X.; Chen, T.; Zhao, D. *Tetrahedron* **2010,** *66,* 8583–8586. doi:10.1016/j.tet.2010.09.061
21. Freitas, C. S.; Barcellos, A. M.; Ricordi, V. G.; Pena, J. M.; Perin, G.; Jacob, R. G.; Lenardão, E. J.; Alves, D. *Green Chem.* **2011,** *13,* 2931–2938. doi:10.1039/c1gc15725f
22. Swapna, K.; Murthy, S. N.; Nageswar, Y. V. D. *Eur. J. Org. Chem.* **2011,** 1940–1946. doi:10.1002/ejoc.201001639
23. Zhao, H.; Hao, W.; Xi, Z.; Cai, M. *New J. Chem.* **2011,** *35,* 2661. doi:10.1039/c1nj20514e
24. Ricordi, V. G.; Freitas, C. S.; Perin, G.; Lenardão, E. J.; Jacob, R. G.; Savegnago, L.; Alves, D. *Green Chem.* **2012,** *14,* 1030–1034. doi:10.1039/c2gc16427b
25. Beletskaya, I. P.; Sigeev, A. S.; Peregudov, A. S.; Petrovskii, P. V.; Khrustalev, V. N. *Chem. Lett.* **2010,** *39,* 720–722. doi:10.1246/cl.2010.720
26. Beletskaya, I. P.; Sigeev, A. S.; Peregudov, A. S.; Petrovskii, P. V. *Russ. J. Org. Chem.* **2001,** *37,* 1463–1475. doi:10.1023/A:1013460213633
27. Ren, K.; Wang, M.; Wang, L. *Org. Biomol. Chem.* **2009,** *7,* 4858–4861. doi:10.1039/b914533h
28. Reddy, K. H. V.; Satish, G.; Ramesh, K.; Karnakar, K.; Nageswar, Y. V. D. *Chem. Lett.* **2012,** *41,* 585–587. doi:10.1246/cl.2012.585
29. Wang, M.; Ren, K.; Wang, L. *Adv. Synth. Catal.* **2009,** *351,* 1586–1594. doi:10.1002/adsc.200900095
30. Hayashi, S.; Yamane, K.; Nakanishi, W. *J. Org. Chem.* **2007,** *72,* 7587–7596. doi:10.1021/jo070988g

31. Beletskaya, I. P.; Sigeev, A. S.; Peregudov, A. S.; Petrovskii, P. V. *Tetrahedron Lett.* **2003,** *44,* 7039–7041. doi:10.1016/S0040-4039(03)01756-8
32. Prasad, C. D.; Balkrishna, S. J.; Kumar, A.; Bhakuni, B. S.; Shrimali, K.; Biswas, S.; Kumar, S. *J. Org. Chem.* **2013,** *78,* 1434–1443. doi:10.1021/jo302480j
33. Suzuki, H.; Matano, Y. *Organobismuth Chemistry;* Elsevier: Amsterdam, 2001.
34. Finet, J. P. *Chem. Rev.* **1989,** *89,* 1487–1501. doi:10.1021/cr00097a005
35. Elliott, G. I.; Konopelski, J. P. *Tetrahedron* **2001,** *57,* 5683–5705. doi:10.1016/S0040-4020(01)00385-4
36. Leonard, N. M.; Wieland, L. C.; Mohan, R. S. *Tetrahedron* **2002,** *58,* 8373–8397. doi:10.1016/S0040-4020(02)01000-1
37. Cho, C. S.; Yoshimori, Y.; Uemura, S. *Bull. Chem. Soc. Jpn.* **1995,** *68,* 950–957. doi:10.1246/bcsj.68.950
38. Arnauld, T.; Barton, D. H. R.; Doris, E. *Tetrahedron* **1997,** *53,* 4137–4144. doi:10.1016/S0040-4020(97)00133-6
39. Arnauld, T.; Barton, D. H. R.; Normant, J.-F.; Doris, E. *J. Org. Chem.* **1999,** *64,* 6915–6917. doi:10.1021/jo9905928
40. Ohe, T.; Tanaka, T.; Kuroda, M.; Cho, C. S.; Ohe, K.; Uemura, S. *Bull. Chem. Soc. Jpn.* **1999,** *72,* 1851–1855. doi:10.1246/bcsj.72.1851
41. Ikegai, K.; Mukaiyama, T. *Chem. Lett.* **2005,** *34,* 1496–1497. doi:10.1246/cl.2005.1496
42. Moiseev, D. V.; Malysheva, Y. B.; Shavyrin, A. S.; Kurskii, Y. A.; Gushchin, A. V. *J. Organomet. Chem.* **2005,** *690,* 3652–3663. doi:10.1016/j.jorganchem.2005.04.051
43. Finet, J.-P.; Fedorov, A. Y. *J. Organomet. Chem.* **2006,** *691,* 2386–2393. doi:10.1016/j.jorganchem.2006.01.022
44. Gagnon, A.; St-Onge, M.; Little, K.; Duplessis, M.; Barabé, F. *J. Am. Chem. Soc.* **2007,** *129,* 44–45. doi:10.1021/ja0676758
45. Ikegai, K.; Fukumoto, K.; Mukaiyama, T. *Chem. Lett.* **2006,** *35,* 612–613. doi:10.1246/cl.2006.612
46. Rao, M. L. N.; Venkatesh, V.; Banerjee, D. *Tetrahedron* **2007,** *63,* 12917–12926. doi:10.1016/j.tet.2007.10.047
47. Gagnon, A.; Duplessis, M.; Alsabeh, P.; Barabé, F. *J. Org. Chem.* **2008,** *73,* 3604–3607. doi:10.1021/jo702377h
48. Rao, M. L. N.; Jadhav, D. N.; Banerjee, D. *Tetrahedron* **2008,** *64,* 5762–5772. doi:10.1016/j.tet.2008.04.011
49. Rahman, A. F. M. M.; Murafuji, T.; Ishibashi, M.; Miyoshi, Y.; Sugihara, Y. *J. Organomet. Chem.* **2004,** *689,* 3395–3401. doi:10.1016/j.jorganchem.2004.07.055
50. Chaudhari, K. R.; Wadawale, A. P.; Jain, V. K. *J. Organomet. Chem.* **2012,** *698,* 15–21. doi:10.1016/j.jorganchem.2011.09.024
51. Barton, D. H. R.; Ozbalik, N.; Ramesh, M. *Tetrahedron* **1988,** *44,* 5661–5668. doi:10.1016/S0040-4020(01)81427-7
52. Rao, M. L. N.; Dasgupta, P. *Tetrahedron Lett.* **2012,** *53,* 162–165. doi:10.1016/j.tetlet.2011.10.156
53. Rao, M. L. N.; Awasthi, D. K.; Talode, J. B. *Tetrahedron Lett.* **2012,** *53,* 2662–2666. doi:10.1016/j.tetlet.2012.03.059
54. Kopinke, F. D.; Zimmermann, G.; Anders, K. *J. Org. Chem.* **1989,** *54,* 3571–3576. doi:10.1021/jo00276a014
55. Hey, D. H.; Shingleton, D. A.; Williams, G. H. *J. Chem. Soc.* **1963,** 5612–5619. doi:10.1039/jr9630005612
56. Yamago, S.; Kayahara, E.; Kotani, M.; Ray, B.; Kwak, Y.; Goto, A.; Fukuda, T. *Angew. Chem., Int. Ed.* **2007,** *46,* 1304–1306. doi:10.1002/anie.200604473
57. Perkins, M. J.; Turner, E. S. *J. Chem. Soc., Chem. Commun.* **1981,** 139–140. doi:10.1039/C39810000139
58. Russell, G. A.; Tashtoush, H. *J. Am. Chem. Soc.* **1983,** *105,* 1398–1399. doi:10.1021/ja00343a069
59. Russell, G. A.; Ngoviwatchai, P.; Tashtoush, H. I.; Pla-Dalmau, A.; Khanna, R. K. *J. Am. Chem. Soc.* **1988,** *110,* 3530–3538. doi:10.1021/ja00219a030
60. Ogawa, A.; Tanaka, H.; Yokoyama, H.; Obayashi, R.; Yokoyama, K.; Sonoda, N. *J. Org. Chem.* **1992,** *57,* 111–115. doi:10.1021/jo00027a021
61. Ogawa, A.; Obayashi, R.; Ine, H.; Tsuboi, Y.; Sonoda, N.; Hirao, T. *J. Org. Chem.* **1998,** *63,* 881–884. doi:10.1021/jo971652h
62. Kawaguchi, S.-i.; Shirai, T.; Ohe, T.; Nomoto, A.; Sonoda, M.; Ogawa, A. *J. Org. Chem.* **2009,** *74,* 1751–1754. doi:10.1021/jo8020067
63. Kawaguchi, S.-i.; Ogawa, A. *J. Synth. Org. Chem., Jpn.* **2010,** *68,* 705–717. doi:10.5059/yukigoseikyokaishi.68.705
64. Kawaguchi, S.-i.; Ohe, T.; Shirai, T.; Nomoto, A.; Sonoda, M.; Ogawa, A. *Organometallics* **2010,** *29,* 312–316. doi:10.1021/om9008982
65. Arnauld, T.; Barton, D. H. R.; Normant, J.-F. *J. Org. Chem.* **1999,** *64,* 3722–3725. doi:10.1021/jo982093x
66. Ogawa, A.; Obayashi, R.; Doi, M.; Sonoda, N.; Hirao, T. *J. Org. Chem.* **1998,** *63,* 4277–4281. doi:10.1021/jo972253p
67. Reich, H. J.; Renga, J. M.; Reich, I. L. *J. Am. Chem. Soc.* **1975,** *97,* 5434–5447. doi:10.1021/ja00852a019
68. Barton, D. H. R.; Bhatnagar, N. Y.; Finet, J. P.; Motherwell, W. B. *Tetrahedron* **1986,** *42,* 3111–3122. doi:10.1016/S0040-4020(01)87378-6

License and Terms

Beilstein Journal of Organic Chemistry

Cascade radical reaction of substrates with a carbon–carbon triple bond as a radical acceptor

Hideto Miyabe[*1,2], Ryuta Asada[2] and Yoshiji Takemoto[*2]

Full Research Paper

Open Access

Address:
[1]School of Pharmacy, Hyogo University of Health Sciences, Minatojima, Chuo-ku, Kobe 650-8530, Japan and [2]Graduate School of Pharmaceutical Sciences, Kyoto University, Yoshida, Sakyo-ku, Kyoto 606-8501, Japan

Email:
Hideto Miyabe[*] - miyabe@huhs.ac.jp; Yoshiji Takemoto[*] - takemoto@pharm.kyoto-u.ac.jp

* Corresponding author

Keywords:
cascade; cyclization; enantioselective; free radical; Lewis acid; radical

Beilstein J. Org. Chem. **2013,** *9,* 1148–1155.
doi:10.3762/bjoc.9.128

Received: 08 April 2013
Accepted: 22 May 2013
Published: 13 June 2013

This article is part of the Thematic Series "Organic free radical chemistry".

Guest Editor: C. Stephenson

Abstract

The limitation of hydroxamate ester as a chiral Lewis acid coordination moiety was first shown in an intermolecular reaction involving a radical addition and sequential allylation processes. Next, the effect of hydroxamate ester was studied in the cascade addition–cyclization–trapping reaction of substrates with a carbon–carbon triple bond as a radical acceptor. When substrates with a methacryloyl moiety and a carbon–carbon triple bond as two polarity-different radical acceptors were employed, the cascade reaction proceeded effectively. A high level of enantioselectivity was also obtained by a proper combination of chiral Lewis acid and these substrates.

Introduction

Strategies involving a cascade process offer the advantage of multiple carbon–carbon and/or carbon–heteroatom bond formations in a single operation. Radical chemistry has been developed as one of the most powerful tools for carbon–carbon bond formation in organic synthesis [1-20]. Particularly, the advantages for utilizing the radical methodologies are the high functional group tolerance and the mild reaction conditions, because radical intermediates are not charged species. Therefore, a number of extensive investigations into sequential radical reactions have been reported over the past fifteen years and significant progress has been made in recent years [21-36]. We have also directed our efforts toward the development of new and efficient cascade approaches for the construction of carbon–carbon/heteroatom bonds based on radical chemistry. These approaches can be classified into two categories according to their reaction mechanism (Figure 1) [37-43].

Enantioselective radical reactions have been intensively studied over the past fifteen years. Compared with stereocontrol studies on intermolecular radical reactions, the enantioselective stereocontrol in radical cyclizations still remains a major challenge [44-68]. We have also investigated a new type of chiral Lewis

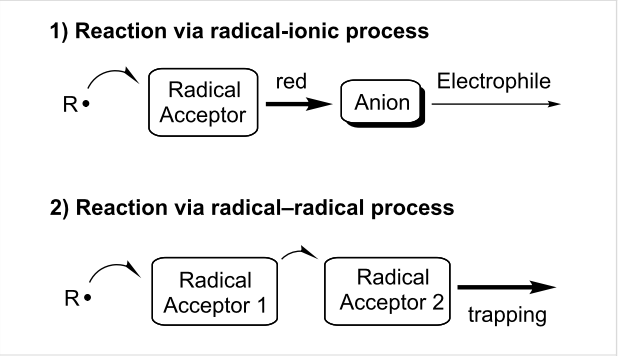

Figure 1: Cascade bond formation based on radical reactions.

acid mediated cyclization approach for cascade bond-forming reactions via sequential radical–radical processes (Figure 2) [39-43]. In these studies, the control of the enantioselectivities was achieved by the introduction of a hydroxamate ester as a two-point-binding coordination tether into the middle of substrates **A**, together with the control of the rotamer population of substrates [39,42]. In this paper, we describe in detail the cascade addition–cyclization–trapping reaction of substrates with a carbon–carbon triple bond as a radical acceptor as well as the effect of hydroxamate ester as a Lewis acid coordination moiety. Some results have been reported in our preliminary communication [39].

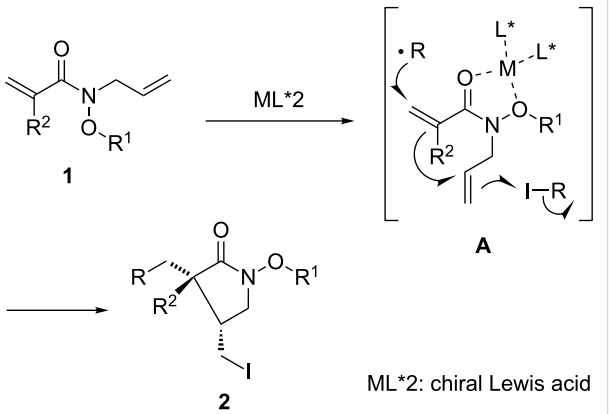

Figure 2: Our method for controlling the geometry of substrates and the stereochemistry of cyclization.

Results and Discussion

Renaud's group showed in 2002 that hydroxamic acid derivatives are useful achiral templates in enantioselective Diels–Alder reactions [69,70]. To study the effect of hydroxamate ester as an achiral template in the intermolecular radical reaction, our experiments began with the investigation of cascade radical addition–allylation of hydroxamate esters **3A**–**C** having an acryloyl moiety (Scheme 1). The reactions were evaluated in CH_2Cl_2 at −78 °C by employing isopropyl iodide, allyltin reagent, and Et_3B as a radical initiator. The enantiomeric purities of products were checked by chiral HPLC analysis. The effect of the substituents R^1 and R^2 of hydroxamate esters **3A**–**C** on yield and selectivity was evaluated in the presence of a chiral Lewis acid prepared from box ligand **L1** and $Zn(OTf)_2$. The results are shown in Scheme 1. Although good enantioselectivities were not observed, the size of the substituents had an impact on enantioselectivity with the larger group leading to lower ee. These observations indicate that the formation of the rigid ternary complex of hydroxamate ester, $Zn(OTf)_2$ and the ligand **L1** is required for enantioselective transformation. A similar trend was observed in our studies on the addition–cyclization–trapping reaction of hydroxamate esters [39,42]. The chiral Lewis acid promoted the reaction of substrate **3A** having a bulky 2-naphthylmethyl group as substituent R^2 to form the product **4A** in 40% yield with 7% ee. Moderate enantioselectivity was observed by employing the substrate **3B** having a benzyl group as R^1 and a methyl group as R^2. Particularly, the steric factor of the fluxional substituent R^1 affected not only enantioselectivity but also the chemical efficiency. The use of **3C** having a 2-naphthylmethyl group as R^1 led to a decrease in the chemical yield, probably because of the steric repulsion by a bulky substituent R^1 leading to the dissociation of the chiral Lewis acid. In these studies, the absolute configuration at newly generated stereocenters has been not determined.

We recently reported in detail the cascade addition–cyclization–trapping reaction of substrates with

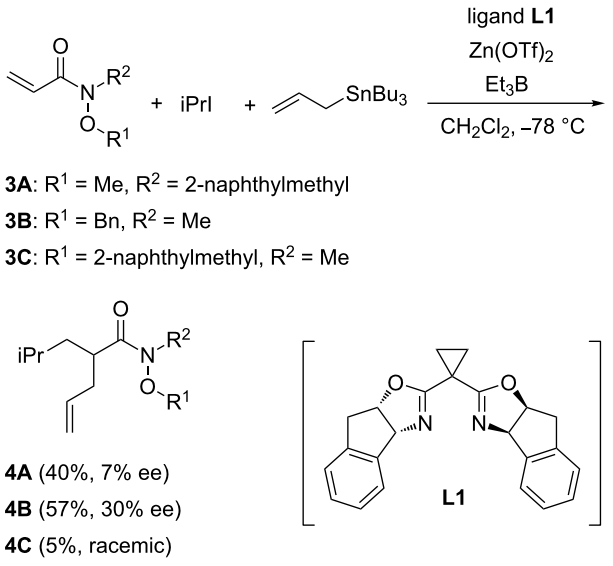

Scheme 1: Effect of hydroxamate ester on intermolecular C–C bond-forming reactions.

carbon–carbon double bonds as two kinds of polarity-different radical acceptors [42]. On the basis of these results, the possibility of the carbon–carbon triple bond as a radical acceptor and the hydroxamate ester functionality as a two-point-binding coordination tether was next studied in detail. To understand the scope and limitation of the cascade transformation of hydroxamate esters with carbon–carbon triple bonds, the substrates of choice were **5**, **6A**–**C**, **7** and **8** having hydroxamate ester functionality (Figure 3).

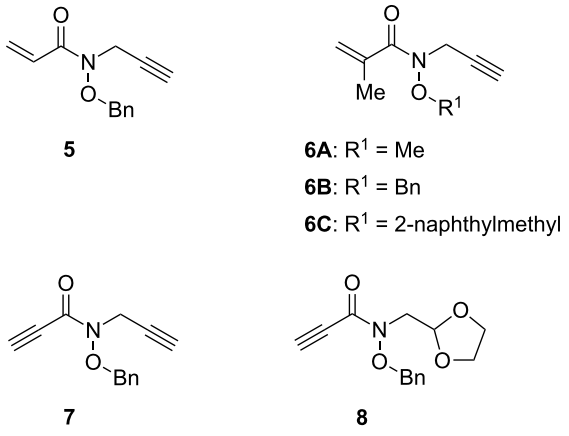

Figure 3: Substrates for testing the cascade transformation.

At first, we studied the cascade reaction of **5** with an acryloyl moiety and **6A**–**C** with a methacryloyl moiety as an electron-deficient acceptor in the absence of a chiral ligand (Scheme 2). To control the rotamer population of substrates, $Zn(OTf)_2$ was used as a Lewis acid to coordinate the hydroxamate ester functionality. The reactions were evaluated in CH_2Cl_2 at 20 °C under the tin-free iodine atom transfer conditions by using isopropyl iodide and Et_3B. The reaction of hydroxamate ester **5** did not give the desired product probably due to polymerization of **5** through the labile acrylamide moiety. In contrast, the reaction of **6A**–**C** proceeded effectively to give the cyclic products **9Aa**–**9Ca** in good yields. Among them, hydroxamate esters **6A** and **6B**, which have a small methyl or benzyl group as R^1, have shown a high reactivity, although a 76% yield of product **9Ca** was obtained even when hydroxamate ester **6C** having a 2-naphthylmethyl group was used. Furthermore, the regiochemical course of the initial radical addition to **6A**–**C** was well controlled. The nucleophilic isopropyl radical reacted selectively with the electron-deficient methacryloyl moiety to give the single isomers **9Aa**–**9Ca**.

It is also important to note that *Z*-isomers **9Aa**–**9Ca** were selectively obtained without the formation of corresponding *E*-isomers. The *E*,*Z*-selectivities are determined by capturing the intermediate vinyl radicals with an atom-transfer reagent

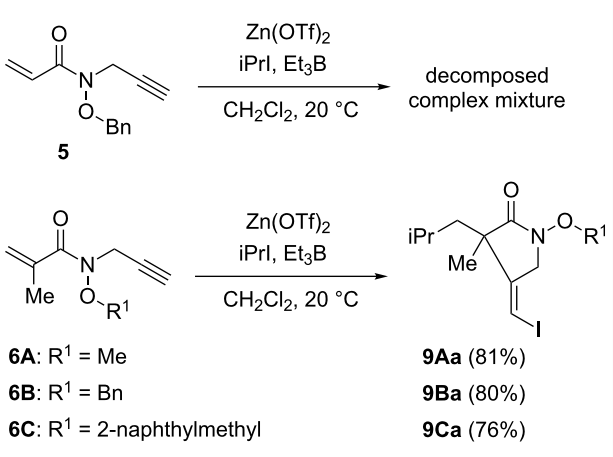

Scheme 2: Cascade radical addition–cyclization–trapping reaction of **5** and **6A**–**C**.

such as isopropyl iodide (Figure 4). These selectivities are controlled by the steric factor around vinyl radicals. The vinyl radicals are σ-radicals in a very fast equilibrium between *E*-isomer **B** and *Z*-isomer **C**. The steric hindrance between the substituents on the α-carbon atom of radical **C** and isopropyl iodide is assumed to lead to selective iodine atom-transfer in radical **B** giving **9Aa**–**9Ca** as single *Z*-isomers.

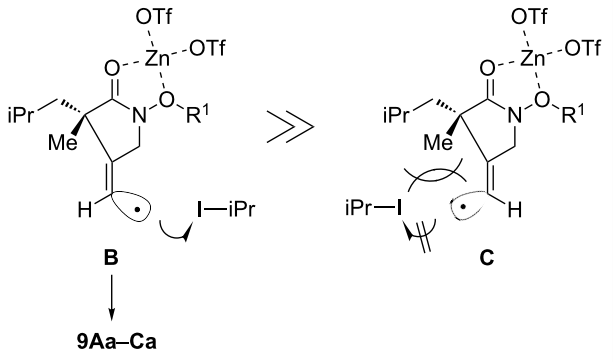

Figure 4: *E*/*Z*-selectivity of **9Aa**–**Ca**.

On the basis of the above results, we next studied the reaction of **6A**–**C** at −78 °C in the presence of $Zn(OTf)_2$ and chiral box ligands **L1**–**L3** (Scheme 3 and Table 1). A stoichiometric amount of chiral Lewis acid prepared from $Zn(OTf)_2$ and ligand **L1** accelerated the reaction of hydroxamate ester **6A** having a methyl group as substituent R^1 (Table 1, entry 1), although the reaction of **6A** did not proceed effectively at −78 °C in the absence of box ligand **L1**. The desired product **9Aa** was isolated as a single isomer in 51% yield with 60% ee after being stirred for 10 h. The use of hydroxamate ester **6B** having a benzyl group led to not only an enhancement in chemical yield but also to an improvement in enantioselectivity to give the pro-

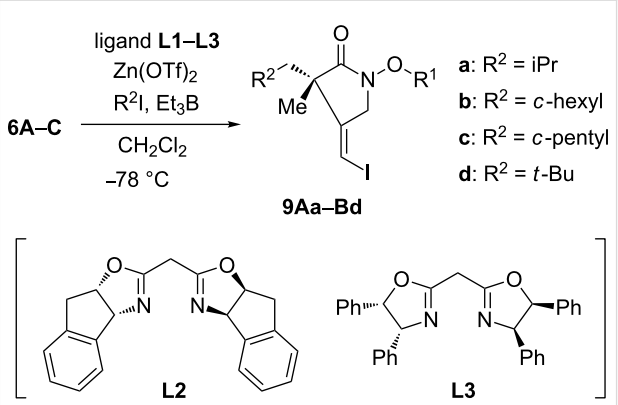

Scheme 3: Enantioselective cascade reaction of **6A**–**C**.

duct **9Ba** in 87% yield with 80% ee (Table 1, entry 2). Next, the catalytic nature of the reactions was examined (Table 1, entries 3–5). The reactions proceeded equally well with 50 and 30 mol % of chiral Lewis acid as with a stoichiometric amount (Table 1, entry 3 and 4). Further reduction of the chiral Lewis acid load to 10 mol % resulted in a decrease of both the chemical yield and enantioselectivity (Table 1, entry 5). In the case of 10 mol % of the chiral Lewis acid, the ternary complex of the ligand, the Lewis acid and the substrate were not effectively formed, and the background reaction giving the racemic product proceeded. Additionally, the high *Z*-selectivity of product **9Ba** indicates that the stereoselective iodine-atom transfer from isopropyl iodide to an intermediate radical proceeded effectively under these catalytic reaction conditions. The reaction using box ligand **L2** instead of **L1** attenuated the enantioselectivity (Table 1, entry 6). A somewhat lower enantioselectivity was obtained by using ligand **L3**, surprisingly resulting in antipode product **9Ba** (Table 1, entry 7). The representative effect of the solvent is shown in Table 1, entries 8–10. No reaction occurred in toluene, owing to the low solubility of the chiral Lewis acid in toluene (Table 1, entry 8). When the reaction was carried out in toluene/CH_2Cl_2 (4:1, v/v), the cyclic product **9Ba** was obtained in 67% yield with 77% ee (Table 1, entry 9). The reaction in the protic solvent MeOH gave the nearly racemic product, although the high *Z*-selectivity was maintained (Table 1, entry 10). These results suggest that the rigid chelation of the chiral Lewis acid to the hydroxamate ester functionality occured in CH_2Cl_2. In the presence of chiral Lewis acid, hydroxamate ester **6C** had also shown good reactivity, although the enantioselectivity diminished to 75% ee (Table 1, entry 11). We next studied the reaction of substrate **6B** with other radical precursors (Table 1, entries 12–14). Reactions with cyclohexyl and cyclopentyl radicals were also facile. Under analogous reaction conditions, an outstanding level of enantioselectivity was observed on employing the bulky *tert*-butyl iodide as a radical precursor (Table 1, entry 14). A good yield of the product **9Bd** was obtained with 92% ee and high *Z*-selectivity.

The absolute configuration at the newly generated stereocenters of **9Aa**–**Bd** was assumed by similarity between the present reaction and the previously reported reaction of substrates having the carbon–carbon double bond [39,42]. In these reactions, a ternary complex of ligand, Lewis acid and substrate would control the three-dimensional arrangement of two radical acceptors. A tetrahedral or *cis*-octahedral geometry around the zinc center was proposed [71,72]. In Figure 5, a tentative model

Table 1: Reaction of **6A**–**C** in the presence of chiral ligand.

entry	substrate	R^2	ligand	Lewis acid (equiv)	product (% yield)	*Z*/*E*	ee (%)
1	**6A**	iPr	**L1**	1.0	**9Aa** (51)	>98:2	60
2 [39]	**6B**	iPr	**L1**	1.0	**9Ba** (87)	>98:2	80
3 [39]	**6B**	iPr	**L1**	0.5	**9Ba** (85)	>98:2	81
4 [39]	**6B**	iPr	**L1**	0.3	**9Ba** (82)	>98:2	81
5 [39]	**6B**	iPr	**L1**	0.1	**9Ba** (49)[a]	>98:2	47
6	**6B**	iPr	**L2**	1.0	**9Ba** (76)	>98:2	71
7	**6B**	iPr	**L3**	1.0	**9Ba** (81)	>98:2	–69
8[b]	**6B**	iPr	**L1**	1.0	no reaction		
9[c]	**6B**	iPr	**L1**	1.0	**9Ba** (67)	>98:2	77
10[d]	**6B**	iPr	**L1**	1.0	**9Ba** (63)	>98:2	rac
11	**6C**	iPr	**L1**	1.0	**9Ca** (83)	>98:2	75
12 [39]	**6B**	*c*-Hex	**L1**	1.0	**9Bb** (82)	>98:2	81
13	**6B**	*c*-Pent	**L1**	1.0	**9Bc** (83)	>98:2	79
14 [39]	**6B**	*t*-Bu	**L1**	1.0	**9Bd** (85)	>98:2	92

[a]starting substrate **6B** was recovered in 29% yield; [b]in toluene; [c]in toluene/CH_2Cl_2 (4:1, v/v); [d]in MeOH.

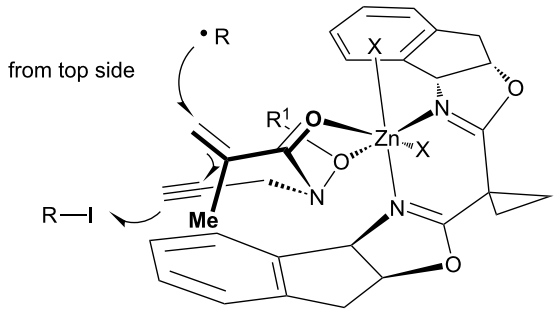

Figure 5: Model for the enantioselective reaction.

of an octahedral complex is shown, in which two oxygen atoms of the hydroxamate ester functionality occupy two equatorial positions.

To study the effect of an electron-deficient acceptor on the cascade process, the reactions of propiolic acid derivatives **7** and **8** were tested (Scheme 4). At first, the reaction of **7** was evaluated under asymmetric reaction conditions. However, the cascade addition–cyclization–trapping reaction did not proceed, and the simple adduct **10** was formed in 57% yield by the addition–trapping process. Next, the reaction of propiolic acid derivative **8** was tested, because we expected the [1,5]-hydrogen shift from 1,3-dioxolane ring into the reactive vinyl radical as shown as **D**. However, the simple adduct **11** was only obtained in 78% yield. The results from these studies show that a carbon–carbon double bond, e.g., a methacryloyl group, of the electron-deficient acceptor is essential for the successful cascade transformation.

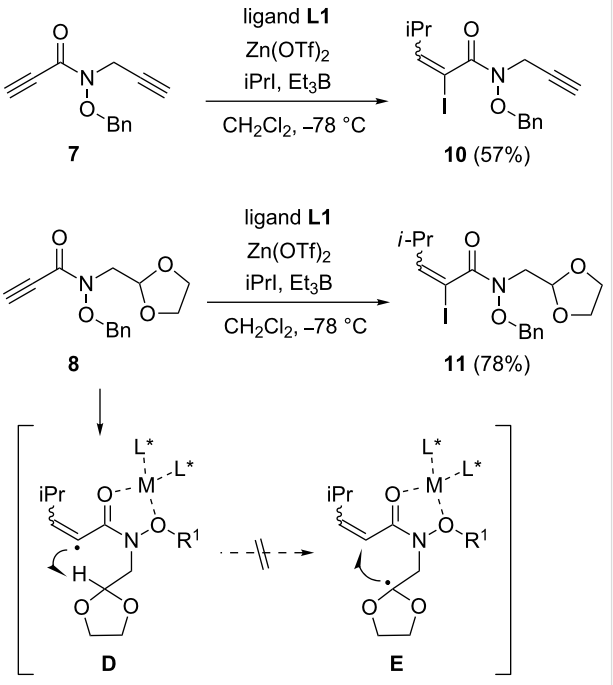

Scheme 4: Reaction of propiolic acid derivatives **7** and **8**.

To gain further insight into the stereocontrol in the cyclization step, we next studied the opposite regiochemical cyclization by using the substrate **12** via the intermediate radical **F** (Scheme 5). The reaction was carried out in the presence of Bu_3SnH under asymmetric reaction conditions. Although the reaction proceeded even at −78 °C, the nearly racemic product **13** was isolated in 60% yield. This observation indicates that the regiochemical course of the cyclization step is an important factor to achieve the highly asymmetric induction.

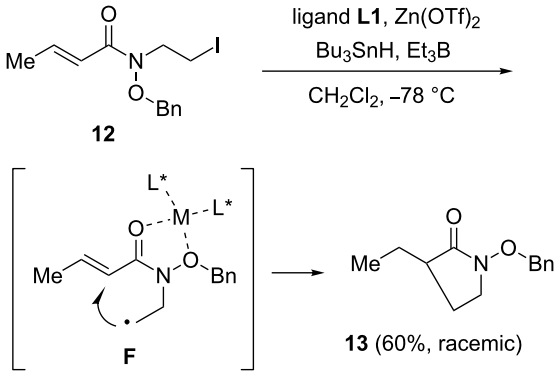

Scheme 5: Opposite regiochemical cyclization using substrate **12**.

We next investigated the reactivity of internal alkynes as electron-rich acceptors (Scheme 6). The internal alkyne **14** has shown a good reactivity comparable to that of the terminal alkynes **6A–C**. In the absence of a chiral ligand, the zinc Lewis acid accelerated the reaction of alkyne **14** with an isopropyl radical at 20 °C to give the desired cyclic product **15a** in 73% yield. Under analogous reaction conditions, both cyclohexyl iodide and cyclopentyl iodide worked well to give **15b** and **15c**

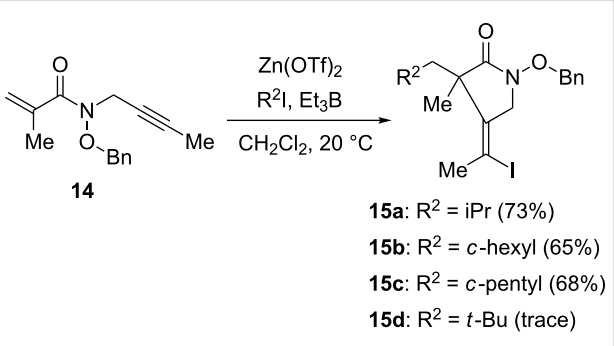

Scheme 6: Cascade reaction of **14**.

in 65% and 68% yields, respectively. However, the reaction with a bulky *tert*-butyl radical did not proceed effectively, probably due to side reactions such as polymerization.

We finally investigated the enantioselective reaction of internal alkynes **14** and **16** (Scheme 7). The reaction of **14** proceeded with good enantioselectivities (Table 2). When a stoichiometric amount of chiral Lewis acid was employed, the reaction with an isopropyl radical gave the desired product **15a** in 86% yield with 83% ee (Table 2, entry 1). The reaction proceeded equally well with 30 mol % of chiral Lewis acid as with a stoichiometric amount (Table 2, entry 2). The secondary radicals, generated from cyclohexyl iodide or cyclopentyl iodide, reacted well to afford **15b** and **15c** with 85% ee and 83% ee, respectively (Table 2, entry 3 and 4). In marked contrast to the reaction in the absence of a chiral ligand (Scheme 6), the use of bulky *tert*-butyl iodide led to not only an enhancement in chemical yield but also to an improvement in enantioselectivity (Table 2, entry 5). These observations indicate that the combination of chiral Lewis acid and hydroxamate ester functionality led the rigid complex promoting the cyclization step and suppressing the background reaction or the undesired side reactions. High chemical yield and enantioselectivity were observed with 50 mol % of chiral Lewis acid (Table 2, entry 6), although further reduction of the catalyst load to 30 mol % resulted in a decrease of yield and enantioselectivity (Table 2, entry 7). Both chemical yield and enantioselectivity decreased by changing Lewis acid from $Zn(OTf)_2$ to MgI_2 (Table 2, entry 8). When the more nucleophilic and stable *tert*-butyl radical was employed, the reaction of substrate **16** having a phenyl group at the terminal position proceeded smoothly to give the desired product **17** in 89% yield with 67% ee (Table 2, entry 9). It is also important to note that the high *Z*/*E*-selectivity of products was observed even when internal alkynes **14** and **16** were employed. These results indicate that the iodine atom-transfer from R^2I to the substituted vinyl radicals proceeded stereoselectively.

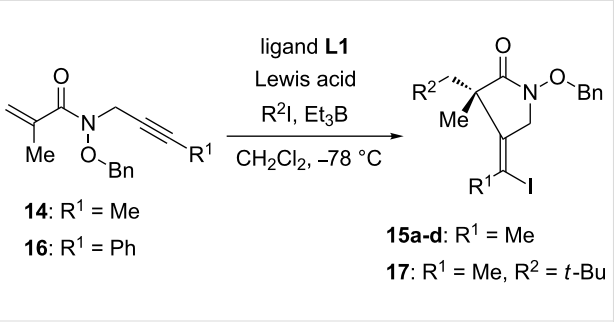

Scheme 7: Enantioselective cascade reaction of **14** and **16**.

Particularly, the substrate **16** having a phenyl group gave the intermediate linear π-radical. Thus, the capture of linear vinyl radical with atom-transfer reagent would be influenced by the steric hindrance around the quaternary carbon atom [43].

Conclusion

We have shown the cascade radical addition–cyclization–trapping reaction of substrates with a carbon–carbon triple bond as a radical acceptor as well as the scope and limitation of hydroxamate ester as a coordination site with a chiral Lewis acid. Synthetic strategies involving enantioselective radical cyclizations would be desirable tools for preparing functionalized cyclic compounds with multiple stereocenters. These studies offer opportunities for further exploration of fascinating possibilities in the realm of cascade radical reactions.

Supporting Information

Supporting Information File 1

General experimental procedures, characterization data of obtained compounds, and preparation of substrates.
[http://www.beilstein-journals.org/bjoc/content/supplementary/1860-5397-9-128-S1.pdf]

Table 2: Reaction of **14** and **16** in the presence of a chiral ligand.

entry	substrate	R^2	Lewis acid (equiv)	yield (%)	ratio	ee (%)
1 [39]	**14**	iPr	$Zn(OTf)_2$ (1.0)	86	>98:2	83
2 [39]	**14**	iPr	$Zn(OTf)_2$ (0.3)	74	>98:2	81
3 [39]	**14**	*c*-Hex	$Zn(OTf)_2$ (1.0)	87	>98:2	85
4	**14**	*c*-Pent	$Zn(OTf)_2$ (1.0)	77	>98:2	83
5 [39]	**14**	*t*-Bu	$Zn(OTf)_2$ (1.0)	94	>98:2	90
6	**14**	*t*-Bu	$Zn(OTf)_2$ (0.5)	94	>98:2	91
7	**14**	*t*-Bu	$Zn(OTf)_2$ (0.3)	75	>98:2	61
8	**14**	*t*-Bu	MgI_2 (1.0)	20	>98:2	54
9	**16**	*t*-Bu	$Zn(OTf)_2$ (1.0)	89	>98:2	67

Acknowledgements

This work was supported in part by a Grant-in-Aid for Scientific Research (C) (H.M.) from the Ministry of Education, Culture, Sports, Science and Technology of Japan.

References

1. Smadja, W. *Synlett* **1994,** 1–26. doi:10.1055/s-1994-22728
2. Fallis, A. G.; Brinza, I. M. *Tetrahedron* **1997,** *53,* 17543–17594. doi:10.1016/S0040-4020(97)10060-6
3. Renaud, P.; Gerster, M. *Angew. Chem., Int. Ed.* **1998,** *37,* 2562–2579. doi:10.1002/(SICI)1521-3773(19981016)37:19<2562::AID-ANIE2562>3.0.CO;2-D
4. Sibi, M. P.; Porter, N. A. *Acc. Chem. Res.* **1999,** *32,* 163–171. doi:10.1021/ar9600547
5. Naito, T. *Heterocycles* **1999,** *50,* 505–541. doi:10.3987/REV-98-SR(H)2
6. Renaud, P.; Sibi, M. P., Eds. *Radicals in Organic Synthesis;* Wiley-VCH: Weinheim, Germany, 2001; Vol. 1 and 2.
7. Bar, G.; Parsons, A. F. *Chem. Soc. Rev.* **2003,** *32,* 251–263. doi:10.1039/b111414j
8. Sibi, M. P.; Manyem, S.; Zimmerman, J. *Chem. Rev.* **2003,** *103,* 3263–3296. doi:10.1021/cr020044l
9. Srikanth, G. S. C.; Castle, S. L. *Tetrahedron* **2005,** *61,* 10377–10441. doi:10.1016/j.tet.2005.07.077
10. Guo, H.-C.; Ma, J.-A. *Angew. Chem., Int. Ed.* **2006,** *45,* 354–366. doi:10.1002/anie.200500195
11. Zimmerman, J.; Sibi, M. P. *Top. Curr. Chem.* **2006,** *263,* 107–162. doi:10.1007/128_027
12. Godineau, E.; Landais, Y. *Chem.–Eur. J.* **2009,** *15,* 3044–3055. doi:10.1002/chem.200802415
13. Rowlands, G. J. *Tetrahedron* **2009,** *65,* 8603–8655. doi:10.1016/j.tet.2009.07.001
14. Rowlands, G. J. *Tetrahedron* **2010,** *66,* 1593–1636. doi:10.1016/j.tet.2009.12.023
15. Perchyonok, V. T. Radical Reactions in Aqueous Media. In *RSC Green Chemistry,* No. 6, RSC Publishing: Cambridge, 2010.
16. Narayanam, J. M. R.; Stephenson, C. R. J. *Chem. Soc. Rev.* **2011,** *40,* 102–113. doi:10.1039/b913880n
17. Yang, Y.-H.; Sibi, P. Stereoselective Radical Reactions. In *Encyclopedia of Radicals in Chemistry, Biology and Materials;* Chatgilialoglu, C.; Studer, A., Eds.; Wiley: Weinheim, Germany, 2012; Vol. 2, pp 655–692. doi:10.1002/9781119953678.rad019
18. Ischay, M. A.; Yoon, T. P. *Eur. J. Org. Chem.* **2012,** 3359–3372. doi:10.1002/ejoc.201101071
19. Shi, L.; Xia, W. *Chem. Soc. Rev.* **2012,** *41,* 7687–7697. doi:10.1039/c2cs35203f
20. Tucker, J. W.; Stephenson, C. R. J. *J. Org. Chem.* **2012,** *77,* 1617–1622. doi:10.1021/jo202538x
21. Nozaki, K.; Oshima, K.; Utimoto, K. *Tetrahedron Lett.* **1988,** *29,* 1041–1044. doi:10.1016/0040-4039(88)85330-9
22. Curran, D. P.; Chen, M. H.; Spletzer, E.; Seong, C. M.; Chang, C. T. *J. Am. Chem. Soc.* **1989,** *111,* 8872–8878. doi:10.1021/ja00206a016
23. Giese, B.; Zehnder, M.; Roth, M.; Zeitz, H.-G. *J. Am. Chem. Soc.* **1990,** *112,* 6741–6742. doi:10.1021/ja00174a061
24. Porter, N. A.; Rosenstein, I. J.; Breyer, R. A.; Bruhnke, J. D.; Wu, W. X.; McPhail, A. T. *J. Am. Chem. Soc.* **1992,** *114,* 7664–7676. doi:10.1021/ja00046a010
25. Marco-Contelles, J. *Chem. Commun.* **1996,** 2629–2630. doi:10.1039/cc9960002629
26. Takai, K.; Matsukawa, N.; Takahashi, A.; Fujii, T. *Angew. Chem., Int. Ed.* **1998,** *37,* 152–155. doi:10.1002/(SICI)1521-3773(19980202)37:1/2<152::AID-ANIE152>3.3.CO;2-#
27. Miyabe, H.; Fujii, K.; Goto, T.; Naito, T. *Org. Lett.* **2000,** *2,* 4071–4074. doi:10.1021/ol006716g
28. Sibi, M. P.; Chen, J. *J. Am. Chem. Soc.* **2001,** *123,* 9472–9473. doi:10.1021/ja016633a
29. Dhimane, A.-L.; Aïssa, C.; Malacria, M. *Angew. Chem., Int. Ed.* **2002,** *41,* 3284–3287. doi:10.1002/1521-3773(20020902)41:17<3284::AID-ANIE3284>3.0.CO;2-Z
30. Yamago, S.; Miyoshi, M.; Miyazoe, H.; Yoshida, J. *Angew. Chem., Int. Ed.* **2002,** *41,* 1407–1409. doi:10.1002/1521-3773(20020415)41:8<1407::AID-ANIE1407>3.0.CO;2-Z
31. Bazin, S.; Feray, L.; Siri, D.; Naubron, J.-V.; Bertrand, M. P. *Chem. Commun.* **2002,** 2506–2507. doi:10.1039/b206695e
32. Tsuchii, K.; Doi, M.; Hirao, T.; Ogawa, A. *Angew. Chem., Int. Ed.* **2003,** *42,* 3490–3493. doi:10.1002/anie.200250790
33. Denes, F.; Chemla, F.; Normant, J. F. *Angew. Chem., Int. Ed.* **2003,** *42,* 4043–4046. doi:10.1002/anie.200250474
34. Yamamoto, Y.; Nakano, S.; Maekawa, H.; Nishiguchi, I. *Org. Lett.* **2004,** *6,* 799–802. doi:10.1021/ol036506e
35. Uenoyama, Y.; Fukuyama, T.; Nobuta, O.; Matsubara, H.; Ryu, I. *Angew. Chem., Int. Ed.* **2005,** *44,* 1075–1078. doi:10.1002/anie.200461954
36. Ueda, U.; Miyabe, H.; Sugino, H.; Miyata, O.; Naito, T. *Angew. Chem., Int. Ed.* **2005,** *44,* 6190–6193. doi:10.1002/anie.200502263
37. Miyabe, H.; Asada, R.; Yoshida, K.; Takemoto, Y. *Synlett* **2004,** 540–542. doi:10.1055/s-2004-815407
38. Miyabe, H.; Asada, R.; Takemoto, Y. *Tetrahedron* **2005,** *61,* 385–393. doi:10.1016/j.tet.2004.10.104
39. Miyabe, H.; Asada, R.; Toyoda, A.; Takemoto, Y. *Angew. Chem., Int. Ed.* **2006,** *45,* 5863–5866. doi:10.1002/anie.200602042
40. Miyabe, H.; Toyoda, A.; Takemoto, Y. *Synlett* **2007,** 1885–1888. doi:10.1055/s-2007-984530
41. Yoshioka, E.; Kentefu; Wang, X.; Kohtani, S.; Miyabe, H. *Synlett* **2011,** 2085–2089. doi:10.1055/s-0030-1261167
42. Miyabe, H.; Asada, R.; Takemoto, Y. *Org. Biomol. Chem.* **2012,** *10,* 3519–3530. doi:10.1039/c2ob25073j
43. Yoshioka, E.; Kohtani, S.; Sawai, K.; Kentefu; Tanaka, E.; Miyabe, H. *J. Org. Chem.* **2012,** *77,* 8588–8604. doi:10.1021/jo3015227
44. Nishida, M.; Hayashi, H.; Nishida, A.; Kawahara, N. *Chem. Commun.* **1996,** 579–580. doi:10.1039/cc9960000579
45. Hiroi, K.; Ishii, M. *Tetrahedron Lett.* **2000,** *41,* 7071–7074. doi:10.1016/S0040-4039(00)01213-2
46. Yang, D.; Gu, S.; Yan, Y.-L.; Zhu, N.-Y.; Cheung, K.-K. *J. Am. Chem. Soc.* **2001,** *123,* 8612–8613. doi:10.1021/ja016383y
47. Yang, D.; Gu, S.; Yan, Y.-L.; Zhao, H.-W.; Zhu, N.-Y. *Angew. Chem., Int. Ed.* **2002,** *41,* 3014–3017. doi:10.1002/1521-3773(20020816)41:16<3014::AID-ANIE3014>3.0.CO;2-J
48. Yang, D.; Zheng, B.-F.; Gao, Q.; Gu, S.; Zhu, N.-Y. *Angew. Chem., Int. Ed.* **2006,** *45,* 255–258. doi:10.1002/anie.200503056
49. Aechtner, T.; Dressel, M.; Bach, T. *Angew. Chem., Int. Ed.* **2004,** *43,* 5849–5851. doi:10.1002/anie.200461222

50. Bauer, A.; Westkämper, F.; Grimme, S.; Bach, T. *Nature* **2005,** *436,* 1139–1140. doi:10.1038/nature03955
51. Breitenlechner, S.; Bach, T. *Angew. Chem., Int. Ed.* **2008,** *47,* 7957–7959. doi:10.1002/anie.200802479
52. Beeson, T. D.; Mastracchio, A.; Hong, J.-B.; Ashton, K.; MacMillan, D. W. C. *Science* **2007,** *316,* 582–585.
53. Jang, H.-Y.; Hong, J.-B.; MacMillan, D. W. C. *J. Am. Chem. Soc.* **2007,** *129,* 7004–7005. doi:10.1021/ja0719428
54. Conrad, J. C.; Kong, J.; Laforteza, B. N.; MacMillan, D. W. C. *J. Am. Chem. Soc.* **2009,** *131,* 11640–11641. doi:10.1021/ja9026902
55. Jui, N. T.; Lee, E. C. Y.; MacMillan, D. W. C. *J. Am. Chem. Soc.* **2010,** *132,* 10015–10017. doi:10.1021/ja104313x
56. Rendler, S.; MacMillan, D. W. C. *J. Am. Chem. Soc.* **2010,** *132,* 5027–5029. doi:10.1021/ja100185p
57. Pham, P. V.; Ashton, K.; MacMillan, D. W. C. *Chem. Sci.* **2011,** *2,* 1470–1473. doi:10.1039/c1sc00176k
58. Jui, N. T.; Garber, J. A. O.; Finelli, F. G.; MacMillan, D. W. C. *J. Am. Chem. Soc.* **2012,** *134,* 11400–11403. doi:10.1021/ja305076b
59. Nicolaou, K. C.; Reingruber, R.; Sarlah, D.; Bräse, S. *J. Am. Chem. Soc.* **2009,** *131,* 2086–2087. doi:10.1021/ja809405c
60. Nicolaou, K. C.; Reingruber, R.; Sarlah, D.; Bräse, S. *J. Am. Chem. Soc.* **2009,** *131,* 6640. doi:10.1021/ja902816z
61. Gansäuer, A.; Shi, L.; Otte, M. *J. Am. Chem. Soc.* **2010,** *132,* 11858–11859. doi:10.1021/ja105023y
62. Gansäuer, A.; Behlendorf, M.; von Laufenberg, D.; Fleckhaus, A.; Kube, C.; Sadasivam, D. V.; Flowers, R. A., II. *Angew. Chem., Int. Ed.* **2012,** *51,* 4739–4742. doi:10.1002/anie.201200431
63. Gansäuer, A.; Klatte, M.; Brändle, G. M.; Friedrich, J. *Angew. Chem., Int. Ed.* **2012,** *51,* 8891–8894. doi:10.1002/anie.201202818
64. Streuff, J.; Feurer, M.; Bichovski, P.; Frey, G.; Gellrich, U. *Angew. Chem., Int. Ed.* **2012,** *51,* 8661–8664. doi:10.1002/anie.201204469
65. Curran, D. P.; Liu, W.; Chen, C. H.-T. *J. Am. Chem. Soc.* **1999,** *121,* 11012–11013. doi:10.1021/ja993329x
66. Nechab, M.; Campolo, D.; Maury, J.; Perfetti, P.; Vanthuyne, N.; Siri, D.; Bertrand, M. P. *J. Am. Chem. Soc.* **2010,** *132,* 14742–14744. doi:10.1021/ja106668d
67. Mondal, S.; Nechab, M.; Campolo, D.; Vanthuyne, N.; Bertrand, M. P. *Adv. Synth. Catal.* **2012,** *354,* 1987–2000. doi:10.1002/adsc.201200045
68. Mondal, S.; Nechab, M.; Vanthuyne, N.; Bertrand, M. P. *Chem. Commun.* **2012,** *48,* 2549–2551. doi:10.1039/c2cc17830c
69. Corminboeuf, O.; Renaud, P. *Org. Lett.* **2002,** *4,* 1731–1734. doi:10.1021/ol025799t
70. Corminboeuf, O.; Renaud, P. *Org. Lett.* **2002,** *4,* 1735–1738. doi:10.1021/ol0257981
71. Sibi, M. P.; Yang, Y.-H. *Synlett* **2008,** 83–88. doi:10.1055/s-2007-992386
72. Evans, D. A.; Kozlowski, M. C.; Tedrow, J. S. *Tetrahedron Lett.* **1996,** *37,* 7481–7484. doi:10.1016/0040-4039(96)01697-8

License and Terms

Beilstein Journal of Organic Chemistry

Copper-catalyzed aerobic aliphatic C–H oxygenation with hydroperoxides

Pei Chui Too, Ya Lin Tnay and Shunsuke Chiba*

Letter

Open Access

Address:
Division of Chemistry and Biological Chemistry, School of Physical and Mathematical Sciences, Nanyang Technological University, Singapore 637371, Singapore. Fax: +65-67911961; Tel: +65-65138013

Email:
Shunsuke Chiba* - shunsuke@ntu.edu.sg

* Corresponding author

Keywords:
copper; 1,4-diols; free radical; 1,5-H radical shift; hydroperoxides; molecular oxygen

Beilstein J. Org. Chem. **2013,** *9,* 1217–1225.
doi:10.3762/bjoc.9.138

Received: 15 April 2013
Accepted: 31 May 2013
Published: 25 June 2013

This article is part of the Thematic Series "Organic free radical chemistry".

Guest Editor: C. Stephenson

Abstract

We report herein Cu-catalyzed aerobic oxygenation of aliphatic C–H bonds with hydroperoxides, which proceeds by 1,5-H radical shift of putative oxygen-centered radicals (O-radicals) derived from hydroperoxides followed by trapping of the resulting carbon-centered radicals with molecular oxygen.

Introduction

Aliphatic sp^3 C–H bonds are ubiquitous components in organic molecules but rather inert towards most of the chemical reactions. It thus remains as one of the most challenging topics in organic synthesis to develop catalytic oxidative sp^3 C–H functionalization with predictable chemo- and regioselectivity [1-4]. To achieve this goal, we have recently utilized 1,5-H-radical shift [5,6] with iminyl radical species (N-radicals) generated under Cu-catalyzed aerobic reaction conditions, in which the resulting carbon-centered radicals (C-radicals) could be trapped by molecular oxygen to form new C–O bonds. For instance, the Cu-catalyzed aerobic reaction of *N*-alkylamidines afforded aminidyl radicals (N-radicals) by single-electron oxidation and deprotonation of the amidine moiety, which was followed by 1,5-H-radical shift to generate the corresponding C-radicals (Scheme 1a) [7]. The successive trapping of the resulting C-radicals with molecular O_2 forms peroxy radicals (the C–O bond formation). Reduction of peroxy radicals generates alkoxides, cyclization of which with the amidine moiety finally affords dihydrooxazoles. Similarly, it was also revealed that the sp^3 C–H oxygenation could proceed directed by the N–H ketimine moieties under Cu-catalyzed aerobic conditions via the corresponding iminyl radical species, where 1,2-diacylbenzenes and amino endoperoxides could be synthesized by C–H oxygenation of secondary and tertiary C–H bonds, respectively (Scheme 1b) [8,9].

Stimulated by these remote sp^3 C–H oxidation reactions using the nitrogen-centered radicals derived from amidines and ketimines, we became interested to utilize oxygen-centered radicals (O-radicals) for the sp^3 C–H functionalization. In this

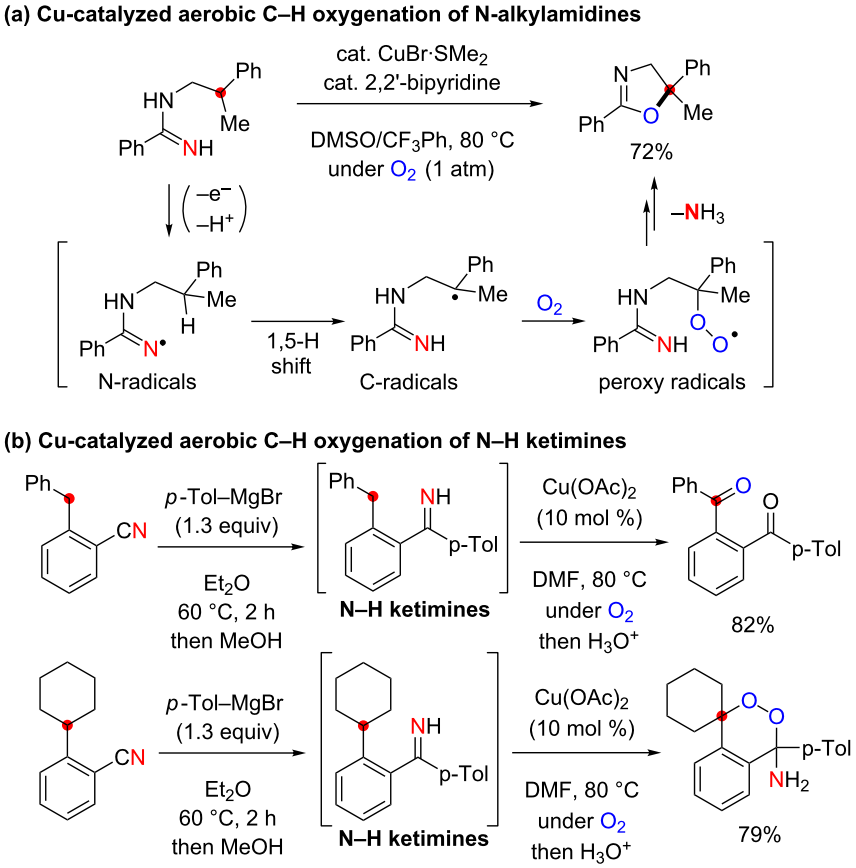

Scheme 1: Aliphatic C–H oxidation with amidines and ketimines by 1,5-H radical shift.

context, we envision employing hydroperoxides as precursors for O-radicals in the presence of Cu salts. The lower valent Cu(I) species could potentially undergo single-electron reduction of hydroperoxides to produce the corresponding O-radicals [10-13]. Ball recently reported CuCl-catalyzed aliphatic C–H chlorination using hydroperoxides as the O-radical source, in which the C-radicals generated by the 1,5-H radical shift were chlorinated (Scheme 2a) [14]. If reductive generation of the O-radicals from hydroperoxides could be achieved under an O_2 atmosphere, the C-radicals generated by 1,5-H radical shift

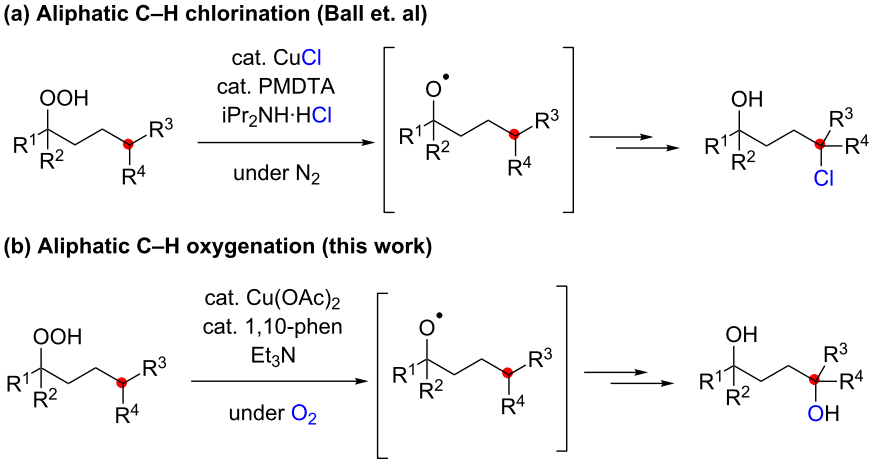

Scheme 2: Aliphatic C–H oxidation with hydroperoxides.

could be trapped by O_2 to form the new C–O bonds. Herein, we report the realization of this concept mainly for the aerobic synthesis of 1,4-diols from hydroperoxides, which could be catalyzed by the $Cu(OAc)_2$-1,10-phenanthroline system in the presence of Et_3N as a terminal reductant of the Cu(II) species (Scheme 2b).

Findings

We commenced our investigation with the Cu-catalyzed aerobic reactions of hydroperoxide **1a** in the presence of Et_3N as a terminal reductant [15] to keep lower valent Cu(I) species in the reaction mixture (Table 1). As expected, when **1a** was treated with $Cu(OAc)_2$ (20 mol %) in the presence of Et_3N (2 equiv) in DMF, the reaction proceeded at room temperature for 17 h to afford C–H oxygenation products, cyclic hemiacetal **2a** and 1,4-diol **3a** in 49% and 8% yields, respectively (Table 1, entry 1). It was found that addition of nitrogen ligands such as 2,2'-bipyridine and 1,10-phenanthroline (1,10-phen) accelerated the reaction (Table 1, entries 2 and 3). The reactions with $CuCl_2$ (Table 1, entry 4) as well as CuCl (Table 1, entry 5)

Table 1: Optimization of the reaction conditions.[a]

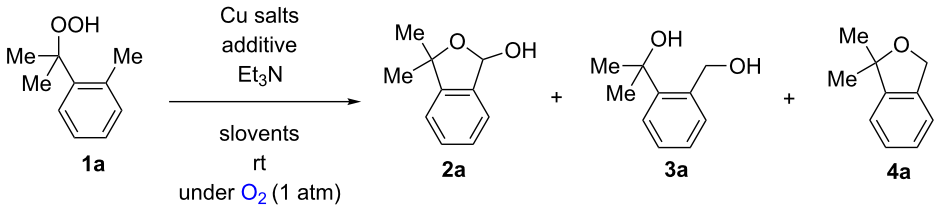

Entry	Cu salts (mol %)	Additive (mol %)	Et_3N (equiv)	Solvent (0.1 M)	Time (h)	Yield (%)[b]		
						2a	**3a**	**4a**
1	$Cu(OAc)_2$ (20)	–	2.0	DMF	17	49	8	0
2	$Cu(OAc)_2$ (20)	2,2'-bipyridine (20)	2.0	DMF	3	49	9	0
3	$Cu(OAc)_2$ (20)	1,10-phen (20)	2.0	DMF	3	53	12	0
4	$CuCl_2$ (20)	1,10-phen (20)	2.0	DMF	6	52	10	0
5	CuCl (20)	1,10-phen (20)	2.0	DMF	3	52	10	0
6	$Cu(OAc)_2$ (20)	1,10-phen (20)	2.0	MeCN	2	55	20	0
7	$Cu(OAc)_2$ (20)	1,10-phen (20)	2.0	benzene	5	71	13	0
8	$Cu(OAc)_2$ (20)	1,10-phen (20)	2.0	toluene	9	70	14	0
9	$Cu(OAc)_2$ (20)	1,10-phen (20)	2.0	benzene/MeCN (5:1)	2	76	11	0
10	$Cu(OAc)_2$ (20)	1,10-phen (20)	0.5	benzene/MeCN (5:1)	3	74	9	0
11	$Cu(OAc)_2$ (20)	1,10-phen (20)	0.5	toluene/MeCN (5:1)	3	74	10	0
12	$Cu(OAc)_2$ (10)	1,10-phen (10)	0.5	toluene/MeCN (5:1)	3	75	16	0
13	$Cu(OAc)_2$ (5)	1,10-phen (5)	0.5	toluene/MeCN (5:1)	3	75	14	0
14[c]	$Cu(OAc)_2$ (5)	1,10-phen (5)	0.5	toluene/MeCN (5:1)	3	–	90	0
15[d]	$Cu(OAc)_2$ (5)	1,10-phen (5)	0.5	toluene/MeCN (5:1)	1	0	0	47

[a]Reactions were carried out using 0.3 mmol of hydroperoxide **1a** in solvents (3 mL, 0.1 M) at room temperature under an O_2 atmosphere. [b]Isolated yields are recorded. [c]After stirring 5 h, the volatile materials were removed in vacuo, and the resulting crude materials were further treated with $LiAlH_4$ (1.2 equiv) in THF at rt for 1 h. [d]The reaction was conducted under a N_2 atmosphere.

resulted in comparable results with that by $Cu(OAc)_2$. Further optimization of the reaction conditions by the solvent screening (Table 1, entries 6–11) revealed that the co-solvent system (benzene/MeCN or toluene/MeCN) performed best to give the highest yield (83–87% combined yields of **2a** and **3a**, Table 1, entries 9–11), in which the amount of Et_3N could be reduced to 0.5 equiv (Table 1, entries 10 and 11). It is worthy of note that the catalytic loading of $Cu(OAc)_2$-1,10-phen could be lowered to 5 mol % while maintaining good combined yields of **2a** and **3a** (89%, Table 1, entry 13). Upon completion of the C–H oxygenation under the reaction conditions in entry 13, the resulting crude residue after removal of the solvents was treated with $LiAlH_4$ in THF, affording 1,4-diol **3a** as the sole product in 90% yield (Table 1, entry 14). The Cu-catalyzed reaction of **1a** under an inert (N_2) atmosphere gave an intramolecular C–H oxygenation product, dihydroisobenzofuran **4a** in 47% yield (Table 1, entry 15).

The proposed reaction pathways for the formation of **2a**, **3a**, and **4a** were described in Scheme 3. Single-electron reduction of the starting $Cu(OAc)_2$ by Et_3N forms the Cu(I) species, which reduces hydroperoxide **1a** to give O-radical **I** along with the generation of the Cu(II) species. 1,5-H-Radical shift of O-radical **I** generates C-radical **II**, which is trapped by molecular O_2 to give peroxy radical **III**. Probably further reaction of **III** with Cu(I) species gives Cu(II)-peroxide **IV**, which undergoes fragmentation to give aldehyde **V** [16-18], which in turn cyclizes to afford hemiacetal **2a**. Protonation of Cu(II)-peroxide **IV** followed by the reduction of the resulting hydroperoxide deliver 1,4-diol **3a**. In the absence of molecular O_2 (under a N_2 atmosphere, Table 1, entry 15), the resulting C-radical **I** is oxidized by the Cu(II) species to give carbocation **VI** [19], which is trapped by the intramolecular hydroxy group to give **4a**.

We next explored the substrate scope of the present aerobic strategy for the synthesis of 1,4-diols by targeting methylene C–H oxygenation with various tertiary hydroperoxides **1** (Table 2). Generally, oxygenation of benzylic methylene C–H bonds proceeded smoothly to give the corresponding 1,4-diols **3** in good to moderate yields (77–51% yields) (Table 2, entries 1–7). Moreover, the present method allowed for oxygenation of nonbenzylic methylene C–H bonds, while yields of obtained 1,4-diols **3** were relatively low (65–40% yields) (Table 2, entries 8–13). In most cases (except for Table 2, entries 3, 6, 7 and 11), either reduced alcohols **5** (up to 23%

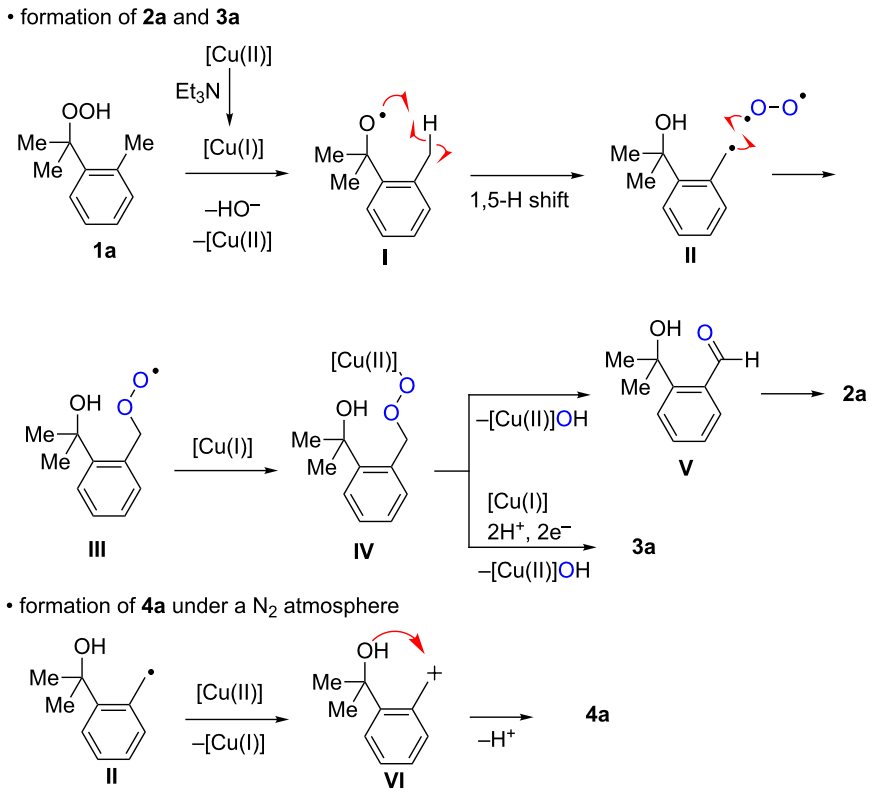

Scheme 3: Proposed reaction mechanisms for the formation of **2a**, **3a**, and **4a**.

Table 2: Substrate scope: oxygenation of secondary C–H bonds.[a]

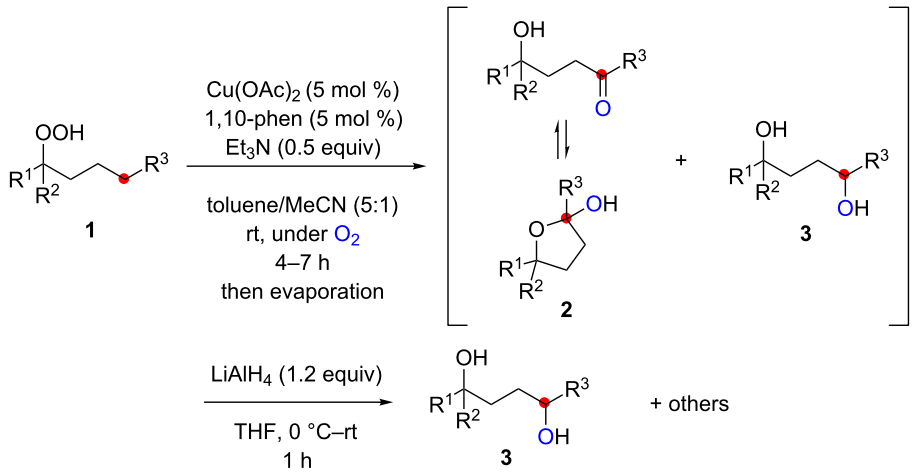

Entry	Hydroperoxides **1**	1,4-Diols **3**	Others	
			Alcohols **5**	Alcohols **6**
	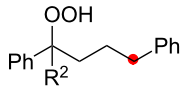	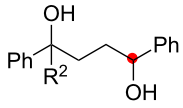		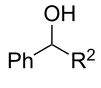
1	**1b** (R^2 = Ph)	**3b** 77%	–	**6b** 8%[b]
2	**1c** (R^2 = Me)	**3c** 72% (1:1)	–	**6c** 8%[b]
3	**1d** (R^2 = Et)	**3d** 51% (1:1)	–	–
	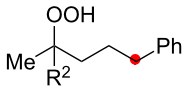	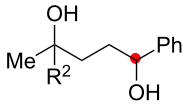	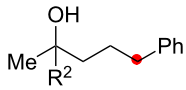	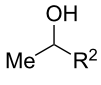
4	**1e** (R^2 = 2-naphthyl)	**3e** 62% (1:1)	**5e** 9%	**6e** 17%[b]
5	**1f** (R^2 = 4-Br-C_6H_4)	**3f** 70% (1:1)	**5f** 15%	**6f** 15%[b]
6	**1g** (R^2 = CH_2CH_2Ph)	**3g** 51% (1:1)	–	–
7	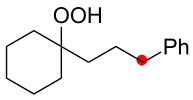 **1h**	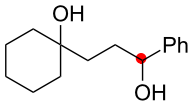 **3h** 56%	–	–
	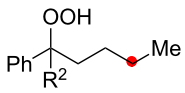	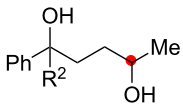	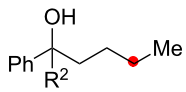	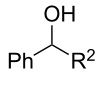
8	**1i** (R^2 = Ph)	**3i** 65%	**5i** 18%	**6b** 14%[b]
9	**1j** (R^2 = Me)	**3j** 62% (1.27:1)	**5j** 23%	**6c** 20%[b]
10	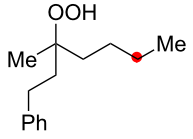 **1k**	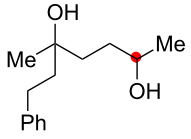 **3k** 40% (1:1)	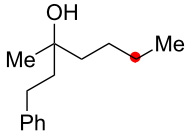 **5k** 16%	–
11	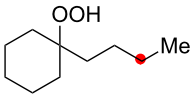 **1l**	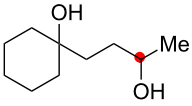 **3l** 48%	–	–

Table 2: Substrate scope: oxygenation of secondary C–H bonds.[a] (continued)

12	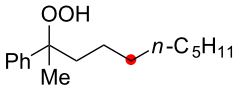 **1m**	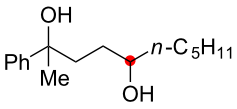 **3m** 45% (1.27:1)	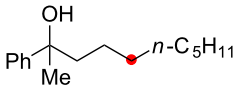 **5m** 18%	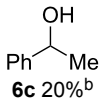 **6c** 20%[b]
13	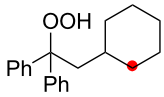 **1n**	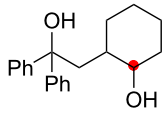 **3n** 51% (*trans*/*cis* = 1.37:1)	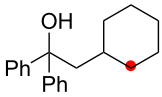 **5n** 13%	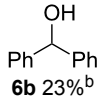 **6b** 23%[b]

[a]Reactions were carried out using 0.5 mmol of hydroperoxides **1** with $Cu(OAc)_2$ (5 mol %), 1,10-phen (5 mol %), and Et_3N (0.5 equiv) in toluene/MeCN (5:1, 0.1 M) at room temperature under an O_2 atmosphere. After stirring for 4–7 h, the volatile materials were removed in vacuo, and the resulting crude materials were further treated with $LiAlH_4$ (1.2 equiv) in THF at rt for 1 h. Isolated yields are recorded. The ratio in parentheses is the diastereomer ratio of the products **3**, where available. [b] ^1H NMR yields with 1,1,2,2-tetrachloroethane as an internal standard.

yield) or fragmented alcohols **6** (up to 23% yield), or both were observed as minor products. The formation of alcohols **5** occurs by two-electron reduction of hydroperoxides **1** followed by protonation or by H-radical abstraction of the transient O-radical generated by one-electron reduction of hydroperoxides **1** prior to the 1,5-H radical shift (Scheme 4). Presumably, radical fragmentation of O-radicals occurs to give the corresponding ketones **7**, which are reduced by $LiAlH_4$ in the next step to give alcohols **6** (Scheme 4).

The reaction of a secondary hydroperoxide such as **1o**, however, afforded C–H oxygenation product **2o** (as a keto form) only in 30% yield along with the formation of the corresponding reduced alcohol **5o** and ketone **8o** in 10% and 43% yields, respectively (Scheme 5).

Oxygenation of tertiary C–H bonds was also examined under the present aerobic conditions (Table 3). In these cases, the Cu-catalyzed aerobic reactions afford hydroperoxides **9** as an

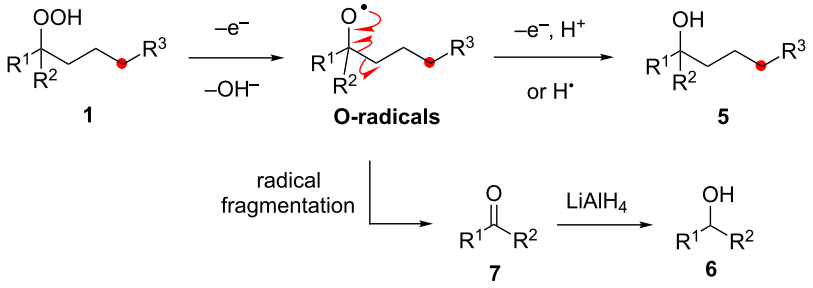

Scheme 4: Proposed reaction mechanisms for the formation of **5** and **6**.

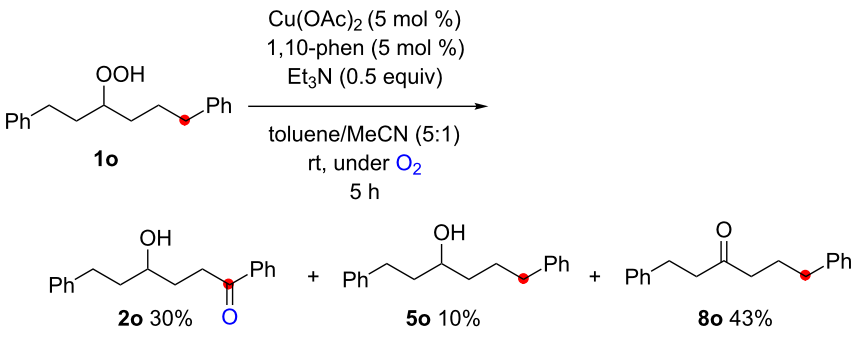

Scheme 5: The reaction of secondary hydroperoxide **1o**.

Table 3: Substrate scope oxygenation of tertiary C–H bonds.[a]

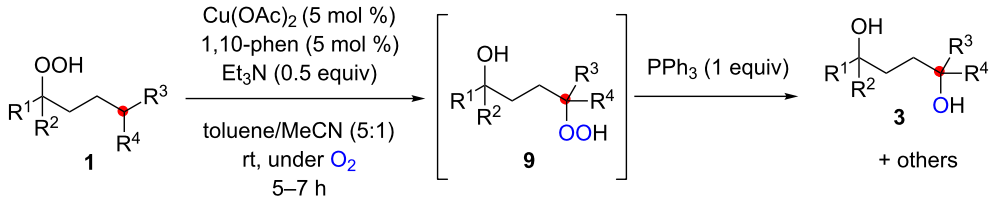

Entry	Hydroperoxides **1**	1,4-Diols **3**	Others	
			Alcohols **5**	Ketones **7**
1	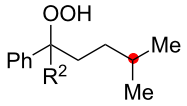 **1p** (R^2 = Ph)	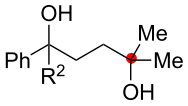 **3p** 52%	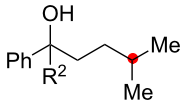 **5p** 16%	 **7b** 28%[b]
2	**1q** (R^2 = Me)	**3q** 45%	**5q** 23%	**7c** 24%[b]
3	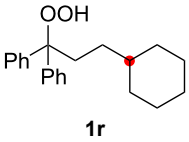 **1r**	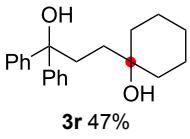 **3r** 47%	–	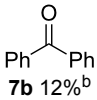 **7b** 12%[b]
4	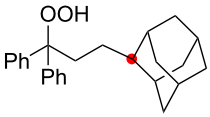 **1s**	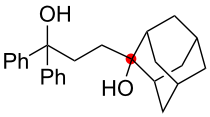 **3s** 23%	–	 **7b** 12%[b]

[a]Reactions were carried out by using 0.5 mmol of hydroperoxides **1** with $Cu(OAc)_2$ (5 mol %), 1,10-phen (5 mol %), and Et_3N (0.5 equiv) in toluene/MeCN (5:1, 0.1 M) at room temperature under an O_2 atmosphere. After stirring for 5–7 h, the reaction mixture was further treated with PPh_3 (1 equiv) at rt. Isolated yields are recorded. [b] ^1H NMR yields with 1,1,2,2-tetrachloroethane as an internal standard.

initial aerobic C–H oxygenation product. After stirring for 5–7 h, the reaction mixtures were successively treated with PPh_3 (1 equiv) for the reduction of **9** to obtain 1,4-diols **3**. Although the desired 1,4-diols **3** were formed with this two-step one-pot procedure, the isolated yields of **3p–3r** were moderate (45–52% yields) (Table 3, entries 1–3). The oxygenation of the adamantyl C–H bond was especially sluggish, giving the desired 1,4-diol **3s** in only 23% yield (Table 3, entry 4). Similarly, in these reactions, the formation of reduced alcohols **5** (for Table 3, entries 1 and 2) and fragmented ketones **7** (for Table 3, entries 1–4) were observed as minor products.

Our next challenge was to develop direct aerobic dioxygenation of alkanes using the present radical strategy. The generation of C-radicals from alkanes at C–H bonds bearing relatively weak bond-dissociation enthalpies (i.e., tertiary alkyl C–H bonds, benzylic C–H bonds, etc.), by phthalimide *N*-oxyl radicals generated oxidatively from *N*-hydroxyphthalimide (NHPI), has been reported [20-22]. The resulting C-radicals could be trapped with molecular oxygen to form hydroperoxides. It could be envisioned that this aerobic C–H bond oxygenation could be combined with the present remote C–H oxygenation with hydroperoxides, presumably resulting in direct formation of 1,4-dioxygenated compounds from nonoxygenated alkanes (Scheme 6).

With this hypothesis, alkane **10** bearing a dibenzylic tertiary C–H bond (marked in green) was treated with the catalytic system of CuCl-1,10-phen (20 mol %) with NHPI in benzene/MeCN solvent under an O_2 atmosphere (1 atm) (Scheme 7). The reaction with 20 mol % of NHPI proceeded as expected at 50 °C to afford a mixture of lactol **2i** and 1,4-diols **3i** in 29% and 3% yields, respectively, via the desired 1,4-dioxygenation, while benzophenone (**7b**) was also formed in 30% yield through fragmentation of the transient alkoxy radical (Scheme 4). Use of 40 mol % of NHPI slightly improved the yields of 1,4-dioxygenation products **2i** and **3i** (40% and 4% yields, respectively).

In conclusion, we have developed the Cu-catalyzed aerobic oxygenation of aliphatic C–H bonds using hydroperoxides by a

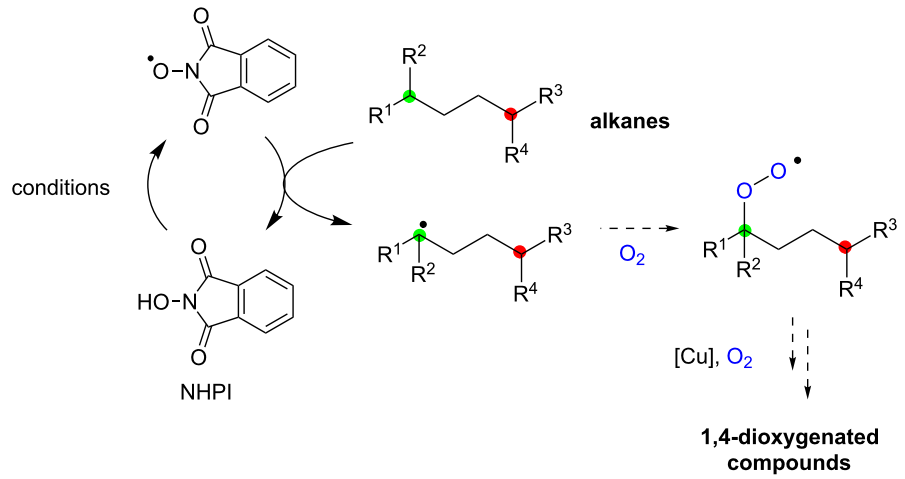

Scheme 6: 1,4-Dioxygenation of alkanes.

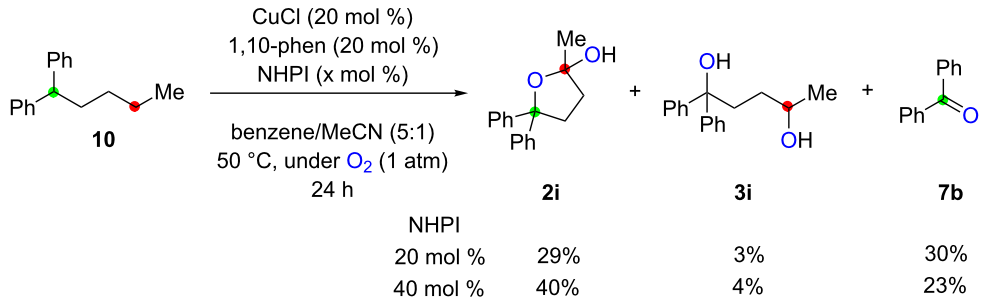

Scheme 7: Aerobic 1,4-dioxygenation of alkanes in the CuCl–NHPI catalytic system.

1,5-H radical shift of putative O-radicals derived from hydroperoxides followed by trapping of the resulting C-radicals with molecular oxygen. A preliminary result involving the direct 1,4-dioxygenation of alkane **10** was demonstrated by using the present method. Further studies will be carried out to develop more robust and efficient catalytic aerobic radical transformations for polyol synthesis from rather simple alkanes.

Supporting Information

Supporting Information File 1

Full experimental details and analytical data.
[http://www.beilstein-journals.org/bjoc/content/supplementary/1860-5397-9-138-S1.pdf]

Acknowledgements

This work was supported by funding from Nanyang Technological University and Singapore Ministry of Education (Academic Research Fund Tier 2: MOE2012-T2-1-014).

References

1. White, M. C. *Science* **2012,** *335,* 807–809. doi:10.1126/science.1207661
2. Davies, H. M. L.; Du Bois, J.; Yu, J.-Q. *Chem. Soc. Rev.* **2011,** *40,* 1855–1856. doi:10.1039/c1cs90010b
3. Newhouse, T.; Baran, P. S. *Angew. Chem., Int. Ed.* **2011,** *50,* 3362–3374. doi:10.1002/anie.201006368
4. Lyons, T. W.; Sanford, M. S. *Chem. Rev.* **2010,** *110,* 1147–1169. doi:10.1021/cr900184e
5. Čeković, Ž. *Tetrahedron* **2003,** *59,* 8073–8090. doi:10.1016/S0040-4020(03)01202-X
6. Majetich, G.; Wheless, K. *Tetrahedron* **1995,** *51,* 7095–7129. doi:10.1016/0040-4020(95)00406-X
7. Wang, Y.-F.; Chen, H.; Zhu, X.; Chiba, S. *J. Am. Chem. Soc.* **2012,** *134,* 11980–11983. doi:10.1021/ja305833a
8. Zhang, L.; Ang, G. Y.; Chiba, S. *Org. Lett.* **2011,** *13,* 1622–1625. doi:10.1021/ol200425c
9. Zhu, P.; Tong, B. M. K.; Wang, R.; Chen, J. P.; Foo, S.; Chong, H. C.; Wang, X. L.; Ang, G. Y.; Chiba, S.; Tan, N. S. *Cell Death Dis.* **2013,** *4,* e552. doi:10.1038/cddis.2013.68
10. Čeković, Ž.; Ilijev, D. *Tetrahedron Lett.* **1988,** *29,* 1441–1444. doi:10.1016/S0040-4039(00)80319-6

11. Čeković, Ž.; Čvetković, M. *Tetrahedron Lett.* **1982,** *23,* 3791–3794. doi:10.1016/S0040-4039(00)87708-4
12. Čeković, Ž.; Dimitrijević, L.; Djokić, G.; Srnić, T. *Tetrahedron* **1979,** *35,* 2021–2026. doi:10.1016/S0040-4020(01)88972-9
13. Čeković, Ž.; Green, M. M. *J. Am. Chem. Soc.* **1974,** *96,* 3000–3002. doi:10.1021/ja00816a059
14. Kundu, R.; Ball, Z. T. *Org. Lett.* **2010,** *12,* 2460–2463. doi:10.1021/ol100472t
15. Li, C.-J. *Acc. Chem. Res.* **2009,** *42,* 335–344. doi:10.1021/ar800164n
16. Zhang, L.; Lee, J.-Y.; Yamazaki, N.; Chiba, S. *Synlett* **2011,** 2167–2170. doi:10.1055/s-0030-1261185
17. Tnay, Y. L.; Chen, C.; Chua, Y. Y.; Zhang, L.; Chiba, S. *Org. Lett.* **2012,** *14,* 3550–3553. doi:10.1021/ol301583y
18. Chiba, S.; Zhang, L.; Lee, J.-Y. *J. Am. Chem. Soc.* **2010,** *132,* 7266–7267. doi:10.1021/ja1027327
19. Kochi, J. K.; Bemis, A.; Jenkins, C. L. *J. Am. Chem. Soc.* **1968,** *90,* 4616–4625. doi:10.1021/ja01019a018
20. Ishii, Y.; Sakaguchi, S.; Iwahama, T. *Adv. Synth. Catal.* **2001,** *343,* 393–427. doi:10.1002/1615-4169(200107)343:5<393::AID-ADSC393>3.0.CO;2-K
21. Roduner, E.; Kaim, W.; Sarjar, B.; Urlacher, V. B.; Pleiss, J.; Gläser, R.; Einicke, W.-D.; Sprenger, G. A.; Beifuß, U.; Klemm, E.; Liebner, C.; Hieronymus, H.; Hsu, S.-F.; Plietker, B.; Laschat, S. *ChemCatChem* **2013,** *5,* 82–112. doi:10.1002/cctc.201200266
22. Recupero, F.; Punta, C. *Chem. Rev.* **2007,** *107,* 3800–3842. doi:10.1021/cr040170k

License and Terms

Beilstein Journal of Organic Chemistry

The synthesis of well-defined poly(vinylbenzyl chloride)-grafted nanoparticles via RAFT polymerization

John Moraes[1], Kohji Ohno[2], Guillaume Gody[1], Thomas Maschmeyer[3] and Sébastien Perrier[*1]

Full Research Paper

Open Access

Address:
[1]Key Centre for Polymers & Colloids, School of Chemistry, The University of Sydney, NSW 2006, Australia, [2]Institute for Chemical Research, Kyoto University, Kyoto 611-0011, Japan and [3]Laboratory of Advanced Catalysis for Sustainability, School of Chemistry, The University of Sydney, NSW 2006, Australia

Email:
Sébastien Perrier[*] - sebastien.perrier@sydney.edu.au

* Corresponding author

Keywords:
core–shell particles; free radical; grafting; RAFT polymerization; silica

Beilstein J. Org. Chem. **2013,** *9,* 1226–1234.
doi:10.3762/bjoc.9.139

Received: 05 April 2013
Accepted: 28 May 2013
Published: 25 June 2013

This article is part of the Thematic Series "Organic free radical chemistry".

Guest Editor: C. Stephenson

Abstract

We describe the use of one of the most advanced radical polymerization techniques, the reversible addition fragmentation chain transfer (RAFT) process, to produce highly functional core–shell particles based on a silica core and a shell made of functional polymeric chains with very well controlled structure. The versatility of RAFT polymerization is illustrated by the control of the polymerization of vinylbenzyl chloride (VBC), a highly functional monomer, with the aim of designing silica core–poly(VBC) shell nanoparticles. Optimal conditions for the control of VBC polymerization by RAFT are first established, followed by the use of the "grafting from" method to yield polymeric brushes that form a well-defined shell surrounding the silica core. We obtain particles that are monodisperse in size, and we demonstrate that the exceptional control over their dimensions is achieved by careful tailoring the conditions of the radical polymerization.

Introduction

The versatility of organic free radical chemistry in terms of functionality and reaction conditions makes it a technique of choice for the synthesis of functional polymeric materials. However, the lack of control over the chain length and chain end of the final polymeric material makes conventional radical processes unsuitable for specific targeted applications. The establishment in the 1990s of living radical polymerization (LRP, defined as reversible deactivation radical polymerization by the IUPAC), has dramatically changed the polymer-synthesis landscape allowing the easy production of well-defined polymeric materials of desired molecular weights with narrow dispersity (<1.5) and complex architectures (i.e., block copoly-

mers) [1]. By exploiting a dormant state of the propagating radical of a growing chain, it is possible to limit the proportion of irreversibly terminated chains in a radical polymerization, and thus to control the final structure of the resulting polymeric chain. Among the many techniques of LRP reported to date, reversible addition–fragmentation chain transfer (RAFT) polymerization is one of the most versatile processes, both in terms of tolerance towards a wide range of monomer functionality and reaction conditions [2]. RAFT polymerization employs a chain transfer agent (CTA, or RAFT agent), which is reversibly transferred from one propagating chain to another in a degenerative process. The rapid exchange of the RAFT agent between propagating chains ensures that each chain grows simultaneously over the course of the polymerization and a final narrow molecular weight distribution of the polymer product ensues. Moreover, the molecular weight of the final material can be easily tuned depending on the amount of CTA initially introduced. This degenerative process is triggered by the presence of radicals, typically obtained from thermal or photoinitiators, the amount of which is kept low in comparison with the amount of CTA introduced (i.e., high ratio CTA/initiator) in order to minimise the fraction of dead chains produced. Therefore, it is commonly assumed that the ratio of monomer to RAFT agent gives the average degree of polymerization (DP, i.e., the number of monomers per chain) [3,4].

RAFT polymerization has been used to generate a very large range of materials ranging from polymeric architectures to nanomaterials and hybrid materials [5-9]. In particular, RAFT has had a major impact in addressing the challenge of preparing highly monodisperse core–shell nanoparticles, which hold great promise for a range of applications such as drug-delivery vectors or colloidal-crystal self-assemblies [10,11]. RAFT polymerization initiated from preformed inorganic nanoparticles enables the grafting of polymer shells from the particle surface and yields well-defined particles from a range of monomeric precursors [12]. While initial work focussed on common monomers such as styrene [13-15] and (meth)acrylates [14-16], several recent papers seek to extend this work to a greater variety of monomers [17-22]. One particular motivation has been the post-polymerization functionalization of the grafted chains to yield functional nanoparticles. Therefore, monomers that allow such post-polymerization functionalization are beginning to attract greater research attention [23,24].

4-Vinylbenzyl chloride (VBC) is one such monomer that offers ready post-polymerization functionalization through the pendant chloride group [25-31], which can readily undergo nucleophilic substitution [25-29] or be used as an initiating site for another LRP system, i.e., atom transfer radical polymerization (ATRP) [30,31]. It has, therefore, been used in a variety of systems as a precursor to glycopolymer stars [29], photo- and pH-responsive nanoparticles [30], nanofibres [28], comb, graft and star polymers [27], and triblock copolymers [26]. While there have been reports of the (co)polymerization of VBC by RAFT techniques [25-30,32], the polymerization of this highly versatile monomer onto solid scaffolds has, thus far, not been described. RAFT polymerization is an ideal radical process technique for VBC as side reactions (such as dissociation of the C–Cl bond, which would be expected if ATRP were used to polymerize VBC) can be avoided [27,32]. For the purposes of this study, high-molecular-weight chains (ca. 20 to 100 kg/mol) are of importance, as the ability to grow high-molecular-weight chains from the surface of the silica particles allows us to increase the number of functionalizable benzyl chloride groups present. Additionally, having a large amount of polymer grown from the particle will allow fine control over the effective diameter of the particle by merely tuning the polymerization conditions to dictate the size of the polymer shell. This cannot be achieved if low molecular weights are targeted, as their comparative contribution to the diameter of the particle is negligible.

This manuscript focuses on two aspects of RAFT polymerization. In the first instance, we explore the use of RAFT polymerization with either thermal autoinitiation of VBC or thermal initiation by an azoinitiator to achieve a well-controlled polymerization of the monomer in solution (Scheme 1). We then use the latter approach to form well-defined core–shell nanoparticles wherein the size of the polymer shell can be varied by changing the degree of polymerization of the grafted polymer chains.

Results and Discussion

Previous literature on the RAFT-mediated polymerization of vinylbenzyl chloride has utilized either thermal autoinitiation [29], or azoinitiators [25-28,32] and photoinitiators [33]. Of these investigations only two were concerned with polymers greater than 20 kg/mol, and hence, our studies focussed on the RAFT polymerization of VBC using either thermal autoinitiation or an azoinitiator [26,29]. The former method is reported to yield faster kinetics due to the higher k_p at elevated temperatures [29] and, thus, initial experiments in this study were conducted at 110 °C in the presence of the RAFT agent 2-(butylthiocarbonothioylthio)propionic acid (PABTC) without any additional initiator. In addition to targeting a high-molecular-weight polymer by choosing a high degree of polymerization (DP), we also prepared polymers of lower molecular weights (DP 100) to serve as a point of comparison.

The two polymerizations showed conventional kinetics features for a radical polymerization, i.e., increase of the monomer conversion with increasing reaction time and linear semilog

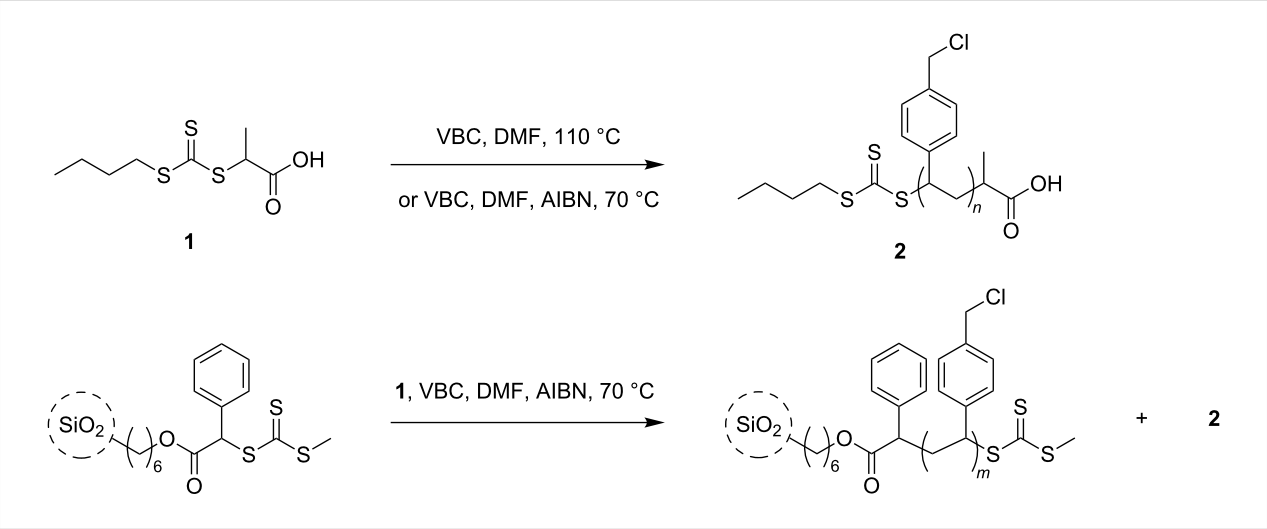

Scheme 1: RAFT polymerization and silica-supported RAFT polymerization of vinylbenzyl chloride (VBC).

kinetics plots (Supporting Information File 1, Figure S1), although significant rate retardation, typically observed in RAFT polymerization [34], was noted for lower DP targeted. Size-exclusion chromatography (SEC) analysis of the polymer chains showed that for both DPs targeted, a linear increase of the molecular weight was noted with increasing conversions of up to ca. 20%. After this point, however, the molecular weights taper off or steadily decrease for polymers of DP 100 and DP 2,500, respectively (Figure 1). We hypothesise that this negative deviation of the experimental molecular weight derived from the large number of thermally initiated chains in solution. In fact, in the case of thermal autoinitiation, since the monomer plays also the role of the initiator, the concentration of initiator would be intimately linked to the monomer concentration. Thus, when high DP are targeted (i.e., low $[CTA]_0$), it is expected that the concentration of monomer-initiated chains (i.e., VBC-derived chains) would greatly outnumber the chains initiated by the R-group of the RAFT agent (i.e., CTA-derived chains). If the number of thermally initiated chains is not negligible in comparison with the number of CTA-derived chains (typically, <10% of the total number of chains is considered negligible) a negative deviation of the theoretical molecular weight is expected, as seen in Equation 1 where $[VBC]_0$ and $[PABTC]_0$ are the initial concentration in VBC and RAFT agent, [thermally initiated chains] is the concentration of generated VBC initiator species, C is the monomer conversion, and $M_{(VBC)}$ and $M_{(PABTC)}$ are the molar masses of monomer and chain transfer agent, respectively.

$$M_{n(Theor.)} = \frac{[VBC]_0 \times C \times M_{(VBC)}}{[PABTC]_0 + [\text{thermally initiated chains}]} + M_{(PABTC)} \quad (1)$$

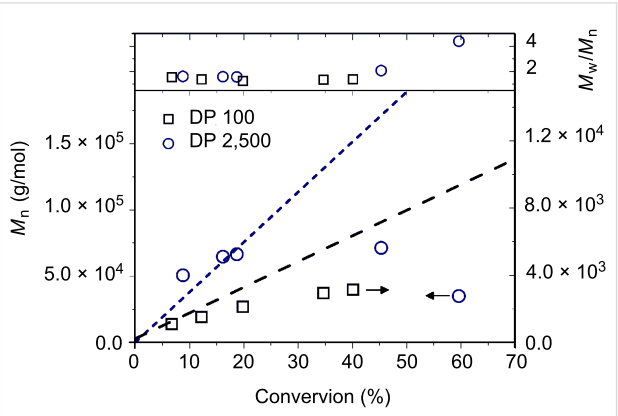

Figure 1: Evolution of number-average molecular weight (M_n) and M_w/M_n values of the poly(VBC) chains obtained by RAFT polymerization with PABTC as CTA and thermal autoinitiation. Dashed lines depict the theoretical molecular weights obtained from Equation 1 without taking into account the thermally initiated chains.

This important feature would also explain the poor uniformity of the final material obtained (cf. the high M_w/M_n values in Figure 1) as the final number of dead chains (chains not possessing a trithiocarbonate, from the RAFT agent ω-end group and thereby nonliving) is related to the total number of VBC-initiated chains. Therefore, when high DPs are targeted, the fraction of VBC-initiated chains (i.e., dead polymer chains) is expected to be very large. It is worth noting that this negative deviation of the experimental molecular weight with the monomer conversion together with high M_w/M_n values when high DPs are targeted has also been previously observed by Chen et al. who prepared star polymers of VBC using thermal autoinitiation [29].

Since thermal autoinitiation resulted in poor control over the polymer chains, we next investigated the use of an azoinitiator, 2,2′-azobis(2-methylpropionitrile) (AIBN). For these experiments, two DPs (100 and 4,100) were targeted, keeping the initial concentration of AIBN and monomer constant so as to obtain similar kinetics for each experiment. As seen in Figure 2, the polymerizations in each case proceeded at almost identical rates (although Figure 2B shows slight retardation at DP 100, as expected for RAFT polymerization targeting lower DPs, see above), irrespective of the DP, while similar linear semilog kinetics plots for each experiment suggest that the radical flux is constant over the time scale of the experiments.

For both polymerizations, the molecular weights of the poly(VBC) chains are close to the theoretical molecular weights (see Table 1). There were two important considerations associated with this finding: (1) the experimental molecular weights of the polymers ($M_{n(Exp.)}$) were determined by using a SEC system calibrated with narrow-molecular-weight poly(styrene) standards. Since this system results in $M_{n(Exp.)}$ values relative to poly(styrene), these $M_{n(Exp.)}$ were corrected by taking into account the difference in molecular weight between VBC and styrene (see Table 1, footnote b). (2) In order to accurately determine the theoretical molecular weight for each experiment, it is crucial to also take into account the concentration of AIBN-

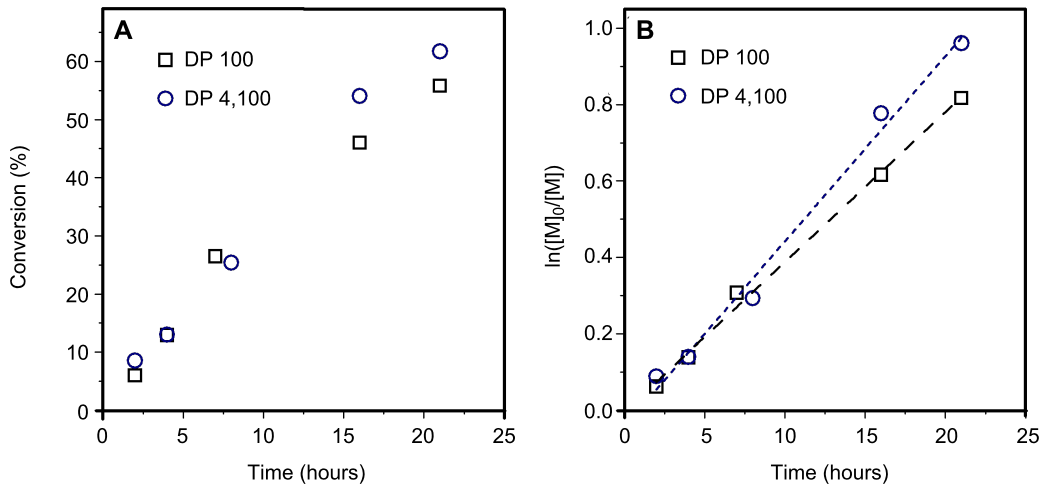

Figure 2: Conversion and ln([M]$_0$/[M]) versus time for AIBN-initiated, PABTC-mediated polymerization of VBC at DP 100 (squares) and DP 4,100 (circles): (A) monomer conversion versus reaction time; (B) semilog kinetics plots with dashed lines indicating linear fits of the data (DP 100, long dashes; DP 4,100, short dashes).

Table 1: Characteristics of polymers produced by the AIBN-initiated, PABTC-mediated polymerization of VBC at 60 °C.

Expt. No.	Time (h)	Conversion[a]	M_n (Theory) (g/mol)	M_n (Exp.) (g/mol)[b]	M_w/M_n	AIBN-initiated chains (%)[c]
1[d]	2	6%	2,000	2,300	1.36	1%
2[d]	4	13%	2,400	2,700	1.42	1%
3[d]	7	26%	3,600	4,000	1.39	2%
4[d]	16	46%	6,000	6,500	1.32	4%
5[d]	21	56%	7,800	8,400	1.27	5%
6[e]	2	8%	40,800	42,800	1.84	24%
7[e]	4	13%	50,900	50,000	1.95	38%
8[e]	8	25%	74,700	72,900	1.77	53%
9[e]	16	54%	113,200	98,800	1.91	67%
10[e]	21	62%	113,300	110,200	1.97	71%

[a]Determined by ^{1}H NMR.
[b]Determined by SEC:

$$M_{n(p(VBC))} = \left(\left(M_{n(SEC)} - M_{(PABTC)} \right) \times \frac{M_{(VBC)}}{M(Sty)} \right) + M_{(PABTC)}$$

[c]From the ratio of AIBN-initiated chains (calculated in a similar manner as in Equation 2) to total chains.
[d]Polymerizations carried out at 60 °C in DMF (10 wt %) and [VBC]$_0$/[PABTC]$_0$/[AIBN]$_0$ = 100/1/0.1.
[e]Polymerizations carried out at 60 °C in DMF (9 wt %) and [VBC]$_0$/[PABTC]$_0$/[AIBN]$_0$ = 4,100/1/5.

initiated chains generated by the decomposition of AIBN throughout the polymerization (see Equation 2 where f is the initiator efficiency (assumed to be 0.5 for AIBN), the term "2" means that 1 molecule of azoinitiator gives two primary radicals, k_d is the dissociation constant of AIBN at 60 °C (9.8×10^{-6} s^{-1}), t is the time in seconds, and f_c is the coupling constant ($f_c = 1$ for 100% termination by combination and $f_c = 0$ for 100% termination by disproportionation), assumed to be 1 in this case since poly(VBC) and poly(styrene) are considered to terminate primarily by combination). This is especially true in the case when high DPs are targeted (for instance 4,100) where the ratio of AIBN to PABTC is 5:1, which results in a substantial proportion (71%) of AIBN-derived chains after 21 h.

$$[\text{AIBN} - \text{initiated chains}] = 2 \times f \times [\text{AIBN}]_0 \times (1 - e^{-k_d t}) \times \left(1 - \frac{f_c}{2}\right) \quad (2)$$

As seen in Table 1, the contribution of the AIBN-initiated chains to the total number of chains becomes significant at higher DPs and explains the negative deviation of $M_{n(Exp.)}$ under these conditions. The presence of these AIBN-initiated chains also adversely affects the M_w/M_n values of the polymers at DP 4,100, which are consistently higher than those at DP 100 (compare experiments 6–10 with experiments 1–5 in Table 1). However, this is an unavoidable consequence of RAFT polymerization under these conditions, when targeting such extremely high DPs. Nonetheless, since a predictable increase in M_n with conversion was demonstrated (a key requirement for the controlled synthesis of core–shell particles), we proceed to undertake the polymerization in the presence of silica-supported RAFT agents.

In the preparation of the silica–polymer hybrid particles, our aim was to form polymer brushes on the surface of the particles. Thus, the so-called "grafting from" approach, where the R-group of the RAFT agent is attached to the silica particle [12,35], was used to obtain a high grafting density [36]. The sulfur content of the particles (hereby SiP–RAFT) was determined by elemental microanalysis, and the grafting density of RAFT–agents on the surface of the particles was calculated to be 0.4 groups·nm^{-2} (see Supporting Information File 1, Equation S1). SiP–RAFT particles were added into the polymerization media such that the particles accounted for 1 wt % of the total mass of the reactants. In addition to the silica-supported RAFT agent, free PABTC was also added to the system in order to maintain control over the polymerization, as previously described [37]. Using the grafting density of the SiP–RAFT, we calculated that the tethered RAFT agent accounts for ca. 10% of the total RAFT agent in the reaction. Thus, two distinct types of RAFT-mediated chains are present in the solution. The first type is derived from the free RAFT agent, while the second type is anchored to the silica surface.

The silica-supported RAFT polymerization was performed at a DP of 4,400 and an initiator concentration of 7.22×10^{-3} mol·L^{-1} (CTA/AIBN ratio of 1/5), conditions analogous to experiments 6–10 in Table 1 above. As seen in Figure 3, the addition of the SiP–RAFT particles to the polymerization media does not have any deleterious effect on the

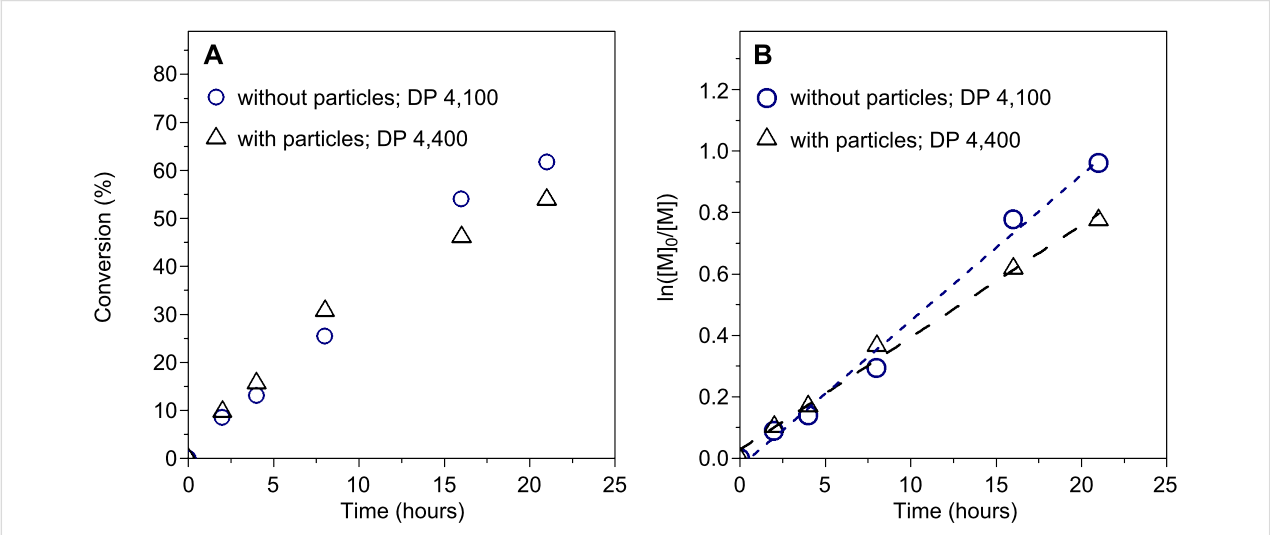

Figure 3: AIBN-initiated, PABTC-mediated polymerization of VBC with (triangles, DP 4,400) and without (circles, DP 4,100) SiP–RAFT particles: (A) monomer conversion versus reaction time; (B) pseudo-first order plots with dashed lines indicating linear fits of the data (long dashes, with particles, DP 4,400; short dashes, without particles, DP 4,100).

polymerization, and similar kinetics are observed in the experiments with and without particles, as expected since SiP–RAFT only accounts for ca. 10% of the total RAFT agent in the reaction.

The free polymer chains are readily separated from the silica particles by dilution of the polymerization mixture with THF and subsequent centrifugation. SEC analysis shows that there is a very close adherence of the molecular weight of the free chains to the theoretically expected values at each step of the polymerization (Figure 4) and the chains maintained a monomodal size distribution throughout the polymerization (see Supporting Information File 1, Figure S2). Grafted chains were liberated from the particles (before being subjected to SEC analysis) by using hydrofluoric acid (HF) to destroy the silica core by etching. These chains show higher $M_{n(Exp.)}$ than the theory and higher M_w/M_n values than for the free polymer chains, particularly at higher conversions. This observation can be attributed either to a poorer control over the RAFT process, for instance the possible occurrence of branching due to chain transfer between grafted polymeric chains and other side reactions occurring during the RAFT process and enhanced by the high local concentration of grafted chains [34,38,39], or the result of the harsh conditions used to etch the silica, which may affect the polymeric chains. Indeed, there were several difficulties encountered during the etching experiments with high pressures being noted in the SEC system when eluting samples. In addition, in contrast to the free polymer chains some bimodality was observed in the etched polymer chains (see Supporting Information File 1, Figure S3 cf. Figure S2). No conclusive elucidation of any degradation to degrafted chains was possible, as the amount of material recovered was insufficient for ^{1}H NMR analysis. The high pressures in the SEC were particularly prevalent in the two samples taken later in the polymerization (at 16 hours and 21 hours). Thus, the SEC data for these two samples may be underestimated (i.e., the longest polymer chains may have been removed during the filtration). What is evident, however, is that in nearly every sample, the molecular weight of the grafted polymer is higher than that of the free polymer. This is similar to what was previously observed in the thermally autoinitiated SiP–RAFT-mediated polymerization of styrene, since the molecular weight of the grafted chains is not affected by the thermally initiated free chains, the presence of which contributes to lower the molecular weight of the nongrafted chains [36]. A thorough analysis of the hybrid nanoparticles at each of the kinetic points was then carried out.

The particles were washed by repeated centrifugation–redispersion cycles in THF in order to completely remove free polymer chains adsorbed onto the particles. The particles (henceforth SiP–p(VBC) particles) were studied by dynamic light scattering (DLS), which showed a monomodal peak indicating well-defined particles with no aggregation (Supporting Information File 1, Figure S4). There is a clear increase in the diameters of the particles as the reaction proceeds, indicating a growth of the polymer shell surrounding the silica core. Plotting the average diameter and polydispersity index (PDI) of the particles against monomer conversion (Figure 5), shows an increase in particle size with increasing conversion. This continues past the first three data points in stark contrast to the M_n of the polymer chains degrafted from the particles. This strongly suggests that the grafted chains do indeed continue to increase in size, despite the plateau observed in the SEC (which could be an artefact of the SEC analysis and the loss of higher-molecular-weight chains on the SEC filters, thereby resulting in the high system pressures mentioned previously). Alternatively, assuming the SEC analysis is an accurate depiction of the polymer chains, it is possible that even though the growth of the

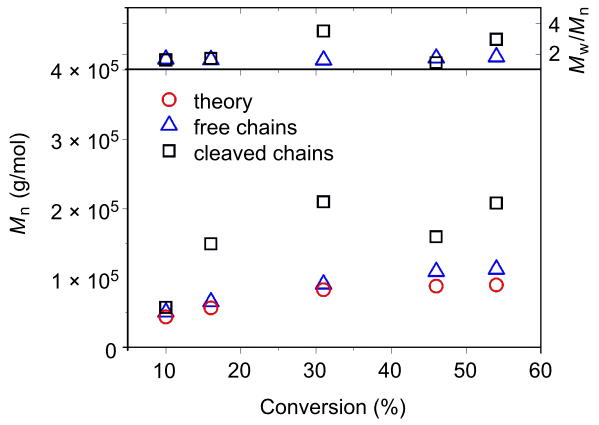

Figure 4: Evolution of molecular weights of free and grafted poly(VBC) chains with conversion.

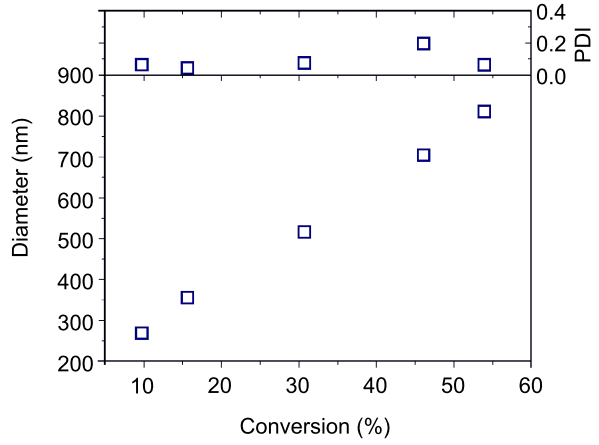

Figure 5: Plot of the average diameter and PDI of particles recovered from silica-supported RAFT polymerization of VBC.

polymer chains slows down at higher conversions, the particles in solution continue to increase in size due to the solvent swelling the grafted polymer chains, thus increasing the apparent particle diameter.

It is also noteworthy that the PDI of the particles remains low throughout the reaction (PDI < 0.2), in contrast to the relatively high PDIs obtained for both the grafted and free polymeric chains from this reaction (Figure 4). This observation shows that despite the high M_w/M_n values for the poly(VBC) chains and the number of initiator-derived chains in the system, a very well controlled growth of particles is achievable and the size of the hybrid particle can be dictated as desired.

Thermogravimetric analysis (TGA) of the hybrid nanoparticles recovered from the reaction showed a steady increase in mass loss with increasing monomer conversion (Supporting Information File 1, Figure S5). Plotting the mass lost against conversion shows an almost linear trend indicating that the addition of polymer to the silica particles proceeds in a controlled manner, thus allowing precise incorporation of the required amount of VBC onto the silica particle. The mass loss on TGA, accompanied with the M_n of the (cleaved) chains measured by SEC allows calculation of the grafting density of the particles (See Supporting Information File 1, Equation S2). As seen in Supporting Information File 1, Figure S5, this remains nearly constant throughout the polymerization with an average value of 0.11 chains/nm^2 (compared to 0.18 chains/nm^2 if the M_n of the free chains is used for calculation).

Transmission electron microscope (TEM) analysis of the particles recovered from the reaction shows that as the reaction proceeds, the polymer shell around the particles increases in size (Figure 6). The polymer shell is visible as the dark grey region between the particles, and it increases in size from 10% conversion (57,600 g/mol, grafted polymer) to 54% conversion (208,000 g/mol, grafted polymer). TEM samples of particles recovered from intermediate stages of the polymerization are included in Supporting Information File 1, Figure S6. It should be noted that TEM images of the particles show the average diameter of the particles to be smaller than that measured by DLS. We ascribe this to the fact that the polymer shell on the particles in DLS analysis is measured in a swollen state with a presumably fully extended chain, whereas the shell visible in the TEM images is desolvated and consequently appears in a shrunken state. We consider the size obtained by DLS as a more accurate depiction of the particles, as this technique assays a much greater number of particles and provides fuller information regarding the distribution of particle sizes in the samples. The pervasive presence of these polymer shells, keeping the particles from aggregating, is evidenced by the uniform distance between the particles. Thus, well-defined core–shell nanoparticles of tunable sizes are readily available using surface-initiated RAFT of VBC.

Conclusion

We have demonstrated the controlled polymerization and grafting onto silica nanoparticles of 4-vinylbenzyl chloride using RAFT polymerization. Whilst thermal autoinitiation of VBC does not lead to well-controlled molecular weight at high conversions, the control is improved by using AIBN as initiator and lower temperatures for DPs around 100, whilst targeting DPs of an order of magnitude higher in similar conditions lead to poorer molecular-weight control, mainly due to the large contribution of terminated polymeric chains. When polymerising VBC in the presence of SiP–RAFT, using AIBN as an

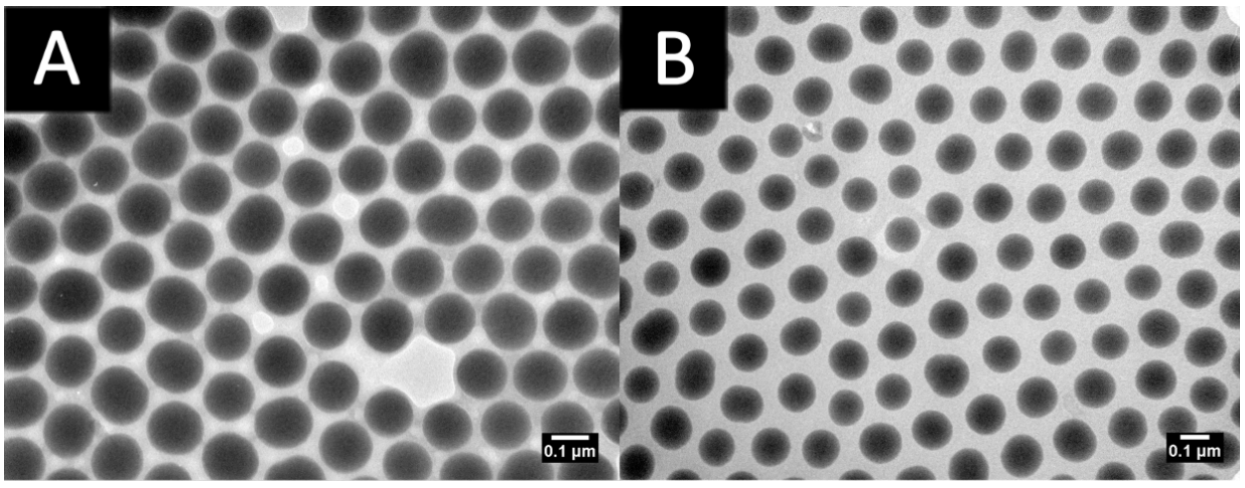

Figure 6: TEM micrographs of particles (A) after 2 hours and (B) after 21 hours of VBC polymerization. Scale bars represent 0.1 µm.

azoinitiator in the reaction medium resulted in a linear evolution of the final particle sizes with conversion. This allowed the desired particles size to be reliably synthesised with a high degree of monodispersity. Indeed, the particles recovered show monomodal particle-size distribution and very low dispersities. Their uniformity results in the formation of well-ordered films, showing long-range two-dimensional order.

Supporting Information

Supporting Information File 1

Experimental procedures, equations, kinetic plots, SEC data, light scattering data, thermolysis data and TEM images.
[http://www.beilstein-journals.org/bjoc/content/supplementary/1860-5397-9-139-S1.pdf]

Acknowledgements

The Australian Research Council's Discovery, Future Fellowship and Linkage Programs are acknowledged by SP and TM for funding, JM acknowledges the Henry Bertie & Florence Mabel Gritton Scholarship, The O'Donnell Young Scientist Prize and CSIRO PhD studentship. GG acknowledges Licella Pty. Ltd. for funding. The authors acknowledge Mr. Yun Huang for help with the preparation of the SiP–RAFT particles. The authors acknowledge the facilities, and the scientific and technical assistance, of the Australian Microscopy & Microanalysis Research Facility at the University of Sydney.

References

1. Matyjaszewski, K.; Davis, T. P. Future Outlook and Perspectives. *Handbook of Radical Polymerization;* John Wiley & Sons, Inc.: Hoboken, 2003; pp 895–900. doi:10.1002/0471220450.ch16
2. Chiefari, J.; Chong, Y. K.; Ercole, F.; Krstina, J.; Jeffery, J.; Le, T. P. T.; Mayadunne, R. T. A.; Meijs, G. F.; Moad, C. L.; Moad, G.; Rizzardo, E.; Thang, S. H. *Macromolecules* **1998,** *31,* 5559–5562. doi:10.1021/ma9804951
3. Moad, G.; Rizzardo, E.; Thang, S. H. *Aust. J. Chem.* **2012,** *65,* 985–1076. doi:10.1071/CH12295
4. Perrier, S.; Takolpuckdee, P. *J. Polym. Sci., Part A: Polym. Chem.* **2005,** *43,* 5347–5393. doi:10.1002/pola.20986
5. Semsarilar, M.; Perrier, S. *Nat. Chem.* **2010,** *2,* 811–820. doi:10.1038/nchem.853
6. Boyer, C.; Stenzel, M. H.; Davis, T. P. *J. Polym. Sci., Part A: Polym. Chem.* **2011,** *49,* 551–595. doi:10.1002/pola.24482
7. Barner-Kowollik, C.; Perrier, S. *J. Polym. Sci., Part A: Polym. Chem.* **2008,** *46,* 5715–5723. doi:10.1002/pola.22866
8. Takolpuckdee, P.; Westwood, J.; Lewis, D. M.; Perrier, S. *Macromol. Symp.* **2004,** *216,* 23–36. doi:10.1002/masy.200451204
9. Gregory, A.; Stenzel, M. H. *Prog. Polym. Sci.* **2012,** *37,* 38–105. doi:10.1016/j.progpolymsci.2011.08.004
10. Cayre, O. J.; Chagneux, N.; Biggs, S. *Soft Matter* **2011,** *7,* 2211–2234. doi:10.1039/c0sm01072c
11. Chaudhuri, R. G.; Paria, S. *Chem. Rev.* **2012,** *112,* 2373–2433. doi:10.1021/cr100449n
12. Radhakrishnan, B.; Ranjan, R.; Brittain, W. J. *Soft Matter* **2006,** *2,* 386–396. doi:10.1039/b516508c
13. Li, C.; Benicewicz, B. C. *Macromolecules* **2005,** *38,* 5929–5936. doi:10.1021/ma050216r
14. Zhao, Y.; Perrier, S. *Macromolecules* **2006,** *39,* 8603–8608. doi:10.1021/ma061586y
15. Li, C.; Han, J.; Ryu, C. Y.; Benicewicz, B. C. *Macromolecules* **2006,** *39,* 3175–3183. doi:10.1021/ma051983t
16. Perrier, S.; Takolpuckdee, P.; Mars, C. A. *Macromolecules* **2005,** *38,* 6770–6774. doi:10.1021/ma0506886
17. Chung, P.-W.; Kumar, R.; Pruski, M.; Lin, V. S.-Y. *Adv. Funct. Mater.* **2008,** *18,* 1390–1398. doi:10.1002/adfm.200701116
18. Lu, C.-H.; Zhou, W.-H.; Han, B.; Yang, H.-H.; Chen, X.; Wang, X.-R. *Anal. Chem.* **2007,** *79,* 5457–5461. doi:10.1021/ac070282m
19. Liu, J.; Zhang, L.; Shi, S.; Chen, S.; Zhou, N.; Zhang, Z.; Cheng, Z.; Zhu, X. *Langmuir* **2010,** *26,* 14806–14813. doi:10.1021/la102994g
20. Zhao, Y.; Perrier, S. *Macromolecules* **2007,** *40,* 9116–9124. doi:10.1021/ma0716783
21. Huang, Y.; Liu, Q.; Zhou, X.; Perrier, S.; Zhao, Y. *Macromolecules* **2009,** *42,* 5509–5517. doi:10.1021/ma900604v
22. Huang, Y.; Hou, T.; Cao, X.; Perrier, S.; Zhao, Y. *Polym. Chem.* **2010,** *1,* 1615–1623. doi:10.1039/c0py00165a
23. Cash, B. M.; Wang, L.; Benicewicz, B. C. *J. Polym. Sci., Part A: Polym. Chem.* **2012,** *50,* 2533–2540. doi:10.1002/pola.26029
24. Li, Y.; Benicewicz, B. C. *Macromolecules* **2008,** *41,* 7986–7992. doi:10.1021/ma801551z
25. Yeh, K.-M.; Chen, Y. *J. Polym. Sci., Part A: Polym. Chem.* **2006,** *44,* 5362–5377. doi:10.1002/pola.21592
26. Strube, O. I.; Schmidt-Naake, G. *Macromol. Symp.* **2009,** *275–276,* 13–23. doi:10.1002/masy.200950102
27. Quinn, J. F.; Chaplin, R. P.; Davis, T. P. *J. Polym. Sci., Part A: Polym. Chem.* **2002,** *40,* 2956–2966. doi:10.1002/pola.10369
28. Fu, G. D.; Xu, L. Q.; Yao, F.; Zhang, K.; Wang, X. F.; Zhu, M. F.; Nie, S. Z. *ACS Appl. Mater. Interfaces* **2009,** *1,* 239–243. doi:10.1021/am800143u
29. Chen, Y.; Chen, G.; Stenzel, M. H. *Macromolecules* **2010,** *43,* 8109–8114. doi:10.1021/ma100919x
30. Feng, H.; Zhao, Y.; Pelletier, M.; Dan, Y.; Zhao, Y. *Polymer* **2009,** *50,* 3470–3477. doi:10.1016/j.polymer.2009.06.017
31. Bayramoglu, G.; Yavuz, E.; Senkal, B. F.; Arica, M. Y. *Colloids Surf., A* **2009,** *345,* 127–134. doi:10.1016/j.colsurfa.2009.04.044
32. Couture, G.; Améduri, B. *Eur. Polym. J.* **2012,** *48,* 1348–1356. doi:10.1016/j.eurpolymj.2012.03.020
33. Zhang, H.; Deng, J.; Lu, L.; Cai, Y. *Macromolecules* **2007,** *40,* 9252–9261. doi:10.1021/ma071287o
34. Barner-Kowollik, C.; Buback, M.; Charleux, B.; Coote, M. L.; Drache, M.; Fukuda, T.; Goto, A.; Klumperman, B.; Lowe, A. B.; Mcleary, J. B.; Moad, G.; Monteiro, M. J.; Sanderson, R. D.; Tonge, M. P.; Vana, P. *J. Polym. Sci., Part A: Polym. Chem.* **2006,** *44,* 5809–5831. doi:10.1002/pola.21589
35. Ranjan, R.; Brittain, W. J. *Macromol. Rapid Commun.* **2007,** *28,* 2084–2089. doi:10.1002/marc.200700428

36. Ohno, K.; Ma, Y.; Huang, Y.; Mori, C.; Yahata, Y.; Tsujii, Y.; Maschmeyer, T.; Moraes, J.; Perrier, S. *Macromolecules* **2011,** *44,* 8944–8953. doi:10.1021/ma202105y
37. Tsujii, Y.; Ejaz, M.; Sato, K.; Goto, A.; Fukuda, T. *Macromolecules* **2001,** *34,* 8872–8878. doi:10.1021/ma010733j
38. Konkolewicz, D.; Hawkett, B. S.; Gray-Weale, A.; Perrier, S. *Macromolecules* **2008,** *41,* 6400–6412. doi:10.1021/ma800388c
39. Konkolewicz, D.; Hawkett, B. S.; Gray-Weale, A.; Perrier, S. *J. Polym. Sci., Part A: Polym. Chem.* **2009,** *47,* 3455–3466. doi:10.1002/pola.23385

License and Terms

Beilstein Journal of Organic Chemistry

Homolytic substitution at phosphorus for C–P bond formation in organic synthesis

Hideki Yorimitsu[1,2]

Review

Open Access

Address:
[1]Department of Chemistry, Graduate School of Science, Kyoto University, Sakyo-ku, Kyoto 606-8502, Japan and [2]ACT-C, Japan Science and Technology Agency, Sakyo-ku, Kyoto 606-8502, Japan

Email:
Hideki Yorimitsu - yori@kuchem.kyoto-u.ac.jp

Keywords:
addition; free radical; homolysis; phosphine; radical; substitution

Beilstein J. Org. Chem. **2013,** *9,* 1269–1277.
doi:10.3762/bjoc.9.143

Received: 22 April 2013
Accepted: 07 June 2013
Published: 28 June 2013

This article is part of the Thematic Series "Organic free radical chemistry".

Guest Editor: C. Stephenson

Abstract

Organophosphorus compounds are important in organic chemistry. This review article covers emerging, powerful synthetic approaches to organophosphorus compounds by homolytic substitution at phosphorus with a carbon-centered radical. Phosphination reagents include diphosphines, chalcogenophosphines and stannylphosphines, which bear a weak P–heteroatom bond for homolysis. This article deals with two transformations, radical phosphination by addition across unsaturated C–C bonds and substitution of organic halides.

Introduction

Organophosphorus compounds constitute an important class of compounds in a wide range of applications in organic chemistry, as reagents, intermediates, ligands, bioactive agents, and functional materials [1-4]. The synthesis of organophosphorus compounds has therefore been extensively investigated (Scheme 1). Classical methods to form a C–P bond include ionic reactions such as nucleophilic substitution of P–X compounds with organometallic reagents, nucleophilic substitution of alkyl halides with phosphorus nucleophiles, and nucleophilic addition to polar unsaturated bonds. Recent advances in transition-metal catalysis have realized catalytic cross-coupling reactions of aryl halides with H–P compounds [5-7] and catalytic addition to nonpolar unsaturated carbon–carbon bonds

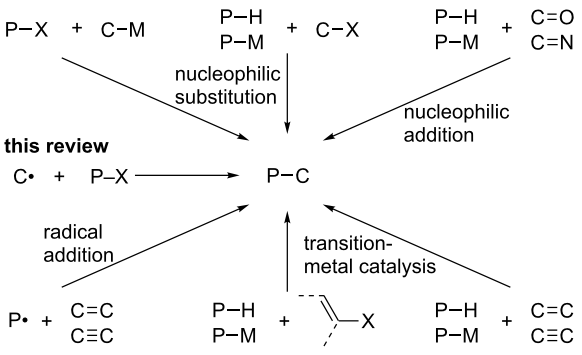

Scheme 1: Representative C–P bond-forming reactions.

[8-11]. In the field of radical chemistry, the addition of phosphorus radicals, mainly from H–P compounds, onto carbon–carbon multiple bonds [12-15] has held a special position since they provide transformations unattainable by polar reactions.

Homolytic substitution is a reaction in which a radical (R•) attacks a saturated atom (X) in a molecule with the liberation of a leaving radical (L•) from the atom (Scheme 2). Homolytic substitution at halogen and chalcogen atoms is well known to proceed and hence has been widely used in organic synthesis [16-19]. In contrast, applications of homolytic substitution to C–P bond formation have been rarely explored. With the growing importance of organophosphorus compounds, increasing attention has been paid to homolytic substitution at phosphorus. The new tool for C–P bond formation has achieved interesting transformations that ionic reactions cannot. This review summarizes homolytic substitution at phosphorus for C–P bond formation in organic synthesis while the relevant mechanistic studies are found in the literature [19-21]. This review deals with two transformations, radical phosphination by addition across unsaturated C–C bonds and substitution of organic halides.

Scheme 2: General equation of homolytic substitution.

Review

Radical addition of phosphination agents

Stannylphosphines of the type $R_3Sn–PR'_2$ are known to undergo radical addition to carbon–carbon unsaturated bonds. Schumann reported the addition of diphenyl(triphenylstannyl)phosphine to allyl chloride, styrene, and phenylacetylene (Scheme 3) [22,23]. The addition is most likely to proceed via a radical process as the absence of AIBN leads to considerable decreases in yield. Mitchell then reported that diphenyl(trimethylstannyl)phosphine reacts not only with terminal alkynes but also with internal alkynes and allenes (Scheme 4) [24,25]. It is noteworthy that the regioselectivity of the radical addition to propynamide is opposite to that of the relevant ionic Michael addition. Considering the regioselectivity, these addition reactions naturally involve C–P bond formation by homolytic substitution at phosphorus (Scheme 5). Studer recently reported similar silylphosphination of phenyl vinyl sulfone with $Me_3Si–PPh_2$ [26].

Tzschach reported that tetraorganodiphosphines $R_2P–PR_2$ add to phenylacetylene under UV irradiation or upon heating in the presence of AIBN (Scheme 6) [27]. The reaction consists of the addition of a diorganophosphanyl radical to phenylacetylene and the homolytic substitution of tetraorganodiphosphine with the resulting vinyl radical to afford the adduct and to regenerate the initial diorganophosphanyl radical (Scheme 7). The high *E* selectivity is attributable to kinetic control of the homolytic substitution, where $R_2P–PR_2$ preferentially approaches the vinyl radical from the roomier side. Although the transformation looks useful to construct an (*E*)-1,2-diphosphanylethene skeleton, the scope of alkyne is limited to phenylacetylene and

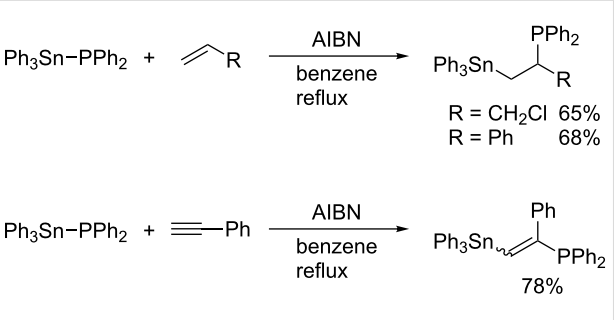

Scheme 3: Addition of diphenyl(triphenylstannyl)phosphine.

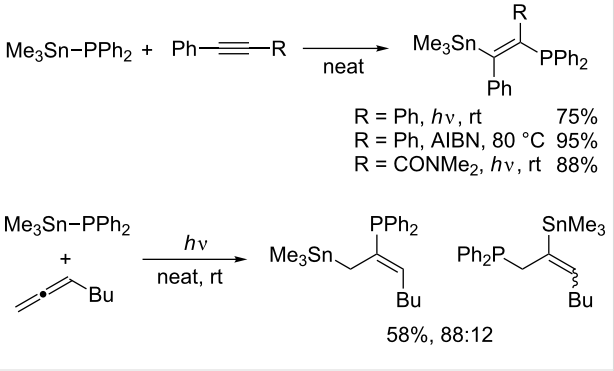

Scheme 4: Addition of diphenyl(trimethylstannyl)phosphine.

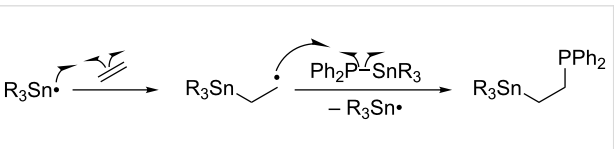

Scheme 5: Plausible mechanism of addition of $R_3Sn–PPh_2$.

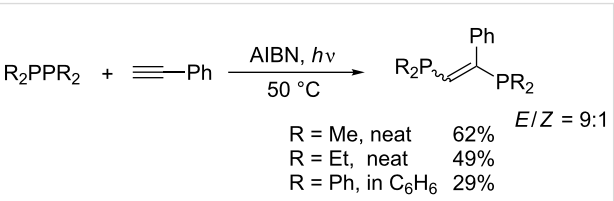

Scheme 6: Addition of tetraorganodiphosphines to phenylacetylene.

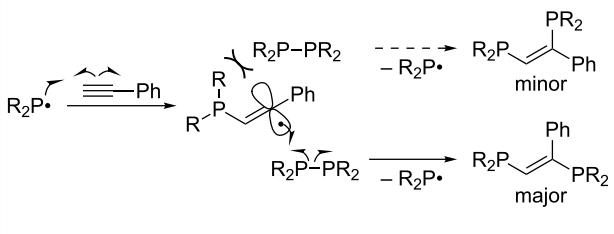

Scheme 7: Plausible mechanism of *anti*-diphosphination.

the reactions result in unsatisfactory yields because of the instability of the products as well as the diphosphines in air.

A more general, facile, and reliable method for diphosphination was later reported by Yorimitsu and Oshima, which utilizes diphosphines generated in situ from chlorophosphine and hydrophosphine in the presence of triethylamine [28]. A variety of terminal alkynes undergo the radical diphosphination (Table 1). The diphosphination was applicable to the synthesis of a new push–pull-type molecule that emits blue fluorescence (Scheme 8). The initially formed diphosphanylethylene derivatives are not very stable in air, and therefore sulfidation or oxidation was performed to accurately assess the efficiency of the diphosphination reactions.

Ogawa independently reported similar diphosphination under UV irradiation (Table 2) [29,30]. The reactions favor the formation of *Z* isomers, which results from photoinduced isomerization of initially formed *E* isomers. Ogawa's diphosphination is thus potentially useful for the synthesis of (*Z*)-1,2-diphosphanyl-1-alkenes, which can serve as bidentate ligands.

Table 1: Radical *anti*-selective diphosphination of terminal alkynes.

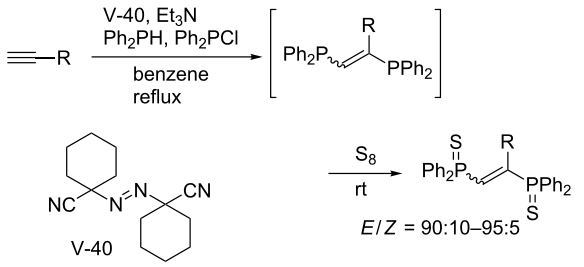

R	Yield (%)
$C_{10}H_{21}$	84
Ph	87
C_6H_4-*p*-OMe	89
C_6H_4-*p*-CO_2Me	95
C_6H_4-*p*-I	83
C_6H_4-*p*-COMe	96
$(CH_2)_3$OBn	78
$(CH_2)_6CO_2Et$	86
$(CH_2)_9$SCOMe	80
$(CH_2)_9$Cl	86

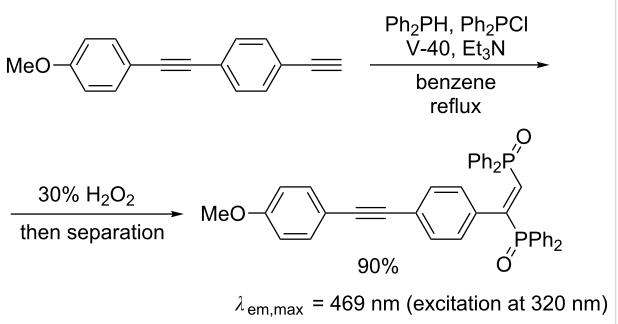

Scheme 8: Radical diphosphination for synthesizing fluorescent material.

Table 2: Photoinduced radical diphosphination of terminal alkynes.

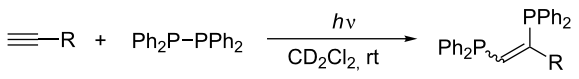

R	Time (h)	Yield (%)	*E*/*Z*
$CH_2CH_2CHMe_2$	39	62	18:82
$(CH_2)_3Cl$	18	55	42:58
Ph	1	45	<1:99

Morse developed photoinduced addition of tetrafluorodiphosphine to alkenes and alkynes in the gas phase (Table 3) [31-34]. The addition provides a series of intriguing bidentate phosphine ligands. The addition to alkynes yields 1:1 mixtures of *E*/*Z* isomers. Due to the high reactivity of a difluorophosphanyl radical, considerable polymerization takes place unless substrates or olefinic products are reasonably inert.

Yorimitsu and Oshima reported radical addition of a P–S bond across alkyne by using diphenyl(organosulfanyl)phosphine (Table 4) [35]. The addition proceeds mainly in an *anti* fashion to afford the adducts bearing a sulfanyl group at the terminal carbon and a phosphanyl group at the internal carbon. The reaction mechanism is similar to that in Scheme 7 (Scheme 9). The regioselective outcome suggests that the homolytic substitution occurs exclusively at phosphorus, not at sulfur. A sulfanyl radical is liberated to add the terminal carbon of alkyne. To reverse the regioselectivity in radical addition of a P–S bond, *S*-thiophosphinyl *O*-ethyl dithiocarbonates were created, although the reversed addition excludes homolytic substitution at phosphorus (Scheme 10) [36].

Table 3: Photoinduced radical diphosphination with tetrafluorodiphosphine.

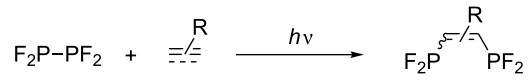

Product	Yield (%)
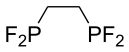	50
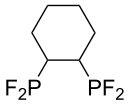	62
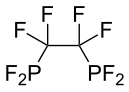	<10
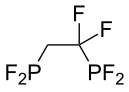	13
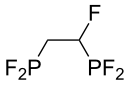	52
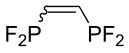	0
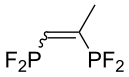	5
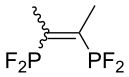	10
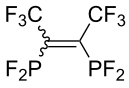	65
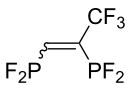	25

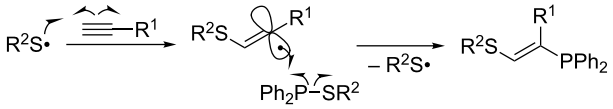

Scheme 9: Mechanism of thiophosphination with diphenyl(organosulfanyl)phosphine.

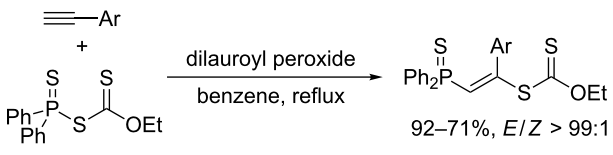

Scheme 10: Thiophosphination with *S*-thiophosphinyl *O*-ethyl dithiocarbonate.

Table 4: Thiophosphination of terminal alkynes.

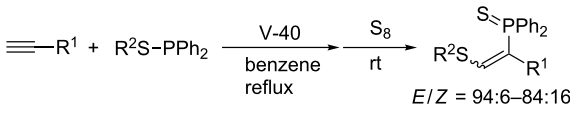

R^1	R^2	Yield (%)
$C_{10}H_{21}$	Ph	75
c-C_6H_{11}	Ph	61
Ph	Ph	83
C_6H_4-*p*-OMe	Ph	75
C_6H_4-*o*-OMe	Ph	85
C_6H_4-*p*-COMe	Ph	69
C_6H_4-*p*-CO_2Me	Ph	73
C_6H_4-*p*-CF_3	Ph	69
C_6H_4-*p*-NH_2	Ph	80
$(CH_2)_3OH$	Ph	66
C_6H_4-*p*-OMe	$C_{12}H_{25}$	70
$C_{10}H_{21}$	$C_{12}H_{25}$	42
$C_{10}H_{21}$	*t*-Bu	51

Kawaguchi, Nomoto, and Ogawa seminally studied the photoinduced radical chalcogenophosphination of alkynes and allenes by means of PhCh–ChPh/Ph_2P–PPh_2 binary systems (Ch = S, Se, Te) [30,37-39]. The regioselective outcome of the photoinduced thio- and selenophosphination of terminal alkynes (Table 5) is similar to that of the thermal thiophosphination (Scheme 9). Detailed mechanistic studies revealed that comproportionation between PhSe–SePh and Ph_2P–PPh_2 occurs smoothly to generate PhSe–PPh_2 as the actual reactive species. Selenophosphination of terminal allene affords (2-phenylselenyl-2-alkenyl)diphenylphosphine regioselectively (Scheme 11). Notably, the sense of the regioselectivity of

Table 5: Photoinduced thio- and selenophosphination by dichalcogen/diphosphine binary system.

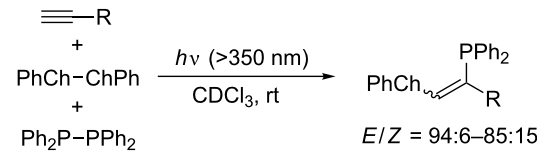

R	Ch	Yield (%)
C_6H_{13}	S	77
C_6H_4-*p*-OMe	S	91
1-cyclohexenyl	S	87
C_6H_4-*p*-Br	Se	96
C_6H_4-*p*-OMe	Se	78
1-cyclohexenyl	Se	83

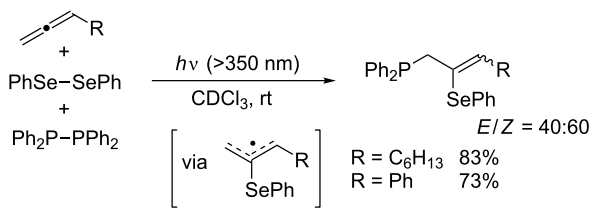

Scheme 11: Photoinduced selenophosphination of allenes.

tellurophosphination by a PhTe–TePh/Ph_2P–PPh_2 system is opposite to those of the thio- and selenophosphination (Scheme 12). This reversal indicates that homolytic substitution at tellurium overwhelms that at phosphorus and that a diphenylphosphanyl radical is more reactive than a phenyltelluranyl radical.

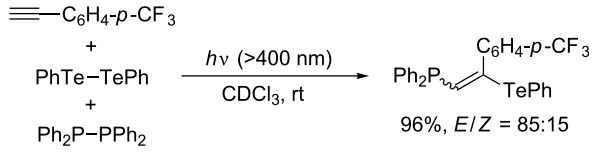

Scheme 12: Photoinduced tellurophosphination.

Substitution of halides (X), carboxys (COOR), or carboxylates (OCOR) with phosphorus

After scattered research efforts into the uncontrolled radical C–H phosphination under harsh reaction conditions [40], Barton elegantly devised radical decarboxylative phosphorylation of carboxylic thiohydroxamic mixed anhydrides (Scheme 13) [41]. Radical addition of a phenylsulfanyl radical to the thiocarbonyl generates the corresponding alkyl radical R•, which undergoes homolytic substitution at the phosphorus of $P(SPh)_3$ to furnish $(PhS)_2$P–R as the initial product (Scheme 14). Oxidative addition of the disulfide byproduct to the initial product furnishes a pentavalent phosphorus species that is eventually hydrolyzed to an *S*,*S*-diphenyl dithiophosphonate upon workup.

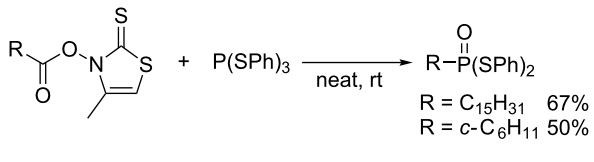

Scheme 13: Decarboxylative phosphorylation of carboxylic acid derivatives.

Barton also reported that white phosphorus reacts with *N*-acyloxythiopyridones, so-called Barton PTOC esters (Scheme 15) [42]. Photolysis of the esters in the presence of white phosphorus followed by oxidation with hydrogen peroxide yields alkylphosphonic acid. The efficient phosphination would stem from the highly strained structure and the weak P–P bonds of white phosphorus.

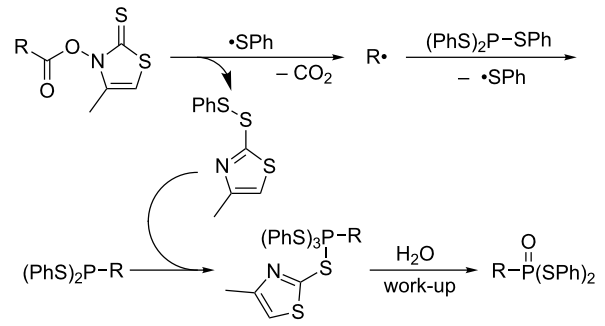

Scheme 14: Plausible mechanism of decarboxylative phosphorylation.

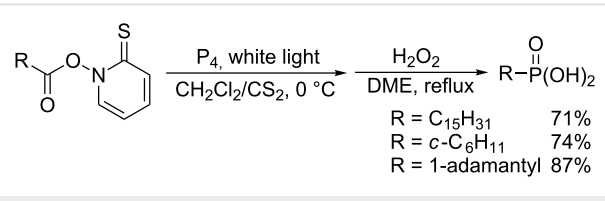

Scheme 15: Radical phosphination of PTOC esters with white phosphorus.

After 13 years of silence, radical substitution reactions of organic halides and related compounds with phosphination agents have now been rapidly developing since 2006. Yorimitsu and Oshima invented radical phosphination of organic halides with tetraphenyldiphosphine (Table 6) [43].

Table 6: Radical phosphination of aryl iodides.

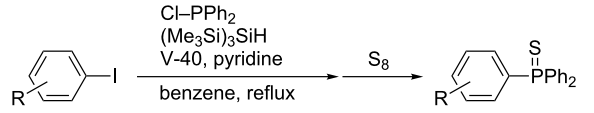

R	Yield (%)
H	88
2,4,6-Me_3	63
2-MeO	65
4-MeO	75
4-CF_3	78
4-Br	66
4-CN	69
4-$COCH_3$	47
4-OTf	68
4-$CO_2CH_2CH{=}CH_2$	78

Tetraphenyldiphosphine is generated in situ by radical reduction of chlorodiphenylphosphine with tris(trimethylsilyl)silane followed by condensation of the resulting diphenylphosphine with the remaining chlorophosphine (Scheme 16, equation 1 and 2). An aryl radical reacts with tetraphenyldiphosphine to liberate a diphenylphosphanyl radical, which abstracts hydrogen from tris(trimethylsilyl)silane to sustain the chain propagation (Scheme 16, equation 3–5). The in situ formations of diphenylphosphine and of tetraphenyldiphosphine can exclude the handling of pyrophoric diphenylphosphine and air-sensitive tetraphenyldiphosphine. The user-friendly conditions are also suitable for dicyclohexylphosphination with $ClP(c\text{-}C_6H_{11})_2$.

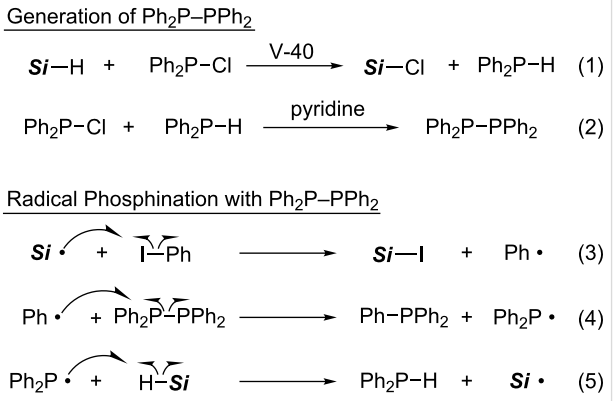

Scheme 16: Plausible mechanism of radical phosphination (***Si*** = $(Me_3Si)_3Si$).

Phosphination of alkyl halides as substrates results in unsatisfactory yields. Instead, Barton's alkyl imidazole-1-carbothioates are good substrates for this radical phosphination (Table 7). Conversion of an optically pure *cis*-carbothioate leads to *trans*-aminophosphine of potential use as a ligand (Scheme 17).

Table 7: Radical phosphination of alkyl imidazole-1-carbothioates.

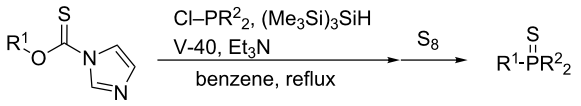

R^1	R^2	Yield (%)
$c\text{-}C_6H_{11}$	Ph	87
$c\text{-}C_6H_{11}$	$c\text{-}C_6H_{11}$	68
$EtOCOCH_2CH(CH_3)$	Ph	89
3-oxacyclopentyl	Ph	87
C_6H_{13}	Ph	63

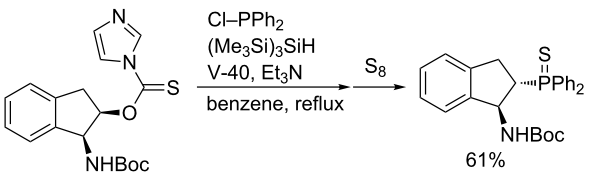

Scheme 17: Stereoselective phosphination leading to (*S*,*S*)-aminophosphine derivative.

Diphosphine approaches the resulting radical from the opposite side of the NHBoc group to invert the original stereochemistry.

Studer developed in 2007 new elegant reagents $Me_3Sn–PPh_2$ and $Me_3Si–PPh_2$ for radical phosphination [44]. The scope of his phosphination with $Me_3Sn–PPh_2$ is wide as summarized in Table 8. Although the low toxicity of $Me_3Si–PPh_2$ is advantageous, phosphination with $Me_3Si–PPh_2$ is limited to alkyl halides or imidazole-1-carbothioate. Density functional theory calculations have clarified the homolytic substitution process is a two-step mechanism via a tetracoordinated phosphorus atom (Figure 1). The spin density in the tetracoordinated phosphorus intermediate is localized mostly on the Sn atom while the remaining spin density is found in the equatorial position of the distorted trigonal prismatic P atom.

Table 8: Radical phosphination with $Me_3Sn–PPh_2$.

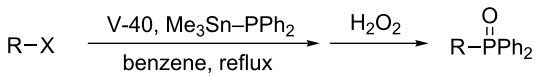

R–X	Yield (%)
$p\text{-}MeOC_6H_4–I$	73
$p\text{-}NCC_6H_4–I$	79
$p\text{-}CF_3C_6H_4–I$	75
$p\text{-}ClC_6H_4–I$	72
$o\text{-}MeOC_6H_4–I$	59
$o\text{-}MeO_2CC_6H_4–I$	73
$CH_3CBr=CH_2$	76
$C_5H_{11}–I$	79
$c\text{-}C_6H_{11}–I$	94
$C_{11}H_{23}–Br$	54
t-Bu–Br	83
$C_5H_{11}–SePh$	60
$c\text{-}C_6H_{11}–OCS\text{-}1\text{-}imidazole$	57

The rate constant for phosphination of an aryl radical with $Me_3Sn–PPh_2$ is calculated to be ca. 9×10^8 $M^{-1}s^{-1}$ by competition kinetics with Bu_3SnH reduction [45]. This large rate constant allows for stereospecific trapping of axially chiral acyl

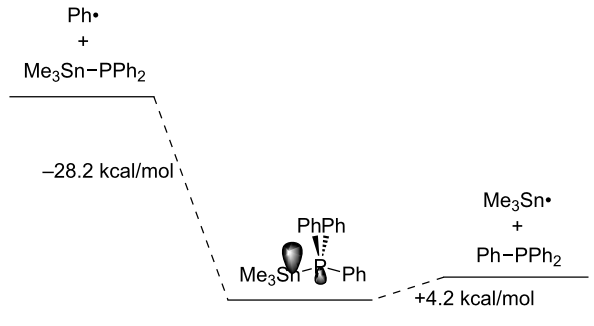

Figure 1: Calculated reaction profile of homolytic substitution between Ph• and $Me_3Sn–PPh_2$ at the B2-PLYP-D/TZVVP//PBE-D/TZVP level. Gray lobes indicate major spin densities.

radicals with $Me_3Sn–PPh_2$ (Scheme 18). Chemodivergent trapping of diastereomers of an *N*-(2-cyclohexenyl)acetanilide derivative is interesting (Scheme 19). One isomer undergoes direct phosphination while the other cyclizes prior to phosphination.

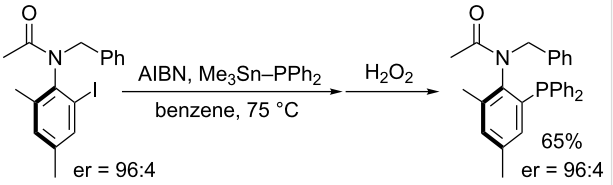

Scheme 18: Phosphination with retention of axial chirality.

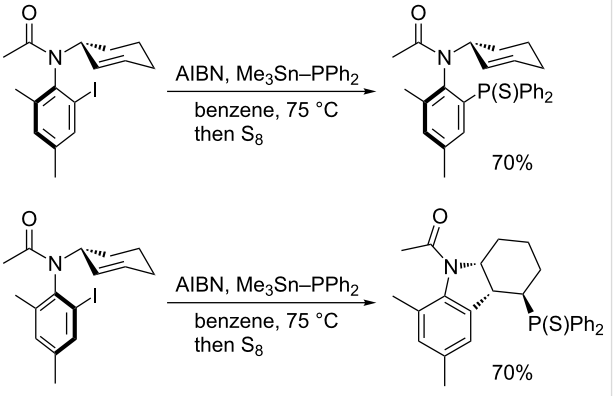

Scheme 19: Chemodivergent phosphination.

Intermolecular phosphinative radical addition of alkyl iodides to activated alkenes proceeds in the presence of $Me_3M–PPh_2$ (M = Sn, Si) and V-40 (Table 9) [26]. Secondary and tertiary alkyl iodides participate in the addition reaction while primary alkyl iodide results in direct phosphination prior to the expected addition. Not only acrylate ester but also acrylamide, vinyl sulfone, and acrylonitrile are good radical acceptors in this addition.

Table 9: Phosphinative radical addition of alkyl iodides to activated alkenes.

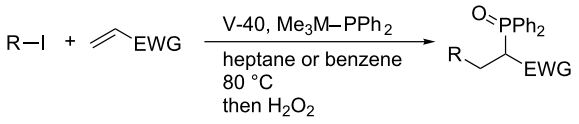

R	*M*	EWG	Yield (%)
c-C_6H_{11}	Si	CO_2t-Bu	72
c-C_6H_{11}	Sn	CO_2t-Bu	64
t-Bu	Si	CO_2t-Bu	76
t-Bu	Sn	CO_2t-Bu	69
C_5H_{11}	Si	CO_2t-Bu	<5
C_5H_{11}	Sn	CO_2t-Bu	<5
c-C_6H_{11}	Sn	SO_2Ph	48
c-C_6H_{11}	Sn	$CONMe_2$	44
c-C_6H_{11}	Sn	CN	79

Studer's stannylphosphine technology is reliable enough to be applied to the construction of interesting π-conjugated frameworks. In collaboration with Yamaguchi, Studer invented a new radical reagent $(Me_3Sn)_2PPh$ for the synthesis of highly strained bis(phosphoryl)-bridged biphenyls (Scheme 20) [46]. Subsequently, Liu reported an efficient synthesis of bis(phosphoryl)-bridged ladder triphenylene by means of the radical clipping with $(Me_3Sn)_2PPh$ (Scheme 21) [47]. In light of the increasing importance of phosphoryl-bridged π-conjugated skeletons in organic material sciences, $(Me_3Sn)_2PPh$ will serve as a key reagent.

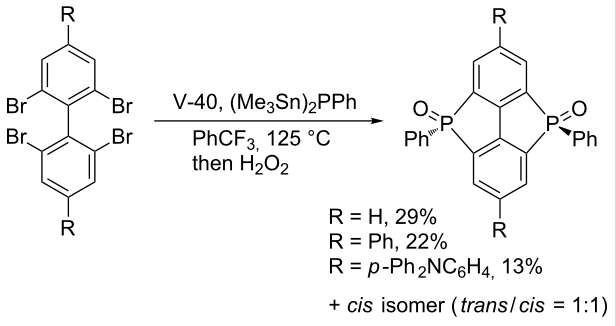

Scheme 20: Bis(phosphoryl)-bridged biphenyls by radical phosphination.

Ogawa developed photoinduced phosphination of perfluoroalkyl iodides with tetraorganodiphosphines (Scheme 22) [48]. Remarkably, the phosphination proceeds quantitatively. The phosphine ligands thus synthesized are fluorophilic. Particu-

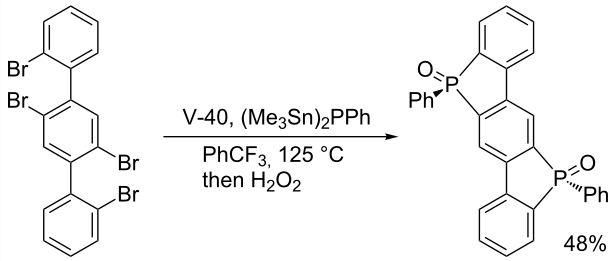

Scheme 21: Bis(phosphoryl)-bridged ladder triphenylene by radical phosphination.

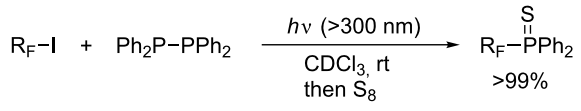

R_F = $C_{10}F_{21}$, C_8F_{17}, C_6F_{13}, C_4F_9,
c-C_6F_{11}, iC_3F_7, -$(CF_2)_6$-, -$(CF_2)_4$-

Scheme 22: Photoinduced phosphination of perfluoroalkyl iodides with tetraphenyldiphosphine.

larly, two molecules of perfluorodecyldiphenylphosphine coordinate to palladium dichloride to form a catalytically active palladium complex that is useful for a fluorous/organic biphasic system.

Cummins devised radical phosphination of bromobenzene or bromocyclohexane with white phosphorus by means of a trivalent titanium complex (Scheme 23) [49]. This represents a unique direct method for preparing triorganophosphine without recourse to any trivalent phosphorus sources such as PCl_3.

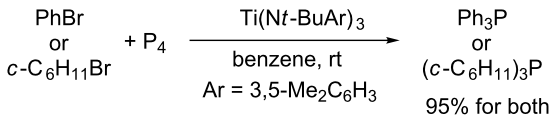

Scheme 23: Ti(III)-mediated radical phosphination of organic bromides with white phosphorus.

Conclusion

Introduction of a phosphorus atom by a radical process has offered an intriguing tool for the synthesis of organophosphorus compounds. Radical addition of a phosphorus-centered radical has been representative so far. A recent dramatic growth in reports of homolytic substitution at phosphorus in organic synthesis has changed the landscape of radical phosphination. Radical addition that involves homolytic substitution at phosphorus always culminates in difunctionalization of a multiple bond. Therefore this methodology will find application in the synthesis of complex phosphines including bidentate ones. Radical substitution of halogen in organic halide with phosphorus will be an alternative to classical ionic substitution. Advantageously, it requires neither highly basic conditions nor transition metals. Homolytic substitution at phosphorus is still in its infancy. In light of the rich chemistry of organophosphorus compounds, it will find wider application in organic synthesis in the future.

Acknowledgements

Preparation of this article and parts of synthetic chemistry in this article were supported by JSPS and MEXT (Grants-in-Aid for Scientific Research, Nos. 24685007, 23655037, 22106523, and 24106721 “Reaction Integration”) and by The Uehara Memorial Foundation, NOVARTIS Foundation for the Promotion of Science, Kinki Invention Center, and Takeda Science Foundation. Special thanks are given to those listed as the coauthors in our papers cited herein, particularly to Dr. Akinori Sato, Dr. Azusa Kondoh, and Professor Koichiro Oshima for their invaluable contributions.

References

1. *Organophosphorus Chemistry;* Royal Society of Chemistry: Cambridge, U.K.; Vol. 1–40.
2. *New Aspects in Phosphorus Chemistry;* Springer: Berlin, Germany; Vol. 1–5.
3. Mathey, F., Ed. *Science of Synthesis: Houben-Weyl Methods of Molecular Transformation;* Thieme: Stuttgart, Germany, 2008; Vol. 42.
4. Murphy, P. J., Ed. *Organophosphorus Reagents;* Oxford University Press: Oxford, U.K., 2004.
5. Beletskaya, I. P.; Kazankova, M. A. *Russ. J. Org. Chem.* **2002,** *38,* 1391–1430. doi:10.1023/A:1022685801622
6. Schwan, A. L. *Chem. Soc. Rev.* **2004,** *33,* 218–224. doi:10.1039/b307538a
7. Tappe, F. M. J.; Trepohl, V. T.; Oestreich, M. *Synthesis* **2010,** 3037–3062. doi:10.1055/s-0030-1257960
8. Wicht, D. K.; Glueck, D. S. Hydrophosphination and Related Reactions. In *Catalytic Heterofunctionalization;* Togni, A.; Grützmacher, H., Eds.; Wiley: Weinheim, Germany, 2001. doi:10.1002/3527600159.ch5
9. Alonso, F.; Beletskaya, I. P.; Yus, M. *Chem. Rev.* **2004,** *104,* 3079–3159. doi:10.1021/cr0201068
10. Tanaka, M. *Top. Curr. Chem.* **2004,** *232,* 25–54. doi:10.1007/b13778
11. Delacroix, O.; Gaumont, A. C. *Curr. Org. Chem.* **2005,** *9,* 1851–1882. doi:10.2174/138527205774913079
12. Baralle, A.; Baroudi, A.; Daniel, M.; Fensterbank, L.; Goddard, J.-P.; Lacôte, E.; Larraufie, M.-H.; Maestri, G.; Malacria, M.; Olivier, C. Main-Group Elements in Radical Chemistry. *In Encyclopedia of Radicals in Chemistry, Biology and Materials;* Wiley: Weinheim, Germany, 2012; Vol. 2, Chapter 28. doi:10.1002/9781119953678.rad023
13. Leca, D.; Fensterbank, L.; Lacôte, E.; Malacria, M. *Chem. Soc. Rev.* **2005,** *34,* 858–865. doi:10.1039/b500511f
14. Walling, C.; Pearson, M. S. *Top. Phosphorus Chem.* **1966,** *3,* 1–56.

15. Stacy, F. W.; Harris, J. F. *Org. React.* **1963,** *13,* 150–376.
16. Kyne, S. H.; Schiesser, C. H. Intramolecular Homolytic Substitution in Synthesis. In *Encyclopedia of Radicals in Chemistry, Biology and Materials;* Chatgilialoglu, C.; Studer, A., Eds.; Wiley: Weinheim, Germany, 2012; Vol. 2, Chapter 24. doi:10.1002/9781119953678.rad018
17. Schiesser, C. H.; Wild, L. M. *Tetrahedron* **1996,** *52,* 13265–13314. doi:10.1016/0040-4020(96)00809-5
18. Crich, D. *Helv. Chim. Acta* **2006,** *89,* 2167–2182. doi:10.1002/hlca.200690204
19. Walton, J. C. *Acc. Chem. Res.* **1998,** *31,* 99–107. doi:10.1021/ar970259v
20. Bentrude, W. G. *Acc. Chem. Res.* **1982,** *15,* 117–125. doi:10.1021/ar00076a004
21. Bentrude, W. G. Chapter 22: Phosphorus Radicals. In *Free Radicals;* Kochi, J. K., Ed.; Wiley: Weinheim, Germany, 1973; Vol. 2.
22. Schumann, H.; Jutzi, P.; Schmidt, M. *Angew. Chem., Int. Ed. Engl.* **1965,** *4,* 869. doi:10.1002/anie.196508692
23. Schumann, H. *Angew. Chem., Int. Ed. Engl.* **1969,** *8,* 937–950. doi:10.1002/anie.196909371
24. Mitchell, T. N.; Belt, H.-J. *J. Organomet. Chem.* **1988,** *345,* C28–C30. doi:10.1016/0022-328X(88)80105-0
25. Mitchell, T. N.; Belt, H.-J. *J. Organomet. Chem.* **1990,** *386,* 167–176. doi:10.1016/0022-328X(90)85241-P
26. Lamas, M.-C.; Studer, A. *Org. Lett.* **2011,** *13,* 2236–2239. doi:10.1021/ol200483p
27. Tzschach, A.; Baensch, S. *J. Prakt. Chem.* **1971,** *313,* 254–258. doi:10.1002/prac.19713130209
28. Sato, A.; Yorimitsu, A.; Oshima, K. *Angew. Chem., Int. Ed.* **2005,** *44,* 1694–1696. doi:10.1002/anie.200462603
29. Kawaguchi, S.-i.; Nagata, S.; Shirai, T.; Tsuchii, K.; Nomoto, A.; Ogawa, A. *Tetrahedron Lett.* **2006,** *47,* 3919–3922. doi:10.1016/j.tetlet.2006.03.165
30. Kawaguchi, S.-i.; Ogawa, A. *J. Synth. Org. Chem., Jpn.* **2010,** *68,* 705–717. doi:10.5059/yukigoseikyokaishi.68.705
31. Morse, K. W.; Morse, J. G. *J. Am. Chem. Soc.* **1973,** *95,* 8469–8470. doi:10.1021/ja00806a057
32. Morse, J. G.; Morse, K. W. *Inorg. Chem.* **1975,** *14,* 565–569. doi:10.1021/ic50145a024
33. Glanville, W. K.; Morse, K. W.; Morse, J. G. *J. Fluorine Chem.* **1976,** *7,* 153–158. doi:10.1016/S0022-1139(00)83992-5
34. Morse, J. G.; Mielcarek, J. J. *J. Fluorine Chem.* **1988,** *40,* 41–49. doi:10.1016/S0022-1139(00)81060-X
35. Wada, T.; Kondoh, A.; Yorimitsu, A.; Oshima, K. *Org. Lett.* **2008,** *10,* 1155–1157. doi:10.1021/ol800059n
36. Sato, A.; Yorimitsu, A.; Oshima, K. *Tetrahedron* **2009,** *65,* 1553–1558. doi:10.1016/j.tet.2008.12.071
37. Shirai, T.; Kawaguchi, S.-i.; Nomoto, A.; Ogawa, A. *Tetrahedron Lett.* **2008,** *49,* 4043–4046. doi:10.1016/j.tetlet.2008.04.068
38. Kawaguchi, S.-i.; Shirai, T.; Ohe, T.; Nomoto, A.; Sonoda, M.; Ogawa, A. *J. Org. Chem.* **2009,** *74,* 1751–1754. doi:10.1021/jo8020067
39. Kawaguchi, S.-i.; Ohe, T.; Shirai, T.; Nomoto, A.; Sonoda, M.; Ogawa, A. *Organometallics* **2010,** *29,* 312–316. doi:10.1021/om9008982
40. Sakurai, H.; Okamoto, Y. *J. Synth. Org. Chem., Jpn.* **1976,** *34,* 203–214.
41. Barton, D. H. R.; Bridon, D.; Zard, S. Z. *Tetrahedron Lett.* **1986,** *27,* 4309–4312. doi:10.1016/S0040-4039(00)94261-8
42. Barton, D. H. R.; Zhu, J. *J. Am. Chem. Soc.* **1993,** *115,* 2071–2072. doi:10.1021/ja00058a082
43. Sato, A.; Yorimitsu, A.; Oshima, K. *J. Am. Chem. Soc.* **2006,** *128,* 4240–4241. doi:10.1021/ja058783h
44. Vaillard, S. E.; Mück-Lichtenfeld, C.; Grimme, S.; Studer, A. *Angew. Chem., Int. Ed.* **2007,** *46,* 6533–6536. doi:10.1002/anie.200701650
45. Bruch, A.; Ambrosius, A.; Fröhlich, R.; Studer, A.; Guthrie, D. B.; Zhang, H.; Curran, D. P. *J. Am. Chem. Soc.* **2010,** *132,* 11452–11454. doi:10.1021/ja105070k
46. Bruch, A.; Fukazawa, A.; Yamaguchi, E.; Yamaguchi, S.; Studer, A. *Angew. Chem., Int. Ed.* **2011,** *50,* 12094–12098. doi:10.1002/anie.201104114
47. Hanifi, D.; Pun, A.; Liu, Y. *Chem.–Asian J.* **2012,** *7,* 2615–2620. doi:10.1002/asia.201200631
48. Kawaguchi, S.-i.; Minamida, Y.; Ohe, T.; Nomoto, A.; Sonoda, M.; Ogawa, A. *Angew. Chem., Int. Ed.* **2013,** *52,* 1748–1752. doi:10.1002/anie.201207383
49. Cossairt, B. M.; Cummins, C. C. *New J. Chem.* **2010,** *34,* 1533–1536. doi:10.1039/c0nj00124d

License and Terms

Beilstein Journal of Organic Chemistry

Metal-free aerobic oxidations mediated by *N*-hydroxyphthalimide. A concise review

Lucio Melone[1,2] and Carlo Punta[*1,2]

Review

Open Access

Address:
[1]Department of Chemistry, Materials, and Chemical Engineering "Giulio Natta", Politecnico di Milano, Piazza L. Da Vinci 32, Milano 20131, Italy and [2]INSTM, National Consortium of Materials Science and Technology, Local Unit Politecnico di Milano, Italy

Email:
Carlo Punta[*] - carlo.punta@polimi.it

* Corresponding author

Keywords:
autoxidation; free-radicals; metal-free; molecular oxygen; *N*-hydroxyphthalimide

Beilstein J. Org. Chem. **2013,** *9,* 1296–1310.
doi:10.3762/bjoc.9.146

Received: 08 May 2013
Accepted: 12 June 2013
Published: 02 July 2013

This article is part of the Thematic Series "Organic free radical chemistry".

Guest Editor: C. Stephenson

Abstract

Since the beginning of the century, *N*-hydroxyphthalimide and related compounds have been revealed to be efficient organocatalysts for free-radical processes and have found ample application in promoting the aerobic oxidation of a wide range of organic substrates. When combined with different co-catalysts, they are activated to the corresponding *N*-oxyl radical species and become able to promote radical chains, involving molecular oxygen, directly or indirectly. Most of the examples reported in the literature describe the use of these *N*-hydroxy derivatives in the presence of transition-metal complexes. However, eco-friendly standards, including the demand for highly selective transformations, impose the development of metal-free processes, especially for large-scale productions, as in the case of the oxygenation of hydrocarbons. For this reason, many efforts have been devoted in the past decade to the design of new protocols for the activation of *N*-hydroxy imides in the presence of nonmetal initiators. Herein we provide a concise overview of the most significant and successful examples in this field, with the final aim to furnish a useful instrument for all scientists actively involved in the O_2-mediated selective oxidation of organic compounds and looking for environmentally safe alternatives to metal catalysis.

Introduction

The development of efficient and cheap catalytic systems for the selective oxidation of organic substrates under mild and environmentally benign conditions represents one of the major challenges in organic synthesis [1]. In this context, the replacement of traditional oxidants, often used in stoichiometric amounts, with molecular oxygen is mandatory in order to improve the beneficial impact of selective oxidation on industrial chemistry [2-5]. Nevertheless, classical autoxidation is usually very slow at low temperatures, and catalysis is required to activate O_2. Transition-metal salts are particularly effective for this scope [6], but their use is often detrimental for the selectivity of the process and they would not meet the standards of

"green chemistry". An alternative catalytic route is based on the use of *N*-hydroxy imides (NHIs), and in particular *N*-hydroxyphthalimide (NHPI), which have found ample application as ideal catalysts for the aerobic oxidation of organic substrates [7-11].

NHPI acts as a precursor of the phthalimide *N*-oxyl (PINO) radical, which is the effective catalyst promoting hydrogen-abstraction processes (Scheme 1).

The reactivity of NHPI and PINO is related to the bond dissociation energy (BDE) of the O–H group, which was estimated at 88.1 kcal/mol [12]. This value is similar to the BDE of O–H in hydroperoxides, suggesting that the faster reactivity of PINO compared to peroxyl radicals should be attributed to an enhanced polar effect involved in the hydrogen abstraction by this nitroxyl radical [13]. Furthermore, NHPI also behaves as a relatively good hydrogen donor even at low temperatures (k_H = 7.2 × 10^3 $M^{-1}s^{-1}$) [12], trapping peroxyl radicals before they undergo termination.

PINO generation represents the key step of the overall process. Many transition metal salts and complexes have been successfully used as co-catalysts for NHPI activation. However, once again their use should be avoided in order to improve the sustainability of the process. For this reason, in the past decade several efforts have been devoted to the development of catalytic systems for the metal-free activation of NHIs under mild conditions. With an overview on the results reported in the literature in the past decade, we aim to describe herein the most significant examples related to the selective oxidation of organic molecules with molecular oxygen, catalyzed by NHIs in the presence of nonmetal cocatalysts. After briefly describing the role of classical radical initiators obtained by thermal decomposition, we will focus on some intriguing redox systems, including nitric oxides, laccase, quinones and aldehydes, which allow operation under very mild conditions, offering efficient alternative solutions to the classical autoxidation processes, especially in the field of the selective oxygenation of hydrocarbons.

Review

Radical initiation by thermal decomposition

Thermal decomposition of peroxides and azo-compounds is a well-known technique generally used to generate radicals in solution. Ishii and co-workers widely investigated the key role of these initiators in promoting the formation of PINO, performing several selective transformations under aerobic or anaerobic conditions.

The combination of NHPI with tiny amounts of dibenzoyl peroxide (BPO) under an atmosphere of argon led to the

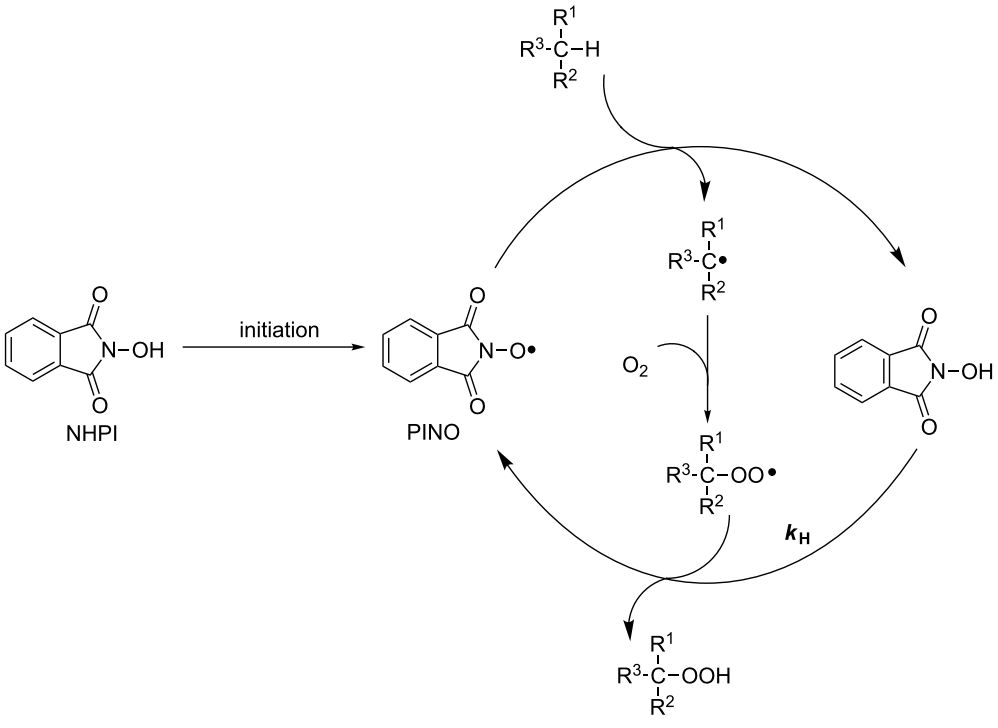

Scheme 1: Catalytic role of NHPI in the selective oxidation of organic substrates.

hydroacylation of simple alkenes by addition of acyl radicals derived from aldehydes and masked aldehydes, such as 1,3-dioxolanes (Scheme 2) [14,15].

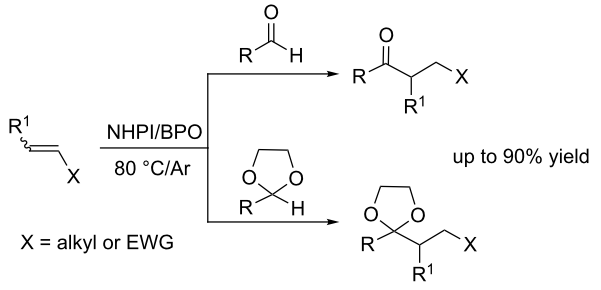

Scheme 2: Radical addition of aldehydes and analogues to alkenes.

The mediating role of NHPI allowed this approach to be extended to electron-deficient olefins [15], preventing the polymerization that easily occurs with these substrates in the presence of radical initiators.

Azo-initiators were mainly employed for the synthesis of phenol derivatives by aerobic oxidation of isopropyl aromatics. For example, the oxidation of 2,6-diisopropylnaphthalene with air in the presence of α,α'-azobisisobutyronitrile (AIBN) and NHPI, followed by decomposition with sulfuric acid of the dihydroperoxide oxidation product, gave the corresponding 2,6-naphthalenediol in 92% yield (Scheme 3) [16].

As expected, the replacement of AIBN with a transition-metal complex ($Co(OAc)_2$) resulted in a collapse of selectivity due to the redox decomposition of the hydroperoxides. This catalytic system was also applied to the oxygenation of 1,3,5-triisopropylbenzene [17]. However, in this case the conversion of all isopropyl groups was far from being reached, with mono- and di-phenols being the major products, while the yield in benzene-1,3,5-triol was close to 1%.

Sheldon and co-workers tested several commercially available azo-compounds (including AIBN and 2,2'-azobis(2,4-dimethylvaleronitrile) (AMVN)) as radical initiators at different temperatures for the NHPI-catalyzed oxidation of cyclohexylbenzene (CHB) to the corresponding hydroperoxides, finding a high selectivity in the oxygenation at the 1-position (CHBHP, Scheme 4) [18]. The selectivity decreased rapidly with increasing conversion and temperature. The use of CHBHP itself as radical initiator in place of azo-compounds required higher temperatures (100–120 °C), leading to conversions up to 20%, but to the detriment of the selectivity (72%).

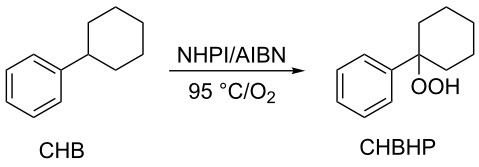

Scheme 4: NHPI/AIBN-promoted aerobic oxidation of CHB.

An analogous catalytic system was employed by Punta et al. [19] for the selective peroxidation of polyunsaturated fatty acids (PUFA), a transformation of high biological interest [20]. The combination of *N*-methylbenzohydroxamic acid (NMBHA) with 2,2'-azobis(4-methoxy-2,4-dimethylvaleronitrile) (MeO-AMVN), an azo initiator that decomposes at physiological temperatures 15 times faster than the corresponding AMVN, allowed the *trans,cis* conjugated hydroperoxides to be obtained exclusively and in good yields by direct oxygenation of the corresponding lipids. In fact, due to its ideal O–H BDE value (79.2 kcal/mol [12]), NMBHA turned out to be a better candidate than NHPI to act both as autoxidation catalyst, promoting the hydrogen abstraction from the bisallylic C–H position of the fatty esters by means of the corresponding amidoxyl radical, and as a good hydrogen donor ($k_H = 1.2 \times 10^5$ $M^{-1}s^{-1}$ [19]) trapping *trans,cis* peroxyl radicals before they underwent β-fragmentation (Scheme 5).

In accordance with this free-radical mechanism, Schmidt and Alexanian more recently reported the aerobic dioxygenation of alkenyl *N*-aryl hydroxamic acids (Scheme 6) [21]. In this case dioxygenation proceeded under 1 atmosphere of O_2 alone, without any additional initiator being required.

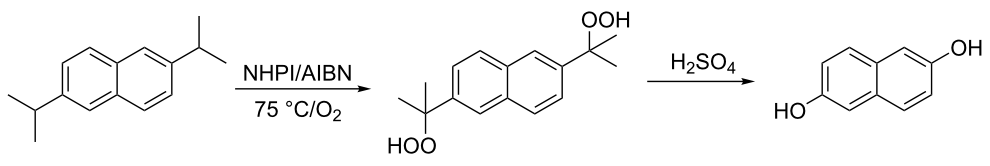

Scheme 3: NHPI/AIBN-promoted aerobic oxidation of 2,6-diisopropylnaphthalene.

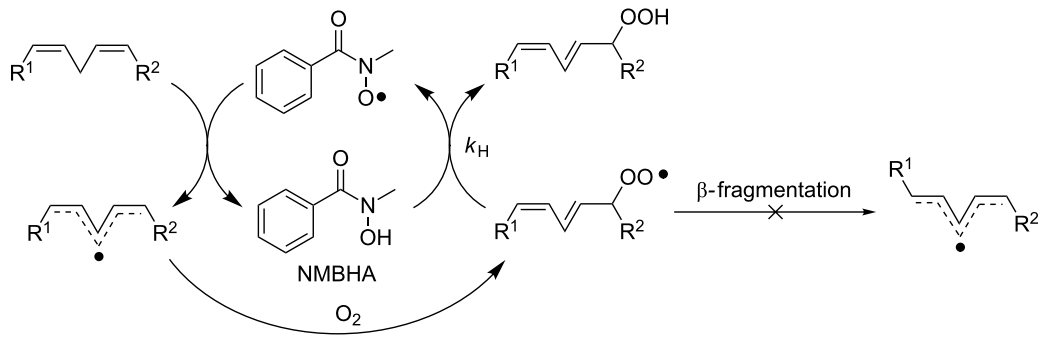

Scheme 5: NMBHA/MeOAMVN promoted aerobic oxidation of PUFA.

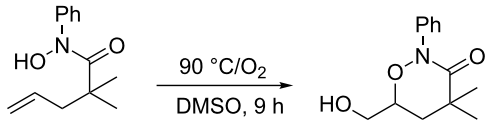

Scheme 6: Alkene dioxygenation by means of *N*-aryl hydroxamic acid and O_2.

Radical initiation by redox processes

Nitrogen oxides and nitric acid

The PINO activation by means of nitric oxide was first reported by Ishii et al. in 1997 [22]. By reacting adamantane in a mixed solvent of benzonitrile and acetic acid under an atmosphere of NO and in the presence of catalytic amounts of NHPI he observed the formation of 1-*N*-adamantylbenzamide as a principal product (Scheme 7), while when operating under the same conditions but in the presence of molecular oxygen, 1-nitroadamantane was achieved in good yields.

Moreover, by simply moving into acetonitrile, they observed the selective oxygenation of phthalane to the corresponding phthalaldehyde in 80% yield [23]. In both cases the reaction proceeds via the formation of a carbocation intermediate (Scheme 7).

The same research group also reported the efficient air-assisted nitration of alkanes [24] and alkyl side-chain aromatic compounds [25] by nitrogen dioxide and nitric acid, under NHPI catalysis (Scheme 8).

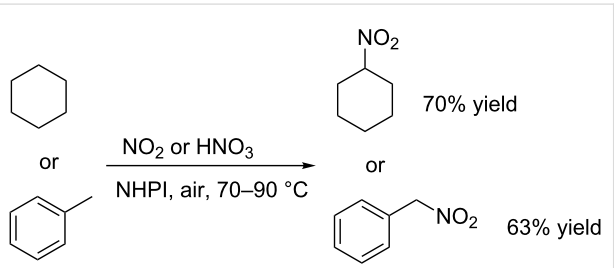

Scheme 8: Nitration of alkanes and alkyl side-chains of aromatics.

Both HNO_3 and NO_2 are able to promote the formation of PINO according to path (a) and (b) reported in Scheme 9. These initiation steps lead to the formation of HNO_2 which, in turn, is

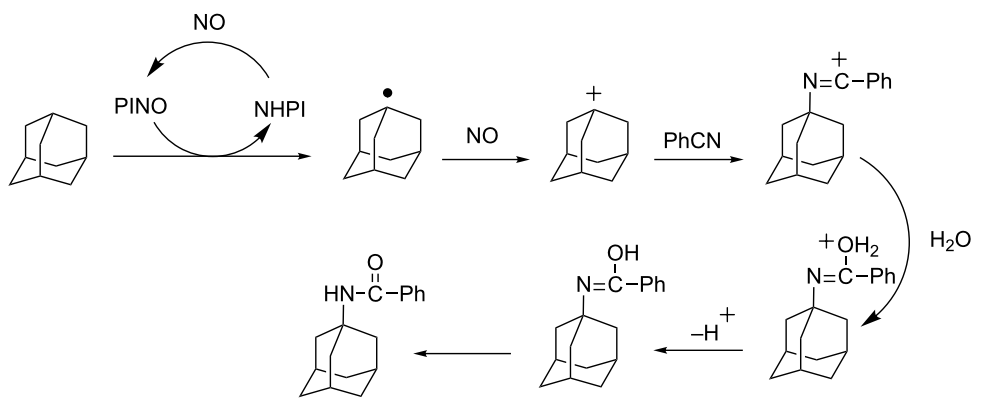

Scheme 7: NHPI-catalyzed reaction of adamantane under NO atmosphere.

converted into HNO_3, H_2O, and NO. The latter is oxidized by molecular oxygen back to NO_2, thus justifying the higher efficiency of the NO_2/air system if compared with anaerobic conditions.

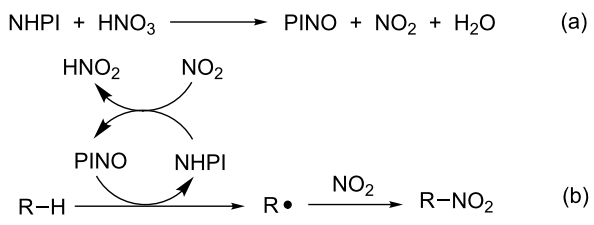

Scheme 9: Radical mechanism for the nitration of alkanes catalyzed by NHPI.

In this context, we reported in 2004 that the $HNO_3/O_2/I_2$ system could promote the nitric aerobic oxidation of alkylbenzenes under NHPI-catalysis, leading to the selective formation of benzyl alcohols through the corresponding acetates, if operating in acetic acid solution (Scheme 10) [26]. According to the proposed mechanism, being that the concentrations of NO_2 and O_2 are much lower than that of I_2, benzyl radicals generated from hydrogen abstraction by PINO react faster with the latter one, forming benzyl iodides selectively. Under the described reaction medium benzyl iodides undergo solvolysis, affording the corresponding benzyl acetates in excellent yields.

Enzyme laccase

Enzyme laccase is a family of "blue-copper" oxidase proteins, containing four copper ions in the active site, which cooperates in the degradation of the biopolymer lignin in woody tissues. With respect to other powerful oxidant enzymes, laccase has a lower redox potential. For this reason, its catalytic action by promoting single-electron oxidation steps is effective only on the phenolic moieties of lignin, with the concomitant reduction of oxygen to water.

Nevertheless, the use of suitable mediators allowed the field of application of this enzyme to be extended to the catalytic oxidation of a wider range of nonphenolic substrates. Among the huge number of mediators, *N*-hydroxy derivatives (NHDs) turned out to be particularly valuable and have been widely investigated. The role of NHDs-mediators in the laccase oxidation is outlined in Scheme 11. They act as electron carriers that, once oxidized by the enzyme, diffuse in the reaction medium and in turn oxidize those organic substrates unable to enter the enzymatic pocket due to their size. Even if the activity of laccase should be ascribed to the Cu(I) inner core, the enzymatic nature of this oxidizing system allows us to consider this approach as an example of the metal-free activation of NHIs, as no further addition of transition-metal complexes is required.

Galli and co-workers [27,28] significantly contributed over the years to the interpretation of the reaction mechanism by comparing NHPI and many other NHDs (Figure 1) with 2,2'-azinobis(3-ethylbenzthiazoline-6-sulfonate) (ABTS), which was

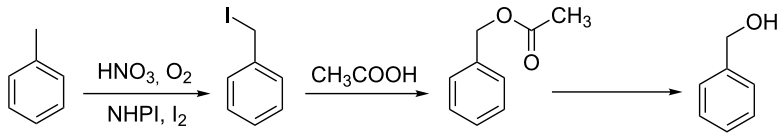

Scheme 10: Benzyl alcohols from alkylbenzenes.

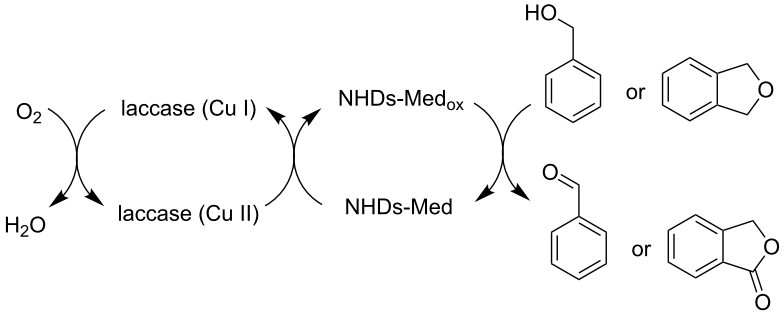

Scheme 11: Catalytic cycle of laccase-NHDs mediator oxidizing system.

the first to be used among mediators of laccase [29]. Laccase-NHDs mediator systems were successfully employed for the aerobic oxidation of nonphenolic substrates such as benzyl alcohols [27,28,30,31] and ethers [32].

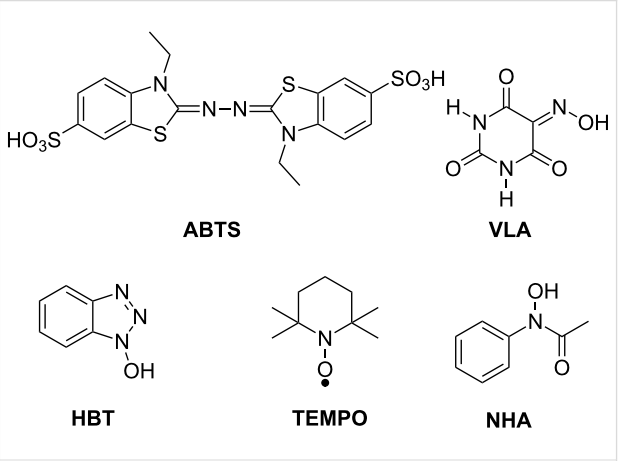

Figure 1: Mediators of laccase.

Whereas laccase-ABTS follows an electron transfer (ET) mechanism, NHPI, VLA, HBT, and NHAmediators promote a hydrogen atom transfer (HAT) route through the formation of the corresponding *N*-oxyl radicals as NHDs-Med_{ox} species (Scheme 11). The same research group also emphasized the specialization of mediators versus the substrate. In fact, the laccase-TEMPO system, which operates through an ionic route by formation of oxammonium ion as NHDs-Med_{ox}, resulted in particularly efficient promotion of the oxidation of benzyl alcohols, while it gave poor performances when applied in the presence of ethers. In contrast, laccase-NHPI and laccase-HBT systems, which follow a radical mechanism, showed high catalytic activity for the oxidation of ethers.

Quinones and analogous derivatives

As stressed before, the promotion of biological oxygenation is usually mediated by one-electron transfers, which lead to the formation of radicals. On the basis of this consideration, Xu and co-workers suggested that quinones, ubiquitous in nature and often involved in ET chains, could be employed to design biomimetic oxygenation models for the activation of NHPI [33]. The catalytic redox cycle is reported in Scheme 12.

The one-electron-transfer interaction of antraquinone (AQ) with NHPI in zeolite HY, followed by hydrogen-atom transfer, successfully led to the formation of the PINO radical, which in turn was responsible for the propagation of the radical chain in the selective oxidation of ethylbenzene to the corresponding acetophenone [33]. Among the different AQ derivatives that were tested, 1,4-diamino-2,3-dichloro-antraquinone (DADCAQ) was the most effective in terms of both conversion and selectivity of the ketone product.

The potential of this catalytic system was proved by extending its application, in the absence of zeolite, for the oxygenation of a wider range of hydrocarbons [34].

Moreover, the electronic effect of substituents on quinones and on the aromatic ring of NHPI was also investigated.

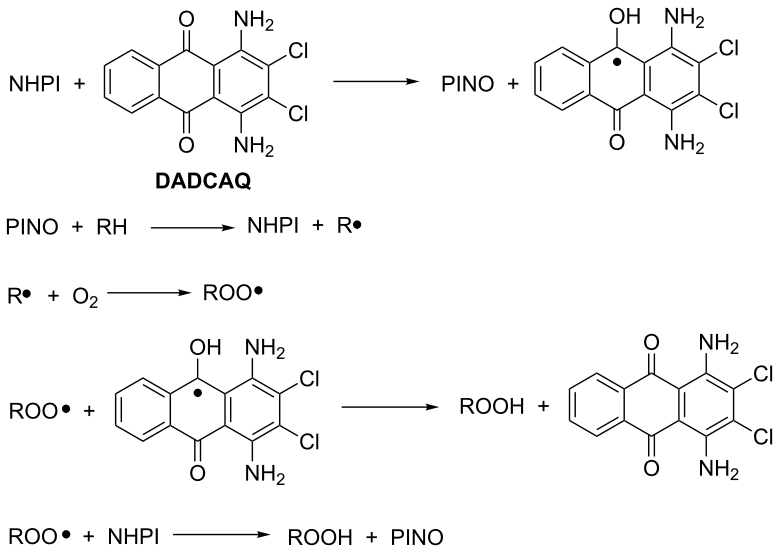

Scheme 12: DADCAQ/NHPI-mediated aerobic oxidation mechanism.

Quinones bearing halogen groups were used in the selective oxidation of alkylarenes, alkenes and alkanes [35], revealing how the moderate electron-withdrawing power of the substituents had a beneficial effect on the ET process. The combined activity of tetrabromo-1,4-benzoquininone (TBBQ) and NHPI afforded the best results.

Aryl-tetrahalogenated NHPI derivatives were also prepared and used in combination with DADCAQ for the oxidation of ethylbenzene [36]. In particular, aryl-tetrachloro-NHPI (TCNHPI) allowed significantly higher conversion and selectivity with respect to the NHPI/DADCAQ classical system (Scheme 13).

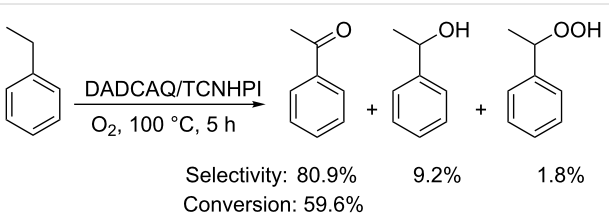

Scheme 13: DADCAQ/TCNHPI mediated aerobic oxidation of ethylbenzene.

More recently, analogous results were achieved by combining NHPI with 2,3-dichloro-5,6-dicyanobenzoquinone (DDQ) [37].

Xu et al. also reported a similar one-electron-transfer activation of NHPI promoted by nonmetal xanthone and tetramethylammonium chloride (TMAC), for the selective oxidation of hydrocarbons (Scheme 14) [38]. In the proposed mechanism, TMAC has the unique role of decomposing the hydroperoxide intermediate, prolonging the free-radical chain [39-41].

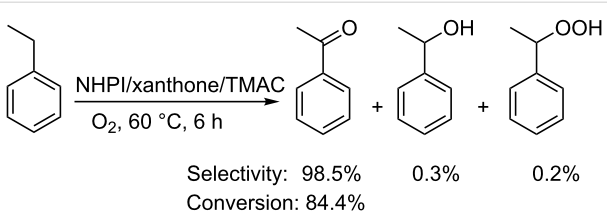

Scheme 14: NHPI/xanthone/TMAC mediated aerobic oxidation of ethylbenzene.

The NHPI-activation by AQ has been also adopted by other research groups. Li and co-workers applied the NHPI/AQ system to promote the metal and solvent-free oxidation of α-isophorone to ketoisophorone, preventing the isomerization process of the substrate to β-isophorone (Scheme 15) [42,43].

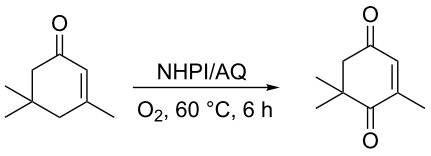

Scheme 15: NHPI/AQ-mediated aerobic oxidation of α-isophorone.

Very recently, Coseri et al. reported that NHPI [44] and other nonpersistent nitroxyl radical precursors, such as VLA, HBT and *N*-hydroxy-3,4,5,6-tetraphenylphthalimide (TPNHPI) [45], were suitable catalysts for the selective oxidation of cellulose fibers promoted by the NaClO/NaBr system (Scheme 16). According to the proposed mechanism PINO radical is oxidized to the corresponding *N*-oxammonium cation, which in turn is responsible for the oxidation of the C6 alcoholic function.

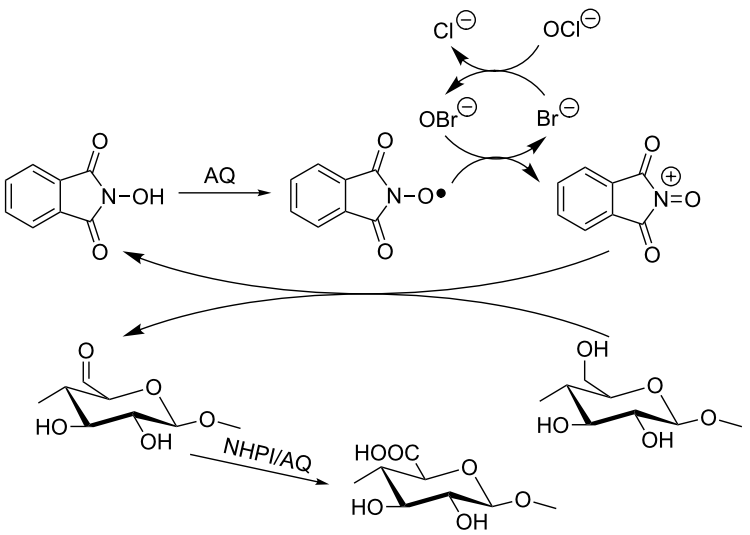

Scheme 16: NHPI/AQ-mediated oxidation of cellulose fibers by NaClO/NaBr system.

The surface modification of cellulose fibers by selectively converting primary hydroxyl groups to the corresponding carboxylic functions, maintaining the original backbone of the polysaccharide, is of major interest for different applications [46,47].

By comparing different activation approaches, including transition-metal complexes, Coseri found that the NHPI/AQ catalytic system allowed higher conversion of hydroxyl groups. A comparison study on the effect of TEMPO and PINO radicals on the oxidation efficiency toward cellulose led to the conclusion that the NHPI/AQ oxidation mediator affords the highest content of carboxylic groups and better preserves the morphology and the molecular weight of the starting material [48].

Moreover, this catalytic system could be employed with dioxygen in place of NaClO as the ultimate oxidizing agent [49]. In this case, the mechanism follows a radical chain via classical HAT by PINO abstraction (Scheme 17).

Aldehydes and the molecule-induced homolysis

Sacrificial reductants have been widely reported in the literature as reactive agents able to promote the autoxidation reaction of less-reactive hydrocarbons. In this context, aldehydes have attracted increasing attention [50].

In principle, the aerobic co-oxidation promoted by aldehydes could be considered a nongreen and expensive process, due to the need for sacrificial reagents. However, this approach for oxygen activation could become competitive for practical application if the high efficiency in substrate conversion, the high selectivity in the final product, and/or the field of application, together with the low cost and environmental impact of the selected aldehyde, were significant enough to justify the reagent sacrifice. Moreover, co-oxidation of aldehydes would become attractive also if the acyl derivatives were not used as stoichiometric reagents, but just in catalytic amounts as initiators of free-radical chains.

The use of aldehydes for the activation of NHPI in an aerobic co-oxidative process was first reported by Einhorn and co-workers in 1997 [51]. The combination of stoichiometric amounts of acetaldehyde with catalytic quantities of NHPI promoted the oxidation of a wide range of hydrocarbons, including cumene and ethylbenzene, to the corresponding carbonyl groups. Under these operative conditions, peracetic acid was directly responsible for the substrate oxidation.

More recently we suggested that the NHPI/aldehyde system could promote the formation of PINO radical following a molecule-induced homolysis mechanism [52]. Molecule-induced initiation is a process driven by a thermodynamic effect and consists of a bimolecular reaction according to which an OH radical, generated from hydroperoxides or peracids, undergoes hydrogen abstraction from a suitable molecule bearing relatively weak X–H bonds. The result is the formation of two radical species and a molecule of water (Scheme 18) [53-55].

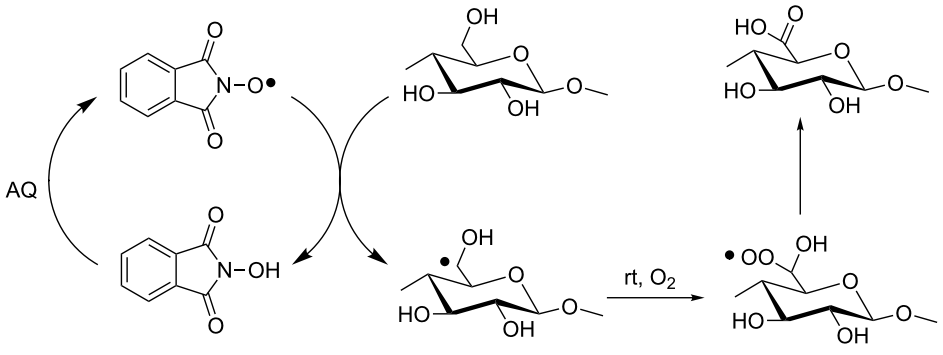

Scheme 17: NHPI/AQ mediated aerobic oxidation of cellulose fibers.

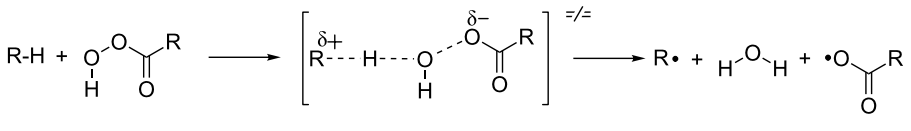

Scheme 18: Molecule-induced homolysis by peracids.

We assumed that an analogous homolysis induced by peracids could occur for this NHPI, leading to the formation of PINO radical under mild and metal-free conditions.

This hypothesis was supported by spectroscopic and analytical evidence. By simply adding NHPI to a solution of acetonitrile containing *m*- chloroperbenzoic acid we could observe the characteristic Electron Paramagnetic Resonance (EPR) spectrum of PINO radical, while *m*-chlorobenzoic acid (90%) and Cl-benzene (10%) resulted as the unique reaction products (Scheme 19, path a) [52]. When the analogous experiment was conducted in benzene as solvent, *m*-chlorobenzoate and *m*-chlorobiphenyl were also detected (Scheme 19, path b).

On the basis of these experimental results, we suggested that the aerobic oxidation of aldehydes could be performed for the in situ generation of the corresponding peracids in the presence of NHPI, promoting co-oxidative processes catalyzed by PINO.

In an early protocol, we reported the NHPI-catalyzed selective aerobic epoxidation of α-olefins and cyclic olefins in the presence of stoichiometric amounts of aldehydes [52].

The experimental results revealed an opposite selectivity with respect to classical epoxidation by peracids, with internal olefins, which were unreactive under our operating conditions. We suggested a free-radical mechanism according to which the acyl peroxyl radical generated in situ is the real epoxidizing agent (Scheme 20).

This protocol was successfully applied on a larger scale (1 liter Büchi glass vessel) for the synthesis of propylene oxide from the corresponding propene [56], and more recently under continuous-flow conditions, by means of a new multijet oscillating disk (MJOD) reactor, designed and developed by Bjørsvik and co-workers [57]. In this latter case we succeeded in accelerating the overall process, shortening the residence time with respect to the batch protocol.

On the basis of this mechanistic evidence, we also decided to investigate the Einhorn's process for the oxidation of cumene and ethylbenzene more thoroughly, as we were expected to find a high selectivity in the corresponding hydroperoxides, which were not mentioned in the first report.

Moreover, we also assumed that high amounts of aldehyde were detrimental for the selectivity of the process, the aldehyde having the unique role of initiating the radical chain by generating PINO radical by molecule-induced homolysis.

Indeed, our hypotheses were confirmed and we succeeded in increasing the selectivity in hydroperoxides up to values higher

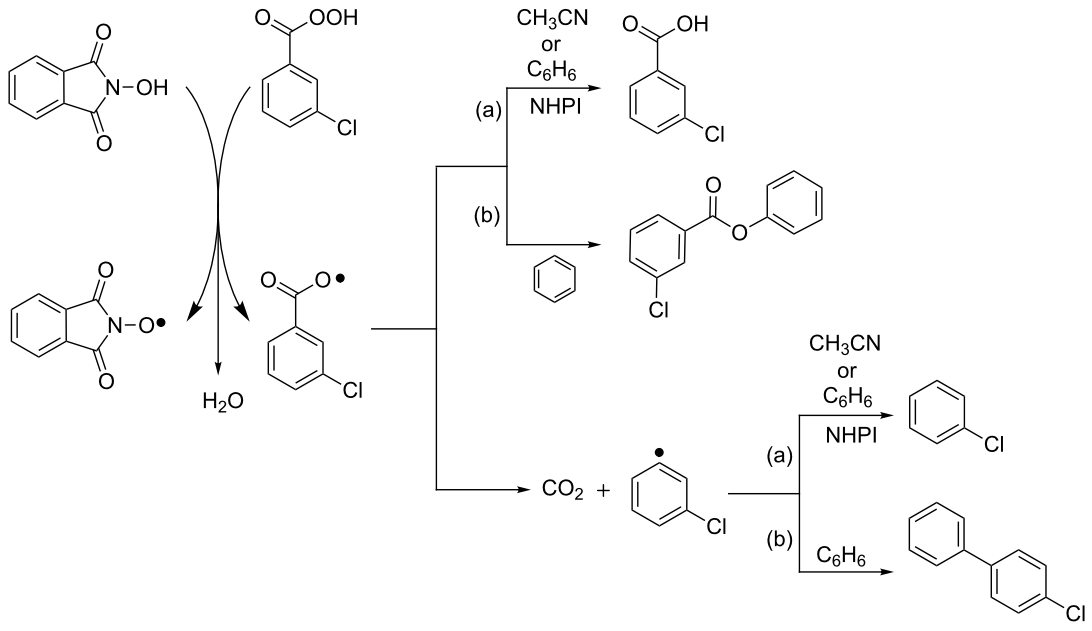

Scheme 19: Molecule-induced homolysis of NHPI/*m*- chloroperbenzoic acid system.

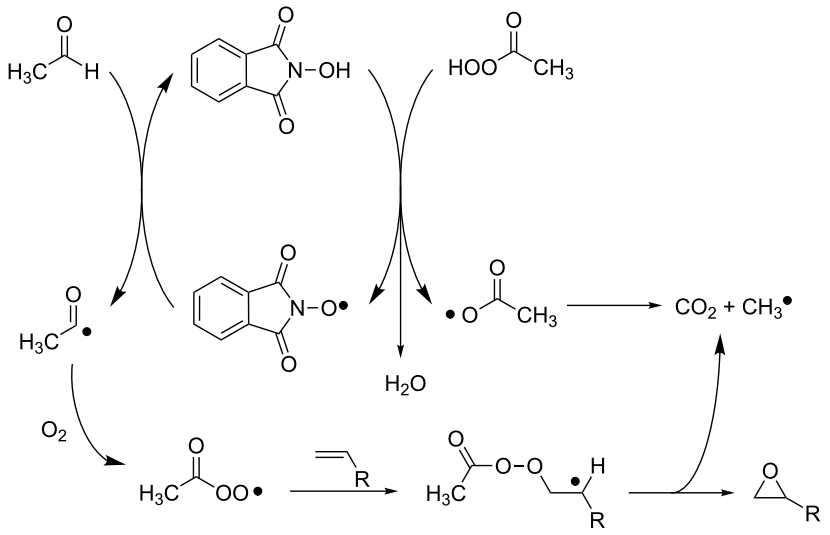

Scheme 20: Proposed mechanism for the NHPI/CH_3CHO/O_2-mediated epoxidation.

than 80% by simply reducing the amount of acetaldehyde to 10% mol ratio with respect to the alkyl aromatic [58,59] (Scheme 21).

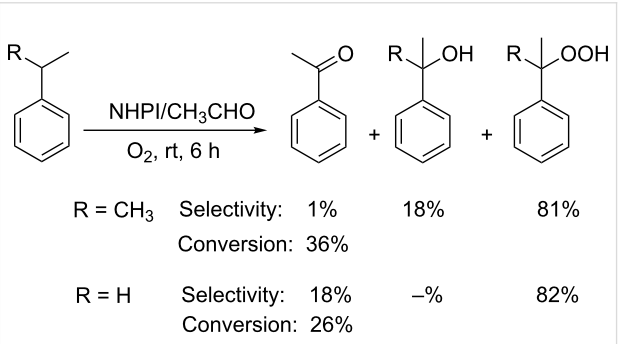

Scheme 21: NHPI/CH_3CHO-mediated aerobic oxidation of alkyl aromatics.

Thus, while the NHPI/AQ catalytic system was particularly effective in converting alkylaromatics to the corresponding carbonyl derivatives, this approach represents a valuable alternative when hydroperoxides are the desired products.

Even if the presence of a polar solvent is crucial to maintain the polar catalyst in solution, it was possible to conduct the aerobic oxidation of cumene at 70 °C in the presence of 1% NHPI, 2% of acetaldehyde, and with a volume ratio cumene/CH_3CN of 5/2, achieving the desired hydroperoxide in 28% yield with 84% of selectivity. Similarly, ethylbenzene was oxidized to the corresponding hydroperoxide with a lower yield (13%), but a higher selectivity (91%), by operating at the same temperature with 2% NHPI, 2% acetaldehyde, and with a volume ratio ethylbenzene/CH_3CN of 1/1. These results are objects of two patent applications [60,61].

Light-induced activation

The first example of light-induced in situ generation of PINO radical was reported in 2007 by Lucarini and co-workers [62]. Irradiation of *N*-alkoxyphthalimides with filtered light ($\lambda >$ 300 nm) from a mercury lamp promoted the selective homolysis of the O–C bond, leading to the formation of the *N*-oxyl radical, as documented by the strong characteristic EPR signal. The efficiency of the initiation approach was documented by measuring the dioxygen consumption during the aerobic oxidation of cumene. In the absence of light, cumene was completely inert, thus proving the intervention of the catalysts in the oxidative cycle.

This process was successfully employed in the selective oxidation of benzyl alcohol at room temperature, affording the corresponding aldehyde in 4 h, in accordance with the results previously reported by our group operating under NHPI/$Co(OAc)_2$ catalysis [63,64] (Scheme 22).

Even if this procedure seems to be particularly valuable, as no further radical mediators or initiators are required, it cannot be applied directly to NHPI.

More recently, Antonietti and co-workers have reported the photocatalytic oxidative activation of NHPI by graphitic carbon nitride (g-C_3N_4) and visible light irradiation [65].

g-C_3N_4, the most stable allotrope of carbon nitride, is a two-dimensional polymer with a tri-*s*-triazine ring unit and a

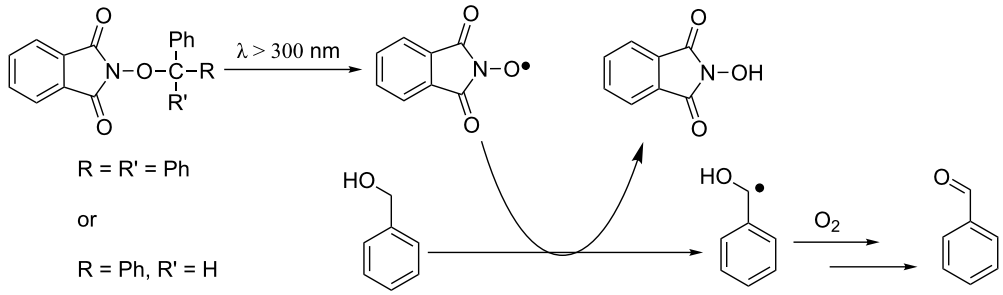

Scheme 22: Light-induced generation of PINO from *N*-alkoxyphthalimides.

π-conjugated layered structure similar to graphene. It is a medium-band-gap semiconductor and has proved to be an efficient photocatalyst for synthetic purposes [66,67].

It has been demonstrated that the excited state of g-C_3N_4, obtained by irradiation with visible light, is able to activate O_2 to the corresponding superoxide radical. The latter could undergo hydrogen abstraction from NHPI, leading to the generation of PINO.

This approach was successfully applied to promote the visible-light-induced metal-free oxidation of allylic substrates (Scheme 23).

Other initiators

In their ongoing research dedicated to NHPI activation towards the aerobic oxidation of hydrocarbons, Xu and co-workers developed other redox initiators in addition to the NHPI/quinone systems previously described.

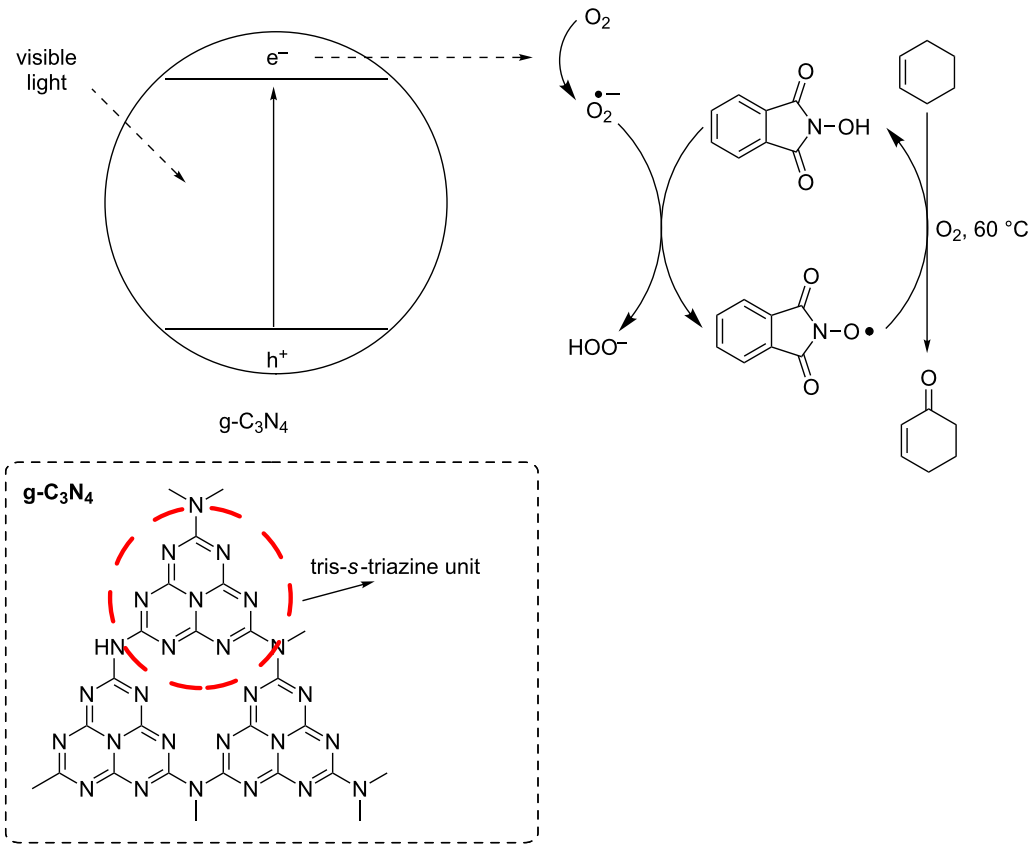

Scheme 23: Visible-light/g-C_3N_4 induced metal-free oxidation of allylic substrates.

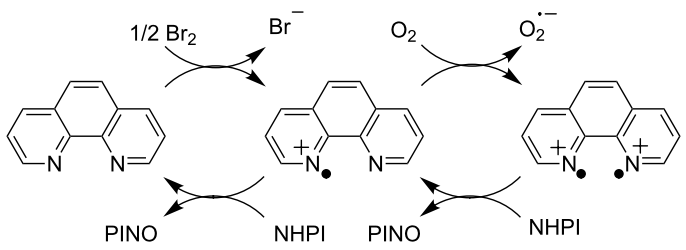

Scheme 24: NHPI/*o*-phenanthroline-mediated organocatalytic system.

In 2005 they reported the selective oxygenation of ethylbenzene to the corresponding acetophenone by means of a NHPI/*o*-phenanthroline-mediated organocatalytic system, in the presence of molecular bromine as a co-catalyst [68] (Scheme 24).

According to the proposed mechanism, Br_2 generates ET processes by oxidizing the *o*-phenanthroline to the corresponding cation radicals. The latter promote in turn ET and HAT processes with NHPI, leading to the formation of PINO.

In 2009 the same research group also performed the oxidation of ethylbenzene and other hydrocarbons by combining NHPI with alkaline-earth chlorides under an aerobic atmosphere [69]. The intervention of the PINO radical in the oxidation mechanism was confirmed by UV–vis and FTIR spectroscopy. $MgCl_2$ was found to be the most effective salt among those tested for this purpose.

An efficient and selective aerobic oxidation of hydrocarbons to their oxygenated products was also achieved by Zheng et al. by combining NHPI with dimethylglyoxime (DMG) [70]. The suggested mechanism is depicted in Scheme 25.

Once again all the approaches described above led to the formation of acetophenone as the major product of ethylbenzene oxidation.

A different result was achieved by Fierro et al. who, in the same year, reported the ethylbenzene oxidation to its hydroperoxide by operating in the presence of NHPI (or other NHIs, i.e., *N*-hydroxysuccinimide, *N*-hydroxymaleimide and *N*-hydroxynaphthalimide) and tiny amounts of sodium hydroxide (5×10^{-3} mol % with respect to ethylbenzene) at 421 K and 0.3 MPa [71]. The addition of NaOH determined a significant increase of selectivity in hydroperoxide (77.3%), while the ethylbenzene conversion slightly decreased from 24.5 to 21.3%.

Very recently NHPI was reported to catalyze selective transformations without requiring additional initiators. Jiao et al. described the catalyzed oxidative cleavage of C=C double bonds using molecular oxygen as the final oxidant [72]. Following this approach α-methylstyrene was converted to acetophenone in 80% yield by operating at 80 °C in *N*,*N*-dimethylacetamide (DMA) as solvent. A plausible mechanism is shown in Scheme 26. It is based on three experimental data sets collected by the research group: (i) The occurrence of a free-radical initiation. In fact, in the presence of the radical scavenger BHT no conversion was observed. (ii) The exclusion that epoxide could be an intermediate of the process. When 2-methyl-2-phenyloxirane was used in place of α-methylstyrene, poor results were obtained in terms of yield in acetophenone. (iii) The proof that the oxygen atom in acetophenone originated from molecular oxygen, by conducting the oxygenation in the presence of $^{18}O_2$.

Finally, Inoue and co-workers reported an efficient C(sp^3)–N bond-forming method consisting of the chemoselective conversion of C(sp^3)–H bonds in the presence of stoichiometric

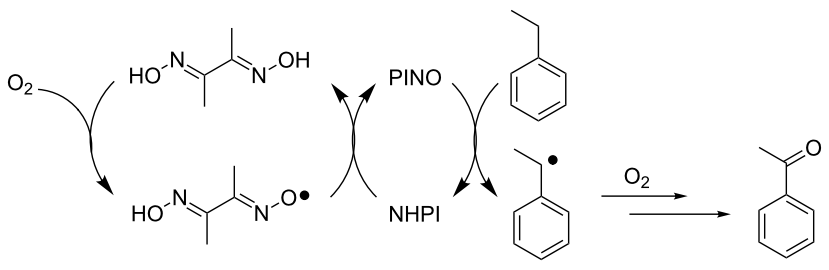

Scheme 25: NHPI/DMG-mediated organocatalytic system.

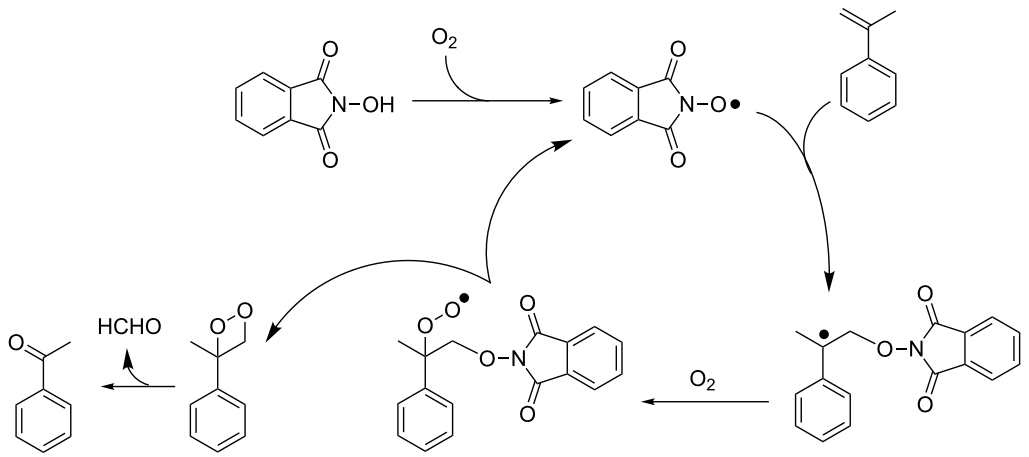

Scheme 26: NHPI catalyzed oxidative cleavage of C=C bonds.

amounts of dialkyl azodicarboxylate reagent [73]. The proposed mechanism (Scheme 27) suggests a double function of the dialkyl azodicarboxylate, which acts both as an oxidant, promoting the oxidation of NHPI to PINO by ET process, and as acceptor of carbon radicals generated via HAT by PINO, leading to the formation of hydrazine derivatives. The scope of the reaction was investigated and its applicability was extended to different C–H bonds, including benzylic, propargylic, and aliphatic ones.

Furthermore, the hydrazine compounds were readily converted to the corresponding carbamates and amines.

Conclusion

Metal-free oxidation catalyzed by *N*-hydroxyphthalimide and analogous *N*-hydroxy imides is becoming an essential tool for all research groups directly involved in the development of selective transformations mediated by molecular oxygen. This increasing interest is testified by several papers that have appeared in the past few years in this field and are herein discussed, describing intriguing free-radical routes for the generation of *N*-oxyl active species under mild conditions. The fields of application range from large-scale production, such as the selective oxidation of alkyl aromatics, to the synthesis of fine chemicals.

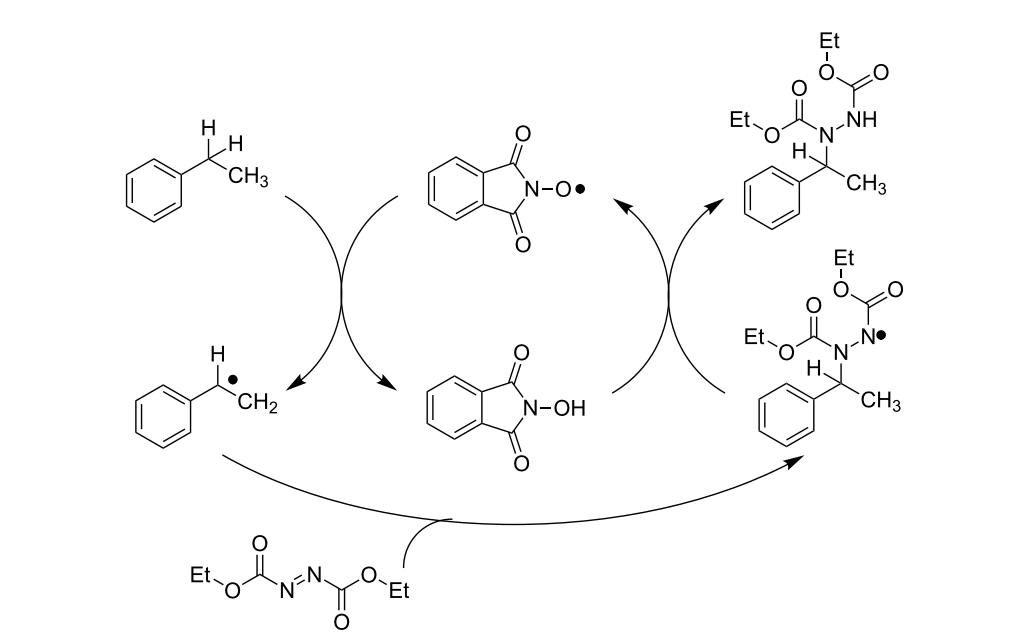

Scheme 27: Synthesis of hydrazine derivatives.

Metal-free PINO activation represents another decisive step towards the consecration of NHPI as the mediator of first choice to perform green and selective aerobic oxidations. The next one would be the engineering of valuable solutions for the complete recovery and recycle of this homogeneous organocatalyst. Once reached, this final goal, combined with the use of molecular oxygen as stoichiometric oxidant under mild operative conditions, would definitely open the way towards much more cost-effective and environmentally friendly oxidative processes.

Acknowledgements

We thank MIUR for the continuing support of our free-radical (PRIN 2010-2011, project 2010PFLRJR_005) and organic (FIRB-Future in Research 2008, project RBFR08XH0H_001) chemistry.

References

1. Bäckvall, J.-E., Ed. *Modern Oxidation Methods;* Wiley-VCH Verlag GmbH & Co. KGaA: Weinheim, Germany, 2005. doi:10.1002/3527603689
2. Hermans, I.; Peeters, J.; Jacobs, P. A. *Top. Catal.* **2008,** *48,* 41–48. doi:10.1007/s11244-008-9051-x
3. Hermans, I.; Peeters, J.; Jacobs, P. A. *Top. Catal.* **2008,** *50,* 124–132. doi:10.1007/s11244-008-9099-7
4. Hermans, I.; Spier, E. S.; Neuenschwander, U.; Turrà, N.; Baiker, A. *Top. Catal.* **2009,** *52,* 1162–1174. doi:10.1007/s11244-009-9268-3
5. Gambarotti, C.; Melone, L.; Caronna, T.; Punta, C. *Curr. Org. Chem.*, in press.
6. Punniyamurthy, T.; Velusamy, S.; Iqbal, J. *Chem. Rev.* **2005,** *105,* 2329–2364. doi:10.1021/cr050523v
7. Recupero, F.; Punta, C. *Chem. Rev.* **2007,** *107,* 3800–3842. doi:10.1021/cr040170k
8. Galli, C.; Gentili, P.; Lanzalunga, O. *Angew. Chem., Int. Ed.* **2008,** *47,* 4790–4796. doi:10.1002/anie.200704292
9. Coseri, S. *Mini-Rev. Org. Chem.* **2008,** *5,* 222–227. doi:10.2174/157019308785161675
10. Coseri, S. *Catal. Rev. - Sci. Eng.* **2009,** *51,* 218–292. doi:10.1080/01614940902743841
11. Punta, C.; Gambarotti, C. *N*-Hydroxy Derivatives: Key Organocatalysts for the Selective Free Radical Aerobic Oxidation of Organic Compounds. In *Ideas in Chemistry and Molecular Sciences: Advances in Synthetic Chemistry;* Pignataro, B., Ed.; Wiley-VCH Verlag GmbH & Co. KGaA: Weinheim, Germany, 2010; pp 3–24. doi:10.1002/9783527630554.ch1
12. Amorati, R.; Lucarini, M.; Mugnaini, M.; Pedulli, G. F.; Minisci, F.; Recupero, F.; Fontana, F.; Astolfi, P.; Greci, L. *J. Org. Chem.* **2003,** *68,* 1747–1754. doi:10.1021/jo026660z
13. Minisci, F.; Recupero, F.; Pedulli, G. F.; Lucarini, M. *J. Mol. Catal. A* **2003,** *204–205,* 63–90. doi:10.1016/S1381-1169(03)00286-3
14. Tsujimoto, S.; Iwahama, T.; Sakaguchi, S.; Ishii, Y. *Chem. Commun.* **2001,** 2352–2353. doi:10.1039/b107548a
15. Tsujimoto, S.; Sakaguchi, S.; Ishii, Y. *Tetrahedron Lett.* **2003,** *44,* 5601–5604. doi:10.1016/S0040-4039(03)01375-3
16. Aoki, Y.; Sakaguchi, S.; Ishii, Y. *Adv. Synth. Catal.* **2004,** *346,* 199–202. doi:10.1002/adsc.200303168
17. Aoki, Y.; Hirai, N.; Sakaguchi, S.; Ishii, Y. *Tetrahedron* **2005,** *61,* 10995–10999. doi:10.1016/j.tet.2005.08.087
18. Arends, I. W. C. E.; Sasidharan, M.; Kühnle, A.; Duda, M.; Jost, C.; Sheldon, R. A. *Tetrahedron* **2002,** *58,* 9055–9061. doi:10.1016/S0040-4020(02)01131-6
19. Punta, C.; Rector, C. L.; Porter, N. A. *Chem. Res. Toxicol.* **2005,** *18,* 349–356. doi:10.1021/tx049685x
20. Porter, N. A. *J. Org. Chem.* **2013,** *78,* 3511–3524. doi:10.1021/jo4001433
21. Schmidt, V. A.; Alexanian, E. J. *Angew. Chem., Int. Ed.* **2010,** *49,* 4491–4494. doi:10.1002/anie.201000843
22. Sakaguchi, S.; Eikawa, M.; Ishii, Y. *Tetrahedron Lett.* **1997,** *38,* 7075–7078. doi:10.1016/S0040-4039(97)01652-3
23. Eikawa, M.; Sakaguchi, S.; Ishii, Y. *J. Org. Chem.* **1999,** *64,* 4676–4679. doi:10.1021/jo982406o
24. Sakaguchi, S.; Nishiwaki, Y.; Kitamura, T.; Ishii, Y. *Angew. Chem., Int. Ed.* **2001,** *40,* 222–224. doi:10.1002/1521-3773(20010105)40:1<222::AID-ANIE222>3.0.CO;2-W
25. Nishiwaki, Y.; Sakaguchi, S.; Ishii, Y. *J. Org. Chem.* **2002,** *67,* 5663–5668. doi:10.1021/jo025632d
26. Minisci, F.; Recupero, F.; Gambarotti, C.; Punta, C.; Paganelli, R. *Tetrahedron Lett.* **2003,** *44,* 6919–6922. doi:10.1016/S0040-4039(03)01687-3
27. Fabbrini, M.; Galli, C.; Gentili, P. *J. Mol. Catal. B: Enzym.* **2002,** *16,* 231–240. doi:10.1016/S1381-1177(01)00067-4
28. Baiocco, P.; Barreca, A. M.; Fabbrini, M.; Galli, C.; Gentili, P. *Org. Biomol. Chem.* **2003,** *1,* 191–197. doi:10.1039/b208951c
29. Branchi, B.; Galli, C.; Gentili, P. *Org. Biomol. Chem.* **2005,** *3,* 2604–2614. doi:10.1039/b504199f
30. Cantarella, G.; Galli, C.; Gentili, P. *New J. Chem.* **2004,** *28,* 366–372. doi:10.1039/b311907f
31. Astolfi, P.; Brandi, P.; Galli, C.; Gentili, P.; Gerini, M. F.; Greci, L.; Lanzalunga, O. *New J. Chem.* **2005,** *29,* 1308–1317. doi:10.1039/b507657a
32. d'Acunzo, F.; Baiocco, P.; Galli, C. *New J. Chem.* **2003,** *27,* 329–332. doi:10.1039/b210978f
33. Yang, G.; Ma, Y.; Xu, J. *J. Am. Chem. Soc.* **2004,** *126,* 10542–10543. doi:10.1021/ja047297b
34. Yang, G.; Zhang, Q.; Miao, H.; Tong, X.; Xu, J. *Org. Lett.* **2005,** *7,* 263–266. doi:10.1021/ol047749p
35. Zhou, L.; Chen, Y.; Yang, X.; Su, Y.; Zhang, W.; Xu, J. *Catal. Lett.* **2008,** *125,* 154–159. doi:10.1007/s10562-008-9537-y
36. Zhang, Q.; Chen, C.; Ma, H.; Miao, H.; Zhang, W.; Sun, Z.; Xu, J. *J. Chem. Technol. Biotechnol.* **2008,** *83,* 1364–1369. doi:10.1002/jctb.1977
37. Yang, X.; Wang, Y.; Zhou, L.; Chen, C.; Zhang, W.; Xu, J. *J. Chem. Technol. Biotechnol.* **2010,** *85,* 564–568. doi:10.1002/jctb.2345
38. Du, Z.; Sun, Z.; Zhang, W.; Miao, H.; Ma, H.; Xu, J. *Tetrahedron Lett.* **2009,** *50,* 1677–1680. doi:10.1016/j.tetlet.2009.01.077
39. Hermans, I.; Vereecken, L.; Jacobs, P. A.; Peeters, J. *Chem. Commun.* **2004,** 1140–1141. doi:10.1039/b401050g
40. Hermans, I.; Jacobs, P. A.; Peeters, J. *Phys. Chem. Chem. Phys.* **2007,** *9,* 686–690. doi:10.1039/b616392k
41. Hermans, I.; Jacobs, P. A.; Peeters, J. *Phys. Chem. Chem. Phys.* **2008,** *10,* 1125–1132. doi:10.1039/b716932a
42. Wang, C.; Wang, G.; Mao, J.; Yao, Z.; Li, H. *Catal. Commun.* **2010,** *11,* 758–762. doi:10.1016/j.catcom.2010.02.010
43. Chen, K.; Sun, Y.; Wang, C.; Yao, J.; Chen, Z.; Li, H. *Phys. Chem. Chem. Phys.* **2012,** *14,* 12141–12146. doi:10.1039/c2cp41617d

44. Coseri, S.; Nistor, G.; Fras, L.; Strnad, S.; Harabagiu, V.; Simionescu, B. C. *Biomacromolecules* **2009,** *10,* 2294–2299. doi:10.1021/bm9004854
45. Biliuta, G.; Fras, L.; Strnad, S.; Harabagiu, V.; Coseri, S. *J. Polym. Sci., Part A: Polym. Chem.* **2010,** *48,* 4790–4799. doi:10.1002/pola.24270
46. Coseri, S.; Biliuta, G.; Simionescu, B. C.; Stana-Kleinschek, K.; Ribitsch, V.; Harabagiu, V. *Carbohydr. Polym.* **2013,** *93,* 207–215. doi:10.1016/j.carbpol.2012.03.086
47. Melone, L.; Altomare, L.; Alfieri, I.; Lorenzi, A.; De Nardo, L.; Punta, C. *J. Photochem. Photobiol., A* **2013,** *261,* 53–60. doi:10.1016/j.jphotochem.2013.04.004.
48. Biliuta, G.; Fras, L.; Drobota, M.; Persin, Z.; Kreze, T.; Stana-Kleinschek, K.; Ribitsch, V.; Harabagiu, V.; Coseri, S. *Carbohydr. Polym.* **2013,** *91,* 502–507. doi:10.1016/j.carbpol.2012.08.047
49. Biliuta, G.; Fras, L.; Harabagiu, V.; Coseri, S. *Digest J. Nanomat. Biostruct.* **2011,** *6,* 291–297.
50. Melone, L.; Punta, C. Co-oxidation processes promoted by *N*-hydroxyphthalimide/aldehyde system. In *New Developments in Aldehydes Research;* Torrioni, L.; Pescasseroni, E., Eds.; Nova Publisher, 2013; pp 121–138.
51. Einhorn, C.; Einhorn, J.; Marcadal, C.; Pierre, J.-L. *Chem. Commun.* **1997,** 447–448. doi:10.1039/a607463d
52. Minisci, F.; Gambarotti, C.; Pierini, M.; Porta, O.; Punta, C.; Recupero, F.; Lucarini, M.; Mugnaini, V. *Tetrahedron Lett.* **2006,** *47,* 1421–1424. doi:10.1016/j.tetlet.2005.12.089
53. Bravo, A.; Bjørsvik, H.-R.; Fontana, F.; Minisci, F.; Serri, A. *J. Org. Chem.* **1996,** *61,* 9409–9416. doi:10.1021/jo961366q
54. Hermans, I.; Jacobs, P. A.; Peeters, J. *Chem.–Eur. J.* **2006,** *12,* 4229–4240. doi:10.1002/chem.200600189
55. Turrà, N.; Neuenschwander, U.; Hermans, I. *ChemPhysChem* **2013,** *14,* 1666–1669. doi:10.1002/cphc.201300130.
56. Punta, C.; Moscatelli, D.; Porta, O.; Minisci, F.; Gambarotti, C.; Lucarini, M. Selective aerobic radical epoxidation of α-olefins catalyzed by *N*-Hydroxyphthalimide. In *Mechanisms in Homogeneous and Heterogeneous Epoxidation Catalysis;* Oyama, S. T., Ed.; Elsevier: Amsterdam, The Netherlands, 2008; pp 217–229. doi:10.1016/B978-0-444-53188-9.00006-7
57. Spaccini, R.; Liguori, L.; Punta, C.; Bjørsvik, H.-R. *ChemSusChem* **2012,** *5,* 261–265. doi:10.1002/cssc.201100262
58. Melone, L.; Gambarotti, C.; Prosperini, S.; Pastori, N.; Recupero, F.; Punta, C. *Adv. Synth. Catal.* **2011,** *353,* 147–154. doi:10.1002/adsc.201000786
59. Melone, L.; Prosperini, S.; Gambarotti, C.; Pastori, N.; Recupero, F.; Punta, C. *J. Mol. Catal. A* **2012,** *355,* 155–160. doi:10.1016/j.molcata.2011.12.009
60. Minisci, F.; Porta, O.; Recupero, F.; Punta, C.; Gambarotti, C.; Pierini, M. Process for the preparation of phenol by means of new catalytic systems. WO2008037435, April 3, 2008.
61. Minisci, F.; Porta, O.; Recupero, F.; Punta, C.; Gambarotti, C.; Spaccini, R. Catalytic process for the preparation of hydroperoxides of alkylbenzenes by aerobic oxidation under mild conditions. WO2009115275, Sept 24, 2009.
62. Lucarini, M.; Ferroni, F.; Pedulli, G. F.; Gardi, S.; Lazzari, D.; Schlingloff, G.; Sala, M. *Tetrahedron Lett.* **2007,** *48,* 5331–5334. doi:10.1016/j.tetlet.2007.05.162
63. Minisci, F.; Punta, C.; Recupero, F.; Fontana, F.; Pedulli, G. F. *Chem. Commun.* **2002,** 688–689. doi:10.1039/b110451a
64. Minisci, F.; Recupero, F.; Cecchetto, A.; Gambarotti, C.; Punta, C.; Faletti, R.; Paganelli, R.; Pedulli, G. F. *Eur. J. Org. Chem.* **2004,** 109–119. doi:10.1002/ejoc.200300332
65. Zhang, P.; Wang, Y.; Yao, J.; Wang, C.; Yan, C.; Antonietti, M.; Li, H. *Adv. Synth. Catal.* **2011,** *353,* 1447–1451. doi:10.1002/adsc.201100175
66. Wang, Y.; Wang, X.; Antonietti, M. *Angew. Chem., Int. Ed.* **2012,** *51,* 68–89. doi:10.1002/anie.201101182
67. Wang, X.; Blechert, S.; Antonietti, M. *ACS Catal.* **2012,** *2,* 1596–1606. doi:10.1021/cs300240x
68. Tong, X.; Xu, J.; Miao, H. *Adv. Synth. Catal.* **2005,** *347,* 1953–1957. doi:10.1002/adsc.200505183
69. Yang, X.; Zhou, L.; Chen, Y.; Chen, C.; Su, Y.; Miao, H.; Xu, J. *Catal. Commun.* **2009,** *11,* 171–174. doi:10.1016/j.catcom.2009.09.019
70. Zheng, G.; Liu, C.; Wang, Q.; Wang, M.; Yang, G. *Adv. Synth. Catal.* **2009,** *351,* 2638–2642. doi:10.1002/adsc.200900509
71. Toribio, P. P.; Gimeno-Gargallo, A.; Capel-Sanchez, M. C.; de Frutos, M. P.; Campos-Martin, J. M.; Fierro, J. L. G. *Appl. Catal., A* **2009,** *363,* 32–39. doi:10.1016/j.apcata.2009.04.023
72. Lin, R.; Chen, F.; Jiao, N. *Org. Lett.* **2012,** *14,* 4158–4161. doi:10.1021/ol3018215
73. Amaoka, Y.; Kamijio, S.; Hoshikawa, T.; Inoue, M. *J. Org. Chem.* **2012,** *77,* 9959–9969. doi:10.1021/jo301840e

License and Terms

Beilstein Journal of Organic Chemistry

Preparation of optically active bicyclodihydrosiloles by a radical cascade reaction

Koichiro Miyazaki[1], Yu Yamane[1], Ryuichiro Yo[1], Hidemitsu Uno[2] and Akio Kamimura[*1]

Full Research Paper

Open Access

Address:
[1]Department of Applied Molecular Bioscience, Graduate School of Medicine, Yamaguchi University, Ube 755-8611, Japan and [2]Department of Chemistry, Graduate School of Science and Engineering, Ehime University, Matsuyama, 790-8577, Japan

Email:
Akio Kamimura[*] - ak10@yamaguchi-u.ac.jp

* Corresponding author

Keywords:
bicyclodihydrosilole; free radical; radical cascade reaction; S_Hi reaction; tris(trimethylsilyl)silane

Beilstein J. Org. Chem. **2013,** *9,* 1326–1332.
doi:10.3762/bjoc.9.149

Received: 27 April 2013
Accepted: 18 June 2013
Published: 04 July 2013

This article is part of the Thematic Series "Organic free radical chemistry".

Guest Editor: C. Stephenson

Abstract

Bicyclodihydrosiloles were readily prepared from optically active enyne compounds by a radical cascade reaction triggered by tris(trimethylsilyl)silane ($(Me_3Si)_3SiH$). The reaction was initiated by the addition of a silyl radical to an α,β-unsaturated ester, forming an α-carbonyl radical that underwent radical cyclization to a terminal alkyne unit. The resulting vinyl radical attacked the silicon atom in an S_Hi manner to give dihydrosilole. The reaction preferentially formed *trans* isomers of bicyclosiloles with an approximately 7:3 to 9:1 selectivity.

Introduction

Radical cyclization occupies a unique position in organic synthesis because it is a useful reaction for the construction of cyclic molecules [1-10]. The radical cascade cyclization process is also an interesting synthetic reaction that often provides an efficient method [11-13]. Recently, we reported a new type of higher-order radical cascade reaction between chiral enyne compounds and Bu_3SnH, which is recognized as a useful reagent in radical reactions [14]. In this reaction, radical addition–cyclization cascade followed by intramolecular radical substitution (S_Hi) occurred in one-pot to give optically active bicyclostannolanes in good yields [15]. We are interested in whether such a cascade S_Hi process might occur with other radical species. We have found that a methylthiyl radical also undergoes such a radical cascade reaction to stereoselectively give bicyclic dihydrothiophenes [16]. We expected that tris(trimethylsilyl)silane $(Me_3Si)_3SiH$ [17], which is a well-known alternative to Bu_3SnH in radical reactions [18-22], would be a good promoter of a similar cascade S_Hi reaction, because there were several reports so far that show such S_Hi reaction on silicon atoms progressing efficiently [23-28]. In this

paper, we report a new synthesis of chiral bicyclodihydrosiloles through an addition–cyclization–S_Hi cascade reaction in one-pot treatment of chiral enyne compounds. A good *trans*-selectivity was observed in the reaction.

Results and Discussion

We examined the cascade process using optically active enyne precursor **1a**, which was prepared by a Michael/aldol domino reaction to chiral sulfinimines followed by thermal elimination and *N*-propargylation [29,30]. We first optimized the reaction conditions. The results are summarized in Table 1.

Treatment of **1** with $(Me_3Si)_3SiH$ in the presence of catalytic amounts of AIBN at 110 °C resulted in the formation of the desired bicyclodihydrosilole **2a** in 14% yield (Table 1, entry 1). The use of one equivalent of AIBN improved the yield of **2a** to 39% (Table 1, entry 2). These results suggest that the radical chain reaction insufficiently progressed during the reaction initiated by AIBN. The product contained two diastereomers, which were separated by chromatography. The use of Et_3B/air as an initiator enhanced the yield of **2a** to 58% (Table 1, entry 3). The enantiomeric excess of *trans*-**2a** was estimated to be 95% by HPLC analysis, which was the same ee level of precursor **1a**. Thus, no epimerization at the C3 chiral center occurred during the reaction. The stereoselectivity was improved to 8:2. The stereoselectivity was sensitive to the reaction temperature, and an 86/14 mixture of *trans*-**2a** and *cis*-**2a** was obtained when the reaction was performed at 0 °C, although the yield was less than that obtained when the reaction was performed at room temperature (Table 1, entry 4).

Having determined the optimized reaction conditions, we examined the generality of the reaction. The results are summarized in Table 2.

For example, the reaction of **1b** smoothly occurred, giving bicyclic dihydrosilole **2b** in 60% yield. HPLC analysis of the reaction mixture revealed that the diastereomeric ratio of **2b** was 84/16. Dihydrosiloles **2c**–**2j** were isolated in good yields from other precursors in a *trans*-selective manner (Table 2, entries 2–9). Their diastereomeric ratios ranged from 9/1 to 7/3. Although we could not determine the enantiomeric excesses for some compounds of **2** because of insufficient separation by chiral HPLC analyses using ChiralPak ID and IC (Table 2, entries 1, 2, and 4), the enantiomeric excesses of most of products **2** were high, and their original values were maintained (Table 2, entries 3, 5, 6, 8, and 9). Interestingly, significant epimerization occurred during the reaction of **1h**; the enantiomeric excess of **2h** was only 68% ee (Table 2, entry 7).

The configuration of **2** was determined in the following manner: The major isomer of **2a** was highly crystalline, which allowed the performance of X-ray crystallography. The observed data clearly showed a *trans*- **2a** structure [31]. The ORTEP structure of major **2a**, which unambiguously indicates a *trans* configuration, is shown in Figure 1. The ^{1}H NMR spectra of *trans*-**2a** and other major **2** showed similar trends, and *trans* configurations for other major **2** were determined unambiguously.

Unfortunately, none of the minor **2** formed suitable crystals, which precluded X-ray analysis of the minor isomers. However, their ^{1}H NMR spectra showed several diagnostic points. For example, the *tert*-butyl group in the ester at the C3a position in minor **2a** appeared at 1.17 ppm; this peak was substantially shifted toward higher field than *trans*-**2a**. Compared with X-ray data for the sulfur analogue of *cis*-**2a**, the *tert*-butyl ester group is located above the aromatic ring at C3, and expected to introduce an anisotropic effect that subsequently causes a high-field

Table 1: Radical cascade reaction under various reaction conditions.

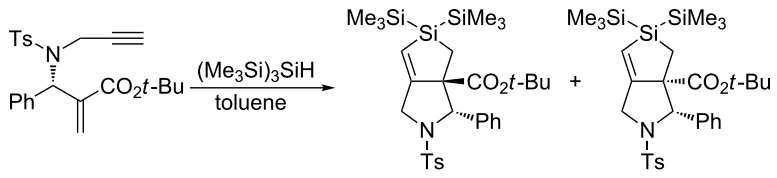

1a (95% ee) *trans*-**2a** *cis*-**2a**

Entry	Initiator (equiv)	Temp (°C)	**2a**; Yield (%)[a]	*trans*/*cis*[b]
1	AIBN (0.1)	110	14	n/a
2	AIBN (1.0)	110	39	69/31
3	Et_3B (3.0)	25	58	80/20 (95)[c]
4	Et_3B (3.0)	0	48	86/14

[a]Isolated yield. [b]Determined by HPLC analyses. [c]Enantiomeric excess for *trans*-**2a**. Determined by chiral HPLC analysis using ChiralPak ID.

Table 2: Preparation of pyrrolidinodihydrosiloles **2**.

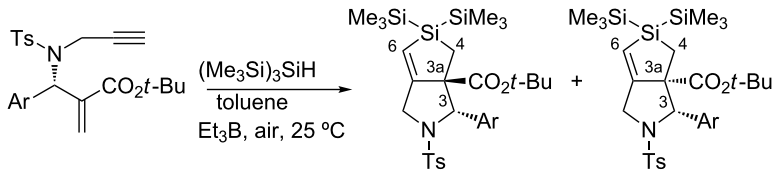

1 *trans*-**2** *cis*-**2**

Entry	Ar	Product	Yield[a] (%)	*trans*/*cis*[b]	ee for *trans*-**2**[c]
1	2-MeC_6H_4	**2b**	60	84/16	nd[d]
2	4-MeC_6H_4	**2c**	53	91/9	nd[d]
3	4-MeOC_6H_4	**2d**	42	86/14	97
4	3-ClC_6H_4	**2e**	42	71/29	nd[d]
5	4-ClC_6H_4	**2f**	51	81/19	90
6	4-FC_6H_4	**2g**	61	80/20	97
7	4-$CF_3C_6H_4$	**2h**	61	80/20	68
8	2-thienyl	**2i**	48	75/25	98
9	2-naphthyl	**2j**	51	81/19	99

[a]Isolated yield. [b]Determined by HPLC analyses. [c]Determined by HPLC analyses with a Chiral-Pak-ID. [d]Not determined owing to insufficient separation by chiral HPLC analyses with ChiralPak ID and IC.

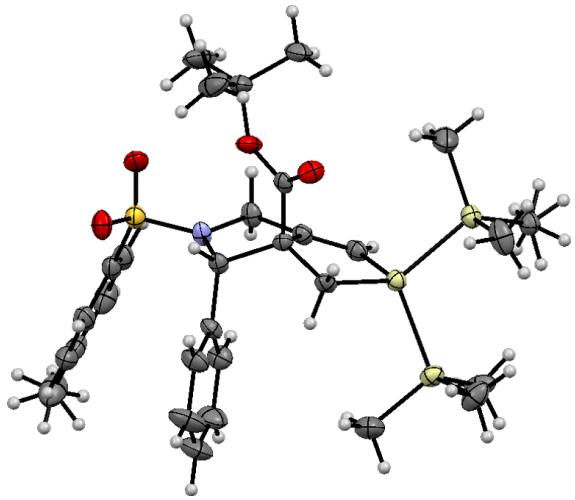

Figure 1: ORTEP structure of *trans*-**2a**.

shift for the *tert*-butyl protons [28]. Other typical differences between the ^{1}H NMR spectra of minor **2a** and major **2a** (= *trans*-**2a**) included the following: The peaks of the CH_2Si group at the C4 position in minor **2a** appeared at 0.92 and 2.00 ppm, whereas the corresponding peaks of *trans*-**2a** were observed at 0.49 and 1.14 ppm. In addition, we found that H6 and H3 appeared at 5.51 and 4.46 ppm, respectively, in the spectrum of minor **2a**. The corresponding protons in *trans*-**2a** appeared at substantially lower-field positions at 5.86 and 5.53 ppm. We assumed that this shift was caused by another anisotropic effect of the Ts group at N2. These trends in the ^{1}H NMR spectra were also observed in the sulfur analogues of *cis*-**2**. Thus, we concluded that the minor isomer of **2** exhibited *cis* configuration.

To explore the reaction mechanism, we examined the reaction of **1a** without additional solvents (Scheme 1).

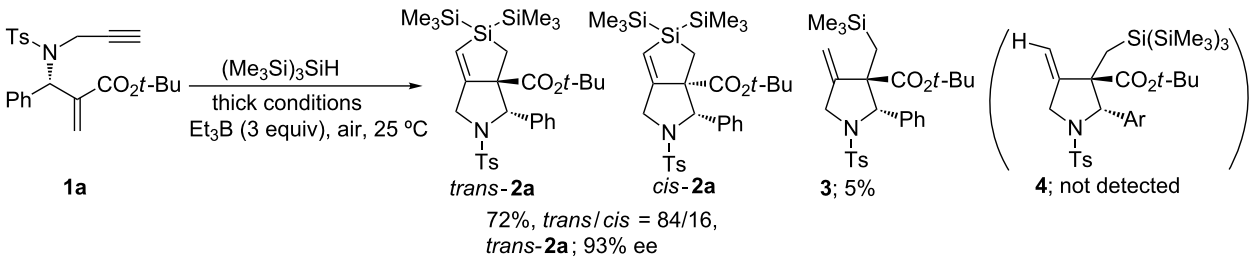

1a *trans*-**2a** *cis*-**2a** **3**; 5% **4**; not detected

72%, *trans*/*cis* = 84/16,
trans-**2a**; 93% ee

Scheme 1: Formation of bicyclic dihydrosilole **2a** under high concentration conditions.

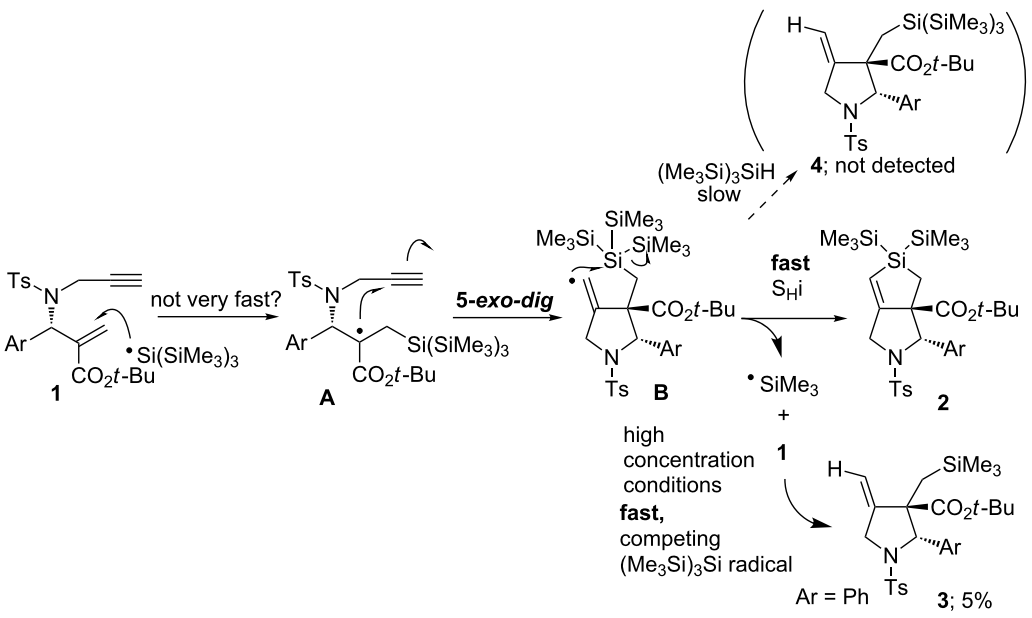

Scheme 2: Plausible reaction mechanism.

The treatment of **1a**, $(Me_3Si)_3SiH$, and Et_3B in hexane under an air atmosphere gave **2a** in 72%. To our surprise, this yield was better than that of the reaction performed under the usual conditions. We expected that *exo*-methylenepyrrolidine **4** would be a side product under these conditions, and we indeed detected an *exo*-methylene compound in 5% yield in the reaction mixture. However, NMR spectra and HRMS results indicated that the isolated product was compound **3,** which contained a Me_3SiCH_2- group instead of a $(Me_3Si)_3SiCH_2$- group. These results suggest that Me_3Si radicals were generated during the cascade reaction, and that a small part of the radical was subsequently trapped by **1** under such conditions.

We believe this process progressed in a similar manner to our previously investigated reaction that involved tributyltin radicals [15]. A plausible reaction mechanism is depicted in Scheme 2.

The $(Me_3Si)_3Si$ radical attacks the β-carbon of the α,β-unsaturated ester in **1,** and α-carbonyl radical **A** is generated. Intermediate **A** undergoes radical cyclization in a 5-*exo-dig* mode giving vinyl radical intermediate **B**, which is potentially reactive for attacking the silyl group in an S_Hi manner to give a Me_3Si radical and **2**. The process from **B** to **2** should be very rapid. Giese and co-workers have reported that the reaction rate for a similar S_Hi process reaches 2.4×10^5 s^{-1} at 80 °C [25]. Although most of the Me_3Si radicals undergo hydrogen abstraction from $(Me_3Si)_3SiH$ to yield a new $(Me_3Si)_3Si$ radical and Me_3SiH, a small fraction of the Me_3Si radicals compete to attack **1**; a similar cascade reaction progresses consequently, and compound **3** is formed in 5% yield under very high concentration conditions. We assume that compound **4** was not detected in the reaction product under such conditions for two reasons: first, as previously mentioned, the S_Hi process from intermediate **B** to **2** is very rapid, and the process occurs faster than intermolecular hydrogen abstraction from $(Me_3Si)_3SiH$, even under high concentration conditions. Second, the addition rate of $(Me_3Si)_3Si$ radicals to alkenes should be relatively slow; the rate competes with the addition rate of Me_3Si radicals to alkenes. This reason is supported by the results that indicated the yield of **2a** to be much improved under high $(Me_3Si)_3SiH$ concentration conditions because the addition rate should be accelerated as the concentration of $(Me_3Si)_3SiH$ increased.

We examined whether a germyl radical might undergo a similar reaction with **1**. Treatment of **1** with Et_3GeH in the presence of Et_3B, however, failed in the formation of the corresponding compound **5**. This failure was probably because a carbon–germanium bond, which is supposed to be stronger than a Si–Si bond, was never cleaved under these conditions (Scheme 3). Another possibility of this failure might be that the addition rate of a triethylgermyl radical to enyne **1a** was slow and less efficient.

Conclusion

In conclusion, we have successfully converted chiral enyne compounds **1**, which were readily available from an asymmetric aza-Morita–Baylis–Hillman equivalent reaction, into

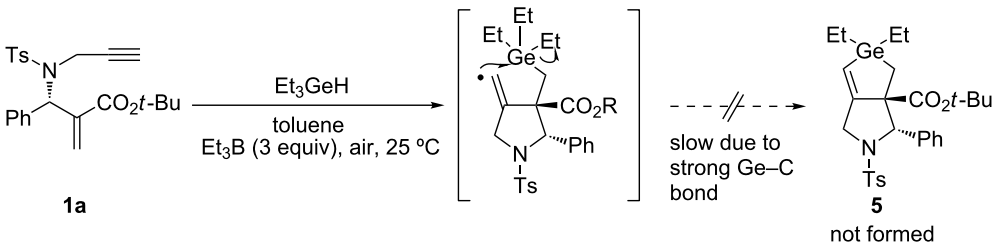

Scheme 3: Reaction **1a** with Et_3GeH.

bicyclic pyrolidinodihydrosiloles **2** in good yields. These reactions progressed in a highly stereoselective manner. Further application of the present silole synthesis is now underway in our laboratory.

Experimental

General methods: All ^1H and ^{13}C NMR spectra were recorded on a JEOL JNM-ECA500 Delta2 (500 MHz for ^1H, 126 MHz for ^{13}C) spectrometer. All the reactions in this study were performed under nitrogen atmosphere unless otherwise noted. CH_2Cl_2 was dried over CaH_2, and distilled under nitrogen before use. High-resolution mass spectra (HRMS) were measured at the Tokiwa Instrumentation Analysis Center, Yamaguchi University.

Preparation of (3*S*)-*tert*-butyl 3-phenyl-2-tosyl-5,5-bis(trimethylsilyl)-1,2,3,3a,4,5-hexahydrosilolo[3,4-*c*]pyrrole-3a-carboxylate (2a). A solution of **1a** (85 mg, 0.201 mmol, 95% ee), $(Me_3Si)_3SiH$ (0.06 mL, 0.195 mmol), and Et_3B (1.0 M in hexane, 0.60 mL, 0.60 mmol) in toluene (20 mL) was stirred at room temperature under air for 15 min. The reaction mixture was concentrated in vacuo, and the residue was purified by flash chromatography (silica gel/hexane–EtOAc 15/1 to 10/1, v/v) to give **2a** in 58% yield (70.2 mg, 0.117 mmol). The two diastereomers, *trans*-**2a** and *cis*-**2a**, were separated by further careful chromatography.

(3*S*,3a*S*)-*tert*-Butyl 3-phenyl-2-tosyl-5,5-bis(trimethylsilyl)-1,2,3,3a,4,5-hexahydrosilolo[3,4-*c*]pyrrole-3a-carboxylate (*trans*-2a). White solid; mp 144–145 °C; $[\alpha]_D$ −31.8 (*c* 0.68, $CHCl_3$); the enantiomeric purity was determined by HPLC analysis, t_R 10.0 min (major), t_R 11.5 min (minor) [CHIRALPAK ID (0.46 cm × 25 cm), hexane/iPrOH, 95/5, 40 °C, 1.0 mL/min] to be 95% ee; ^1H NMR (500 MHz, $CHCl_3$) δ 7.32 (d, *J* = 8.2 Hz, 2H), 7.26 (s, 3H), 7.24–7.07 (m, 2H), 7.03 (d, *J* = 7.8 Hz, 2H), 5.86 (s, 1H), 5.23 (s, 1H), 4.42 (d, *J* = 13.0 Hz, 1H), 3.95 (d, *J* = 13.0 Hz, 1H), 2.32 (s, 3H), 1.51 (s, 9H), 1.15 (d, *J* = 14.9 Hz, 1H), 0.50 (d, *J* = 14.8 Hz, 1H), 0.07 (s, 9H), −0.20 (s, 9H); ^{13}C NMR (126 MHz, $CHCl_3$) δ 173.9, 157.6, 142.6, 138.6, 137.1, 129.1 (2C), 128.3 (br, 4C), 127.5, 127.0 (2C), 124.2, 82.3, 71.1, 69.7, 50.5, 28.0 (3C), 21.5, 12.2, −0.3 (3C), −0.9 (3C); HRMS–ESI (positive mode; M + Na) *m*/*z* 622.2282, calcd for $C_{30}H_{45}NNaO_4SSi_3$, 622.2275.

(3*S*,3a*R*)-*tert*-Butyl 3-phenyl-2-tosyl-5,5-bis(trimethylsilyl)-1,2,3,3a,4,5-hexahydrosilolo[3,4-c]pyrrole-3a-carboxylate (*cis*-2a). Pale yellow oil; $[\alpha]_D$ +97.3 (c 0.27, $CHCl_3$); ^1H NMR (500 MHz, $CHCl_3$) δ 7.63 (d, *J* = 7.8 Hz, 2H), 7.57–7.50 (m, 2H), 7.33–7.22 (m, 5H), 5.51 (s, 1H), 4.60 (d, *J* = 14.3 Hz, 1H), 4.23 (s, 1H), 4.11 (dd, *J* = 14.3, 1.6 Hz, 1H), 2.39 (s, 3H), 2.00 (d, *J* = 12.8 Hz, 1H), 1.17 (s, 9H), 0.92 (d, *J* = 15.0 Hz, 1H), 0.04 (s, 9H), −0.11 (s, 9H); ^{13}C NMR (126 MHz, $CHCl_3$) δ 169.5, 157.8, 143.8, 138.1, 133.1, 129.9 (2C), 128.0 (2C), 127.7 (2C), 127.7, 127.1 (br, 2C), 122.8, 82.1, 75.2, 72.5, 53.7, 27.9 (3C), 21.6, 17.4, 0.3 (3C), −1.4 (3C); HRMS–ESI (positive mode; M + Na) *m*/*z* 622.2292, calcd for $C_{30}H_{45}NNaO_4SSi_3$, 622.2275.

Preparation of 2a under no solvent conditions (Scheme 3, neat condition). A solution of **1a** (85 mg, 0.201 mmol), $(Me_3Si)_3SiH$ (0.07 mL, 0.228 mmol), and Et_3B (1.0 M in hexane, 0.60 mL, 0.60 mmol) was stirred at room temperature for 15 min under air. The reaction mixture was concentrated in vacuo, and the yellow residue was purified by flash chromatography (silica gel/hexane–EtOAc 30/1 to 20/1 v/v) to give **2a** in 72% yield (85.6 mg, 0.143 mmol). The *trans*-**2a**/*cis*-**2a** ratio was determined to be 84/16. Careful separation of these two diastereomers gave pure *trans*-**2a** and minor isomers that contained *cis*-**2a** and **3** in a 74/26 ratio. The separation of **3** was achieved using a recycling GPC apparatus, giving pure **3** in 5% yield (5.1 mg, 0.011 mmol).

(2*S*,3*S*)-*tert*-Butyl 3-((trimethylsilyl)methyl)-4-methylene-2-phenyl-1-tosylpyrrolidine-3-carboxylate (3). Pale yellow oil; $[\alpha]_D$ +3.0 (c 0.01, $CHCl_3$); ^1H NMR (500 MHz, $CHCl_3$) δ 7.20–7.09 (m, 5H), 7.00–6.94 (m, 4H), 5.36 (s, 1H), 5.21 (t, *J* = 1.8 Hz, 1H), 5.14 (dd, *J* = 2.7, 1.5 Hz, 1H), 4.36 (dt, *J* = 13.0, 2.5 Hz, 1H), 3.90 (dt, *J* = 13.0, 1.5 Hz, 1H), 2.29 (s, 3H), 1.50 (s, 9H), 0.90 (d, *J* = 14.6 Hz, 1H), 0.48 (d, *J* = 14.7 Hz, 1H), −0.13 (s, 9H); ^{13}C NMR (126 MHz, $CHCl_3$) δ 172.4, 148.8,

142.4, 138.2, 136.7, 129.0 (4C), 128.1 (2C), 127.8, 127.0 (2C), 110.0, 82.4, 70.2, 61.0, 51.5, 27.9 (3C), 21.5, 19.6, 0.7 (3C); HRMS–ESI (positive mode; M + Na) *m/z* 522.2108, calcd for $C_{27}H_{37}NNaO_4SSi$, 522.2110.

Supporting Information

Supporting Information File 1

Experimental procedures and ^1H and ^{13}C NMR spectra.
[http://www.beilstein-journals.org/bjoc/content/supplementary/1860-5397-9-149-S1.pdf]

Supporting Information File 2

CIF data for *trans*-**2a**.
[http://www.beilstein-journals.org/bjoc/content/supplementary/1860-5397-9-149-S2.cif]

Acknowledgements

We are grateful to financial assistance from the Sasakawa Scientific Research Grant (to K. M.) and Yamaguchi University under the YU Strategic Program for Fostering Research Activities (2010–2011, 2013–2014).

References

1. Zimmerman, J.; Halloway, A.; Sibi, M. P. Free Radical Cyclization Reactions. In *Handbook of Cyclization Reactions;* Ma, S., Ed.; Wiley-VCH: Weinheim, Germany, 2010; Vol. 2, pp 1099–1148.
2. Majumdar, K. C.; Mukhopadhyay, P. P.; Basu, P. K. *Heterocycles* **2004,** *63,* 1903. doi:10.3987/REV-04-577
3. Majumdar, K. C.; Basu, P. K.; Mukhopadhyay, P. P. *Tetrahedron* **2004,** *60,* 6239. doi:10.1016/j.tet.2004.05.001
4. Majumdar, K. C.; Basu, P. K.; Mukhopadhyay, P. P. *Tetrahedron* **2005,** *61,* 10603. doi:10.1016/j.tet.2005.07.079
5. Ishibashi, H. *Chem. Rec.* **2006,** *6,* 23–31. doi:10.1002/tcr.20069
6. Barrero, A. F.; Quilez del Moral, J. F.; Sanchez, E. M.; Arteaga, J. F. *Eur. J. Org. Chem.* **2006,** 1627. doi:10.1002/ejoc.200500849
7. Majumdar, K. C.; Basu, P. K.; Chattopadhyay, S. K. *Tetrahedron* **2007,** *63,* 793. doi:10.1016/j.tet.2006.09.049
8. Yoshioka, E.; Kohtani, S.; Miyabe, H. *Heterocycles* **2009,** *79,* 229. doi:10.3987/REV-08-SR(D)8
9. Rowlands, G. J. *Tetrahedron* **2010,** *66,* 1593. doi:10.1016/j.tet.2009.12.023
10. Galli, C. *Chem. Rev.* **1988,** *88,* 765. doi:10.1021/cr00087a004
11. Curran, D. P.; Kim, D.; Liu, H. T.; Shen, W. *J. Am. Chem. Soc.* **1988,** *110,* 5900. doi:10.1021/ja00225a052
12. Snieckus, V.; Cuevas, J.-C.; Sloan, C. P.; Liu, H.; Curran, D. P. *J. Am. Chem. Soc.* **1990,** *112,* 896. doi:10.1021/ja00158a075
13. Dènés, F.; Beaufils, F.; Renaud, P. *Synlett* **2008,** 2389. doi:10.1055/s-2008-1078016
14. Chatgilialoglu, C.; Newcomb, M. *Adv. Organomet. Chem.* **1999,** *44,* 67. doi:10.1016/S0065-3055(08)60620-6
See for a review om tin hydride and related hydride reagents.
15. Kamimura, A.; Ishikawa, S.; Noguchi, F.; Moriyama, T.; So, M.; Murafuji, T.; Uno, H. *Chem. Commun.* **2012,** *48,* 6592. doi:10.1039/c2cc31753b
16. Kamimura, A.; Miyazaki, K.; Yamane, Y.; Yo, R.; Ishikawa, S.; Uno, H. submitted.
17. Gilman, H.; Atwell, W. H.; Sen, P. K.; Smith, C. L. *J. Organomet. Chem.* **1965,** *4,* 163. doi:10.1016/S0022-328X(00)84384-3
18. Chatgilialoglu, C. *Chem.–Eur. J.* **2008,** *14,* 2310. doi:10.1002/chem.200701415
19. Kanabus-Kaminska, J. M.; Hawari, J. A.; Griller, D.; Chatgilialoglu, C. *J. Am. Chem. Soc.* **1987,** *109,* 5267. doi:10.1021/ja00251a035
20. Chatgilialoglu, C.; Griller, D.; Lesage, M. *J. Org. Chem.* **1988,** *53,* 3641. doi:10.1021/jo00250a051
21. Chatgilialoglu, C. *Acc. Chem. Res.* **1992,** *25,* 188. doi:10.1021/ar00016a003
22. Chatgilialoglu, C. *Organosilanes in Radical Chemistry;* Wiley: Chichester (UK), 2004. doi:10.1002/0470024755
23. Miura, K.; Oshima, K.; Utimoto, K. *Chem. Lett.* **1992,** *21,* 2477. doi:10.1246/cl.1992.2477
24. Miura, K.; Oshimaa, K.; Utimoto, K. *Bull. Chem. Soc. Jpn.* **1993,** *66,* 2348. doi:10.1246/bcsj.66.2348
25. Kulicke, K.; Chatgilialoglu, C. S.; Kopping, B.; Giese, B. *Helv. Chim. Acta* **1992,** *75,* 935. doi:10.1002/hlca.19920750327
26. Studer, A. *Angew. Chem., Int. Ed.* **1998,** *37,* 462. doi:10.1002/(SICI)1521-3773(19980302)37:4<462::AID-ANIE462>3.0.CO;2-M
27. Studer, A.; Steen, H. *Chem.–Eur. J.* **1999,** *5,* 759. doi:10.1002/(SICI)1521-3765(19990201)5:2<759::AID-CHEM759>3.0.CO;2-V
28. Rouquet, G.; Robert, F.; Méreau, R.; Castet, F.; Renaud, P.; Landais, Y. *Chem.–Eur. J.* **2012,** *18,* 940. doi:10.1002/chem.201102318
29. Kamimura, A.; Okawa, H.; Morisaki, Y.; Ishikawa, S.; Uno, H. *J. Org. Chem.* **2007,** *72,* 3569. doi:10.1021/jo062251h
30. Ishikawa, S.; Noguchi, F.; Kamimura, A. *J. Org. Chem.* **2010,** *75,* 3578. doi:10.1021/jo100315j
31. Crystallographic data (excluding structure factors) for the structures of *trans* **2a** have been deposited with the Cambridge Crystallographic Data Centre under supplementary publication numbers CCDC 931894. Copies of the data can be obtained, free of charge, upon request from the CCDC, 12 Union Road, Cambridge CB2 1EZ, UK [fax: +44(0)-1223-336033 or email: deposit@ccdc.cam.ac.uk].

Beilstein Journal of Organic Chemistry

A construction of 4,4-spirocyclic γ-lactams by tandem radical cyclization with carbon monoxide

Mitsuhiro Ueda[1], Yoshitaka Uenoyama[1], Nozomi Terasoma[1], Shoko Doi[1], Shoji Kobayashi[2], Ilhyong Ryu[*1] and John A. Murphy[*3]

Letter

Open Access

Address:
[1]Department of Chemistry, Graduate School of Science, Osaka Prefecture University, Sakai, Osaka 599-8531, Japan, [2]Department of Applied Chemistry, Faculty of Engineering, Osaka Institute of Technology, 5-16-1 Ohmiya, Asahi-ku, Osaka 535-8585, Japan and [3]Department of Pure and Applied Chemistry, University of Strathclyde, 295 Cathedral Street, Glasgow G1 1XL, UK

Email:
Mitsuhiro Ueda - ueda@c.s.osakafu-u.ac.jp; Ilhyong Ryu[*] - ryu@c.s.osakafu-u.ac.jp; John A. Murphy[*] - john.murphy@strath.ac.uk

* Corresponding author

Keywords:
4,4-spirocyclic indol γ-lactams; carbon monoxide; free radical; iodoaryl allyl azides; tandem radical cyclization

Beilstein J. Org. Chem. **2013,** *9,* 1340–1345.
doi:10.3762/bjoc.9.151

Received: 27 April 2013
Accepted: 17 June 2013
Published: 05 July 2013

This article is part of the Thematic Series "Organic free radical chemistry".

Guest Editor: C. Stephenson

Abstract

A straightforward synthesis of 4,4-spirocyclic indol γ-lactams by tandem radical cyclization of iodoaryl allyl azides with CO was achieved. The reaction of iodoaryl allyl azides, TTMSS and AIBN under CO pressure (80 atm) in THF at 80 °C gave the desired 4,4-spirocyclic indoline, benzofuran, and oxindole γ-lactams in moderate to good yields.

Introduction

4,4-Spirocyclic oxindole γ-lactams containing a quaternary carbon center are key structures for the synthesis of biologically active natural products and the related analogues [1-4]. Therefore, the development of an efficient synthesis of this spiro structure is of continued interest for synthetic chemists. Recently, Comesse and Daïch reported the synthesis of 4,4-spirocyclic oxindole γ-lactams by tandem spirocyclization via nucleophilic halide displacement and amide coupling [4]. Shaw and co-workers reported the synthesis of 4,4-spirocyclic oxindole γ-lactams by the cycloaddition of imines and succinic anhydrides [5]. Tandem radical cyclization can also provide a powerful tool for the construction of heterocycles [6-12]. One of us previously reported on the construction of spirocyclic pyrrolidinyl oxindoles by the tandem reaction of iodoaryl alkenyl azides under radical conditions (Scheme 1) [13,14]. Curran et al. reported the synthesis of spirocyclic pyrrolidinyl dihydroquinolinones by tandem radical cyclization [15,16].

In this study we report a radical cyclization/annulation approach to 4.4-spirocyclic γ-lactams in which CO was intro-

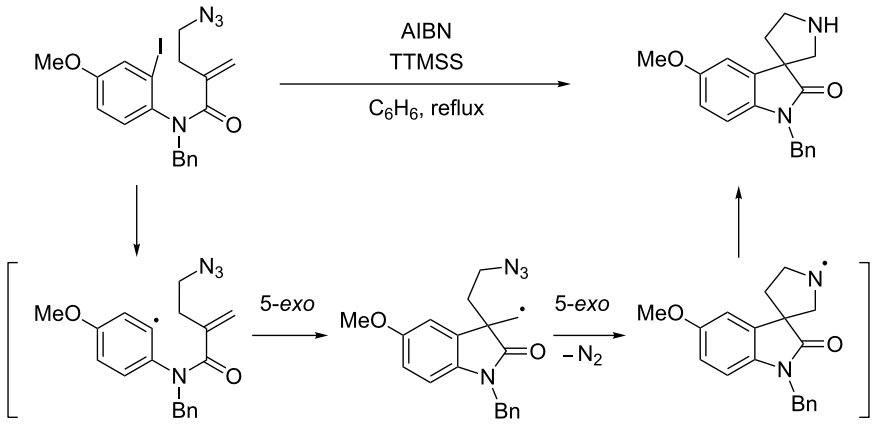

Scheme 1: A construction of spirocyclic pyrrolidinyl oxindole by tandem radical cyclization with azide [14].

duced as the lactam carbonyl moiety [17-23]. Our approach consists of a sequence of aryl radical cyclization, radical carbonylation [24-27], and spirocyclization of the resulting acyl radical onto an azide group, which can give 4,4-spirocyclic γ-lactams (Scheme 2).

Results and Discussion

For the first model reaction in our investigation of the development of a novel tandem radical cyclization/annulation strategy, we prepared *N*-(2-(azidomethyl)allyl)-*N*-(2-iodophenyl)-4-methylbenzenesulfonamide (**1a**) according to the methods shown in Scheme 3. The reaction of **1a** with Bu_3SnH (2.0 equiv) and AIBN (2,2'- azobisisobutyronitrile, 0.3 equiv) was carried out under CO pressure (80 atm) in THF (0.02 M) at 80 °C for 12 h, which gave the desired 4,4-spirocyclic indoline γ-lactam **2a** in 48% yield (Scheme 4). We found that the modest improvement in the yield of **2a** to 53% was achieved by changing the mediator from Bu_3SnH to TTMSS [tris(trimethylsilyl)silane].

The tandem spirocyclization with CO was investigated with several 2-iodoaryl compounds having an allyl azide moiety. Results are summarized in Table 1. The reaction of *N*-(2-(azidomethyl)allyl)-*N*-(2-iodo-5-methoxyphenyl)-4-methylbenzenesulfonamide (**1b**) with CO gave the corresponding spiro lactam **2b** in 53% yield (Table 1, entry 2). *N*-(2-(Azidomethyl)allyl)-*N*-(2-iodophenyl)methanesulfonamide (**1c**) showed a comparable reactivity with **1a** and **1b** (Table 1, entry 3). The reaction of 1-(2-(azidomethyl)allyloxy)-2-iodobenzene (**1d**) also gave the spiro benzofuran lactam **2d** in 58% yield (Table 1, entry 4). On

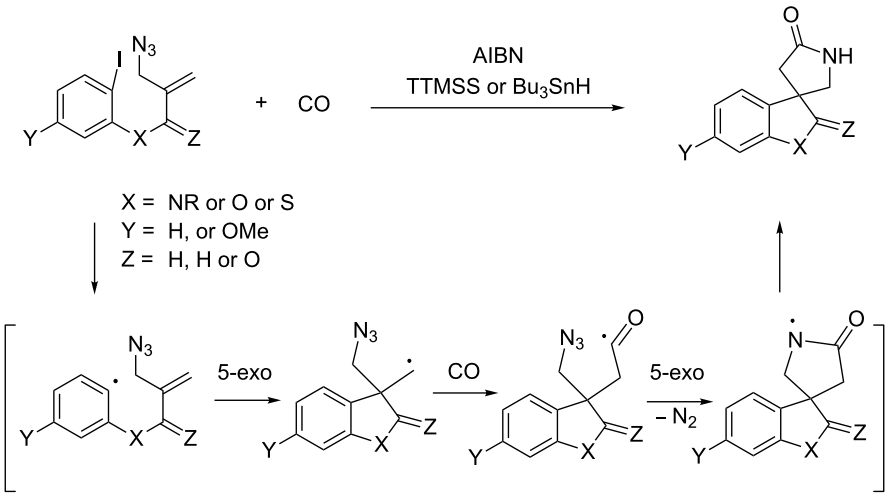

Scheme 2: A tandem radical cyclization/annulation strategy for the synthesis of 4,4-spirocyclic γ-lactams with the incorporation of CO.

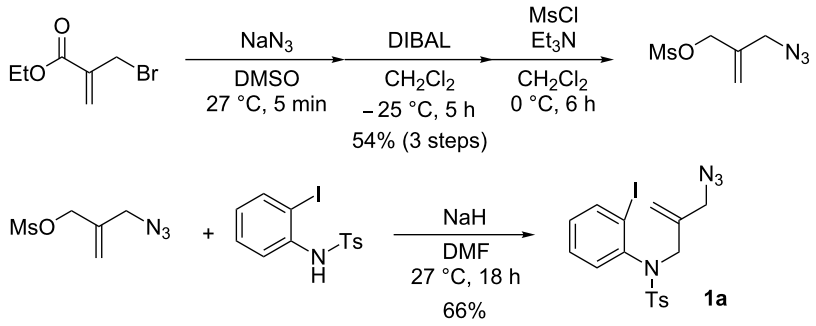

Scheme 3: The synthetic methods of **1a**.

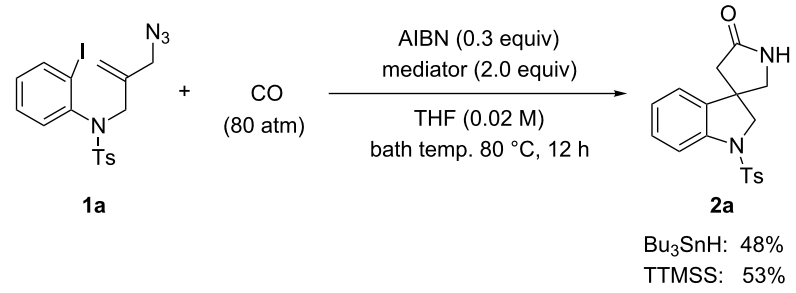

Scheme 4: The tandem radical spirocyclization reaction of *N*-(2-(azidomethyl)allyl)-*N*-(2-iodophenyl)-4-methylbenzenesulfonamide (**1a**) with CO.

Table 1: Synthesis of 4,4-spirocyclic γ-lactams **2** by tandem radical spirocyclization of **1** with CO.[a]

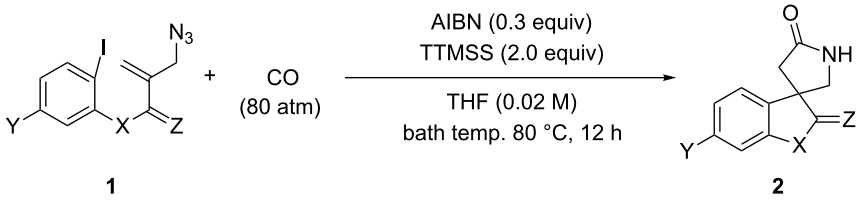

Entry	Substrate (**1**)	Product (**2**)	Yield (%)
1[b]	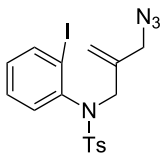 **1a**	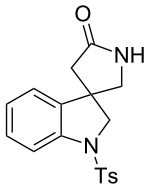 **2a**	53
2[b]	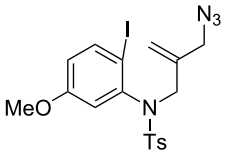 **1b**	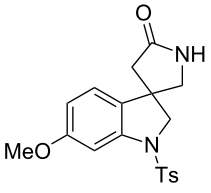 **2b**	53

Table 1: Synthesis of 4,4-spirocyclic γ-lactams **2** by tandem radical spirocyclization of **1** with CO.[a] (continued)

3	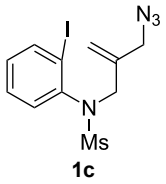 **1c**	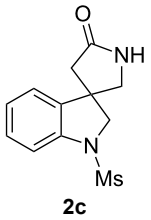 **2c**	55
4	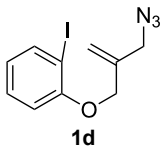 **1d**	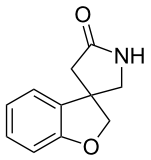 **2d**	58
5[c]	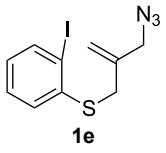 **1e**	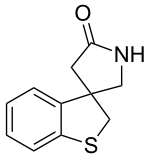 **2e**	19
6	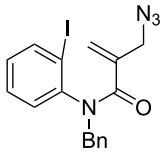 **1f**	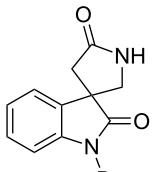 **2f**	62
7	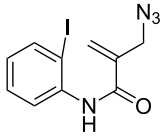 **1g**	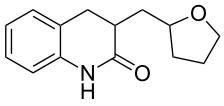 dr = 1:1 **3**	60[d]

[a]Reaction conditions: **1** (1.0 equiv), CO (80 atm), AIBN (0.3 equiv), TTMSS (2.0 equiv), THF (0.02 M), bath temperature 80 °C, 12 h. [b]Reaction time: 24 h. [c]The reaction was carried out at a bath temperature of 110 °C. [d]Yield of **3**.

the other hand, 2-(azidomethyl)allyl(2-iodophenyl)sulfane (**1e**) gave a low yield of the corresponding spiro thiobenzofuran lactam (19%, Table 1, entry 5), which may be rationalized by the less effective cyclization due to the longer C–S bonds.

We then tried to extend the tandem spirocyclization approach to obtain 4,4-spirocyclic oxindole γ-lactam and tested two substrates, 2-(azidomethyl)-*N*-benzyl-*N*-(2-iodophenyl)acrylamide (**1f**) and the nitrogen-unprotected analogue **1g**. The reaction of **1f** was smooth to give the desired 4,4-spirocyclic oxindole γ-lactam **2f** in 62% yield (Table 1, entry 6). On the other hand, the reaction of **1g** gave the cyclized product in only a trace amount, and instead THF-incorporating 6-*endo* cyclization product **3** was obtained in 60% yield (Table 1, entry 7) [28].

Based on the known chemistry of radical cyclization and carbonylation reactions, a possible mechanism for the spirocyclization of **1f** with CO is shown in Scheme 5. The iodoaryl allyl azide **1f** is converted to an aryl radical **A** via the iodine atom abstraction by the $(TMS)_3Si$ radical. The subsequent 5-*exo* cyclization of aryl radical **A** gives an alkyl radical **B**, which adds to CO to give an acyl radical **C**. Finally, the 5-*exo* addition of acyl radical **C** onto an azide group takes place with the liberation of dinitrogen to give a cyclized amidyl radical **D** [29,30], which abstracts hydrogen from TTMSS, affording the 4,4-spirocyclic indoline γ-lactam **2f** and a $(TMS)_3Si$ radical, thus creating a radical chain.

On the other hand, the unusual formation of THF-incorporating lactam **3** from **1g** may be rationalized by the consecutive 6-*endo*

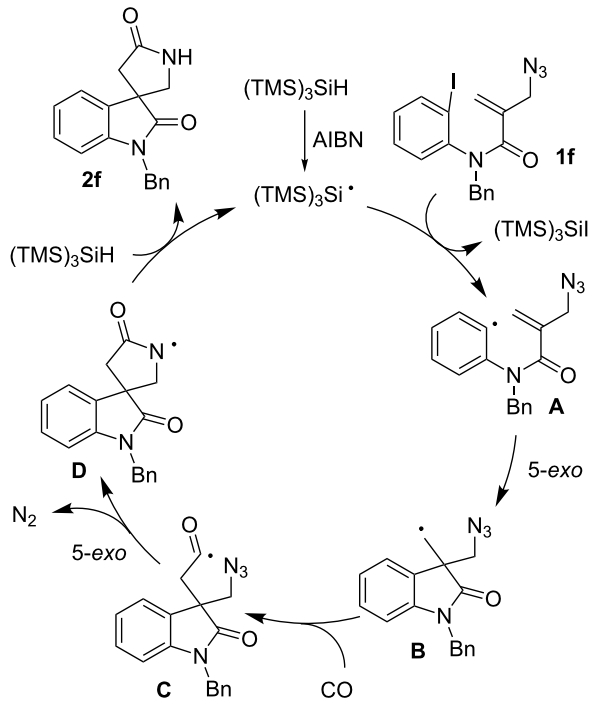

Scheme 5: Proposed mechanism for a construction of 4,4-spirocyclic indoline γ-lactam **2f** by the tandem radical cyclization of **1f** with CO.

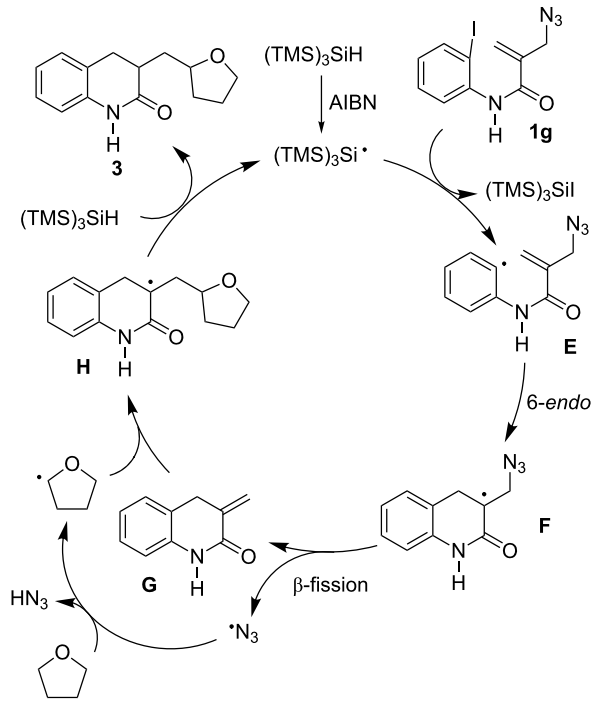

Scheme 6: Proposed mechanism for the formation of THF-incorporating product **3** from **1g**.

cyclization of **E** and β-elimination of an azidyl radical from the resulting **F**, to give 2-methylene lactam **G** (Scheme 6). Then, the THF radical is formed via the α-hydrogen abstraction by the azidyl radical [31-34], which is attached to **G** to give α-carbonyl radical **H**. Finally, **H** abstracts hydrogen from TTMSS, affording the THF-incorporating product **3** and the $(TMS)_3Si$ radical, which participates in the next chain reaction.

Conclusion

We have examined a TTMSS-mediated 5-*exo* radical cyclization/carbonylation/spirocyclization sequence to synthesize 4,4-spirocyclic rings. By using this protocol, indoline, benzofuran and oxindole γ-lactams can be conveniently prepared in moderate to good yields. As shown in the contrasting results of acrylic amides **1f** and **1g**, to cause the requisite 5-*exo* cyclization of aryl radicals onto allylic azide in preference to the 6-*endo* cyclization, the angle compression caused by the substitution on the nitrogen has to be considered carefully. Nevertheless, our method can provide a steady tool for the ring formation of 4,4-spirocyclic γ-lactams with the incorporation of CO as a carbonyl group.

Experimental

Typical procedure for a construction of 4,4-spirocyclic γ-lactams by tandem radical cyclization with CO: A magnetic stirring bar, 2-(azidomethyl)-*N*-benzyl-*N*-(2-iodophenyl)acrylamide (**1f**) (150.0 mg, 0.36 mmol), AIBN (2,2'-azobisisobutyronitrile, 17.7 mg, 0.11 mmol), TTMSS ([tris(trimethylsilyl)silane], 178.3 mg, 0.72 mmol) and THF (17.9 mL; 0.02 M) were placed in a 50 mL stainless steel autoclave. The autoclave was closed, purged three times with CO, pressurized with 80 atm of CO, and then heated at 80 °C (bath temperature) for 12 h. Excess CO was discharged after the reaction. The reaction mixture was concentrated in vacuo. The resulting residue was purified by column chromatography on silica gel (hexane/EtOAc 2:1) to give the desired 4,4-spirocyclic oxindole γ-lactam product **2f** as a colorless oil in 62% yield (65.3 mg, 0.22 mmol). ^{1}H NMR (400 MHz, $CDCl_3$) δ 7.39–7.16 (m, 7H), 7.07 (t, J = 7.6 Hz, 1H), 6.79 (d, J = 7.6 Hz, 1H), 5.89 (s, 1H), 4.93 (s, 2H), 3.91 (d, J = 9.2 Hz, 1H), 3.50 (d, J = 9.2 Hz, 1H) 3.02 (d, J = 16.8 Hz, 1H), 2.51 (d, J = 16.8 Hz, 1H); ^{13}C NMR (100 MHz, $CDCl_3$) δ 177.5, 175.4, 141.9, 135.5, 133.2, 129.1, 129.0, 128.0, 127.4, 123.6, 122.3, 109.7, 51.1, 49.7, 44.3, 40.4; IR (neat): 3418, 3061, 2927, 1696, 1613, 1488, 1467, 1455, 1380, 1368, 1177 cm^{-1}; HRMS–FAB (m/z): $[M + H]^+$ calcd for $C_{18}H_{17}N_2O_2$, 293.1290; found, 293.1299.

Acknowledgements

This work was supported by a Grant-in-Aid for Scientific Research from the MEXT and JSPS.

References

1. Edmondson, S.; Danishefsky, S. J.; Sepp-Lorenzino, L.; Rosen, N. *J. Am. Chem. Soc.* **1999,** *121,* 2147–2155. doi:10.1021/ja983788i
2. Cravotto, G.; Giovenzana, G. B.; Pilati, T.; Sisti, M.; Palmisano, G. *J. Org. Chem.* **2001,** *66,* 8447–8453. doi:10.1021/jo015854w
3. Marti, C.; Carreira, E. M. *Eur. J. Org. Chem.* **2003,** 2209–2219. doi:10.1002/ejoc.200300050
4. Allous, I.; Comesse, S.; Berkeš, D.; Alkyat, A.; Daïch, A. *Tetrahedron Lett.* **2009,** *50,* 4411–4415. doi:10.1016/j.tetlet.2009.02.114
5. Tan, D. Q.; Atherton, A. L.; Smith, A. J.; Soldi, C.; Hurley, K. A.; Fettinger, J. C.; Shaw, J. T. *ACS Comb. Sci.* **2012,** *14,* 218–223. doi:10.1021/co2001873
6. Beckwith, A. L. J. *Chem. Soc. Rev.* **1993,** *22,* 143–151. doi:10.1039/cs9932200143
7. Ishibashi, H.; Sato, T.; Ikeda, M. *Synthesis* **2002,** 695–713. doi:10.1055/s-2002-25759
8. Srikanth, G. S. C.; Castle, S. L. *Tetrahedron* **2005,** *61,* 10377–10441. doi:10.1016/j.tet.2005.07.077
9. Fallis, A. G.; Brinza, I. M. *Tetrahedron* **1997,** *53,* 17543–17594. doi:10.1016/S0040-4020(97)10060-6
10. Friestad, G. K. *Tetrahedron* **2001,** *57,* 5461–5496. doi:10.1016/S0040-4020(01)00384-2
11. Bowman, W. R.; Fletcher, A. J.; Potts, G. B. S. *J. Chem. Soc., Perkin Trans. 1* **2002,** 2747–2762. doi:10.1039/B108582B
12. Minozzi, M.; Nanni, D.; Spagnolo, P. *Chem.–Eur. J.* **2009,** *15,* 7830–7840. doi:10.1002/chem.200802710
13. Patro, B.; Murphy, J. A. *Org. Lett.* **2000,** *2,* 3599–3601. doi:10.1021/ol006477x
14. Lizos, D. E.; Murphy, J. A. *Org. Biomol. Chem.* **2003,** *1,* 117–122. doi:10.1039/b208114h
15. González-López de Turiso, F.; Curran, D. P. *Org. Lett.* **2005,** *7,* 151–154. doi:10.1021/ol0477226
16. Zhang, H.; Curran, D. P. *J. Am. Chem. Soc.* **2011,** *133,* 10376–10378. doi:10.1021/ja2042854
17. Ryu, I.; Matsu, K.; Minakata, S.; Komatsu, M. *J. Am. Chem. Soc.* **1998,** *120,* 5838–5839. doi:10.1021/ja980731n
18. Ryu, I.; Miyazato, H.; Kuriyama, H.; Matsu, K.; Tojino, M.; Fukuyama, T.; Minakata, S.; Komatsu, M. *J. Am. Chem. Soc.* **2003,** *125,* 5632–5633. doi:10.1021/ja034896u
19. Tojino, M.; Otsuka, N.; Fukuyama, T.; Matsubara, H.; Schiesser, C. H.; Kuriyama, H.; Miyazato, H.; Minakata, S.; Komatsu, M.; Ryu, I. *Org. Biomol. Chem.* **2003,** *1,* 4262–4267. doi:10.1039/b309944j
20. Tojino, M.; Otsuka, N.; Fukuyama, T.; Matsubara, H.; Ryu, I. *J. Am. Chem. Soc.* **2006,** *128,* 7712–7713. doi:10.1021/ja0623865
21. Kyne, S. H.; Lin, C. Y.; Ryu, I.; Coote, M. L.; Schiesser, C. H. *Chem. Commun.* **2010,** *46,* 6521–6523. doi:10.1039/c0cc01262a
22. Ryu, I.; Fukuyama, T.; Tojino, M.; Uenoyama, Y.; Yonamine, Y.; Terasoma, N.; Matsubara, H. *Org. Biomol. Chem.* **2011,** *9,* 3780–3786. doi:10.1039/c1ob05145h
23. Fukuyama, T.; Nakashima, N.; Okada, T.; Ryu, I. *J. Am. Chem. Soc.* **2013,** *135,* 1006–1008. doi:10.1021/ja312654q
24. Ryu, I.; Sonoda, N. *Angew. Chem., Int. Ed. Engl.* **1996,** *35,* 1050–1066. doi:10.1002/anie.199610501
25. Ryu, I.; Sonoda, N.; Curran, D. P. *Chem. Rev.* **1996,** *96,* 177–194. doi:10.1021/cr9400626
26. Ryu, I. *Chem. Soc. Rev.* **2001,** *30,* 16–25. doi:10.1039/a904591k
27. Chatgilialogu, C.; Crich, D.; Komatsu, M.; Ryu, I. *Chem. Rev.* **1999,** *99,* 1991–2070. doi:10.1021/cr9601425
28. Jones, K.; Wilkinson, J. *J. Chem. Soc., Chem. Commun.* **1992,** 1767–1769. doi:10.1039/C39920001767
    Similar 6-*endo* cyclization was reported previously.
29. Kim, S.; Joe, G. H.; Do, J. Y. *J. Am. Chem. Soc.* **1994,** *116,* 5521–5522. doi:10.1021/ja00091a087
30. Benati, L.; Leardini, R.; Minozzi, M.; Nanni, D.; Spagnolo, P.; Strazzari, S.; Zanardi, G. *Org. Lett.* **2002,** *4,* 3079–3081. doi:10.1021/ol026366t
31. Viuf, C.; Bols, M. *Angew. Chem., Int. Ed.* **2001,** *40,* 623–625. doi:10.1002/1521-3773(20010202)40:3<623::AID-ANIE623>3.0.CO;2-G
32. Marinescu, L. G.; Pedersen, C. M.; Bols, M. *Tetrahedron* **2005,** *61,* 123–127. doi:10.1016/j.tet.2004.10.040
33. Pedersen, C. M.; Marinescu, L. G.; Bols, M. *Org. Biomol. Chem.* **2005,** *3,* 816–822. doi:10.1039/b500037h
34. Klima, R. F.; Jadhav, A. V.; Singh, P. N. D.; Chang, M.; Vanos, C.; Sankaranarayanan, J.; Vu, M.; Ibrahim, N.; Ross, E.; McCloskey, S.; Murthy, R. S.; Krause, J. A.; Ault, B. S.; Gudmundsdóttir, A. D. *J. Org. Chem.* **2007,** *72,* 6372–6381. doi:10.1021/jo070558q

License and Terms

Beilstein Journal of Organic Chemistry

Copper(II)-salt-promoted oxidative ring-opening reactions of bicyclic cyclopropanol derivatives via radical pathways

Eietsu Hasegawa*, Minami Tateyama, Ryosuke Nagumo, Eiji Tayama and Hajime Iwamoto

Full Research Paper

Open Access

Address:
Department of Chemistry, Faculty of Science, Niigata University, Ikarashi-2 8050, Niigata 950-2181, Japan

Email:
Eietsu Hasegawa* - ehase@chem.sc.niigata-u.ac.jp

* Corresponding author

Keywords:
copper(II) salt; cyclopropanol; electron transfer; free radical; radical ion probe

Beilstein J. Org. Chem. **2013,** *9,* 1397–1406.
doi:10.3762/bjoc.9.156

Received: 30 April 2013
Accepted: 19 June 2013
Published: 11 July 2013

This article is part of the Thematic Series "Organic free radical chemistry".

Guest Editor: C. Stephenson

Abstract

Copper(II)-salt-promoted oxidative ring-opening reactions of bicyclic cyclopropanol derivatives were investigated. The regioselectivities of these processes were found to be influenced by the structure of cyclopropanols as well as the counter anion of the copper(II) salts. A mechanism involving rearrangement reactions of radical intermediates and their competitive trapping by copper ions is proposed.

Introduction

Radical ions are key intermediates in electron-transfer (ET) reactions of organic molecules [1-5] and they often undergo fragmentations to yield free radicals and ions [6-10]. The ensuing reaction pathways followed by the resulting radicals are governed not only by their intrinsic nature but also by the nature of co-existing redox reagents. In principle, radical intermediates in ET-promoted reactions have a tendency to participate in further ET processes to generate ionic species when stoichiometric amounts of redox reagents are used (Scheme 1) [1-10]. In contrast, radical intermediates formed by a photoinduced ET (PET) are less likely to undergo these secondary reactions, because steady-state concentrations of PET-generated redox

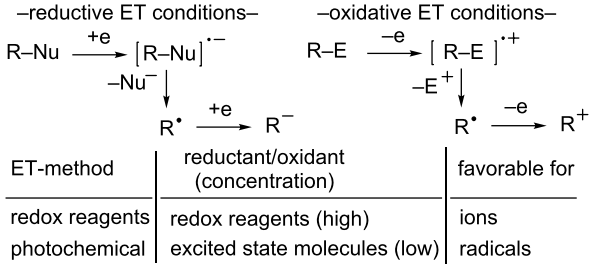

Scheme 1: Comparison of fragmentation reaction pathways of organic radical ions generated under the redox-reagent-promoted ET and PET conditions.

reagents are low [11-19]. When radical intermediates and ions derived from their precursor radical ions undergo different rearrangement reactions, it is often possible to distinguish respective reaction pathways of radicals and ions by examining the product distributions of the reactions of substrates that contain appropriate probe moieties (Scheme 2).

In past studies, we developed unique families of substances (exemplified by probes **I** and **II** in Figure 1) that act as radical ion probes [20] and found that radical intermediates in their reaction pathways undergo efficient 5-*exo* hexenyl radical cyclization reactions [21], (Figure 1) [22-30]. For example, PET reactions of probe **I** with amines were observed to produce a spirocyclic ketone product while its reduction reaction induced by samarium diiodide (SmI_2) gives rise to a cyclopropanol (left in Scheme 3) [22,24,27]. On the other hand, the same spirocyclic ketone is obtained in the 9,10-dicyanoanthracene (DCA) and biphenyl (BP) sensitized PET reaction of probe **II**, while reactions of this substrate with certain oxidants afford ring-expanded ketone and enone products (right in Scheme 3) [23,25,26,28-30].

Careful examination of the reaction of probe **II** with $FeCl_3$ revealed that a small quantity of the spirocyclic ketone was also formed [23,28]. This observation prompted us to explore the possibility that the free radical rearrangement route becomes more predominant when oxidizing reagents weaker than Fe(III) are used to promote the reaction. Based on a consideration of the redox potentials of Fe and Cu ions (E^o in H_2O, V versus NHE), +0.77 for Fe(III)/Fe(II), +0.17 for copper(II)/copper(I) [31], we chose to explore the use of copper(II) reagents in this effort. Although various ET reagents have been employed to promote reactions of cyclopropanol derivatives [32-47], the employment of copper(II) reagents to induce reactions has not been extensively studied [36,39]. In the investigation described below, we have explored copper(II)-salt-promoted oxidative ring-opening reactions of selected bicyclic cyclopropanol derivatives.

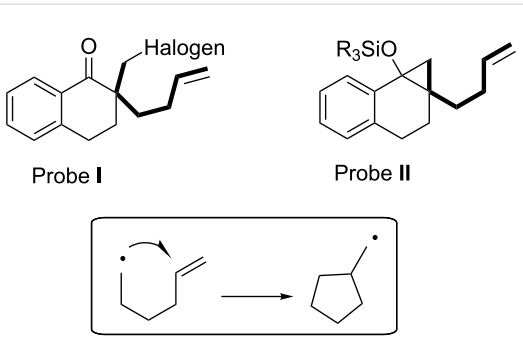

Figure 1: Radical anion and cation probe substances **I** and **II**, possessing 5-hexenyl structures.

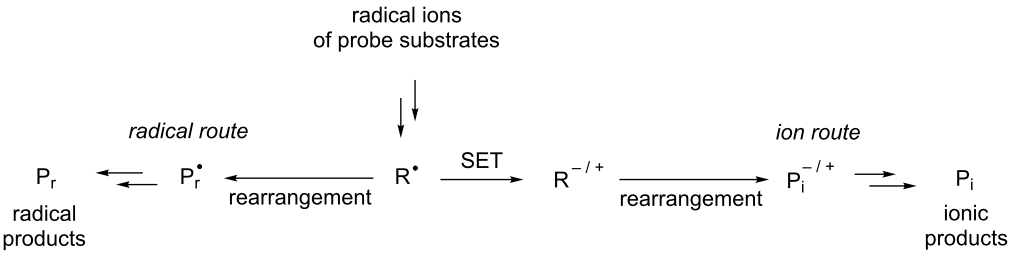

Scheme 2: Using rearrangements of radicals and ions to distinguish mechanistic pathways for ET-reactions.

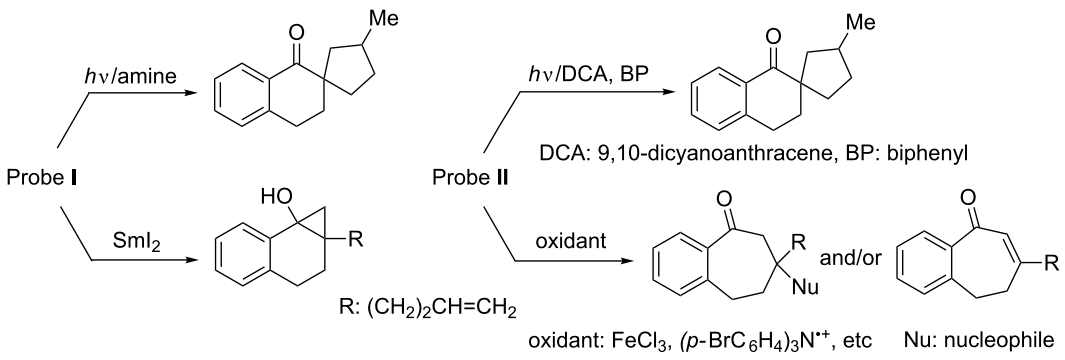

Scheme 3: Reductive ET reactions of the probe **I** (left) and oxidative ET reactions of probe **II** (right).

Results and Discussion

In the initial phase of this effort, we examined the reaction of cyclopropyl silyl ether **1a** (0.40 mmol) with copper(II) acetate, $Cu(OAc)_2$, (1.1 equiv) for 1 h at room temperature (Scheme 4). Under these conditions no reaction takes place, which we attribute to the steric bulk of the silyl substituent causing interference in the reaction of the substrate with $Cu(OAc)_2$. In accordance with this reasoning, we found that inclusion of *n*-Bu_4NF (1.2 equiv) in the reaction mixture led to a reaction that completely consumes **1a** and produced the expected spirocyclic ketone **2**, albeit in low yield, and spirocyclic ketone **3** possessing an *exo*-methylene moiety as the major product. Interestingly, ketone **3** was previously observed as a product of the DCA–BP-sensitized PET reaction of **1a** in the presence of $Cu(OAc)_2$ [25]. Only a trace amount of ring-expanded enone **4** along with small amounts of desilylated alcohol **1b** (ca. 8%) and ketone **5** were detected in the product mixture by using ^{1}H NMR analysis. Treatment of **1a** (0.19 mmol) with *n*-Bu_4NF (2.0 equiv) in THF for 1 h followed by hydrolysis gave a mixture of **1b** and **5** (12:88). Therefore, **5** may not result from the copper(II)-oxidation reaction.

Based on the above observations, we anticipated that sterically less hindered cyclopropanols would more efficiently undergo copper(II)-induced oxidation reactions than the corresponding silyl ethers. To probe this prediction, cyclopropanols **1**, prepared by SmI_2-promoted intramolecular Barbier reaction of the corresponding α-bromomethyl cycloalkanones **6** [28], were subjected to reactions promoted by various copper(II) salts, CuX_2 (Scheme 5).

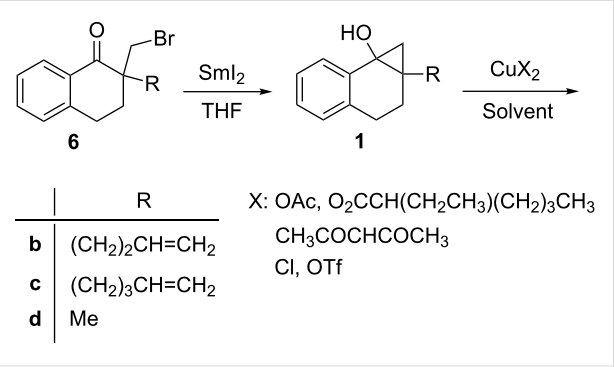

Scheme 5: SmI_2-promoted preparation of **1** and subsequent reaction with CuX_2.

The results of the reaction of **1b** with $Cu(OAc)_2$ (Scheme 6) are summarized in Table 1. As expected, this process produces ketone **3** as the major product along with both **2** and ring-expanded enone **4** as minor products. Moreover, the order of addition of **1b** and $Cu(OAc)_2$ does not significantly affect the product distribution (compare Table 1, entry 1 to entry 2). An exploration of solvent effects revealed that MeCN is more suitable than DMF while the solubility of $Cu(OAc)_2$ is higher in the latter solvent (compare Table 1, entry 1 to entry 5). In entry 5 (Table 1), ring-opened ketone **5** was obtained. In other experiments (see below), the formations of **5** (see Table 2), and other ring-opened ketones **22** (see Table 3) and **25** (see Scheme 11) are also observed. These products might be formed by deprotonation of the corresponding cyclopropanols **1**. It should be noted that THF is not an appropriate solvent for this reaction (Table 1, entry 8), a finding that is in contrast to the previous

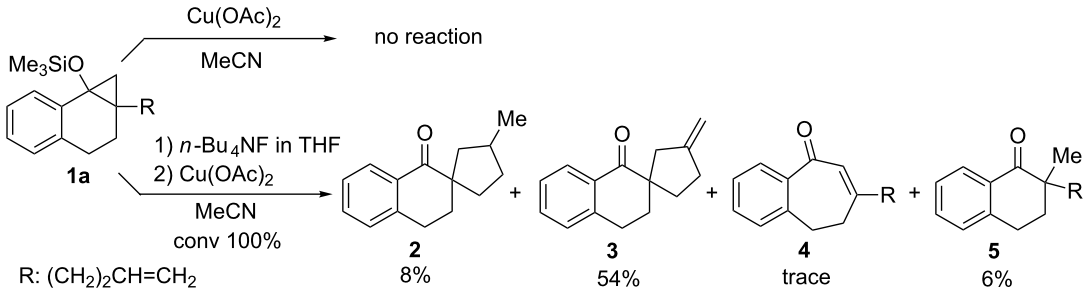

Scheme 4: Reaction of silyl ether **1a** with $Cu(OAc)_2$ in the absence or presence of *n*-Bu_4NF.

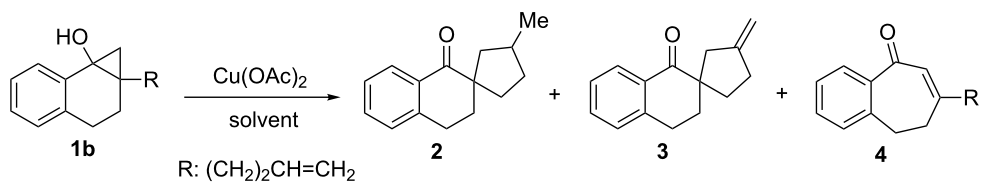

Scheme 6: Reaction of cyclopropanol **1b** with $Cu(OAc)_2$.

Table 1: Reaction of cyclopropanol **1b** with $Cu(OAc)_2$.[a]

entry	$Cu(OAc)_2$ (equiv)	solvent	conv of **1b**[b] (%)	yields[c] (%)		
				2	**3**	**4**
1	1.1	MeCN	91	0	70	~5[d]
2[e]	1.1	MeCN	100	0	70	~8[d]
3	0.5	MeCN	82	5	47	~2[d]
4[e]	2.2	MeCN	100	0	62	4
5[f]	1.1	DMF	60	0	35	trace
6	2.2	DMF	69	1	40	~1[d]
7[e]	1.1	CH_2Cl_2	85	10	38	trace
8	1.1	THF	28	trace	6	trace

[a]**1b** derived from **6b** (0.40 mmol) was added to $Cu(OAc)_2$ in a solvent (4 mL). [b]Determined by ^{1}H NMR based on the yield of the isolated products (see Experimental). [c]Isolated or determined by ^{1}H NMR. [d]Crude yields. [e]$Cu(OAc)_2$ was added to **1b** in a solvent. [f]Ketone **5** (~5%) was obtained.

observation that ether is a better solvent than MeCN and DMF in $Cu(BF_4)_2$-promoted ring-opening reactions of cyclopropylsilyl ethers [39]. When CH_2Cl_2 is employed as solvent, formation of **2** becomes more efficient while the yield of **3** remains moderate (Table 1, entry 7). Although the effect of the quantity of $Cu(OAc)_2$ on the reaction is not great, a decrease in the amount of $Cu(OAc)_2$ causes a small increase in the yield of **2** and a decrease in the yield of **3** (compare Table 1, entry 3 to entry 1). By using more $Cu(OAc)_2$, the yield of **3** is increased in DMF (compare Table 1, entry 6 to entry 5) while it is decreased in MeCN (compare Table 1, entry 4 to entry 2).

The observations described above suggest that the mechanism for this reaction shown in Scheme 7 is plausible. Because copper(II) is a relatively weak outer-sphere SET oxidant [1], addition of the hydroxy group of **1b** to $Cu(OAc)_2$ takes place initially to produce Lewis base–acid complex **7**, followed by inner-sphere ET involving elimination of CuOAc and AcOH, which gives cyclopropoxy radical **8**. Either external or internal bond cleavage of **8** generates the respective primary alkyl radical **9** or tertiary alkyl radical **10**. An equilibrium interconverting **9** and **10** through **8** [22-30] might occur (see below). A mechanism on the fragmentation of initially formed

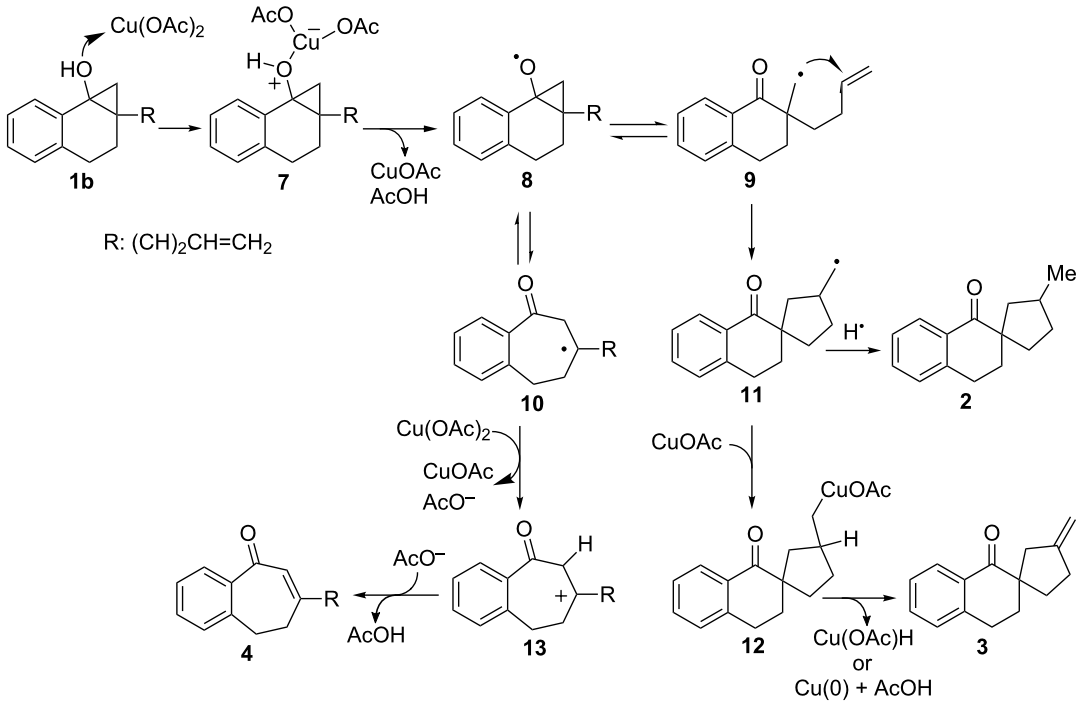

Scheme 7: Plausible reaction pathways for the reaction of **1b** with $Cu(OAc)_2$.

metal–organic complexes, giving β-ketoalkyl radicals [40], cyclopropoxy radicals [25,28,48-50], or β-metalated carbonyls [39], is still controversial [35-47]. Thus, we believe the reaction follows the pathways shown in Scheme 7 although the possibility of direct formations of **9** and **10**, a concerted ET and cyclopropane ring opening, cannot be ruled out. Rapid 5-*exo* cyclization of hexenyl radical moiety in **9** produces spirocyclic primary alkyl radical **11**. Hydrogen-atom abstraction by **11** then leads to formation of spirocyclic ketone product **2**, while trapping of **11** by CuOAc followed by β-H elimination (either hydride elimination or deprotonation) [39] of the resulting organocopper intermediate **12** generates the exocyclic methylene analogue **3** as the major product [25]. Protonation of **12** might be an alternative route for the formation of **2** (not shown in Scheme 7). Reactions of alkyl radicals with copper(II) are well documented [51,52], and it has been also suggested that copper(I) efficiently reacts with alkyl radicals [39]. As described, 1.1 equiv of $Cu(OAc)_2$ leads to nearly complete reaction of **1b** (see entry 1 and entry 2 in Table 1). Thus, CuOAc which is generated after initial ET between $Cu(OAc)_2$ and **1b** may capture the primary alkyl radical **11**. In addition, although not predominant, oxidation of **10** by $Cu(OAc)_2$ gives rise to tertiary carbocation **13** [51,52], which is then deprotonated to form enone **4**.

Studies of the effect of the counter ion on copper(II)-promoted reactions of **1b** (Scheme 8) gave the results summarized in Table 2. While no reaction occurred when copper(II) acetylacetonate, $Cu(acac)_2$, is used, (Table 2, entry 1), copper(II) 2-ethylhexanoate, $Cu(ehex)_2$, serves as an effective oxidant in transforming **1b** to **3** in a yield that is comparable to the process promoted by $Cu(OAc)_2$ (compare Table 2, entry 2 to entry 3). Noticeable amounts of **2** are also generated in this reaction. When $CuCl_2$ is employed to oxidize **1b**, only ring-expanded ketones **4** and **14** are produced along with a lesser amount of chloro ketone **15**, and competitive formation of **2** and **3** does not occur (Table 2, entry 4). An increase in the amount of $CuCl_2$ causes a slight increase in the conversion of **1b** and the total yield of ring-expanded products **4** and **14** (compare Table 2, entry 5 to entry 4). Interestingly, $CuCl_2$ (1.1 equiv) could also promote the reaction of silyl ether **1a** to produce **4** (23%), **14** (4%) and **15** (3%) at 89% conversion of **1a**. Although the origin

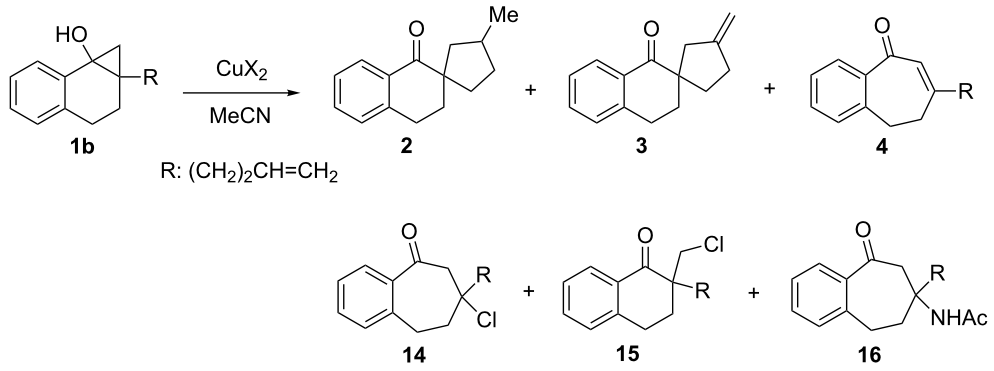

Scheme 8: Reaction of cyclopropanol **1b** with various copper(II) salts (CuX_2).

Table 2: Reaction of cyclopropanol **1b** with various copper(II) salts (CuX_2).[a]

entry	X	Conv of **1b**[b] (%)	yields[c] (%)		
			2	**3**	**4**
1	acetyl acetonate (acac)	0		No reaction	
2[d]	2-ethyl hexanoate (ehex)	94	5	63	~4[e]
3[f]	OAc	91	0	70	~5[e]
4[g]	Cl	63	0	0	~25[e](9)[h]
5[i]	Cl	71	0	0	34(6)[h]
6[j]	OTf	77	trace	0	~11[e](34)[k]

[a]**1b** derived from **6b** (0.40 mmol) was added to CuX_2 (1.1 equiv for entries 1–4,6; 2.2 equiv for entry 5) in MeCN (4 mL). [b]Determined by ^{1}H NMR based on the yield of the isolated products (see Experimental). [c]Isolated or determined by ^{1}H NMR. [d]Ketone **5** (13%) was obtained. [e]Crude yield. [f]Same as entry 1 in Table 1. [g]Ketone **5** (9%) and chloro ketone **15** (4%) were obtained. [h]Number in the parenthesis is the yield of chloro adduct **14**. [i]Ketone **5** (13%) and chloro ketone **15** (11%) were obtained. [j]Ketone **5** (~2%) was obtained. [k]Number in parentheses is the yield of acetoamide **16**.

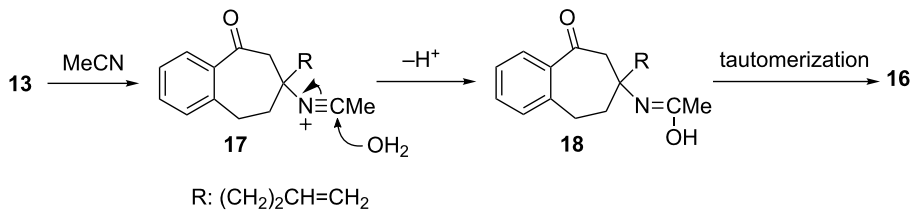

Scheme 9: Formation of acetoamide **16** from the cation **13**.

of **15** is uncertain, one possibility is that it is formed by halogen substitution of unconverted bromide **6b** to **1b** by SmI_2. The formation of chloro ketone **23** (see Table 3) may be similarly explained. Finally, reaction of **1b** with $Cu(OTf)_2$ leads to formation of ring-expanded products **4** and **16** and a negligible amount of **2** (Table 2, entry 6). Acetamide **16** is probably produced in this process through a Ritter reaction between cation **13** and the solvent acetonitrile (Scheme 9).

Hypothetically, both the Lewis acidity and oxidizing ability of CuX_2 should depend on the basicity of the counter ion (X^-: conjugate base of HX). Based on the acidity order HX, TfOH > HCl > AcOH ~ 2-ethyl hexanoic acid > acetylacetone [53,54], it is possible to assign $Cu(acac)_2$, which is ineffective in promoting the reaction, as the weakest oxidant. On the other hand, $CuCl_2$ and $Cu(OTf)_2$ induce reactions that follow a different pathway from those promoted by copper(II) carboxylates. These observations suggest that a rapid equilibrium does indeed exist between isomeric radical intermediates **9** and **10** (Scheme 7) and that the thermodynamically less stable isomer **9** undergoes fast hexenyl-radical cyclization leading to the formation of **11** in reactions promoted by copper(II) carboxylates. On the other hand, a fast oxidation of the more stable isomer **10** by stronger oxidants such as $CuCl_2$ or $Cu(OTf)_2$ occurs to give the stable tertiary carbocation **13**, which is then captured by Cl^- or MeCN.

In order to explore the generality of the proposed counter-anion-dependent reactivity switch in the nature of copper(II)-promoted reactions of **1**, the pentenyl-substituted cyclo-

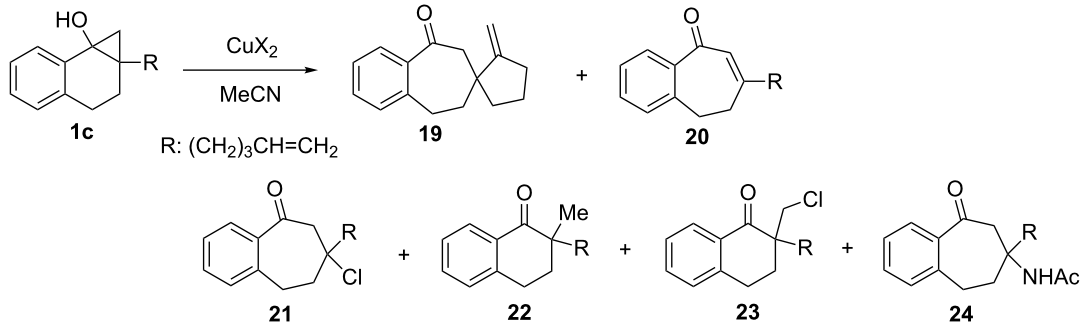

Scheme 10: Reaction of cyclopropanol **1c** with various copper(II) salts (CuX_2).

Table 3: Reaction of cyclopropanol **1c** with various copper(II) salts (CuX_2).[a]

entry	X	additive	conv of **1c**[b] (%)	yields[c] (%)	
				19	**20**
1	OAc	–	95	55	0
2	OAc	pyridine (1.2 equiv)	~65[d]	33	0
3	ehex	–	100	33	0
4[e]	Cl	–	63	0	28(8)[f]
5	OTf	–	~93[d]	0	13(33)[g]

[a]CuX_2 (1.1 equiv) was added to **1c** derived from **6c** (0.4 mmol) in MeCN (4 mL). [b]Determined by ^{1}H NMR based on the yield of the isolated products (see Experimental). [c]Isolated or determined by ^{1}H NMR. [d]Based on the crude yield of **1c**. [e]Ketone **22** (14%) and chloro ketone **23** (5%) were obtained. [f]Number in parentheses is the yield of chloro adduct **21**. [g]Number in parentheses is the yield of acetoamide **24**.

propanol **1c** was employed as the substrate (Scheme 10 and Table 3). A major product of the reaction of **1c** promoted by $Cu(OAc)_2$ was observed to be the *exo*-methylene containing spirocyclic ketone **19** (Table 3, entry 1), which is produced in the DCA–BP sensitized PET reaction of silyl ether of **1c** in the presence of $Cu(OAc)_2$ [25]. Contrary to the expectation that a base could assist the deprotonation of the complex between copper and **1c** (similar to **7** in Scheme 7), the addition of pyridine was found to decelerate the reaction (Table 3, entry 2). This observation suggests that coordination of pyridine to copper reduces the oxidizing ability of $Cu(OAc)_2$. $Cu(ehex)_2$ was also effective to give **19** although the yield was relatively low (Table 3, entry 3). Reaction of **1c** with $CuCl_2$ was observed to form ring-expanded ketones **20** and **21**, along with small amounts of **22** and **23**. However, competitive generation of **19** does not take place (Table 3, entry 4). Finally, reaction of **1c** with $Cu(OTf)_2$ leads to the formation of ring-expanded enone **20** and acetoamide **24** (Table 3, entry 5).

As described above, observation of the occurrence of hexenyl-radical cyclization processes serves as good evidence for the involvement of radical intermediates in mechanistic pathways for reactions of **1b** and **1c**. In order to gain more information about these processes, we explored an oxidation reaction of substrate **1d**, which does not contain an alkene tether and whose reaction pathway, thus, cannot involve radical intermediates that undergo hexenyl-radical cyclization. We observed that reaction of the methyl-substituted cyclopropanol **1d** with $Cu(OAc)_2$ leads to formation of the ring-expanded enone **25** as a major product along with a trace amount of ketone **26** (Scheme 11).

The $Cu(OAc)_2$-promoted reactions of **1c** and **1d** are compared in Scheme 12. The ring-expanded tertiary alkyl radical **27**, formed as an intermediate in the reaction of **8** (R = $(CH_2)_3CH{=}CH_2$), undergoes rapid 5-*exo* hexenyl cyclization along the route for the production of spirocyclic ketone **19**. Thus, oxidation of **27** followed by deprotonation to give enone **20** is a minor contributor. If an external bond cleavage of **8** occurs, cyclization of heptenyl-radical moiety in the resulting primary alkyl radical (not shown in Scheme 12) is expected. However, the *exo*-cyclization of heptenyl radical is two orders of magnitude slower than that of the hexenyl radical [55]. In contrast, because no competitive radical-rearrangement process exists, the corresponding radical intermediate **28** formed from **8** (R = Me) undergoes sequential oxidation and deprotonation to give enone **25** as a major product.

Conclusion

Various copper(II) salts promote ring-opening reactions of bicyclic cyclopropanol derivatives. Using substrates that possess hexenyl moieties, we observed that the nature of the counter anion of copper(II) salts has a significant impact on the product distributions. The results suggest that reaction pathways followed by radical intermediates derived from these substrates are strongly influenced by post ring-opening steps.

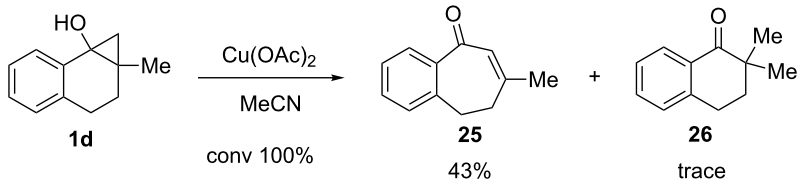

Scheme 11: Reaction of cyclopropanol **1d** with various $Cu(OAc)_2$.

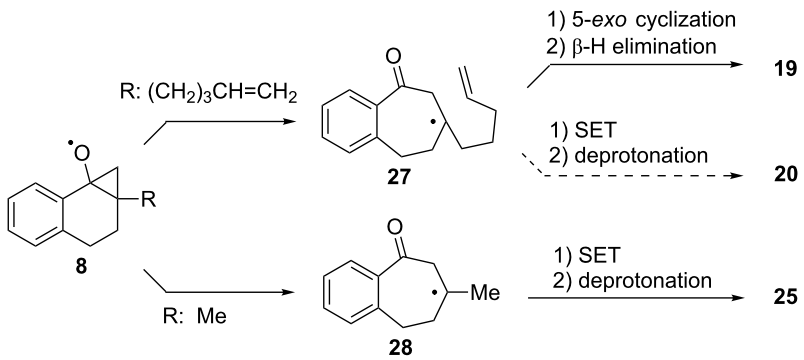

Scheme 12: Comparison of reaction pathways of ring-expanded radical **27** and **28**.

Thus, cyclopropane bond cleavage, which is reversible, does not serve as a product-determining step if a rapid follow-up reaction like hexenyl-radical cyclization does not exist. The results show that by using a proper choice of copper(II) salts it is possible to control the reaction pathways followed by radical and ionic intermediates derived from the initially formed Lewis base–acid complexes if the radicals and ions are capable of undergoing different rearrangement reactions.

Experimental

General: NMR spectra were recorded in $CDCl_3$ with Me_4Si as an internal standard at 400 MHz for ^1H NMR and 100 MHz for ^{13}C NMR. Column chromatography was performed with silica gel (Wakogel C-200). Preparative TLC was performed on 20 cm × 20 cm plates coated with silica gel (Wakogel B-5F). MeCN was distilled over P_2O_5 and subsequently distilled with K_2CO_3. CH_2Cl_2 was treated with H_2SO_4, water, 5% NaOH, water, and $CaCl_2$, and then distilled with CaH_2. THF was distilled over sodium benzophenone under N_2. Anhydrous DMF was purchased and used without distillation. Other reagents and solvents were purchased and used without further purification. Substrates **1a** [25], **1b** [29], **1d** [29], **6b** [24], and **6d** [28] and products **2** [24], **3** [25], **4** [25], **5** [29], **19** [25], **20** [26], **25** [25], and **26** [25] are known compounds. Spectral data of **1c**, **6c**, **14**, **15**, **16**, **21**, **22**, and **23** are presented below.

Preparation of cyclopropanols 1: Cyclopropanol derivatives **1** were prepared from the corresponding bromo ketones **6** by using SmI_2 following previously reported procedures [25,28]. Silyl ether **1a** was prepared by the treatment of alcohol **1b** with TMSCl and Et_3N. The synthesized alcohols **1b**, **1c** and **1d** were directly used for the reactions owing to their instabilities during silica-gel chromatography.

1-Hydroxy-3-(4-pentenyl)-6,7-benzobicyclo[4.1.0]heptane (1c): White solid; mp 71.5–72.9 °C; ^1H NMR (400 MHz, $CDCl_3$) δ 7.67–7.64 (m, 1H), 7.23–7.17 (m, 1H), 7.11–7.05 (m, 1H), 7.03–6.99 (m, 1H), 5.88–5.76 (m, 1H), 5.05–4.93 (m, 2H), 2.62 (ddd, *J* = 15.2, 5.2, 1.6 Hz, 1H), 2.52 (bs, 1H), 2.38 (td, *J* = 15.2, 5.2 Hz, 1H), 2.14–2.04 (m, 2H), 1.96 (ddd, *J* = 12.8, 5.6, 2.0 Hz, 1H), 1.66–1.46 (m, 5H), 1.20 (d, *J* = 6.0 Hz, 1H), 0.81 (d, *J* = 5.6 Hz, 1H); ^{13}C NMR (100 MHz, $CDCl_3$) δ 140.8, 138.9, 133.0, 127.9, 126.2, 125.3, 123.8, 114.4, 58.6, 33.9, 32.1, 30.5, 26.9, 26.4, 23.3, 21.3; IR (neat) ν_{max} (cm^{-1}): 3278, 3188, 3072, 2921, 1640, 1444, 1278, 1228, 1194, 990, 908, 740; LRMS–EI *m*/*z* (% relative intensity): 228 (M^+, 6), 160 (100); HRMS–EI (*m*/*z*): $[M]^+$ calcd for $C_{16}H_{20}O$, 228.1514; found, 228.1511.

2-Bromomethyl-2-(4-pentenyl)-1-tetralone (6c): Pale yellow oil; ^1H NMR (400 MHz, $CDCl_3$) δ 8.05–8.02 (m, 1H), 7.51–7.46 (m, 1H), 7.34–7.23 (m, 2H), 5.77–5.70 (m, 1H), 5.00–4.91 (m, 2H), 3.77 (d, *J* = 10.4 Hz, 1H), 3.64 (d, *J* = 10.4 Hz, 1H), 3.13–2.90 (m, 2H), 2.34–2.16 (m, 2H), 2.04–1.98 (m, 2H), 1.78–1.24 (m, 4H); ^{13}C NMR (100 MHz, $CDCl_3$) δ 198.7, 143.0, 138.0, 133.5, 131.3, 128.8, 128.1, 126.8, 115.0, 48.6, 39.3, 33.9, 32.7, 30.9, 24.8, 22.7; IR (neat) ν_{max} (cm^{-1}): 2938, 1680, 1600, 1454, 1304, 1224, 991, 910, 743; HRMS–ESI (*m*/*z*): $[M + H]^+$ calcd for $C_{16}H_{19}O^{79}Br$, 307.0692; found, 307.0687; $[M + H]^+$ calcd for $C_{16}H_{19}O^{81}Br$, 309.0672; found, 306.0665.

Reaction of cyclopropanols 1 with copper(II) salts: A typical experiment using **1b** is described (Table 1, entry 1). To $Cu(OAc)_2$ (79.9 mg, 0.44 mmol) in MeCN (4 mL) was added **1b** (85.7 mg, 0.40 mmol). In some experiments, the order of addition was reversed (see entry 2 in Table 1 and Table 3). The resulting mixture was stirred under N_2 at room temperature for 1 h, diluted with water and extracted with Et_2O. The extract was washed with water, saturated aqueous $Na_2S_2O_3$, saturated aqueous $NaHCO_3$, and brine, dried over anhydrous $MgSO_4$, and concentrated in vacuo giving a residue that was subjected to TLC (AcOEt:*n*-hexane 20/1), and **3** (59.3 mg, 0.28 mmol, 70%) and **4** (~5 mg, ~0.02 mmol, ~5%) were obtained. Other reactions were performed in a similar manner. Because cyclopropanols **1** have a tendency to partially decompose during silica-gel chromatography, their conversion in reactions was determined by using ^1H NMR analysis of the crude reaction mixtures. When product isolations were not performed, yields were also determined by ^1H NMR, and crude yields are reported in some cases.

3-(3-Butenyl)-3-chloro-1-benzosuberone (14): Brown liquid; ^1H NMR (400 MHz, $CDCl_3$) δ 7.80 (d, *J* = 7.6 Hz, 1H), 7.41 (t, *J* = 6.6 Hz, 1H), 7.32–7.29 (m, 2H), 5.88–5.78 (m, 1H), 5.10–4.98 (m, 2H), 3.51–3.40 (m, 2H), 3.16 (dd, *J* = 12.0, 1.6 Hz, 1H), 3.03 (dd, *J* = 17.0, 8.2 Hz, 1H), 2.55 (dd, *J* = 15.4, 8.2 Hz, 1H), 2.47–2.38 (m, 1H), 2.34–2.25 (m, 1H), 2.10–1.96 (m, 3H); ^{13}C NMR (100 MHz, $CDCl_3$) δ 197.8, 143.9, 137.5, 137.2, 132.0, 130.3, 128.9, 126.5, 115.2, 72.8, 55.8, 43.1, 42.8, 31.0, 28.7; IR (neat) ν_{max} (cm^{-1}): 2939, 1681, 1602, 1453, 1299, 1226, 915, 749; HRMS–ESI (*m*/*z*): $[M + H]^+$ calcd for $C_{15}H_{17}O^{35}Cl$, 249.1041; found, 249.1038; $[M + H]^+$ calcd for $C_{15}H_{17}O^{37}Cl$, 250.1074; found, 250.1071.

2-(3-Butenyl)-2-chloromethyl-1-tetralone (15): Colorless oil; ^1H NMR (400 MHz, $CDCl_3$) δ 8.03 (d, *J* = 8.4 Hz, 1H), 7.48 (t, *J* = 6.8 Hz, 1H), 7.31 (t, *J* = 7.6 Hz, 1H), 7.23 (d, *J* = 7.6 Hz, 1H), 5.78–5.68 (m, 1H), 5.01–4.91 (m, 2H), 3.87 (d, *J* = 11.6 Hz, 1H), 3.79 (d, *J* = 11.2 Hz, 1H), 3.13–3.05 (m, 1H), 2.96 (dt, *J* = 17.4, 5.0 Hz, 1H), 2.35–2.28 (m, 1H), 2.22–2.06 (m, 2H), 2.01–1.92 (m, 1H), 1.88–1.72 (m, 2H); ^{13}C NMR

(100 MHz, $CDCl_3$) δ 198.8, 142.8, 137.6, 133.5, 131.3, 128.7, 128.0, 126.8, 115.0, 49.1, 49.0, 31.6, 29.9, 27.7, 24.7; IR (neat) ν_{max} (cm^{-1}) 2940, 1680, 1601, 1453, 1225, 914, 748; HRMS–ESI (*m*/*z*): $[M + H]^+$ calcd for $C_{15}H_{17}O^{35}Cl$, 249.1041; found, 249.1041; $[M + H]^+$ calcd for $C_{15}H_{17}O^{37}Cl$, 251.1011; found, 251.1006.

3-(Acetylamino)-3-(3-butenyl)-1-benzosuberone (16): Yellow solid; mp 105.0–107.0 °C; ^1H NMR (400 MHz, $CDCl_3$) δ 7.77 (d, *J* = 6.4 Hz, 1H), 7.41 (t, *J* = 6.8 Hz, 1H), 7.30 (t, *J* = 6.4 Hz, 1H), 7.25 (d, *J* = 8.0 Hz, 1H), 5.87–5.77 (m, 1H), 5.56 (bs, 1H), 5.06–4.95 (m, 2H), 3.12–2.97 (m, 4H), 2.46–2.40 (m, 1H), 2.27–2.20 (m, 1H), 2.10–2.03 (m, 3H), 1.99–1.95 (m, 4H); ^{13}C NMR (100 MHz, $CDCl_3$) δ 201.3, 169.9, 144.2, 138.2, 138.1, 132.1, 130.3, 128.6, 126.6, 115.0, 57.5, 50.9, 39.3, 36.1, 31.2, 28.3, 24.2; IR (neat) ν_{max} (cm^{-1}) 3308, 3209, 2246, 1665, 1599, 1548, 1450, 1298, 1232, 912, 732; HRMS–ESI (*m*/*z*): $[M + Na]^+$ calcd for $C_{17}H_{21}NO_2$, 271.1567; found, 294.1463.

3-Chloro-3-(4-pentenyl)-1-benzosuberone (21): Brown oil; ^1H NMR (400 MHz, $CDCl_3$) δ 7.81 (d, *J* = 7.6 Hz, 1H), 7.42 (t, *J* = 7.6 Hz, 1H), 7.32–7.26 (m, 2H) , 5.87–5.76 (m, 1H), 5.07–4.96 (m, 2H), 3.51–3.41 (m, 2H), 3.16 (dd, *J* = 12.0, 1.6 Hz, 1H), 3.03 (dd, *J* = 16.0, 8.0 Hz, 1H), 2.55 (dd, *J* = 15.4, 8.4 Hz, 1H), 2.13–2.08 (m, 2H), 1.98–1.62 (m, 5H); ^{13}C NMR (100 MHz, $CDCl_3$) δ 198.0, 144.0, 138.0, 137.6, 132.0, 130.3, 128.9, 126.5, 115.0, 73.3, 55.8, 43.2, 43.1, 33.4, 31.1, 23.6; IR (neat) ν_{max} (cm^{-1}) 2943, 1680, 1600, 1449, 1297, 913, 751; HRMS–ESI (*m*/*z*): $[M + H]^+$ calcd for $C_{16}H_{19}O^{35}Cl$, 263.1197; found, 263.1191; $[M + H]^+$ calcd for $C_{16}H_{19}O^{37}Cl$, 265.1168; found, 265.1168.

2-Methyl-2-(4-pentenyl)-1-tetralone (22): Pale yellow oil; ^1H NMR (400 MHz, $CDCl_3$) δ 8.03 (d, *J* = 8.0 Hz, 1H), 7.45 (t, *J* = 7.6 Hz, 1H), 7.30 (t, *J* = 8.0 Hz, 1H), 7.21 (d, *J* = 8.0 Hz, 1H), 5.82–5.72 (m, 1H), 3.00–2.94 (m, 2H), 2.11–2.00 (m, 1H), 1.96–1.89 (m, 3H), 1.71–1.62 (m, 1H), 1.56–1.48 (m, 1H), 1.43–1.34 (m, 2H), 1.18 (s, 3H); ^{13}C NMR (100 MHz, $CDCl_3$) δ 202.6, 143.3, 138.6, 132.9, 131.7, 128.6, 128.0, 126.6, 114.6, 44.6, 35.9, 34.2, 33.6, 25.4, 23.3, 22.2; IR (neat) ν_{max} (cm^{-1}): 2933, 2859, 1682, 1601, 1454, 1222, 909, 741; HRMS–ESI (*m*/*z*): $[M + H]^+$ calcd for $C_{16}H_{20}O$, 229.1587; found, 229.1593.

2-Chloromethyl-2-(4-pentenyl)-1-tetralone (23): Pale yellow oil; ^1H NMR (400 MHz, $CDCl_3$) δ 8.03 (d, *J* = 8.0 Hz, 1H), 7.48 (t, *J* = 7.6 Hz, 1H), 7.31 (t, *J* = 8.0 Hz, 1H), 7.23 (d, *J* = 7.6 Hz, 1H), 5.78–5.68 (m, 1H), 5.00–4.90 (m, 2H), 3.82 (d, *J* = 11.2 Hz, 1H), 3.77 (d, *J* = 11.2 Hz, 1H), 3.12–3.04 (m, 1H), 2.95 (dt, *J* = 18.0, 4.8 Hz, 1H), 2.34–2.28 (m, 1H), 2.22–2.16 (m, 2H), 2.03–1.97 (m, 2H), 1.78–1.72 (m, 2H), 1.45–1.30 (m, 2H); ^{13}C NMR (100 MHz, $CDCl_3$) δ 199.1, 142.9, 138.0, 133.5, 131.4, 128.7, 128.0, 126.8, 115.0, 49.2, 49.1, 33.9, 31.9, 29.9, 24.7, 22.7; IR (neat) ν_{max} (cm^{-1}): 2939, 1680, 1600, 1454, 1222, 911, 746; HRMS–ESI (*m*/*z*): $[M + H]^+$ calcd for $C_{16}H_{19}O^{35}Cl$, 263.1195; found, 263.1197; $[M + H]^+$ calcd for $C_{16}H_{19}O^{37}Cl$, 265.1168; found, 265.1168.

3-(*N*-Acetylamino)-3-(4-pentenyl)-1-benzosuberone (24): Viscous yellow oil; ^1H NMR (400 MHz, $CDCl_3$) δ 7.77 (d, *J* = 7.6 Hz, 1H), 7.40 (t, *J* = 7.6 Hz, 1H), 7.28 (t, *J* = 7.6 Hz, 1H), 7.24 (d, *J* = 7.2 Hz, 1H), 5.84–5.74 (m, 1H), 5.55 (bs, 1H), 5.04–4.94 (m, 2H), 3.11–2.96 (m, 4H), 2.42–2.36 (m, 1H), 2.11–2.04 (m, 4H), 1.93 (s, 3H), 1.91–1.83 (m, 1H) , 1.43–1.35 (m, 2H) ppm; ^{13}C NMR (100 MHz, $CDCl_3$) δ 201.3, 169.8, 144.2, 138.4, 138.2, 132.0, 130.3, 128.5, 126.5, 114.8, 57.6, 50.9, 39.2, 36.6, 33.7, 31.2, 24.2, 23.1 ppm; IR (neat) ν_{max} (cm^{-1}): 3301, 3204, 2246, 1660, 1599, 1547, 1449, 1298, 1229, 912, 731; HRMS–ESI (*m*/*z*): $[M + Na]^+$ calcd for $C_{18}H_{23}NO_2$, 308.1621; found, 308.1622.

Acknowledgements

This study was partly supported by a grant from the Sasaki Environment Technology Foundation. We thank Professor Masaki Kamata (Niigata University) for his useful comments, and Professor James M. Tanko (Virginia Polytechnic Institute and State University, USA) for his suggestion on radical ion probes. We also thank Mr. Junichi Sakai (Niigata University) for his assistance in making HRMS (EI) measurements.

References

1. Eberson, L. *Electron Transfer Reactions in Organic Chemistry;* Reactivity and Structure Concepts in Organic Chemistry, Vol. 25; Springer Verlag: Berlin, Germany, 1987. doi:10.1007/978-3-642-72544-9
2. Mariano, P. S., Ed. *Advances in Electron Transfer Chemistry;* JAI Press: Greenwich, 1991–1999; Vol. 1–6.
3. Balzani, V., Ed. *Electron Transfer in Chemistry;* Wiley-VCH: Weinheim, Germany, 2001; Vol. 1–5.
4. Lund, H.; Hammerich, O. *Organic Electrochemistry,* 4th ed.; Marcel Dekker: New York, NY, 2001.
5. Procter, D. J.; Flowers, R. A., Eds. Electron Transfer Reagents in Organic Synthesis. *Tetrahedron* **2009,** *65,* 10725–10950.
6. Schmittel, M.; Burghart, A. *Angew. Chem., Int. Ed. Engl.* **1997,** *36,* 2550–2589. doi:10.1002/anie.199725501
7. Berger, D. J.; Tanko, J. M. In *The Chemistry of Double-Bonded Functional Groups;* Patai, S., Ed.; John Wiley & Sons: New York, NY, 1997; pp 1281–1354. doi:10.1002/0470857234.ch22
8. Roth, H. D. In *Reactive Intermediate Chemistry;* Moss, R. A.; Platz, M. S.; Jones, M., Jr., Eds.; John Wiley & Sons: Hoboken, NJ, USA, 2004; pp 205–272.
9. Floreancig, P. E., Ed. The Chemistry of Radical Ions. *Tetrahedron* **2006,** *62,* 6447–6594.
10. Todres, Z. V. *Ion-Radical Organic Chemistry Principles and Applications,* 2nd ed.; CRC Press: Boca Raton, FL, 2009.

11. Fox, M. A.; Channon, M., Eds. *Photoinduced Electron Transfer;* Elsevier: Amsterdam, The Netherlands, 1988. Parts A–D.
12. Kavarnos, G. J. *Fundamental of Photoinduced Electron Transfer;* VCH Press: New York, NY, USA, 1993.
13. Horspool, W. M.; Lenci, F., Eds. *CRC Handbook of Organic Photochemistry and Photobiology,* 2nd ed.; CRC Press: Boca Raton, FL, USA, 2004.
14. Hasegawa, E. *J. Photosci.* **2003,** *10,* 61–69.
15. Cossy, J.; Beloti, D. *Tetrahedron* **2006,** *62,* 6459–6470. doi:10.1016/j.tet.2006.03.062
16. Griesbeck, A. G.; Hoffmann, N.; Warzecha, K.-D. *Acc. Chem. Res.* **2007,** *40,* 128–140. doi:10.1021/ar068148w
17. Floreancig, P. E. *Synlett* **2007,** 191–203. doi:10.1055/s-2007-968021
18. Waske, P. A.; Tzvetkov, N. T.; Mattay, J. *Synlett* **2007,** 669–685. doi:10.1055/s-2007-970777
19. Cho, D. W.; Yoon, U. C.; Mariano, P. S. *Acc. Chem. Res.* **2011,** *44,* 204–215. doi:10.1021/ar100125j
20. Tanko, J. M.; Drumright, R. E. *J. Am. Chem. Soc.* **1990,** *112,* 5362–5363. doi:10.1021/ja00169a060 See for the originally proposed term radical ion probe.
21. Griller, D.; Ingold, K. U. *Acc. Chem. Res.* **1980,** *13,* 317–323. doi:10.1021/ar50153a004
22. Hasegawa, E.; Takizawa, S.; Iwaya, K.; Kurokawa, M.; Chiba, N.; Yamamichi, K. *Chem. Commun.* **2002,** 1966–1967. doi:10.1039/B205781F
23. Hasegawa, E.; Tsuchida, H.; Tamura, M. *Chem. Lett.* **2005,** *34,* 1688–1689. doi:10.1246/cl.2005.1688
24. Hasegawa, E.; Takizawa, S.; Seida, T.; Yamaguchi, A.; Yamaguchi, N.; Chiba, N.; Takahashi, T.; Ikeda, H.; Akiyama, K. *Tetrahedron* **2006,** *62,* 6581–6588. doi:10.1016/j.tet.2006.03.061
25. Hasegawa, E.; Yamaguchi, N.; Muraoka, H.; Tsuchida, H. *Org. Lett.* **2007,** *9,* 2811–2814. doi:10.1021/ol0709937
26. Hasegawa, E.; Ogawa, Y.; Kakinuma, K.; Tsuchida, H.; Tosaka, E.; Takizawa, S.; Muraoka, H.; Saikawa, T. *Tetrahedron* **2008,** *64,* 7724–7728. doi:10.1016/j.tet.2008.06.012
27. Hasegawa, E.; Hirose, H.; Sasaki, K.; Takizawa, S.; Seida, T.; Chiba, N. *Heterocycles* **2009,** *77,* 1147–1161. doi:10.3987/COM-08-S(F)94
28. Tsuchida, H.; Tamura, M.; Hasegawa, E. *J. Org. Chem.* **2009,** *74,* 2467–2475. doi:10.1021/jo802749g
29. Hasegawa, E.; Kakinuma, K.; Yanaki, T.; Komata, S. *Tetrahedron* **2009,** *65,* 10876–10881. doi:10.1016/j.tet.2009.09.108
30. Tsuchida, H.; Hasegawa, E. *Tetrahedron* **2010,** *66,* 3447–3451. doi:10.1016/j.tet.2010.03.029
31. Lange, N. A. In *Lange's Handbook of Chemistry,* 13th ed.; Dean, J. A., Ed.; McGraw-Hill: New York, NY, USA, 1985. Section 6.
32. Gibson, D. H.; DePuy, C. H. *Chem. Rev.* **1974,** *74,* 605–623. doi:10.1021/cr60292a001
33. Kuwajima, I.; Nakamura, E. Metal homoenolates from siloxycyclopropanes. In *Small Ring Compounds in Organic Synthesis IV;* de Meijere, A., Ed.; Topics in Current Chemistry, Vol. 155; Springer Verlag: Berlin, Germany, 1990; pp 1–39. doi:10.1007/3-540-52422-3_1
34. Kulinkovich, O. G. *Chem. Rev.* **2003,** *103,* 2597–2632. doi:10.1021/cr010012i
35. Ito, Y.; Fujii, S.; Saegusa, T. *J. Org. Chem.* **1976,** *41,* 2073–2074. doi:10.1021/jo00873a055
36. Ryu, I.; Ando, M.; Ogawa, A.; Murai, S.; Sonoda, N. *J. Am. Chem. Soc.* **1983,** *105,* 7192–7194. doi:10.1021/ja00362a041
37. Paolobelli, A. B.; Gioacchini, F.; Ruzziconi, R. *Tetrahedron Lett.* **1993,** *34,* 6333–6336. doi:10.1016/S0040-4039(00)73745-2
38. Iwasawa, N.; Hayakawa, S.; Funahashi, M.; Isobe, K.; Narasaka, K. *Bull. Chem. Soc. Jpn.* **1993,** *66,* 819–827. doi:10.1246/bcsj.66.819
39. Ryu, I.; Matsumoto, K.; Kameyama, Y.; Ando, M.; Kusumoto, N.; Ogawa, A.; Kambe, N.; Murai, S.; Sonoda, N. *J. Am. Chem. Soc.* **1993,** *115,* 12330–12339. doi:10.1021/ja00079a013
40. Booker-Milburn, K. I.; Thompson, D. F. *J. Chem. Soc., Perkin Trans. 1* **1995,** 2315–2321. doi:10.1039/P19950002315
41. Iwasawa, N.; Funahashi, M.; Hayakawa, S.; Ikeno, T.; Narasaka, K. *Bull. Chem. Soc. Jpn.* **1999,** *72,* 85–97. doi:10.1246/bcsj.72.85
42. Highton, A.; Volpicelli, R.; Simpkins, N. S. *Tetrahedron Lett.* **2004,** *45,* 6679–6683. doi:10.1016/j.tetlet.2004.06.115
43. Kirihara, M.; Kakuda, H.; Ichinose, M.; Ochiai, Y.; Takizawa, S.; Mokuya, A.; Okubo, K.; Hatano, A.; Shiro, M. *Tetrahedron* **2005,** *61,* 4831–4839. doi:10.1016/j.tet.2005.03.033
44. Chiba, S.; Cao, Z.; El Bialy, S. A. A.; Narasaka, K. *Chem. Lett.* **2006,** *35,* 18–19. doi:10.1246/cl.2006.18
45. Jiao, J.; Nguyen, L. X.; Patterson, D. R.; Flowers, R. A., II. *Org. Lett.* **2007,** *9,* 1323–1326. doi:10.1021/ol070159h
46. Jida, M.; Guillot, R.; Ollivier, J. *Tetrahedron Lett.* **2007,** *48,* 8765–8767. doi:10.1016/j.tetlet.2007.10.003
47. Wang, Y. F.; Toh, K. K.; Ng, E. P. J.; Chiba, S. *J. Am. Chem. Soc.* **2011,** *133,* 6411–6421. doi:10.1021/ja200879w
48. Ryu, I.; Fukushima, H.; Okuda, T.; Matsu, K.; Kambe, N.; Sonoda, N.; Komatsu, M. *Synlett* **1997,** 1265–1268. doi:10.1055/s-1997-1554
49. Chatgilialoglu, C.; Ferreri, C.; Lucarini, M.; Venturini, A.; Zavitsas, A. *Chem.–Eur. J.* **1997,** *3,* 376–387. doi:10.1002/chem.19970030309
50. Cooksy, A. L.; King, H. F.; Richardson, W. H. *J. Org. Chem.* **2003,** *68,* 9441–9452. doi:10.1021/jo035085b
51. Kochi, J. K. *Acc. Chem. Res.* **1974,** *7,* 351–360. doi:10.1021/ar50082a006
52. Snider, B. B. *Chem. Rev.* **1996,** *96,* 339–364. doi:10.1021/cr950026m
53. Smith, M. B.; March, J. *March's Advanced Organic Chemistry,* 6th ed.; John Wiley & Sons: Hoboken, NJ, USA, 2007.
54. Howells, R. D.; McCown, J. D. *Chem. Rev.* **1977,** *77,* 69–92. doi:10.1021/cr60305a005
55. Beckwith, A. L. J.; Schiesser, C. H. *Tetrahedron* **1985,** *41,* 3925–3941. doi:10.1016/S0040-4020(01)97174-1

License and Terms

Beilstein Journal of Organic Chemistry

Diastereoselective radical addition to γ-alkyl-α-methylene-γ-butyrolactams and the synthesis of a chiral pyroglutamic acid derivative

Tomoko Yajima*, Eriko Yoshida and Masako Hamano

Full Research Paper

Open Access

Address:
Department of Chemistry, Ochanomizu University, Otsuka, Bunkyo-ku, Tokyo, 112-8610, Japan

Email:
Tomoko Yajima* - yajima.tomoko@ocha.ac.jp

* Corresponding author

Keywords:
chelation controlled reaction; diastereoselective reaction; free radical; lactams; pyroglutamic acid derivative; radical alkylation

Beilstein J. Org. Chem. **2013,** *9,* 1432–1436.
doi:10.3762/bjoc.9.161

Received: 23 May 2013
Accepted: 25 June 2013
Published: 17 July 2013

This article is part of the Thematic Series "Organic free radical chemistry".

Guest Editor: C. Stephenson

Abstract

The *cis*- and *trans*-stereoselective radical additions to α-methylene-γ-alkyl- γ-lactams were investigated and the scope and limitation of the reaction were also revealed. This stereoselective radical reaction was used for synthesis of chiral pyroglutamic acid derivatives starting from a commercially available chiral amino acid.

Introduction

γ-Lactams exist in many natural products and biologically active compounds and are one of the most important classes of compounds for drug discovery [1-3]. Substituted γ-lactams, in particular, have potential application in drug synthesis, but the development of stereoselective synthesis of chiral γ-lactams remains a challenge [4,5]. Developing effective and simple synthetic methods is important so that the drug candidates can be screened. A stereoselective addition to a γ-lactam skeleton provides a direct and efficient method for synthesizing various γ-lactam derivatives. However, the most commonly used methods for synthesizing chiral γ-lactams are based on the cyclization or cycloaddition of *N*-containing precursors, which are synthesized stereoselectively, and there are limited studies on the stereoselective additions to γ-lactam skeletons [6-8] and no reports on radical addition.

We have already investigated diastereoselective alkyl radical additions to α-methylene-γ-phenyl- γ-lactam and reported that the *N*-unsubstituted lactam yields *cis*-α,γ-disubstituted lactams using $(Me_3Si)_3SiH$ under UV irradiation, whereas the reactions of *N*-pivaloyllactams with Et_3B and Bu_3SnH in the presence of $Yb(OTf)_3$ yields *trans*-α,γ-disubstituted lactams, both reactions involving various alkyl radicals (Scheme 1) [9]. Although this method allows the stereoselective introduction of various substituents into γ-lactams, only γ-phenyl-γ-lactam was used as a substrate. Therefore, we were interested in whether our reac-

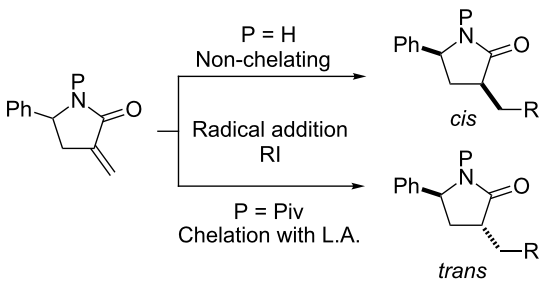

Scheme 1: Radical addition to α-methylene-γ-phenyl-γ-butyrolactams.

tion conditions would be suitable for γ-alkyl substrates and would allow the efficient synthesis of chiral *N*-containing compounds.

Here, we report *cis*- and *trans*-stereoselective radical additions to α-methylene-γ-alkyl- γ-lactams and the synthesis of chiral pyroglutamic acid derivatives using our reaction, starting from a commercially available chiral amino acid.

Results and Discussion

First, *cis*-selective isopropyl radical additions to α-methylene-γ-alkyl-γ-lactams were investigated (Table 1). The lactams **1a**–**1d** were synthesized following published procedures [10]. The conditions used in our previous study [9] were used as the starting point, and the reactions of **1a**–**1d** (1 equiv) with isopropyl iodide (3 equiv) in CH_2Cl_2 by using AIBN (0.2 equiv) as a radical initiator and $(Me_3Si)_3SiH$ (TTMSS) (2 equiv) as a H-donor were performed at room temperature under UV irradiation. The reactions of **1a** and **1b** yielded strong *cis*-diastereoselectivities, but the reactions of **1c** and **1d** were less diastereoselective.

Next, isopropyl radical additions to *N*-pivaloyl substrates **3a**–**3d** in the presence of a Lewis acid were investigated (Table 2). The

Table 1: Radical addition to **1** under non-chelating conditions.

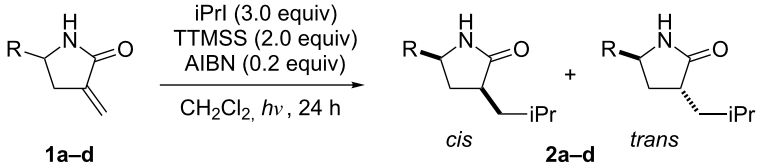

1a–d **2a–d**

entry	**1**	R	**2**	yield (%)	*cis*/*trans*
1	**1a**	iPr	**2a**	82	91:9
2	**1b**	*c*-Hex	**2b**	55	92:8
3	**1c**	iBu	**2c**	52	80:20
4	**1d**	$PhCH_2CH_2$	**2d**	49	84:16

Table 2: Radical addition to **3** under chelating conditions.

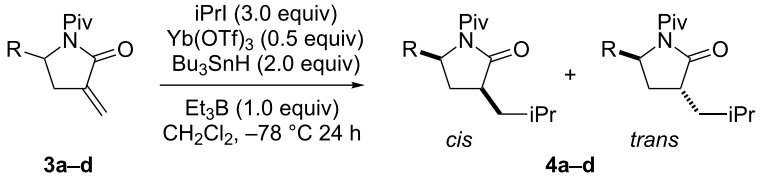

3a–d **4a–d**

entry	**3**	R	**4**	yield (%)	*cis*/*trans*
1	**3a**	iPr	**4a**	90	45:55
2	**3b**	*c*-Hex	**4b**	42	75:25
3[a]	**3b**	*c*-Hex	**4b**	62	88:12
4[b]	**3b**	*c*-Hex	**4b**	46	80:20
5	**3c**	iBu	**4c**	85	36:64
6	**3d**	$PhCH_2CH_2$	**4d**	71	50:50

[a]Without $Yb(OTf)_3$. [b]1.0 equiv of $Yb(OTf)_3$ was used.

reactions of **3a**–**3d** (1 equiv) with isopropyl iodide (3 equiv) in CH_2Cl_2 in the presence of Et_3B (1 equiv), Bu_3SnH (2 equiv), and $Yb(OTf)_3$ (0.5 equiv) were performed at −78 °C. The reactions of **3a**, **3c,** and **3d** were almost nondiastereoselective, while that of **3b** was *cis*-selective. The selectivity was almost the same as when the reaction was performed without a Lewis acid (Table 2, entry 3). Using an excess of $Yb(OTf)_3$ did not affect the diastereoselectivity (Table 2, entry 2).

We then changed the protecting group of the lactam nitrogen from the pivaloyl to the acetyl group and investigated the reaction in the presence of a Lewis acid (Table 3). The reactions of **5c** and **5d** yielded strong *trans*-selectivities, but *cis*-selectivities were observed in the reactions of **5a** and **5b**. The use of $MgBr_2$–OEt_2 instead of $Yb(OTf)_3$ enhanced the yield but did not affect the diastereoselectivity (Table 3, entry 2).

The direction of hydrogen transfer from the H-donor (*n*-Bu_3SnH or TTMSS) to the intermediate radical determined the stereochemistry of the product. In the case of the reaction of unprotected lactam by using a bulky H-donor (Table 1), hydrogen transferred from the opposite side of the γ-alkyl group and the *cis*-product was obtained. The less hindered primary isobutyl or phenethyl substrates (**1c** or **1d**) yielded poorer stereoselectivities than did **1a** or **1b**. *Trans*-selectivity was expected for the amide type *N*-protecting group reaction because of the coordinating carbonyl oxygens. The carbonyl oxygen of lactam and that of the *N*-protecting group (pivaloyl or acetyl) bidentately coordinate to the Lewis acid to form a six-membered chelate. The Lewis acid coordinates from the opposite side of the γ-alkyl group, and hydrogen transfer occurred from the same face as the γ-alkyl substituent to give *trans*-selectivity. However, strong *trans*-selectivities were not observed for substrates with pivaloyl groups, and it appears that steric hindrance between the pivaloyl group and the lactam γ-alkyl disturbs chelation. Using the acetyl group, which is less sterically hindered than the pivaloyl group, improved the chelate formation of γ-isobutyl or γ-phenethyl substrates and the reactions of **5c** and **5d** were *trans*-selective. In contrast, relatively bulky isopropyl or cyclohexyl groups could not form the six-membered chelate because of the steric repulsion between the acetyl and tertiary alkyl group (Figure 1).

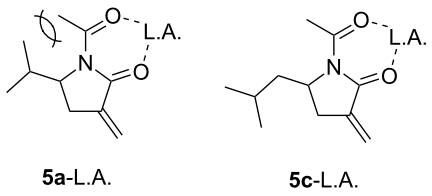

Figure 1: Chelation of **5a** and **5d**.

Finally, we attempted to synthesize the chiral pyroglutamic acid derivatives starting from a commercially available chiral amino acid. The reaction of benzaldehyde and (*S*)-phenylglycinol in the presence of $MgSO_4$ (used as a dehydrating reagent) gave a chiral imine, and the subsequent Reformatsky reaction with bromide **7** afforded butyl acrylate **8** as a single diastereomer [11,12] (Scheme 2). Hydrolysis with CF_3CO_2H and converting the hydroxy group to the chloride yielded the corresponding lactam **9** [13]. The chiral auxiliary was removed by DBU-assisted elimination to the enamine and subsequent hydrolysis [14]. Introducing the pivaloyl group, because *N*-pivaloyl gave high trans-selectivity of γ-phenyl substrate, yielded the chiral radical substrate **10**.

The *trans*-selective ethyl radical addition proceeded, yielding **11** with high diastereoselectivity, as we previously reported [9]. The *trans*-isomer was isolated by silica-gel column chromatography. The *N*-pivaloyl group on **11** was converted to the Boc

Table 3: Radical addition to **5** under chelating conditions.

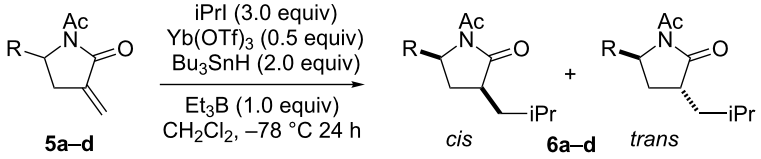

entry	5	R	6	yield (%)	*cis*/*trans*
1	**5a**	iPr	**6a**	37	78:22
2[a]	**5a**	iPr	**6a**	84	66:39
3	**5b**	*c*-Hex	**6b**	51	62:38
4	**5c**	iBu	**6c**	97	20:80
5	**5d**	$PhCH_2CH_2$	**6d**	92	25:75

[a]3.0 equiv of $MgBr_2$–OEt_2 was used instead of $Yb(OTf)_3$.

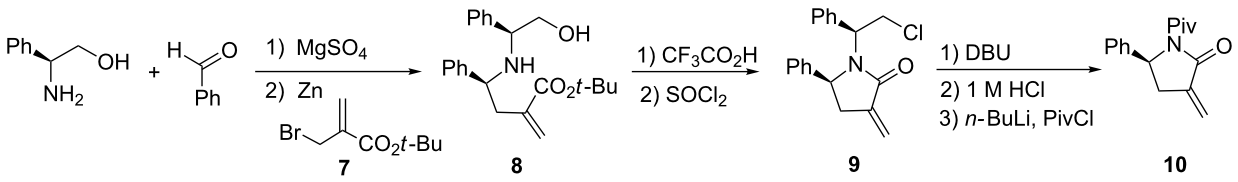

Scheme 2: Synthesis of chiral substrate **10**.

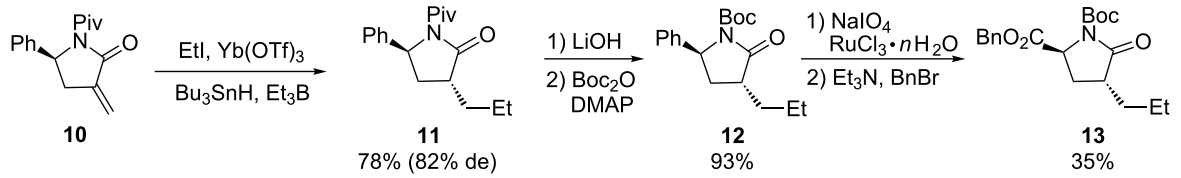

Scheme 3: Synthesis of chiral 4-butyl-L-pyroglutamic acid **13**.

group, because ruthenium oxidation did not proceed on using the pivaloyl-protected substrate **11**. The phenyl group was oxidized to the carboxylic acid by using ruthenium trichloride [15,16], and the benzylation of the carboxyl group yielded the pyroglutamic acid derivative **13** as a single stereoisomer (Scheme 3).

Conclusion

In this study, we investigated the *cis*- and *trans*-stereoselective radical additions to α-methylene-γ-alkyl- γ-lactams. Strong *cis*-selectivities were observed using various γ-substituents under non-chelating conditions. The reactions of pivaloyl protected substrates in the presence of a Lewis acid were not *trans*-selective, although pivaloyl protected γ-phenyl substrates gave high *trans*-selectivity in our previous report. The poor selectivities were attributed to the steric repulsion between the pivaloyl group and the γ-substituent on the substrate. The reactions using *N*-acetyl substrates instead of pivaloyl substrates yielded better *trans*-selectivities with γ-isobutyl and γ-phenethyl substrates, because acetyl is sufficiently small to allow chelation with the Lewis acid and lactam carbonyl. We used the reaction to synthesize chiral pyroglutamic acid derivatives starting from (*S*)-phenylglycinol.

Supporting Information

Supporting Information File 1

Experimental procedures and characterization data for compounds **2a**–**d**, **6a**–**d** and **9**–**13**.
[http://www.beilstein-journals.org/bjoc/content/supplementary/1860-5397-9-161-S1.pdf]

References

1. Catalani, M. P.; Alvaro, G.; Bernasconi, G.; Bettini, E.; Bromidge, S. M.; Heer, J.; Tedesco, G.; Tommasi, S. *Bioorg. Med. Chem. Lett.* **2011,** *21,* 6899–6904. doi:10.1016/j.bmcl.2011.07.116
2. Lee, C.; Choi, E.; Cho, M.; Lee, B.; Oh, S. J.; Park, S.-K.; Lee, K.; Kim, H. M.; Han, G. *Bioorg. Med. Chem. Lett.* **2012,** *22,* 4189–4192. doi:10.1016/j.bmcl.2012.04.045
3. Cornut, D.; Lemoine, H.; Kanishchev, O.; Okada, E.; Albrieux, F.; Beavogui, A. H.; Bienvenu, A.-L.; Picot, S.; Bouillion, J.-P.; Médebielle, M. *J. Med. Chem.* **2013,** *56,* 73–83. doi:10.1021/jm301076q
4. Zhao, X.; DiRocco, D. A.; Rovis, T. *J. Am. Chem. Soc.* **2011,** *133,* 12466–12469. doi:10.1021/ja205714g
5. Comesse, S.; Sanselme, M.; Daïch, A. *J. Org. Chem.* **2008,** *73,* 5566–5569. doi:10.1021/jo702752w
6. Zhang, Y.; Shao, Y.-L.; Xu, H.-S.; Wang, W. *J. Org. Chem.* **2011,** *76,* 1472–1474. doi:10.1021/jo102223v
7. Shao, C.; Yu, H.-J.; Wu, N.-Y.; Tian, P.; Wang, R.; Feng, C.-G.; Lin, G.-Q. *Org. Lett.* **2011,** *13,* 788–791. doi:10.1021/ol103054a
8. Lin, L.; Zhang, J.; Ma, X.; Fu, X.; Wang, R. *Org. Lett.* **2011,** *13,* 6410–6413. doi:10.1021/ol202713f
9. Yajima, T.; Hamano, M.; Nagano, H. *Tetrahedron Lett.* **2009,** *50,* 1301–1302. doi:10.1016/j.tetlet.2009.01.007
10. Pertrini, M.; Profeta, R.; Righi, P. *J. Org. Chem.* **2002,** *67,* 4530–4535. doi:10.1021/jo025606f
11. Dembélé, Y. A.; Belaud, C.; Hitchcock, P.; Villiéras, J. *Tetrahedron: Asymmetry* **1992,** *3,* 351–354. doi:10.1016/S0957-4166(00)80272-4
12. Dembélé, Y. A.; Belaud, C.; Villiéras, J. *Tetrahedron: Asymmetry* **1992,** *3,* 511–514. doi:10.1016/S0957-4166(00)80253-0
13. Obrecht, D.; Bohdal, U.; Daly, J.; Lehmann, C.; Schönholzer, P.; Müller, K. *Tetrahedron* **1995,** *51,* 10883–10900. doi:10.1016/0040-4020(95)00665-U
14. Agami, C.; Couty, F.; Evano, G. *Tetrahedron Lett.* **1999,** *40,* 3709–3712. doi:10.1016/S0040-4039(99)00594-8
15. Clayden, J.; Menet, C. J.; Tchabanenko, K. *Tetrahedron* **2002,** *58,* 4727–4733. doi:10.1016/S0040-4020(02)00379-4

16. Clayden, J.; Watson, D. W.; Helliwell, M.; Chambers, M. *Chem. Commun.* **2003,** 2582–2583. doi:10.1039/b308029c

License and Terms

Beilstein Journal of Organic Chemistry

Development of an additive-controlled, SmI_2-mediated stereoselective sequence: Telescoped spirocyclisation, lactone reduction and Peterson elimination

Brice Sautier, Karl D. Collins and David J. Procter*

Full Research Paper

Open Access

Address:
University of Manchester, School of Chemistry, Oxford Road, Manchester M13 9PL, United Kingdom

Email:
David J. Procter* - david.j.procter@manchester.ac.uk

* Corresponding author

Keywords:
cyclisation; free radical; Peterson elimination; reduction; samarium; telescoped process

Beilstein J. Org. Chem. **2013,** *9,* 1443–1447.
doi:10.3762/bjoc.9.163

Received: 20 May 2013
Accepted: 28 June 2013
Published: 18 July 2013

This article is part of the Thematic Series "Organic free radical chemistry".

Guest Editor: C. Stephenson

Abstract

Studies on SmI_2-mediated spirocyclisation and lactone reduction culminate in a telescoped sequence in which additives are used to "switch on" individual steps mediated by the electron transfer reagent. The sequence involves the use of two activated SmI_2 reagent systems and a silicon stereocontrol element that exerts complete diastereocontrol over the cyclisation and is removed during the final stage of the sequence by Peterson elimination. The approach allows functionalised cyclopentanols containing two vicinal quaternary stereocentres to be conveniently prepared from simple starting materials.

Introduction

Samarium diiodide (SmI_2) has become an essential tool for chemists since its introduction by Kagan [1,2], efficiently mediating a wide range of reductive transformations [3]. The reagent's versatility and the high degree of control usually observed in SmI_2-mediated reactions make it the first choice for an array of reductive electron transfer processes [4-13]. Cyclisations are one of the most notable classes of transformation induced by SmI_2 and have been widely employed in natural-product syntheses [8-10]. Importantly, fine tuning of the reagent's reduction potential through the use of additives allows complex, polyfunctionalised starting materials to be manipulated selectively [3-16].

Recently, we reported the use of a C–Si bond to control the stereochemical course of SmI_2-mediated cyclisations. For example, complete diastereocontrol was achieved in the construction of cyclobutanols [13,17-22] and spirocyclopentanols (Scheme 1) [23-28]. The use of MeOH as an additive with SmI_2 was key to the success of these cyclisations [24].

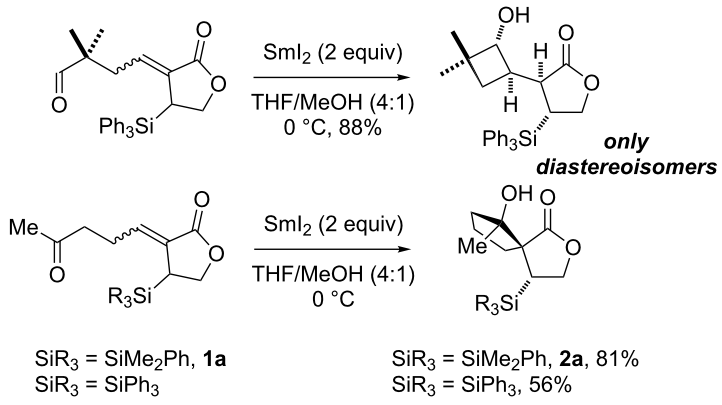

Scheme 1: SmI_2-mediated cyclisations directed by a C–Si bond.

In the case of spirocyclopentanol products **2**, further manipulation was hampered by their sensitivity to standard reductive conditions, and initially their reduction could only be achieved in two steps via the corresponding lactols [28]. An alternative solution for the manipulation of spirocyclopentanols **2** arose from our recent introduction of SmI_2−H_2O−amine [29-39] as a mild and efficient reagent system for the electron transfer reduction of carboxylic acid derivatives [40-42]. Pleasingly, SmI_2−H_2O−amine provided direct access to highly functionalised triols such as **3b** from spirocyclopentanol **2b** (Scheme 2) [42].

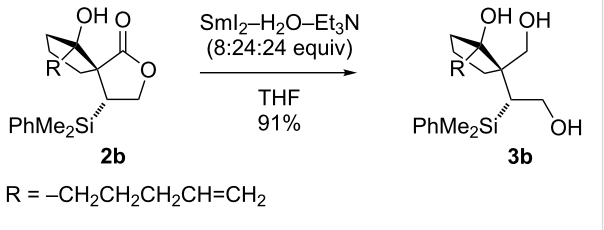

Scheme 2: Reduction of a spirocyclic lactone using SmI_2−H_2O−Et_3N.

In this manuscript, we report studies on SmI_2-mediated cyclisation and lactone reduction that culminate in a "telescoped" sequence, i.e., a sequence of steps carried out on a single reaction mixture by the sequential addition of various reagents. In the sequence, additives are used with SmI_2 to "switch on" individual steps: spirocyclisation, lactone reduction and Peterson elimination allow rapid access to functionalised cyclopentanols, containing two vicinal quaternary stereocentres, from simple starting materials. The sequence involves the use of two activated SmI_2 reagent systems, and a silicon stereocontrol element exerts complete diastereocontrol over the cyclisation and is removed during the final stage of the sequence.

Results and Discussion

Spirocyclisation

We first set out to examine the scope of the reductive-aldol spirocyclisation [23-27] directed by a C–Si bond, by varying the nature and functionalisation of the side chain. The ratio of **2b**/**4b** was optimized by adjusting the SmI_2/MeOH ratio and the reaction time to minimise retro-aldol reaction and the formation of saturated ketolactone byproduct **4b** (Table 1). Lowering the amount of SmI_2 and MeOH used and shortening the reaction time resulted in improved selectivity for spirolactone **2b**. We believe that spirolactones such as **2b** undergo retro-aldol fragmentation (to give products such as **4b**) upon prolonged exposure to Lewis acidic Sm(II)/(III)-species present in the reaction mixture.

Pleasingly, the process proved general, affording the desired spirocycles **2** in good yields and as single diastereoisomers with only small amounts of saturated ketolactone byproducts (cf. **4b**) observed. No byproducts arising from reaction of the additional functional groups present were formed (Scheme 3). Of particular note, keto-lactone **1f** bearing an ester-containing side chain gave the expected spirocycle **2f**, albeit with low conversion (unoptimized). As expected, no products arising from the reduction of the ester were observed [40-42].

Telescoped spirocyclisation/lactone reduction

Although the reduction of the spirocycles **2** proceeds smoothly with SmI_2−H_2O−Et_3N [40-42], we recognised the advantages of performing both SmI_2-mediated steps in a telescoped fashion. The strongly coordinating H_2O and amine additives used to activate SmI_2 [29-42] in the second lactone reduction step suggested that this far more reducing system would tolerate the presence of samarium(III) salts and a less-activating additive (MeOH) from the first reduction step. Pleasingly, when

Table 1: Optimisation of SmI_2–mediated spirocyclisation conditions.

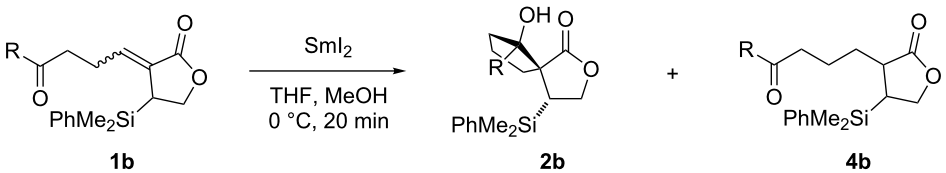

1b **2b** **4b**

R = $–CH_2CH_2CH_2CH=CH_2$

Entry	SmI_2[a] (equiv)	MeOH (equiv)	SmI_2/MeOH	**2b**/**4b**[b]
1	2.2	128	1:58	1.8:1
2	2.5	128	1:52	1.9:1
3	3	128	1:43	2.4:1
4	4	128	1:32	2.6:1
5	2.2	70	1:32	3.2:1
6	2.5	80	1:32	3.3:1
7	3	96	1:32	3.2:1
8[c]	2.5	80	1:32	4:1
9[c]	2.5	96	1:38	4:1

[a]0.1 M solution in THF. [b]From ^1H NMR of crude product mixture. [c]Reaction time 3–5 min.

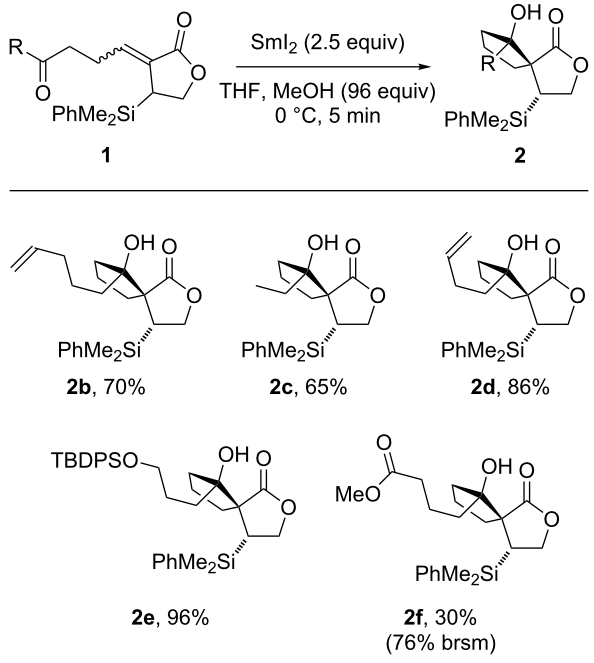

1 **2**

2b, 70% **2c**, 65% **2d**, 86%

2e, 96% **2f**, 30% (76% brsm)

Scheme 3: Stereoselective spirocyclisation of functionalised keto-lactone substrates directed by a C–Si bond.

subjected to the telescoped sequence, substrates **1** gave the desired triols **3** in comparable yields to those obtained from the stepwise process, without any need for further optimisation (Scheme 4).

The process is carried out by transferring the reaction mixture after the first reduction stage (SmI_2–MeOH) to a preformed solution of SmI_2–H_2O–Et_3N. The telescoped procedure proved robust and was scaled up to 1.2 g (3.5 mmol) without any drop in yield.

Telescoped spirocyclisation/lactone reduction/Peterson elimination

With an efficient process combining spirocyclisation and lactone reduction in hand, we proposed that manipulation of the triol products by Peterson elimination [43,44] could be added to the telescoped sequence. Crucially, Peterson elimination of triols **3** would result in removal of the silicon stereocontrol element used to control the stereochemical course of C–C bond formation. In early studies, treatment of triol **3b** with *t*-BuOK gave vinyl cyclopentanol **5b** in moderate yield [45], but the reaction suffered from poor reproducibility. Following a screen of reaction conditions, moderate but consistent yields were obtained when eliminations were performed in an open vessel, using undried solvents.

When combined with the spirocyclisation and lactone reduction sequence, the Peterson elimination gave diols **5**, with good overall yields comparable to those obtained for the stepwise process (Scheme 5).

We are currently exploring the use of the telescoped route to cyclopentanols **5** in an asymmetric approach [46] to the anti-tumor natural product pseudolaric acid B [47].

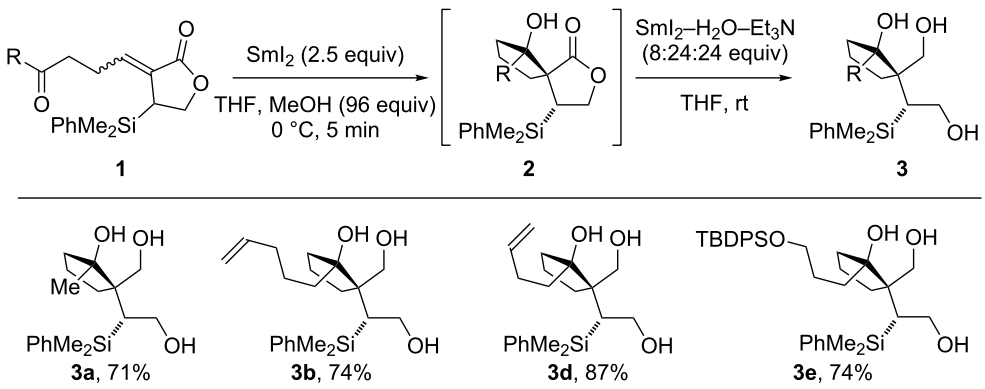

Scheme 4: Telescoped stereoselective spirocyclisation/lactone reduction.

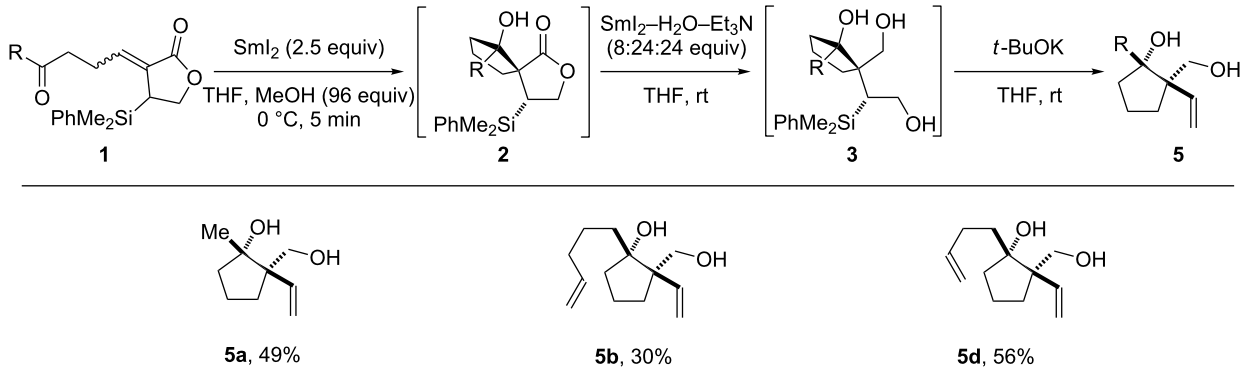

Scheme 5: Telescoped stereoselective spirocyclisation/lactone reduction/Peterson elimination.

Conclusion

In summary, we have developed a convenient, telescoped, three-step sequence to access functionalised cyclopentanols bearing two vicinal quaternary stereocentres from simple keto-lactone starting materials. The process involves the use of two activated SmI_2 reagent systems and a silicon stereocontrol element that results in complete diastereocontrol and is removed in the final stage of the sequence. The procedure is scalable and the overall yields of the telescoped sequences compare well to the combined yields of the analogous stepwise processes. The use of additives to "switch on" individual steps in a particular sequence mediated by the same electron transfer reagent constitutes an exciting new opportunity for efficient synthesis.

Supporting Information

Supporting Information File 1

General experimental procedures and characterisation data.
[http://www.beilstein-journals.org/bjoc/content/supplementary/1860-5397-9-163-S1.pdf]

Acknowledgements

We thank the EPSRC (project studentship, B.S.), Astrazeneca (CASE award, K.D.C.), and the University of Manchester.

References

1. Namy, J. L.; Girard, P.; Kagan, H. B. *Nouv. J. Chim.* **1977,** *1,* 5.
2. Girard, P.; Namy, J. L.; Kagan, H. B. *J. Am. Chem. Soc.* **1980,** *102,* 2693. doi:10.1021/ja00528a029
3. Procter, D. J.; Flowers, R. A., II; Skrydstrup, T. *Organic Synthesis using Samarium Diiodide: A Practical Guide;* RSC Publishing: Cambridge, 2009.
4. Kagan, H. B. *Tetrahedron* **2003,** *59,* 10351. doi:10.1016/j.tet.2003.09.101
5. Molander, G. A.; Harris, C. R. *Chem. Rev.* **1996,** *96,* 307. doi:10.1021/cr950019y
6. Krief, A.; Laval, A.-M. *Chem. Rev.* **1999,** *99,* 745. doi:10.1021/cr980326e
7. Steel, P. G. *J. Chem. Soc., Perkin Trans. 1* **2001,** 2727. doi:10.1039/A908189E
8. Edmonds, D. J.; Johnston, D.; Procter, D. J. *Chem. Rev.* **2004,** *104,* 3371. doi:10.1021/cr030017a
9. Nicolaou, K. C.; Ellery, S. P.; Chen, J. S. *Angew. Chem., Int. Ed.* **2009,** *48,* 7140. doi:10.1002/anie.200902151

10. Szostak, M.; Procter, D. J. *Angew. Chem., Int. Ed.* **2011,** *50,* 7737. doi:10.1002/anie.201103128
11. Flowers, R. A., II. *Synlett* **2008,** 1427. doi:10.1055/s-2008-1078414
12. Beemelmanns, C.; Reissig, H.-U. *Chem. Soc. Rev.* **2011,** *40,* 2199. doi:10.1039/c0cs00116c
13. Harb, H. Y.; Procter, D. J. *Synlett* **2012,** 6. doi:10.1055/s-0031-1290093
14. Dahlén, A.; Hilmersson, G. *Eur. J. Inorg. Chem.* **2004,** 3393. doi:10.1002/ejic.200400442
15. Sautier, B.; Procter, D. J. *Chimia* **2012,** *66,* 399. doi:10.2533/chimia.2012.399
16. Szostak, M.; Spain, M.; Parmar, D.; Procter, D. J. *Chem. Commun.* **2012,** *48,* 330. doi:10.1039/c1cc14252f
17. Johnston, D.; McCusker, C. M.; Procter, D. J. *Tetrahedron Lett.* **1999,** *40,* 4913. doi:10.1016/S0040-4039(99)00910-7
18. Johnston, D.; McCusker, C. F.; Muir, K.; Procter, D. J. *J. Chem. Soc., Perkin Trans. 1* **2000,** 681. doi:10.1039/A909549G
19. Johnston, D.; Francon, N.; Edmonds, D. J.; Procter, D. J. *Org. Lett.* **2001,** *3,* 2001. doi:10.1021/ol015976a
20. Johnston, D.; Couché, E.; Edmonds, D. J.; Muir, K. W.; Procter, D. J. *Org. Biomol. Chem.* **2003,** *1,* 328. doi:10.1039/b209066j
21. Edmonds, D. J.; Muir, K. W.; Procter, D. J. *J. Org. Chem.* **2003,** *68,* 3190. doi:10.1021/jo026827o
22. Baker, T. M.; Edmonds, D. J.; Hamilton, D.; O'Brien, C. J.; Procter, D. J. *Angew. Chem., Int. Ed.* **2008,** *47,* 5631. doi:10.1002/anie.200801900
23. Hutton, T. K.; Muir, K.; Procter, D. J. *Org. Lett.* **2002,** *4,* 2345. doi:10.1021/ol0260472
24. Hutton, T. K.; Muir, K. W.; Procter, D. J. *Org. Lett.* **2003,** *5,* 4811. doi:10.1021/ol0358399
25. Sloan, L. A.; Baker, T. M.; Macdonald, S. J. F.; Procter, D. J. *Synlett* **2007,** 3155. doi:10.1055/s-2007-1000821
26. Guazzelli, G.; Duffy, L. A.; Procter, D. J. *Org. Lett.* **2008,** *10,* 4291. doi:10.1021/ol8017209
27. Baker, T. M.; Sloan, L. A.; Choudhury, L. H.; Murai, M.; Procter, D. J. *Tetrahedron: Asymmetry* **2010,** *21,* 1246. doi:10.1016/j.tetasy.2010.03.047
28. Harb, H. Y.; Collins, K. D.; Altur, J. V. G.; Bowker, S.; Campbell, L.; Procter, D. J. *Org. Lett.* **2010,** *12,* 5446. doi:10.1021/ol102278c
29. Cabri, W.; Candiani, I.; Colombo, M.; Franzoi, L.; Bedeschi, A. *Tetrahedron Lett.* **1995,** *36,* 949. doi:10.1016/0040-4039(94)02398-U
30. Dahlén, A.; Hilmersson, G. *Tetrahedron Lett.* **2002,** *43,* 7197. doi:10.1016/S0040-4039(02)01673-8
31. Dahlén, A.; Hilmersson, G. *Chem.–Eur. J.* **2003,** *9,* 1123. doi:10.1002/chem.200390129
32. Dahlén, A.; Sundgren, A.; Lahmann, M.; Oscarson, S.; Hilmersson, G. *Org. Lett.* **2003,** *5,* 4085. doi:10.1021/ol0354831
33. Dahlén, A.; Hilmersson, G.; Knettle, B. W.; Flowers, R. A., II. *J. Org. Chem.* **2003,** *68,* 4870. doi:10.1021/jo034173t
34. Davis, T. A.; Chopade, P. R.; Hilmersson, G.; Flowers, R. A., II. *Org. Lett.* **2005,** *7,* 119. doi:10.1021/ol047835p
35. Dahlén, A.; Hilmersson, G. *J. Am. Chem. Soc.* **2005,** *127,* 8340. doi:10.1021/ja043323u
36. Dahlén, A.; Nilsson, A.; Hilmersson, G. *J. Org. Chem.* **2006,** *71,* 1576. doi:10.1021/jo052268k
37. Ankner, T.; Hilmersson, G. *Tetrahedron* **2009,** *65,* 10856. doi:10.1016/j.tet.2009.10.086
38. Wettergren, J.; Ankner, T.; Hilmersson, G. *Chem. Commun.* **2010,** *46,* 7596. doi:10.1039/c0cc02009e
39. Ankner, T.; Hilmersson, G. *Org. Lett.* **2009,** *11,* 503. doi:10.1021/ol802243d
40. Szostak, M.; Spain, M.; Procter, D. J. *Chem. Commun.* **2011,** *47,* 10254. doi:10.1039/c1cc14014k
41. Szostak, M.; Spain, M.; Procter, D. J. *Org. Lett.* **2012,** *14,* 840. doi:10.1021/ol203361k
42. Szostak, M.; Collins, K. D.; Fazakerley, N. J.; Spain, M.; Procter, D. J. *Org. Biomol. Chem.* **2012,** *10,* 5820. doi:10.1039/c2ob00017b
43. Peterson, D. J. *J. Org. Chem.* **1968,** *33,* 780. doi:10.1021/jo01266a061
44. Ager, D. J. *Synthesis* **1984,** 384. doi:10.1055/s-1984-30849
45. Performed by opening the vessel to air to quench the remaining SmI_2 and adding *t*-BuOK portionwise to the reaction mixture until completion by TLC.
46. Pace, V.; Rae, J. P.; Harb, H. Y.; Procter, D. J. *Chem. Commun.* **2013,** *49,* 5150. doi:10.1039/c3cc42160k
47. Chiu, P.; Leung, L. T.; Ko, B. C. B. *Nat. Prod. Rep.* **2010,** *27,* 1066. doi:10.1039/b906520m

License and Terms

Beilstein Journal of Organic Chemistry

Mechanistic studies on the CAN-mediated intramolecular cyclization of δ-aryl-β-dicarbonyl compounds

Brian M. Casey, Dhandapani V. Sadasivam and Robert A. Flowers II*

Full Research Paper

Open Access

Address:
Department of Chemistry, Lehigh University, Bethlehem, PA 18015, USA

Email:
Robert A. Flowers II* - rof2@lehigh.edu

* Corresponding author

Keywords:
CAN oxidation; β-dicarbonyls; free radical; radical arylations; tetralones

Beilstein J. Org. Chem. **2013,** *9,* 1472–1479.
doi:10.3762/bjoc.9.167

Received: 25 April 2013
Accepted: 13 June 2013
Published: 23 July 2013

This article is part of the Thematic Series "Organic free radical chemistry".

Guest Editor: C. Stephenson

Abstract

The synthesis of 2-tetralones through the cyclization of δ-aryl-β-dicarbonyl substrates by using CAN is described. Appropriately functionalized aromatic substrates undergo intramolecular cyclizations generating 2-tetralone derivatives in moderate to good yields. DFT computational studies indicate that successful formation of 2-tetralones from δ-aryl-β-dicarbonyl radicals is dependent on the stability of the subsequent cyclohexadienyl radical intermediates. Furthermore, DFT computational studies were used to rationalize the observed site selectivity in the 2-tetralone products.

Introduction

2-Tetralones are important intermediates or components of several natural products and biologically relevant molecules [1-7]. They are typically synthesized through transition-metal-mediated processes or preformed tetralin or naphthyl precursors [8,9]. Radical approaches can also be used to synthesize substituted 2-tetralones, and single-electron oxidations employing δ-aryl-β-dicarbonyl compounds have been carried out on arenes containing pendant β-ketoesters [10,11]. When Mn(III)-based oxidants are employed, secondary oxidations of the 2-tetralone products can occur [10,11].

Cerium(IV) ammonium nitrate (CAN) is a versatile, inexpensive and nontoxic single-electron oxidizing reagent commonly used in organic synthesis [12-14]. In a previous study, we showed that when 6-phenyl-2,4-hexanedione (**1a**) is oxidized by CAN in MeCN in the absence of a radicophile, 3-phenylpropionic acid (**2a***) is obtained exclusively over the cyclized 2-tetralone product **2a** (Scheme 1) [15]. Using this method, a variety of 1,3-dicarbonyl compounds can be mildly converted to carboxylic acids in moderate to excellent yields. In follow up studies, we found that 2-tetralone **2a** could be obtained as the major product when **1a** was oxidized by CAN in MeOH [16]. In addition, when 2.2 equivalents of CAN were employed, no products of secondary oxidations were obtained. Based on this observation, the single-electron oxidations of a variety of δ-aryl-β-dicarbonyl substrates with CAN in MeOH were

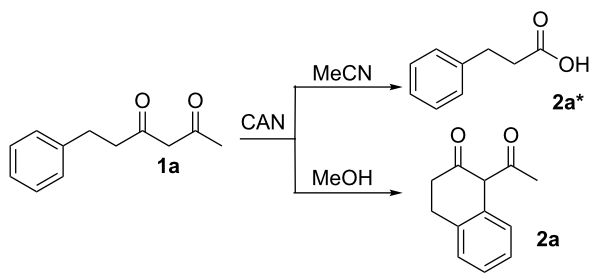

Scheme 1: Oxidative conversion of 1,3-dicarbonyl compounds to carboxylic acids with CAN.

performed to determine the scope of the reaction. DFT calculations were used to rationalize the observed impact of substitution on the δ-aryl ring on cyclization. The results of the synthetic and computational studies are presented herein.

Results and Discussion

In an initial experiment, compound **1a** was treated with 2.2 equivalents of CAN in MeOH producing 2-tetralone **2a** in a 73% yield. To examine the breadth of this method, a series of δ-aryl-β-dicarbonyl substrates was prepared by a previously reported procedure [17]. As shown in Table 1, the intramolecular cyclization of δ-aryl-β-diketones with unsubstituted aryl rings (Table 1, entries 1 and 3) afforded 2-tetralone products in moderate to good yields. Additionally, cyclization of the β-ketoester **1b** proceeded efficiently, generating **2b** in an 85% yield.

Previous work by Rickards and co-workers on a related system reported strong electronic effects when electron-donating substituents were incorporated onto the δ-aryl ring of the starting material [10,11]. To probe the impact of electron density of the δ-aryl ring on intramolecular cyclization, several substrates with either electron-donating or electron-withdrawing groups were synthesized and subjected to our reaction conditions. The results of these experiments are summarized in Table 2. As shown in Table 2, entry 1, dimethoxylated substrate **1d** oxidatively cyclized to the 2-tetralone derivative in a 76% yield. However, when only one methoxy group was incorporated onto the δ-aryl ring, the expected 2-tetralone derivative was obtained only when the methoxy group was at the *meta* position (Table 2, entry 4). For substrates **1e** and **1f** with the methoxy group at either the *ortho* or *para* position, respectively, methyl esters **2e** and **2f** (Table 2, entries 2 and 3) were the major products. Additionally, intramolecular cyclizations with electron-deficient δ-aryl rings (Table 2, entries 5 and 6) did not occur, and oxidation of **1h** and **1i** instead favored the formation of methyl esters **2h** and **2i**. Finally, the tricyclic product **2j** was generated in an isolated yield of 61% when substrate **1j** was

Table 1: CAN-mediated oxidation of δ-aryl-β-dicarbonyl compounds in MeOH[a].

Entry	Substrate	Product[b]	Yield (%)[c]
1	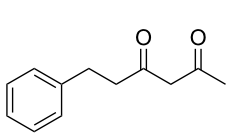 **1a**	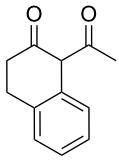 **2a**	73
2	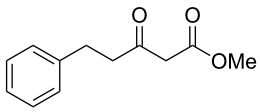 **1b**	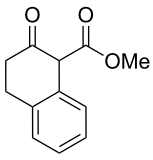 **2b**	85
3	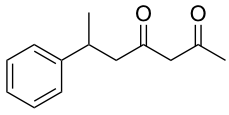 **1c**	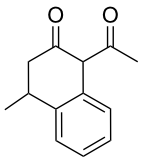 **2c**	59

[a]Reaction conditions: 1 equiv δ-aryl-β-dicarbonyl, 2.2 equiv CAN, MeOH, rt, N_2, 4 h. [b]Products exist predominantly in the enol form by ^{1}H NMR. [c]Isolated yield.

oxidized. It is important to note that products **2g** and **2j** were isolated as single isomers. Moreover, the isomers formed from these reactions result from cyclization occurring at the more hindered carbon atom of the δ-aryl ring. This observed site selectivity is consistent with previous research by both MacMillan and Nicolaou on the α-arylation of aldehydes through organo-SOMO activation [18-21]. The preferential formation of these isomers will be discussed below.

While the nucleophilicity of alkyl radicals is well-documented [22-24], the radicals generated from β-dicarbonyl compounds have been shown to display more electrophilic character [25-27]. As a consequence, these radicals should favor coupling with more nucleophilic, electron-rich carbon centers. The observation that intramolecular cyclization did not occur in either of the electron-deficient substrates (compounds **1h** and **1i**) is consistent with electrophilic radical intermediates.

To obtain a better understanding of the impact of arene substitution on the intramolecular cyclization, DFT calculations were performed at UB3LYP/6-31G(d) level by using Gaussian 03/09 [28]. Previous research from our group has shown that the oxidation of the enol tautomer of a diketone initially forms a radical cation, which is deprotonated readily by MeOH to form the radical under the reaction conditions [15,16].

Table 2: Impact of ring substituents on the CAN-mediated oxidation of δ-aryl-β-dicarbonyl compounds in MeOH[a].

Entry	Substrate	Product[b]	Yield (%)[c]
1	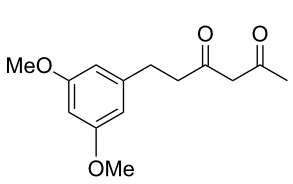 **1d**	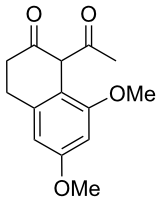 **2d**	76
2	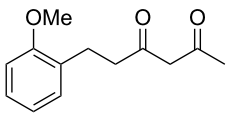 **1e**	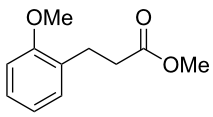 **2e**	–[d]
3	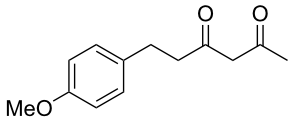 **1f**	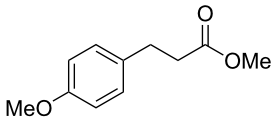 **2f**	–[d]
4	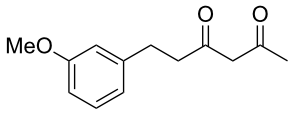 **1g**	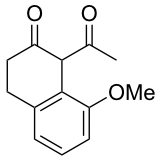 **2g**	83
5	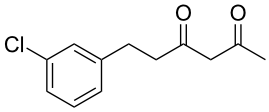 **1h**	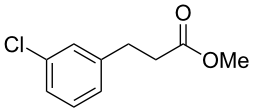 **2h**	–[d]
6	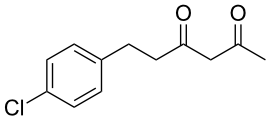 **1i**	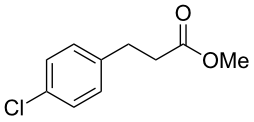 **2i**	–[d]
7	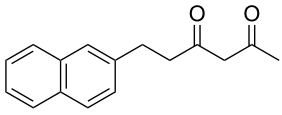 **1j**	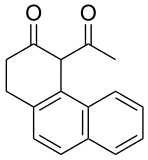 **2j**	61

[a]Reaction conditions: 1 equiv δ-aryl-β-dicarbonyl, 2.2 equiv CAN, MeOH, rt, N_2, 4 h. [b]Products exist predominantly in the enol form by ^{1}H NMR. [c]Isolated yield. [d]GC data indicated that the major products (50–80% conversion) were the methyl esters. Attempts were not made to isolate the methyl esters.

To probe the origin of the effect of substitution on cyclization, the key step of the reaction, namely the cyclization of the β-dicarbonyl radical onto the aromatic ring, was investigated. Energy barriers for the transition structures of the *ortho* cyclization leading to their corresponding product cyclohexadienyl radicals were determined.

All structures were fully optimized and identified as minima on potential energy surfaces with frequency calculations. Transition structures were identified with one imaginary frequency. Intrinsic reaction coordinate (IRC) calculations were performed to connect the transition structures to their respective minima on either side of the first-order saddle point. In some cases, the

lowest energy structures obtained from IRCs were further optimized to obtain the minima.

For the aryl diketone radical, two conformers for the ketones were considered, one with the carbonyl groups *syn* to each other and the other with the carbonyl groups in the *anti* orientation. For every substrate, two transition structures were identified on the energy surface along the reaction coordinate. The first one is a rotational transition structure for the rotation around the C–C bond beta to the dicarbonyl to go from the minimum to a geometry from which an addition to the aromatic ring is viable. The second transition structure corresponds to the addition of the radical intermediate to the aromatic ring.

Recently, Houk, MacMillan and co-workers showed that for the organo-SOMO-catalyzed oxidative α-arylation of aldehydes, the preference for the attack of the intermediate enamine radical cation on the substituted aromatic ring leading to *ortho*/*para* cyclization depends on the greater stabilization of the intermediate cyclohexadienyl radical [19]. The oxidative cyclization of δ-aryl-β-dicarbonyl substrates should proceed through a similar intermediate. As a result, the same rationale can be applied here. While MacMillan and Houk performed detailed computational studies to explain the site-selective radical cyclizations with *m*-methoxylated rings, the selectivity of naphthyl substrates was not investigated.

The energy values for the cyclization of all substituents are given in Table 3, and their corresponding energy diagrams are given in Figure 1. For unsubstituted **1a'**, the initial rotational transition structure **TS1a'** has a barrier of 2.5 kcal/mol, and the corresponding radical intermediate **2a'** is 0.6 kcal/mol above **1a'**. For the radical addition to the aromatic ring, the energy barrier is 15.8 kcal/mol, and the product cyclohexadienyl radical **3a'** is 8.8 kcal/mol higher in energy. The *syn* isomer of **1a'** is 4.5 kcal/mol higher in energy compared to the *anti* isomer (see Table S2 in Supporting Information File 1). Only the energies of the *anti* isomers are discussed here.

In the case of the electron-rich *m*-methoxy substituent **1g'**, the energy barrier for the cyclization is 12.0 kcal/mol, which is approximately 4 kcal/mol lower than **TS2a'**. Due to the electrophilic character of the diketo radical intermediate, electron-rich systems are expected to favor cyclization. Similarly, the cyclized cyclohexadienyl radical **3g'** is approximately 3.0 kcal/mol more stable compared to **3a'**. The stability of the cyclized radical is reflected in the activation barrier, and rotational transition structure **TS1g'** has a barrier of 2.5 kcal/mol. For the electron-withdrawing chloro-substituted arene **1h'**, the energy barrier for the cyclization on the aromatic ring is 16.9 kcal/mol, nearly 5 kcal/mol higher compared to the *m*-methoxy substituent. The corresponding cyclohexadienyl radical **3h'** is 10.2 kcal/mol higher in energy compared to the parent β-dicarbonyl radical **1h'**. The rotational transition structure has an energy barrier of 2.4 kcal/mol, which is similar to other radical intermediates. The higher barrier for cyclization is consistent with synthetic data showing that no cyclized product is obtained in this case. In the case of the naphthyl system (**1j'**), the energy barrier for the cyclization is 12.6 kcal/mol. The cyclized product radical **3j'** is only 4.0 kcal/mol higher in energy when compared to the parent aryl diketone radical, and

Table 3: Energies (R. E. kcal/mol) of calculated structures. Energies are relative to the open form of the radical.

	R. E.[a]	R. E. + ZPVE[b]	low frequency[c]
1a'	0.0	0.0	21.4
TS1a'	2.3	2.5	46.7i
2a'	0.2	0.6	19.7
TS2a'	15.0	15.8	477.2i
3a'	7.7	8.8	35.4
1g'	0.0	0.0	13.30
TS1g'	2.4	2.5	41.8i
2g'	0.4	0.7	16.6
TS2g'	11.0	12.0	446.3i
3g'	4.2	5.7	37.5
1g"	0.0	0.0	13.3
TS1g"	2.3	2.4	45.0i
2g"	0.3	0.6	13.5
TS2g"	13.1	13.9	437.5i
3g"	7.3	8.5	34.2
1f'	0.0	0.0	21.3
TS1f'	2.4	2.4	42.3i
2f'	0.2	0.5	15.9
TS2f'	15.8	16.4	473.0i
3f'	9.1	10.0	36.1
1h'	0.0	0.0	15.1
TS1h'	2.3	2.4	40.3i
2h'	0.2	0.4	19.1
TS2h'	16.2	16.9	489.8i
3h'	8.8	10.2	36.2
1j'	0.0	0.0	17.45
TS1j'	2.4	2.5	42.1i
2j'	0.2	0.5	16.5
TS2j'	11.8	12.6	445.9i
3j'	2.4	4.0	34.9
1j"	0.0	0.0	17.5
TS1j"	2.2	2.3	41.3i
2j"	0.3	0.6	11.5
TS2j"	13.4	14.1	463.8i
3j"	4.9	6.2	35.7

[a]UB3LYP/6-31G(d) geometry optimized. [b]From (a) with unscaled zero-point vibrational energy (ZPVE) corrections. [c]Low or imaginary frequencies (cm^{-1}).

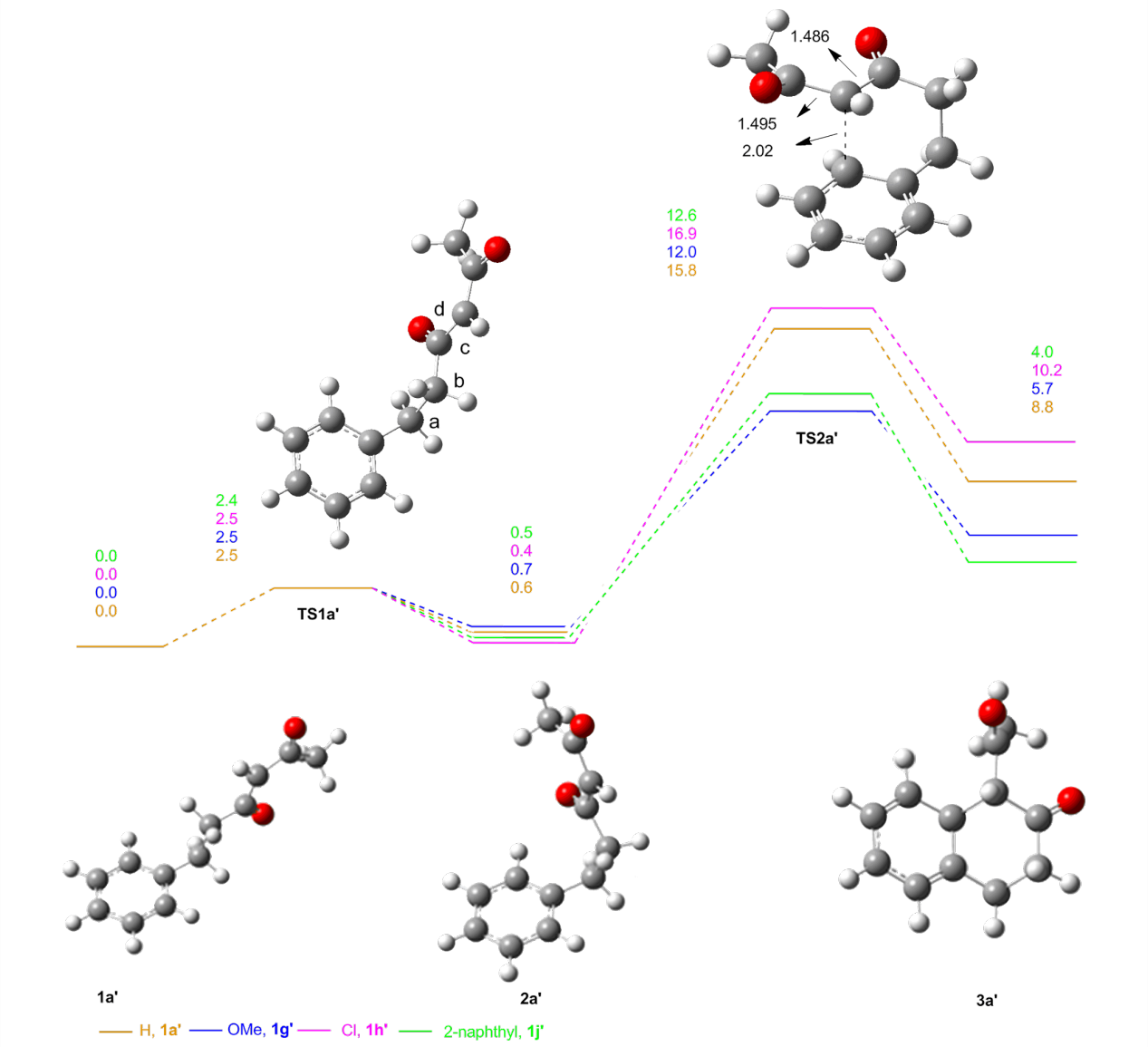

Figure 1: Energy diagram for the unsubstituted arene with the carbonyl groups *anti* to each other. For **TS1a'** the dihedral angle between atoms *abcd* = 6.4°. *The energy values for **1a'**, **1g'**, **1h'** and **1j'** are shown. **1g"**, **1f'** and **1j"** were not included for clarity.

the rotational transition structure has a comparable barrier of 2.5 kcal/mol.

While it is evident why electron-rich systems should more readily cyclize, the observed site selectivity in products **2g** and **2j** warranted further investigation. For these substrates, there are two possible sites of *ortho* cyclization (Figure 2). For the *m*-methoxy substrate **1g**, the energy barrier for the cyclization (**TS2g''**), which would lead to product **2g"**, is 1.9 kcal/mol higher relative to the other *ortho* cyclization (**TS2g'**). This finding is consistent with the synthetic observation that **3g'** is the only product observed. A similar trend was observed for the 2-naphthyl substrate **1j**. The barrier for **TS2j"**, which would form anthracene-derived product **2j"**, is 1.5 kcal/mol higher

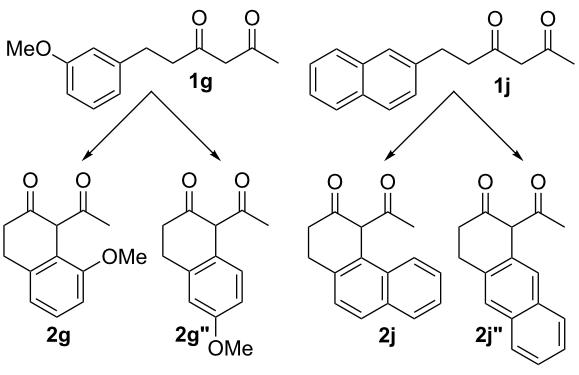

Figure 2: Possible products from the *ortho* cyclization of **1g** and **1j**.

than **TS2j'** and provides a rationale for the selective formation of the phenanthrene-derived product (**2j**).

Finally, in order to better understand how the position of the methoxy group on the δ-aryl ring affects the formation of the β-tetralone product, the energies of the intermediates for the *p*-methoxy substrate **1f** were calculated. The energy barrier for the cyclization (**TS2f'**) is 16.4 kcal/mol, 4.4 kcal/mol higher than the corresponding **TS2g'**. Furthermore, the product cyclohexadienyl radical **3f'** is 10.0 kcal/mol less stable than the parent **1f'**, a value very close to the 10.2 kcal/mol for the electron-poor *m*-chloro substrate **3h'**. Taken together, these data support the experimental observations that oxidative cyclization occurs only for the methoxy substrate substituted at the *meta* position.

Overall the DFT calculations show that the origin of the reactivity as well as the selectivity in these reactions depends on the stability of the product cyclohexadienyl radical, which is reflected in the activation barriers (**TS2's**) for the cyclization, consistent with previous studies of MacMillan and Houk [19]. The *m*-methoxy substituent on the aromatic ring provides the lowest barrier for cyclization, and the corresponding cyclized cyclohexadienyl radical is more stable. Conversely, the electron-withdrawing *m*-chloro substituent has the highest barrier among the systems studied and leads to the least stable cyclohexadienyl radical. For the unsubstituted arene substrate, the energy barrier to cyclization as well as the energy of the cyclohexadienyl radical intermediate falls between the calculated values for the *m*-chloro and *m*-methoxy systems. For the 2-naphthyl system, delocalization of the cyclized radical intermediate results in a more stable product and hence a lower barrier providing a pathway to formation of phenanthrene-derived **2j**.

In a previous study by our research group, the rates of oxidation of several β-diketones and their related silyl enol ethers by CAN and the more lipophilic ceric tetra-*n*-butylammonium nitrate (CTAN) were measured in MeOH, MeCN and CH_2Cl_2 by using stopped-flow spectrophotometry [16]. In these experiments, initial oxidation of substrates generated radical cation intermediates. The rates of formation and subsequent decay of these radical cations were measured in all three solvents. The results from these studies [15,16] provide two important insights into the mechanism of the oxidation of δ-aryl-β-dicarbonyl compounds in MeOH. First, MeOH is intimately involved in the decay of the initial radical cation through solvent-assisted deprotonation. Second, intramolecular cyclization of **1a'** occurs after the rate-limiting step of the reaction.

Based on the synthetic and computational data presented herein and findings from previous studies, the mechanism in Scheme 2 is proposed for the oxidation of δ-aryl-β-dicarbonyl compounds in MeOH with CAN. Initial oxidation of the enol tautomer (**4'**) by CAN produces protonated radical **5**. Intermediate **5** is deprotonated by MeOH to radical species **6**. When the radical

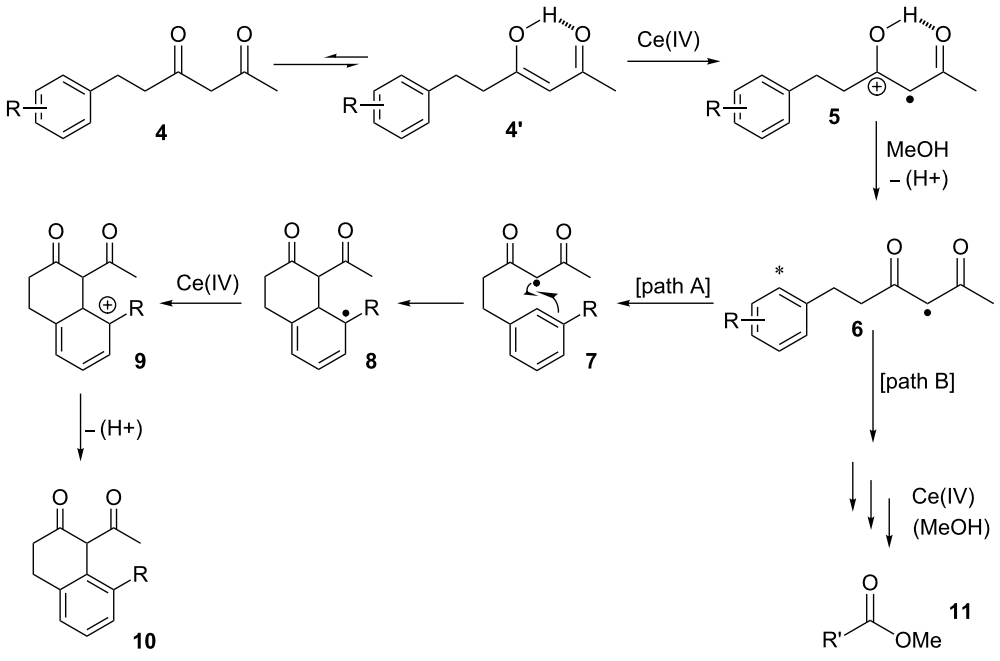

Scheme 2: Proposed mechanism for the conversion of δ-aryl-β-dicarbonyl compounds to β-tetralones (path A) and methyl esters (path B).

contains a δ-aryl group with an appropriate substitution at the *meta* position, path A is followed. Intramolecular cyclization of **7** occurs through radical addition to the aromatic ring forming intermediate **8**. As demonstrated by the oxidation of substrate **1j**, intramolecular cyclization of this radical occurs at the more electron-rich carbon atom of the δ-aryl rings. A second equivalent of CAN oxidizes **8** to cation **9**. Rearomatization through deprotonation of intermediate **9** yields the 2-tetralone derivative **10**. Conversely, when the δ-aryl ring has electron-withdrawing substituents (Table 2, entries 5 and 6), the reaction follows path B [16,29-31].

Conclusion

A protocol for the conversion of δ-aryl-β-tetralones using CAN has been developed. The Ce(IV)-mediated synthesis of 2-tetralones has short reaction times and affords the desired products in moderate to very good yields under mild conditions. While 2-tetralones were not generated for all substrates, cyclization does occur for the unsubstituted arene **1a** suggesting that the electrophilicity of the radical provides some driving force for the cyclization. The DFT computational studies indicated that the formation of 2-tetralones from the cyclization of δ-aryl-β-dicarbonyl radicals is dependent on the stability of the product cyclohexadienyl radicals.

Experimental

General methods and materials. Methanol (MeOH) was degassed with argon and dried with activated 3 Å molecular sieves prior to use. THF was purified with a Pure Solv solvent purification system from Innovative Technology Inc. CAN was purchased commercially and used without further purification. The glassware was flame dried prior to use. Unless otherwise stated, reactions were performed under an inert atmosphere of nitrogen. Products were separated by using prepacked silica gel columns with a gradient elution of ether/hexanes in an automated CombiFlash® Rf system from Teledyne Isco, Inc. All new compounds were characterized by ^{1}H NMR, ^{13}C NMR, GC–MS, IR, and LC–HRMS. Known compounds were characterized by ^{1}H NMR, ^{13}C NMR and GC–MS. ^{1}H NMR and ^{13}C NMR spectra were recorded on a Bruker 500 MHz spectrometer. Mass spectra were obtained by using a HP 5890 series GC–MS instrument. A Satellite FTIR from Thermo-Mattson was used to obtain IR spectra. LC–HRMS data were recorded at the Mass Spectrometry Facility at Notre Dame University.

General procedure for the synthesis of δ-aryl-β-dicarbonyl compounds 1a–j. Sodium hydride (11 mmol) was suspended in 25 mL of THF and cooled to 0 °C. Next, 10 mmol of 2,4-pentanedione (or methyl acetoacetate for **1b**) was added dropwise to the flask, evolving H_2 gas and forming an opaque, white solution. After stirring for 10 min, 10.5 mmol of butyllithium was added dropwise forming a clear yellow solution, which was stirred for an additional 10 min. The appropriate organohalide (11 mmol) was dissolved in 2 mL of THF and rapidly injected into the reaction at 0 °C. The reaction mixture was warmed gradually to room temperature over 30 min. The reaction was slowly quenched with an HCl solution (2 mL of concentrated HCl in 5 mL H_2O). The organic layer was separated, and the aqueous layer was washed three times with ether. The organic layers were combined, washed with brine, dried with $MgSO_4$, filtered, and concentrated. The crude product was purified by automated flash chromatography.

General procedure for the oxidation of δ-aryl-β-dicarbonyl compounds with CAN in MeOH. CAN (1.1 mmol) was dissolved in 4 mL MeOH. This CAN solution was then added dropwise in 1 min to the δ-aryl-β-dicarbonyl compound (0.5 mmol), which was dissolved in 15 mL of MeOH. The reaction was stirred for 30 min. The solvent was then removed by rotary evaporation. Ice-cold H_2O (15 mL) was poured into the reaction and extracted three times with ether. The organic layers were combined, dried with $MgSO_4$, filtered, and concentrated. The crude product was purified by automated flash chromatography.

Supporting Information

Supporting Information File 1

Characterization data for all compounds, copies of ^{1}H and ^{13}C NMR spectra of final products, computational details, absolute energies, and Cartesian coordinates of all optimized structures.
[http://www.beilstein-journals.org/bjoc/content/supplementary/1860-5397-9-167-S1.pdf]

Acknowledgements

R.A.F. is grateful to the National Institutes of Health (1R15GM075960-03) for support of this work.

References

1. Taber, D. F.; Neubert, T. D.; Rheingold, A. L. *J. Am. Chem. Soc.* **2002,** *124,* 12416–12417. doi:10.1021/ja027882h
2. Gemma, S.; Butini, S.; Fattorusso, C.; Fiorini, I.; Nacci, V.; Bellebaum, K.; McKissic, D.; Saxena, A.; Campiani, G. *Tetrahedron* **2003,** *59,* 87–93. doi:10.1016/S0040-4020(02)01449-7
3. Goel, A.; Verma, D.; Pratap, R.; Taneja, G.; Hemberger, Y.; Knauer, M.; Raghunandan, R.; Maulik, P. R.; Ram, V. J.; Bringmann, G. *Eur. J. Org. Chem.* **2011,** 2940–2947. doi:10.1002/ejoc.201001565
4. Silveira, C. C.; Machado, A.; Braga, A. L.; Lenardão, E. J. *Tetrahedron Lett.* **2004,** *45,* 4077–4080. doi:10.1016/j.tetlet.2004.03.154

5. Lucas, S.; Heim, R.; Ries, C.; Schewe, K. E.; Birk, B.; Hartmann, R. W. *J. Med. Chem.* **2008,** *51,* 8077–8087. doi:10.1021/jm800888q
6. Nguyen, T. X.; Kobayashi, Y. *J. Org. Chem.* **2008,** *73,* 5536–5541. doi:10.1021/jo800793s
7. Yao, B.; Ji, H.; Cao, Y.; Zhou, Y.; Zhu, J.; Lü, J.; Li, Y.; Chen, J.; Zheng, C.; Jiang, Y.; Liang, R.; Tang, H. *J. Med. Chem.* **2007,** *50,* 5293–5300. doi:10.1021/jm0701167
8. Silveira, C. C.; Braga, A. L.; Kaufmanb, T. S.; Lenardão, E. J. *Tetrahedron* **2004,** *60,* 8295–8328. doi:10.1016/j.tet.2004.06.080
9. Hon, Y.-S.; Devulapally, R. *Tetrahedron Lett.* **2009,** *50,* 2831–2834. doi:10.1016/j.tetlet.2009.03.185
10. Citterio, A.; Pesce, L.; Sebastiano, R.; Santi, R. *Synthesis* **1990,** 142–144. doi:10.1055/s-1990-26814
11. Jamie, J. F.; Rickards, R. W. *J. Chem. Soc., Perkin Trans. 1* **1996,** 2603–2613. doi:10.1039/P19960002603
12. Nair, V.; Deepthi, A. *Tetrahedron* **2009,** *65,* 10745–10755. doi:10.1016/j.tet.2009.10.083
13. Nair, V.; Deepthi, A. *Chem. Rev.* **2007,** *107,* 1862–1891. doi:10.1021/cr068408n
14. Casey, B. M.; Eakin, C. A.; Flowers, R. A., II. *Tetrahedron Lett.* **2009,** *50,* 1264–1266. doi:10.1016/j.tetlet.2008.12.114
15. Zhang, Y.; Jiao, J.; Flowers, R. A., II. *J. Org. Chem.* **2006,** *71,* 4516–4520. doi:10.1021/jo0602975
16. Jiao, J.; Zhang, Y.; Devery, J. J., III; Xu, L.; Deng, J.; Flowers, R. A., II. *J. Org. Chem.* **2007,** *72,* 5486–5492. doi:10.1021/jo0625406
17. Huckin, S. N.; Weiler, L. *J. Am. Chem. Soc.* **1974,** *96,* 1082–1087. doi:10.1021/ja00811a023
18. Conrad, J. C.; Kong, J.; Laforteza, B. N.; MacMillan, D. W. C. *J. Am. Chem. Soc.* **2009,** *131,* 11640–11641. doi:10.1021/ja9026902
19. Um, J. M.; Gutierrez, O.; Schoenebeck, F.; Houk, K. N.; MacMillan, D. W. C. *J. Am. Chem. Soc.* **2010,** *132,* 6001–6005. doi:10.1021/ja9063074
20. Nicolaou, K. C.; Reingruber, R.; Sarlah, D.; Bräse, S. *J. Am. Chem. Soc.* **2009,** *131,* 2086–2087. doi:10.1021/ja809405c
21. Nicolaou, K. C.; Reingruber, R.; Sarlah, D.; Bräse, S. *J. Am. Chem. Soc.* **2009,** *131,* 6640. doi:10.1021/ja902682t
22. Minisci, F. Recent aspects of homolytic aromatic substitutions. In *Synthetic and Mechanistic Organic Chemistry;* Minisci, F.; Hendrickson, J. B.; Wentrup, C., Eds.; Topics in Current Chemistry, Vol. 62; Springer: Berlin, Germany, 1976; pp 1–48. doi:10.1007/BFb0046046
23. Citterio, A.; Arnoldi, A.; Minisci, F. *J. Org. Chem.* **1979,** *44,* 2674–2682. doi:10.1021/jo01329a017
24. Citterio, A.; Minisci, F.; Porta, O.; Sesana, G. *J. Am. Chem. Soc.* **1977,** *99,* 7960–7968. doi:10.1021/ja00466a031
25. Heiba, E.-A. I.; Dassau, R. M. *J. Org. Chem.* **1974,** *39,* 3456–3457. doi:10.1021/jo00937a052
26. Fristad, W. E.; Hershberger, S. S. *J. Org. Chem.* **1985,** *50,* 1026–1031. doi:10.1021/jo00207a024
27. Corey, E. J.; Kang, M. C. *J. Am. Chem. Soc.* **1984,** *106,* 5384–5385. doi:10.1021/ja00330a076
28. *Gaussian 09,* Revision C.01; Gaussian, Inc.: Wallingford, CT, 2010.
29. Goswami, P.; Chowdhury, P. *New J. Chem.* **2000,** *24,* 955–957. doi:10.1039/b005908k
30. Iranpoor, N.; Shekarriz, M. *Bull. Chem. Soc. Jpn.* **1999,** *72,* 455–458. doi:10.1246/bcsj.72.455
31. Pan, W.-B.; Chang, F.-R.; Wei, L.-M.; Wu, M.-J.; Wu, Y.-C. *Tetrahedron Lett.* **2003,** *44,* 331–334. doi:10.1016/S0040-4039(02)02578-9

License and Terms

Beilstein Journal of Organic Chemistry

Stability of SG1 nitroxide towards unprotected sugar and lithium salts: a preamble to cellulose modification by nitroxide-mediated graft polymerization

Guillaume Moreira[1], Laurence Charles[1], Mohamed Major[1], Florence Vacandio[2], Yohann Guillaneuf[1], Catherine Lefay[*1] and Didier Gigmes[*1]

Full Research Paper

Open Access

Address:
[1]Aix-Marseille Université, CNRS, ICR UMR 7273, 13397 Marseille, France and [2]Aix-Marseille Université, CNRS, MADIREL UMR 7246, 13397 Marseille, France

Email:
Catherine Lefay[*] - catherine.lefay@univ-amu.fr; Didier Gigmes[*] - didier.gigmes@univ-amu.fr

* Corresponding author

Keywords:
ESR; glucose; lithium salt; nitroxide; SG1; stability

Beilstein J. Org. Chem. **2013,** *9,* 1589–1600.
doi:10.3762/bjoc.9.181

Received: 28 April 2013
Accepted: 06 July 2013
Published: 06 August 2013

This article is part of the Thematic Series "Organic free radical chemistry".

Guest Editor: C. Stephenson

Abstract

The range of applications of cellulose, a glucose-based polysaccharide, is limited by its inherently poor mechanical properties. The grafting of synthetic polymer chains by, for example, a “grafting from” process may provide the means to broaden the range of applications. The nitroxide-mediated polymerization (NMP) method is a technique of choice to control the length, the composition and the architecture of the grafted copolymers. Nevertheless, cellulose is difficult to solubilize in organic media because of inter- and intramolecular hydrogen bonds. One possibility to circumvent this limitation is to solubilize cellulose in *N*,*N*-dimethylformamide (DMF) or *N*,*N*-dimethylacetamide (DMA) with 5 to 10 wt % of lithium salts (LiCl or LiBr), and carry out grafted polymerization in this medium. The stability of nitroxides such as SG1 has not been studied under these conditions yet, even though these parameters are of crucial importance to perform the graft modification of polysaccharide by NMP. The aim of this work is to offer a model study of the stability of the SG1 nitroxide in organic media in the presence of unprotected glucose or cellobiose (used as a model of cellulose) and in the presence of lithium salts (LiBr or LiCl) in DMF or DMA.

Contrary to TEMPO, SG1 proved to be stable in the presence of unprotected sugar, even with an excess of 100 molar equivalents of glucose. On the other hand, lithium salts in DMF or DMA clearly degrade SG1 nitroxide as proven by electron-spin resonance measurements. The instability of SG1 in these lithium-containing solvents may be explained by the acidification of the medium by the hydrolysis of DMA in the presence of LiCl. This, in turn, enables the disproportionation of the SG1 nitroxide into an unstable hydroxylamine and an oxoammonium ion.

Once the conditions to perform an SG1-based nitroxide-mediated graft polymerization from cellobiose have been established, the next stage of this work will be the modification of cellulose and cellulose derivatives by NMP.

Introduction

With the rising costs and prospective shortage of fossil fuels, an increasing interest is dedicated to the elaboration of materials derived from renewable resources and in particular from natural polysaccharides [1,2]. However, one of the main drawbacks of polysaccharides is their inherently poor mechanical properties and heat resistance. To circumvent these limitations, one solution is the modification of polysaccharides by grafting synthetic polymers [3]. Three main strategies are generally reported to graft polymer chains onto polysaccharides, namely (i) the "grafting to" approach based on the end-functionalization of a preformed synthetic polymer chain grafted to the polysaccharide backbone, (ii) the "grafting through" method, which consists of copolymerizing premade vinyl-functionalized polysaccharides with a comonomer and (iii) the "grafting from" strategy where the grafted polymer chains grow from the polysaccharide backbone. This last method is the most convenient one as it is less sensitive to steric hindrance problems, which can limit the grafting process. The development of controlled/living radical polymerization (CLRP) techniques, such as atom transfer radical polymerization (ATRP) [4-7], reversible addition-fragmentation chain transfer (RAFT) [8-10], and nitroxide-mediated polymerization (NMP) [11], has opened new prospects in this research field, and permits precise tailoring of the synthetic chain length, the composition and the architecture [12].

Contrary to pullulan, dextran and locust bean gum, cellulose is not soluble in water and hardly soluble in few organic media. Consequently, its modification by polymer grafting proceeds either in organic media under homogeneous conditions or under heterogeneous conditions (surface-initiated polymerization from cellulose fibre, pulp, nanocrystals, etc.) [2,13]. Working under homogeneous conditions allows for following the kinetics of the grafting copolymerization by size-exclusion chromatography (SEC) or NMR for instance. This is of crucial importance to prove the living/controlled character of a polymerization performed by a CLRP technique. A strategy to modify cellulose by polymer grafting under homogeneous conditions consists in previously modified cellulose into organosoluble cellulose-derivatives such as cellulose acetate, methyl, ethyl or hydroxypropylcellulose. The main drawback of this method of cellulose solubilisation is the loss of the initial polysaccharide, namely cellulose. Another strategy that has drawn interest in the scientific community is the use of ionic liquids [14]. However, these solvents usually are very expensive or must be specifically synthesized. A more convenient media, which has proven to be efficient to solubilize polysaccharides, is DMA in the presence of LiCl (generally 5 to 10 wt % versus DMA) [15]. This system has already been reported to successfully solubilize cellulose before grafting modification by ATRP in dimethyl sulfoxide (DMSO) [16], but not in the case of NMP yet. Indeed, to our knowledge, only hydroxyisopropylcellulose (HPC) has been modified by NMP under homogeneous conditions with the 2,2,6,6-tetramethyl-1-piperidinyloxy radical (TEMPO) (Figure 1) as a control agent and by using Barton ester intermediates [17]. Several hydroxyisopropylcellulose-grafted polystyrene (HPC-g-PS) were reported and the grafted PS chains, analysed by SEC after acid hydrolysis of the cellulose backbone, proved to be efficient to control the polymerization (number-average molar mass M_n ranging from 28,000 to 62,000 g·mol^{-1} and polydispersity index PDI ranging from 1.28 to 1.52). To our knowledge, the modification of free cellulose, i.e., cellulose with unprotected hydroxy groups, by NMP graft polymerization has not been studied yet. It has to be noted that sugar and in particular glucose have been used by Georges and co-workers [18] to degrade the TEMPO nitroxide to enhance the kinetics of styrene polymerization mediated by this nitroxide. In the case of a polysaccharide, this degradation reaction could be detrimental to the success of the grafted polymerization. In particular, the stability of the acyclic β-phosphorylated nitroxide *N*-(2-methylpropyl)-*N*-(1-diethylphosphono-2,2-dimethylpropyl)-*N*-oxyl) named SG1 by Tordo et al. [19,20], which is now recognized as the most potent nitroxide for NMP, in the presence of sugar and lithium-containing solvents has

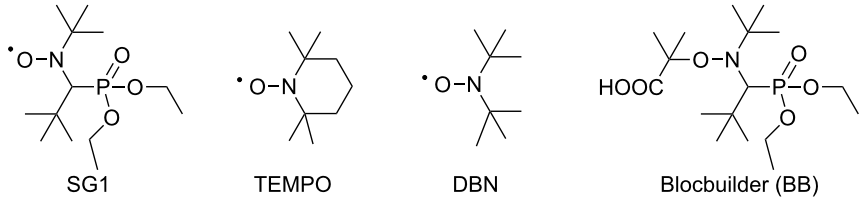

Figure 1: Structure of the SG1, TEMPO and DBN nitroxides and the BlocBuilder MA alkoxyamine.

never been reported (Figure 1). It is noteworthy that the SG1 stability is a crucial parameter to ensure the success of the nitroxide-mediated polymerization.

The aim of this work is to propose a model study of the modification of unprotected cellulose by SG1-based nitroxide-mediated graft polymerization. In this study, glucose and cellobiose were used as a model of cellulose. The stability of the SG1 nitroxide was studied in the presence of unprotected glucose and lithium salts (LiBr and LiCl) in DMF or DMA by electron spin resonance (ESR). NMP of styrene was then performed with two SG1-based alkoxyamines (BlocBuilder MA alkoxyamine (BB)) and a cellobiose-BB alkoxyamine (called cello-SG1) with or without lithium salts. This study clearly proves that SG1 is stable in the presence of unprotected hydroxy functions, but that lithium salts in DMF or DMA degrade SG1. Two degradation mechanisms have been investigated, namely (i) redox reactions involving the SG1, (ii) the acid-catalyzed disproportionation of SG1 nitroxide into an unstable hydroxylamine and an oxoammonium ion.

Results and Discussion

Stability of SG1 in presence of glucose

The NMP is based on a dynamic equilibrium between a propagating radical (P•) and a dormant form unable to propagate (alkoxyamine, i.e., radical end-capped by a nitroxide) in the presence of a nitroxide, which acts as a control agent (Figure 2). This reversible termination decreases the propagating radical concentration in the media and consequently the occurrence of irreversible terminations. Once the equilibrium between the dormant and active species is established, namely, the activation–deactivation equilibrium, all the chains grow at the same rate affording a living/controlled polymerization.

Several nitroxides have been synthesized since their first development in the 1980s [11]. In particular, the cyclic nitroxide TEMPO has been intensely studied [21,22] in the polymerization of styrene derivatives. Another important property of TEMPO is that it is reduced by reducing sugars such as glucose [18]. The consumption of nitroxides by reducing agents such as a sugar or a polysaccharide is of prime importance when aiming at the synthesis of glycopolymers or the graft polymerization onto polysaccharides. To our knowledge, Fukuda et al. were the only ones to polymerize by NMP an unprotected glycomonomer [23]. *N*-*(p*-Vinylbenzyl)-[*O*-β-D-galactopyranosyl-(1→4)]-D-gluconamide (VLA), a styrene derivative with an oligosaccharide moiety, was polymerized in DMF solution at 90 °C with di-*tert*-butyl nitroxide (DBN) as a control agent (Figure 1). The acetylation of VLA enabled the synthesis of well-defined glycopolymers with molar mass ranging from 2,000 to 40,000 g·mol^{-1} along with PDI values of about 1.1, whereas the NMP of VLA could not exceed M_n higher than 6,000, with PDI values increasing with conversion. According to the authors, chain transfer to the hydroxy groups of VLA was responsible for this phenomenon and lead to dead polymer chains and broad PDI values.

The first part of this work was devoted to studying the stability of SG1 in the presence of D-glucose. SG1 (1.5×10^{-2} mol·L^{-1}) in DMA was heated at 120 °C for 5 hours in the presence of different amounts of D-glucose. Samples were regularly withdrawn from the media and diluted in *tert*-butylbenzene (*t*-BuPh) before analysis by ESR. Irrespective of the number of molar equivalents of glucose (from 1 to 100 versus SG1), an increase of the SG1 consumption was not observed when compared to the experiment without glucose (Figure 3). In contrast, the concentration of TEMPO decreased by 50% after 5 hours in the

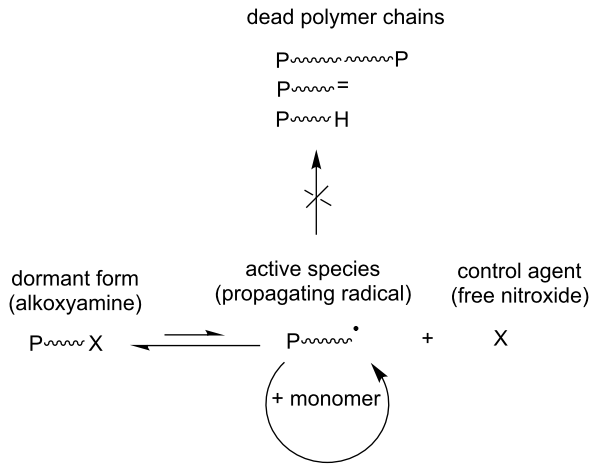

Figure 2: Key equilibrium between active and dormant species involved in the nitroxide-mediated (NMP) polymerization technique.

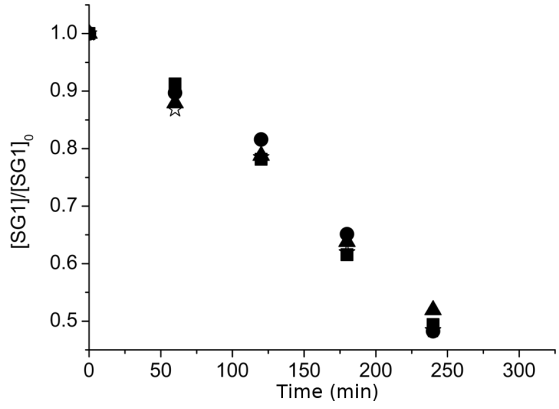

Figure 3: Degradation of the SG1 nitroxide versus time in the presence of 0 (empty stars), 1 (filled squares), 10 (filled triangles) and 100 (filled circles) mol equivalents of D-glucose as measured by ESR in *t*-BuPh at 25 °C (samples heated in DMA at 120 °C and then diluted in *t*-BuPh).

presence of 10 mol equivalents of D-glucose (Figure 4). These ESR results prove the lack of interaction of the SG1 with unprotected sugars leading to extra degradation of the nitroxide. Furthermore, these results are very encouraging to envision the modification of unprotected polysaccharides by grafting synthetic polymer chains by the SG1-based NMP technique.

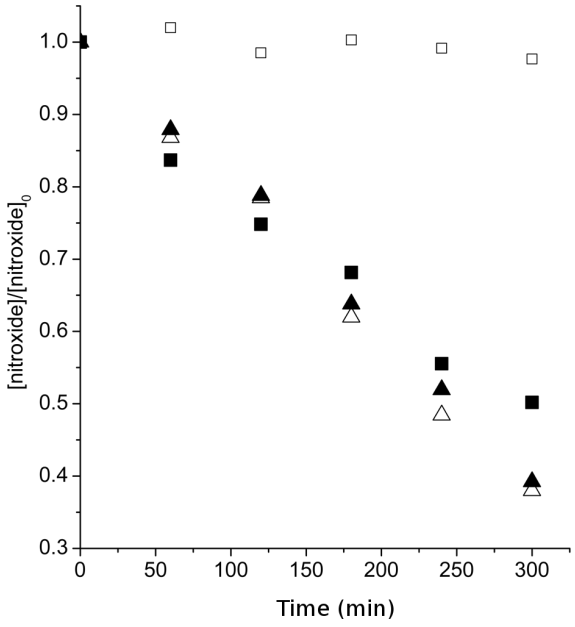

Figure 4: Degradation of the SG1 (triangles) and TEMPO (squares) nitroxides versus time in the presence of 0 (empty symbols) and 10 (filled symbols) mol equivalents of D-glucose as measured by ESR in *t*-BuPh at 25 °C (samples heated in DMA at 120 °C and then diluted in *t*-BuPh).

Stability of SG1 in the presence of lithium salts

The system DMA/LiCl has been largely reported for the analysis of cellulose and for the preparation of a wide variety of its derivatives [15]. This system is of particular interest for analysis as it is colourless and efficient to dissolve polysaccharides without or at least with negligible degradation even in the case of high molar mass. Even though it is not proven yet, replacing the DMA molecules as complexing agents around the Li^+ ions by cellulose-hydroxy groups is the proposed mechanism to explain the cellulose dissolution [14].

Although many nitroxide-mediated polymerizations were performed in pure DMA or DMF [24-27], such polymerizations have never been performed in DMF or DMA in the presence of LiCl or LiBr. In particular, the stability of SG1 nitroxide has never been studied in DMA or DMF in the presence of LiCl or LiBr. The stability of the SG1 nitroxide in various solvents (DMA, DMF, MeOH and *t*-BuPh) without

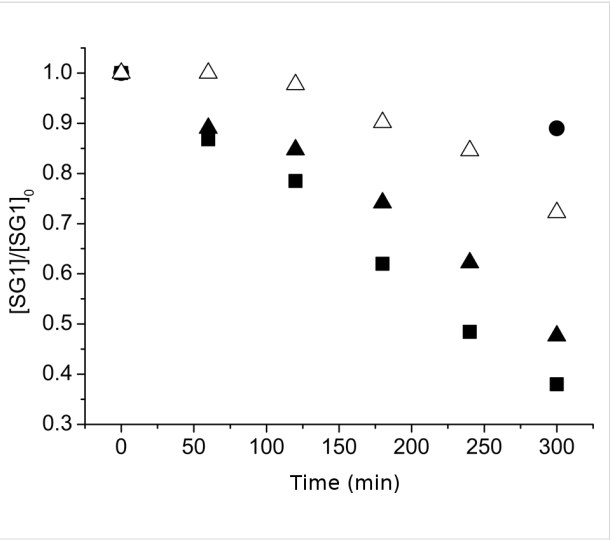

Figure 5: Degradation of the SG1 nitroxide versus time in DMA (filled squares), DMF (filled triangles), MeOH (filled circles) and *t*-BuPh (empty triangles) as measured by ESR in *t*-BuPh at 25 °C (samples heated in DMA, DMF, MeOH or *t*-BuPh at 120 °C, removed after 1 to 5 hours and diluted in *t*-BuPh).

lithium salt was first investigated by ESR (Figure 5). In accordance with previous experiments, SG1 solutions in DMA, DMF, MeOH or *t*-BuPh (1.5×10^{-2} mol·L^{-1}) were heated at 120 °C and then diluted in *t*-BuPh for ESR analysis at 25 °C. The SG1 degradation is clearly faster in DMA or DMF compared to *t*-BuPh and MeOH. After 5 hours of heating at 120 °C, only 10 and 25% of SG1 were consumed in MeOH and *t*-BuPh, respectively, whereas 50 and 60% of SG1 degraded in DMF and DMA, respectively. SG1 is therefore less stable in DMF or DMA than in MeOH or *t*-BuPh.

The influence of the lithium salt concentration (LiCl or LiBr) was then investigated at 4.5 and 10 wt % in DMF and DMA (Figure 6).

Figure 6 clearly proves that irrespective of the counter ion (Cl^- or Br^-), SG1 was totally consumed within 1 hour with 4.5 or 10 wt % of lithium salt in DMF or DMA. In contrast to LiCl and LiBr, NaCl did not seem to catalyse the SG1 degradation. It is noteworthy that this experiment was performed under heterogeneous conditions since NaCl is not soluble in DMA. Although LiCl or LiBr degrades the SG1 nitroxide in DMF or DMA, degradation does not occur when these lithium salts are dissolved in methanol (Figure 6). The combination of the solvent (DMF or DMA) with the lithium salt (LiCl or LiBr) is, thus, responsible for the SG1 degradation and not the lithium salt alone. Two possible SG1 degradation mechanisms will be discussed in the last part of this work. Nevertheless, one notices that contrary to SG1, the TEMPO nitroxide proved to be stable in DMA even with 4.5 wt % of LiCl (Figure 7). The instability

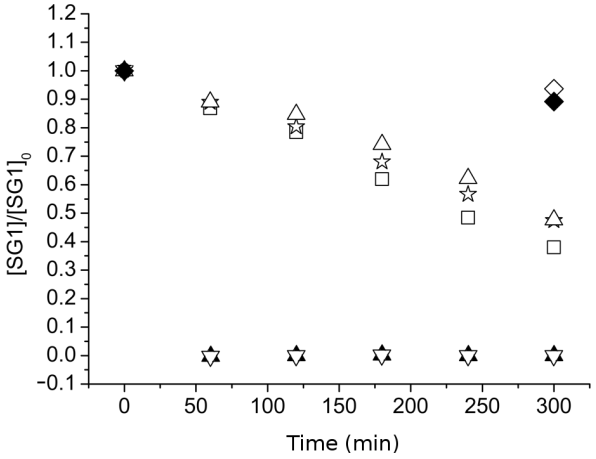

Figure 6: Degradation of the SG1 nitroxide versus time in the presence of 0% of lithium salt in DMA (empty squares); DMF (empty triangles) and MeOH (empty diamonds), 4.5 or 10 wt % of LiCl in DMA or DMF (filled triangles), 4.5 wt % of LiBr in DMA (reverse filled triangles), 4.5 wt % of LiCl in MeOH (filled diamonds) and 4.5 wt % of NaCl in DMA (empty stars) as measured by ESR in t-BuPh at 25 °C (samples heated in DMA, DMF or MeOH at 120 °C, removed after 1 to 5 hours and diluted in t-BuPh).

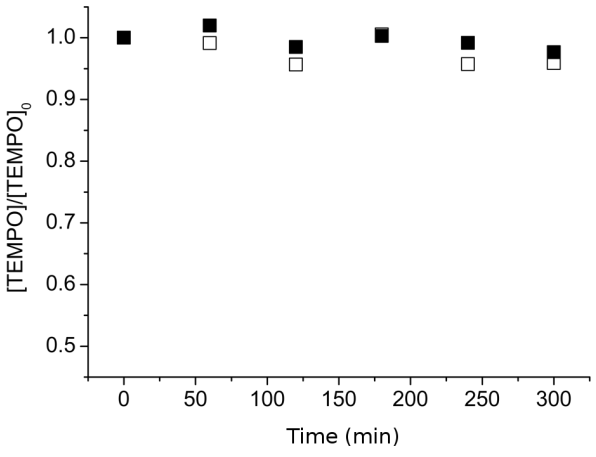

Figure 7: Degradation of the TEMPO nitroxide versus time in DMA in the presence of 0% lithium salt (empty squares) and 4.5 wt % LiCl (filled squares) as measured by ESR in *t*-BuPh at 25 °C (samples heated at 120 °C in DMA, removed after 1 to 5 hours and diluted in *t*-BuPh).

of SG1 in lithium-containing solvents such as DMF, DMA/LiCl or LiBr can consequently not be extended to all nitroxides.

According to these ESR results, it is not a good option to carry out a controlled/living polymerization by SG1-based NMP in DMA/LiCl or DMF/LiCl. As expected, with the BlocBuilder MA alkoxyamine as an initiator (Figure 1), the NMP of styrene performed in DMA at 120 °C without LiCl fulfilled the criteria of a controlled polymerization (PDI values < 1.5, linear increase of M_n values with conversion (Figure 8a), and a regular shift of the molar mass distribution towards high M_n (Figure 8b)). In contrast, the control of the polymerization was lost under the same conditions after 1.5 hours in the presence of 4.5 wt % of LiCl (PDI > 1.5, M_n values constant around 8,000 g·mol^{-1} (Figure 8c), and a broadening of the molar mass distribution (Figure 8d)).

To mimic a cellulose chain functionalized by a SG1-based alkoxyamine, we coupled the commercially available BlocBuilder MA alkoxyamine and cellobiose to prepare a compound called cello-SG1 (Scheme 1). As the aim was to prepare a model of cellulose, we targeted the grafting of one BB unit onto cellobiose but without selecting one specific position. Indeed, in the case of cellulose polysaccharide, it is very challenging to selectively modify only one type of hydroxy function (C_2-OH, C_3-OH or C_6-OH).

The procedure of elaboration of this alkoxyamine has already been described elsewhere [28]. Briefly, the synthesis of the cello-SG1 alkoxyamine is performed in two steps: (i) acroylation of one hydroxy function of cellobiose to graft one acrylate function, (ii) intermolecular 1,2-radical addition (1,2-IRA) of the SG1-based BlocBuilder MA alkoxyamine onto the acrylate function. Nevertheless, in the case of cellobiose the first step of acroylation has to be performed in DMA with a minimal amount of LiCl to ensure the cellobiose solubilization. The cello-SG1 alkoxyamine was then used to initiate the NMP of styrene in DMA at 120 °C. Figure 9a and Figure 9b prove that a successful controlled/living polymerization could be achieved in these conditions (linear increase of the number-average molar mass with conversion, PDI values < 1.5, and regular shift of the molar mass distribution) until 40% of conversion. For higher conversion values, the PDI values increase (>1.5), and the molar mass distribution broadens because of SG1 degradation due to residual lithium salt in the media that is very difficult to fully eliminate after the 1,2-IRA step.

This study therefore clearly proves that lithium salt can be used to solubilize sugar, oligo- or polysaccharides, but that they have to be carefully removed before performing a SG1-based NMP. In addition, the successful NMP initiated by the cellobiose-derivative alkoxyamine is a very promising result to envision the modification of fully or partially unprotected polysaccharide by SG1-based nitroxide-mediated graft (co)polymerization.

Mechanism of the degradation of the SG1 nitroxide in DMF or DMA/LiCl or LiBr solvent

ESR experiments proved that the SG1 nitroxide was degraded in DMF or DMA with 4.5 wt % of LiCl or LiBr. Two

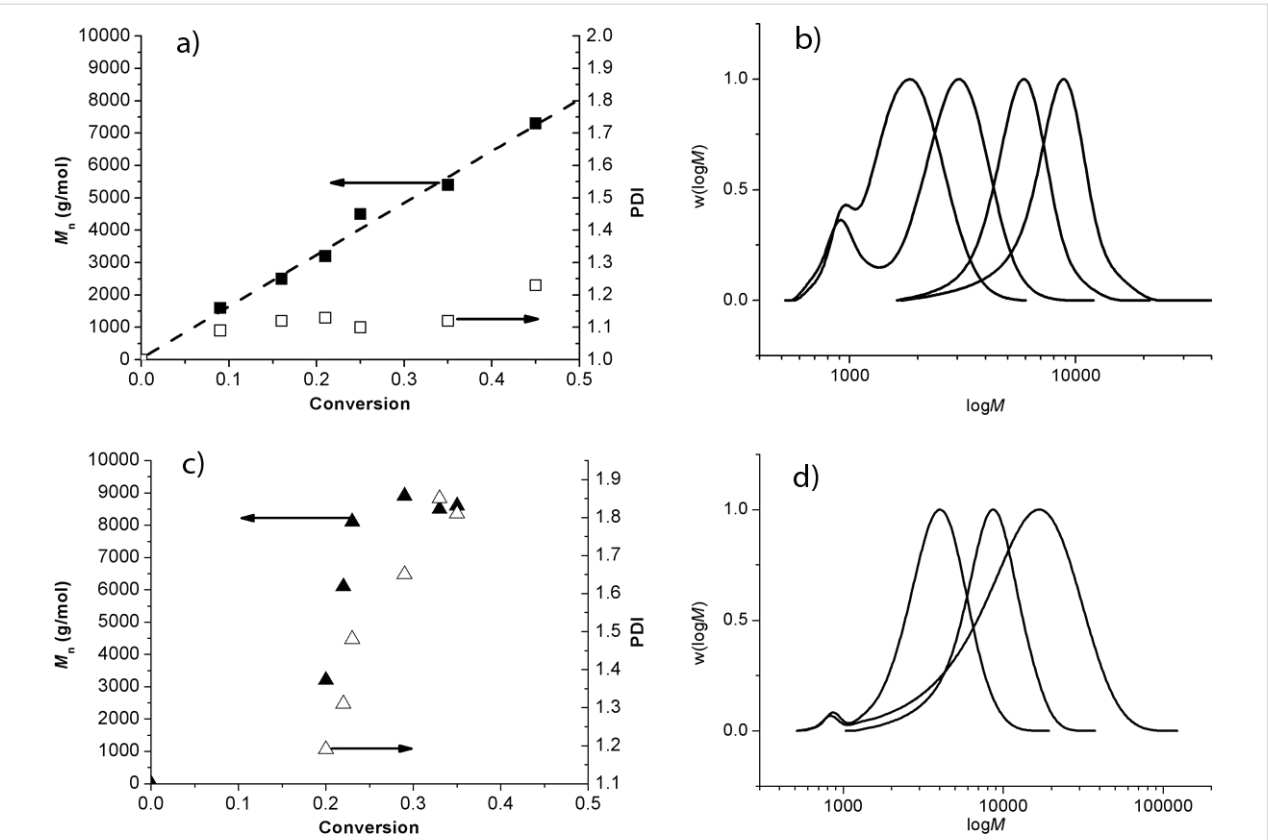

Figure 8: NMP of styrene initiated by the BlocBuilder MA alkoxyamine at 120 °C in DMA without LiCl salt. (a) Evolution of the number-average molar mass (M_n: filled symbols, linear fit: dash lines) and polydispersity indexes (PDI: empty symbols) with conversion. (b) Molar mass distribution (w(log$M$) versus log$M$) of the polystyrene chains at various conversions. NMP of styrene initiated by the BB alkoxyamine at 120 °C in DMA with 4.5 wt % of LiCl. (c) Evolution of the number-average molar mass (M_n: filled symbols) and polydispersity indexes (PDI: empty symbols) with conversion. (d) Molar mass distribution (w(logM) versus logM) of the polystyrene chains at various conversions.

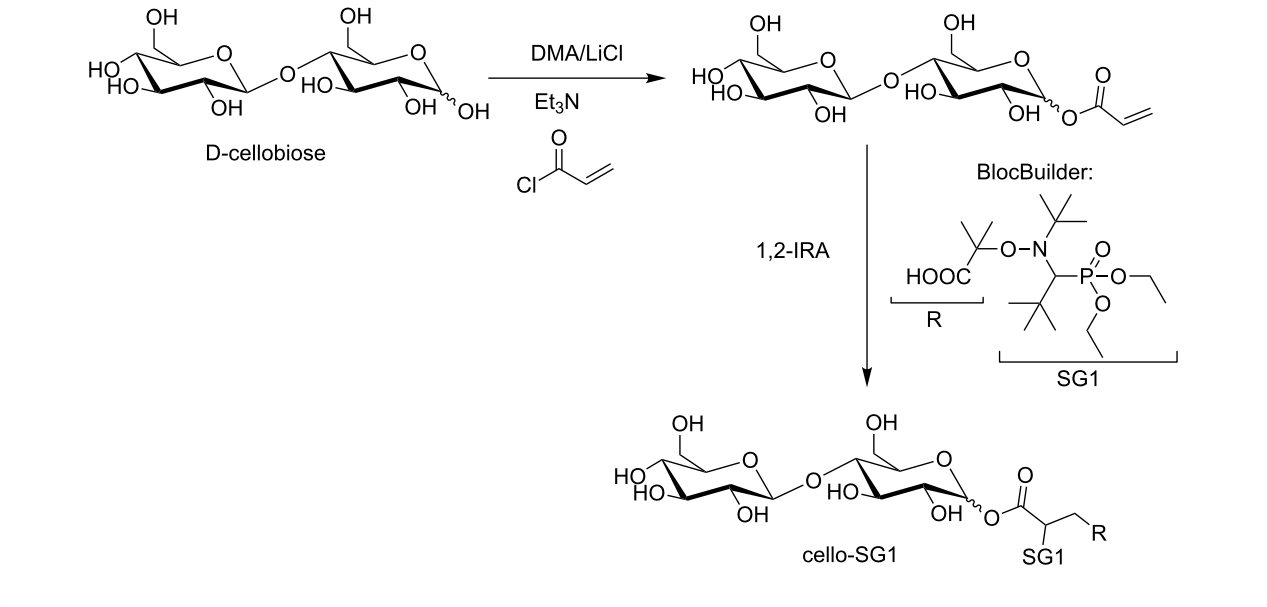

Scheme 1: Synthesis of the cellobiose and SG1-based alkoxyamine (cello-SG1). The shown regioisomer exhibits an acroylation in C1 since this OH group is known to be more reactive, but all regioisomers are possible.

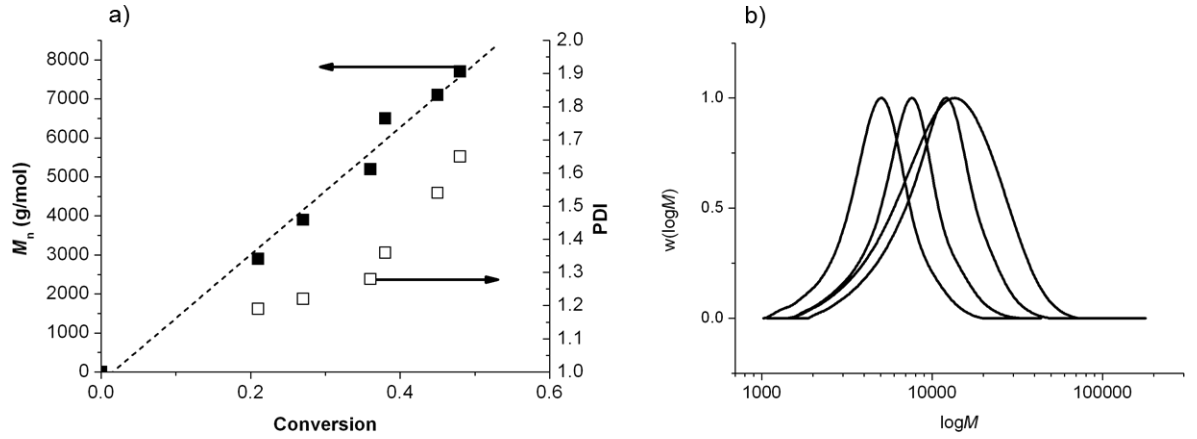

Figure 9: (a) Evolution of the number-average molar mass (M_n: filled symbol, linear fit: dash lines) and polydispersity index (PDI: empty symbols) with styrene conversion by using cello-SG1 as initiator. (b) Molar mass distribution (w(log$M$) versus log$M$) of the polystyrene chains at various conversions (DMA, 120 °C, $[\text{cello-SG1}]_0 = 1.5 \times 10^{-2}$ mol·L^{-1}, $[\text{styrene}]_0 = 1.4$ mol·L^{-1}).

hypotheses could be postulated to explain this degradation: (i) the SG1 undergoes an oxidation reaction, (ii) LiCl catalyses the hydrolysis of DMA (or DMF) that degrades the SG1 into unstable species.

Oxidation of the SG1 nitroxide

Nitroxide can be readily oxidized into an oxoammonium ion and reduced to hydroxylamine (Scheme 2) [29]. This feature was extensively used by many researchers for developing a pure organic battery based on the nitroxide functionality [30]. The redox potentials of cyclic nitroxides and in particular TEMPO are well-known in acetonitrile, but there was only one measurement for SG1 in acetonitrile and no measurement in DMA or DMF as a solvent. The aim of the study was to measure the redox potentials of the SG1 and LiCl/solvent and to conclude if a redox reaction could happen between these species.

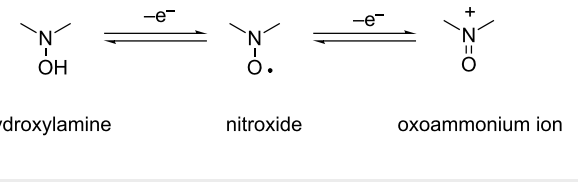

Scheme 2: (Reversible) redox system of nitroxide.

The redox potentials of SG1 and LiCl (4.5 wt %) in DMF and MeOH were then determined by cyclic voltammetry with a platinum electrode and are listed in Table 1. The cyclic voltammograms of SG1 and LiCl in DMF and MeOH are presented in Figure 10. The redox potential of the reduction of Li^+/Li in DMF is around −2.1 V as already reported [31].

Table 1: Experimental redox potential of the oxidation (E_{ox}) and of the reduction (E_{red}) in DMF and MeOH.[a]

	E_{ox} or E_{red} (vs Ag/AgCl)
SG1 (DMF)	$E_{ox} = 0.64$ $E_{red} = 0.00$
Cl_2/Cl^- (DMF)	E_{ox} / $E_{red} = 0.86$
SG1 (MeOH)	$E_{ox} = 0.64$ $E_{red} = 0.00$
Cl_2/Cl^- (MeOH)	$E_{ox} = 1.10$ $E_{red} = 0.84$

[a]Glassy carbon electrode, Ag/AgCl, Pt, sweep rate 50 mV·s^{-1}.

Initially only the SG1 nitroxide, Li^+ and Cl^- were present in the media. The only possible redox reaction is the one involving the reduction of the in situ formed Cl_2 to Cl^- and the oxidation of the nitroxide to an oxoammonium ion. In conclusion, if Cl_2 can be formed in the system, then the oxidation of the SG1 nitroxide is possible. However, this hypothesis is challenging to validate since Cl_2 is a gas and thus difficult to quantify. We tried to prove the formation of Br_2 by heating DMF/4.5 wt % LiBr solutions for 14 hours. A comparison with the same solution but with heating for only 30 min did not show any difference by cyclic voltammetry. In particular, the reduction wave of Br_2 into Br^- did not increase with prolonged heating time (Figure 11). Since the formation of Cl_2 or Br_2 in the case of DMA/LiCl or DMA/LiBr was not straightforward, the hypothesis of the SG1 degradation by a redox phenomenon was hardly acceptable. A different explanation was then investigated, namely the disproportionation of the SG1 nitroxide into unstable species in acidic media.

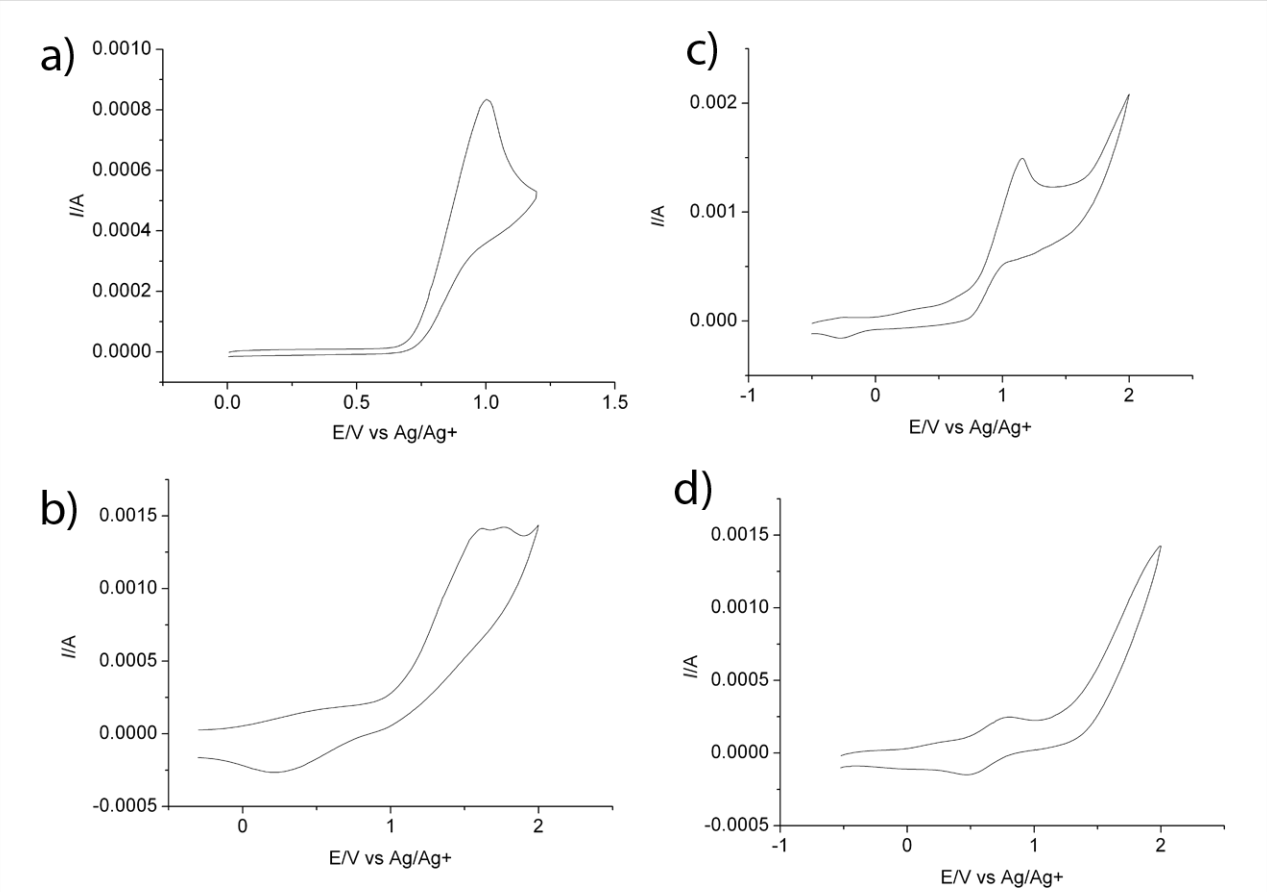

Figure 10: Cyclic voltammograms in DMF of (a) SG1 (10^{-2} M)/ $NaClO_4$ (10^{-1} M) and (b) LiCl (10^{-2} M)/$TBAPF_6$ (10^{-1} M). Cyclic voltammograms in MeOH of (c) SG1 (10^{-2} M)/$TBAPF_6$ (10^{-1} M) and (d) LiCl (10^{-2} M)/$TBAPF_6$ (10^{-1} M). Glassy carbon electrode, Ag/AgCl, Pt, sweep rate 50 mV·s^{-1}.

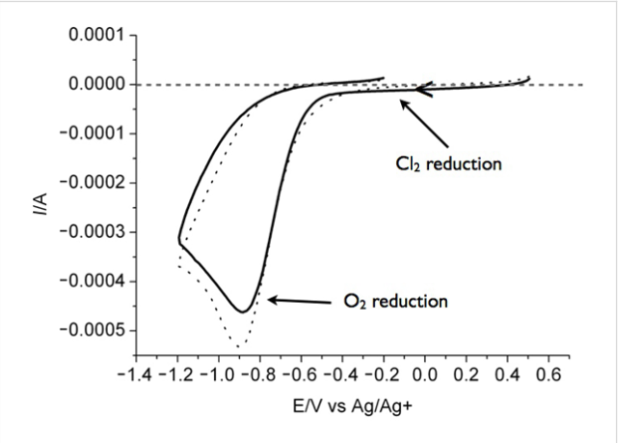

Figure 11: Cyclic voltammograms of DMF/4.5 wt % LiBr solution heated at 80 °C for 30 min (plain line) and 14 hours (dotted line). Glassy carbon electrode, Ag/AgCl, Pt, sweep rate 50 mV·s^{-1}.

Disproportionation of SG1 nitroxide into unstable species in acidic media

LiCl has proven to catalyze the hydrolysis of DMA [32]. In particular, heating wet DMA in the presence of LiCl produces dimethylammonium acetate and its conjugated base dimethylamine (Scheme 3). The DMA/LiCl solution becomes more acidic with time as the dimethylamine is volatile and gradually evaporates, and the acetic acid accumulates (pH decreases from 7 to 4–5). The increase of the acidity accelerates the DMA hydrolysis since the reaction mechanism between water and DMA becomes an acid-catalyzed process.

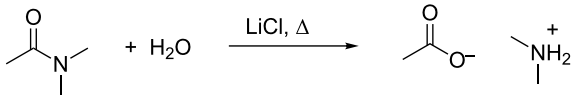

Scheme 3: Hydrolysis of DMA in the presence of LiCl.

The disproportionation of TEMPO nitroxide in acidic media is a well-documented degradation process [33,34]. In particular, in the presence of an excess of acid HX (X = BF_4, Cl^-, Br^-, Br_3^-, OCl_4^-), the disproportionation of TEMPO gives rise to the oxoammonium salt along with the protonated hydroxylamine (Scheme 4).

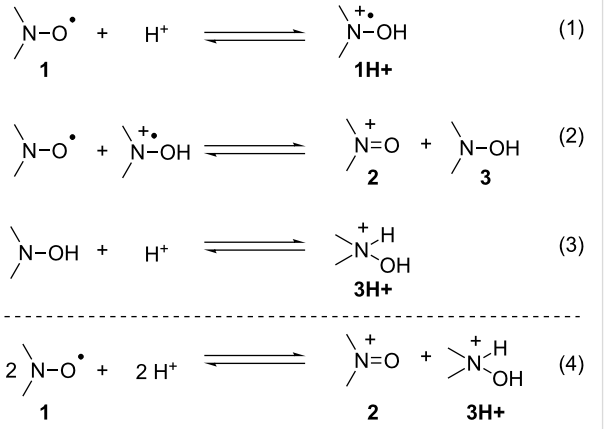

Scheme 4: Disproportionation of nitroxide **1** by acid treatment.

Concerning the hydrolysis of DMA and the disproportionation of TEMPO in acidic media, we could postulate that the hydrolysis of DMA in the presence of LiCl forms HCl, which in turn, degrades SG1 into oxoammonium salt and hydroxylamine. However, Bagryanskaya et al. [35] proved that the hydroxylamine derivative from SG1 is unstable. The cyclic voltammogram of SG1 also proved the instability of the SG1 oxoammonium cation since its reversible reduction is not observed (Figure 10). In conclusion, the degradation of SG1 in DMA/LiCl solutions could be explained by a disproportionation mechanism in the presence of HCl giving rise to an unstable hydroxylamine and an oxoammonium cation. It is noteworthy that the instability of SG1 has already been observed at 75 °C at pH 3.5 in the presence of methacrylic acid [36].

To confirm the instability of the SG1 in acidic media and to explain the difference between SG1 and TEMPO when heated in DMA/LiCl (see ESR experiments and Figure 6 and Figure 7), SG1 and TEMPO MeOH solutions (1.5×10^{-2} mol·L^{-1}) were heated at 120 °C in the presence of HCl (3.7 mol % equivalents). Samples were withdrawn regularly and diluted in *t*-BuPh for ESR analysis (Figure 12). In accordance with previous observations in DMA/LiCl, the kinetics of the consumption of SG1 and TEMPO in the presence of HCl are very different. TEMPO degrades very quickly in the first seconds of the experiment (Figure 12c) to reach an equilibrium (TEMPO concentration constant with time for 5 h, Figure 12a), whereas the SG1 consumption is slower (Figure 12c) but complete since all the nitroxide is consumed after 5 h at 120 °C (Figure 12b). This experiment proves that the acidity of the media (DMA/LiCl) is responsible for the SG1 degradation. The difference between TEMPO and SG1 nitroxides could be explained by a disproportionation mechanism that quickly gives a stable hydroxylamine and an oxoammonium ion in the case of TEMPO and slowly gives the same but unstable species in the case of SG1. The equilibrium (1) and (3) (Scheme 4) are then shifted towards (**1H**+) and (**3H**+) formation up to the complete consumption of the SG1 nitroxide.

Conclusion

This study proved that contrary to TEMPO nitroxide, SG1 was stable in the presence of unprotected glucose. More specifically, SG1 was stable in the presence of up to 100 mol equivalents of glucose when heated at 120 °C in DMA. In contrast, SG1 degraded in DMF or DMA in the presence of LiCl or LiBr lithium salts, whereas TEMPO remained stable. ESR analyses proved that the lithium salt itself was not responsible for the nitroxide degradation, but that the degradation was caused by the combination of the solvent (DMF or DMA) with the lithium salt (LiCl or LiBr).

The first hypothesis to explain the SG1 consumption in DMA/LiCl was based on the SG1 oxidation by Cl_2 (or Br_2 in the case of LiBr lithium salt). However, the study by cyclic voltammetry of the redox potential of SG1 and LiCl could not attest to

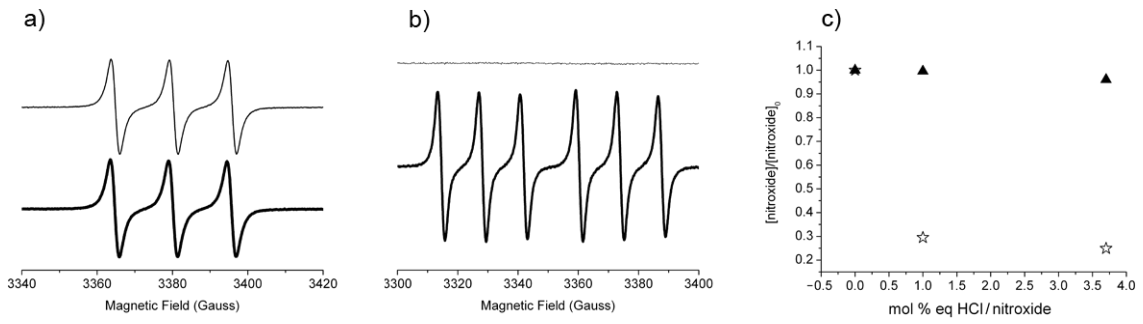

Figure 12: Degradation of the nitroxides (SG1 and TEMPO) in the presence of HCl. (a) TEMPO ESR signal in the presence of 3.7 mol % equivalents of HCl at *t* = 0 (thick line) and *t* = 5 h (thin line). (b) SG1 ESR signal in the presence of 3.7 mol % equivalents of HCl at *t* = 0 (thick line) and *t* = 5 h (thin line). c) SG1 (filled triangles) and TEMPO (empty stars) initial degradation (*t* = 0) in the presence of 0, 1 and 3.7 mol % equivalent of HCl versus nitroxide (ESR in *t*-BuPh at 25 °C, samples heated at 120 °C in MeOH, and diluted in *t*-BuPh).

this hypothesis, since the presence of Cl_2 (or Br_2) in the media could not be proven.

Ultimately, the instability of SG1 in DMA/LiCl was attributed to the disproportionation of the nitroxide in acidic media forming hydroxylamine and an oxoammonium ion, which were stable in the case of TEMPO and unstable in the case of SG1.

The successful nitroxide-mediated polymerization of styrene in DMA from an alkoxyamine based on cellobiose and SG1 confirmed the ability to perform SG1-based NMP in DMA (without lithium salts) in the presence of unprotected sugars, and consequently opened the way to the modification of cellulose polymer chains by NMP.

Experimental

Materials and general experimental details

Triethylamine (Et_3N, Aldrich, 99+%), acryloyl chloride (Aldrich, 97+%), D-glucose (Aldrich, 99.5%), D-cellobiose (Alfa Aesar, 98+%), lithium chloride (LiCl, Aldrich, 99+%), lithium bromide (LiBr, Aldrich, 99+%), sodium perchlorate ($NaClO_4$, Aldrich, ACS reagent ≥98%), tetrabutylammonium hexafluorophosphate ($TBAPF_6$, Fluka, 98+%), TEMPO (Aldrich, 98%), styrene (Aldrich, 99+%), *N*,*N*-dimethylformamide (DMF, SDS, Analytical grade), *N*,*N*-dimethylacetamide (DMA, Aldrich, 99.5+%), sodium chloride (NaCl, Carlo Erba), ethyl acetate (EtOAc, Carlo Erba), triethyl phosphite ($P(O)(OEt)_3$, Aldrich, 99+%), and *tert*-butylbenzene (*t*-BuPh, Aldrich, 99%) were used as received. The 2-methyl-2-(*N*-*tert*-butyl-*N*-(1-diethoxyphosphoryl-2,2-dimethylpropyl)aminoxy)-propionic acid alkoxyamine (BlocBuilder MA, BB) was kindly supplied by Arkema.

The styrene conversion was estimated by ^1H NMR experiments on a Bruker Avance 400 spectrometer (DMSO-d_6 as solvent, 400 MHz; chemical shifts are given relative to TMS used as an internal reference). ^{31}P and ^1H NMR analyses were performed on a Bruker Avance 400 spectrometer in DMSO-d_6.

The size-exclusion chromatography analyses were performed by using an EcoSEC system from TOSOH equipped with a differential refractometer detector. THF was used as an eluent with 0.25 vol % toluene as a flow marker at a flow rate of 0.3 mL·min^{-1} after filtration on Alltech PTFE membranes with a porosity of 0.2 μm. The column oven was kept at 40 °C, and the injection volume was 20 μL. One ResiPore Pre-column (50 mm, 4.6 mm) and two ResiPore columns (250 mm, 4.9 mm) from Polymer Laboratories were used in series. The system was calibrated by using polystyrene standards in the range 100–400,000 g·mol^{-1}, purchased from Agilent.

Electron spin resonance experiments were performed on a Bruker EMX 300 spectrometer and *t*-BuPh was used as a solvent. SG1 (or TEMPO) solutions (1.5×10^{-2} mol·L^{-1}) were deoxygenated under argon and then heated at 120 °C for 5 hours in Schlenk tubes. Samples (134 μL) were regularly withdrawn and diluted in 20 mL of *t*-BuPh for analysis at 25 °C under air.

The electrochemical experiments were conducted in a three-electrode glass cell. A glassy carbon disk electrode (1 cm^2) and a platinum wire were used as the working and the counter electrodes, respectively. The potentials were referred to Ag/AgCl. The cyclic voltammograms were collected at room temperature and atmosphere at a potential sweep rate of 50 mV·s^{-1} generated by a potentiostat/galvanostat (Solartron analytical SI 1287). In all the experiments, the concentration of SG1 and LiCl was 10^{-2} mol·L^{-1} and that of the supporting electrolyte ($NaCLO_4$ or $TBAPF_6$) 0.1 mol·L^{-1}.

High-resolution mass spectrometry experiments were performed by using a QStar Elite mass spectrometer (Applied Biosystems SCIEX, Concord, ON, Canada) equipped with an electrospray ionization source operated in the positive mode. The capillary voltage was set to +5,500 V and the cone voltage to +20 V. Air was used as the nebulizing gas (10 psi), while nitrogen was the curtain gas (20 psi). In this hybrid instrument, ions were measured by using an orthogonal acceleration time-of-flight (oa-TOF) mass analyser. Instrument control, data acquisition, and data processing were achieved by using Analyst software (QS 2.0) provided by Applied Biosystems. The sample solution (i.e., cello-SG1 diluted in methanol containing 3 mM of ammonium acetate) was introduced in the ionization source at a 5 μL min^{-1} flow rate by using a syringe pump.

Synthesis of the cellobiose and SG1-based alkoxyamine (Cello-SG1)

D-cellobiose (10 g, 29 mmol) was dissolved in a solution of DMA/LiCl (94 mL/1.5 g) at 100 °C for 20 min under argon atmosphere. After cooling, Et_3N (4.5 mL, 32 mmol) was added at room temperature, and acryloyl chloride (2.4 mL, 29 mmol) was introduced dropwise at 0 °C for 10 min (0.24 mL/min). The temperature was kept at 0 °C for 20 min. The mixture was then heated at 40 °C for 2 h. Triethylammonium chloride was removed by filtration at room temperature and the filtrate (98 mL) was kept for the next step. ESI^+ (mass spectrometry) analyses proved the presence of a mixture of cellobiose mono, di- and tri-acroylated, acrylic acid (resulting from the hydrolysis of acryloyl chloride), and free cellobiose. It is noteworthy that this reaction is not regioselective, so that several regioisomers are formed, which are very difficult to separate and quan-

tify. BB (4.8 g, 12.6 mmol) was added to the previous filtrate (50 mL). After deoxygenation by argon bubbling for 20 min at room temperature, the solution was heated at 80 °C for 3 h. After cooling, EtOAc was added to the media and the product was recovered by precipitation. The obtained white solid was dried under reduced pressure to give the cellobiose-based alkoxyamine cello-SG1 (two steps yield reaction: 13%, measured by ^{31}P NMR with P(O)(OEt)$_3$ as an internal reference).

The E_a value of the cello-SG1 homolysis was determined by ^{31}P NMR as already described (E_a = 122 kJ·mol^{-1}) [37,38].

The protonated molecule ($C_{32}H_{61}NO_{18}P^+$, m/z_{theo} 778.3621) was accurately mass measured with a relative error of ±0.3 ppm by using two reference ions from a poly(propylene glycol) as internal standards.

Nitroxide-mediated polymerization of styrene in *N*,*N*-dimethylacetamide

After the addition of styrene (2.16 g, 20.7 mmol) to the alkoxyamine solution (BB or Cello-SG1, 0.23 mmol, previously dissolved in 15 mL of DMA), the solution was deoxygenated by argon bubbling for 20 min at room temperature and then heated at 120 °C for 5 h. Aliquots were periodically withdrawn during the reaction time and cooled in an iced water bath to quench the polymerization. For all of them, the monomer conversion was determined by ^{1}H NMR analysis of the raw polymerization medium in DMSO-d_6 solution, whereas the M_n and the PDI of the polystyrene chains were measured by SEC/THF.

Acknowledgements

The authors thank the Agence Nationale de la Recherche for financial support, grant number ANR-10-CDII-09. ARKEMA is acknowledged for kindly providing BlocBuilder MA alkoxyamine.

References

1. Gandini, A. *Macromolecules* **2008,** *41,* 9491–9504. doi:10.1021/ma801735u
2. Roy, D.; Semsarilar, M.; Guthrie, J. T.; Perrier, S. *Chem. Soc. Rev.* **2009,** *38,* 2046–2064. doi:10.1039/b808639g
3. Jenkins, D. W.; Hudson, S. M. *Chem. Rev.* **2001,** *101,* 3245–3274. doi:10.1021/cr000257f
4. Kato, M.; Kamigaito, M.; Sawamoto, M.; Higashimura, T. *Macromolecules* **1995,** *28,* 1721–1723. doi:10.1021/ma00109a056
5. Wang, J.-S.; Matyjaszewski, K. *J. Am. Chem. Soc.* **1995,** *117,* 5614–5615. doi:10.1021/ja00125a035
6. Matyjaszewski, K.; Xia, J. *Chem. Rev.* **2001,** *101,* 2921–2990. doi:10.1021/cr940534g
7. Kamigaito, M.; Ando, T.; Sawamoto, M. *Chem. Rev.* **2001,** *101,* 3689–3746. doi:10.1021/cr9901182
8. Chiefari, J.; Chong, Y. K.; Ercole, F.; Krstina, J.; Jeffery, J.; Le, T. P. T.; Mayadunne, R. T. A.; Meijs, G. F.; Moad, C. L.; Moad, G.; Rizzardo, E.; Thang, S. H. *Macromolecules* **1998,** *31,* 5559–5562. doi:10.1021/ma9804951
9. Destarac, M.; Charmot, D.; Franck, X.; Zard, S. Z. *Macromol. Rapid Commun.* **2000,** *21,* 1035–1039. doi:10.1002/1521-3927(20001001)21:15<1035::AID-MARC1035>3.0.CO;2-5
10. Moad, G.; Rizzardo, E.; Thang, S. H. *Aust. J. Chem.* **2005,** *58,* 379–410. doi:10.1071/CH05072
11. Nicolas, J.; Guillaneuf, Y.; Lefay, C.; Bertin, D.; Gigmes, D.; Charleux, B. *Prog. Polym. Sci.* **2013,** *38,* 63–235. doi:10.1016/j.progpolymsci.2012.06.002
12. Tizzotti, M.; Charlot, A.; Fleury, E.; Stenzel, M.; Bernard, J. *Macromol. Rapid Commun.* **2010,** *31,* 1751–1772. doi:10.1002/marc.201000072
13. Stenstad, P.; Andresen, M.; Tanem, B. S.; Stenius, P. *Cellulose* **2008,** *15,* 35–45. doi:10.1007/s10570-007-9143-y
14. Lindman, B.; Karlström, G.; Stigsson, L. *J. Mol. Liq.* **2010,** *156,* 76–81. doi:10.1016/j.molliq.2010.04.016
15. Heinze, T.; Liebert, T. *Prog. Polym. Sci.* **2001,** *26,* 1689–1762. doi:10.1016/S0079-6700(01)00022-3
16. Yan, L.; Ishihara, K. *J. Polym. Sci., Part A: Polym. Chem.* **2008,** *46,* 3306–3313. doi:10.1002/pola.22670
17. Daly, W. H.; Evenson, T. S.; Iacono, S. T.; Jones, R. W. *Macromol. Symp.* **2001,** *174,* 155–164. doi:10.1002/1521-3900(200109)174:1<155::AID-MASY155>3.0.CO;2-O
18. Keoshkerian, B.; Georges, M.; Quinlan, M.; Veregin, R.; Goodbrand, B. *Macromolecules* **1998,** *31,* 7559–7561. doi:10.1021/ma971686r
19. Finet, J.-P.; Grimaldi, S.; Le Moigne, F.; Nicol, P.; Plechot, M.; Tordo, P. Polymerisation en presence d'un radical nitroxide β-substitue. WO Patent WO 1996/024620 A1, Aug 15, 1996.
20. Benoit, D.; Grimaldi, S.; Robin, S.; Finer, J.-P.; Tordo, P.; Gnanou, Y. *J. Am. Chem. Soc.* **2000,** *122,* 5929–5939. doi:10.1021/ja991735a
21. Georges, M. K.; Veregin, R. P. N.; Kazmaier, P. M.; Hamer, G. K. *Macromolecules* **1993,** *26,* 2987–2988. doi:10.1021/ma00063a054
22. Hawker, C. J. *J. Am. Chem. Soc.* **1994,** *116,* 11185–11186. doi:10.1021/ja00103a055
23. Ohno, K.; Tsujii, Y.; Miyamoto, T.; Fukuda, T.; Goto, M.; Kobayashi, K.; Akaike, T. *Macromolecules* **1998,** *31,* 1064–1069. doi:10.1021/ma971329g
24. Lessard, B. H.; Guillaneuf, Y.; Mathew, M.; Liang, K.; Clement, J.-L.; Gigmes, D.; Hutchinson, R. A.; Marić, M. *Macromolecules* **2013,** *46,* 805–813. doi:10.1021/ma3023525
25. Lessard, B. H.; Savelyeva, X.; Marić, M. *Polymer* **2012,** *53,* 5649–5656. doi:10.1016/j.polymer.2012.10.020
26. Handké, N.; Trimaille, T.; Luciani, E.; Rollet, M.; Delair, T.; Verrier, B.; Bertin, D.; Gigmes, D. *J. Polym. Sci., Part A: Polym. Chem.* **2011,** *49,* 1341–1350. doi:10.1002/pola.24553
27. Kuo, K.-H.; Chiu, W.-Y.; Cheng, K.-C. *Polym. Int.* **2008,** *57,* 730–737. doi:10.1002/pi.2400
28. Lefay, C.; Guillaneuf, Y.; Moreira, G.; Thevarajah, J. J.; Castignolles, P.; Ziarelli, F.; Bloch, E.; Major, M.; Charles, L.; Gaborieau, M.; Bertin, D.; Gigmes, D. *Polym. Chem.* **2013,** *4,* 322–328. doi:10.1039/c2py20544k
29. Yamasaki, T.; Mito, F.; Ito, Y.; Pandian, S.; Kinoshita, Y.; Nakano, K.; Murugesan, R.; Sakai, K.; Utsumi, H.; Yamada, K. *J. Org. Chem.* **2011,** *76,* 435–440. doi:10.1021/jo101961m

30. Oyaizu, K.; Nishide, H. *Adv. Mater.* **2009,** *21,* 2339–2344. doi:10.1002/adma.200803554
31. Lund, H.; Michel, M.-A.; Simonet, J. *Acta Chem. Scand., Ser. B* **1975,** *29,* 217–220.
32. Potthast, A.; Rosenau, T.; Buchner, R.; Röder, T.; Ebner, G.; Bruglachner, H.; Sixta, H.; Kosma, P. *Cellulose* **2002,** *9,* 41–53. doi:10.1023/A:1015811712657
33. Sen, V. D.; Golubev, V. A. *J. Phys. Org. Chem.* **2009,** *22,* 138–143. doi:10.1002/poc.1439
34. Tebben, L.; Studer, A. *Angew. Chem., Int. Ed.* **2011,** *50,* 5034–5068. doi:10.1002/anie.201002547
35. Edeleva, M.; Marque, S. R. A.; Kabytaev, K.; Guillaneuf, Y.; Gigmes, D.; Bagryanskaya, E. *J. Polym. Sci., Part A: Polym. Chem.* **2013,** *51,* 1323–1336. doi:10.1002/pola.26500
36. Brusseau, S.; D'Agosto, F.; Magnet, S.; Couvreur, L.; Chamignon, C.; Charleux, B. *Macromolecules* **2011,** *44,* 5590–5598. doi:10.1021/ma2008282
37. Bertin, D.; Gigmes, D.; Marque, S.; Tordo, P. *e-Polym.* **2003,** 002.
38. Brémond, P.; Marque, S. R. A. *Chem. Commun.* **2011,** *47,* 4291–4293. doi:10.1039/c0cc05637e

License and Terms

Beilstein Journal of Organic Chemistry

Organotellurium-mediated living radical polymerization under photoirradiation by a low-intensity light-emitting diode

Yasuyuki Nakamura and Shigeru Yamago*

Full Research Paper

Open Access

Address:
Institute for Chemical Research, Kyoto University, Gokasyo, Uji, Kyoto 611-0011, Japan, and Core Research for Evolutional Science and Technology (CREST), Japan Science and Technology Agency (JST)

Email:
Shigeru Yamago* - yamago@scl.kyoto-u.ac.jp

* Corresponding author

Keywords:
free radical; light-emitting diode; living radical polymerization; organotellurium compound; photopolymerization; tellurium; visible light

Beilstein J. Org. Chem. **2013,** *9,* 1607–1612.
doi:10.3762/bjoc.9.183

Received: 05 June 2013
Accepted: 12 July 2013
Published: 07 August 2013

This article is part of the Thematic Series "Organic free radical chemistry".

Guest Editor: C. Stephenson

Abstract

A low-intensity (6 W) light-emitting diode (LED) effectively activated an organotellurium chain transfer agent and the dormant species, promoting well-controlled radical polymerization. The use of the LED provided many advantages over the previously reported high-intensity Hg lamp, including high energy efficiency during the polymerization, and easy availability of the low-cost light source. Structurally well-defined poly(methyl methacrylate), poly(methyl acrylate), and polystyrene, with narrow molecular weight distributions, were synthesized under LED irradiation with or without a neutral density filter.

Introduction

Living radical polymerization (LRP) is one of the most powerful methods for the synthesis of structurally well-defined polymers because of its robustness and high versatility, which allows for the polymerization of a wide variety of vinyl monomers with various functionalities [1-3]. LRP relies on the reversible generation of polymer-end radicals from a dormant species. One approach to the activation of the dormant species is the use of photostimulation. This has been widely employed in conventional radical polymerization for various applications such as coatings, adhesives, gels and microelectronics [4-7]. The major motivation for the utilization of photochemistry in LRP is that it enables the dormant species to be activated under mild thermal conditions [8-11]. In addition, photochemical activation is beneficial for increasing the fidelity of the polymer-end structure [12]. However, the experimental setup required for the reaction provides problems, as distinctive light sources such as γ-rays or high-intensity UV irradiation are required [13-21].

We have previously developed organotellurium-mediated LRP (TERP), which has several synthetic advantages over other LRP methods [22-24]. These include high monomer versatility [25-27], good compatibility with polar functional groups and solvents [28,29], and facile living-end transformation for the

synthesis of block copolymers [30-34] and end-functional polymers [35,36]. Furthermore, we recently reported that photochemical stimuli were efficient in the activation of organotellurium dormant species, and that TERP proceeded under mild thermal conditions to give highly controlled polymers [37]. The polymerization proceeded by irradiation with a weak-intensity light source such as a 60–100 W black lamp or sunlight, but we routinely used a high-intensity light source, namely, a 500 W high pressure Hg lamp, combined with a light cutoff filter. However, control of the light intensity was difficult under such conditions. For example, when light of a relatively high intensity was used to prepare a polyisoprene using TERP, a radical coupling reaction occurred because of the efficient formation of the polymer-end radical [38]. In addition, when ditellurides were added to the TERP reaction in order to increase the level of control over the polymerization of methacrylates, optimization of the conditions was difficult, because ditellurides have a stronger absorption coefficient than the organotellurium compounds (Figure 1). This resulted in the generation of tellurium radicals, which activate the organotellurium dormant species [30,39]. Therefore, the development of new photochemical conditions which employ a weak-intensity, readily available light source is necessary for expanding the utility of photo-TERP. We focused on a light emitting diode (LED) due to its high power conversion efficiency, low heat generation, narrow and tunable wavelength range of the emitted light, and ease of availability. Herein, we report on the use of photo-TERP with a 6 W white, household LED (Scheme 1). Attention was focused on the TERP of methyl methacrylate (MMA) in the presence of ditelluride, but other typical conjugated monomers, namely, methyl acrylate and styrene, were also evaluated. TERP of these monomers proceeded efficiently in a controlled manner by adjusting the light intensity using ND filters. The results clearly demonstrate the extremely high sensitivity of organotellurium compounds for generating radical species by photostimulation.

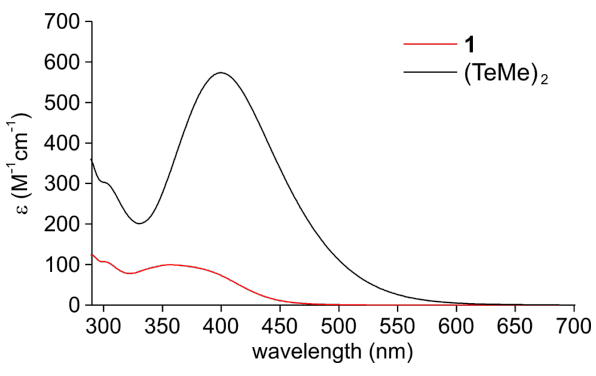

Figure 1: UV–vis absorption spectra of organotellurium chain transfer agent **1** and dimethyl ditelluride in toluene.

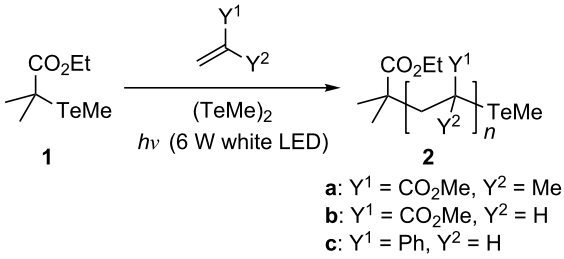

Scheme 1: Photopolymerization in the presence of organotellurium chain transfer agent **1**.

Based on these findings, we also adjust our previous statements regarding the effect of ditelluride on TERP.

Results and Discussion

The polymerization of MMA (100 equiv) was first conducted in the presence of organotellurium chain transfer agent **1** (1 equiv) and dimethyl ditelluride (1 equiv) under 6 W white LED at 70 °C (Scheme 1 and Table 1, run 1). The polymerization progressed rapidly, reaching 93% monomer conversion after 1 h. However, the number-average molecular weight (M_n) of the resulting polymer (**2a**, $M_{n(exp)}$ = 11900) deviated slightly from the theoretical value, as calculated from the monomer/**1** ratio and the monomer conversion ($M_{n(theo)}$ = 9400). In addition, the control of molecular weight distribution (MWD, M_w/M_n = 1.26; M_w refers to weight average molecular weight) was moderate.

We have previously reported that the intensity of irradiating light is critical for gaining control of the polymerization [37]. Therefore, we investigated the effect of the light intensity by using ND filters (Figure 2). When a 50% transmittance ND filter was used, the MWD improved to 1.20 from 1.26, while 2 h was required to reach >90% monomer conversion (Table 1, run 2). The MWD control was further improved when the light intensity was reduced by using 30% and 20% transmittance ND filters (M_w/M_n = 1.18–1.19), although the monomer conversion further slowed down with this order (Table 1, runs 3 and 4). The MWD control reached a plateau when a 10% transmittance ND filter was used, while the polymerization rate was further decelerated (Table 1, run 5). In the absence of light irradiation, the polymerization was extremely slow, reaching only 36% monomer conversion, even after 12 h (Table 1, run 6). These results clearly demonstrate that weak light intensity was sufficient for activating the organotellurium compounds. The concentration of the radical species was roughly proportional to the light intensity. The monomer conversion after 1 h increased nearly linearly by the use of ND filters with higher transmittance (25, 36, 47, 62, and 93% monomer conversion by using 10, 20, 30,

Table 1: Photopolymerization of MMA in the presence of **1** under LED irradiation.[a]

Run	MMA/**1** ratio	ND filter[b]	Time (h)	Conv. (%)[c]	$M_{n(theo)}$	$M_{n(exp)}$[d]	M_w/M_n[d]
1	100	none	1.0	93	9400	11900	1.26
2	100	50	2.0	92	9300	10700	1.20
3	100	30	2.5	93	9400	9800	1.19
4	100	20	4.0	92	9300	9500	1.18
5	100	10	5.5	93	9500	10400	1.18
6[e]	100	none	12	36	3700	2500	1.27
7[f]	100	20	6.0	94	9500	10400	1.18
8[g]	100	20	3.0	91	9200	9600	1.19
9[h]	100	20	2.5	93	9400	9900	1.19
10	200	20	4.0	92	18500	20500	1.17
11	300	20	4.5	94	28400	31900	1.14
12[i]	500	10	5.0	94	47200	52400	1.14
13[i]	1000	10	5.5	91	91200	109700	1.25

[a]A solution of **1**, dimethyl ditelluride (1 equiv) and monomer (100 equiv) was irradiated with a 6 W LED with or without a ND filter at 70 °C. [b]% Transmittance is shown. [c]Determined by ^{1}H NMR. [d]Determined by GPC calibrated with PMMA standards. [e]The reaction was carried out in the dark. [f]The polymerization was carried out at 60 °C. [g]The polymerization was carried out at 80 °C. [h]The polymerization was carried out at 90 °C. [i]2 equiv of dimethyl ditelluride was used.

50% ND filter and direct irradiation, respectively). The poor MWD control under high-intensity light is probably due to the increase in undesired termination reactions of the polymer-end radicals. When the termination is negligible, the level of MWD control is determined by the rate of deactivation of the polymer-end radicals by ditelluride forming a dormant species [39] which is independent of the light intensity.

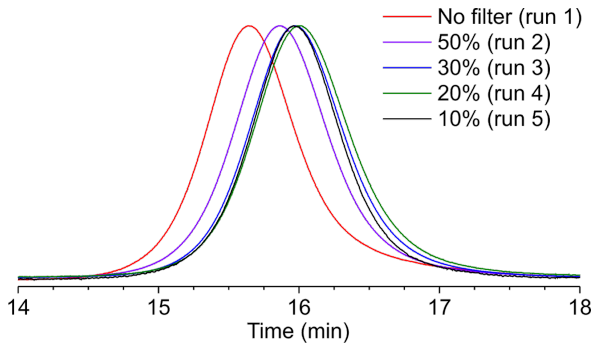

Figure 2: GPC traces for the polymerizations of MMA (Table 1). The percentages in the legend refer to the ND filters used.

The synthetic scope of MMA polymerization was next examined (Table 1, runs 7–13). As the generation of the polymer-end radical from the organotellurium dormant species does not require thermal stimuli, the reaction temperature can be arbitrarily selected depending on the propagation rate of the particular monomer. For example, the same polymerization proceeded over the range of 60–90 °C under otherwise identical conditions, affording structurally well controlled PMMAs in all cases (Table 1, runs 7–9). The conversion of the monomer was slow at lower temperatures because of the decrease in propagation rate, but the MWDs were identical in all cases, within the experimental error. Due to the high propagation rate at high temperatures the polymerization at 90 °C reached >90% monomer conversion within 2.5 h, affording PMMA with a narrow MWD (M_w/M_n = 1.19, Table 1, run 9).

Structurally well controlled, high-molecular-weight PMMAs were also prepared by changing the monomer/**1** ratio (Table 1, runs 10–13). When 200–1000 equivalents of MMA over **1** were employed, monomer conversion reached >90% in all cases within 5.5 h, and PMMAs with a M_n, of 20500–109700 with a narrow MWD ($M_w/M_n \leq 1.25$) were synthesized. When more than 500 equivalents of monomer were employed, the addition of two equivalents of dimethyl ditelluride, as well as the use of a 10% transmittance ND filter, resulted in improved MWDs (Table 1, runs 12 and 13).

The use of the LED was also found to be effective for the efficient and controlled polymerization of other monomers (Table 2). For example, TERP of methyl acrylate (100 equiv) without ditelluride reached 91% monomer conversion after 1.6 h irradiation with the LED without an ND filter at 50 °C. Structurally well-defined poly(methyl acrylate) (PMA) with M_n = 10100 and a narrow MWD (M_w/M_n = 1.11) was obtained (Table 2, run 1). High-molecular-weight PMAs with narrow MWDs (M_n = 90200, M_w/M_n = 1.13 and M_n = 166000, M_w/M_n = 1.15) were also prepared by changing the monomer/**1** ratio under LED irradiation through a 50% transmittance ND filter (Table 2, runs 2 and 3).

Table 2: Photopolymerization in the presence of **1** under LED irradiation.[a]

Run	Monomer (equiv)[b]	ND filter (% transmittance)	Temp. (°C)	Time (h)	Conv. (%)[c]	$M_{n(theo)}$	$M_{n(exp)}$[d]	M_w/M_n[d]
1	MA (100)	none	50	1.6	91	8000	10100	1.11
2	MA (1000)	50	50	5	93	80100	90200	1.13
3	MA (2000)	50	50	8	86	148100	166000	1.15
4	St (100)	none	90	6	96	10100	18200	1.36
5	St (100)	20	90	9	98	10300	11600	1.09
6	St (500)	10	90	14	95	49500	47400	1.18
7	St (1000)	10	90	16	83	86500	87500	1.33

[a]A solution of **1** and monomer (100 equiv) was irradiated with a 6 W LED with or without a ND filter. [b]Monomer abbreviations: MA, methyl acrylate; St, styrene. [c]Determined by ^{1}H NMR. [d]Determined by GPC calibrated with PMMA or polystyrene standards.

Next, the polymerization of styrene was examined at 90 °C, as the propagation rate constant of styrene is much lower than those of acrylates and methacrylates. Polymerization in the absence of a filter quantitatively converted the monomer to the polymer within 6 h (96%), but the $M_{n(exp)}$ of the resulting polystyrene (18100) was significantly different from the $M_{n(theo)}$ (10100), and the MWD control was unsatisfactory (M_w/M_n = 1.36) (Table 2, run 4). On the other hand, when the polymerization was carried out through a 20% transmittance ND filter, although the monomer conversion was slower, the resulting polystyrene had a $M_{n(exp)}$ close to $M_{n(theo)}$, and a very narrow MWD (M_w/M_n = 1.09) (Table 2, run 5). High-molecular-weight polystyrene of M_n = 47400 and 87500, with narrow MWDs (M_w/M_n = 1.18 and 1.33, respectively) were successfully synthesized by using a 10% transmittance ND filter (Table 2, runs 6 and 7).

When the ditelluride is absent, polymerization is initiated by the direct photolysis of the carbon–tellurium bond of the organotellurium dormant species, P–TeMe (Scheme 2, reaction 1, P denotes polymer) [37]. Once the polymer radical is generated, it predominantly undergoes a degenerative chain transfer-mediated polymerization reaction (Scheme 2, reaction 2, P′ refers to a polymer with either the same or different chain length as P) [25,40]. When the ditelluride is present, its activation produces two molecules of methyltellanyl radical (Scheme 2, reaction 3). As ditelluride possesses a higher absorption coefficient in the UV region than organotellurium compounds such as **1** (Figure 1), the preferential activation of ditelluride over organotellurium compounds should occur. Once a methyltellanyl radical forms, it activates P–TeMe, giving a polymer end-radical and a ditelluride (Scheme 2, reaction 4).

We have previously reported that the addition of ditelluride accelerates the TERP and that the activation of P–TeMe by a methyltellanyl radical is the origin of this rate enhancement [39]. However, the mechanism by which this occurs has not been fully elucidated. As we have deduced that the activation of ditelluride successfully proceeds under very weak intensity light irradiation, the tellanyl radical should also be formed by the photons from interior fluorescent lighting. Indeed, TERP of MMA in the presence of ditelluride completed in approximately 13 h at 80 °C, without any special caution under interior fluorescent lighting [30], whereas the same experiment completely protected from all light sources took 22 h.

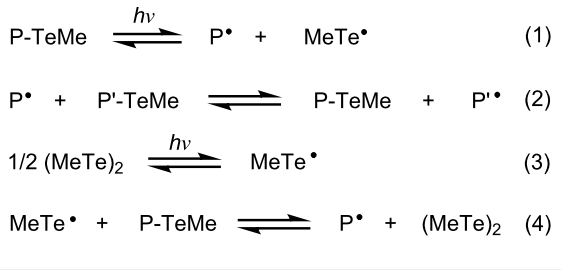

Scheme 2: Activation and deactivation mechanism of dormant (P-TeMe) and ditelluride.

Conclusion

A new and efficient procedure for photoinduced TERP was developed by using a low energy (6 W) visible LED as the light source. Compared to previously employed photoinduced TERP by using a 60–500 W light source, the energy efficiency was significantly improved. As the TERP of MMA and styrene was best controlled in combination with 10 or 20% transmittance ND filters, light with an intensity below 6 W should also be usable. Improvement in the MWD could be achieved by appropriate tuning of the light intensity. As activation of the organotellurium compounds has been shown to be possible with a low power and readily available LED, implementation to large scale synthesis should be feasible. Furthermore, the activation of the dormant species does not require thermal stimuli, and so independent control of the initiation (radical generation) and the propagation should be possible.

Experimental

General: All reactions involving oxygen and moisture sensitive compounds were carried out in a dry reaction vessel under a nitrogen atmosphere. A 6 W white LED (Panasonic) was used as the light source in combination with a neutral density (ND) filter (Sigma Koki). ^{1}H NMR (400 MHz) spectra were measured for a $CDCl_3$ solution of the sample and are reported in ppm (δ) from an internal of tetramethylsilane. Gel permeation chromatography (GPC) was performed on a machine equipped with two linearly connected polystyrene mixed gel columns (Shodex LF-604) at 40 °C by using UV and refluctive index (RI) detectors with chloroform as the eluent. The number-average molecular weight (M_n) is reported in g·mol^{-1}. PMMA and poly(methyl acrylate) were calibrated with PMMA standards, and polystyrene was calibrated with polystyrene standards.

Materials: Unless otherwise noted, chemicals obtained from commercial suppliers were used as received. Methyl methacrylate (MMA), methyl acrylate and styrene were washed with 5% NaOH aqueous solution and were distilled over CaH_2. Ethyl 2-methyltellanylisobutylate (**1**) and dimethyl ditelluride were prepared as reported [22]. The UV–vis spectra of **1** and dimethyl ditelluride are shown in Figure 1.

Typical procedure for photopolymerization: A solution of MMA (1.0 mL, 9.4 mmol), **1** (16.5 μL, 0.094 mmol), and dimethyl ditelluride (10.0 μL, 0.094 mmol) was irradiated with a 6 W white LED equipped with a 20% ND filter at 70 °C for 4 h under a nitrogen atmosphere in a capped tube (Figure 3). A small portion of the reaction mixture was then removed, and the conversion of the monomer (92%) was determined by using ^{1}H NMR spectroscopy. The reaction mixture was analyzed by using GPC, and the M_n (9500) and M_w/M_n (1.18) were determined. Chloroform was subsequently added to the mixture, and the resulting solution was poured into hexane with vigorous stirring. The product was collected by suction filtration and dried under vacuum to give the final PMMA product (810 mg).

Figure 3: Experimental setup for the photopolymerization using the LED.

References

1. Matyjaszewski, K.; Davis, T. P. *Handbook of Radical Polymerization;* John Wiley and Sons: Hoboken, 2002.
2. Matyjaszewski, K.; Moeller, M.; Sawamoto, M.; Coates, G. W., Eds. *Chain Polymerization of Vinyl Monomers;* Polymer Science: A Comprehensive Reference, Vol. 3; Elsevier BV: Amsterdam, 2012.
3. *Polymers and Materials;* Chatgilialoglu, C.; Studer, A., Eds.; *Encyclopedia of Radicals in Chemistry, Biology and Materials*; John Wiley and Sons, 2012.
4. Fouassier, J.-P. *Photoinitiation, Photopolymerization, and Photocuring: Fundamentals and Applications;* Hanser-Gardner Publications: Munich, 1995.
5. Tasdelen, M. A.; Yagci, Y. *Aust. J. Chem.* **2011,** *64,* 982–991. doi:10.1071/CH11113
6. Yamago, S.; Nakamura, Y. *Polymer* **2013,** *54,* 981–994. doi:10.1016/j.polymer.2012.11.046
7. Tasdelen, M. A.; Çiftci, M.; Uygun, M.; Yagci, Y. *Progress in controlled radical polymerization: materials and applications*. Matyjaszewski, K.; Sumerlin, B. S.; Tsarevsky, N. V., Eds.; American Chemical Society: Washington DC, 2012; p 59.
8. Konkolewicz, D.; Schröder, K.; Buback, J.; Bernhard, S.; Matyjaszewski, K. *ACS Macro Lett.* **2012,** *1,* 1219–1223. doi:10.1021/mz300457e
9. Fors, B. P.; Hawker, C. J. *Angew. Chem., Int. Ed.* **2012,** *51,* 8850–8853. doi:10.1002/anie.201203639
10. Ohtsuki, A.; Goto, A.; Kaji, H. *Macromolecules* **2013,** *46,* 96–102. doi:10.1021/ma302244j
11. Zhao, Y.; Yu, M.; Fu, X. *Chem. Commun.* **2013,** *49,* 5186–5188. doi:10.1039/c3cc41466c
12. Nakamura, Y.; Kitada, Y.; Kobayashi, Y.; Ray, B.; Yamago, S. *Macromolecules* **2011,** *44,* 8388–8397. doi:10.1021/ma201761q
13. Bai, R.-K.; You, Y.-Z.; Pan, C.-Y. *Macromol. Rapid Commun.* **2001,** *22,* 315–319. doi:10.1002/1521-3927(20010301)22:5<315::AID-MARC315>3.0.CO;2-O
14. Quinn, J. F.; Barner, L.; Davis, T. P.; Thang, S. H.; Rizzardo, E. *Macromol. Rapid Commun.* **2002,** *23,* 717–721. doi:10.1002/1521-3927(20020801)23:12<717::AID-MARC717>3.0.CO;2-I
15. Barner, L.; Quinn, J.; Barner-Kowollik, C.; Vana, P.; Davis, T. P. *Eur. Polym. J.* **2003,** *39,* 449–459. doi:10.1016/S0014-3057(02)00247-1
16. Millard, P.-E.; Barner, L.; Stenzel, M. H.; Davis, T. P.; Barner-Kowollik, C.; Müller, A. H. E. *Macromol. Rapid Commun.* **2006,** *27,* 821–828. doi:10.1002/marc.200600115
17. Chen, G.; Zhu, X.; Zhu, J.; Cheng, Z. *Macromol. Rapid Commun.* **2004,** *25,* 818–824. doi:10.1002/marc.200300266
18. Quinn, J. F.; Barner, L.; Barner-Kowollik, C.; Rizzardo, E.; Davis, T. P. *Macromolecules* **2002,** *35,* 7620–7627. doi:10.1021/ma0204296

19. Lu, L.; Yang, N.; Cai, Y. *Chem. Commun.* **2005,** 5287–5288. doi:10.1039/b512057h
20. Muthukrishnan, S.; Pan, E. H.; Stenzel, M. H.; Barner-Kowollik, C.; Davis, T. P.; Lewis, D.; Barner, L. *Macromolecules* **2007,** *40,* 2978–2980. doi:10.1021/ma0703094
21. Tasdelen, M. A.; Durmaz, Y. Y.; Karagoz, B.; Bicak, N.; Yagci, Y. *J. Polym. Sci., Part A: Polym. Chem.* **2008,** *46,* 3387–3395. doi:10.1002/pola.22686
22. Yamago, S.; Iida, K.; Yoshida, J. *J. Am. Chem. Soc.* **2002,** *124,* 2874–2875. doi:10.1021/ja025554b
23. Yamago, S. *Chem. Rev.* **2009,** *109,* 5051–5068. doi:10.1021/cr9001269
24. Yamago, S.; Nakamura, Y. Other Degenerative Transfer Systems. In *Chain Polymerization of Vinyl Monomers;* Matyjaszewski, K.; Möller, M., Eds.; Polymer Science: A Comprehensive Reference, Vol. 3; Elsevier BV: Amsterdam, 2012; pp 227–247. doi:10.1016/B978-0-444-53349-4.00067-4
25. Goto, A.; Kwak, Y.; Fukuda, T.; Yamago, S.; Iida, K.; Nakajima, M.; Yoshida, J. *J. Am. Chem. Soc.* **2003,** *125,* 8720–8721. doi:10.1021/ja035464m
26. Mishima, E.; Tamura, T.; Yamago, S. *Macromolecules* **2012,** *45,* 8998–9003. doi:10.1021/ma301570r
27. Mishima, E.; Tamura, T.; Yamago, S. *Macromolecules* **2012,** *45,* 2989–2994. doi:10.1021/ma300325r
28. Mishima, E.; Yamago, S. *Macromol. Rapid Commun.* **2011,** *32,* 893–898. doi:10.1002/marc.201100089
29. Sugihara, Y.; Kagawa, Y.; Yamago, S.; Okubo, M. *Macromolecules* **2007,** *40,* 9208–9211. doi:10.1021/ma071363n
30. Yamago, S.; Iida, K.; Yoshida, J. *J. Am. Chem. Soc.* **2002,** *24,* 13666–13667. doi:10.1021/ja027599i
31. Ray, B.; Kotani, M.; Yamago, S. *Macromolecules* **2006,** *39,* 5259–5265. doi:10.1021/ma060248u
32. Yusa, S.; Yamago, S.; Sugahara, M.; Morikawa, S.; Yamamoto, T.; Morishima, Y. *Macromolecules* **2007,** *40,* 5907–5915. doi:10.1021/ma070769x
33. Kumar, S.; Changez, M.; Murthy, C. N.; Yamago, S.; Lee, J.-S. *Macromol. Rapid Commun.* **2011,** *32,* 1576–1582. doi:10.1002/marc.201100277
34. Mishima, E.; Yamada, T.; Watanabe, H.; Yamago, S. *Chem.–Asian J.* **2011,** *6,* 445–451. doi:10.1002/asia.201000402
35. Yamada, T.; Mishima, E.; Ueki, K.; Yamago, S. *Chem. Lett.* **2008,** *37,* 650–651. doi:10.1246/cl.2008.650
36. Yamago, S.; Kayahara, E.; Yamada, H. *React. Funct. Polym.* **2009,** *69,* 416–423. doi:10.1016/j.reactfunctpolym.2009.03.008
37. Yamago, S.; Ukai, Y.; Matsumoto, A.; Nakamura, Y. *J. Am. Chem. Soc.* **2009,** *131,* 2100–2101. doi:10.1021/ja8099689
38. Nakamura, Y.; Arima, T.; Tomita, S.; Yamago, S. *J. Am. Chem. Soc.* **2012,** *134,* 5536–5539. doi:10.1021/ja300869x
39. Kwak, Y.; Tezuka, M.; Goto, A.; Fukuda, T.; Yamago, S. *Macromolecules* **2007,** *40,* 1881–1885. doi:10.1021/ma0623385
40. Kwak, Y.; Goto, A.; Fukuda, T.; Kobayashi, Y.; Yamago, S. *Macromolecules* **2006,** *39,* 4671–4679. doi:10.1021/ma060295m

License and Terms

Beilstein Journal of Organic Chemistry

Computational study of the rate constants and free energies of intramolecular radical addition to substituted anilines

Andreas Gansäuer*[1], Meriam Seddiqzai[1], Tobias Dahmen[1], Rebecca Sure[2] and Stefan Grimme*[2]

Full Research Paper

Open Access

Address:
[1]Kekulé-Institut für Organische Chemie und Biochemie der Rheinischen-Friedrich-Wilhelms-Universität Bonn, Gerhard-Domagk-Straße 1, D-53121 Bonn, Germany and [2]Mulliken Center for Theoretical Chemistry, Institut für Physikalische und Theoretische Chemie der Rheinischen-Friedrich-Wilhelms-Universität Bonn, Beringstraße 4, D-53115 Bonn, Germany

Email:
Andreas Gansäuer* - andreas.gansaeuer@uni-bonn.de;
Stefan Grimme* - grimme@thch.uni-bonn.de

* Corresponding author

Keywords:
aromatic substitution; computational chemistry; DFT-D3; free radical; polar effects; radical reaction

Beilstein J. Org. Chem. **2013,** *9,* 1620–1629.
doi:10.3762/bjoc.9.185

Received: 14 May 2013
Accepted: 17 July 2013
Published: 08 August 2013

This article is part of the Thematic Series "Organic free radical chemistry".

Guest Editor: C. Stephenson

Abstract

The intramolecular radical addition to aniline derivatives was investigated by DFT calculations. The computational methods were benchmarked by comparing the calculated values of the rate constant for the 5-*exo* cyclization of the hexenyl radical with the experimental values. The dispersion-corrected PW6B95-D3 functional provided very good results with deviations for the free activation barrier compared to the experimental values of only about 0.5 kcal mol^{-1} and was therefore employed in further calculations. Corrections for intramolecular London dispersion and solvation effects in the quantum chemical treatment are essential to obtain consistent and accurate theoretical data. For the investigated radical addition reaction it turned out that the polarity of the molecules is important and that a combination of electrophilic radicals with preferably nucleophilic arenes results in the highest rate constants. This is opposite to the Minisci reaction where the radical acts as nucleophile and the arene as electrophile. The substitution at the N-atom of the aniline is crucial. Methyl substitution leads to slower addition than phenyl substitution. Carbamates as substituents are suitable only when the radical center is not too electrophilic. No correlations between free reaction barriers and energies ($\Delta G^{\ddagger}$ and ΔG_R) are found. Addition reactions leading to indanes or dihydrobenzofurans are too slow to be useful synthetically.

Introduction

The development of efficient catalytic reactions is one of the central issues of chemistry [1,2]. Radical-based transformations are amongst the most attractive methods for the use in catalytic cycles due to the ease of radical generation, high functional group tolerance, and selectivity in C–C bond formation [3-5]. Recently, we have reported a novel catalytic reaction, a radical arylation of epoxides [6-8] proceeding via catalysis in single electron steps (for experimental results see Scheme 1) [9,10]. The C–C bond forming step of the catalytic cycle is an intramolecular alkyl radical addition to substituted anilines. Even though only rarely used, reaction sequences employing such steps in an intermolecular or intramolecular manner have been employed in some transformations that are highly useful. Prominent examples are the Minisci reaction [11-15] for the preparation of mainly nitrogen heterocycles and Zard's homolytic substitution reactions at nitrogen heterocycles with xanthates as radical precursors [16-20].

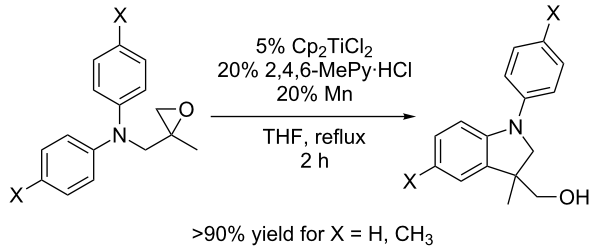

Scheme 1: Experimental results for the radical arylation of epoxides.

Despite this usefulness only few studies have been concerned with the determination of absolute rate constants of radical additions to arenes. These were carried out in mechanistic studies of the Minisci reaction [21,22]. It was found that the butyl radical adds to benzene with a rate constant of 3.8×10^2 M^{-1} s^{-1} at 79 °C. In this study it was also demonstrated that the rate constants for addition reactions to electron deficient (protonated) heteroarenes can be much higher due to polar effects. Despite these insightful investigations a more general picture of the kinetics of radical addition to arenes is still elusive and, to the best of our knowledge, thermodynamic data (free energies) for radical additions to arenes are not available.

In this study, we have investigated the rate constants and free energies of intramolecular radical addition to substituted anilines that constitutes the C–C bond forming event of indoline synthesis via homolytic substitution with computational methods. The results are of general interest for the understanding of radical addition to electron rich arenes and should be helpful in the design of novel radical reactions.

The aim of theoretical thermochemistry is to describe the energetics of a chemical process with an accuracy of 1 kcal mol^{-1} or even better. At the same time, the methods applied should not be too demanding in terms of computational costs in order to be still applicable to chemically interesting systems. Kohn–Sham density functional theory (KS-DFT) has been proven to yield good accurate thermochemical properties within acceptable computation times [23-25]. However, the number of the proposed approximate exchange–correlation functionals to choose from is huge and they can suffer from severe problems, e.g., self-interaction error (SIE) leading to underestimated reaction barriers and the lack of long-range electron correlation (London dispersion) effects. Regarding the latter problem, one of the most successful and widely used dispersion correction schemes is DFT-D3, in which a damped, atom-pair wise potential is added to a standard DFT result [26]. A thorough energy benchmark study of various density functionals for general main group thermochemistry, kinetics and non-covalent interactions (GMTKN30 benchmark set) [27] showed that Zhao and Truhlar's PW6B95 functional [28] in combination with DFT-D3 (termed PW6B95-D3 from now on) is the most robust and accurate general purpose hybrid functional and is therefore used also in this work. As a meta-hybrid functional it partially avoids the SIE by admixture of non-local Fock-exchange (28%) leading to reasonable reaction barriers [27] which are normally underestimated (in particular for radical species) with semi-local GGAs.

We conducted a DFT study using the above mentioned state-of-the-art quantum chemical methods which are applied successfully to various thermochemical problems in our group since several years. This well established protocol consists of gas phase structure optimization at the dispersion-corrected DFT-D3 level using large triple-zeta AO basis sets (TPSS-D3/def2-TZVP) followed by accurate single-point energy calculations at the meta-hybrid level with a further extended AO basis set (PW6B95-D3/def2-QZVP), thermo-statistical corrections from energy to free energy at a given temperature and corrections for solvation free energy by the reliable (DFT-based) COSMO-RS continuum solvation model [29,30]. For recent applications of this procedure see [31-33]. The estimated accuracy is 1–2 kcal mol^{-1} for absolute free enthalpies and relative values for different compounds (trends) should have an error <1 kcal mol^{-1}.

Results and Discussion

Theoretical methods and benchmarking

Computational details

The quantum chemical calculations have been performed with the TURBOMOLE 6.4 suite of programs [34]. All geometry

optimizations were performed on the DFT level using the TPSS density functional [35] along with the polarized triple-zeta def2-TZVP basis set [36]. This choice avoids major basis set superposition errors (BSSE) without employing counter-poise corrections and gives theoretically consistent energies and structures. Single point energies were obtained on the PW6B95 [28] level together with the extended quadruple-zeta basis set def2-QZVP [36]. For the small benchmark on the 5-*exo* cyclization of the 5-hexenyl radical the functionals BP86 [37,38] and B3LYP [39-41] also have been applied together with the def2-QZVP basis set. CCSD(T) calculations with the def2-TZVPP[36] basis set have been performed and extrapolated to the complete basis set limit (CBS) [42] via MP2 [43] calculations with the def2-TZVPP and def2-QZVPP basis sets. CCSD-F12 [44] calculations with perturbative triples (CCSD-F12(T)) together with the correlation-consistent basis set cc-pVDZ-F12 [43] for explicitly correlated wave function methods have been calculated using TURBOMOLE 6.5 [45].

For all calculations the resolution-of-identity (RI) approximation for the Coulomb integrals [46] with matching default auxiliary basis sets [47] was applied. The numerical quadrature grid *m4* was employed for integration of the exchange-correlation contribution. For all geometry optimizations as well as single-point calculations the D3 dispersion correction scheme [26] applying Becke–Johnson (BJ) damping [48-50] was used.

Computations of the harmonic vibrational frequencies were performed analytically using the TURBOMOLE module *aoforce*. Thermal corrections from energy to free enthalpy were calculated within the standard harmonic-oscillator approximation for each molecule in the gas phase. The vibrational frequencies were used unscaled. The HOMO–SOMO energy gaps were evaluated using the TPSS-D3/TZVP orbitals. The COSMO-RS model [29,30] was used as implemented in COSMO therm [51] to obtain all solvation free energies. Single point calculations employing the default BP86 [37,38]/def-TZVP [52] level of theory were performed on the optimized gas phase geometries. The solvation contribution was then added to the gas phase free energies.

The 5-*exo* cyclization as benchmark

In order to find reliable computational methods for the description of the radical additions, we sought for systems for benchmarking that are structurally related to our system and that are experimentally well investigated. An ideal radical reaction in this respect is the 5-*exo* cyclization (Scheme 2) of the 5-hexenyl radical.

The reaction is preparatively highly important and has been used in many syntheses of complex molecules [3-5]. Moreover,

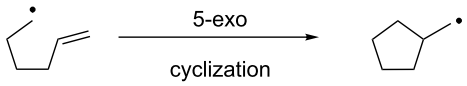

$k_{298} = 2.2 \times 10^5\ s^{-1}$

$\log k_{10} = (10.37 \pm 0.32) - (6.85 \pm 0.42)/\Theta$

$\Theta = 2.3\ RT/\ \text{kcal mol}^{-1}$

Scheme 2: 5-*exo* cyclization of the hexenyl radical.

the kinetics of the 5-*exo* cyclization has been studied very thoroughly and the rate constant has been determined by a number of approaches. The value currently accepted as 'best' for the rate constant is $k = 2.2 \times 10^5\ s^{-1}$ at 25 °C [53]. The Arrhenius equation for the 5-hexenyl cyclization has been determined to be $\log k_{10}/s^{-1} = (10.37 \pm 0.32) - (6.85 \pm 0.42)/\theta$ with $\theta = 2.3\ RT/$ kcal mol^{-1}. This implies that k lies between $5.1 \times 10^4\ s^{-1}$ and $9.3 \times 10^5\ s^{-1}$ at 25 °C and $6.1 \times 10^5\ s^{-1}$ and $8.2 \times 10^6\ s^{-1}$ at 100 °C.

Moreover, the geometry of the transition state of the 5-*exo* cyclization has been the subject of investigation [54,55]. In the transition state, the length of the forming C–C bond is assumed to be 2.341 Å and the attack of the radical at the olefin occurs at an angle of 105.8°. This value is close to the tetrahedral angle and the Bürgi–Dunitz angle [56].

In this study, the absolute free energy of activation as well as the free energy of the 5-*exo* cyclization of the hexenyl radical were calculated using the TPSS and PW6B95 functionals as described in computational details. From these values the absolute rate constants at 298 K (25 °C) in benzene were computed as summarized in Table 1 together with the experimental value for k at 25 °C. The experimental free enthalpy of activation was derived from the rate constant. We furthermore

Table 1: Experimental and computed rate constants and free energies of activation of the 5-*exo* cyclization of the hexenyl radical in benzene at 25 °C.

	ΔE [kcal mol^{-1}]	$\Delta G^{\ddagger}$ [kcal mol^{-1}]	k [s^{-1}]
Experiment		10.18	2.20×10^5
TPSS-D3	4.60	8.07	7.83×10^6
BP86-D3	4.05	7.52	1.99×10^7
B3LYP	9.81	13.28	1.18×10^3
B3LYP-D3	7.46	10.94	6.18×10^4
PW6B95	7.86	11.33	3.19×10^4
PW6B95-D3	7.16	10.63	1.03×10^5
CCSD(T)/CBS	9.46	12.93	2.12×10^3
CCSD-F12(T)	9.51	13.02	1.83×10^3

give zero-point and solvation exclusive pure electronic activation energies which are more convenient for a straightforward comparison of theoretical methods.

From our data it is clear that the semi-local TPSS and BP86 functionals strongly underestimate the activation energy of the 5-*exo* cyclization (by about 3 kcal mol^{-1}) due to the SIE but this behavior is as expected for functionals of this type. The hybrid functional B3LYP slightly overestimates the activation barrier when the D3 correction is used and highly overestimates the barrier (by about 3 kcal mol^{-1}) without the D3 correction. The plain PW6B95 functional without the dispersion correction still overestimates the barrier by 0.7 kcal mol^{-1}. However, the use of PW6B95-D3 provided an energy of activation that differs from the experimental value by only 0.5 kcal mol^{-1}. This deviation (about 5%) is within the typical error limits of DFT-D3 and the experimental methods. In passing it is noted that the D3-dispersion correction to the barrier even for this relatively small molecule is substantial (decrease by 0.7 kcal mol^{-1} for PW6B95 and 2.4 kcal mol^{-1} for B3LYP, respectively) and quantitative agreement between theory and experiment cannot be obtained with uncorrected standard density functionals. The encouraging observation that two different hybrid density functionals yield the same barrier to within 0.3 kcal mol^{-1} is mainly an effect of the D3-correction (plain PW6B95 and B3LYP differ by 2 kcal mol^{-1}). Although the stabilizing influence of intramolecular London dispersion on the transition state due to its 'closer' (more dense) structure is partially quenched by solvation, we think that reliable predictions ('the right answer for the right reason') can only be achieved when both effects are accounted for by, e.g., the D3 and COSMO-RS models.

Extrapolated CCSD(T)/CBS via MP2/CBS calculations and estimating the basis set limit by explicitly correlated CCSD-F12(T)/cc-pVDZ-F12 yield an almost identical energy of activation of 12.93 and 13.02 kcal mol^{-1}, respectively, which is very encouraging. Presently the origin of the difference to the experimental barrier of 2.4 kcal mol^{-1} is not clear to us. We noted some spin contamination of the Hartee–Fock reference wave function for the transition state structure ($S^2 \approx 1$) but it seems unlikely that this influences the highly accurate CCSD(T) calculations so significantly.

We also investigated the influence of the choice of the geometries and vibrations on the energy of activation and optimized the 5-hexenyl radical as well as the transition state also on the B3LYP-D3/def2-TZVP level. The obtained thermal correction to the free energy of activation is 2.44 kcal mol^{-1} compared to the value based on TPSS geometries of 2.84 kcal mol^{-1}. Single-point calculations on the PW6B95/def2-QZVP level for the electronic barrier show that this change by 0.4 kcal mol^{-1} is compensated by a higher ΔE of 7.58 kcal mol^{-1} compared to 7.16 kcal mol^{-1} for the TPSS geometries. With an almost identical solvation free enthalpy for the activation process (0.62 and 0.64 kcal mol^{-1}) the free energy of activation is practically the same for the TPSS structures (10.63 kcal mol^{-1}) and the B3LYP geometries (10.67 kcal mol^{-1}). The total influence of the geometries and vibrations on $\Delta G^{\ddagger}$ is therefore small (0.1–0.2 kcal mol^{-1} at most) and this technical detail cannot explain the discrepancy of the CCSD(T) barrier and the experimental value.

The 5-*exo* cyclisation of 5-hexenyl has been studied before using the G3-(MP2)-RAD protocol and a value of 7.6×10^4 s^{-1} was reported for the rate constant at 21 °C [57]. This high-level composite method was designed to yield accurate gas-phase thermochemical data for free radicals [58]. Nevertheless this protocol does not include solvation effects, which might be an explanation for the better agreement of the rate constant presented in this work compared to the experimental value [53]. In order to increase the validity of the benchmarking, the rate constants k were calculated for a number of temperatures and compared to the values obtained from the Arrhenius equation reported as most reliable (Table 2).

Table 2: Rate constants of the 5-*exo* cyclization of the hexenyl radical in benzene at different temperatures calculated at the PW6B95-D3/QZVP//TPSS-D3/def2-TZVP level of theory.

T [°C]	$k_{exp.}$ [s^{-1}]	$k_{calc.}$ [s^{-1}]
25	2.20×10^5	1.02×10^5
40	3.83×10^5	1.99×10^5
60	7.43×10^5	4.36×10^5
80	1.34×10^6	8.76×10^5
100	2.26×10^6	1.62×10^6

The results demonstrate that the agreement between calculated and experimental values is becoming even better with increasing temperature. This suggests that the (small) error in the calculated values is due to a slight overestimation of the enthalpy of activation. When employing the COSMO-RS model to simulate different media (THF and benzene) we found that the rate constant at 40 °C for the two solvents is almost identical (2.02×10^5 s^{-1} and 1.99×10^5 s^{-1}). This is in agreement with experimental results indicating the insensitivity of k to solvent effects. On an absolute scale, however, inclusion of these effects is important as the free energy barrier computed for the gas phase is increased by about 0.6 kcal mol^{-1} in THF or benzene. This improves the agreement between theory and experiment. As documented in the Supporting Information, even the sign of solvent correction varies for different systems

and differences on the order of 1 kcal mol^{-1} are found and it hence can be concluded that they should be included by default in accurate computational work.

Finally, the literature transition state geometry and our geometry are very similar. The length of the forming bond is 2.30 Å and the angle of attack to the double bond is 108.2° in our treatment. These values are slightly different than the values used in the modeling based calculations of radical cyclization (2.34 Å and 105.8°) that were derived from values of the attack of alkyl radicals on ethane and propene, however [54,55].

In summary, it can be concluded that the calculations employing the PW6B95-D3/QZVP//TPSS-D3/TZVP method on the 5-*exo* cyclization of the hexenyl radical are in excellent agreement with the experimental and previous computational results. Therefore, this approach was employed in the investigations of the following intramolecular radical additions to arenes.

Investigation of the radical addition to substituted anilines

In our preparative work, we have been mostly concerned with the catalytic synthesis of indolines via addition reactions of epoxide derived radicals [59,60] and thus, radical additions to substituted anilines are investigated in this study.

Substitution at nitrogen

Radicals **1**–**3** (Scheme 3) are simple models for the addition steps of these sequences and were therefore studied first (Table 3).

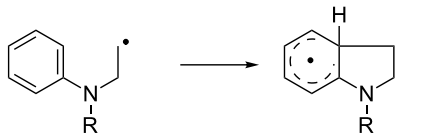

R = Ph: **1**
R = CO_2Me: **2**
R = Me: **3**

R = Ph: **4**
R = CO_2Me: **5**
R = Me: **6**

Scheme 3: Intramolecular radical additions of simple aniline derivatives.

Table 3: Calculated kinetic and thermodynamic data (on the PW6B95-D3/QZVP//TPSS-D3/def2-TZVP level) and HOMO-SOMO gap $\Delta E_{H\text{-}S}$ (on the TPSS-D3/TZVP level) of the reactions of **1**–**3** in benzene at 40 °C.

Subst.	k [s^{-1}]	$\Delta G^{‡}$ [kcal mol^{-1}]	ΔG_R [kcal mol^{-1}]	$\Delta E_{H\text{-}S}$ [eV]
1	3.56×10^3	13.3	−10.3	−0.77
2	5.62×10^3	13.0	−9.9	−1.40
3	3.88×10^2	14.7	−10.2	−1.14

Somewhat surprisingly for us, all addition reactions are considerably exergonic and all ΔG_R values are fairly similar. Thus, radical stabilization in **4**–**6** provides a substantial thermodynamic driving force for the addition. Despite the similarity of the ΔG_R values the rate constants of the addition differ significantly. For **1** and **3** the difference in k can be ascribed to the lower HOMO–SOMO gap and hence more favorable polar effects for **1**. For **2** having the highest rate constant this is not the case. We suggest that the electron withdrawing substituent on N reduces the aromaticity of the aniline and hence facilitates radical attack.

For **1** and **2** the addition is about as fast as the 6-*endo* cyclization of the hexenyl radical. Such reactions and other even slower cyclizations are well documented in titanocene mediated and catalyzed radical processes [61-69]. Therefore, the relatively high computational rate constant for the addition of **1** readily explains the excellent synthetic results with epoxides derived from aryl substituted anilines in the radical arylation of epoxides. The reaction of **3** is too slow to be useful in typical radical chain reactions. However, reactions under our catalytic reaction conditions [6] with radicals similar to **3** were successful, too (see Scheme 4). Nevertheless, the transformations are, in agreement with the calculations, clearly more demanding than those with radicals similar to **1** and thus, more elaborate catalysts and the use of additives to enhance catalyst stability is essential.

In accordance with intuition, all transition states are ‘later’ than that of the 5-*exo* cyclization as indicated by the shorter distances between the radical center and the C-atom attacked for

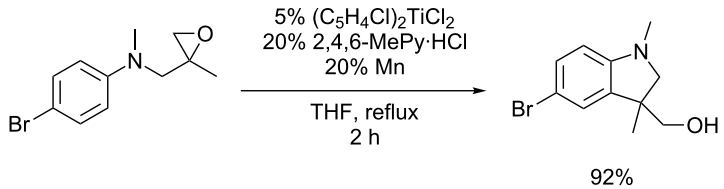

92%

Scheme 4: Successful catalytic radical addition to an *N*-methyl substituted aniline.

1–3 (2.15–2.17 Å vs 2.30 in the 5-*exo* cyclization). Moreover, the trajectory of attack on the arene is very similar for **1–3** (121–123°). This angle is substantially larger than for the 5-*exo* cyclization (108.2°). This is shown for the addition of **1** in Figure 1.

Substitution at the radical center

We investigated the influence of radical substitution on the rate and the free energy of the addition reaction next. In order to ensure comparability the examples were chosen with phenyl substitution at N. They are shown in Scheme 5 and the results are summarized in Table 4.

The notion that the radical acts as an electrophile and the arene as nucleophile is further corroborated by the highest rate constant for the addition reaction of **9** that has the most electrophilic radical center due to ester substitution. The more nucleophilic radicals **8** and **10** react slower than **1**. The –OMe group in **10** is a better electron donor than the –Me group in **8**, which should make it more nucleophilic and lead to a slower radical addition. The calculated rate constant for **10** still is higher than for **8**, which leads to the conclusion that the electron withdrawing inductive effect of the –OMe group overcomes its +M-effect. However, the difference in $\Delta G^{\ddagger}$ is below 0.5 kcal mol^{-1} and thus within the error margin of the theoretical method. The addition of the stabilized benzyl radical is slowest and also endergonic. As above, no correlation between k and ΔG_R is obvious. The polarity of the radical [70-72] and the arene is reversed in comparison with the Minisci reaction [11]. With alkyl substitution at N (as in **3**) similar trends are observed. This indicates that for compounds derived from **3** the SOMO–HOMO interaction is decisive, too. Finally, care has to be taken in transferring effects from one series of substrates to another. As shown in Scheme 6, radical **15** adds to the arene to give **16** substantially slower than **9**. Thus, the combination of an electron deficient radical with an electron withdrawing substitution on N leads to a mismatching of polar effects with respect to k.

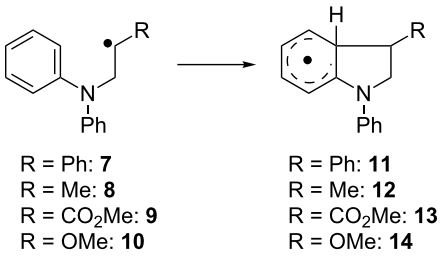

R = Ph: **7**
R = Me: **8**
R = CO_2Me: **9**
R = OMe: **10**

R = Ph: **11**
R = Me: **12**
R = CO_2Me: **13**
R = OMe: **14**

Scheme 5: Intramolecular radical additions of simple aniline derivatives.

Table 4: Calculated kinetic and thermodynamic data (on the PW6B95-D3/QZVP//TPSS-D3/def2-TZVP level) and HOMO–SOMO gap $\Delta E_{H\text{-}S}$ (on the TPSS-D3/TZVP level) of the reactions of **7–10** in benzene at 40 °C.

Subst.	k [s^{-1}]	$\Delta G^{\ddagger}$ [kcal mol^{-1}]	ΔG_R [kcal mol^{-1}]	$\Delta E_{H\text{-}S}$ [eV]
7	7	17.2	+2.7	−1.07
8	8.94×10^2	14.2	−6.7	−0.90
9	2.17×10^4	12.2	−3.3	−0.83
10	1.70×10^3	13.8	−3.9	−1.14

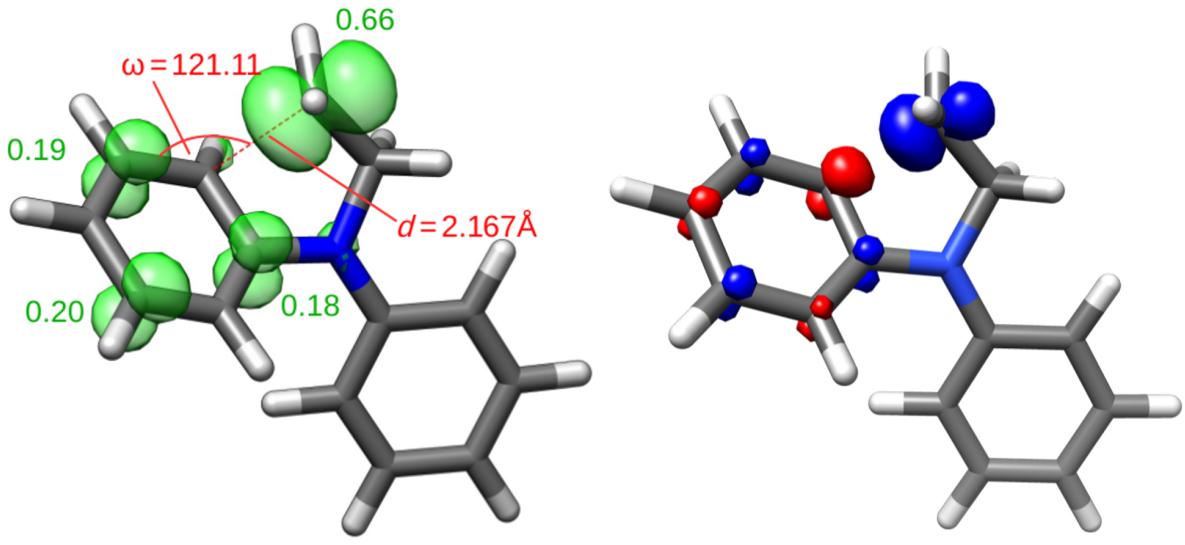

Figure 1: Optimized structure of the transition state of the radical addition of **1** (left: spin density plot and atomic spin-density populations; right: SOMO).

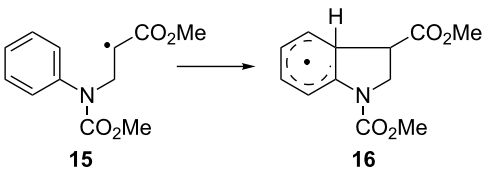

15 **16**

k_{25} = 5259 s^{-1}; $\Delta G^{‡}$ = 13.0 kcal mol^{-1}
ΔG_r = –2.7 kcal mol^{-1}

Scheme 6: Mismatching of polar effects.

Effect of arene substitution

The results obtained so far strongly suggest that a matching of the nucleophilicity of the arene and the electrophilicity of the radical center are decisive for the magnitude of *k*. We investigated this issue by the introduction of substituents either in the *p*-position or both *m*-positions of the anilines.

Effect of *p*-substitution

The examples of *p*-substitution investigated are summarized in Scheme 7 and Table 5.

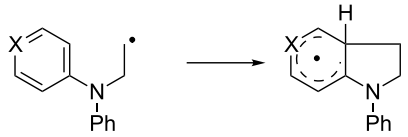

X = C–CH_3: **17**
X = C–OCH_3: **18**
X = C–F: **19**
X = C–$COCH_3$: **20**
X = NH^+: **21**

X = C–CH_3: **22**
X = C–OCH_3: **23**
X = C–F: **24**
X = C–$COCH_3$: **25**
X = NH^+: **26**

Scheme 7: Examples of *p*-substituted anilines investigated.

Table 5: Calculated kinetic and thermodynamic data (on the PW6B95-D3/QZVP//TPSS-D3/def2-TZVP level) and HOMO–SOMO gap $\Delta E_{H\text{-}S}$ (on the TPSS-D3/TZVP level) of the reactions of **17**–**21** in benzene at 40 °C.

Subst.	*k* [s^{-1}]	$\Delta G^{‡}$ [kcal mol^{-1}]	ΔG_R [kcal mol^{-1}]	$\Delta E_{H\text{-}S}$ [eV]
17	2.52 × 10^4	12.1	−11.2	−0.77
18	7.25 × 10^3	12.8	−9.4	−0.74
19	5.54 × 10^3	13.0	−11.4	−0.70
20	9.04 × 10^2	14.1	−8.7	−0.89
21	5.44 × 10^2	14.5	−8.9	−0.98

Methyl substitution in **17** leads by far to the highest value of *k*. For **18** and **19** higher values than for **1** were obtained. However, the effect of –OCH_3 and –F substitution is surprisingly small and within the error margin of the computational method. Electron withdrawing substituents (**20** and **21**) strongly retard the addition. In these cases larger SOMO–HOMO gaps are involved. The radicals act as electrophiles in all cases. Thus, compared to the Minisci reaction our addition has a reversed polar effect.

Changing the substituent at N from Ph to CH_3 leads to similar trends with lower absolute values of *k* as expected. These results are summarized in Supporting Information File 1.

Effect of *m*,*m*'-disubstitution

The second substitution pattern investigated is the *m*,*m*'-disubstitution. By adding both substituents, the problem of the regioselectivity of addition to the arene is circumvented. The examples and results are summarized in Scheme 8 and Table 6.

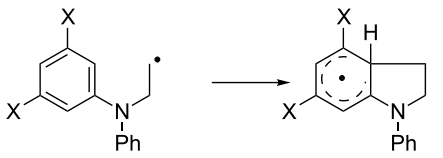

X = CH_3: **27**
X = OCH_3: **28**
X = F: **29**

X = CH_3: **30**
X = OCH_3: **31**
X = F: **32**

Scheme 8: Examples of *m*,*m*'-disubstituted anilines investigated.

Table 6: Calculated kinetic and thermodynamic data (on the PW6B95-D3/QZVP//TPSS-D3/def2-TZVP level) and HOMO–SOMO gap $\Delta E_{H\text{-}S}$ (on the TPSS-D3/TZVP level) of the reactions of **27**–**29** in benzene at 40 °C.

Subst.	*k* [s^{-1}]	$\Delta G^{‡}$ [kcal mol^{-1}]	ΔG_R [kcal mol^{-1}]	$\Delta E_{H\text{-}S}$ [eV]
27	1.01 × 10^4	12.6	−10.2	−0.80
28	5.46 × 10^2	14.5	−9.8	−1.46
29	1.62 × 10^2	15.2	−8.7	−1.30

As above, methyl substitution (in **27**) leads to a higher value for *k*. The introduction of two –OCH_3 (in **28**) or two –F substituents (in **29**) results in a reduction of the value of *k* compared to **1**. While this could be indicative of a weak negative inductive effect, the differences in $\Delta G^{‡}$ are low and within the errors of the computational method.

Radical additions leading to dihydrobenzofurans and indanes

So far, all radicals investigated contained a substituted aniline and the importance of the nucleophilicity of the arene has become obvious for a number of examples. To conclude our

study we therefore investigated an O atom and a CH_2 group in the chain linking the radical center and the arene as shown in Scheme 9. The results are summarized in Table 7.

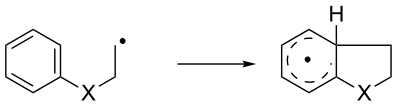

X = O: **33**
X = CH_2: **34**

X = O: **35**
X = CH_2: **36**

Scheme 9: Addition reactions leading to dihydrobenzofuran and an indane.

Table 7: Calculated kinetic and thermodynamic data (on the PW6B95-D3/QZVP//TPSS-D3/def2-TZVP level) and HOMO–SOMO gap $\Delta E_{H\text{-}S}$ (on the TPSS-D3/TZVP level) of the reactions of **33** and **34** in benzene at 40 °C.

Subst.	k [s^{-1}]	$\Delta G^{‡}$ [kcal mol^{-1}]	ΔG_R [kcal mol^{-1}]	$\Delta E_{H\text{-}S}$ [eV]
33	51	15.9	−6.0	−1.61
34	2	17.9	−1.8	−2.22

For both **33** and **34** the calculated rate constants are substantially lower than for **1** and **3**. This can be attributed to the much higher SOMO–HOMO gap that indicates much weaker polar effects for the reactions of **33** and **34**. Thermodynamically, both addition reactions are favorable and once again, no correlation between ΔG_r and k is obvious. Thus, for our simple model systems the combination of only weakly nucleophilic arenes and an electrophilic radical center is disadvantageous. This is in agreement with preliminary synthetic results that suggest that dihydrobenzofurans and indanes are not accessible via the titanocene catalyzed radical arylation.

Conclusion

The intramolecular radical addition to substituted anilines was studied computationally with the aid of the PW6B95-D3 functional in combination with the large quadruple-zeta basis set def2-QZVP. This method was chosen after benchmarking on the 5-*exo* cyclization of the hexenyl radical. It provides sufficiently accurate values for the rate constant of the cyclization over a wide range of temperatures.

For the radical addition to anilines it was found that polar effects are highly important and a combination of electrophilic radicals with preferably nucleophilic arenes results in the highest rate constants. In general, the relative rates correlate with a low SOMO–HOMO gap. Thus, the polarity of the radical and the arene is reversed in comparison with the related Minisci reaction. The substitution at the N-atom of the aniline is crucial. Methyl substitution leads to slower addition than phenyl substitution. Carbamates as substituents are suitable only when the radical center is not too electrophilic. Concerning the substitution pattern of the arene it was found that electron releasing substituents accelerate the addition whereas strongly electron withdrawing substituents like acyl groups retard the addition. Para-substitution has a stronger influence than meta-substitution. Addition reactions leading to indanes or dihydrobenzofurans are too slow to be useful.

Supporting Information

Supporting Information File 1

Energies and coordinates of all radicals and transition states, tables with data on radicals with Me-substitution on N analogous to Tables 4, 5, and 6.
[http://www.beilstein-journals.org/bjoc/content/supplementary/1860-5397-9-185-S1.pdf]

Acknowledgements

We thank the DFG (SFB 813, ‘Chemistry at Spin Centers’) and the Jürgen Manchot Stiftung (Fellowship to T. D.) for support.

References

1. Trost, B. M. *Science* **1991,** *254,* 1471–1477. doi:10.1126/science.1962206
2. Trost, B. M. *Angew. Chem., Int. Ed. Engl.* **1995,** *34,* 259–281. doi:10.1002/anie.199502591
3. Curran, D. P.; Porter, N. A.; Giese, B. *Stereochemistry of Radical Reactions;* VCH: Weinheim, 1996.
4. Renaud, P.; Sibi, M. P., Eds. *Radicals in Organic Synthesis;* Wiley-VCH: Weinheim, 2001.
5. Zard, S. Z. *Radical Reactions in Organic Synthesis;* Oxford University: Oxford, 2003.
6. Gansäuer, A.; Behlendorf, M.; von Laufenberg, D.; Fleckhaus, A.; Kube, C.; Sadasivam, D. V.; Flowers, R. A., II. *Angew. Chem., Int. Ed.* **2012,** *51,* 4739–4742. doi:10.1002/anie.201200431
7. Wipf, P.; Maciejewski, J. P. *Org. Lett.* **2008,** *10,* 4383–4386. doi:10.1021/ol801860s
8. Maciejewski, J. P.; Wipf, P. *ARKIVOC* **2011,** No. (vi), 92–119.
9. Gansäuer, A.; Rinker, B.; Ndene-Schiffer, N.; Pierobon, M.; Grimme, S.; Gerenkamp, M.; Mück-Lichtenfeld, C. *Eur. J. Org. Chem.* **2004,** 2337–2351. doi:10.1002/ejoc.200400001
10. Gansäuer, A.; Fleckhaus, A.; Alejandre Lafont, M.; Okkel, A.; Kotsis, K.; Anoop, A.; Neese, F. *J. Am. Chem. Soc.* **2009,** *131,* 16989–16999. doi:10.1021/ja907817y
11. Duncton, M. A. J. *MedChemComm* **2011,** *2,* 1135–1161. doi:10.1039/c1md00134e
12. Lynch, B. M.; Chang, H. S. *Tetrahedron Lett.* **1964,** *5,* 617–620. doi:10.1016/0040-4039(64)83015-X
13. Minisci, F.; Galli, R.; Cecere, M.; Malatesta, V.; Caronna, T. *Tetrahedron Lett.* **1968,** *9,* 5609–5612. doi:10.1016/S0040-4039(00)70732-5

14. Gagosz, F.; Zard, S. Z. *Org. Lett.* **2002,** *4,* 4345–4348. doi:10.1021/ol0270024
15. Du, W.; Kaskar, B.; Blumbergs, P.; Subramanian, P. K.; Curran, D. P. *Bioorg. Med. Chem.* **2003,** *11,* 451–458. doi:10.1016/S0968-0896(02)00437-6
16. El Qacemi, M.; Petit, L.; Quiclet-Sire, B.; Zard, S. Z. *Org. Biomol. Chem.* **2012,** *10,* 5707–5719. doi:10.1039/c2ob25169h
17. Biechy, A.; Hachisu, S.; Quiclet-Sire, B.; Richard, L.; Zard, S. Z. *Angew. Chem., Int. Ed.* **2008,** *47,* 1436–1438. doi:10.1002/anie.200704996
18. Biechy, A.; Zard, S. Z. *Org. Lett.* **2009,** *11,* 2800–2803. doi:10.1021/ol900996k
19. Petit, L.; Botez, I.; Tizot, A.; Zard, S. Z. *Tetrahedron Lett.* **2012,** *53,* 3220–3224. doi:10.1016/j.tetlet.2012.04.020
20. Petit, L.; Zard, S. Z. *Chem. Commun.* **2010,** *46,* 5148–5150. doi:10.1039/c0cc00680g
21. Citterio, A.; Minisci, F.; Porta, O.; Sesana, G. *J. Am. Chem. Soc.* **1977,** *99,* 7960–7968. doi:10.1021/ja00466a031
22. Citterio, A.; Arnoldi, A.; Minisci, F. *J. Org. Chem.* **1979,** *44,* 2674–2682. doi:10.1021/jo01329a017
23. Koch, W.; Holthausen, M. C. *A Chemist's Guide to Density Functional Theory;* Wiley-VCH: New York, 2001.
24. Schwabe, T.; Grimme, S. *Acc. Chem. Res.* **2008,** *4,* 569–579. doi:10.1021/ar700208h
25. Zhao, Y.; Truhlar, D. G. *Acc. Chem. Res.* **2008,** *41,* 157–167. doi:10.1021/ar700111a
26. Grimme, S.; Antony, J.; Ehrlich, S.; Krieg, H. *J. Chem. Phys.* **2010,** *132,* 154104. doi:10.1063/1.3382344
27. Goerigk, L.; Grimme, S. *Phys. Chem. Chem. Phys.* **2011,** *13,* 6670–6688. doi:10.1039/c0cp02984j
28. Zhao, Y.; Truhlar, D. G. *J. Phys. Chem. A* **2005,** *109,* 5656–5667. doi:10.1021/jp050536c
29. Klamt, A. *J. Chem. Phys.* **1995,** *99,* 2224–2235. doi:10.1021/j100007a062
30. Eckert, F.; Klamt, A. *AIChE J.* **2002,** *48,* 369–385. doi:10.1002/aic.690480220
31. Grimme, S. *Chem.–Eur. J.* **2012,** *18,* 9955–9964. doi:10.1002/chem.201200497
32. Greb, L.; Oña-Burgos, P.; Schirmer, B.; Grimme, S.; Stephan, D. W.; Paradies, J. *Angew. Chem., Int. Ed.* **2012,** *51,* 10164–10168. doi:10.1002/anie.201204007
33. Sajid, M.; Klose, A.; Birkmann, B.; Liang, L.; Schirmer, B.; Wiegand, T.; Eckert, H.; Lough, A. J.; Frohlich, R.; Daniliuc, C. G.; Grimme, S.; Stephan, D. W.; Kehra, G.; Erker, G. *Chem. Sci.* **2013,** *4,* 213–219. doi:10.1039/c2sc21161k
34. *TURBOMOLE 6.4;* Universität Karlsruhe, 2012, http://www.turbomole.com.
35. Tao, J.; Perdew, J.; Staroverov, V.; Scuseria, G. *Phys. Rev. Lett.* **2003,** *91,* 146401. doi:10.1103/PhysRevLett.91.146401
36. Weigend, F.; Ahlrichs, R. *Phys. Chem. Chem. Phys.* **2005,** *7,* 3297–3305. doi:10.1039/b508541a
37. Becke, A. D. *Phys. Rev. A* **1988,** *38,* 3098–3100. doi:10.1103/PhysRevA.38.3098
38. Perdew, J. P. *Phys. Rev. B* **1986,** *33,* 8822–8824. doi:10.1103/PhysRevB.33.8822
39. Becke, A. D. *J. Chem. Phys.* **1993,** *98,* 5648–5652. doi:10.1063/1.464913
40. Lee, C.; Yang, W.; Parr, R. G. *Phys. Rev. B* **1988,** *37,* 785–789. doi:10.1103/PhysRevB.37.785
41. Stephens, P. J.; Devlin, F. J.; Chabalowski, C. F.; Frisch, M. J. *J. Phys. Chem.* **1994,** *98,* 11623–11627. doi:10.1021/j100096a001
42. Halkier, A.; Helgaker, T.; Jørgensen, P.; Klopper, W.; Koch, H.; Olsen, J.; Wilson, A. K. J. *Chem. Phys. Lett.* **1998,** *286,* 243–252. doi:10.1016/S0009-2614(98)00111-0
43. Hättig, C.; Tew, D. P.; Köhn, A. *J. Chem. Phys.* **2010,** *132,* 231102. doi:10.1063/1.3442368
44. Peterson, K. A.; Adler, T. B.; Werner, H.-J. *J. Chem. Phys.* **2008,** *128,* 084102. doi:10.1063/1.2831537
45. TURBOMOLE V6.5 2013, a development of University of Karlsruhe and Forschungszentrum Karlsruhe GmbH, 1989-2007, TURBOMOLE GmbH, since 2007; available from http://www.turbomole.com.
46. Eichkorn, K.; Treutler, O.; Öhm, H.; Häser, M.; Ahlrichs, R. *Chem. Phys. Lett.* **1995,** *242,* 652–660. doi:10.1016/0009-2614(95)00838-U
47. Weigend, F. *Phys. Chem. Chem. Phys.* **2006,** *8,* 1057–1065. doi:10.1039/b515623h
48. Grimme, S.; Ehrlich, S.; Goerigk, L. *J. Comput. Chem.* **2011,** *32,* 1456–1465. doi:10.1002/jcc.21759
49. Becke, A. D.; Johnson, E. R. *J. Chem. Phys.* **2005,** *123,* 154101. doi:10.1063/1.2065267
50. Johnson, E. R.; Becke, A. D. *J. Chem. Phys.* **2005,** *123,* 24101. doi:10.1063/1.1949201
51. *COSMOtherm,* Version C3.0, Release 12.01; COSMOlogic GmbH & Co. KG: Leverkusen, Germany, 2010.
52. Schäfer, A.; Huber, C.; Ahlrichs, R. *J. Chem. Phys.* **1994,** *100,* 5829–5835. doi:10.1063/1.467146
53. Chatgilialoglu, C.; Ingold, K. U.; Scaiano, J. C. *J. Am. Chem. Soc.* **1981,** *103,* 7739–7742. doi:10.1021/ja00416a008
54. Beckwith, A. L. J.; Schiesser, C. H. *Tetrahedron* **1985,** *41,* 3925–3941. doi:10.1016/S0040-4020(01)97174-1
55. Spellmeyer, D. C.; Houk, K. N. *J. Org. Chem.* **1987,** *52,* 959–974. doi:10.1021/jo00382a001
56. Bürgi, H. B.; Dunitz, J. D.; Lehn, J. M.; Wipff, G. *Tetrahedron* **1974,** *30,* 1563–1572. doi:10.1016/S0040-4020(01)90678-7
57. Lobachevsky, S.; Schiesser, C. H.; Lin, C. Y.; Coote, M. L. *J. Phys. Chem. A* **2008,** *112,* 13622–13627. doi:10.1021/jp806535z
58. Henry, D. J.; Sullivan, M. B.; Radom, L. *J. Chem. Phys.* **2003,** *118,* 4849–4860. doi:10.1063/1.1544731
59. RajanBabu, T. V.; Nugent, W. A. *J. Am. Chem. Soc.* **1994,** *116,* 986–997. doi:10.1021/ja00082a021
60. Gansäuer, A.; Bluhm, H.; Pierobon, M. *J. Am. Chem. Soc.* **1998,** *120,* 12849–12859. doi:10.1021/ja981635p
61. Gansäuer, A.; Pierobon, M. *Synlett* **2000,** 1357–1359. doi:10.1055/s-2000-7133
62. Barrero, A. F.; Rosales, A.; Cuerva, J. M.; Oltra, J. E. *Org. Lett.* **2003,** *5,* 1935–1938. doi:10.1021/ol034510k
63. Gansäuer, A.; Lauterbach, T.; Geich-Gimbel, D. *Chem.–Eur. J.* **2004,** *10,* 4983–4990. doi:10.1002/chem.200400685
64. Friedrich, J.; Dolg, M.; Gansäuer, A.; Geich-Gimbel, D.; Lauterbach, T. *J. Am. Chem. Soc.* **2005,** *127,* 7071–7077. doi:10.1021/ja050268w
65. Justicia, J.; Oller-Lopez, J. L.; Campaña, A. G.; Oltra, J. E.; Cuerva, J. M.; Buñuel, E.; Cárdenas, D. J. *J. Am. Chem. Soc.* **2005,** *127,* 14911–14921. doi:10.1021/ja054316o
66. Barrero, A. F.; del Moral, J. F. Q.; Sanchez, E. M.; Arteaga, J. F. *Eur. J. Org. Chem.* **2006,** 1627–1641. doi:10.1002/ejoc.200500849
67. Friedrich, J.; Walczak, K.; Dolg, M.; Piestert, F.; Lauterbach, T.; Worgull, D.; Gansäuer, A. *J. Am. Chem. Soc.* **2008,** *130,* 1788–1796. doi:10.1021/ja077596b

68. Gansäuer, A.; Worgull, D.; Knebel, K.; Huth, I.; Schnakenburg, G. *Angew. Chem., Int. Ed.* **2009,** *48,* 8882–8885. doi:10.1002/anie.200904428
69. Gansäuer, A.; Knebel, K.; Kube, C.; van Gastel, M.; Cangönül, A.; Daasbjerg, K.; Hangele, T.; Hülsen, M.; Dolg, M.; Friedrich, J. *Chem.–Eur. J.* **2012,** *18,* 2591–2599. doi:10.1002/chem.201102959
70. Giese, B. *Angew. Chem., Int. Ed. Engl.* **1983,** *22,* 753–764. doi:10.1002/anie.198307531
71. Giese, B.; Lachhein, S. *Angew. Chem., Int. Ed. Engl.* **1982,** *21,* 768–769. doi:10.1002/anie.198207681
72. Aitken, H. M.; Hancock, A. N.; Schiesser, C. H. *Chem. Commun.* **2012,** *48,* 8326–8328. doi:10.1039/c2cc33856d

License and Terms

Beilstein Journal of Organic Chemistry

Anodic coupling of carboxylic acids to electron-rich double bonds: A surprising non-Kolbe pathway to lactones

Robert J. Perkins, Hai-Chao Xu, John M. Campbell and Kevin D. Moeller*

Full Research Paper

Open Access

Address:
Washington University in Saint Louis, Saint Louis, Missouri 63130, United States

Email:
Kevin D. Moeller* - moeller@wustl.edu

* Corresponding author

Keywords:
carboxylic acid; cyclization; electrolysis; free radical; kolbe; radical cation

Beilstein J. Org. Chem. **2013,** *9,* 1630–1636.
doi:10.3762/bjoc.9.186

Received: 12 June 2013
Accepted: 18 July 2013
Published: 09 August 2013

This article is part of the Thematic Series "Organic free radical chemistry".

Guest Editor: C. Stephenson

Abstract

Carboxylic acids have been electro-oxidatively coupled to electron-rich olefins to form lactones. Kolbe decarboxylation does not appear to be a significant competing pathway. Experimental results indicate that oxidation occurs at the olefin and that the reaction proceeds through a radical cation intermediate.

Introduction

Anodic cyclization reactions of the general type shown in Scheme 1 can provide a powerful method for the synthesis of a variety of ring systems [1,2]. The reactions effectively reverse the polarity of an electron-rich functional group and in so doing open up entirely new opportunities for bond formation. In addition, the oxidative reactions lead to products that either preserve or increase the level of functionality found in the initial substrate. This provides synthetic handles for further development of the cyclic products generated.

Such reactions can be used to build a variety of fused, bridged, and spirocyclic carbocyclic systems [3], cyclic amino acid derivatives [4], cyclic ethers [5,6], and lactones [7,8]. In most of these examples, the reactions can be viewed as arising from an oxidation that forms an olefinic radical cation that is then rapidly trapped by a nucleophile. This triggers a cascade of reactions that typically involve the loss of two protons (or a silyl group), a second oxidation of a radical intermediate, and solvent trapping. This reaction cascade leads to formation of the final product.

A combination of computational studies and competition experiments has begun to identify both cyclization reactions that proceed through different mechanistic pathways and cyclization reactions where the cascade of reactions downstream from the cyclization plays an important role in product formation [9].

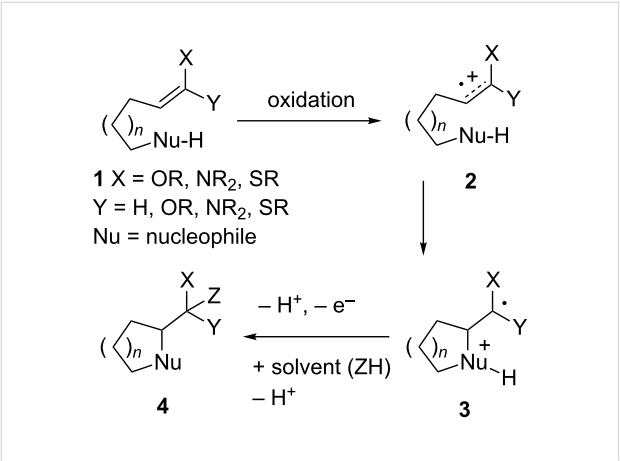

Scheme 1: General scheme for anodic cyclization reactions.

For example, consider the competition experiment highlighted in Scheme 2. In this experiment, an electron-rich olefin was coupled to one of two competing nucleophiles, a sulfonamide and an alcohol (**5**). When the oxidation was run with 2,6-lutidine as a base (not shown), the reaction led to the formation of a radical cation from the electron-rich olefin followed by trapping by the alcohol nucleophile to form product **9**. No product from sulfonamide trapping (**8**) was observed. However, when the reaction was run under more basic conditions (0.5 equivalents of lithium methoxide) cyclic voltammetry data indicated that the oxidative cyclizations were initiated by the oxidation of sulfonamide anion. This led to initial formation of N-localized radical **6**. Depending on the reaction conditions, the experiment favoured either a sulfonamide or alcohol based cyclization. Density functional theory (DFT) calculations suggested that sulfonamide based cyclizations proceed by addition of the N-localized radical to the electron-rich double bond, a reaction that led to product **8**. In a competitive process, an intramolecular electron-transfer reaction occurred that led to formation of a radical cation from the olefin **7** and regeneration of the sulfonamide anion. Formation of a radical cation from the olefin led to the possibility of alcohol trapping and the formation of cyclic ether product **9**. Experimental data suggested that the alcohol trapping pathway provided the kinetic product but that the cyclization was reversible. The sulfonamide radical pathway afforded the thermodynamic product. In a very interesting development, we found that the reaction could be shifted toward the alcohol-trapping product by increasing the current passed through the cell. The increased current appeared to accelerate the removal of a second electron from an initial cyclic product like **3** (Scheme 1), a change that reduced the reversibility of the cyclization.

Clearly, the use of basic reaction conditions with the acidic substrate led to dramatic mechanistic changes to our early, simplified view of the reactions. It is tempting to suggest that similar situations would arise with other acidic substrates. For example, would the oxidation of a substrate having a carboxylic acid and an electron-rich olefin lead to a carboxy radical pathway or a radical cation type reaction? To date, we have been hesitant to try such an experiment, and in fact we typically avoid substrates with carboxylic acid functional groups [5]. This action was taken because of the well-known Kolbe electrolysis reaction (Scheme 3) [10,11]. In the Kolbe electrolysis (Scheme 3, reac-

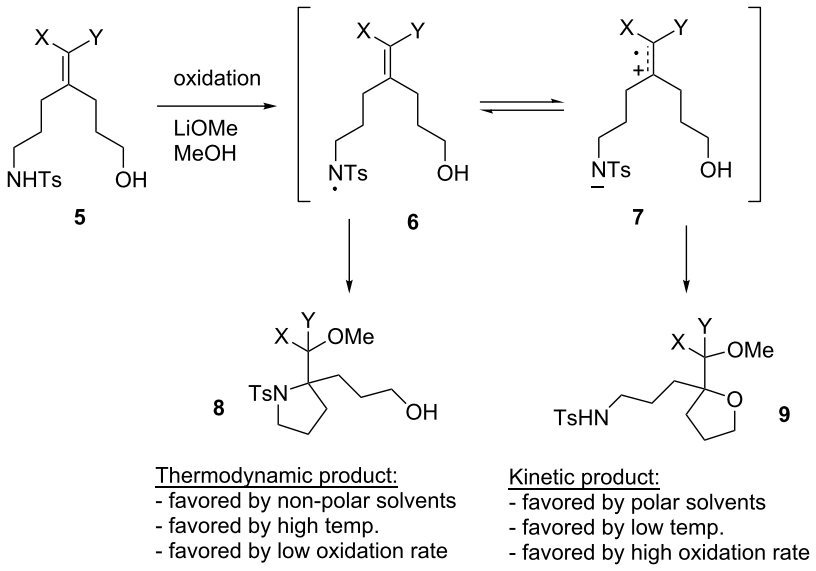

Scheme 2: Anodic cyclization competition study.

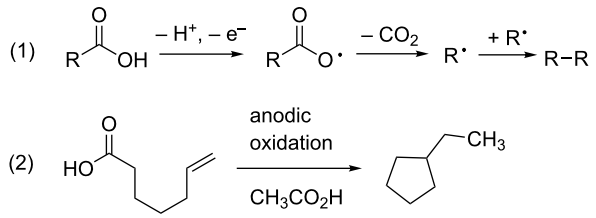

Scheme 3: Kolbe electrolysis reactions.

tion 1), a carboxylic acid is oxidized. A decarboxylation reaction then leads to the formation of a radical that is subsequently trapped by a second radical formed in solution. The reaction has been used to form dimers [12], as well as in some cases cyclic products (Scheme 3, reaction 2) [13-15].

However, the chemistry highlighted in Scheme 2 suggests that a Kolbe-type decarboxylation reaction might not interfere at all with an oxidative coupling reaction between a carboxylic acid and an electron-rich olefin. Examples in the literature of the coupling of carboxylic acids to aromatic rings, though limited in scope, were also encouraging [16-20].

There are three mechanistic possibilities which would allow for a successful reaction. First, if the carboxy radical **10** is formed, then it may simply add to the electron-rich olefin to give **12** faster than it undergoes a decarboxylation reaction (Scheme 4).

Second, it is possible for a carboxy radical like **10** to undergo an intramolecular electron-transfer reaction analogous to that observed in the case of the sulfonamide-based radical. One might suspect the electron-transfer to form radical cation **11** to be even more favorable in the present case due to the stability of the resulting carboxylate anion. The electron-transfer would minimize the risk of decarboxylation and lead to carboxylate trapping of the radical cation to again form the cyclic radical **12**.

A third mechanistic possibility is a direct oxidation of the elctron-rich olefin to form radical cation **11** followed by carboxylate trapping. All three mechanistic variations would then require a successful single-electron oxidation of **12** to ultimately lead to **13**, the product of a direct oxidative coupling between the carboxylic acid moiety and the electron-rich olefin.

We report here that this is the case and that the direct oxidative coupling of a carboxylic acid and an electron-rich olefin can be accomplished in good yield. In all cases, the reactions appear to proceed through an olefinic radical cation intermediate.

Results and Discussion

Initial cyclization studies

The compatibility of the carboxylic acid with the anodic cyclization was initially studied by examining the anodic oxidation of substrates **14a–c** (Table 1). The oxidation of **14a** nicely afforded the five-membered ring product using either lithium methoxide or 2,6-lutidine as a base. Clearly, decarboxylation of the carboxylate anion was not a problem. In fact, cyclic voltammetry data suggest that the reaction originated from an oxidation of the ketene dithioacetal. The oxidation potential ($E_{p/2}$) for **14a** was measured to be +0.68 V versus Ag/AgCl. For comparison, the oxidation potential measured for 10-undecenoic acid was +1.91 V versus Ag/AgCl in DMF solvent and +1.85 V versus Ag/AgCl in acetonitrile. When 0.5 equivalents of benzyltrimethylammonium hydroxide was added to the cyclic voltammetry solutions in order to generate the carboxylate and mimic the preparative oxidation conditions used for the reaction originating from **14a**, the oxidation potential of the 10-undecenoic acid fell to 1.36–1.40 V versus Ag/AgCl for the DMF solution and 1.38 V versus Ag/AgCl for

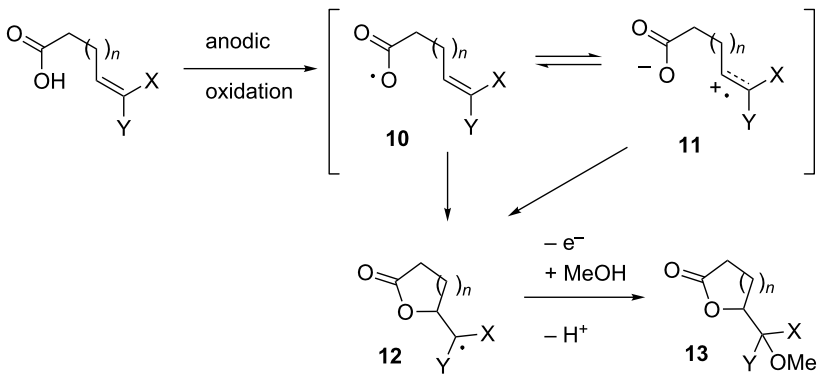

Scheme 4: Oxidative coupling between a carboxylic acid and electron-rich olefin.

Table 1: Anodic coupling of ketene dithioacetals and carboxylic acids.

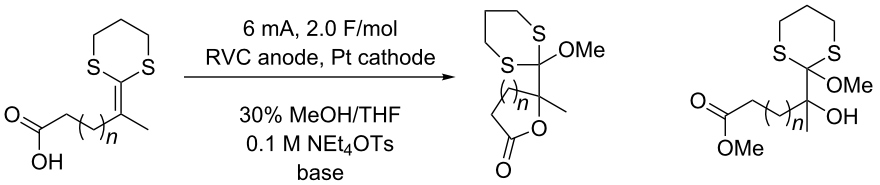

14 **15** **16**

Substrate	*n*	$E_{p/2}$[a]	Base (0.5 equiv)	Yield (**15**)
14a	1	0.68	LiOMe	87%
14a	1		2,6-lutidine	74%
14b	2	0.71	LiOMe	0%[b]
14b	2		2,6-lutidine	72%
14c	3	1.06	LiOMe	0%[c]
14c	3		2,6-lutidine	0%

[a]Cyclic voltammetry data were obtained relative to a Ag/AgCl reference electrode with a sweep rate of 50 mV/s. [b]87% of the ring opened methyl ester **16b** was obtained. [c]30% of the ring opened methyl ester **16c** was obtained.

the acetonitrile solution. The carboxylate was only partially soluble in acetonitrile. While the formation of the carboxylate significantly lowered the oxidation potential of the acid moiety, it did not lower it close to the oxidation potential measured for substrate **14a** or even the oxidation potential of a ketene dithioacetal (ca. +1.06 V versus Ag/AgCl) [21]. Hence, the oxidation potential measured for **14a** is most consistent with a fast cyclization originating from oxidation of the olefin. Fast cyclization reactions are known to significantly lower the oxidation potential of a ketene dithioacetal. For example, the trapping of a ketene dithioacetal derived radical cation by an amine was shown to lower the oxidation potential measured for the ketene dithioacetal by 460 mV [21], a value consistent with the potential measured here for **14a**.

The oxidation of **14b** to afford the six-membered ring product also proceeded well. When 2,6-lutidine was used as the base for the reaction, a 72% isolated yield of the desired product was obtained. In this case, the use of the more nucleophilic lithium methoxide as the base led to cyclization followed by opening of the lactone ring to form methyl ester product **16b**. This product did have the olefin functionalized with an alcohol and a methoxy group indicating that the initial oxidative cyclization had occurred. In this case, the slightly higher oxidation potential measured for the substrate (+0.71 V versus Ag/AgCl) is consistent with a slightly slower cyclization reaction.

Attempts to generate seven-membered ring products using the oxidative cyclization were not successful. While 30% of a methoxide opened product **16c** could be obtained with lithium methoxide as the base, no cyclic product was observed when 2,6-lutidine was employed. The reactions were quite messy and consistent with the formation of a radical cation followed by a cyclization that was too slow to compete with decomposition. The cyclic voltammetry data obtained were consistent with this observation. The +1.06 V versus Ag/AgCl oxidation potential measured for substrate **14c** was the same as that measured for the ketene dithioacetal in the absence of a trapping group [21].

The anodic coupling of a carboxylic acid group with a vinyl sulfide and an enol ether were also examined (Table 2). As with earlier alcohol and amine based cyclizations, reactions with the vinyl sulfide coupling partner proceeded much better than did their enol ether counterparts [21,22]. In the previous cases, the argument was made that less polar radical cations underwent better trapping reactions with heteroatomic nucleophiles [23], and a similar argument can be made here.

Table 2: Extension to other electron-rich olefins.

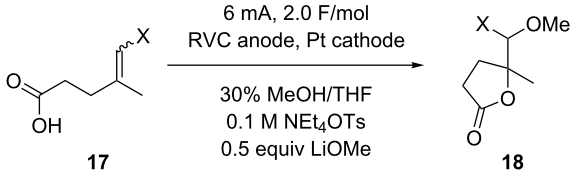

17 **18**

substrate	-X	Yield
17a	-SMe	74%
17b	-OMe	66%

The oxidation potential for the vinyl sulfide used in substrate **17a** is +1.08 V versus Ag/AgCl [9] and the oxidation potential of the enol ether in substrate **17b** is +1.18 versus Ag/AgCl [9]. Both oxidation potentials are lower than the potential measured for the carboxylate suggesting that both reactions proceed through the olefinic radical cation. While an intramolecular electron-transfer to form the carboxy radical can occur, the difference in oxidation potentials suggests that the equilibrium would lie on the side of the oxidized olefin.

Styrene substrates and additional insights

With the ketene dithioacetal, vinyl sulfide, and enol ether substrates, it appeared clear that the initial oxidation was occurring at the olefin instead of at the carboxylate. We wondered how the reaction might change if the olefin had a higher oxidation potential. With this in mind, a series of carboxylic acid substituted styrene substrates were examined (Table 3).

The first substrate studied was the simple styrene derivative **19a** (R = H). Cyclic voltammetry suggested that in the presence of base the initial oxidation should occur at the carboxylate ($E_{p/2}$ = +1.38 in acetonitrile) since the $E_{p/2}$ value measured for substrate **19a** under neutral conditions was +1.52 V versus Ag/AgCl. Several sets of conditions were attempted to achieve the cyclization. However, in no case was the yield of cyclic product obtained more than 33%. Proton NMR data taken of the crude reaction mixture showed no evidence for decarboxylation. Instead, all products appeared to arise from a styrene derived radical cation, an intermediate that might be formed by an intramolecular electron-transfer. Furthermore, the recovery of starting material after 2 F/mol of current had been passed through the reaction mixture indicated poor current efficiency. Why might an increase in the oxidation potential of the olefin hurt the reaction?

Past experience suggests that in such cases the low yield of product obtained might arise from either a slow initial cyclization or the formation of a stable cyclic radical that then struggles to undergo the second oxidation. Both pathways might lead to the formation of a polymer or decomposition, and in so doing lower the mass balance for the reaction as observed. Also, diffusion of a stable radical or radical cation to the cathode would

Table 3: Extension to styrene derivatives.

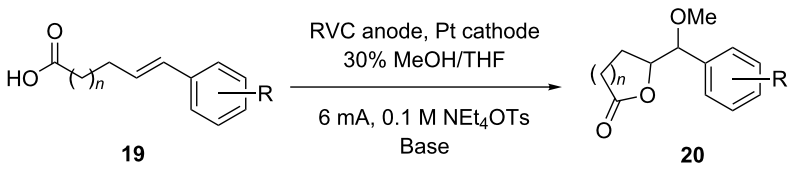

19 **20**

Substrate	R	*n*	$E_{p/2}$[a]	Base/Temperature	F/mol	Yield
19a	H	1	1.52	0.5 equiv LiOMe/rt	2	15%
19a	H	1	1.52	0.5 equiv LiOMe/rt	10	27%
19a	H	1	1.52	None/40 °C	10	33%
19b	H	3	1.73	NA[b]	NA	NA
19c	4-OMe	1	1.31	0.5 equiv LiOMe/rt	2	56%
19c	4-OMe	1	1.31	None/40 °C	2	76%
19d	4-OMe	3	1.42	NA	NA	NA
19e	2-OMe	1	1.39[c]	0.5 equiv LiOMe/rt	2	48%
19e	2-OMe	1	1.39[c]	None/40 °C	2	59%
19f	2-OMe	3	1.39[c]	NA	NA	NA
19g	3-OMe	1	1.42[c]	0.5 equiv LiOMe/rt	2	4% (NMR)
19g	3-OMe	1	1.42[c]	0.5 equiv LiOMe/rt	10	35%
19g	3-OMe	1	1.42[c]	None/40 °C	10	23%
19h	3-OMe	3	1.50	NA	NA	NA
19i	2,4-OMe	1	1.09	0.5 equiv LiOMe/rt	2	48%
19i	2,4-OMe	1	1.09	None/40 °C	2	45%
19i	2,4-OMe	1	1.09	1.0 equiv LiOMe/rt	2	74%
19j	2,4-OMe	3	1.11	NA	NA	NA

[a]Conditions: Substrates were dissolved in acetonitrile to a concentration of 0.025 M in a solution that contained 0.1 M tetraethylammonium tosylate. Cyclic voltammetry was performed at a sweep rate of 50 mV/s using a platinum anode. Half-wave oxidation potentials were measured versus a Ag/AgCl reference electrode. [b]Not applicable. [c]Lithium perchlorate was used as the electrolyte.

result in a reduction to give the starting material, a scenario that would lead to low current efficiency. Of the two mechanistic explanations for these observations, we believe that a slow second oxidation step is the problem.

The possibility of a slow cyclization was eliminated by consideration of the observed half-wave oxidation potential measured for **19a**. The oxidation potential ($E_{p/2}$) of +1.52 V for **19a** (measured under neutral conditions) was significantly lower than that measured for **19b** (+1.73 V), a similar styrene with a longer tether between the coupling partners. This observation is consistent with the oxidation of **19a** leading to a fast cyclization that rapidly removes the radical cation from the electrode surface, resulting in a lower observed oxidation potential [21]. The seven-membered ring cyclization arising from the oxidation of **19b** would be significantly slower, giving rise to a higher oxidation potential.

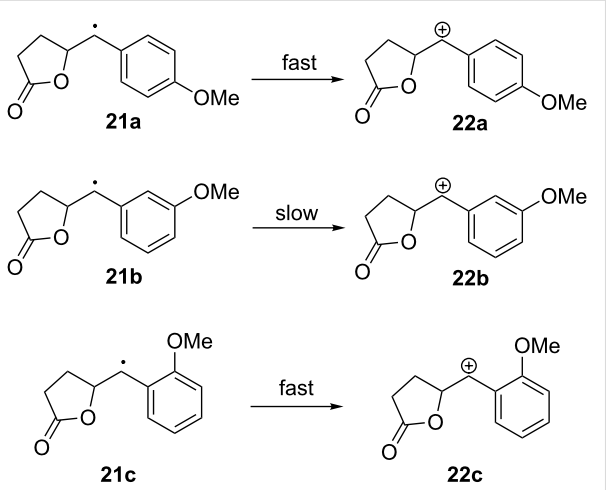

Scheme 5: Predicted relative rates of single-electron oxidation based on resonance stabilization of the resulting cation.

Given the evidence for a fast cyclization reaction, we attributed the challenges associated with the styrene cyclizations to a problem with the second single-electron oxidation. This idea was supported by our next set of experiments. Methoxy-substituted styrenes **19c** (R = 4-OMe), **19e** (R = 2-OMe), and **19g** (R = 3-OMe) were prepared. Substrate **19c** has a *p*-methoxy substituent positioned perfectly for aiding in the removal of a second electron from cyclic radical **21a** (Scheme 5). Indeed, the reactions of **19c** proceeded better than the cyclizations originating from **19a**, giving acceptable yields and complete consumption of the starting material after 2 F/mol of current had been passed. In this case, the reaction benefited strongly from using less basic reaction conditions and slightly elevated temperatures. When more basic reaction conditions were used, an overoxidized product derived from the elimination of the lactone ester to form a methoxy styrene from product **20c** was obtained. The elevated temperatures are known to assist the intramolecular cyclization. The significantly lower oxidation potential measured for **19c** relative to that measured for its seven-membered ring counterpart **19d** was again consistent with a fast initial cyclization.

We believe that the primary advantage of the methoxy group is to facilitate the second electron oxidation, rather than merely stabilizing an olefinic radical cation. To demonstrate this, the position of the methoxy group on the ring was altered systematically (see Table 3). Cyclic radical **21b**, arising from the reaction of *m*-methoxy substituted styrene **19g** (Table 3), would not be expected to oxidize as readily as radical **21a**. Indeed, the anodic oxidation of **19g** gave low yields and poor current efficiency, mirroring the results obtained from the oxidation of unsubstituted styrene **19a**. As with other substrates, the oxidation potential of **19g** was lower than that of its seven-membered ring counterpart **19h**, indicating a fast cyclization. Hence, the poor yield obtained from the oxidation of **19g** was not due to a problem with the first step.

Good yields and efficient consumption of starting material were regained upon moving the methoxy group to the *ortho* position (**19e**). Interestingly, **19e** showed no oxidation potential drop from the analogous long-chain substrate **19f**. It is tempting to assign this to a slow cyclization, but we do not believe that this is necessarily the case. The relatively low oxidation potentials for **19e** and **19f** (as well as the potentials measured for **19i** and **19j**) may be due to an interaction between the *o*-methoxy substituent and the radical cation (Figure 1). Such a stabilizing interaction would be expected to lower the oxidation potential of the olefin.

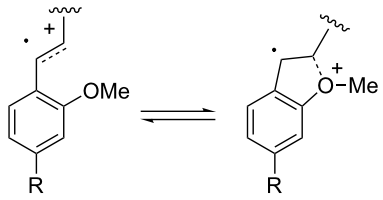

Figure 1: Radical cation stabilization by an *o*-methoxy substituent.

We also investigated the reactivity of the *o*,*p*-dimethoxy substituted styrene **19i** towards the coupling reaction. This reaction also led to a good yield of product and efficient consumption of the starting material. Surprisingly, the optimized conditions for the oxidation of **19i** were different from those optimized for the oxidation of either **19c** or **19e**, and the initial yields for the cyclization of **19i** were not good. The cyclization originating

from **19i** benefited from the use of more base. It appears that the use of base reduced the formation of a quinone methide from the product. For example, when a full equivalent of base was used for the reaction, the desired product was obtained in 74% isolated yield.

It is clear that the success of the styrene derived coupling reaction depends strongly on the position of the methoxy group on the aromatic ring. *Ortho* and *para* substitution leads to a successful cyclization while *meta* substitution does not. This observation is best explained by the reaction being dependent upon the ease with which the cyclic benzyl radicals **21a–c** are oxidized.

Conclusion

It was found that carboxylic acid nucleophiles can be coupled to electron-rich olefins to form lactone products in good yield without interference from competitive decarboxylation reactions. The reactions are consistent with carboxylate trapping of an olefin-derived radical cation intermediate and depend strongly on the ease with which the second oxidation step in the mechanism occurs. This is particularly true when styrene-based substrates are used. Finally, optimization of reaction pH required careful consideration of product stability.

Supporting Information

Supporting Information File 1

Procedures for electrolysis and cyclic voltammetry experiments, characterization of electrolysis products, procedures for synthesis and characterization of electrolysis starting materials.
[http://www.beilstein-journals.org/bjoc/content/supplementary/1860-5397-9-186-S1.pdf]

Acknowledgements

We thank the National Science Foundation (CHE-1151121) for their generous support of this work.

References

1. Sperry, J. B.; Wright, D. L. *Chem. Soc. Rev.* **2006,** *35,* 605–621. doi:10.1039/b512308a
2. Yoshida, J.; Kataoka, K.; Horcajada, R.; Nagaki, A. *Chem. Rev.* **2008,** *108,* 2265–2299. doi:10.1021/cr0680843
3. Moeller, K. D. *Synlett* **2009,** 1208–1218. doi:10.1055/s-0028-1088126
4. Xu, H.-C.; Moeller, K. D. *J. Am. Chem. Soc.* **2010,** *132,* 2839–2844. doi:10.1021/ja910586v
5. Sutterer, A.; Moeller, K. D. *J. Am. Chem. Soc.* **2000,** *122,* 5636–5637. doi:10.1021/ja001063k
6. Liu, B.; Duan, S.; Sutterer, A. C.; Moeller, K. D. *J. Am. Chem. Soc.* **2002,** *124,* 10101–10111. doi:10.1021/ja026739l
7. Brandt, J. D.; Moeller, K. D. *Org. Lett.* **2005,** *7,* 3553–3556. doi:10.1021/ol051296m
8. Xu, H.-C.; Brandt, J. D.; Moeller, K. D. *Tetrahedron Lett.* **2008,** *49,* 3868–3871. doi:10.1016/j.tetlet.2008.04.075
9. Campbell, J. M.; Xu, H.-C.; Moeller, K. D. *J. Am. Chem. Soc.* **2012,** *134,* 18338–18344. doi:10.1021/ja307046j
10. Torii, S.; Tanaka, H. Carboxylic Acids. In *Organic Electrochemistry,* 4th ed.; Lund, H.; Hammerich, O., Eds.; Marcel Dekker: New York, 2001; pp 499–543.
11. Schäfer, H. J. Recent Contributions of Kolbe Electrolysis to Organic Synthesis. In *Electrochemistry IV;* Steckhan, E., Ed.; Topics in Current Chemistry, Vol. 152; Springer-Verlag: New York, 1990; pp 91–151.
12. Schäfer, H. J. *Chem. Phys. Lipids* **1979,** *24,* 321–333. doi:10.1016/0009-3084(79)90117-8
13. Lebreux, F.; Buzzo, F.; Markó, I. E. *Synlett* **2008,** 2815–2820. doi:10.1055/s-0028-1083547
14. Huhtasaari, M.; Schäfer, H. J.; Becking, L. *Angew. Chem., Int. Ed. Engl.* **1984,** *23,* 980–981. doi:10.1002/anie.198409801
15. Matzeit, A.; Schäfer, H. J.; Amatore, C. *Synthesis* **1995,** 1432–1444. doi:10.1055/s-1995-4112
16. Scott, A. I.; Dodson, P. A.; McCapra, F.; Meyers, M. B. *J. Am. Chem. Soc.* **1963,** *85,* 3702–3704. doi:10.1021/ja00905a040
17. Coutts, I. G. C.; Edwards, M.; Musto, D. R.; Richards, D. J. *Tetrahedron Lett.* **1980,** *21,* 5055–5056. doi:10.1016/S0040-4039(00)71131-2
18. Coutts, I. G. C.; Culbert, N. J.; Edwards, M.; Hadfield, J. A.; Musto, D. R.; Pavlidis, V. H.; Richards, D. J. *J. Chem. Soc., Perkin Trans. 1* **1985,** 1829–1836. doi:10.1039/P19850001829
19. Thomas, H. G.; Schwager, H.-W. *Tetrahedron Lett.* **1984,** *25,* 4471–4474. doi:10.1016/S0040-4039(01)81469-6
20. Deffieux, D.; Fabre, I.; Courseille, C.; Quideau, S. *J. Org. Chem.* **2002,** *67,* 4458–4465. doi:10.1021/jo020023r
21. Xu, H.-C.; Moeller, K. D. *Angew. Chem., Int. Ed.* **2010,** *49,* 8004–8007. doi:10.1002/anie.201003924
22. Xu, G.; Moeller, K. D. *Org. Lett.* **2010,** *12,* 2590–2593. doi:10.1021/ol100800u
23. Tang, F.; Moeller, K. D. *Tetrahedron* **2009,** *65,* 10863–10875. doi:10.1016/j.tet.2009.09.028

License and Terms

Beilstein Journal of Organic Chemistry

Bromination of hydrocarbons with CBr_4, initiated by light-emitting diode irradiation

Yuta Nishina*[1], Bunsho Ohtani[2] and Kotaro Kikushima[1]

Letter

Open Access

Address:
[1]Research Core for Interdisciplinary Science, Okayama University, Tsushimanaka, Kita-ku, Okayama 700-8530, Japan and [2]Catalysis Research Center, Hokkaido University, Sapporo 001-0021, Japan

Email:
Yuta Nishina* - nisina-y@cc.okayama-u.ac.jp

* Corresponding author

Keywords:
bromination; free radical; hydrocarbon; light-emitting diode; photo irradiation

Beilstein J. Org. Chem. **2013,** *9,* 1663–1667.
doi:10.3762/bjoc.9.190

Received: 26 April 2013
Accepted: 25 July 2013
Published: 14 August 2013

This article is part of the Thematic Series "Organic free radical chemistry".

Guest Editor: C. Stephenson

Abstract

The bromination of hydrocarbons with CBr_4 as a bromine source, induced by light-emitting diode (LED) irradiation, has been developed. Monobromides were synthesized with high efficiency without the need for any additives, catalysts, heating, or inert conditions. Action and absorption spectra suggest that CBr_4 absorbs light to give active species for the bromination. The generation of $CHBr_3$ was confirmed by NMR spectroscopy and GC–MS spectrometry analysis, indicating that the present bromination involves the homolytic cleavage of a C–Br bond in CBr_4 followed by radical abstraction of a hydrogen atom from a hydrocarbon.

Introduction

Bromination reactions of organic compounds are fundamental reactions for providing a wide variety of organic precursors for industrial materials [1-8]. Generally, the bromination of saturated hydrocarbons proceeds through radical abstraction of hydrogen atoms and trapping with bromide, whereas the bromination reactions of aromatic and unsaturated hydrocarbons are induced by electrophilic addition of bromine and/or a cationic bromide. Combinations of *N*-bromosuccinimide (NBS) with azobisisobutyronitrile or benzoyl peroxide as radical initiators are typical conditions for Wohl–Ziegler bromination [9-12] and are widely used for the bromination of benzylic and allylic positions, despite the need for heating and the generation of equimolar amounts of waste. To avoid these drawbacks, several efforts have been focused on benzylic bromination using Br_2 or bromide salts as highly efficient bromine sources [13-17]. However, the direct bromination of non-activated C–H bonds is still a challenging task. Although Br_2 [13], CBr_4 [18-20], R_4NBr [21,22] and LiBr [23] have been reported to serve as bromine sources for the bromination of saturated hydrocarbons, these reactions exhibit low selectivity or reactivity. Efficient bromination using Br_2 as a bromine source combined with a stoichiometric base [24], an excess of MnO_2 [25], or a catalytic amount of Li_2MnO_3 [26] has been reported to give high reactivity and selectivity. The combination of CBr_4 with a copper catalyst at high temperature also achieves effective bromination of hydrocarbons [27].

We have focused on CBr_4, which is solid and easy to handle, as a bromine source. CBr_4 has been used in organic synthesis to give useful bromide-containing precursors. For instance, alkyl alcohols can be converted to alkyl bromides in the presence of CBr_4 and triphenylphosphine; this is known as the Appel reaction [28]. This combination can also be used to transform aldehydes into dibromoalkenes, which are useful precursors for the Corey–Fuchs reaction [29], to obtain terminal alkynes. Although CBr_4 has been used for various bromination reactions including radical brominations, these reactions need further additives to proceed. Here, we disclose the efficient bromination of saturated hydrocarbons, using CBr_4 as a bromine source without any additives, through radical reactions induced by irradiation with light from commonly used light-emitting diodes (LEDs) [30]. In this reaction, additives, catalysts, heating, and inert reaction conditions are all unnecessary.

Results and Discussion

First, the bromination of cyclohexane under LED irradiation was investigated using 1.0 mL of cyclohexane with 0.20 mmol CBr_4 (Table 1). The desired monobrominated product was obtained in 77% yield, based on CBr_4, after 2 h, and no dibromide was observed (Table 1, entry 1). It was found that the yield of cyclohexyl bromide exceeded 100% after 3 h (Table 1, entry 2). When the mixture was irradiated for 4 h, the product yield reached 148% and had almost peaked (Table 1, entry 3). Further improvements were not observed, even after 24 h (Table 1, entry 5). These results indicate that during the reaction one or more bromine atoms originated from one CBr_4. It is considered that $CHBr_3$ generated through radical abstraction of a hydrogen atom by a tribromomethyl radical served as a bromine source. To test this hypothesis the reaction was repeated with $CHBr_3$ instead of CBr_4 and the product was obtained in a low yield (Table 1, entry 6), whereas the reaction with CH_2Br_2 produced no bromination product at all under these conditions (Table 1, entry 7). Other bromination reagents such as NBS also gave the desired product in moderate yield (Table 1, entry 8). In the case of tetrabutylammonium bromide, no brominated product was obtained (Table 1, entry 9), showing that the present reaction was a radical reaction. Based on the assumption that the initial formation of bromine radicals would be important, addition of catalytic amounts of CBr_4 along with various bromination sources was examined (Table 1, entries 10–12). The combination of catalytic CBr_4 with $CHBr_3$ or CH_2Br_2 resulted in slight improvements in the yields (Table 1, entries 10 and 11), showing these bromides also could serve as bromination sources in the presence of the radical species. The combination of CBr_4 with NBS gave the desired product in a moderate yield (Table 1, entry 12). On the other hand, the reaction was inhibited by the addition of water (Table 1, entry 13) and performing the reaction under inert argon atmosphere led to a decreased yield of 87% (Table 1, entry 14).

Table 1: Bromination of cyclohexane using CBr_4 under LED irradiation.[a]

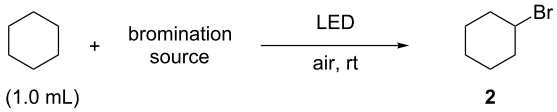

1 (1.0 mL) **2**

entry	bromination source (mmol)	time (h)	yield (%)[b]
1	CBr_4 (0.20)	2	77
2	CBr_4 (0.20)	3	108
3	CBr_4 (0.20)	4	148
4	CBr_4 (0.20)	5	148
5	CBr_4 (0.20)	24	150
6	$CHBr_3$ (0.20)	24	27
7	CH_2Br_2 (0.20)	24	0
8	NBS (0.20)	24	31
9	Bu_4NBr (0.20)	24	0
10	CBr_4 (0.02)/$CHBr_3$ (0.20)	24	39
11	CBr_4 (0.02)/CH_2Br_2 (0.20)	24	16
12	CBr_4 (0.02)/NBS (0.20)	24	79
13[c]	CBr_4 (0.20)	24	0
14[d]	CBr_4 (0.20)	24	87

[a]Conditions: 1.0 mL of cyclohexane, bromination sources, under LED irradiation, rt. [b]Yields were determined by GC analysis based on the mole of CBr_4. [c]In the presence of 0.10 mL water. [d]Under Ar.

Based on the above experiments, the bromination of other substrates was examined with CBr_4 under LED irradiation. Cyclooctane underwent bromination under the optimized conditions to furnish the monobromide in 178% yield, based on CBr_4, without contamination by dibromide (Table 2, entry 1). The bromination of *n*-hexane produced three bromides: 1-bromohexane (14%), 2-bromohexane (84%), and 3-bromohexane (41%) (Table 2, entry 2). On the other hand, no bromination of toluene occurred under LED irradiation. In this case, light would be absorbed by the aromatic ring of toluene, suppressing the activation of CBr_4. Using sunlight in place of LED light, however, resulted in the bromination of the benzylic position to give benzyl bromide in 140% yield (Table 2, entry 3).

To investigate the wavelength dependency of the present reaction, the action spectrum of the bromination of cyclohexane in the presence of CBr_4 was obtained by plotting the apparent quantum efficiency against wavelength (Figure 1, red line) [31]. It was found that the present reaction was promoted by irradiation with ultraviolet (UV) light and deactivated under visible-light (>475 nm) irradiation. CBr_4 shows strong absorption in the UV region (Figure 1, blue line), and this overlaps with the

Table 2: Bromination of other substrates using CBr_4 under LED irradiation.[a]

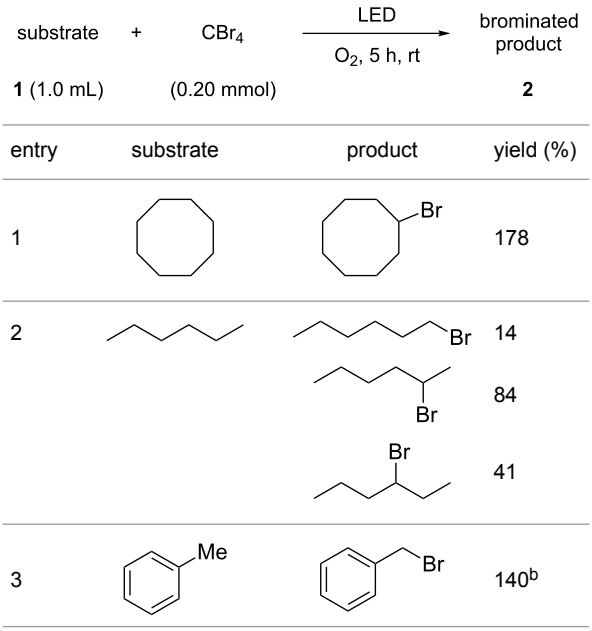

entry	substrate	product	yield (%)
1			178
2			14
			84
			41
3			140[b]

[a]Conditions: 1.0 mL of substrate, 0.20 mmol of CBr_4, under LED irradiation. Yields were determined by GC using dodecane as an internal standard. [b]Under sunlight irradiation.

above-mentioned action spectrum. The activation of CBr_4 is therefore considered to be induced by photo-irradiation, initiating the reaction. Although other light sources could also activate CBr_4, we adopted LED light due to safety, mildness, and availability. We have confirmed that fluorescent room light could also promote the reaction.

A plausible mechanism for the present bromination is illustrated in Scheme 1. First, photo-irradiation generates a bromine radical and a CBr_3 radical (Scheme 1, reaction 1), which abstracts a hydrogen atom from the substrate to form $CHBr_3$ (Scheme 1, reaction 2). Finally, the radical species derived from the substrate reacts with the bromine radical or CBr_4 to afford the brominated product (Scheme 1, reactions 3 and 4). Additionally, the in situ generated $CHBr_3$ releases a bromine radical upon LED irradiation, thus serving as a bromine source (Scheme 1, reaction 5). Alternatively the radical species derived from the substrate abstracts a bromine atom from $CHBr_3$ (Scheme 1, reaction 6).

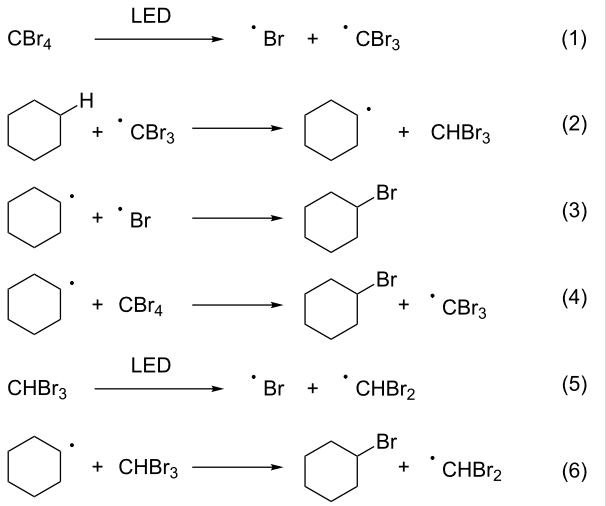

Scheme 1: Plausible mechanism for bromination of cyclohexane with CBr_4 induced by LED irradiation.

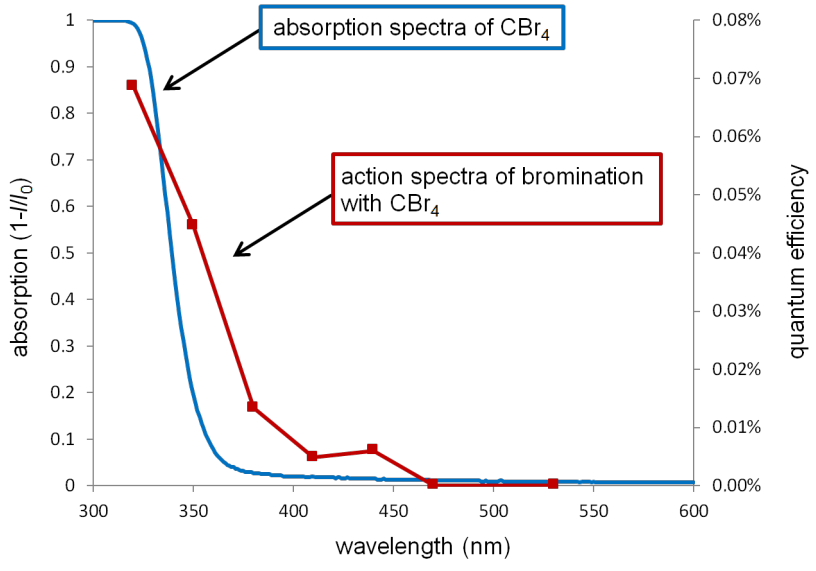

Figure 1: Action spectrum of bromination with CBr_4, induced by LED irradiation (red line), and absorption spectrum of CBr_4 (blue line).

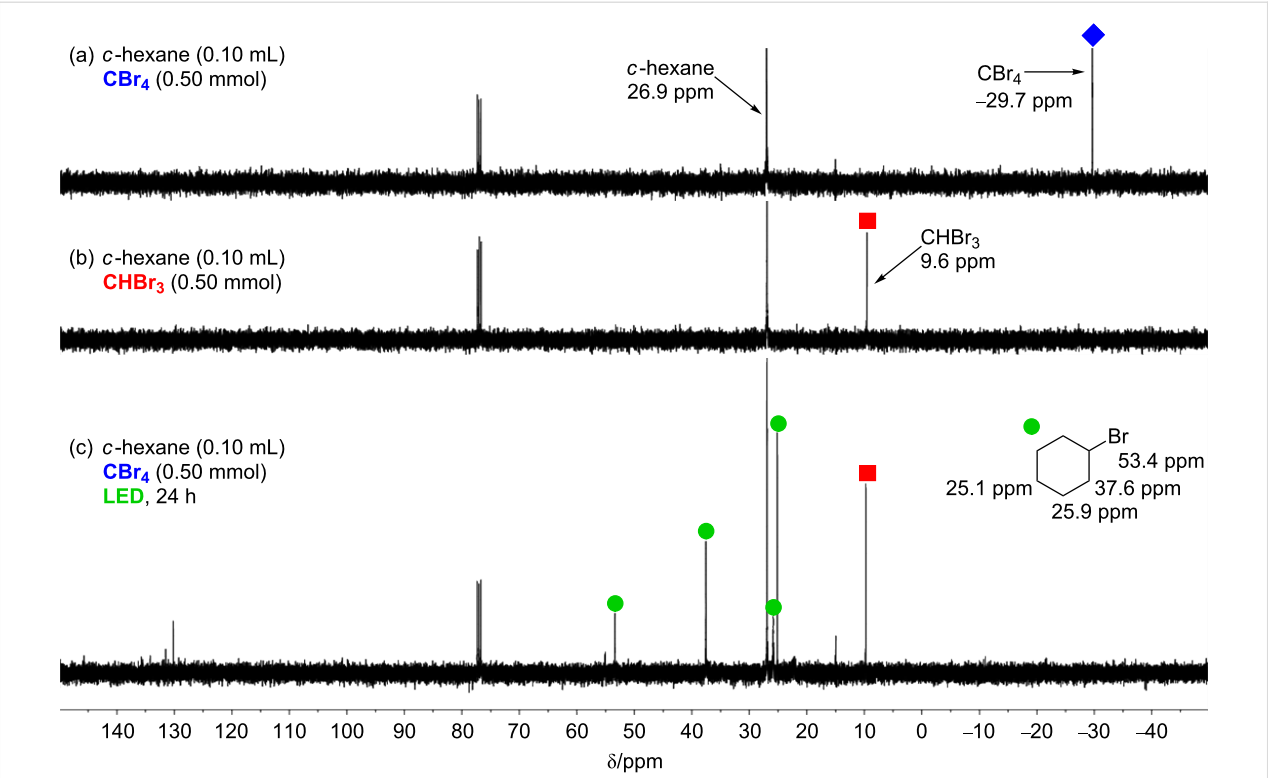

Figure 2: ^{13}C NMR monitoring of reaction mixtures: (a) 0.50 mmol of CBr_4, 0.10 mL of cyclohexane, and 0.40 mL of $CDCl_3$, (b) 0.5 mmol of $CHBr_3$, 0.10 mL of cyclohexane, and 0.40 mL of $CDCl_3$, (c) 0.50 mmol of CBr_4 and 0.10 mL of cyclohexane, LED irradiation for 24 h, and then addition of 0.40 mL of $CDCl_3$.

To examine the above hypothesis, the bromination of cyclohexane was monitored using ^{13}C NMR spectroscopy (Figure 2). CBr_4 (0.50 mmol) dissolved in cyclohexane (0.10 mL) and $CDCl_3$ (0.40 mL) was observed at −29.7 ppm (Figure 2a). After stirring a reaction mixture of CBr_4 (0.50 mmol) and cyclohexane (0.10 mL) under LED irradiation for 24 h, peaks assigned to bromocyclohexane (53.4, 37.6, 25.9, and 25.1 ppm) and another strong peak at 9.6 ppm appeared (Figure 2c). The latter peak was found to be consistent with the peak of $CHBr_3$ (0.50 mmol) dissolved in cyclohexane (0.10 mL) and $CDCl_3$ (0.40 mL) (Figure 2b). Additionally, the generation of $CHBr_3$ in the present bromination was confirmed by ^1H NMR spectroscopy and GC–MS spectrometry. These results support the reaction pathway described above, although the chemical species after the second bromination was not assigned at this point.

Conclusion

In conclusion, we have developed a method for the hydrocarbon bromination induced by LED irradiation using CBr_4 as a bromine source. The present reaction system did not require any additives, catalysts, heating, or inert conditions, and is therefore an extremely simple procedure. An action spectrum and NMR measurements showed that the LED irradiation activates CBr_4 to generate bromine radicals, which initiate the bromination reaction. Further elucidation of the detailed mechanism and the use of LED irradiation in other reaction systems are under investigation in our laboratory.

Experimental

General information

All commercially available compounds were purchased and used as received. Cyclohexane, cyclooctane, *n*-hexane, and toluene were purchased from Wako Pure Chemical Industries and used as received. ^1H (400 MHz) and ^{13}C (100 MHz) NMR spectra were recorded using a JEOL JNM-LA400 spectrometer. Proton chemical shifts are reported relative to residual solvent peak of $CDCl_3$ at δ 7.26 ppm. Carbon chemical shifts are reported relative to $CDCl_3$ at δ 77.00 ppm. Gas chromatographic analysis was conducted with Shimadzu GC-2014 equipped with FID detector. The chemical yields were determined using dodecane as an internal standard. The NMR data of all brominated products match those reported.

General procedure for the bromination induced by LED irradiation

A reaction tube was charged with CBr_4 (66.33 mg, 0.20 mmol) and a hydrocarbon (1.0 mL). The reaction mixture was stirred

under white LED (7 W) irradiation. To this was added dodecane (45.2 μL, 0.20 mmol) and the yield was determined by GC analysis with dodecane as an internal standard.

Acknowledgements

Financial support for this study was provided by the Development of Human Resources in Science and Technology, The Circle for the Promotion of Science and Engineering, and the Cooperative Research Program of Catalysis Research Center, Hokkaido University (Grant #11B2001). We also received generous support from Mr. Junya Miyata, Mr. Ryota Watanabe, and Dr. Tomoka Kawase on this research.

References

1. Rosseels, G.; Houben, C.; Kerckx, P. Synthesis of a metabolite of fantofarone. In *Advances in Organobromine Chemistry II;* Desmurs, J. R.; Gérard, B.; Goldstein, M. J., Eds.; Elsevier: Amsterdam, New York, 1995; pp 152–159. doi:10.1016/S0926-9614(05)80016-4
2. Cristau, H. J.; Desmurs, J. R. Arylation of hard heteroatomic nucleophiles using bromoarenes substrates and Cu, Ni, Pd-catalysts. In *Advances in Organobromine Chemistry II;* Desmurs, J. R.; Gérard, B.; Goldstein, M. J., Eds.; Elsevier: Amsterdam, New York, 1995; pp 240–263. doi:10.1016/S0926-9614(05)80024-3
3. Rakita, P. E. In *Handbook of Grignard Reagents;* Silverman, G. S.; Rakita, P. E., Eds.; Marcel Dekker: New York, 1996; pp 1 ff.
4. Echavarren, A. M.; Cárdenas, D. J. Mechanistic Aspects of Metal-Catalyzed C,C- and C,X-Bond-Forming Reactions. In *Metal-Catalyzed Cross-Coupling Reactions, 2nd ed.;* de Meijere, A.; Diederich, F., Eds.; Wiley-VCH: Weinheim, Germany, 2004; pp 1 ff. doi:10.1002/9783527619535.ch1
5. Knochel, P.; Dohle, W.; Gommermann, N.; Kneisel, F. F.; Kopp, F.; Korn, T.; Sapountzis, I.; Vu, V. A. *Angew. Chem., Int. Ed.* **2003,** *42,* 4302–4320. doi:10.1002/anie.200300579
6. Parham, W. E.; Bradsher, C. K. *Acc. Chem. Res.* **1982,** *15,* 300–305. doi:10.1021/ar00082a001
7. Gribble, G. W. *Acc. Chem. Res.* **1998,** *31,* 141–152. doi:10.1021/ar9701777
8. Gribble, G. W. *Chem. Soc. Rev.* **1999,** *28,* 335–346. doi:10.1039/a900201d
9. Wohl, A. *Ber. Dtsch. Chem. Ges.* **1919,** *52,* 51–63. doi:10.1002/cber.19190520109
10. Ziegler, K.; Schenck, G.; Krockow, E. W.; Siebert, A.; Wenz, A.; Weber, H. *Justus Liebigs Ann. Chem.* **1942,** *551,* 1–79. doi:10.1002/jlac.19425510102
11. Djerassi, C. *Chem. Rev.* **1948,** *43,* 271–317. doi:10.1021/cr60135a004
12. Horner, L.; Winkelman, E. M. *Angew. Chem.* **1959,** *71,* 349–365. doi:10.1002/ange.19590711102
13. Shaw, H.; Perlmutter, H. D.; Gu, C.; Arco, S. D.; Quibuyen, T. O. *J. Org. Chem.* **1997,** *62,* 236–237. doi:10.1021/jo950371b
14. Kikuchi, D.; Sakaguchi, S.; Ishii, Y. *J. Org. Chem.* **1998,** *63,* 6023–6026. doi:10.1021/jo972263q
15. Mestres, R.; Palenzuela, J. *Green Chem.* **2002,** *4,* 314–316. doi:10.1039/b203055a
16. Podgoršek, A.; Stavber, S.; Zupana, M.; Iskra, J. *Tetrahedron Lett.* **2006,** *47,* 7245–7247. doi:10.1016/j.tetlet.2006.07.109
17. Adimurthy, S.; Ghosh, S.; Patoliya, P. U.; Ramachandraiah, G.; Agrawal, M.; Gandhi, M. R.; Upadhyay, S. C.; Ghosh, P. K.; Ranu, B. C. *Green Chem.* **2008,** *10,* 232–237. doi:10.1039/b713829f
18. Schreiner, P. R.; Lauenstein, O.; Kolomitsyn, I. V.; Nadi, S.; Fokin, A. A. *Angew. Chem., Int. Ed.* **1998,** *37,* 1895–1897. doi:10.1002/(SICI)1521-3773(19980803)37:13/14<1895::AID-ANIE1895>3.0.CO;2-A
19. Barton, D. H. R.; Csuhai, E.; Doller, D. *Tetrahedron* **1992,** *48,* 9195–9206. doi:10.1016/S0040-4020(01)85610-6
20. Wiedenfeld, D. *J. Chem. Soc., Perkin Trans. 1* **1997,** 339–348. doi:10.1039/A600172F
21. Kojima, T.; Matsuo, H.; Matsuda, Y. *Chem. Lett.* **1998,** *27,* 1085–1086. doi:10.1246/cl.1998.1085
22. He, Y.; Goldsmith, C. R. *Synlett* **2010,** 1377–1380. doi:10.1055/s-0029-1219832
23. Shaikh, T. M.; Sudalai, A. *Tetrahedron Lett.* **2005,** *46,* 5589–5592. doi:10.1016/j.tetlet.2005.06.033
24. Montoro, R.; Wirth, T. *Synthesis* **2005,** 1473–1478. doi:10.1055/s-2005-865322
25. Jiang, X.; Shen, M.; Tang, Y.; Li, C. *Tetrahedron Lett.* **2005,** *46,* 487–489. doi:10.1016/j.tetlet.2004.11.113
26. Nishina, Y.; Morita, J.; Ohtani, B. *RSC Adv.* **2013,** *3,* 2158–2162. doi:10.1039/c2ra22197g
27. Smirnov, V. V.; Zelikman, V. M.; Beletskaya, I. P.; Golubeva, E. N.; Tsvetkov, D. S.; Levitskii, M. M.; Kazankova, M. A. *Russ. J. Org. Chem.* **2002,** *38,* 962–966. doi:10.1023/A:1020889209717
28. Appel, R. *Angew. Chem., Int. Ed. Engl.* **1975,** *14,* 801–811. doi:10.1002/anie.197508011
29. Corey, E. J.; Fuchs, P. L. *Tetrahedron Lett.* **1972,** *13,* 3769–3772. doi:10.1016/S0040-4039(01)94157-7
30. Nobuta, T.; Fujiya, A.; Hirashima, S.; Tada, N.; Miura, T.; Itoh, A. *Tetrahedron Lett.* **2012,** *53,* 5306–5308. doi:10.1016/j.tetlet.2012.07.091
31. Torimoto, T.; Nakamura, N.; Ikeda, S.; Ohtani, B. *Phys. Chem. Chem. Phys.* **2002,** *4,* 5910–5914. doi:10.1039/b207448f

License and Terms

Beilstein Journal of Organic Chemistry

Aerobic radical multifunctionalization of alkenes using *tert*-butyl nitrite and water

Daisuke Hirose[1] and Tsuyoshi Taniguchi[*2]

Letter

Open Access

Address:
[1]Graduate School of Natural Science and Technology, Kanazawa University, Kakuma-machi, Kanazawa 920-1192, Japan, and [2]School of Pharmaceutical Sciences, Institute of Medical, Pharmaceutical and Health Sciences, Kanazawa University, Kakuma-machi, Kanazawa 920-1192, Japan

Email:
Tsuyoshi Taniguchi[*] - tsuyoshi@p.kanazawa-u.ac.jp

* Corresponding author

Keywords:
C−H oxidation; free radical; nitration; oxygen; radicals; water

Beilstein J. Org. Chem. **2013,** *9,* 1713–1717.
doi:10.3762/bjoc.9.196

Received: 19 June 2013
Accepted: 30 July 2013
Published: 20 August 2013

This article is part of the Thematic Series "Organic free radical chemistry".

Guest Editor: C. Stephenson

Abstract

Water induces a change in the product of radical multifunctionalization reactions of aliphatic alkenes involving an sp^3 C–H functionalization by an 1,5-hydrogen shift using *tert*-butyl nitrite and molecular oxygen. The reaction without water, reported previously, gives nitrated γ-lactols, whereas the reaction in the presence of water produces 4-hydroxy-5-nitropentyl nitrate or 4-hydroxy-3-nitropentyl nitrate derivatives.

Introduction

Multifunctionalization reactions of simple organic molecules are useful methods because they can provide a shortcut to desired products. Various methods used widely, such as organometallic reactions, cycloaddition reactions and multicomponent reactions, are utilized for multifunctionalization [1-5]. If direct functionalization reactions of inactivated bonds, such as simple multiple bonds or C–H bonds, are combined with multifunctionalization processes, they would become more efficient synthetic methods [6-9]. In this regard, radical reactions are capable of realizing multifunctionalization of inactivated organic molecules due to their high reactivity. Addition reactions of radical species to multiple bonds in the presence of appropriate trapping reagents give double functionalized compounds [10,11]. In addition, a radical methodology is a powerful tool for sp^3 C–H functionalization [12-16]. It is frequently achieved by intramolecular radical hydrogen transfer reactions. An 1,5-hydrogen shift is the most favourable process [17], and useful methods such as the Barton reaction and the Hofmann–Löffler–Freytag reaction have been reported [18-20]. Recently, we reported a novel radical multifunctionalization reaction of aliphatic alkenes using *tert*-butyl nitrite (*t*-BuONO) and oxygen [21]. In this reaction, three positions including an unreactive sp^3 C–H bond are functionalized in alkenes to produce nitrated γ-lactols in one step. For instance, treatment of alkene **1** with 5 equivalents of *t*-BuONO in a dried solvent under an oxygen atmosphere directly gave γ-lactol **2**

(Scheme 1). On the other hand, we found in the course of this study that addition of water altered the products to a non-cyclic functionalized compound **3** (Scheme 1). In this letter, we report water-induced multifunctionalization reactions of alkenes by aerobic radical oxynitration.

Results and Discussion

Our investigation started with the screening of solvents in the reaction of alkene **1** with *t*-BuONO (3 equiv) and oxygen in the presence of water (3 equiv). Although dimethyl sulfoxide (DMSO) was the best solvent in the reaction without water to obtain γ-lactol **2** [21], it worked inefficiently in the presence of water, and triple functionalized product **3** was obtained in low yield along with a large amount of oxynitration product **4** (Table 1, entry 1). The use of other polar solvents such as *N*,*N*-dimethylformamide (DMF) and tetrahydrofuran (THF) also did not give better results (Table 1, entries 2 and 3), whereas the use of dichloromethane (CH_2Cl_2) improved the ratio of **3** and **4** (ca. 1:2), though the isolated yield of **3** was still low (entry 4). Encouraged by this observation, we tested the reaction in pentane and obtained an improved ratio (ca. 1:1) and improved yield (26%) of **3** (entry 5). Eventually, the reaction with an excess of water (30 equiv) and with a longer reaction time (12 h) somewhat improved the yield (33%) of **3**. This reaction was reproducible on a larger scale (6 mmol) and gave **3** in 37% yield. Water was insoluble in the organic solvent, but it seemed to cause no problem with the reproducibility. Although we tried to further optimize the conditions, such as amounts of reagents, concentration, temperature and sonication, no better results were obtained. Efforts for optimizations are still being continued.

Table 1: The effect of solvents.

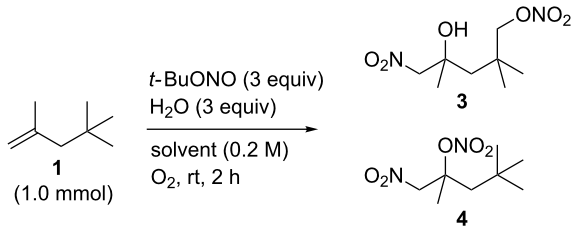

entry	solvent	yield (%)[a] 3	4
1	DMSO	15	54
2	DMF	15	43
3	THF	18	52
4	CH_2Cl_2	13	28
5	pentane	26	28
6[b]	pentane	33 (37)[c]	37 (38)[c]

[a]Isolated yield. [b]30 equiv of H_2O, 12 h. [c]6.0 mmol scale.

Next, our interest focused on the multifunctionalization reactions of various alkenes **5**–**14** (Table 2). The oxynitration of olefins and the direct oxygenation of methyl C–H bonds of branched aliphatic alkenes **5**–**10** occurred to afford triple functionalized products **15**–**20** (Table 2, entries 1–6). In the reactions of alkenes **5** and **7**, a remarkable diastereoselectivity was observed (Table 2, entries 1 and 3, and vide infra). We found that the multifunctionalization of monosubstituted alkene **8** took place to give **18** unlike the reaction without water [21], though the yield was not high (entry 4). The reaction of 1,1,3,3-tetramethyl-5-methylenecyclohexane (**9**) gave the mutifunctionalized product **19** as a single isomer. The stereochemistry of **19** could be presumably assigned by considering the 1,5-hydrogen shift mechanism (entry 5) [17]. The reaction of alkene **10** bearing a methyl ester moiety gave γ-lactone **20** by intramolecular transesterification with a tertiary hydroxy group arising from hydration of the olefin (entry 6). Functionalization reactions involving oxygenation of methylene C–H bonds of alkenes **11**–**13** also proceeded to afford secondary nitrate compounds **21**–**23**, though no diastereoselectivity was observed (Table 2, entries 7–9). Unfortunately, no tertiary nitrate ester **24** was detected in the reaction of **14**. This implies that the 1,5-hydrogen shift on the methine site is not so fast (entry 10). Typically, in the radical hydrogen abstraction, a methine C–H bond is more reactive than methyl and methylene sites, whereas it might be difficult for substrates having a methine group to form an organized transition state to induce the 1,5-hydrogen shift because they have only one hydrogen atom that can be abstracted [17]. In short, entropy factors might be dominant in the present reaction.

We attempted to transform the product obtained by the present reaction into a valuable compound. As a represent example,

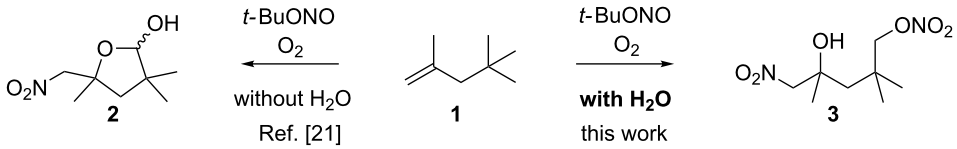

Scheme 1: The effect of water in radical multifunctionalization reactions.

Table 2: Reactions of various alkenes[a].

entry	alkene	product	yield[b]
1	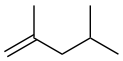 **5**	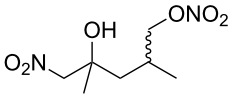 **15**	40%; dr, 90:10
2	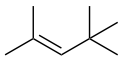 **6**	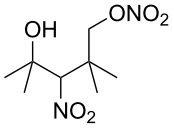 **16**	29%
3	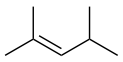 **7**	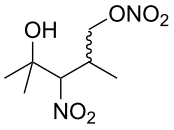 **17**	38%; dr, >95:5
4[c]	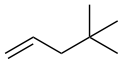 **8**	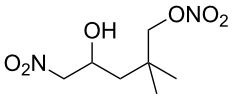 **18**	16%
5[c]	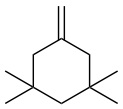 **9**	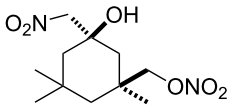 **19**	28%
6[b]	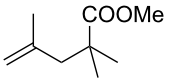 **10**	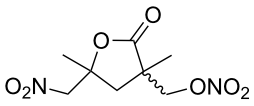 **20**	31%; dr, 50:50
7	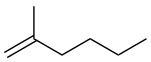 **11**	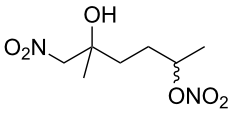 **21**	31%; dr, 50:50
8	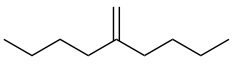 **12**	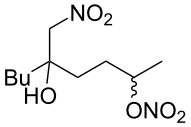 **22**	33%; dr, 50:50
9	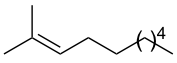 **13**	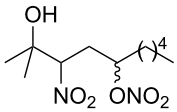 **23**	37%; dr, 50:50
10	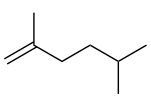 **14**	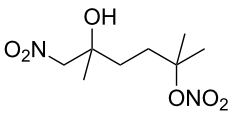 **24**	not detected

[a]Reaction conditions: alkene (1.0 mmol), *t*-BuONO (3.0 mmol), H_2O (30 mmol) in pentane (5 mL) under an oxygen atmosphere (balloon) for 12 h.
[b]Isolated yield. Diastereomeric ratio (dr) was approximately estimated by ^1H NMR analysis. [c]3 equiv (3.0 mmol) of H_2O was used.

compound **3** was exposed to typical hydrogenation conditions using 10% palladium on carbon to obtain the corresponding 5-amino-1,4-diol compound. Since this is a highly polar compound, diol **25** was isolated after protection of the amino group by subsequent treatment of the crude product with di-*tert*-butyl dicarbonate (Boc_2O) (Scheme 2). This experiment emphasised the potential of the present multifunctionalization method because the simple unsaturated hydrocarbon **1** can be converted into the highly polar amino-1,4-diol compound in only two steps.

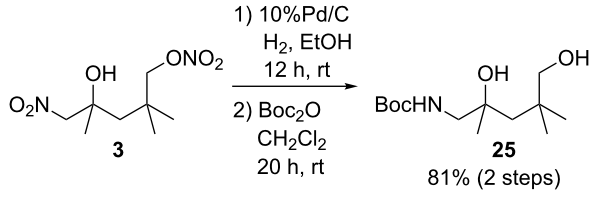

Scheme 2: Transformation of **3** into 5-amino-1,4-diol derivative **25**.

The plausible mechanism is fundamentally the same as the previously proposed one (Scheme 3) [21-23]. Certainly, the present reaction is triggered by addition of nitrogen dioxide (NO_2) generated by aerobic decomposition of *t*-BuONO to the olefin of **1**. After the resultant tertiary carbon radical has been trapped by molecular oxygen, an alkoxy radical **26** is formed from the peroxynitrite intermediate (ROONO) generated by the reaction of the peroxy radical (ROO•) intermediate with *t*-BuONO. The alkoxy radical causes an 1,5-hydrogen shift to give the corresponding alkyl radical **27** followed by formation of another alkoxy radical **28** through a similar process. An important issue in the current work is the effect of water to determine the destiny of **28**. In the absence of water, the alkoxy radical **28** was merely oxidized to aldehyde **29**, which was converted into γ-lactol **2** [21]. On the other hand, if **28** is caught by NO_2 more rapidly than the oxidation, nitrate ester **3** is produced, and it was really observed in the presence of water. These observations clearly indicate that a difference in the concentration of NO_2 in situ affects the results of each reaction. In other words, water may promote the generation of NO_2 from *t*-BuONO, and this observation has already been reported in previous radical oxynitration reactions of alkenes [22]. In addition, when alkene **1** was subjected to nitrous acid (HNO_2), that was formed from sodium nitrite ($NaNO_2$; 3 equiv) and acetic acid (3 equiv), and oxygen in water (30 equiv) and pentene (0.2 M), production of compound **3** was observed, though the yield was low (7%). Since this system is an alternative method for the generation of NO_2, this may support the formation of same intermediate species such as HNO_2 and NO_2 in the reaction using *t*-BuONO, oxygen and water [24].

The high diastereoselectivity in reactions of alkenes **5** and **7** could be rationalized by six-membered transition states **30** and **31** in the 1,5-hydrogen shift. If chair forms were postulated in both cases, more substituents should be arranged at equatorial positions to form more stable transition states. According to this presumption, the configurations of the major isomers of products **15** and **17** can be tentatively assigned as shown in Scheme 3.

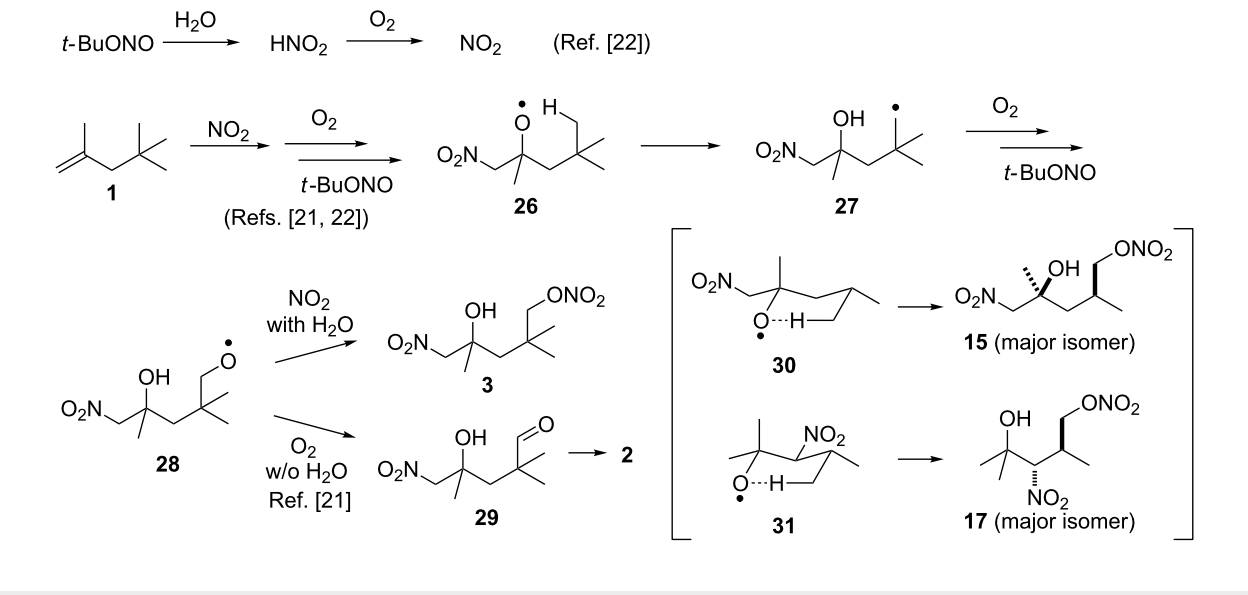

Scheme 3: Proposed reaction mechanism.

Conclusion

We found in multifunctionalization reactions of alkenes with *t*-BuONO and oxygen that water induced the production of another triple functionalized compound that is a nitrate ester. This can be a precursor of a 5-amino-1,4-diol, and the access from simple aliphatic alkenes in one step is unprecedented. The functionalization of unreactive sp^3 C–H bonds using a radical 1,5-hydrogen shift is an old methodology compared with modern transition metal-catalyzed C–H activation reactions [25-27], but the current work has shown that this old methodology still has a large potential. The development of other direct C–H functionalization reactions based on radical chemistry is currently on-going together with further optimization of the presented reaction in our laboratory.

Supporting Information

Supporting Information File 1

Experimental details, characterization data of all products, and copies of NMR spectra.
[http://www.beilstein-journals.org/bjoc/content/supplementary/1860-5397-9-196-S1.pdf]

Acknowledgements

Authors thank Mr. Yuki Sugiura (Kanazawa University) for performing some preliminary experiments. Authors are also grateful to Drs. Shigeyoshi Kanoh, Katsuhiro Maeda, and Tomoyuki Ikai (Kanazawa University) for helpful discussions. This work was partially supported by a Grant-in-Aid for Scientific Research (C) (25460011) from The Ministry of Education, Culture, Sports, Science and Technology, Japan.

References

1. Pellissier, H. *Chem. Rev.* **2013,** *113,* 442–524. doi:10.1021/cr300271k
2. Matsuo, Y.; Isobe, H.; Tanaka, T.; Murata, Y.; Murata, M.; Komatsu, K.; Nakamura, E. *J. Am. Chem. Soc.* **2005,** *127,* 17148–17149. doi:10.1021/ja056077a
3. Hilt, G.; Hess, W.; Harms, K. *Org. Lett.* **2006,** *8,* 3287–3290. doi:10.1021/ol061153f
4. Jiang, B.; Tu, S.-J.; Kaur, P.; Wever, W.; Li, G. *J. Am. Chem. Soc.* **2009,** *131,* 11660–11661. doi:10.1021/ja904011s
5. Arai, S.; Koike, Y.; Hada, H.; Nishida, A. *J. Am. Chem. Soc.* **2010,** *132,* 4522–4523. doi:10.1021/ja910451j
6. Muñiz, K.; Martínez, C. *J. Org. Chem.* **2013,** *78,* 2168–2174. doi:10.1021/jo302472w
7. Souto, J. A.; Becker, P.; Iglesias, Á.; Muñiz, K. *J. Am. Chem. Soc.* **2012,** *134,* 15505–15511. doi:10.1021/ja306211q
8. Li, Y.-M.; Sun, M.; Wang, H.-L.; Tian, Q.-P.; Yang, S.-D. *Angew. Chem., Int. Ed.* **2013,** *52,* 3972–3976. doi:10.1002/anie.201209475
9. Egami, H.; Shimizu, R.; Kawamura, S.; Sodeoka, M. *Angew. Chem., Int. Ed.* **2013,** *52,* 4000–4003. doi:10.1002/anie.201210250
10. Renaud, P.; Sibi, M. P., Eds. *Radicals in Organic Synthesis;* Wiley-VCH: Weinheim, Germany, 2001. doi:10.1002/9783527618293
11. Tojino, M.; Ryu, I. Free-Radical-Mediated Multicomponent Coupling Reactions. In *Multicomponent Reactions;* Zhu, J.; Bienaymé, H., Eds.; Wiley-VCH: Weinheim, Germany; pp 169–198. doi:10.1002/3527605118.ch6
12. Wille, U. *Chem. Rev.* **2013,** *113,* 813–853. doi:10.1021/cr100359d
13. Recupero, F.; Punta, C. *Chem. Rev.* **2007,** *107,* 3800–3842. doi:10.1021/cr040170k
14. Ishihara, Y.; Baran, P. S. *Synlett* **2010,** 1733–1745. doi:10.1055/s-0030-1258123
15. Chen, H.; Sanjaya, S.; Wang, Y.-F.; Chiba, S. *Org. Lett.* **2013,** *15,* 212–215. doi:10.1021/ol303302r
16. Amaoka, Y.; Nagatomo, M.; Inoue, M. *Org. Lett.* **2013,** *15,* 2160–2163. doi:10.1021/ol4006757
17. Čeković, Ž. *Tetrahedron* **2003,** *59,* 8073–8090. doi:10.1016/S0040-4020(03)01202-X
18. Barton, D. H. R.; Beaton, J. M.; Geller, L. E.; Pechet, M. M. *J. Am. Chem. Soc.* **1960,** *82,* 2640–2641. doi:10.1021/ja01495a061
19. Barton, D. H. R.; Beaton, J. M.; Geller, L. E.; Pechet, M. M. *J. Am. Chem. Soc.* **1961,** *83,* 4076–4083. doi:10.1021/ja01480a030
20. Wolff, M. E. *Chem. Rev.* **1963,** *63,* 55–64. doi:10.1021/cr60221a004
21. Taniguchi, T.; Sugiura, Y.; Hatta, T.; Yajima, A.; Ishibashi, H. *Chem. Commun.* **2013,** *49,* 2198–2200. doi:10.1039/C3CC00130J
22. Taniguchi, T.; Yajima, A.; Ishibashi, H. *Adv. Synth. Catal.* **2011,** *353,* 2643–2647. doi:10.1002/adsc.201100315
23. Maity, S.; Naveen, T.; Sharma, U.; Maiti, D. *Org. Lett.* **2013,** *15,* 3384–3387. doi:10.1021/ol401426p
24. Shiri, M.; Zolfigol, M. A.; Kruger, H. G.; Tanbakouchian, Z. *Tetrahedron* **2010,** *66,* 9077–9106. doi:10.1016/j.tet.2010.09.057
25. Chen, X.; Engle, K. M.; Wang, D.-H.; Yu, J.-Q. *Angew. Chem., Int. Ed.* **2009,** *48,* 5094–5115. doi:10.1002/anie.200806273
26. Lyons, T. W.; Sanford, M. S. *Chem. Rev.* **2010,** *110,* 1147–1169. doi:10.1021/cr900184e
27. Ackermann, L. *Chem. Rev.* **2011,** *111,* 1315–1345. doi:10.1021/cr100412j

License and Terms

Beilstein Journal of Organic Chemistry

Iron-catalyzed decarboxylative alkenylation of cycloalkanes with arylvinyl carboxylic acids via a radical process

Jincan Zhao[1], Hong Fang[1], Jianlin Han[*1,2] and Yi Pan[*1]

Full Research Paper

Open Access

Address:
[1]School of Chemistry and Chemical Engineering, State of Key Laboratory of Coordination, Nanjing University, Nanjing, 210093, China and [2]Institute for Chemistry & BioMedical Sciences, Nanjing University, Nanjing, 210093, China

Email:
Jianlin Han[*] - hanjl@nju.edu.cn; Yi Pan[*] - yipan@nju.edu.cn

* Corresponding author

Keywords:
alkenylation; cycloalkanes; decarboxylative; $Fe(acac)_3$; free radical; sp^3 C–H bonds

Beilstein J. Org. Chem. **2013,** *9,* 1718–1723.
doi:10.3762/bjoc.9.197

Received: 01 July 2013
Accepted: 02 August 2013
Published: 21 August 2013

This article is part of the Thematic Series "Organic free radical chemistry".

Guest Editor: C. Stephenson

Abstract

A $Fe(acac)_3$-catalyzed decarboxylative coupling of 2-(aryl)vinyl carboxylic acids with cycloalkanes was developed by using DTBP as an oxidant through a radical process. This reaction tolerates a wide range of substrates, and products are obtained in good to excellent yields (71–95%). The reaction also shows excellent stereoselectivity, and only *trans*-isomers are obtained.

Introduction

Direct C–H functionalization has become one of the most useful and attractive tools in organic chemistry because it can construct carbon–carbon or carbon–heteroatom bonds in a highly atom economical manner [1-8]. Among all these C–H functionalization methods, the direct $C(sp^3)$–H functionalization attracts particular attention due to its low reactivity and challenging activation [9-11]. In previous studies, numerous transition-metal-catalyzed processes, such as Pd [12-18], Cu [19-23], Ru [24-27], Rh [28-31], Co [32-34], Au [35,36], Ir [37-39], Fe [40-43] and other metals [44-47], have been developed for sp^3 C–H activation reactions. Additionally, metal-free methodologies, which use TBHP, $PhI(OAc)_2$, TBAI, I_2 or Lewis/Brønsted acids, have also been employed for cross-dehydrogenative coupling reactions [48-57].

Owing to the general low reactivity of cycloalkane $C(sp^3)$–H bonds, the direct alkenylation of cycloalkanes with high selectivity and stereospecificity remains a great challenge and attracted a lot of attention in the past years. In 1996, the Fuchs group described the alkenylation of cyclohexane by a radical reaction with vinyl triflone [58]. In 2003, the Yao group reported that styryl cycloalkanes were prepared based on a radical substitution of cyclohydrocarbon units to (*E*)-β-nitrostyrenes by using the radical initiator benzoyl peroxide

[59]. Recently, the Liu group developed a copper-catalyzed decarboxylative coupling of vinylic carboxylic acids with simple alcohols and ethers in high yields. Cycloalkanes were also investigated in this catalytic system, though only moderate yields were obtained [60].

Several other groups have also found that Pd, Ag or Cu could catalyze the decarboxylative coupling of various aromatic, alkenyl, and alkynyl carboxylic acids [61-68]. Our group was surprised to find that low-cost $Fe(acac)_3$ could catalyze the direct alkenylation of cyclohexane sp^3 C–H bonds by decarboxylative couplings with high efficiency.

Results and Discussion

We initiated our investigation by reacting cinnamic acid (**1a**, 0.3 mmol) with cyclohexane (**2a**, 2 mL) in the presence of iron(II) chloride tetrahydrate (20 mol %) and 2.0 equiv of di-*tert*-butyl peroxide (DTBP) as the oxidant at 120 °C under nitrogen, which provided the expected (*E*)-(2-cyclohexylvinyl)benzene (**3a**), but in a moderate 54% yield (Table 1, entry 1). The use of aqueous TBHP as oxidant instead of DTBP reduced the yield to only 38% (Table 1, entry 2). With the help of 1,10-phenanthroline (30 mol %) as the ligand, the yield could be slightly improved to 68% (Table 1, entry 3). Iron(III) acetylacetonate provided a superior yield (91%) compared to the other Fe salts such as $FeCl_3$, ferrocene, Fe_2O_3 and Fe_3O_4 tested (Table 1, entries 4–8). Application of other oxidants such as $K_2S_2O_8$, H_2O_2 (30% aqueous solution) or TBPB did not afford any improvements (Table 1, entries 9–11). A decreased loading of $Fe(acac)_3$ to 10 mol % or an increased amount of DTBP to 5.0 equiv and a lower temperature (110 °C), decreased the yield to 63%, 69% and 79%, respectively (Table 1, entries 12–14). The reaction did not proceed without the iron catalyst or DTBP (Table 1, entries 15 and 16).

We then examined the substrate scope and limitation of the procedure by reacting cyclohexane with a variety of substituted cinnamic acid derivatives under the optimized conditions (Table 1, entry 8). As shown in Scheme 1, almost all of the tested substrates worked well in this reaction. Several substituents on the aromatic ring were tolerated and the position of these substituents showed almost no effect on the chemical yield. We also observed that electron-donating substituents, such as methyl or methoxy groups at any position of the ring, efficiently took part in the reaction with a slightly decreased yield in case of ortho-substituted products (Scheme 1, **3b**–**g**).

Table 1: Optimization of typical reaction conditions.[a]

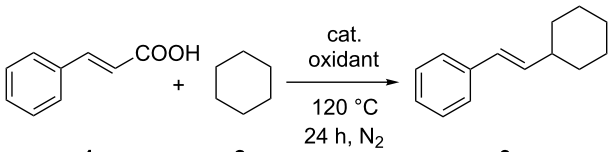

1a **2a** **3a**

Entry	cat. (mol %)	oxidant	yield (%)[b]
1	$FeCl_2{\cdot}4H_2O$ (20)	DTBP	54
2	$FeCl_2{\cdot}4H_2O$ (20)	TBHP	38
3	$FeCl_2{\cdot}4H_2O$ (20)	DTBP	68[c]
4	$FeCl_3$ (20)	DTBP	Trace
5	Ferrocene (20)	DTBP	74
6	Fe_2O_3 (20)	DTBP	78
7	Fe_3O_4 (20)	DTBP	80
8	$Fe(acac)_3$ (20)	DTBP	91
9	$Fe(acac)_3$ (20)	$K_2S_2O_8$	N.D.
10	$Fe(acac)_3$ (20)	H_2O_2[d]	21
11	$Fe(acac)_3$ (20)	TBPB	49
12	$Fe(acac)_3$ (10)	DTBP[e]	63
13[f]	$Fe(acac)_3$ (20)	DTBP	69
14	$Fe(acac)_3$ (20)[g]	DTBP	79
15	$Fe(acac)_3$ (20)	–	N.D.
16	–	DTBP	N.D.

[a]Catalytic conditions: cinnamic acid (0.3 mmol), cyclohexane (2 mL), iron catalyst (20 mol %), oxidant (2.0 equiv), 120 °C, 24 h, N_2. [b]Isolated yields based on cinnamic acid. [c]Using 1,10-phenanthroline (30 mol %) as the ligand. [d]30% aqueous solution. [e]5 equiv. [f]12 h. [g]110 °C.

Furthermore, a reaction of 2,6-disubstituted cinnamic acid **1m** lead to the expected product **3m**, which was obtained in a lower yield due to steric hindrance. In addition, heteroaryl-substituted acrylic acids can also be efficiently converted under these conditions. This was shown by the reaction of 3-(thiophen-2-yl)acrylic acid (**1p**) with cyclohexane furnishing the product **3p** in 89% yield. In general, the stereoselectivity of this reaction was excellent and only *trans*-isomers were obtained in all cases.

Next, other cycloalkanes, including cyclopentane, cycloheptane and cyclooctane, were reacted with different cinnamic acids **1**, giving products **4a**–**f** in 83–95% chemical yield (Scheme 2). As already shown for cyclohexane as a substrate, the reaction of other cycloalkanes performs equally well with a variety of cinammic acid derivatives under these conditions. It is noteworthy, that the decarboxylative cross-coupling with cyclooctane showed a higher efficiency than with smaller cycloalkanes.

Finally two control experiments were carried out to shed light on the reaction mechanism. Addition of the radical scavenger 2,2,6,6-tetramethylpiperidine *N*-oxide (TEMPO) or azobisisobutyronitrile (AIBN) completely inhibited the reaction, and almost no desired product was obtained. Based on these results and literature reports [69,70], a plausible mechanism for the radical oxidative coupling is illustrated in Scheme 3. At the beginning, Fe-catalyzed cleavage of DTBP by Fe(III) in the presence of cinnamic acid, gives *tert*-butoxy radical **A**, intermediate **B** and one acac. Next, a cyclohexane radical **C** is generated by the reaction between *tert*-butoxy radical **A** and cyclohexane. Subsequently, addition of cyclohexane radical **C** to the α-position of the double bond in **B** gives intermediate **D**. Finally, the radical intermediate **D** is oxidatively decarboxylated by Fe(III) to give product **3**, Fe(II) and carbon dioxide. The Fe(III) catalyst is then reformed via DTBP oxidation [71].

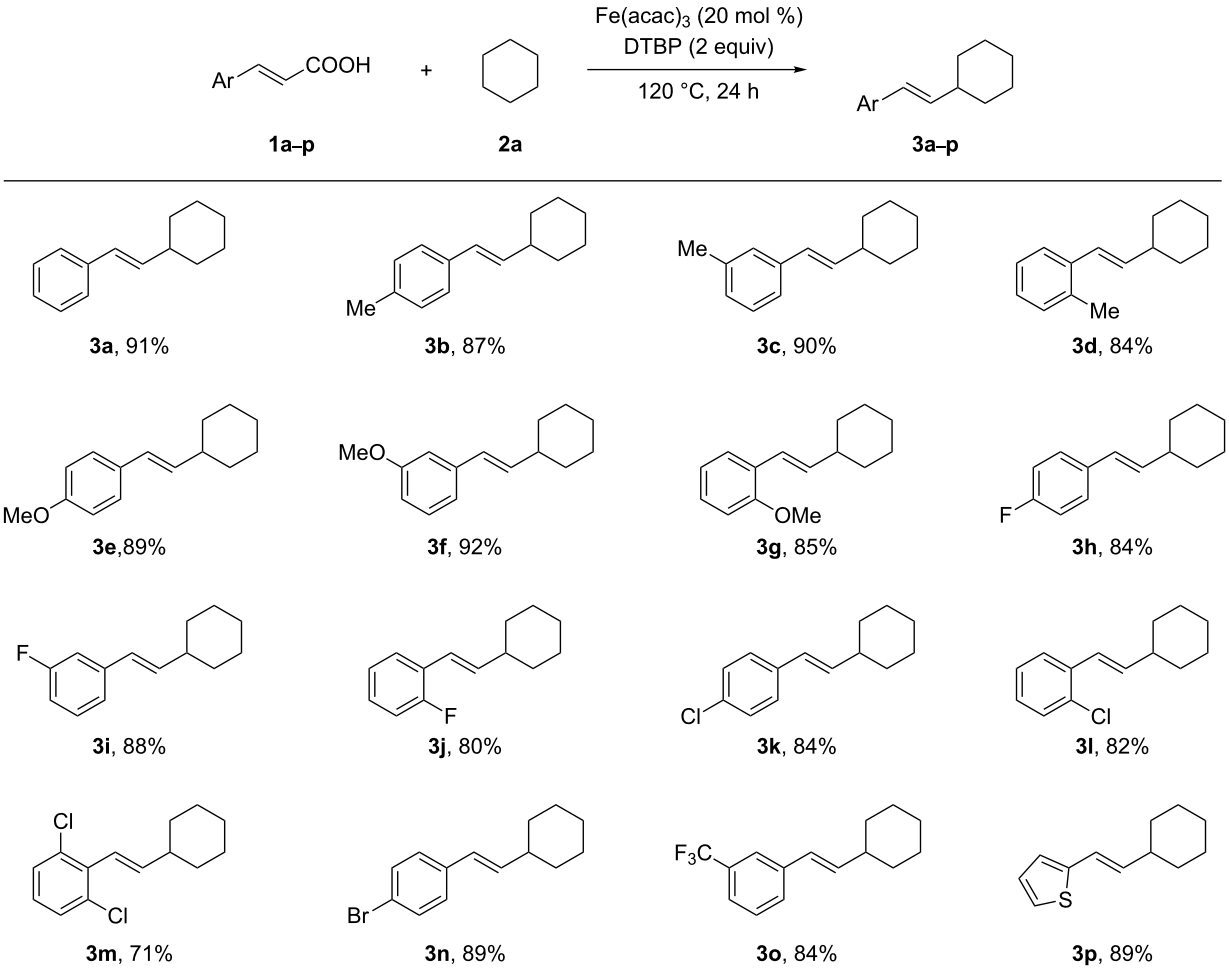

Scheme 1: $Fe(acac)_3$-catalyzed alkenylation of cyclohexane. Catalytic conditions: cinnamic acid (**1**) (0.3 mmol), cyclohexane (2 mL), $Fe(acac)_3$ (20 mol %), DTBP (2.0 equiv), 120 °C, 24 h, N_2. Yields are isolated yields based on cinnamic acid.

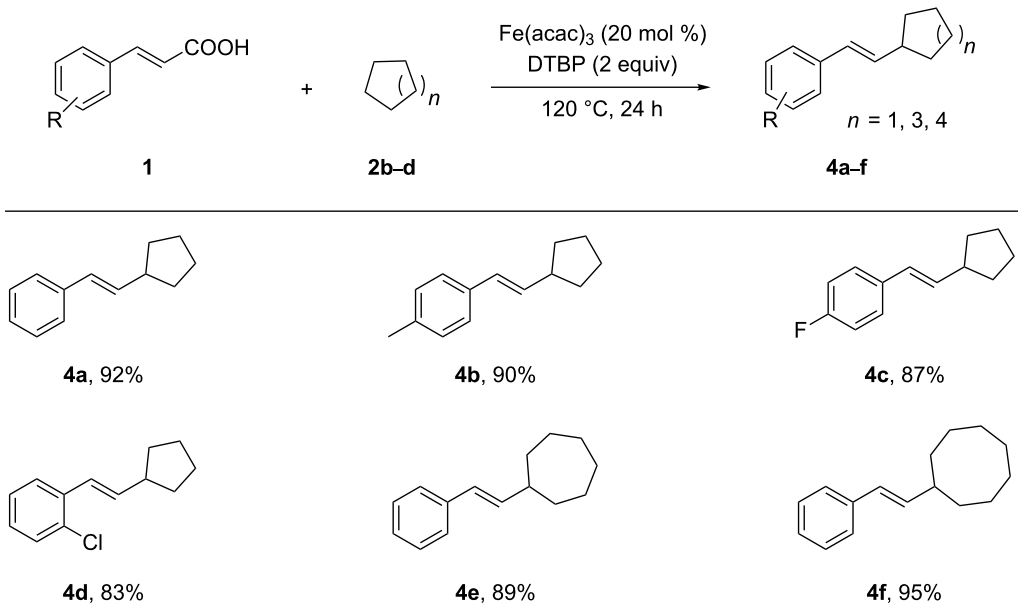

Scheme 2: $Fe(acac)_3$-catalyzed alkenylation of cyclopentan, cycloheptane and cyclooctane. Catalytic conditions: cinnamic acid (**1**) (0.3 mmol), cycloalkanes (2.0 mL), $Fe(acac)_3$ (20 mol %), DTBP (2 equiv), 120 °C, 24 h, N_2. Yields are isolated yields based on cinnamic acid.

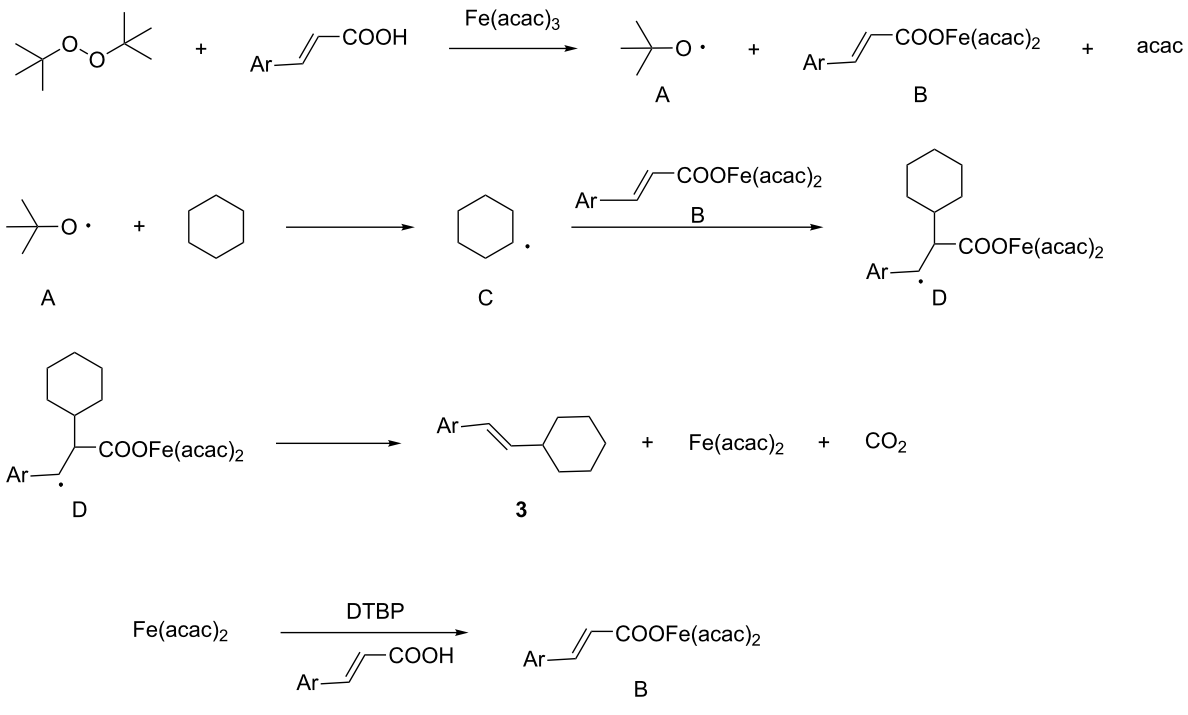

Scheme 3: A plausible pathway for the reaction.

Conclusion

In conclusion, an efficient procedure for the $Fe(acac)_3$-catalyzed direct alkenylation of sp^3 C–H bonds of cycloalkanes with DTBP as an oxidant has been reported. This method provides a useful strategy for the stereospecific synthesis of substituted *E*-alkenes. Various cinnamic acids and cycloalkanes are well-tolerated in this catalytic system with good to excellent chemical yields. The mechanism of this reaction has also been

studied, and a radical mechanism was proposed. Further studies on the alkenylation of other sp^3 C–H substrates are currently investigated in our laboratory.

Experimental

General procedure for the iron-catalyzed decarboxylative alkenylation of cycloalkanes: To a Schlenk tube equipped with a magnetic stir bar were added $Fe(acac)_3$ (21.2 mg, 0.06 mmol) and cinnamic acid (0.3 mmol) under a nitrogen atmosphere. Cycloalkane (2.0 mL, 15–25 mmol) and DTBP (di-*tert*-butyl peroxide, 0.6 mmol, 113 μL) were added under a nitrogen atmosphere and the resulting reaction mixture was stirred at 120 °C for 24 h. After cooling to room temperature and removal of volatiles, the products were isolated by flash column chromatography (PE).

Supporting Information

Supporting Information File 1

Experimental details and spectral data.
[http://www.beilstein-journals.org/bjoc/content/supplementary/1860-5397-9-197-S1.pdf]

Acknowledgements

We gratefully acknowledge the financial support from the National Natural Science Foundation of China (No. 21102071) and the Fundamental Research Funds for the Central Universities (No. 1107020522 and No. 1082020502). The Jiangsu 333 program (for Pan) and Changzhou Jin-Feng-Huang program (for Han) are also acknowledged.

References

1. Chen, X.; Engle, K. M.; Wang, D.-H.; Yu, J.-Q. *Angew. Chem., Int. Ed.* **2009,** *48,* 5094–5115. doi:10.1002/anie.200806273
2. Daugulis, O.; Do, H.-Q.; Shabashov, D. *Acc. Chem. Res.* **2009,** *42,* 1074–1086. doi:10.1021/ar9000058
3. Li, C.-J. *Acc. Chem. Res.* **2009,** *42,* 335–344. doi:10.1021/ar800164n
4. Coperet, C. *Chem. Rev.* **2010,** *110,* 656–680. doi:10.1021/cr900122p
5. Werner, H. *Angew. Chem., Int. Ed.* **2010,** *49,* 4714–4728. doi:10.1002/anie.201000306
6. Sun, C.-L.; Li, B.-J.; Shi, Z.-J. *Chem. Rev.* **2011,** *111,* 1293–1314. doi:10.1021/cr100198w
7. Campbell, A. N.; Stahl, S. S. *Acc. Chem. Res.* **2012,** *45,* 851–863. doi:10.1021/ar2002045
8. Kozhushkov, S. I.; Ackermann, L. *Chem. Sci.* **2013,** *4,* 886–896. doi:10.1039/c2sc21524a
9. Chatani, N.; Asaumi, T.; Yorimitsu, S.; Ikeda, T.; Kakiuchi, F.; Murai, S. *J. Am. Chem. Soc.* **2001,** *123,* 10935–10941. doi:10.1021/ja011540e
10. Jiang, X. F.; Shen, M.; Tang, Y.; Li, C. *Tetrahedron Lett.* **2005,** *46,* 487–489. doi:10.1016/j.tetlet.2004.11.113
11. Song, C.-X.; Cai, G.-X.; Farrell, T. R.; Jiang, Z.-P.; Li, H.; Gan, L.-B.; Shi, Z.-J. *Chem. Commun.* **2009,** 6002–6004. doi:10.1039/b911031c
12. Guin, S.; Rout, S. K.; Banerjee, A.; Nandi, S.; Patel, B. K. *Org. Lett.* **2012,** *14,* 5294–5297. doi:10.1021/ol302438z
13. Rousseaux, S.; Liégault, B.; Fagnou, K. *Chem. Sci.* **2012,** *3,* 244–248. doi:10.1039/c1sc00458a
14. Solé, D.; Mariani, F.; Fernández, I.; Sierra, M. A. *J. Org. Chem.* **2012,** *77,* 10272–10284. doi:10.1021/jo301924e
15. Wasa, M.; Chan, K. S. L.; Zhang, X.-G.; He, J.; Miura, M.; Yu, J.-Q. *J. Am. Chem. Soc.* **2012,** *134,* 18570–18572. doi:10.1021/ja309325e
16. Yin, Z.; Sun, P. *J. Org. Chem.* **2012,** *77,* 11339–11344. doi:10.1021/jo302125h
17. Saget, T.; Perez, D.; Cramer, N. *Org. Lett.* **2013,** *15,* 1354–1357. doi:10.1021/ol400380y
18. Zhang, S.-Y.; He, G.; Nack, W. A.; Zhao, Y.; Li, Q.; Chen, G. *J. Am. Chem. Soc.* **2013,** *135,* 2124–2127. doi:10.1021/ja312277g
19. Li, Z.; Li, C.-J. *J. Am. Chem. Soc.* **2004,** *126,* 11810–11811. doi:10.1021/ja0460763
20. Xie, J.; Huang, Z.-Z. *Angew. Chem., Int. Ed.* **2010,** *49,* 10181–10185. doi:10.1002/anie.201004940
21. Yang, F.; Li, J.; Xie, J.; Huang, Z.-Z. *Org. Lett.* **2010,** *12,* 5214–5217. doi:10.1021/ol102252n
22. Rout, S. K.; Guin, S.; Ghara, K. K.; Banerjee, A.; Patel, B. K. *Org. Lett.* **2012,** *14,* 3982–3985. doi:10.1021/ol301756y
23. Xia, R.; Niu, H.-Y.; Qu, G.-R.; Guo, H.-M. *Org. Lett.* **2012,** *14,* 5546–5549. doi:10.1021/ol302640e
24. Pastine, S. J.; Gribkov, D. V.; Sames, D. *J. Am. Chem. Soc.* **2006,** *128,* 14220–14221. doi:10.1021/ja064481j
25. Rankin, M. A.; Schatte, G.; McDonald, R.; Stradiotto, M. *J. Am. Chem. Soc.* **2007,** *129,* 6390–6391. doi:10.1021/ja071684e
26. Deng, G.; Zhao, L.; Li, C.-J. *Angew. Chem., Int. Ed.* **2008,** *47,* 6278–6282. doi:10.1002/anie.200801544
27. Wang, M.-Z.; Zhou, C.-Y.; Wong, M.-K.; Che, C.-M. *Chem.–Eur. J.* **2010,** *16,* 5723–5735. doi:10.1002/chem.200902387
28. Shi, L.; Tu, Y.-Q.; Wang, M.; Zhang, F.-M.; Fan, C.-A.; Zhao, Y.-M.; Xia, W.-J. *J. Am. Chem. Soc.* **2005,** *127,* 10836–10837. doi:10.1021/ja0528331
29. Jo, E.-A.; Lee, J.-H.; Jun, C.-H. *Chem. Commun.* **2008,** 5779–5781. doi:10.1039/b814166e
30. Rakshit, S.; Patureau, F. W.; Glorius, F. *J. Am. Chem. Soc.* **2010,** *132,* 9585–9587. doi:10.1021/ja104305s
31. Kuninobu, Y.; Nakahara, T.; Takeshima, H.; Takai, K. *Org. Lett.* **2013,** *15,* 426–428. doi:10.1021/ol303353m
32. Harden, J. D.; Ruppel, J. V.; Gao, G.-Y.; Zhang, X. P. *Chem. Commun.* **2007,** 4644–4646. doi:10.1039/b710677g
33. Hung-Low, F.; Krogman, J. P.; Tye, J. W.; Bradley, C. A. *Chem. Commun.* **2012,** *48,* 368–370. doi:10.1039/c1cc15458c
34. Lu, H.; Hu, Y.; Jiang, H.; Wojtas, L.; Zhang, X. P. *Org. Lett.* **2012,** *14,* 5158–5161. doi:10.1021/ol302511f
35. Horino, Y.; Yamamoto, T.; Ueda, K.; Kuroda, S.; Toste, F. D. *J. Am. Chem. Soc.* **2009,** *131,* 2809–2811. doi:10.1021/ja808780r
36. Bhunia, S.; Ghorpade, S.; Huple, D. B.; Liu, R.-S. *Angew. Chem., Int. Ed.* **2012,** *51,* 2939–2942. doi:10.1002/anie.201108027
37. DeBoef, B.; Pastine, S. J.; Sames, D. *J. Am. Chem. Soc.* **2004,** *126,* 6556–6557. doi:10.1021/ja049111e
38. Pan, S.; Endo, K.; Shibata, T. *Org. Lett.* **2011,** *13,* 4692–4695. doi:10.1021/ol201907w
39. Obora, Y.; Ogawa, S.; Yamamoto, N. *J. Org. Chem.* **2012,** *77,* 9429–9433. doi:10.1021/jo3019347
40. Wang, Z.; Zhang, Y.; Fu, H.; Jiang, Y.; Zhao, Y. *Org. Lett.* **2008,** *10,* 1863–1866. doi:10.1021/ol800593p

41. Zhang, S.-Y.; Tu, Y.-Q.; Fan, C.-A.; Zhang, F.-M.; Shi, L. *Angew. Chem., Int. Ed.* **2009,** *48,* 8761–8765. doi:10.1002/anie.200903960
42. Pan, S.; Liu, J.; Li, H.; Wang, Z.; Guo, X.; Li, Z. *Org. Lett.* **2010,** *12,* 1932–1935. doi:10.1021/ol100670m
43. Bloom, S.; Pitts, C. R.; Woltornist, R.; Griswold, A.; Holl, M. G.; Lectka, T. *Org. Lett.* **2013,** *15,* 1722–1724. doi:10.1021/ol400424s
44. Vadola, P. A.; Sames, D. *J. Am. Chem. Soc.* **2009,** *131,* 16525–16528. doi:10.1021/ja906480w
45. Yoshikai, N.; Mieczkowski, A.; Matsumoto, A.; Ilies, L.; Nakamura, E. *J. Am. Chem. Soc.* **2010,** *132,* 5568–5569. doi:10.1021/ja100651t
46. Qian, B.; Xie, P.; Xie, Y.; Huang, H. *Org. Lett.* **2011,** *13,* 2580–2583. doi:10.1021/ol200684b
47. Liu, X.; Sun, B.; Xie, Z.; Qin, X.; Liu, L.; Lou, H. *J. Org. Chem.* **2013,** *78,* 3104–3112. doi:10.1021/jo4000674
48. Chen, L.; Shi, E.; Liu, Z.; Chen, S.; Wei, W.; Li, H.; Xu, K.; Wan, X. *Chem.–Eur. J.* **2011,** *17,* 4085–4089. doi:10.1002/chem.201100192
49. He, T.; Yu, L.; Zhang, L.; Wang, L.; Wang, M. *Org. Lett.* **2011,** *13,* 5016–5019. doi:10.1021/ol201779n
50. Huang, J.; Li, L.-T.; Li, H.-Y.; Husan, E.; Wang, P.; Wang, B. *Chem. Commun.* **2012,** *48,* 10204–10206. doi:10.1039/c2cc35450k
51. Li, L.-T.; Li, H.-Y.; Xing, L.-J.; Wen, L.-J.; Wang, P.; Wang, B. *Org. Biomol. Chem.* **2012,** *10,* 9519–9522. doi:10.1039/c2ob26636a
52. Mai, W.-P.; Wang, H.-H.; Li, Z.-C.; Yuan, J.-W.; Xiao, Y.-M.; Yang, L.-R.; Mao, P.; Qu, L.-B. *Chem. Commun.* **2012,** *48,* 10117–10119. doi:10.1039/c2cc35279f
53. Feng, J.; Liang, S.; Chen, S.-Y.; Zhang, J.; Fu, S.-S.; Yu, X.-Q. *Adv. Synth. Catal.* **2012,** *354,* 1287–1292. doi:10.1002/adsc.201100920
54. Shi, E.; Shao, Y.; Chen, S.; Hu, H.; Liu, Z.; Zhang, J.; Wan, X. *Org. Lett.* **2012,** *14,* 3384–3387. doi:10.1021/ol3013606
55. Wang, F.-F.; Luo, C.-P.; Wang, Y.; Deng, G.; Yang, L. *Org. Biomol. Chem.* **2012,** *10,* 8605–8608. doi:10.1039/c2ob26604k
56. Zhu, Y.-p.; Jia, F.-c.; Liu, M.-c.; Wu, L.-m.; Cai, Q.; Gao, Y.; Wu, A.-x. *Org. Lett.* **2012,** *14,* 5378–5381. doi:10.1021/ol302613q
57. Zhu, Y.-p.; Liu, M.-c.; Jia, F.-c.; Yuan, J.-j.; Gao, Q.-h.; Lian, M.; Wu, A.-x. *Org. Lett.* **2012,** *14,* 3392–3395. doi:10.1021/ol301366p
58. Xiang, J.; Fuchs, P. L. *J. Am. Chem. Soc.* **1996,** *118,* 11986–11987. doi:10.1021/ja962790b
59. Jang, Y.-J.; Shih, Y.-K.; Liu, J.-Y.; Kuo, W.-Y.; Yao, C.-F. *Chem.–Eur. J.* **2003,** *9,* 2123–2128. doi:10.1002/chem.200204571
60. Cui, Z.; Shang, X.; Shao, X.-F.; Liu, Z.-Q. *Chem. Sci.* **2012,** *3,* 2853–2858. doi:10.1039/c2sc20712e
61. Forgione, P.; Brochu, M.-C.; St-Onge, M.; Thesen, K. H.; Bailey, M. D.; Bilodeau, F. *J. Am. Chem. Soc.* **2006,** *128,* 11350–11351. doi:10.1021/ja063511f
62. Gooßen, L. J.; Rudolphi, F.; Oppel, C.; Rodríguez, N. *Angew. Chem., Int. Ed.* **2008,** *47,* 3043–3045. doi:10.1002/anie.200705127
63. Kim, H.; Lee, P. H. *Adv. Synth. Catal.* **2009,** *351,* 2827–2832. doi:10.1002/adsc.200900502
64. Wang, Z.; Ding, Q.; He, X.; Wu, J. *Org. Biomol. Chem.* **2009,** *7,* 863–865. doi:10.1039/b821870f
65. Zhang, F.; Greaney, M. F. *Angew. Chem., Int. Ed.* **2010,** *49,* 2768–2771. doi:10.1002/anie.200906921
66. Wang, Z. T.; Zhu, L.; Yin, F.; Su, Z. Q.; Li, Z.; Li, C. *J. Am. Chem. Soc.* **2012,** *134,* 4258–4263. doi:10.1021/ja210361z
67. Yin, F.; Wang, Z.; Li, Z.; Li, C. *J. Am. Chem. Soc.* **2012,** *134,* 10401–10404. doi:10.1021/ja3048255
68. Liu, X.; Wang, Z.; Cheng, X.; Li, C. *J. Am. Chem. Soc.* **2012,** *134,* 14330–14333. doi:10.1021/ja306638s
69. Liu, Z.-Q.; Sun, L.; Wang, J.-G.; Han, J.; Zhao, Y.-K.; Zhou, B. *Org. Lett.* **2009,** *11,* 1437–1439. doi:10.1021/ol900145u
70. Yang, H.; Yan, H.; Sun, P.; Zhu, Y.; Lu, L.; Liu, D.; Rong, G.; Mao, J. *Green Chem.* **2013,** *15,* 976–981. doi:10.1039/c3gc37131j
71. Chowdhury, S.; Roy, S. *J. Org. Chem.* **1997,** *62,* 199–200. doi:10.1021/jo951991f

License and Terms

Beilstein Journal of Organic Chemistry

Damage of polyesters by the atmospheric free radical oxidant $NO_3^{\bullet}$: a product study involving model systems

Catrin Goeschen and Uta Wille*

Full Research Paper

Open Access

Address:
ARC Centre of Excellence for Free Radical Chemistry and Biotechnology, School of Chemistry and Bio21 Institute, The University of Melbourne, 30 Flemington Road, Parkville, VIC 3010, Australia

Email:
Uta Wille* - uwille@unimelb.edu.au

* Corresponding author

Keywords:
environmental oxidants; free radicals; nitrate radicals; polyester degradation; product studies; reaction mechanisms

Beilstein J. Org. Chem. **2013,** *9,* 1907–1916.
doi:10.3762/bjoc.9.225

Received: 12 July 2013
Accepted: 23 August 2013
Published: 20 September 2013

This article is part of the Thematic Series "Organic free radical chemistry".

Guest Editor: C. Stephenson

Abstract

Manufactured polymer materials are used in increasingly demanding applications, but their lifetime is strongly influenced by environmental conditions. In particular, weathering and ageing leads to dramatic changes in the properties of the polymers, which results in decreased service life and limited usage. Despite the heavy reliance of our society on polymers, the mechanism of their degradation upon exposure to environmental oxidants is barely understood. In this work, model systems of important structural motifs in commercial high-performing polyesters were used to study the reaction with the night-time free radical oxidant $NO_3^{\bullet}$ in the absence and presence of other radical and non-radical oxidants. Identification of the products revealed 'hot spots' in polyesters that are particularly vulnerable to attack by $NO_3^{\bullet}$ and insight into the mechanism of oxidative damage by this environmentally important radical. It is suggested that both intermediates as well as products of these reactions are potentially capable of promoting further degradation processes in polyesters under environmental conditions.

Introduction

Polymers are without doubt the most important industrial materials, which have benefited our society in numerous ways. Improving the performance of polymers by making them long lasting and durable is therefore highly desirable not only for the consumer but also for the environment, because expensive waste removal strategies can be avoided or at least reduced. The most important way to improve polymer longevity is a detailed knowledge of the mechanism by which they undergo degradation upon exposure to the environment. It is quite surprising that, despite the heavy reliance of our society on polymeric materials, the chemical mechanism of polymer degradation is by far not fully understood.

It has generally been assumed that polymer degradation involves a radical-mediated autoxidation mechanism, which propagates through hydrogen abstraction by an intermediate peroxyl radical ROO$^\bullet$. Although this autoxidation mechanism was initially proposed only for a limited number of polymers that contain activated allylic hydrogen atoms (for example rubber materials) [1-5], it has been universally adapted as general mechanism for polymer degradation. However, recent comprehensive high-level theoretical studies by Coote et al. clearly revealed that polymers possessing only saturated alkyl chains, for example polyesters, will not propagate autoxidation, particularly because the ROO–H bond-dissociation energy (BDE) is usually less than the BDE for unactivated R–H bonds [6].

Polymer surface coatings, which are widely used in the building, automotive and aircraft industries to protect the underlying material from degradation, are commonly high-performing polyesters, which are exposed to significant environmental stress, in particular high temperatures, humidity and UV irradiation. These materials are in direct contact with the troposphere, which is the lowest part of the atmosphere and a highly oxidizing environment. While the oxidation power during daytime can be assigned to the presence of hydroxyl radicals, HO$^\bullet$, the highly electrophilic nitrate radical, $NO_3^\bullet$, is responsible for the tropospheric transformation processes at night. $NO_3^\bullet$, which is formed through reaction of the atmospheric pollutants nitrogen dioxide, $NO_2^\bullet$, with ozone, O_3 (Scheme 1a) [7,8], reacts with organic compounds through various pathways, such as hydrogen abstraction (HAT) and addition to π systems. Most importantly, $NO_3^\bullet$ is one of the strongest free-radical oxidants known [$E(NO_3^\bullet/NO_3^-)$ = 2.3–2.5 V vs NHE] [9], and recent product studies by us revealed that $NO_3^\bullet$ readily damages aromatic amino acids and pyrimidine nucleosides through an oxidative pathway [10-13]. Thus, the ease by which model compounds of biologically important macromolecules are attacked by $NO_3^\bullet$ leads inevitably to the question, how resistant synthetic polymers are towards oxidative damage by this environmental free-radical species, in particular in conjunction with other atmospheric radical and non-radical oxidants, which are in direct contact with these materials. Is it possible that such reactions could lead to structural modifications in the polymer that may render the material more susceptible to further damage, for example through photodegradation and/or autoxidation? To our knowledge, the role of environmental free-radical oxidants as mediator of polymer degradation has barely been assessed so far.

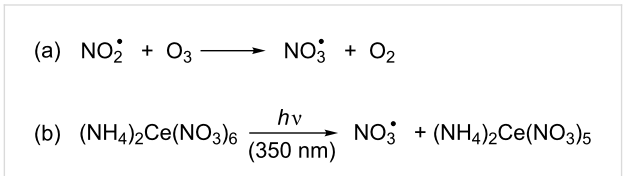

Scheme 1: Generation of $NO_3^\bullet$ (a) in the atmosphere, (b) under experimental conditions.

In light of this, we have now performed the first product study of the reaction of $NO_3^\bullet$ with model substrates relevant to the polymeric structures in high-performing polyesters in the presence and absence of other oxidants, in particular $NO_2^\bullet$, O_2 and O_3. This work not only reveals new insight into the degradation mechanism in polyesters upon exposure to important environmental oxidants, but it also enables identification of vulnerable sites ('hot spots') in the polymer, which could open up new pathways to polyester degradation under environmental conditions that have not been considered before. This study might therefore be regarded as a first step on a long journey towards a revised mechanistic scheme for polymer degradation, which is crucial for the development of improved materials.

Results and Discussion

Experimental conditions

The compounds that served in this work as models for substructures typically found in surface-coating polyesters are shown in Figure 1. These comprise aromatic moieties, such as phthalic and benzoic esters **1** and **3**, respectively, as well as aliphatic diesters of type **2**. The esters were used as methylates or neopentylates, where the latter provided a simplified model for diesters of neopentyl glycol, which is the commonly used diol component in such polyesters.

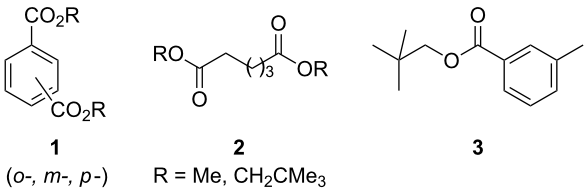

Figure 1: Polyester-model systems studied in this work.

All experiments were performed in solution, using two different methods to produce $NO_3^\bullet$ in situ in the presence of the respective substrate **1**–**3**. In experiments where $NO_3^\bullet$ was used in the absence of other radical and non-radical oxidants, $NO_3^\bullet$ was generated at room temperature from cerium(IV) ammonium nitrate (CAN) through photo-induced electron transfer at an irradiation wavelength of λ = 350 nm (Scheme 1b) [11-13].

In a typical experiment, the polyester-model substrate and four equivalents of CAN were dissolved in acetonitrile and the solu-

tions degassed by sonicating under a continuous argon stream, followed by irradiation and aqueous work-up. Control experiments performed under exclusion of light showed no reaction, which ensured that the observed products indeed resulted from the reaction involving $NO_3^•$ and not from CAN, which is also an oxidizing agent [$E^0(Ce^{4+}/Ce^{3+})$ = 1.61 V vs. NHE] [14].

In another set of experiments, $NO_3^•$ was obtained through the reaction shown in Scheme 1a, where to a solution of the respective polyester-model substrate in anhydrous dichloromethane at 10 °C an excess of liquid $NO_2^•$ was added and ozonized O_2 was bubbled through the mixture at a low flow rate, followed by aqueous work-up. Through control experiments it was revealed that none of the various polyester-model compounds reacted to a noticeable extent with $NO_2^•$ or ozonized O_2 in isolation. Reactions with this $NO_3^•$ source in acetonitrile gave identical products to those in dichloromethane. However, additional products were also obtained in small amounts, which could not be identified. It is possible that these resulted from hydrolysis of dinitrogen pentoxide, N_2O_5, which is formed through reversible recombination of $NO_2^•$ with $NO_3^•$, by trace amounts of water present in acetonitrile, but this was not further explored. By performing the radical reactions in dichloromethane, potentially interfering reactions involving the solvent, which could complicate the reaction outcome and mechanic considerations, were avoided. It should also be noted that $NO_2^•$ is in equilibrium with its dimer dinitrogen tetroxide, N_2O_4. In solution the $NO_2^•/N_2O_4$ equilibrium constant favours the dimer [15], and N_2O_4 can be oxidized with O_3 to give N_2O_5. Gas-phase kinetic studies revealed that N_2O_5 reacts with unsaturated compounds several orders of magnitude slower than $NO_3^•$ [16] and does not readily nitrate deactivated aromatic compounds in solution [17].

In all experiments we have used $NO_3^•$ in excess in order to obtain sufficient amounts of material to enable product separation by preparative HPLC using UV detection at wavelengths of λ = 214 and 230 nm and identification by spectroscopic characterization. Details are given in the Experimental section. HPLC chromatograms of the relevant raw reaction mixtures are shown in Supporting Information File 1. Although under natural conditions $NO_3^•$ will be present in much lower concentrations compared to the polyester, our experimental procedure ensured that vulnerable sites in the polyester-model systems could be located with certainty. Due to the repeated purification by HPLC, yields could not be obtained for any of these reactions. However, since this study is aimed at obtaining insight into the nature of the products in order to qualitatively assess how such chemical modifications might affect polymer stability under environmental conditions, exact yields are not required. It is reasonable to assume that only very few damaged sites are initially required in the polyester to promote further degradation on a large scale through chain and other processes.

Reaction of polyester-model compounds **1**–**3** with $NO_3^•$ from CAN photolysis

Study of the products formed in the reaction of $NO_3^•$ obtained from CAN photolysis provides the opportunity to gain insight into the mechanism of oxidative damage in the absence of other radical and non-radical oxidants. In Scheme 2 the products of the reaction of the polyester-model compounds **1**–**3** with $NO_3^•$ are shown.

It was interesting to note that no reaction occurred with the isomeric phthalates **1** and the adipic acid derivatives **2**. In the case of the former this could be explained by the fact that the aromatic ring is very deactivated due to the two electron-withdrawing ester substituents, so that oxidative electron transfer (ET) by $NO_3^•$ is not possible. Also, $NO_3^•$ induced HAT from the ester, particularly the neopentyl moiety, which is a potential pathway that should most likely occur at the methylene groups α to the ester oxygen atom [18-20], is apparently not a feasible pathway. This finding is of potential relevance for the autoxidation mechanism, which proposes hydrogen abstraction by $ROO^•$ as propagating step. Thus, although $NO_3^•$ is not only much more reactive than $ROO^•$ [7,8], and the BDE for the O_2NO–H bond is with 427 kJ mol^{-1} also considerably higher than that of

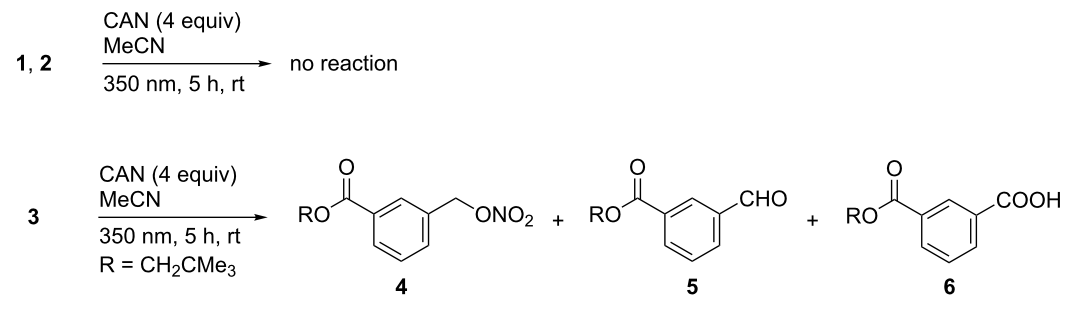

Scheme 2: Products of the reaction of polyester model compounds **1**–**3** with $NO_3^•$ in the absence of other radical and non-radical oxidants.

the ROO–H bond (which is about 360 ± 20 kJ mol^{-1}) [21], the fact that no hydrogen abstraction from the ester units was observed in the reactions with $NO_3^•$ demonstrates that saturated alkyl groups are quite inert to radical attack.

On the other hand, in the case of neopentyl ester of *m*-toluic acid (**3**), which differs from the phthalates by replacement of one ester group by a σ-donating methyl group, reaction with $NO_3^•$ leads to selective oxidative modification of the methyl side chain, while a reaction at the ester moiety was, again, not observed. Analytical HPLC of the raw reaction mixture recorded at λ = 230 nm revealed besides unreacted starting material **3** (which was identified by comparison with an authentic sample but not isolated), nitrate **4**, aldehyde **5** and carboxylic acid **6** as most important products (see Supporting Information File 1). Other products were formed in too minor amounts to enable isolation. Further, HPLC analysis revealed that shorter reaction times or a smaller excess of CAN shifted the product ratio towards the nitrate **4** at expense of the higher oxidized products **5** and **6** (data not shown).

The observed side-chain oxidation in **3** by $NO_3^•$ is similar to the outcome of the reaction of thymidine nucleosides with $NO_3^•$, where oxidative transformation of the methyl substituent in the heterocyclic base occurs exclusively [13]. Concentration–time profiles revealed for the latter reactions that formation of a nitrate occurs first, which is converted to an aldehyde and subsequently into a carboxylic acid [13]. It is not unreasonable to assume that such a step-wise oxidation also occurs in the reaction involving **3**, which could be rationalized by the mechanism shown in Scheme 3.

Because of the high oxidation power of $NO_3^•$, it is proposed that the reaction is initiated by ET at the aromatic ring through an addition–elimination pathway, as has been suggested from time-resolved transient spectroscopic studies for the reaction of $NO_3^•$ with alkylaromatic compounds [22,23]. In the absence of any reactants the resulting radical cation $\mathbf{3}^{•+}$ undergoes deprotonation to give benzyl radical **7**, in analogy to the mechanism of the $NO_3^•$-induced oxidation of aromatic amino acids and nucleosides [10-13]. This mechanism is supported by findings by Steenken et al., who showed that in the reaction of alkylaromatic compounds with $NO_3^•$ ET and deprotonation can occur practically in a concerted fashion in the case of highly electron-rich arenes, while in the case of less activated alkylaromatic compounds the intermediate radical cation has a lifetime on the nanosecond time scale [23]. It was further demonstrated that deprotonation of arylradical cations is accelerated by nitrate (NO_3^-) that is present in the reaction system as 'byproduct' of the oxidation process and as ligand in CAN, and which acts as a Brønsted base [23]. It is important to note that the formation of radical intermediate **7** could principally also occur in one step through $NO_3^•$-induced benzylic HAT in **3** (not shown). However, it appears from the outcome of the reactions with the neopentyl derivatives of **1** and **2** that HAT by $NO_3^•$ is not competitive with $NO_3^•$-induced ET in these systems [7,8,24,25].

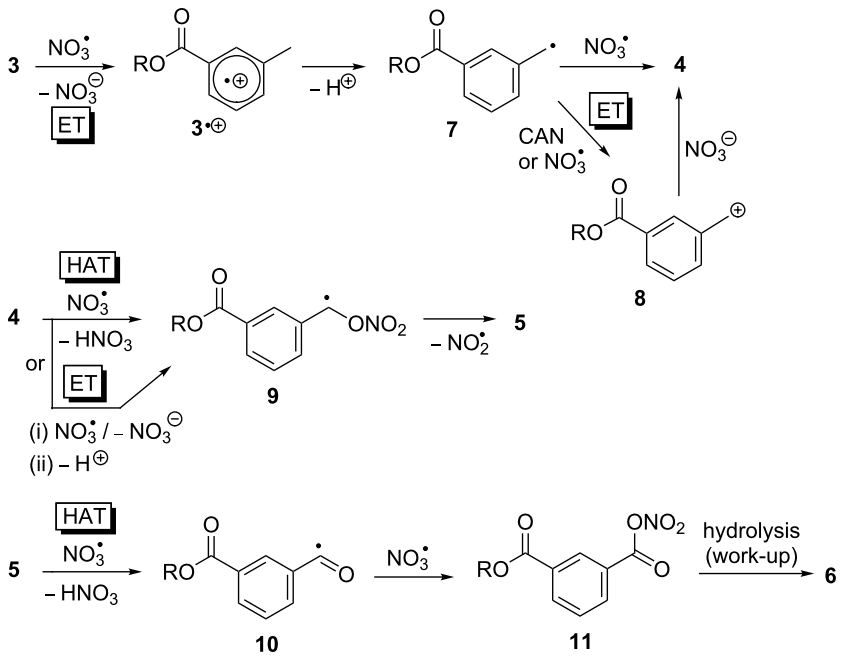

Scheme 3: Proposed mechanism for the reaction of *m*-toluic acid neopentyl ester (**3**) with $NO_3^•$ in the absence of radical and non-radical oxidants.

An initial ET step and formation of an intermediate radical cation $\mathbf{3}^{\bullet+}$ is further supported by the outcomes of the reaction of **3** with $NO_3^\bullet$ in the presence of $NO_2^\bullet$, which will be outlined below.

Formation of nitrate **4** could principally occur via two different pathways, e.g. through direct trapping of **7** by $NO_3^\bullet$ or in a two-step process by first $NO_3^\bullet$ or CAN-induced ET, followed by quenching of the resulting benzyl cation **8** through ligand exchange from CAN. Although the nature of the intermediate was not further explored in this work, our previous experiments involving thymidines provided strong indications that the reaction likely involves a cationic intermediate [13].

Conversion of the nitrate ester **4** into the aldehyde **5** could proceed through either an intermediate benzyl radical **9**, which could be formed through a direct HAT by $NO_3^\bullet$ [26], or through a sequential ET–deprotonation pathway in analogy to the initial reaction step. The labile O–NO_2 bond in **9** is expected to undergo rapid β-scission to give aldehyde **5** with release of $NO_2^\bullet$ [27,28]. The latter is too unreactive to initiate a radical process in this system, which has been confirmed through independent control experiments.

Oxidation of aldehyde **5** to the carboxylic acid **6** under the experimental conditions could by initiated through abstraction of the aldehyde hydrogen atom by $NO_3^\bullet$ [29], followed by trapping of the resulting acyl radical **10** by $NO_3^\bullet$ to give the mixed anhydride **11**, which could be hydrolysed to the acid **6** during aqueous work-up and/or purification by HPLC.

The mechanism in Scheme 3 shows that more than one equivalent of $NO_3^\bullet$ is required to produce the observed products **4**–**6**. Such multiple attacks seem unlikely under environmental conditions, where [$NO_3^\bullet$] is low [7,8]. However, from the previous work on $NO_3^\bullet$-induced oxidative damage of biological molecules, it appears that an already damaged compound is more prone to attack by another $NO_3^\bullet$ than an undamaged substrate [11-13].

Reaction of polyester-model compounds **1**–**3** with $NO_3^\bullet$ from $NO_2^\bullet/O_3$

Under environmental conditions, however, $NO_3^\bullet$ is not an isolated reactant, but is always accompanied by other radicals and non-radical oxidants, such as $NO_2^\bullet$, O_3, and O_2, respectively, which principally could become involved in these reactions through trapping of reactive intermediates. Thus, in order to explore the role of such additional reactants on the outcome of $NO_3^\bullet$-induced oxidative damage of polyester-model compounds, we have used the reaction in Scheme 1a to produce $NO_3^\bullet$.

Similar to the reaction with $NO_3^\bullet$ in isolation, no reaction of $NO_3^\bullet$ with phthalates **1** and adipic esters **2** was observed in the presence of $NO_2^\bullet$, O_3, and O_2, which is a further confirmation for the low reactivity of saturated alkyl chains. On the other hand, the reaction with the *m*-toluic acid ester **3** was very fast. According to the HPLC spectrum of the raw reaction mixture (see Supporting Information File 1), the starting material was completely consumed and considerably more products were obtained in the presence of $NO_2^\bullet$, O_3, and O_2 compared to the reaction of $NO_3^\bullet$ in isolation.

The main reaction pathways lead to products possessing a nitroaromatic ring, such as the isomeric mono-nitroaromatic compounds **12a**–**d**, the dinitrated product **13** and two isomeric species **14a**,**b**, which carry both a nitro and a hydroxy substituent (Scheme 4). The nitro compound **15** appears to be the only product that results from oxidative modification of the methyl substituent at the aromatic ring. HPLC analysis indicated that additional products were formed in this reaction (see Supporting Information File 1), but their amounts were too small to enable isolation and identification. The proposed mechanism leading to the various products **12**–**15** is outlined in Scheme 5.

Similar to the mechanism shown in Scheme 3, initial ET should lead to the radical cation $\mathbf{3}^{\bullet+}$. However, in contrast to the reaction with $NO_3^\bullet$ in isolation, where benzylic deprotonation occurred exclusively, in the presence of excess $NO_2^\bullet$ the radical cation $\mathbf{3}^{\bullet+}$ is trapped prior to deprotonation to form the isomeric σ-complexes **16** [30]. The aromatic ring is restored through loss of a proton, which leads to the nitroaromatic products **12a**–**d**. The proposed competition in radical cation $\mathbf{3}^{\bullet+}$ between trapping by $NO_2^\bullet$ and benzylic deprotonation is supported by the fact that the nitromethylene compound **15** is obtained as byproduct in this reaction. The latter likely results from recombination of $NO_2^\bullet$ with benzyl radical **7**, which is obviously formed in small amounts. Thus, in contrast to the reaction of **3** with $NO_3^\bullet$ in isolation, formation of stable reaction products in the presence of $NO_2^\bullet$, O_3 and O_2, such as the nitroaromatic compounds **12**, requires only one equivalent of $NO_3^\bullet$ and should readily occur even at low atmospheric [$NO_3^\bullet$].

Formation of the tetrasubstituted products **13** and **14** proceeds likely through a second $NO_3^\bullet$-induced ET in the mono-nitrated compounds **12a**,**b**, where the intermediately formed radical cation $\mathbf{12}^{\bullet+}$ can be trapped by $NO_2^\bullet$ to give the dinitro compound **13** after deprotonation. This mechanism is supported by previous findings in the reaction of aromatic amino acids with $NO_3^\bullet$ in the presence of $NO_2^\bullet$, O_3, and O_2, where it was shown that dinitrated products result from a step-wise nitration of the aromatic ring [10]. On the other hand, to our knowledge, forma-

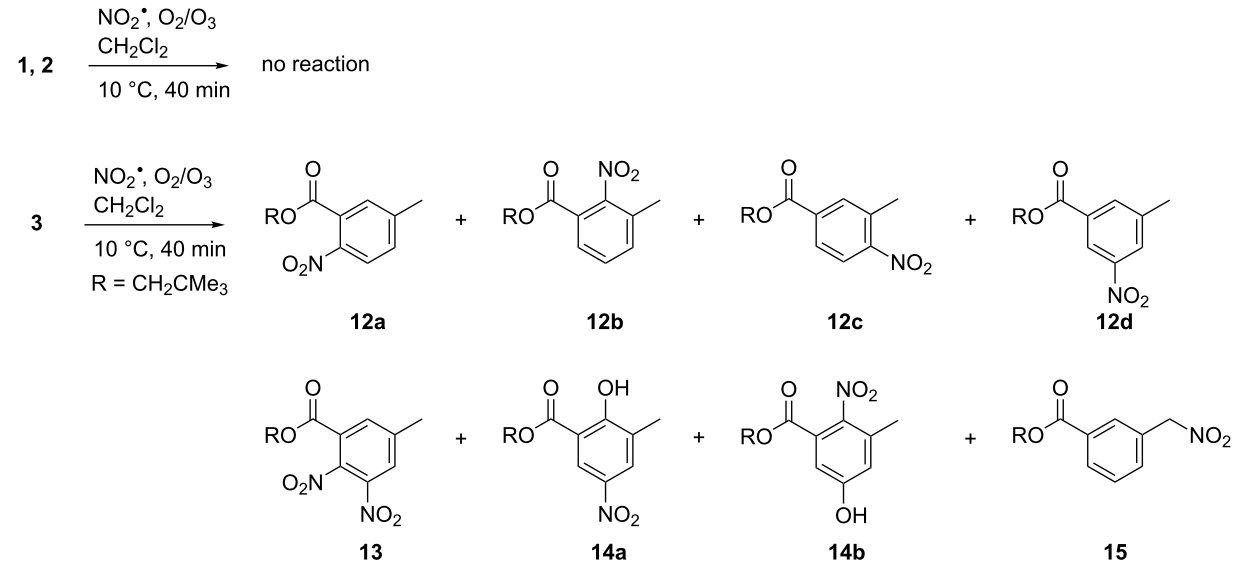

Scheme 4: Products of the reaction of polyester-model compounds **1**–**3** with $NO_3^•$ in presence of $NO_2^•$, O_3, and O_2.

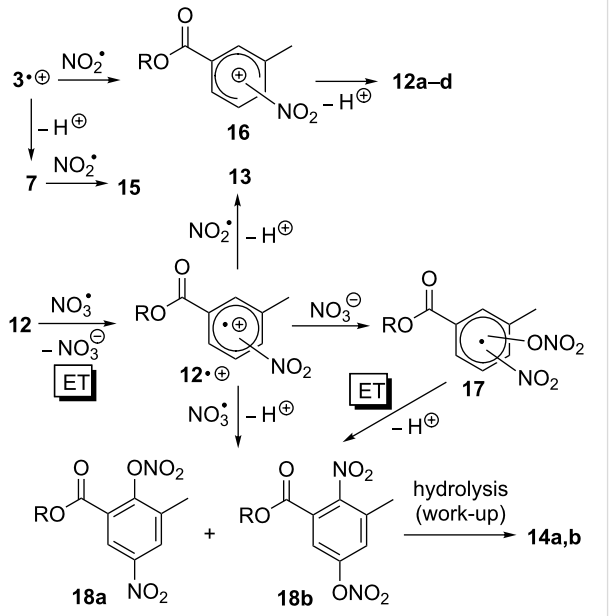

Scheme 5: Proposed mechanism for the reaction of *m*-toluic acid neopentyl ester (**3**) with $NO_3^•$ in presence of $NO_2^•$, O_3 and O_2.

tion of hydroxylated products of type **14** in the reaction of $NO_3^•$ with aromatic compounds is unprecedented. We propose that these compounds result from hydrolysis of the corresponding nitrates **18** during work-up and/or HPLC purification. Potential pathways to the latter could involve either trapping of the radical cation $\mathbf{12}^{•+}$ by $NO_3^•$, followed by deprotonation, or recombination of $\mathbf{12}^{•+}$ with NO_3^- (the byproduct of the $NO_3^•$-induced ET). The resulting radical adduct **17** could be oxidized in a subsequent step by either $NO_3^•$ or $NO_2^•$ [$E(NO_2^•/NO_2^-)$ = 1.04 V vs NHE] [31], which is followed by deprotonation to restore the aromatic system.

Conclusion

We have shown for the first time that certain aromatic moieties in commercial polyesters (e.g. alkylated benzoic acid derivatives of type **3**) are vulnerable to damage by the environmental free-radical oxidant $NO_3^•$. The reaction is most likely initiated by ET to give a highly reactive aryl radical cation intermediate $\mathbf{3}^{•+}$, whose fate depends strongly on the reaction conditions. In the absence of radical-trapping agents, in particular $NO_2^•$, benzylic deprotonation is the exclusive pathway that ultimately leads to oxidative functionalization of the alkyl side chain through formation of nitrates **4**, aldehydes **5** and carboxylic acids **6**. In this work we have not specifically explored the role of O_2 on the reaction outcome, but our recent studies on the $NO_3^•$-induced oxidative damage in thymidines showed that any residual O_2 present in the system solely accelerates production of the higher oxidized compounds **5** and **6**, while no different products are formed [13]. It is reasonable to expect a similar outcome for the reaction of $NO_3^•$ with **3** in the presence of O_2. On the other hand, when the reaction of $NO_3^•$ with **3** is performed in the presence of $NO_2^•$, benzylic deprotonation in radical cation $\mathbf{3}^{•+}$ can hardly compete with trapping of the latter by $NO_2^•$, which leads to formation of the isomeric nitroaromatic compounds **12a**–**d** as well as the dinitro and hydroxylated products **13** and **14**, respectively, that result from further $NO_3^•$-induced oxidation of **12**. An additional, however only minor pathway yields the nitromethylene compound **15**, which

is formed via benzyl radical **7**. Although we have not studied the nature of the reactive intermediates formed in these reactions, it is difficult to rationalize formation of the ring-substituted products **12**–**14** through a mechanism that involves benzylic HAT by $NO_3^•$. The reaction must therefore be initiated by oxidation of the aromatic ring, which is in accordance with literature findings [22,23].

The different outcome of the reaction of $NO_3^•$ with **3** under the various conditions could be explained by the different concentration of $NO_2^•$ and NO_3^- in these systems. Thus, CAN photolysis generates $NO_3^•$ in the presence of excess NO_3^-, which acts as Brønsted base and mediates deprotonation of the initial radical cation $\mathbf{3}^{•+}$ to give benzyl radical **7** [23], followed by transformation to the products **4**–**6**. In the $NO_2^•/O_3$ system, on the other hand, $[NO_3^-] = [\mathbf{3}^{•+}]$ and deprotonation in $\mathbf{3}^{•+}$ cannot complete with its trapping by excess $NO_2^•$, which leads to the nitroaromatic species **12**–**14**.

In contrast to the high reactivity of the aromatic ring in **3**, phthalate-building blocks as well as ester moieties possessing only saturated alkyl chains appear to be inert to attack by $NO_3^•$ through either ET or HAT, respectively, under the various conditions explored. Our observation that $NO_3^•$-induced HAT in the ester moieties does not occur, although $NO_3^•$ is much more reactive than $ROO^•$ and the O_2NO–H bond is considerably stronger than the ROO–H bond, could be taken as indication that an autoxidation mechanism involving $ROO^•$ as chain carrier cannot operate in intact polyesters with saturated alkyl chains, which is in support of the theoretical findings by Coote et al. [6].

None of the various polyester-model compounds explored in this work reacted with $NO_2^•$ and O_3 in isolation. However, this outcome is not unexpected, since the reactivity of $NO_2^•$ is much lower than that of $NO_3^•$. In particular, the oxidation power of $NO_2^•$ is not sufficient to induce ET in deactivated aromatic compounds [31]. Likewise, although O_3 is a strong oxidant, it does not react via ET transfer. Rapid reactions are only expected for π systems, such as alkenes, which are not present in intact polyester materials (however, it should be noted that these structural motifs may be formed in the polymer through degradation processes).

What are the potential implications of $NO_3^•$-induced oxidative damage in aromatic building blocks for polyester stability? Although there are no experimental data available yet, it is possible to make some predictions from the outcome of this work, which can be used to guide future studies on polyester stability upon exposure to the environment. It is important to realize that under environmental conditions only few sites of initial damage are required to trigger degradation of the polymer material on a large scale. Identification of the reaction products using simplified model systems enables to obtain some general insight into the mechanism of radical-induced oxidative damage in these materials. Thus, in the reaction of the aromatic ester **3** with $NO_3^•$ it could be speculated that both intermediates as well as products could principally promote further damage in the polymer. For example, the radical cation $\mathbf{3}^{•+}$ is itself a highly oxidizing intermediate, which could, when embedded in the polyester matrix, induce an ET cascade across the polymer involving aromatic moieties, where oxidative damage may end up at positions remote from the initial site of attack. The benzyl radical **7** resulting from deprotonation in $\mathbf{3}^{•+}$ on the other hand, could be trapped by O_2 and be involved as chain carrier in subsequent transformations that lead to degradation.

Of the various products formed in the reaction of $NO_3^•$ with **3** under the different reaction conditions, in particular the aldehyde **5** and the nitroaromatic species **12**–**14** are expected to be photochemically active compounds. Exposure of the carbonyl or nitro moieties to UV light leads to photoexcited intermediates, which are strong hydrogen-atom abstractors in Norrish-type II photoreactions [32,33]. In the polymer matrix, where the various polyester chains are tightly packed, both intra- and interstrand reactions are likely to occur, such as photo-induced hydrogen abstractions, which could provide pathways to C-radicals in unactivated alkyl chains that would usually be inert to attack by peroxyl radicals.

To conclude, this work provides strong indications for a number of so far unexplored pathways that could promote degradation of high-performing polyesters under environmental conditions. It is obvious that detailed kinetic data and product analyses from exposure studies involving both simple as well as more complex model systems, including melamine cross-linker moieties, are required (for example from smog chamber experiments), to obtain further insight into the role of environmental free-radical oxidants, such as $NO_3^•$ and $HO^•$, in promoting polyester degradation.

Experimental

General procedures

The irradiations were performed under a continuous gas flow (argon) in a Rayonet photochemical reactor (λ = 350 nm). Before the irradiations, residual oxygen was removed from the reaction mixture by bubbling argon through the solution while sonicating. ^1H and ^{13}C NMR spectra were taken on a Varian Unity Inova 500 spectrometer [500 MHz (^1H), 125 MHz (^{13}C)] or on an Agilent MR 400 spectrometer [400 MHz (^1H), 100 MHz (^{13}C)] in deuterated DMSO. If necessary the assignment of the chemical shifts was confirmed by utilising 2D NMR

techniques. GC–MS (EI, 70 eV) analysis was run on an Agilent 7890A GC/5975C MSD, column from SUPELCO 30 m, 0.32 mm ID, 0.25 μm film thickness fused silica capillary column, using the temperature program $70_5 \rightarrow 250_{17}$ heating rate 5 ºC min^{-1} (40 min in total). HRMS was conducted by ionising the samples via ESI into a Thermo-Finnigan LTQ FT–ICR hybrid mass spectrometer or an Agilent 6520 LC/Q-TOF mass spectrometer with an electrospray ionizing source coupled to an Agilent 1100 LC system equipped with a variable wavelength detector. The crude products were purified by reversed-phase HPLC (Phenomenex C18, 150 × 21.2 mm, 5 micron, preparative column, 8 mL min^{-1}) using an Agilent 1100 LC system equipped with a variable wavelength detector by running a gradient from 50% water in acetonitrile to 100% acetonitrile within 2–3 hours. UV detection was performed at λ = 214 and 230 nm. Purity was assessed by analytical RP HPLC on an SGE Protecol C18 5 μM 250 × 4.6 mm column.

Reactions with $NO_3^\bullet$ from CAN photolysis

In a typical experiment 1.0 mmol of the model substrate and 4.0 mmol of CAN were dissolved in 5 and 95 mL of absolute acetonitrile, respectively, and the individual solutions degassed by sonicating under a continuous argon stream. The solutions were combined and irradiated (λ = 350 nm) for a period of 5 h at room temperature. The reaction was quenched by addition of brine (50 mL) and water (50 mL) and extracted with ethyl acetate. The combined organic fractions were dried ($MgSO_4$) and the solvent removed in vacuum. The crude product mixture was separated by reversed-phase HPLC.

Neopentyl 3-(nitratomethyl)benzoate (**4**): ^{1}H NMR (DMSO-d_6, 500 MHz) δ 8.08 (td, = 1.8, 0.6 Hz, 1H), 8.01 (ddd, *J* = 7.8, 1.8, 1.2 Hz, 1H), 8.75 (dtd, *J* = 7.6, 1.2, 0.6 Hz, 1H), 7.60 (td, *J* = 7.7, 0.5 Hz, 1H), 5.66, (s, 2H), 3.99 (s, 2H), 0.99 (s, 9H); ^{13}C NMR (DMSO-d_6, 125 MHz) δ 165.7, 134.5, 133.7, 130.7, 130.3, 130.2, 129.9, 74.9, 74.2, 31.8, 26.7; HRMS (*m*/*z*): calcd for $C_{13}H_{17}NO_5$ + H, 268.1185; found, 268.1181; HRMS (*m*/*z*): calcd for $C_{12}{}^{13}CH_{17}NO_5$ + H, 269.1219; found, 269.1212.

Neopentyl 3-formylbenzoate (**5**): ^{1}H NMR (DMSO-d_6, 500 MHz) δ 10.10 (s, 1H), 8.45 (td, *J* = 1.7, 0.5 Hz, 1H), 8.27 (ddd, *J* = 7.7, 1.8, 1.2 Hz, 1H), 8.17 (td, *J* = 7.7, 1.5 Hz, 1H), 7.77 (td, *J* = 7.7, 0.5 Hz, 1H), 4.02 (s, 2H), 1.00 (s, 9H); ^{13}C NMR (DMSO-d_6, 125 MHz) δ 192.8, 164.9, 136.5, 134.5, 133.6, 130.7, 130.0, 129.9, 73.9, 31.4, 26.2; HRMS (*m*/*z*): calcd for $C_{13}H_{16}O_3$ + H: 221.1178. Found: 221.1170; HRMS (*m*/*z*): calcd for $C_{12}{}^{13}CH_{16}O_3$ + H, 222.1211; found, 222.1204.

Neopentyl 3-carboxylbenzoate (**6**): ^{1}H NMR (DMSO-d_6, 500 MHz) δ 13.28 (s(br), 1H), 8.49 (td, *J* = 1.8, 0.5 Hz, 1H), 8.19 (d, *J* = 1.7 Hz, 1H), 8.18 (dd, *J* = 1.8, 0.5 Hz, 1H), 7.66 (td, *J* = 7.8, 0.6 Hz, 1H), 4.00 (s, 2H), 0.98 (s, 9H); ^{13}C NMR (DMSO-d_6, 125 MHz) δ 166.9, 165.4, 134.2, 133.6, 131.9, 130.7, 130.1, 129.9, 74.2, 31.8, 26.7; HRMS (*m*/*z*): calcd for $C_{13}H_{16}O_4$ + Na, 259.0946; found, 259.0940; HRMS (*m*/*z*): calcd for $C_{12}{}^{13}CH_{16}O_4$ + Na, 260.0980; found, 260.0974.

Reactions with $NO_3^\bullet$ generated from $NO_2^\bullet/O_3$

In a typical experiment 0.5 mL liquid $NO_2^\bullet$ (15 mmol) was added to 1.00 mmol of the model substrate in anhydrous dichloromethane (15 mL) at 10 °C, and ozonised O_2 was bubbled through the mixture at a low flow rate. After 40 min the reaction was quenched by addition of 10 mL aq $NaHCO_3$, the phases were separated and the aqueous phase extracted with dichloromethane. The combined organic fractions were dried over $MgSO_4$, concentrated and the reaction products isolated and purified by repeated preparative HPLC. It was not possible to state the exact [$NO_2^\bullet$] in these experiments, since an indeterminable amount evaporated prior to its reaction with O_3.

Neopentyl 5-methyl-2-nitrobenzoate (**12a**): ^{1}H NMR (DMSO-d_6, 500 MHz) δ 7.95 (d, *J* = 8.3 Hz, 1H), 7.65 (dd, *J* = 1.8, 0.9 Hz, 1H), 7.60 (ddd, *J* = 8.3, 1.9, 0.9 Hz, 1H), 3.94 (s, 2H), 2.45 (s, 3H), 0.92 (s, 9H); ^{13}C NMR (DMSO-d_6, 100 MHz) δ 165.4, 145.2, 133.3, 130.5, 127.1, 124.6, 75.5, 31.6, 26.5, 21.2. The signal of the carbon atom carrying the nitro substituent (C-2) could not be observed; MS (EI, 70 eV) *m*/*z* (%): 251.1 (1) [M^+], 164.1 (100) [$M^+ - OCH_2C(CH_3)_3$], 57.2 (31) [$C(CH_3)_3^+$]; IR (cm^{-1}) ν: 2960, 1730, 1527, 1367, 1347, 1257,1200, 1072, 833.

Neopentyl 3-methyl-2-nitrobenzoate (**12b**): ^{1}H NMR (DMSO-d_6, 500 MHz) δ 7.89 (d, *J* = 7.7 Hz, 1H), 7.76 (d, *J* = 7.6 Hz, 1H), 7.67 (d, *J* = 7.7 Hz, 1H), 3.95 (s, 2H), 2.30 (s, 3H), 0.94 (s, 9H); ^{13}C NMR (DMSO-d_6, 100 MHz) δ 163.6, 136.7, 131.4, 130.7, 129.2, 123.1, 75.5, 31.6, 26.5, 16.8. The signal of the carbon atom carrying the nitro substituent (C-2) could not be observed; MS (EI, 70 eV) *m*/*z* (%): 251.1 (1) [M^+], 164.1 (100) [$M^+ - OCH_2C(CH_3)_3$], 57.1 (40) [$C(CH_3)_3^+$]; IR (cm^{-1}) ν: 2958, 1727, 1533, 1369, 1287.

Neopentyl 3-methyl-4-nitrobenzoate (**12c**): ^{1}H NMR (DMSO-d_6, 500 MHz) δ 8.08 (d, *J* = 8.5 Hz, 1H), 8.06 (d, *J* = 1.5 Hz, 1H), 8.00 (dd, *J* = 8.5, 1.9 Hz, 1H), 4.03 (s, 2H), 2.56 (s, 3H), 1.01 (s, 9H); ^{13}C NMR (DMSO-d_6, 100 MHz) δ 164.7, 152.2, 138.8, 133.7, 133.5, 128.4, 125.3, 74.6, 31.8, 26.7, 19.5; MS (EI, 70 eV) *m*/*z* (%): 251.1 (4) [M^+], 164.1 (100) [$M^+ - OCH_2C(CH_3)_3$], 57.1 (90) [$C(CH_3)_3^+$]; IR (cm^{-1}) ν: 2960, 1723, 1526, 1367, 1259,1192, 118, 1026, 839, 735.

Neopentyl 5-methyl-3-nitrobenzoate (**12d**): ^{1}H NMR (DMSO-d_6, 500 MHz) δ 8.45 (m, 1H), 8.35 (ddd, *J* = 2.5, 1.5,

0.8 Hz, 1H), 8.20 (dt, J = 1.8, 1.1 Hz, 1H), 4.05 (s, 2H), 2.53 (s, 3H), 1.01 (s, 9H); ^{13}C NMR (DMSO-d_6, 100 MHz) δ 164.5, 148.4, 141.7, 136.0, 131.6, 128.4, 121.3, 74.7, 31.8, 26.7, 21.0; MS (EI, 70 eV) m/z (%): 251.1 (1) [M^+], 164.1 (91) [$M^+ - OCH_2C(CH_3)_3$], 57.1 (100) [$C(CH_3)_3^+$]; IR (cm^{-1}) ν: 2960, 1656, 1541, 1289.

Neopentyl 5-methyl-2,3-dinitrobenzoate (**13**): ^{1}H NMR (DMSO-d_6, 500 MHz) δ 8.14 (t, J = 1.7 Hz, 1H), 8.05 (dt, J = 7.8, 1.4 Hz, 1H), 7.79 (ddd, J = 7.7, 1.8, 1.3 Hz, 1H), 5.88 (s, 2H), 4.01 (s, 2H), 1.01 (s, 9H); ^{13}C NMR (DMSO-d_6, 125 MHz) δ 163.3, 145.8, 140.7, 138.6, 133.9, 132.6, 124.7, 75.3, 31.9, 26.6, 17.0; MS (EI, 70 eV) m/z (%): 296.1 (1) [M^+], 209.0 (34) [$M^+ - OCH_2C(CH_3)_3$], 57.1 (100) [$C(CH_3)_3^+$]; IR (cm^{-1}) ν: 2958, 1724, 1548, 1347, 756.

Neopentyl 2-hydroxy-3-methyl-5-nitrobenzoate (**14a**): ^{1}H NMR (DMSO-d_6, 500 MHz) δ 11.57 (s(br), 1H), 8.48 (d, J = 2.9 Hz, 1H), 8.35 (dd, J = 2.7, 1.2 Hz, 1H), 4.11 (s, 2H), 2.30 (s, 3H), 1.02 (s, 9H); ^{13}C NMR (DMSO-d_6, 100 MHz) δ 168.5, 164.2, 130.8, 129.0, 123.7, 112.4, 75.1, 31.8, 26.6, 15.9. The signal of the carbon atom carrying the nitro substituent (C-5) could not be observed. MS (EI, 70 eV) m/z (%): 267.1 (24) [M^+], 180.0 (100) [$M^+ - OCH_2C(CH_3)_3$], 57.1 (25) [$C(CH_3)_3^+$]; IR (cm^{-1}) ν: 2966, 1676, 1335, 1173.

Neopentyl 5-hydroxy-3-methyl-2-nitrobenzoate (**14b**): ^{1}H NMR (DMSO-d_6, 500 MHz) δ 10.74 (s(br), 1H), 7.12 (dd, J = 2.7, 0.6 Hz, 1H), 6.99 (dd, J = 2.6, 0.8 Hz, 1H), 3.91 (s, 2H), 2.25 (s, 3H), 0.93 (s, 9H); ^{13}C NMR (DMSO-d_6, 100 MHz) δ 164.2, 159.3, 142.4, 133.6, 126.7, 121.5, 114.9, 75.4, 31.6, 26.5, 17.7; MS (EI, 70 eV) m/z (%): 267.1 (21) [M^+], 180.0 (100) [$M^+ - OCH_2C(CH_3)_3$], 57.1 (69) [$C(CH_3)_3^+$]; IR (cm^{-1}) ν: 2959, 1724, 1532, 1370, 1347, 1333, 1238, 1097.

Neopentyl 3-(nitromethylene)benzoate (**15**): ^{1}H NMR (DMSO-d_6, 500 MHz) δ 8.53 (d, J = 1.7 Hz, 1H), 8.48 (dd, J = 2.1 Hz, 1H), 4.08 (s, 2H), 2.47 (s, 3H), 1.02 (s, 9H); ^{13}C NMR (DMSO-d_6, 125 MHz) δ 165.7, 135.9, 131.8, 131.7, 130.7, 130.5, 129.8, 78.7, 74.2, 31.8, 26.7; MS (EI, 70 eV) m/z (%): 205.1 (100) [$M^+ - NO_2$], 164.1 (34) [$M^+ - OCH_2C(CH_3)_3$], 57.1 (31) [$C(CH_3)_3^+$]; IR (cm^{-1}) ν: 2963, 1720, 1557, 1370, 1282, 1198.

Supporting Information

Supporting Information File 1

HPLC chromatograms of raw reaction mixtures.
[http://www.beilstein-journals.org/bjoc/content/supplementary/1860-5397-9-225-S1.pdf]

Acknowledgements

The work was supported by the Australian Research Council under the Centre of Excellence Program. We thank Philip Barker for helpful discussions.

References

1. Bolland, J. L. *Proc. R. Soc. London, Ser. A* **1946,** *186,* 218–236. doi:10.1098/rspa.1946.0040
2. Bolland, J. L.; Gee, G. *Trans. Faraday Soc.* **1946,** *42,* 244–252. doi:10.1039/tf9464200244
3. Bolland, J. L.; ten Have, P. *Discuss. Faraday Soc.* **1947,** *2,* 252–260. doi:10.1039/df9470200252
4. Bateman, L. *Q. Rev., Chem. Soc.* **1954,** *8,* 147–167.
5. Bolland, J. L.; Gee, G. *Trans. Faraday Soc.* **1946,** *42,* 236–243. doi:10.1039/tf9464200236
6. Gryn'ova, G.; Hodgson, J. L.; Coote, M. L. *Org. Biomol. Chem.* **2011,** *9,* 480–490. doi:10.1039/c0ob00596g
7. Wayne, R. P.; Barnes, I.; Biggs, P.; Burrows, J. P.; Canosa-Mas, C. E.; Hjorth, J.; Le Bras, G.; Moortgat, G. K.; Perner, D.; Restelli, G.; Sidebottom, H. *Atmos. Environ., Part A* **1991,** *25,* 1–203. doi:10.1016/0960-1686(91)90192-A
8. Wayne, R. P.; Barnes, I.; Biggs, P.; Burrows, J. P.; Canosa-Mas, C. E.; Hjorth, J.; Le Bras, G.; Moortgat, G. K.; Perner, D.; Restelli, G.; Sidebottom, H. *The Nitrate Radical: Physics, Chemistry and the Atmosphere - Air Pollution Report 31;* CEC: Brussels, 1991.
9. Neta, O.; Huie, R. E. *J. Phys. Chem.* **1986,** *90,* 4644–4648. doi:10.1021/j100410a035
10. Goeschen, C.; Wibowo, N.; White, J. M.; Wille, U. *Org. Biomol. Chem.* **2011,** *9,* 3380–3385. doi:10.1039/c0ob01186j
11. Sigmund, D. C. E.; Wille, U. *Chem. Commun.* **2008,** 2121–2123. doi:10.1039/b803456g
12. Goeschen, C.; White, J. M.; Gable, R. W.; Wille, U. *Aust. J. Chem.* **2012,** *65,* 427–437. doi:10.1071/CH11446
13. Wille, U.; Goeschen, C. *Aust. J. Chem.* **2011,** *64,* 833–842. doi:10.1071/CH11102
14. Nair, V.; Deepthi, A. *Chem. Rev.* **2007,** *107,* 1862–1891. doi:10.1021/cr068408n
15. Redmond, T. F.; Wayland, B. B. *J. Phys. Chem.* **1968,** *72,* 1626–1629. doi:10.1021/j100851a040
16. Pfrang, C.; Martin, R. S.; Canosa-Mas, C. E.; Wayne, R. P. *Phys. Chem. Chem. Phys.* **2006,** *8,* 354–363. doi:10.1039/b510835g
17. Bak, R. R.; Smallridge, A. J. *Tetrahedron Lett.* **2001,** *42,* 6767–6769. doi:10.1016/S0040-4039(01)01378-8
18. Lindsay Smith, J. R.; Nagatomi, E.; Stead, A.; Waddington, D. J.; Bévière, S. D. *J. Chem. Soc., Perkin Trans. 2* **2000,** 1193–1198. doi:10.1039/b000507j
19. Lindsay Smith, J. R.; Nagatomi, E.; Waddington, D. J. *J. Chem. Soc., Perkin Trans. 2* **2000,** 2248–2258. doi:10.1039/b004589f
20. Lindsay Smith, J. R.; Nagatomi, E.; Stead, A.; Waddington, D. J. *J. Chem. Soc., Perkin Trans. 2* **2001,** 1527–1533. doi:10.1039/b103555j
21. Luo, Y. R. *Comprehensive Handbook of Chemical Bond Energies;* CRC Press: Boca Raton, Florida, 2007. doi:10.1201/9781420007282
22. Ito, O.; Akiho, S.; Iino, M. *J. Org. Chem.* **1989,** *54,* 2436–2440. doi:10.1021/jo00271a038
23. Del Giacco, T.; Baciocchi, E.; Steenken, S. *J. Phys. Chem.* **1993,** *97,* 5451–5456. doi:10.1021/j100123a003

24. Atkinson, R. *J. Phys. Chem. Ref. Data* **1991,** *20,* 459–507. doi:10.1063/1.555887
25. Wayne, R. P. Experimental study of the nitrate radical. In *N-Centered Radicals;* Alfassi, Z. B., Ed.; John Wiley & Sons: New York, 1998; pp 207–258.
26. Shono, T.; Yamamoto, Y.; Takigawa, K.; Maekawa, H.; Ishifune, M.; Kashimura, S. *Chem. Lett.* **1994,** *23,* 1045–1048. doi:10.1246/cl.1994.1045
27. Wille, U. *J. Phys. Org. Chem.* **2011,** *24,* 672–681. doi:10.1002/poc.1808
28. Wille, U. *Chem. Rev.* **2013,** *113,* 813–853. doi:10.1021/cr100359d
29. D'Anna, B.; Andresen, Ø.; Gefen, Z.; Nielsen, C. J. *Phys. Chem. Chem. Phys.* **2001,** *3,* 3057–3063. doi:10.1039/b103623h
30. Suzuki, H.; Mori, T. *J. Chem. Soc., Perkin Trans. 2* **1997,** 1265–1274. doi:10.1039/a700326i
And literature cited therein.
31. Shafirovich, V.; Cadet, J.; Gasparutto, D.; Dourandin, A.; Geacintov, N. E. *Chem. Res. Toxicol.* **2001,** *14,* 233–241. doi:10.1021/tx000204t
32. Takami, M.; Matsuura, T.; Saito, I. *Tetrahedron Lett.* **1974,** *15,* 661–662. doi:10.1016/S0040-4039(01)82298-X
33. Petersen, W. C.; Letsinger, R. L. *Tetrahedron Lett.* **1971,** *12,* 2197–2200. doi:10.1016/S0040-4039(01)96818-2

License and Terms

Beilstein Journal of Organic Chemistry

The chemistry of amine radical cations produced by visible light photoredox catalysis

Jie Hu, Jiang Wang, Theresa H. Nguyen and Nan Zheng*

Review

Open Access

Address:
Department of Chemistry, University of Arkansas, Fayetteville, AR 72701, USA

Email:
Nan Zheng* - nzheng@uark.edu

* Corresponding author

Keywords:
α-amino radical; amine radical cation; catalysis; distonic ion; free radical; iminium ion; photoredox; visible light

Beilstein J. Org. Chem. **2013,** *9,* 1977–2001.
doi:10.3762/bjoc.9.234

Received: 01 July 2013
Accepted: 29 August 2013
Published: 01 October 2013

This article is part of the Thematic Series "Organic free radical chemistry".

Guest Editor: C. Stephenson

Abstract

Amine radical cations are highly useful reactive intermediates in amine synthesis. They have displayed several modes of reactivity leading to some highly sought-after synthetic intermediates including iminium ions, α-amino radicals, and distonic ions. One appealing method to access amine radical cations is through one-electron oxidation of the corresponding amines under visible light photoredox conditions. This approach and subsequent chemistries are emerging as a powerful tool in amine synthesis. This article reviews synthetic applications of amine radical cations produced by visible light photocatalysis.

Introduction

Amine radical cations, which are an odd-electron species, are of great utility in amine syntheses [1-8]. They can be formed by loss of an electron from the corresponding amines. This one-electron oxidation process has been realized by using electrochemistry [9-11], chemical oxidants [12-14], metal-catalyzed oxidation [15-18], UV light-mediated photochemistry [7,19-21], and visible light-mediated photochemistry [22,23]. Recently, the last approach has become a major research focus in organic chemistry. The enthusiasm surrounding this approach is partially driven not only by its green characteristics (i.e. using visible light), but also more importantly by its unique ability to achieve unconventional bond formation.

Like most organic compounds, amines do not absorb visible light efficiently, unless they have a chromophore (e.g., conjugated π-bond systems). Therefore, a photocatalyst is often required to initialize electron-transfer reactions with amines. Some of the frequently used photocatalysts include ruthenium [24-26] and iridium [27,28] polypyridyl complexes as well as organic dyes [29,30] that are absorbed in the visible-light region. They all share one common characteristic: a facile intersystem crossing (ISC) that allows the conversion of the initially formed singlet photoexcited state to the relatively long-lived triplet photoexcited state. The triplet photoexcited state's long lifetime permits it to engage in single-electron transfer with

organic molecules such as amines. The photoexcited state is both more oxidizing and more reducing than the ground state. It can be quenched reductively by accepting an electron from an electron donor or oxidatively by donating an electron to an electron acceptor. Amines are often used as an electron donor to reductively quench the photoexcited state while they are oxidized to amine radical cations. This single-electron transfer process was investigated intensively in the late 1970s and early 1980s because amines were used as a sacrificial electron donor in water splitting [31,32] and carbon dioxide reduction [33,34]. Since 2008, seminal works from MacMillan, Yoon, and Stephenson have reinvigorated the field of visible light photoredox catalysis [35-42]. The use of amines as both the electron donor and the substrate, rather than just the electron donor, has become a major approach to exploit synthetic utility of photogenically produced amine radical cations.

Reductive quenching of the photoexcited state of a photocatalyst (M) by amine **1** is governed by the reduction potentials of the photoexcited state and the amine (Scheme 1). The amine's reduction potential, which can be readily measured by cyclic voltammetry, should be less positive than that of the photoexcited M. The solvent also has a significant impact on the oxidation and the subsequent reactions [43,44]. A polar solvent is generally favored for electron-transfer reactions involving amine radical cations, but identification of the optimal solvent requires experimentation. Once formed, amine radical cation **2** has been shown to have four modes of reactivity. The first mode is the back electron transfer reaction, which involves amine radical cation **2** giving back one electron to M(n−1). This is a major side reaction competing against the other productive downstream reactions of **2**. To circumvent this side reaction, two approaches or a combination thereof can be exploited [45,46]. One approach involves modifying the structure of the ligand on M to retard the back electron transfer. The other involves designing fast and/or irreversible downstream reactions of **2**. The second mode involves hydrogen atom abstraction from **2** to produce iminium ion **4**, when a good hydrogen atom acceptor is present in the reaction. The use of amine radical cation **2** as the source of a hydrogen radical has been applied to a number of visible light-mediated reductions such as reductive dehalogenation [47-51], reductive radical cyclization [52-54], reduction of activated ketones [49], and reduction of aromatic azides [55]. The third mode involves deprotonation of amine radical cation **2** to form α-amino radical **3**, which is converted to iminium ion **4** by another one-electron oxidation. The acidifying effect of one-electron oxidation on the α-C–H bond remains debatable [56-60]. The rate for deprotonation of amine radical cation **2** has been measured experimentally by several groups, and a broad range has been obtained [61,62]. α-Amino radical **3** is strongly reducing [45,63], thus making the second one-electron oxidation facile. The last mode involves cleavage of a C–C bond α to the nitrogen atom, yielding a neutral free radical **6** and iminium ion **5**. Iminium ion **4**, an excellent electrophile, is amenable to interception by a variety of nucleophiles to directly install a new bond at the position α to the nitrogen atom. In contrast, α-amino radical **3** is nucleophilic. It tends to add to electron-deficient alkenes to form a C–C bond, also at the position α to the nitrogen atom.

This review will summarize the work to date on the use of amine radical cations generated under visible light photoredox conditions as a key intermediate to trigger downstream reactions. The work is grouped based on the key intermediates

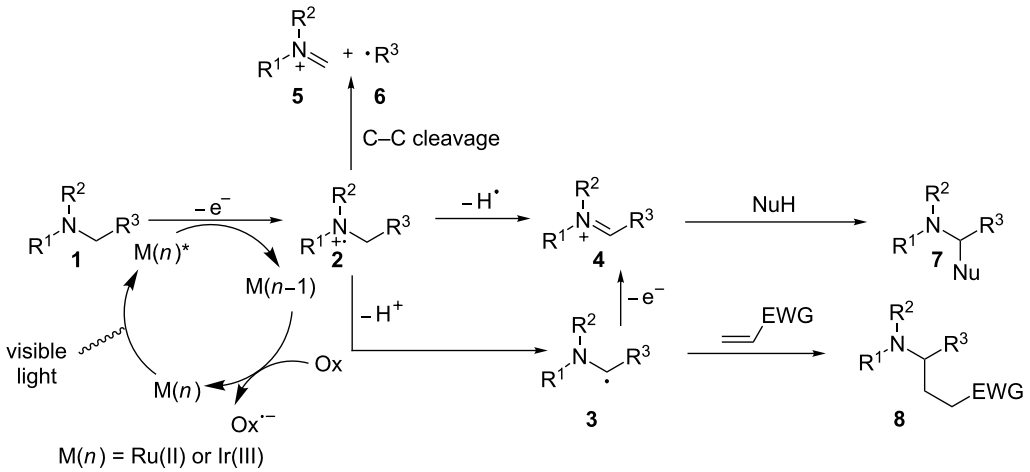

Scheme 1: Amine radical cations' mode of reactivity.

(iminium ions and α-amino radicals) or processes (cleavage of C–C and N–N bonds) involved. The chemistries that have focused on the use of amines as a sacrificial electron donor only or as a hydrogen radical donor only will not be discussed in the review. These chemistries have been recently reviewed [22,23,35-42]. Photooxidation of amines to amine radical cations can also be achieved using UV light with a sensitizer. This approach and subsequent chemistries are also outside the scope of this review. Interested readers are referred to these reviews [7,19-21].

Review

Iminium ions

Intercepted by carbon nucleophiles

One of the major modes of reactivity for amine radical cations is their conversion to the powerful electrophilic iminium ions, which can be intercepted by a range of pronucleophiles to form a number of important bonds such as C–C, C–N, C–O, and C–P. The chemistry involving iminium ions has seen the most synthetic applications so far.

The Whitten group provided some early studies to establish the conversion of amine radical cations to iminium ions. In 1980, Giannotti and Whitten reported that irradiation of triethylamine with three ruthenium polypyridyl complexes using visible light in the presence of water yielded acetaldehyde, presumably formed by the hydrolysis of iminium ion **12** (Scheme 2) [46]. They proposed that reductive quenching of the photoexcited Ru(II) complex by triethylamine produced Ru(I) and amine radical cation **9**. Then amine radical cation **9** can either abstract a hydrogen atom from the solvent (CH_3CN) to form carbon radical **10**, or lose a proton to another molecule of triethylamine to form α-amino radical **11**. Carbon radical **10** is converted to α-amino radical **11** by abstracting a hydrogen atom from a second molecule of triethylamine and CH_3CN is ultimately regenerated. Finally, one electron oxidation of α-amino radical **11** furnishes iminium ion **12** that is hydrolyzed to acetaldehyde. Although the authors were not able to detect amine radical cation **12** spectroscopically, they were able to use ESR (electron spin resonance) techniques to detect Ru(I) and α-amino radical **11** with the aid of a spin trap, nitrosodurene.

In 2010, Stephenson and coworkers reported a visible light-mediated aza-Henry reaction that harnesses the synthetic potential of iminium ions. Using only 1 mol % of $[Ir(ppy)_2(dtbbpy)](PF_6)$ and visible light, a variety of *N*-aryltetrahydroisoquinolines were oxidatively coupled with nitroalkanes to provide the aza-Henry products in excellent yields (Scheme 3) [64]. They suggested that reductive quenching of the Ir(III) photoexcited state by *N*-aryltetrahydroisoquinolines **13** leads to the formation of amine radical cation **14** and the powerful reducing agent Ir(II) (Ir(III)/Ir(II), −1.51 V vs SCE). The Ir(II) catalyst then reduces nitromethane or oxygen to a radical anion that may abstract a hydrogen atom from amine radical cation **14** to form the iminium ion **15**. Interception of the iminium ion by the anion of nitromethane affords the aza-Henry product **16**.

Oxygen has been the most often used stoichiometric oxidant in the formation of iminium ions under photoredox conditions. However, this use has some limitations. The catalyst turnover mediated by O_2 is often slow, resulting in long reaction time. O_2 can also intercept α-amino radicals, one of the key intermediates in the formation of iminium ions, to produce amides and thus compromise the formation of iminium ions [65,66]. The Stephenson group sought an alternative stoichiometric oxidant to overcome the limitations encountered by O_2 (Scheme 4) [58]. $BrCCl_3$ was identified as such an alternative and iminium ions were produced cleanly within 3 hours. A broad range of nucleophiles, including nitroalkanes, was shown to add to iminium ions. The authors proposed two possible mechanisms for the formation of iminium ions based on the two

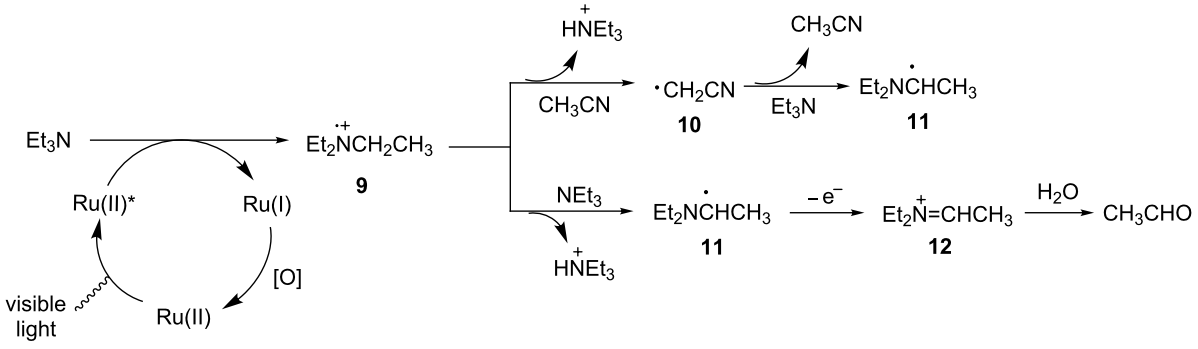

Scheme 2: Reductive quenching of photoexcited Ru complexes by Et_3N.

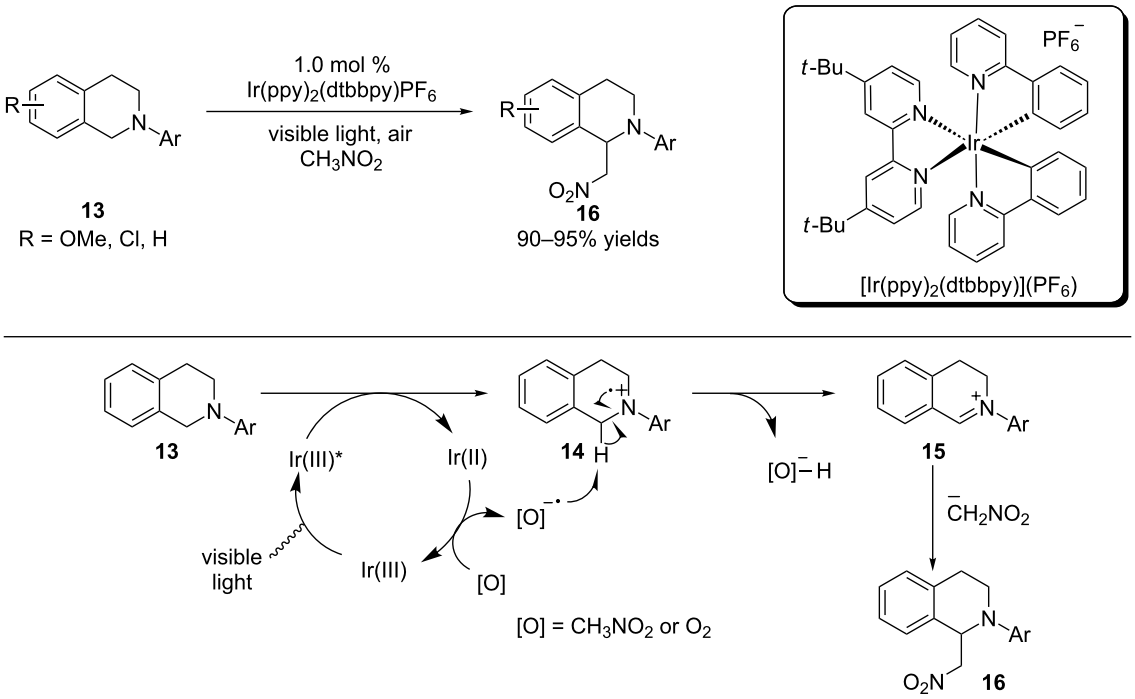

Scheme 3: Photoredox aza-Henry reaction.

divergent pathways for the conversion of amine radical cations to iminium ions. The first mechanism is based on the pathway involving abstraction of a hydrogen atom from amine radical cation **14**. The hydrogen atom acceptor is a trichloromethyl radical, which is formed via one-electron reduction of $BrCCl_3$ by Ru(I). The second is centered on the pathway involving deprotonation of amine radical cation **14** followed by one-electron oxidation. $BrCCl_3$ is the one-electron oxidant via electron transfer or atom transfer. The trichloromethyl radical, which is generated by this oxidation, then abstracts a hydrogen atom of another molecule of *N*-aryltetrahydroisoquinoline to produce the α-amino radical **17**, which once again enters the radical chain process with $BrCCl_3$.

König and coworkers showed that the same aza-Henry reaction can be catalyzed by the organic dye Eosin Y to afford the aza-Henry product **18** (Scheme 5) [67]. In addition to nitroalkanes, dialkyl malonates and malononitrile can be used as pronucleophiles to provide β-diester amine **19** and α-aminonitrile **20**. The authors proposed a mechanism similar to that proposed by Stephenson and coworkers for the aza-Henry reaction catalyzed by the Ir complex (Scheme 3). The Tan group simultaneously reported that another organic dye, Rose Bengal (RB), can be used in place of Eosin Y to catalyze the aza-Henry reaction [68].

The Wu group concurrently developed the Eosin Y-catalyzed aza-Henry reaction as reported by König and also performed mechanistic studies on the reaction. Their proposed catalytic cycle for the reaction is detailed in Scheme 6 [69]. Wu and coworkers were able to obtain experimental evidence to lend support to some of the key steps in the catalytic cycle. An oxygen uptake experiment showed that 0.75 equiv of O_2 was consumed for the complete conversion of *N*-phenyltetrahydroisoquinoline **13**. This data strongly supports the role of O_2 as the stoichiometric oxidant. Flash photolysis studies established that reductive quenching of the triplet excited state of Eosin Y by *N*-phenyltetrahydroisoquinoline **13** produced the Eosin Y radical anion. An ESR study on the irradiated solution of DMPO (5,5-dimethyl-1-pyrroline-*N*-oxide), Eosin Y, and *N*-phenyltetrahydroisoquinoline in air-saturated CH_3CN detected the adduct of superoxide to DMPO. In contrast, an ESR study on the same solution but with DMPO being replaced by TEMP (2,3,6,6-tetramethylpiperidine) did not detect TEMPO, the oxidation product of TEMP by singlet oxygen. However, TEMPO was detected in the absence of *N*-phenyltetrahydroisoquinoline. The results from these ESR studies are consistent with the notion that singlet oxygen is not formed in the presence of *N*-phenyltetrahydroisoquinoline and the Eosin Y radical anion reduces oxygen to superoxide. Finally, the yield of the product **18** increased when the reaction mixture was kept

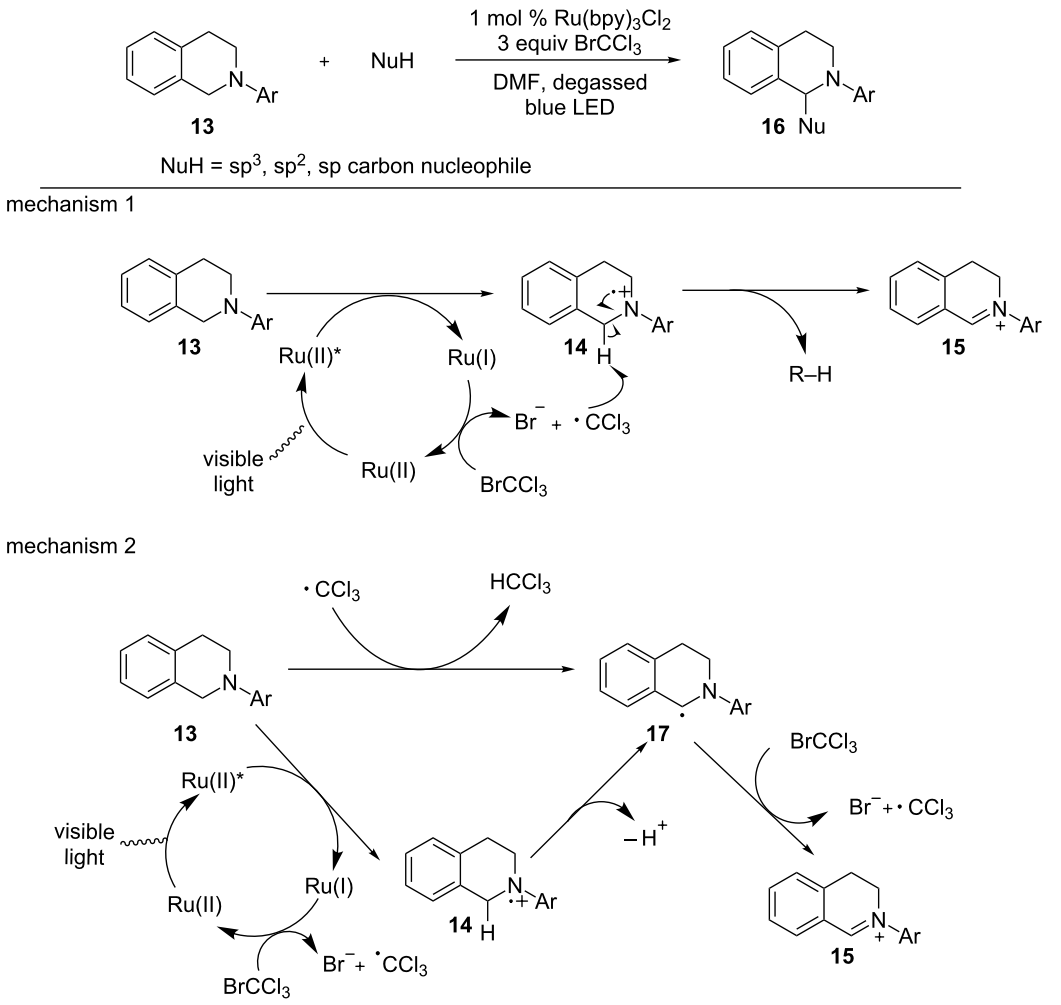

Scheme 4: Formation of iminium ions using $BrCCl_3$ as stoichiometric oxidant.

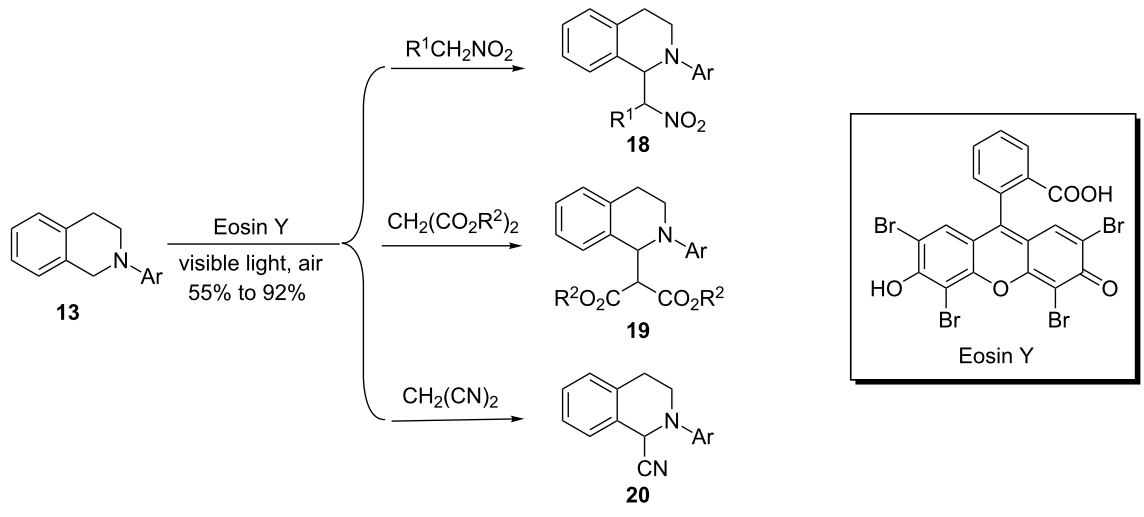

Scheme 5: Oxidative functionalization of *N*-aryltetrahydroisoquinolines using Eosin Y.

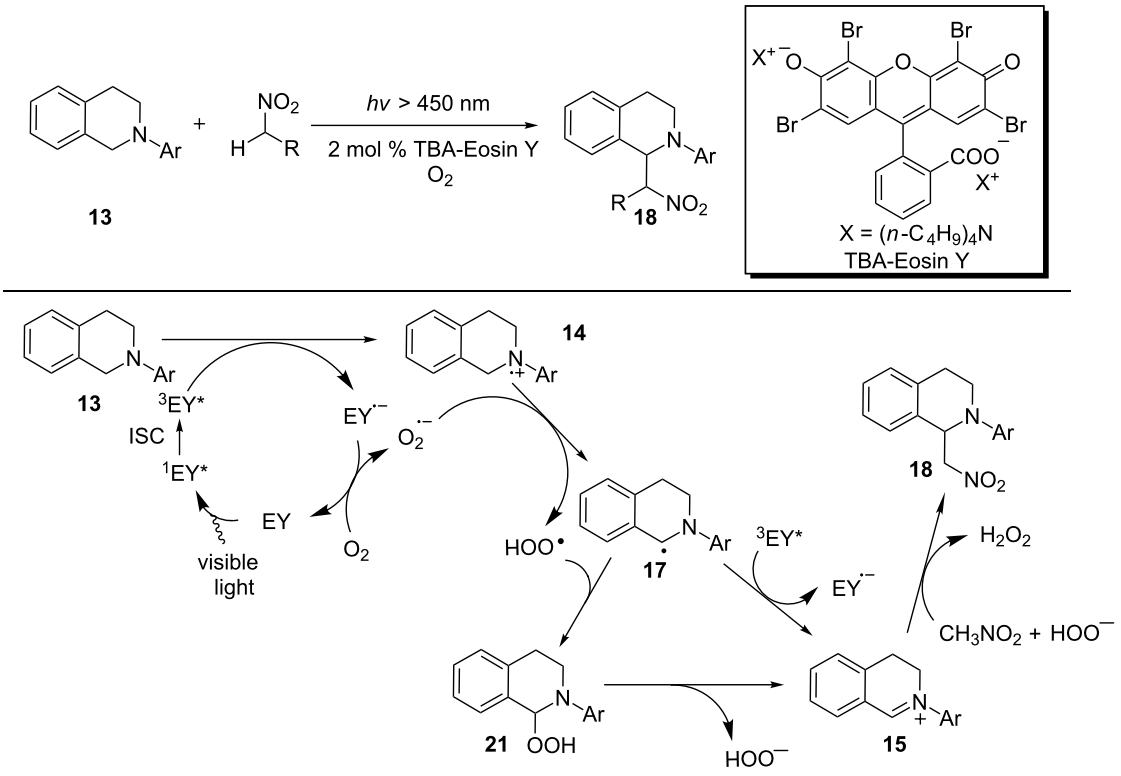

Scheme 6: Synthetic and mechanistic studies of Eosin Y-catalyzed aza-Henry reaction.

stirring in the dark after 4 h irradiation. This observation supports the formation of hydroperoxide intermediate **21**.

Tan and coworkers employed a cocatalyst system composed of the organic dye Rose Bengal and graphite oxide (GO) for α-cyanation of *N*-aryltetrahydroisoquinolines (Scheme 7) [70]. The use of GO as carbocatalyst, pioneered by the Bielawski group, has been shown to facilitate a variety of reactions including oxidation, reduction, dehydration, and C–C bond formation [71-74]. GO was found to improve the yields of the α-cyanation reaction, and this was the first example of using GO to promote visible light-mediated reactions. The synergistic effect between carbocatalysis and visible light-mediated photocatalysis has the potential to be further explored in other photocatalyzed reactions.

Since visible light photocatalysis is often orthogonal to or compatible with a number of common catalytic processes, merging it with another type of catalysis has become a recent development in the field of visible light photocatalysis. One

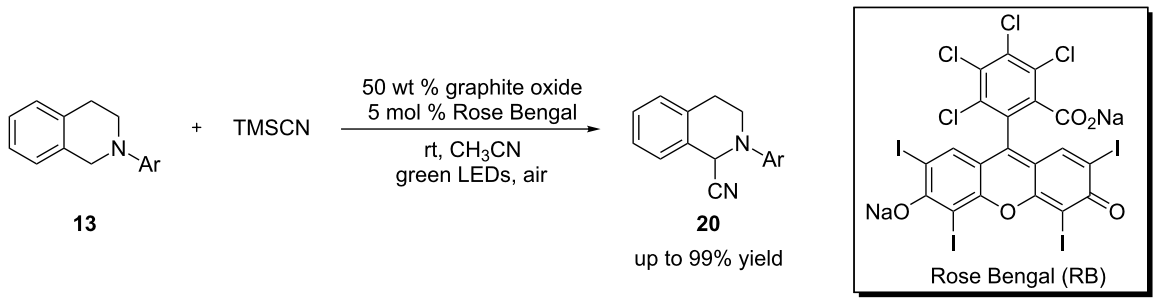

Scheme 7: Oxidative functionalization of *N*-aryltetrahydroisoquinolines using RB and GO.

direct benefit of this dual catalysis approach is to allow expansion of the types of nucleophiles capable of adding to the iminium ions generated under photoredox conditions.

In 2011, Rueping and coworkers described a dual catalytic system combining photoredox and Lewis base catalysis for the functionalization of C–H bonds α to the nitrogen atom of *N*-aryltetrahydroisoquinoline **13** (Scheme 8) [65]. In the presence of a Lewis base, a ketone is converted to enamine nucleophile **28** in situ, which is then added to photogenically formed iminium ion **27** to yield the Mannich product **23**. The Mannich reaction was sluggish without the Lewis base, and a side reaction, formation of the oxidized isoquinoline, became significant. The choice of Lewis base was found to be also crucial for the outcome of the reaction and proline was more effective than pyrrolidine. Additionally, to maximize the yields, the optimal rates for the two catalytic processes need to be similar. Since formation of the iminium ions is much faster than the addition of the enamine nucleophiles, higher yields were realized with slower formation of the iminium ions. This was achieved by use of $[Ru(bpy)_3](PF_6)_2$ in conjunction with a weak light source (5 W fluorescence bulb).

The Che group synthesized a photoactive gold(III) complex that was shown to catalyze α-cyanation of *N*-aryltetrahydroisoquinolines [75]. Very recently, Zhu and coworkers used an analogous gold(III) complex to catalyze the reactions similar to those reported by the Rueping group (Scheme 9) [76]. A 5 W blue LED was used as the light source. One advantage of using the gold complex over $[Ru(bpy)_3](PF_6)_2$ is that long-chain ali-

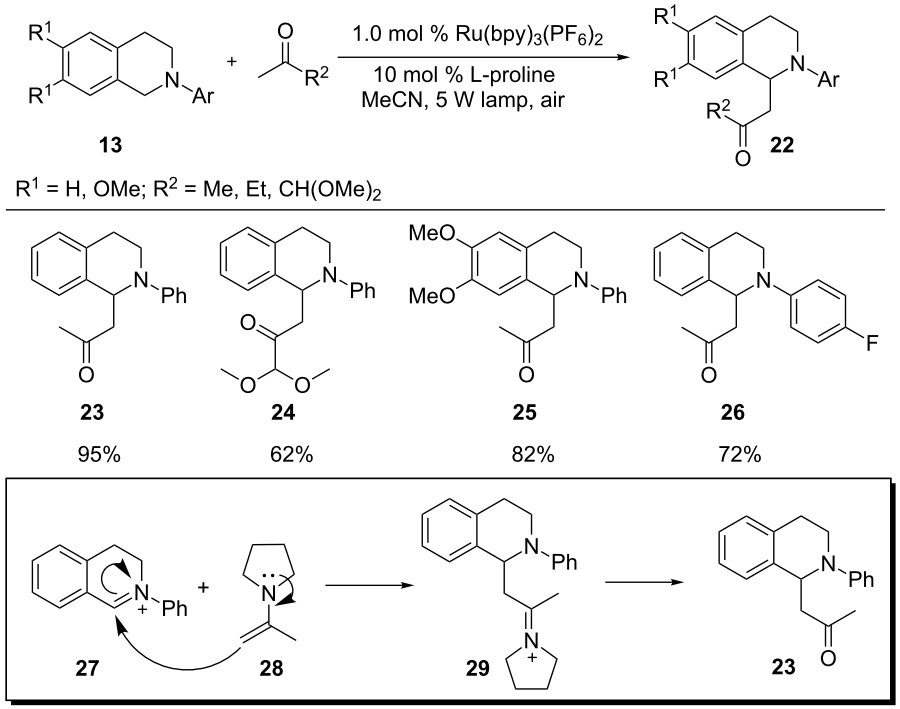

Scheme 8: Merging Ru-based photoredox catalysis and Lewis base catalysis for the Mannich reaction.

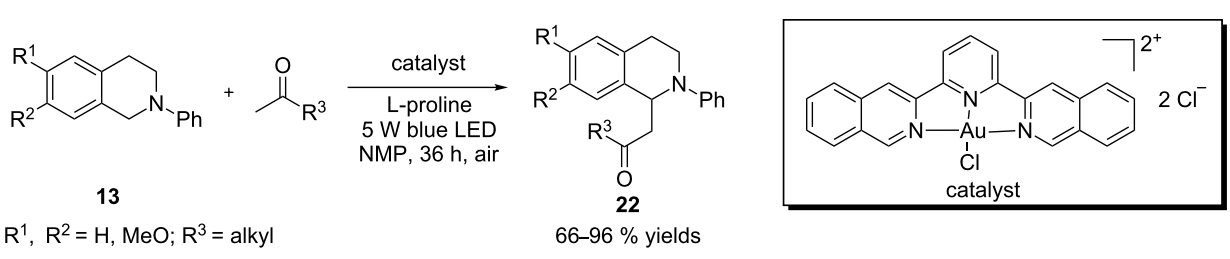

Scheme 9: Merging Au-based photoredox catalysis and Lewis base catalysis for the Mannich reaction.

phatic ketones work much better using the former catalyst. Other types of pronucleophiles such as malonates are also effective in the Mannich reaction.

The Rueping group extended the concept of dual catalysis by merging visible light photocatalysis with a metal-catalyzed process (Scheme 10) [77]. To make this approach work, several hurdles need to be addressed. First, a labile carbon–metal bond is desired in order to have an efficient turnover of the metal. Second, the metal complex needs to be compatible with the strongly reducing intermediates (e.g., superoxide) produced in the photocatalytic cycle. Third, the rates of the two catalytic cycles have to be comparable, as iminium ions are known to be converted to amides by superoxide [65,66]. Rueping and coworkers discovered that using a weak light source (5 W fluorescent bulb), copper acetylide **31**, formed in situ by $(MeCN)_4CuPF_6$, was added efficiently to the photogenically-produced iminium ion **27a**, thus achieving the formation of Csp^3–Csp bonds.

Rovis and coworkers recently developed another mode of dual catalysis involving visible light photocatalysis with chiral *N*-heterocyclic carbene catalysis, which allows catalytic asymmetric α-acylation of *N*-aryltetrahydroisoquinoline **13** with an aliphatic aldehyde (Scheme 11) [78]. In the presence of a *N*-heterocyclic carbene (NHC), the aldehyde is converted to a chiral acyl anion or homoenolate equivalent **37**, which is then added to the iminium ion **27** to form Csp^3–Csp^2 bonds asymmetrically. It is interesting to note that the use of *m*-dinitrobenzene (*m*-DNB) is critical to achieve the desirable conversion and yield of the expected product **32**. *m*-DNB is proposed to act as an electron acceptor to promote an oxidative quenching cycle of $Ru(bpy)_3^{2+}$* to $Ru(bpy)_3^{3+}$. *N*-aryltetrahydroisoquinoline **13** is then oxidized by $Ru(bpy)_3^{3+}$. This is in contrast to the majority of reported examples in which the conversion to the iminum ion such as **27** is realized in a reductive quenching cycle of $Ru(bpy)_3^{2+}$* to $Ru(bpy)_3^{1+}$, where *N*-aryltetrahydroisoquinoline **13** is oxidized by $Ru(bpy)_3^{2+}$* instead.

Xiao [79] and Rueping [80] independently reported that when tetrahydroisoquinolines (e.g., **41** and **45**) were substituted with a methylene group attached to one or two esters, the initially formed iminium ions were readily converted to azomethine ylides. They subsequently underwent 1,3-dipolar cycloaddition with a range of dipolarophiles to form fused pyrrolidines **43** and **47** (Scheme 12). Xiao also showed that the pyrrolidine ring of **43** could be further oxidized to a fused pyrrole **44** under the same photoredox conditions or by treatment with NBS. Both $Ru(bpy)_3Cl_2$ and $Ir(bpy)(ppy)_2$ were found to be effective catalysts.

A plausible mechanism for the 1,3-dipolar cycloaddition is shown in Scheme 13. The reaction commences with oxidation of tetrahydroisoquinoline **41** to amine radical cation **48** by the photoexcited state of Ru^{2+}. Subsequently, abstraction of a hydrogen atom α to the nitrogen atom of **48** yields iminium ion **49**, which is then converted to azomethine ylide **50** by loss of a proton. 1,3-Dipolar cycloaddition of **50** with a dipolarophile **46** furnishes fused pyrrolidine **51** that is further oxidized to pyrrole **52**.

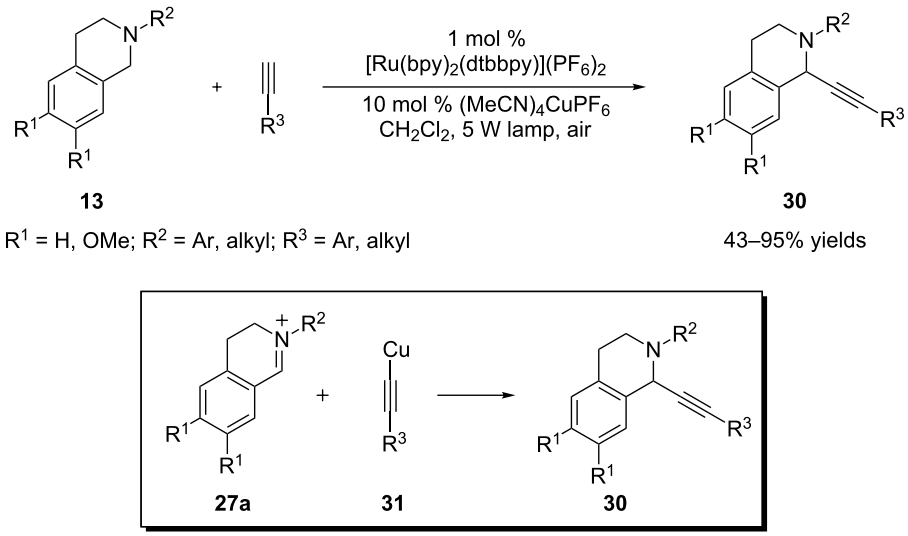

Scheme 10: Merging Ru-based photoredox catalysis and Cu-catalyzed alkynylation reaction.

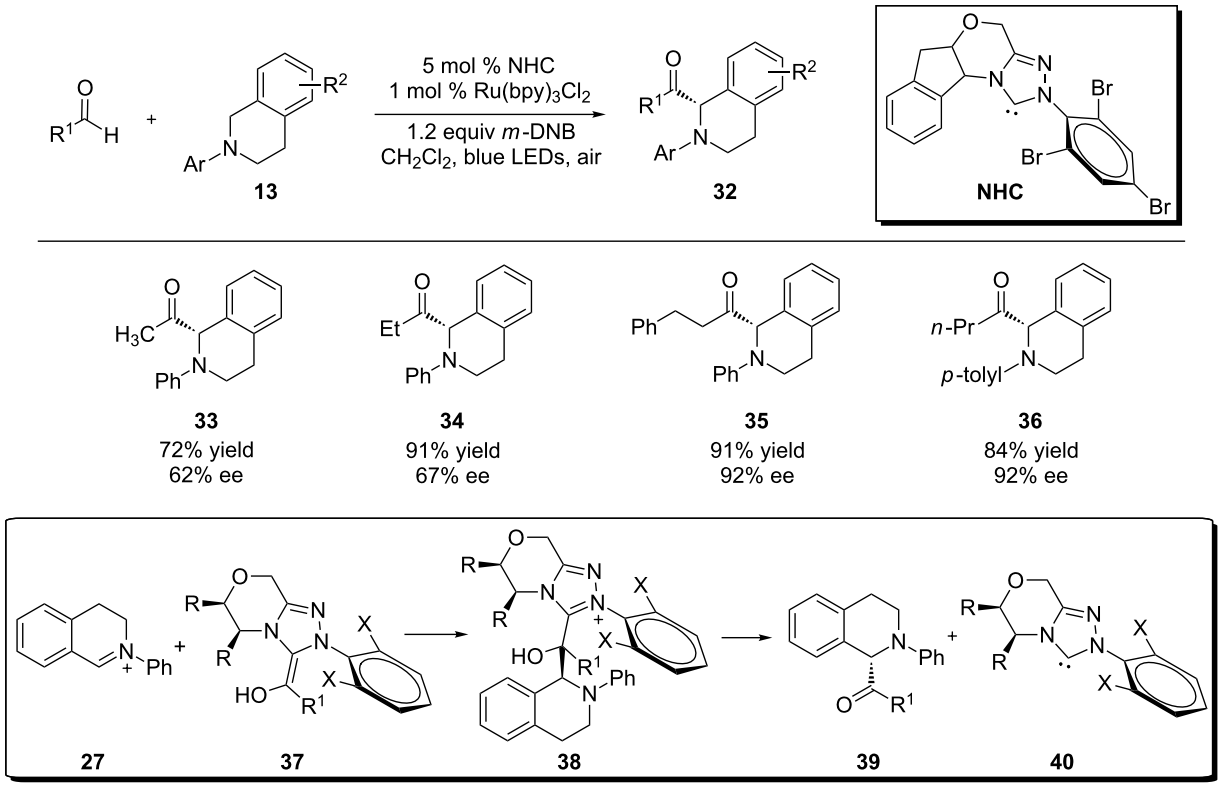

Scheme 11: Merging Ru-based photoredox catalysis and NHC catalysis.

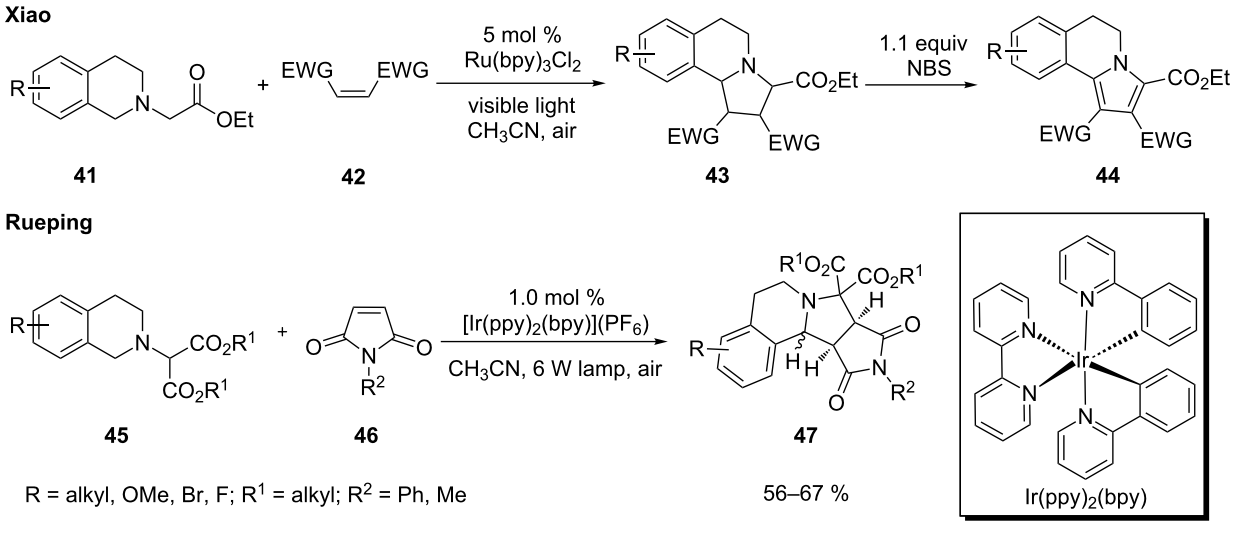

Scheme 12: 1,3-Dipolar cycloaddition of photogenically formed azomethine ylides.

The Zhu group discovered that the use of α-ketoester **53** as a pronucleophile to intercept the iminium ion of **13** triggered a new cascade reaction en route to fused isoxazolidine **54** in excellent diastereoselectivity (>20:1, Scheme 14) [81]. Alcohols were found to be the solvent of choice for this reaction. Among the three alcohols screened, iPrOH was more effective than MeOH or EtOH, resulting in a shorter reaction time. The addition of a catalytic amount of TfOH had marginally beneficial effects on the reaction time and yields. Interestingly, depending on the electronic character of the *N*-aryl group,

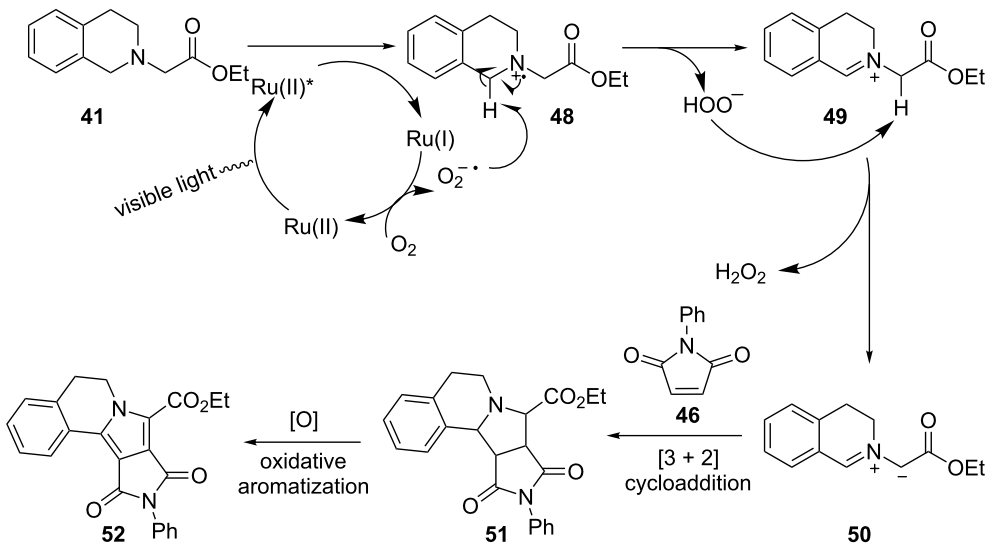

Scheme 13: Plausible mechanism for photoredox 1,3-dipolar cycloaddition.

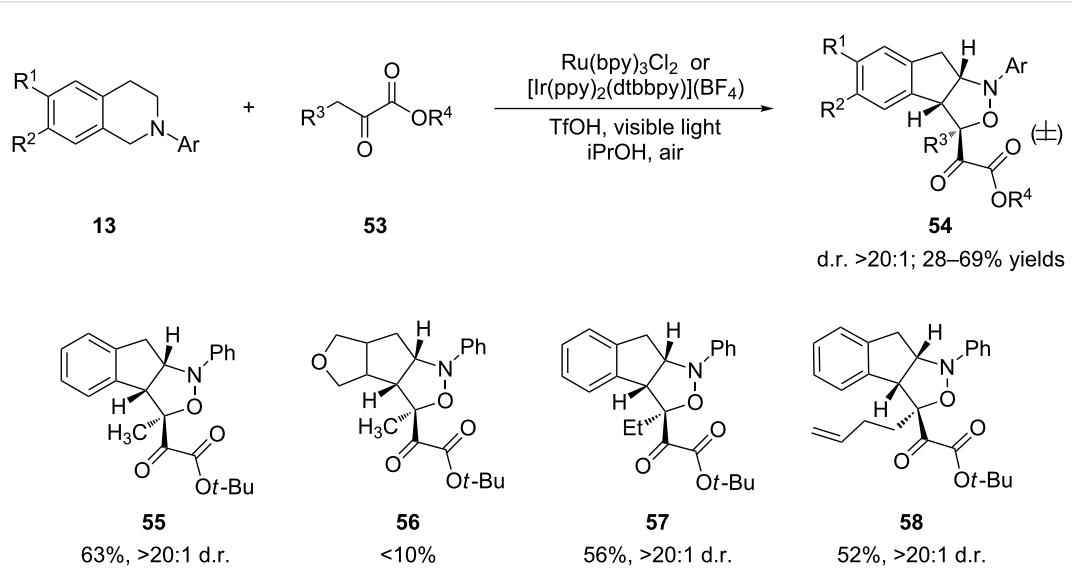

Scheme 14: Photoredox-catalyzed cascade reaction for the synthesis of fused isoxazolidines.

$[Ir(ppy)_2(dtbbpy)](BF_4)$ or $Ru(bpy)_3Cl_2$ was used to obtain optimal yields. The former catalyst worked better with electron-poor *N*-aryl groups while the latter was more effective for electron-rich *N*-aryl groups.

The authors proposed a possible mechanism that starts with reductive quenching of the photoexcited state of Ru(II) or Ir(III) by *N*-phenyltetrahydroisoquinoline **13** (Scheme 15). The initially formed amine radical cation **14** is converted to iminium ion **15** by abstraction of a hydrogen atom directly. The addition of the enol form of α-ketoester **59** to **15** furnishes the Mannich adduct **60**. A retro-aza-Michael reaction via enol **61** allows cleavage of the C–N bond to yield secondary aniline **62**. Aniline **62** is first oxidized to imine **63**, which is further oxidized to nitrone **64**. Finally, an intramolecular 1,3-dipolar cycloaddition of **64** furnishes isoxazolidine **55**.

Tetrahydroisoquinolines are arguably the most exploited amines in visible light photoredox catalysis. However, efforts towards expanding the scope of amines have been recently reported. Li [82] and Rueping [83] independently reported that *N*-aryl-glycine derivatives **65** are viable substrates (Scheme 16). They

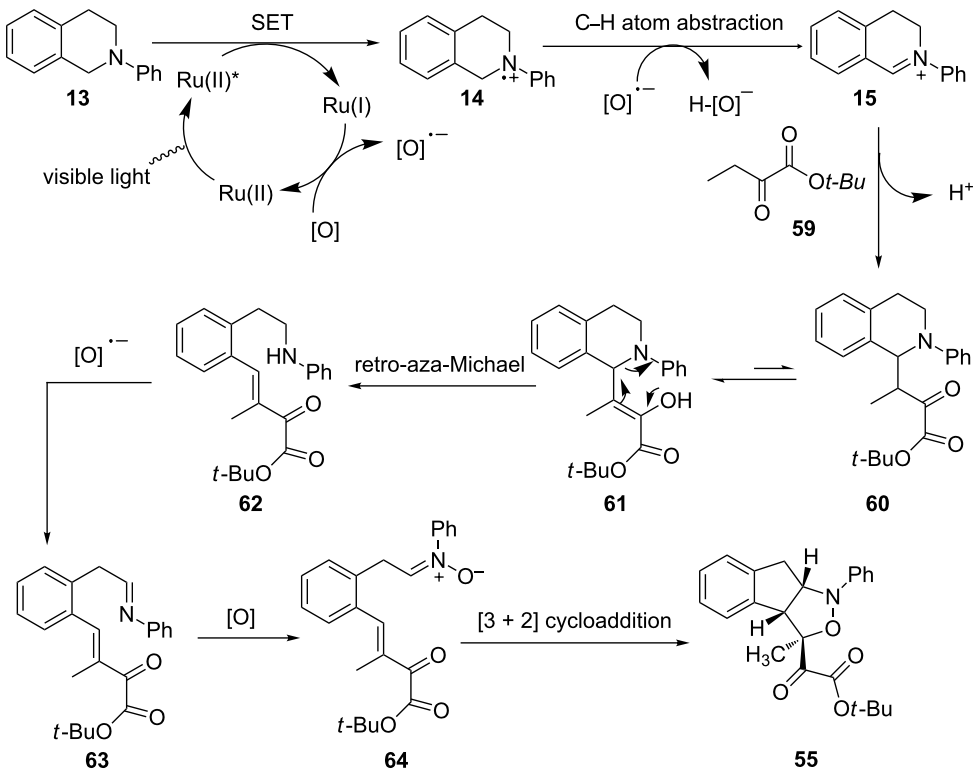

Scheme 15: Plausible mechanism for the photoredox-catalyzed cascade reaction.

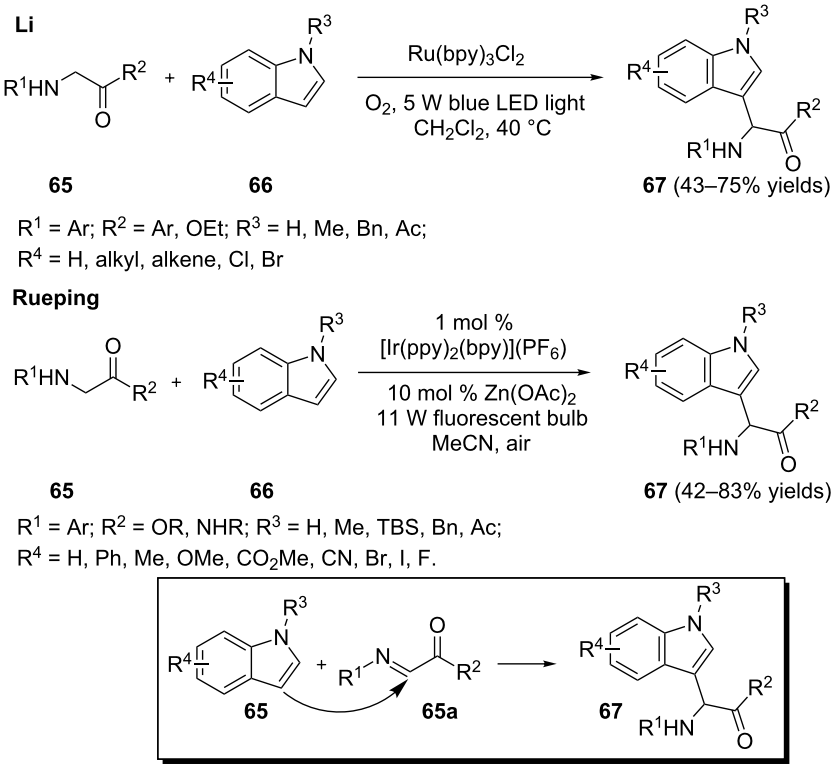

Scheme 16: Photoredox-catalyzed α-arylation of glycine derivatives.

are presumably converted to imines **65a** that are intercepted by indoles to give the Mannich-like adducts **67**. The conditions used by Li were 10 mol % $Ru(bpy)_3Cl_2$ and 1 atm O_2 at 40 °C with a 5 W blue LED as the light source. *N*-arylglycine derivatives **65**, including esters and ketones, were successfully converted to the products **67**. Rueping used $Ir(ppy)_2(bpy)PF_6$ as the photocatalyst, air, and an 11 W fluorescent bulb as the light source. Additionally, $Zn(OAc)_2$ was employed as a Lewis acid cocatalyst. It was postulated that $Zn(OAc)_2$ facilitates the conversion of the initially formed amine radical cation to the imine **65a** and subsequently activates the imine for nucelophilic attack. *N*-arylglycine esters and *N*-arylglycine derived dipeptides worked quite well under these conditions. However, the ketones failed to provide the desired products.

Amides **68** are generally much more difficult to be oxidized than amines. Their reduction potentials range from 1.2–1.5 V (vs SCE) for tertiary amides to 2.0 V (vs SCE) for primary amides [84] which makes them less susceptible to oxidation by the photoexcited state of Ru(II) or Ir(III) complexes ($Ru(bpy)_3^{2+}$*/Ru^{1+}: 0.77 V vs SCE; $Ir(ppy)_2(dtbbpy)^+$*/$Ir(ppy)_2(dtbbpy)$, 0.66 V vs SCE) [35]. Stephenson and coworkers devised a strategy by reversing the order of oxidation and C–H abstraction to overcome this issue (Scheme 17) [85]. The first intermediate formed is a strongly reducing α-amino radical **68a** that is oxidizable by the photoexcited state of Ru(II) or Ir(III). The α-amino radical **68a** is formed via C–H abstraction by the sulfate radical anion ($SO_4^{-\bullet}$), which is generated by exposure of Ru^{2+}* to persulfate ($S_2O_8^{2-}$), an oxidative quencher. Electron-rich arenes and indoles are then added to the *N*-acyliminium ions **68b** to provide the amidoalkylation products **69**. Alternatively, the use of only persulfate at 55 °C afforded the same products. However, higher yields and better selectivities were generally observed with the photocatalytic process.

Intercepted by nitrogen, oxygen, or phosphorus nucleophiles

In addition to carbon nucleophiles, heteronucleophiles including nitrogen, oxygen, and phosphorus are susceptible to interception of the photogenically formed iminium ions. The Xiao group developed a highly diastereroselective route to substituted tetrahydroimidazoles **72** based on intramolecular interception of the iminium ions by a tethered sulfonamide (**71**, Scheme 18) [86]. $Ru(bpy)_3Cl_2$ was employed as the photocatalyst with oxygen as the stoichiometric oxidant. The use of a base in an alcohol solvent, such as MeOH, was also the key to the success of this reaction. The diastereoselectivities were greatly improved by prolonging the reaction time, which would allow for epimerization leading to the thermodynamically more stable products. The starting materials, 1,2-diamines **70**, were readily prepared from natural amino acids in enantiomerically pure form.

Xiao and coworkers then applied the same strategy to prepare two other types of heterocycles, isoquino[2,1-*a*][3,1]oxazine

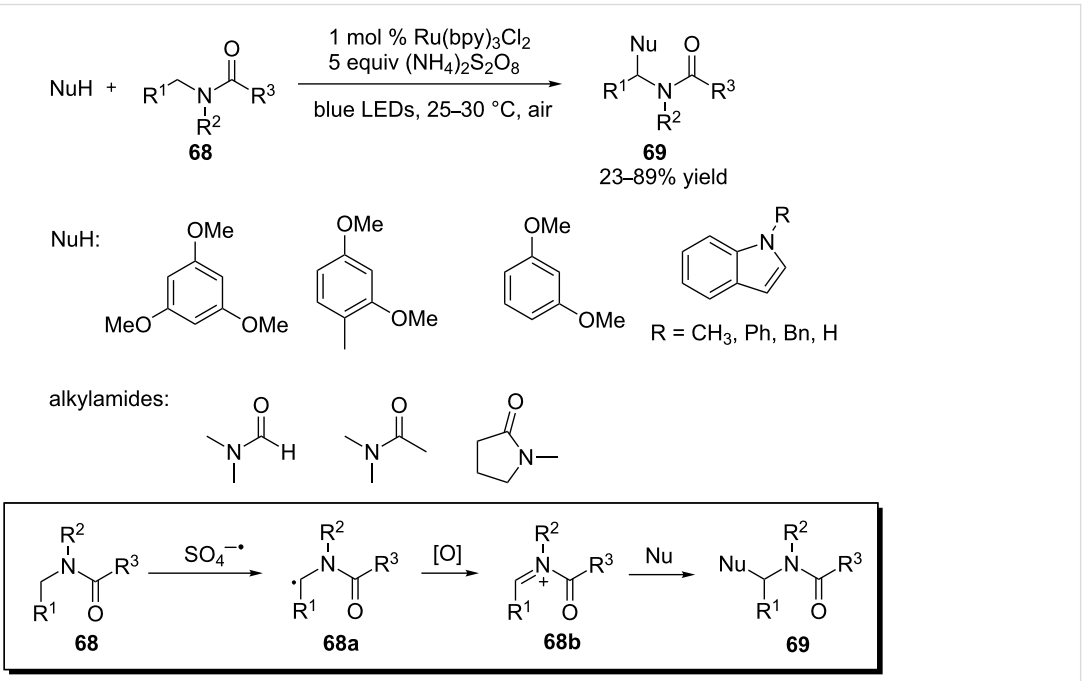

Scheme 17: Photoredox-catalyzed α-arylation of amides.

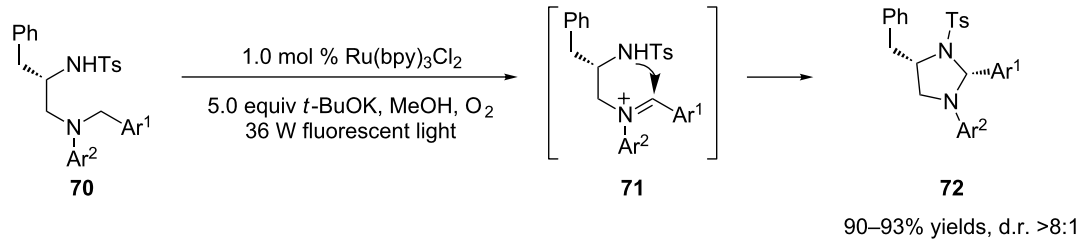

Scheme 18: Intramolecular interception of iminium ions by sulfonamides.

and isoquino[2,1-*a*]pyrimidine (**75**, Scheme 19) [87]. The use of $[Ir(ppy)_2(dtbbpy)](PF_6)$ with air as the external oxidant was found to be optimal for catalyzing the reaction. Later, the Marvin group reported an identical synthesis of isoquino[2,1-*a*][3,1]oxazine using $Ru(bpy)_3Cl_2$ instead [88]. The tethered nucleophiles, primary alcohols or sulfonamides, are part of the *N*-aryl group of tetrahydroisoquinolines **73**. Similar to the synthesis of tetrahydroimidazoles **72**, MeOH was the optimal solvent. No external base was needed when the alcohol was the nucleophile. However, if the sulfonamide was the nucleophile, an external base such as *t*-BuOK was required presumably to increase the nucleophilicity of the sulfonamide.

The Rueping group trapped the iminium ions using phosphites **76** to produce α-amino phosphonates **78** (Scheme 20) [89]. $[Ir(ppy)_2(bpy)](PF_6)$ was found to be the most effective catalyst. Interestingly, a biphasic mixture of toluene and water turned out to be the optimal solvent. The often-observed byproducts, amides derived from over-oxidation of the iminium ions, were suppressed [65,66]. The reactions were also sensitive to the steric and electronic nature of phosphites. Phosphites are quite acidic; their pK_as are similar to alcohols. Less sterically hindered phosphites reacted faster as did more acidic phosphites (e.g., diphenylphosphite).

The König group applied the organic dye Eosin Y as the photocatalyst to catalyze the same reactions (Scheme 21) [67]. The reactions were irradiated in DMF with green LED light, which overlapped with the λ_{max} of Eosin Y. The yields are comparable for the two catalyst systems, but the reactions catalyzed by Eosin Y are much faster (note: the conclusion is based on 2 mol % Eosin Y vs 1 mol % $[Ir(ppy)_2(bpy)](PF_6)$).

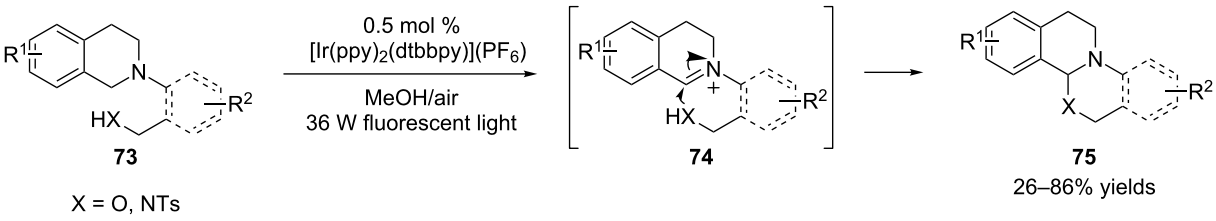

Scheme 19: Intramolecular interception of iminium ions by alcohols and sulfonamides.

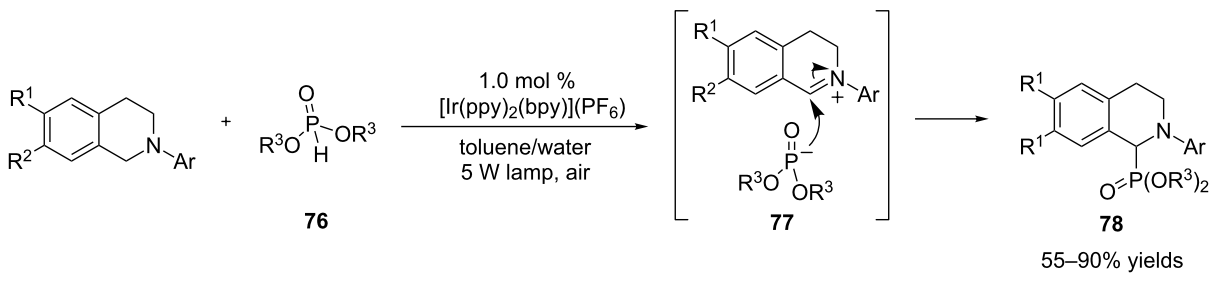

Scheme 20: Intermolecular interception of iminium ions by phosphites.

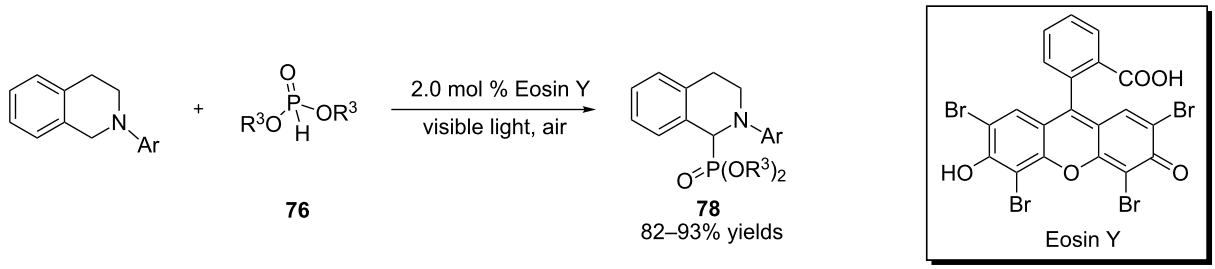

Scheme 21: Photoredox-catalyzed oxidative phosphonylation by Eosin Y.

α-Amino radicals

α-Amino radicals are another class of downstream intermediates produced from amine radical cations. They are also the key intermediate in one of two potential pathways for the conversion of amine radical cations to iminium ions (Scheme 1). In contrast to the electrophilic nature of iminum ions, α-amino radicals are nulceophilic. They tend to add to Michael acceptors in a 1,4 fashion. Since the addition is overall redox neutral, no external oxidant is required. Most of these addition reactions are conducted under degassing conditions. This is in contrast to the chemistries involving iminium ions, which are often performed with exposure to air or oxygen. The reactivity umpolung at the carbon α to the nitrogen atom has expanded the repertoire of amine radical cations' modes of reactivity. Compared to iminium ions, α-amino radicals have been much less exploited as synthetic intermediates. Their synthetic applications remain limited.

Pandey and Reiser revealed that α-amino radicals derived from *N*-aryltetrahydroisoquinolines were added intermolecularly to Michael acceptors (Scheme 22) [66]. A blue LED was used as the light source. Both $Ru(bpy)_3Cl_2$ and $[Ir(ppy)_2(dtbbpy)](PF_6)$ were found to catalyze the reactions. However, in some of the examples, the Ir catalyst gave better yields. Mechanistically, reductive quenching of the photoexcited Ru(II) or Ir(III) complex by *N*-aryltetrahydroisoquinolineamine yields amine radical cation **14**, which is converted to α-amino radical **17**. Conjugated addition of **17** to methyl vinyl ketone produces radical **79**, which is reduced by the Ru(I) or Ir(II) complex with concomitant regeneration of the Ru(II) or Ir(III) complex. Protonation of the resulting enolate furnishes the adduct **80**, thus completing the catalytic cycle. The authors performed two control studies to probe the involvement of the α-amino radical **17**. The first study was to irradiate *N*-phenyltetrahydroisoquinoline **13** in the absence of the Michael acceptor under otherwise identical conditions. The dimer, **81**, was formed as a mixture of diastereomers. The second study involved irradiation of *N*-phenyltetrahydroisoquinoline **13** only without degassing the reaction solution. The amide, **82**, was produced instead. Both findings lend credence to the intermediacy of the α-amino radical **17**.

The Yoon group independently discovered that the efficiency of the same Michael reaction was greatly improved in the presence of a Brønsted acid (Scheme 23) [90]. Some of the improvements included shorter reaction time, higher yields, and use of a weaker light source (CFL). The most effective acid catalysts, of which TFA was found to be optimal, lie within a narrow range of pK_a values. The authors suggested that TFA protonates the enone **83**, thus accelerating the addition of the α-amino radical to the enone (**84**).

The Nishibayashi group reported that α-amino radicals generated from a different class of amines, anilines **87**, were also added intermolecularly to Michael acceptors **86** (Scheme 24) [91]. In this reaction, the Michael acceptors **86** were limited to those activated by two electron-withdrawing groups. $[Ir(ppy)_2(dtbbpy)](BF_4)$ was found to be the most effective photocatalyst. Solvents were also critical to the outcome of the reaction; NMP produced much higher yields of the products **89** than DMF, while no products were formed in MeCN or MeOH. The authors interrogated the intermediacy of the α-amino radical **88** by treatment of diphenylmethylaniline with a Michael acceptor incorporating a cyclopropyl ring **95**. The ring-opening product **98** was isolated in 64% yield, which is consistent with the involvement of the α-amino radical **88**.

Oxygen has been suggested to play multiple roles in the oxidation of amines under photoredox conditions (vide supra). The Rueping group recently reported a new role that oxygen played in the intermolecular addition of α-amino radicals to Michael acceptors (Scheme 25) [92]. Oxygen was found to act as a chemical switch to two competing reaction pathways from the same starting anilines. Irradiation of a degassed solution of aniline **99**, 2-benzylidenemalononitrile **100**, 5 mol % $Ir(ppy)_2(bpy)](PF_6)$ in MeCN furnished the typical Michael adduct **102**. This result is similar to those reported by Pandey

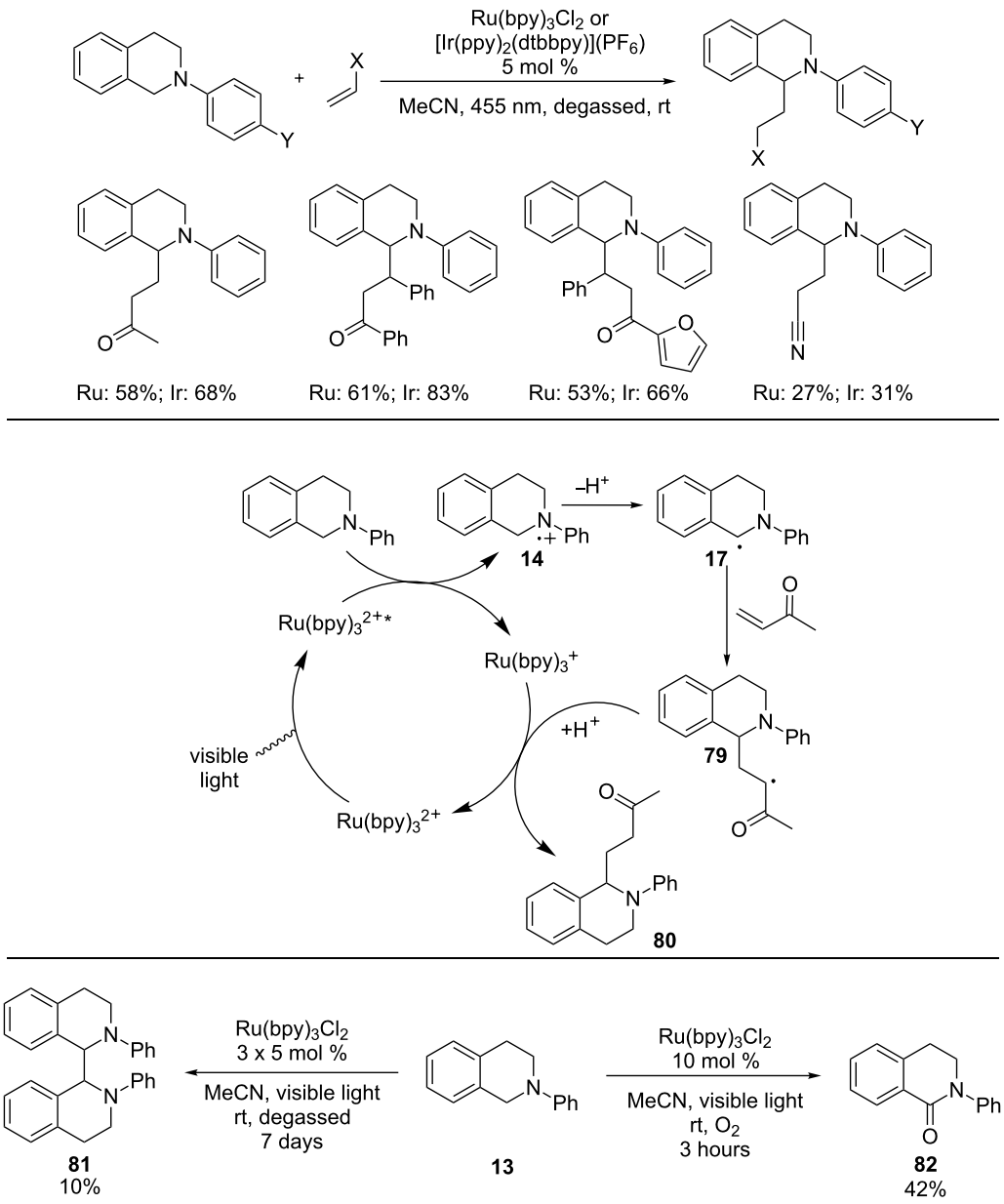

Scheme 22: Conjugated addition of α-amino radicals to Michael acceptors.

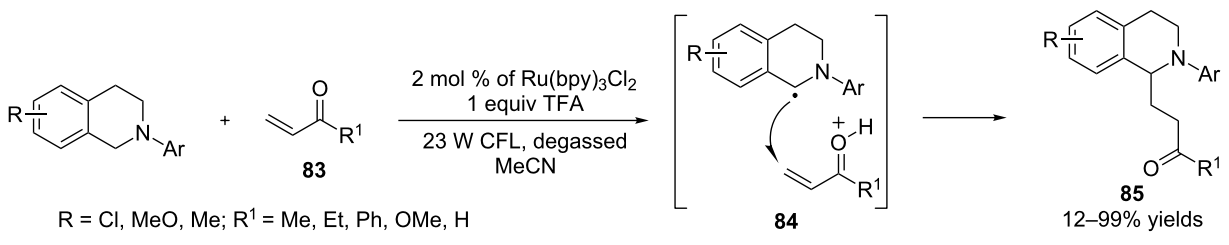

Scheme 23: Conjugated addition of α-amino radicals to Michael acceptors assisted by a Brønsted acid.

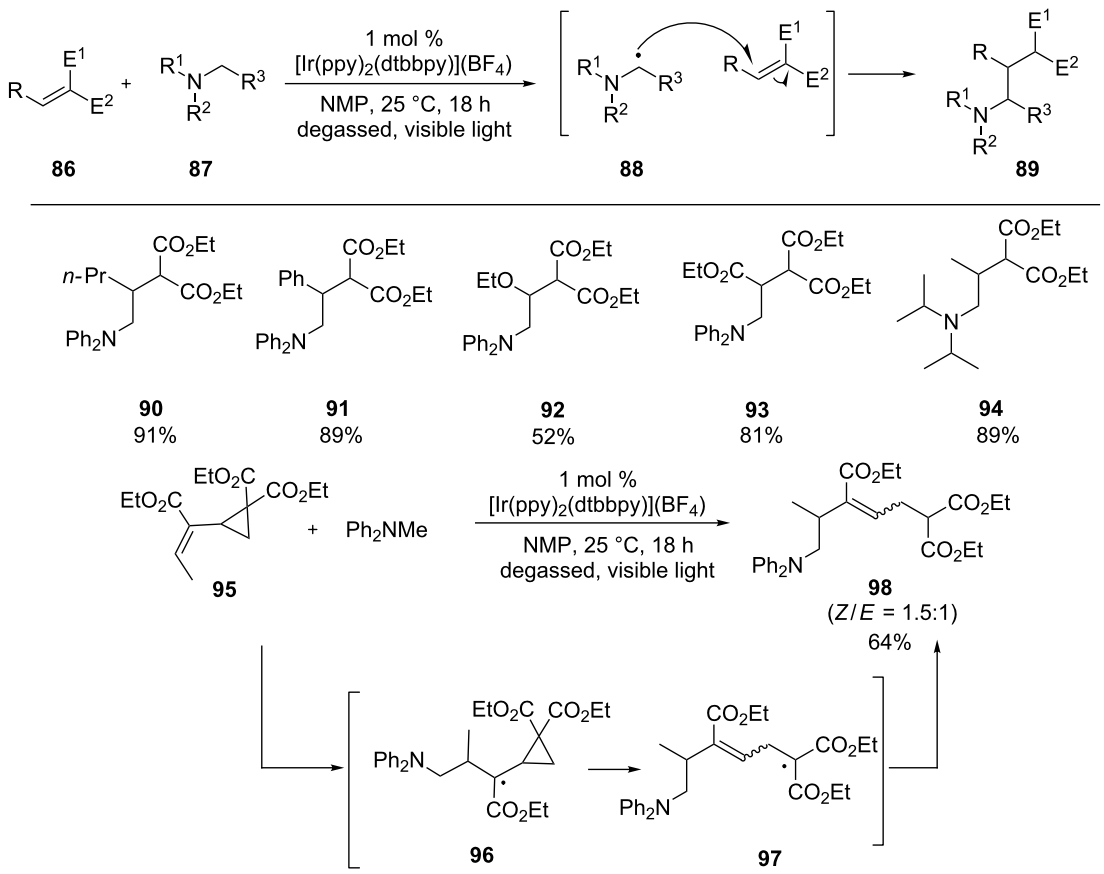

Scheme 24: Conjugated addition of α-amino radicals derived from anilines to Michael acceptors.

and Reiser [66], and Nishibayashi [91]. However, when the irradiation was conducted in the presence of air, a different reaction pathway occurred, resulting in the formation of *N*-alkyltetrahydroquinoline **101**. The two reaction pathways diverge from the radical intermediate **105** generated from the Michael addition of α-amino radical **104** to 2-benzylidenemalononitrile **100**. Without oxygen, the radical undergoes a one-electron reduction by Ir(II) to produce a stabilized anion, which is protonated to afford the Michael adduct **106**. Alternatively, the radical is added onto arene to form a cyclohexadienyl radical **107**. This step is reversible in the absence of oxygen. However, in the presence of oxygen, superoxide is formed via one-electron reduction of oxygen by Ir(II). The cyclohexadienyl radical **107** is converted to the cyclization product **108** irreversibly by giving one electron and one proton to the superoxide.

The Nishibayashi group also successfully trapped α-amino radicals derived from *N*-aryltetrahydroquinolines and *N*-arylindolines using di-*tert*-butyl azodicarboxylate **110** to form *N*,*N*-acetal products **111** (Scheme 26) [93]. Functionalization of the sp^3 C–H bond α to the nitrogen atom in tetrahydroquinolines and indolines via iminium ions is challenging because the corresponding iminium ions are enolizable and thus tend to tautomerize to enamines [94,95] and/or aromatize [96,97]. The authors adopted a strategy to bypass the iminium ions and use α-amino radicals such as **112** instead to construct C–N bonds. Treatment of *N*,*N*-acetal product **111** with Grignard reagents (Scheme 26, entry 1) or indoles in the presence of TsOH (Scheme 26, entry 2) provided nucleophilic substitution products at the α carbon. This provides an indirect approach for α-C–H functionalization of *N*-aryltetrahydroquinolines and *N*-arylindolines. Based on the feasibility of oxidation of aromatic amines as well as reduction of di-*tert*-butyl azodicarboxylate (**110**) by the photoexcited Ir(III) complex [98,99], the authors favored a mechanism that does not involve the direct addition of α-amino radical **112** to di-*tert*-butyl azodicarboxylate (**110**). Oxidation of *N*-phenyltetrahydroquinoline by the photoexcited Ir(III) complex followed by deprotonation provides α-amino radical **112** with the concomitant formation of the Ir(II) complex. Di-*tert*-butyl azodicarboxylate (**110**) is reduced by the Ir(II) complex to generate radical anion **113**, which couples with α-amino radical **112** to yield nitrogen anion **114**. Concurrently, the Ir(III) complex is regenerated. Protonation of **114** furnishes *N*,*N*-acetal **111**.

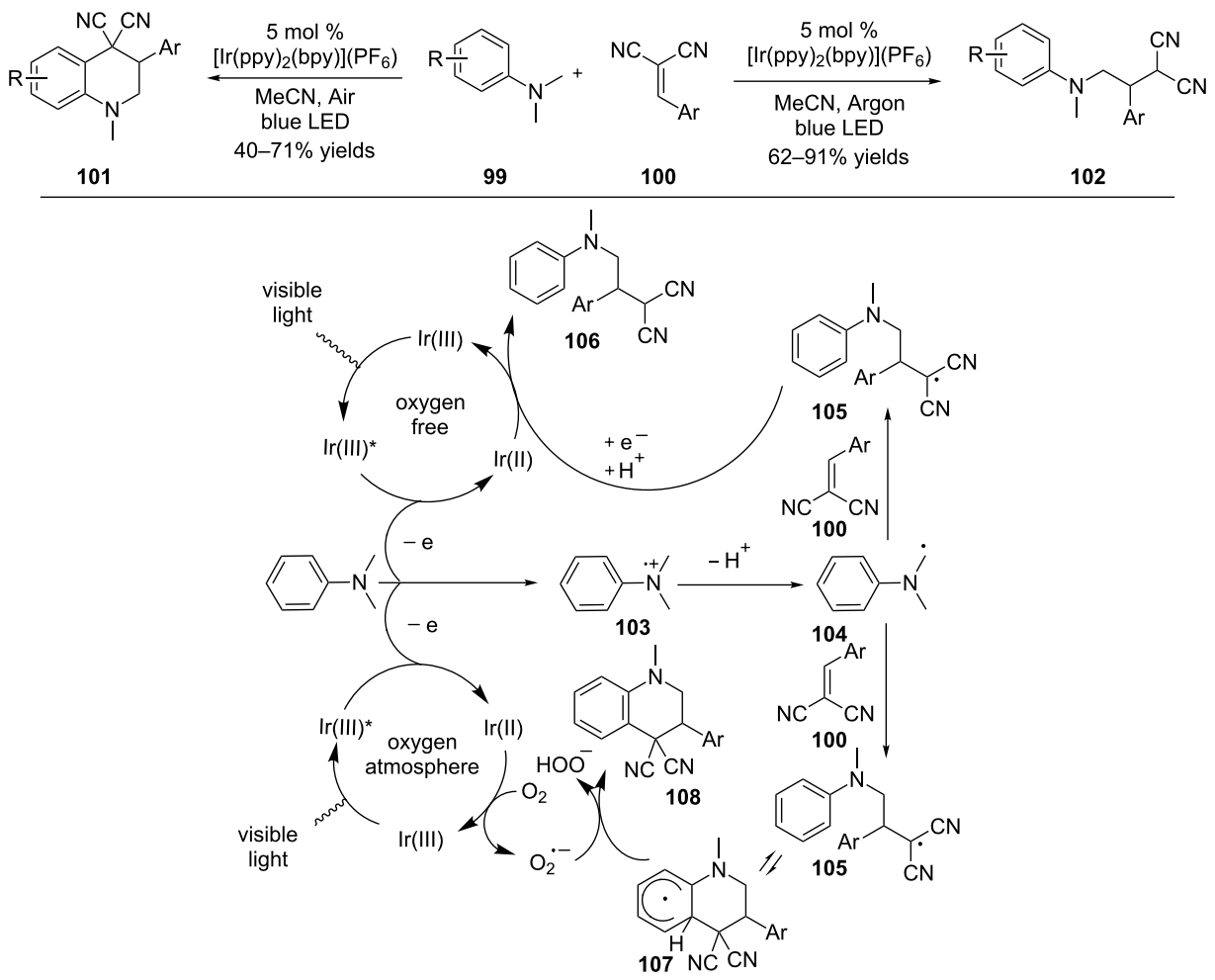

Scheme 25: Oxygen switch between two pathways involving α-amino radicals.

α-Amino radicals have been mainly used in conjugate addition reactions. Recently, the MacMillan group has nicely expanded the scope of the reactions to include addition of the radicals to aryl rings (Scheme 27) [100]. Using $Ir(ppy)_3$ as the photocatalyst and a 26 W fluorescent light bulb as the light source, cyclic amines with a variety of ring sizes and acyclic amines underwent the α-arylation reaction to provide benzylic amines. The arylating reagents were benzonitriles substituted with an electron-withdrawing group. The nitrile group functioned as the leaving group. In some classes of five-membered heteroaromatics, a chloride was capable of replacing the nitrile group as the leaving group.

The authors proposed a mechanistic pathway that is initiated by oxidative quenching of the photoexcited state of $Ir(ppy)_3$ by benzonitrile **121** to generate radical anion **123** and $Ir^{4+}(ppy)_3$ (Scheme 28). Amine **122** is then oxidized to amine radical cation **124** by $Ir^{4+}(ppy)_3$ that is reduced to the initial catalyst, $Ir(ppy)_3$. Deprotonation of amine radical cation **124** by NaOAc produces α-amino radical **125**, which is coupled with radical anion **123** to form the key C–C bond in **126**. Finally, aromatization via expulsion of the nitrile group provides benzylic amine **127**.

Cleavage of C–C and N–N bonds

The dominant reaction pathway involving the photogenically formed amine radical cations is deprotonation at the carbon α to the nitrogen atom to produce the strongly reducing α-amino radicals (e.g., **128** to **129**). α-Amino radicals can be then intercepted by Michael acceptors or undergo one-electron oxidation to yield iminium ions (vide supra). An alternative yet much less exploited reaction pathway concerning amine radical cations **129** is the cleavage of the C–C bond α to the nitrogen atom to generate a neutral carbon radical (e.g., **130**) and an iminium ion (e.g., **131**). The iminum ion is subsequently reduced to α-amino radical **132** by Ru(I). Back in 1986, the Whitten group established this pathway by irradiation of three substituted tertiary amines with $Ru[4,4'\text{-}CO_2Et(bpy)]_3(PF_6)_2$ respectively using

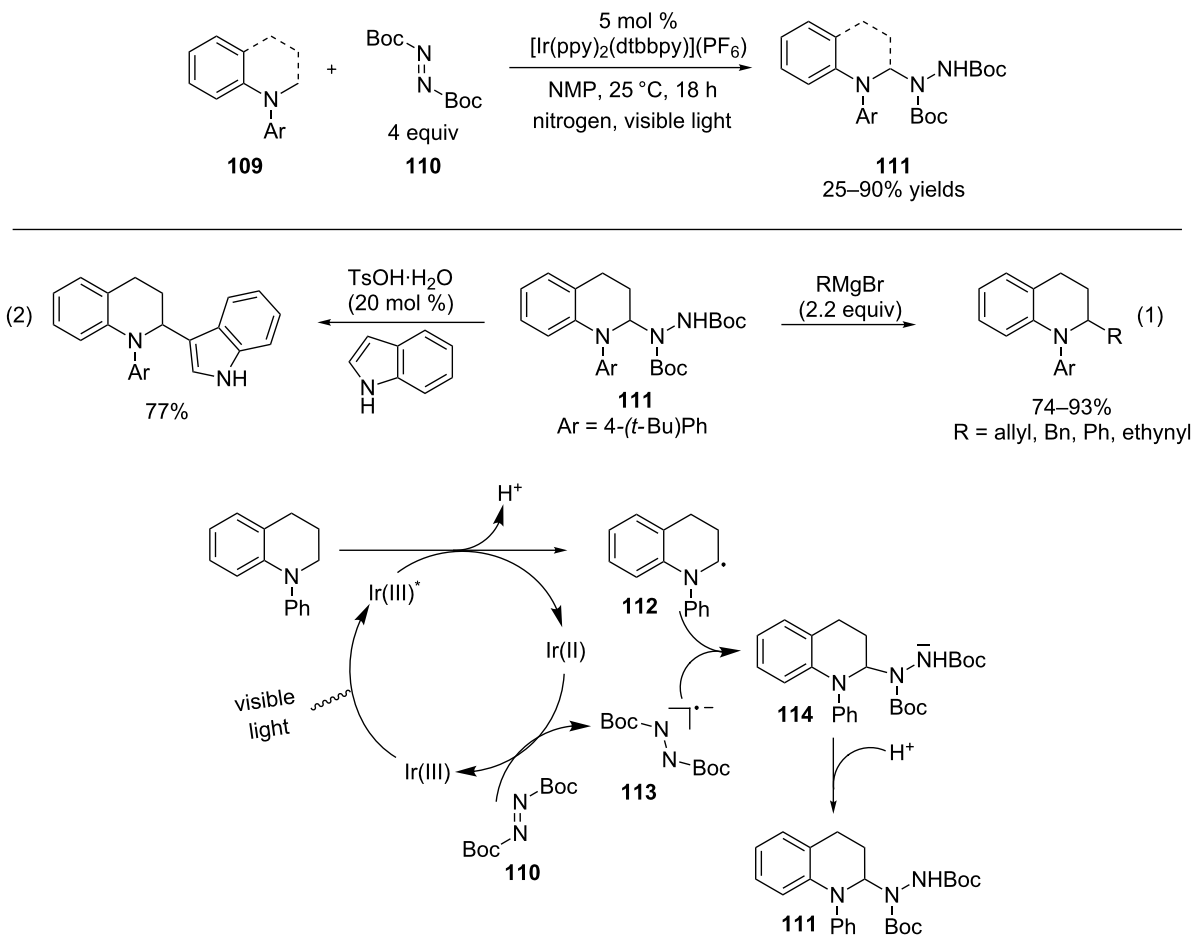

Scheme 26: Interception of α-amino radicals by azodicarboxylates.

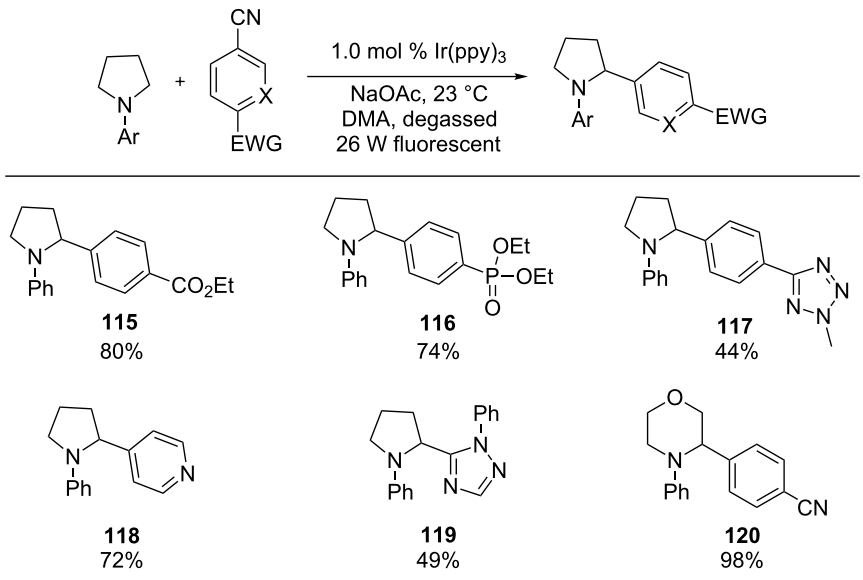

Scheme 27: α-Arylation of amines.

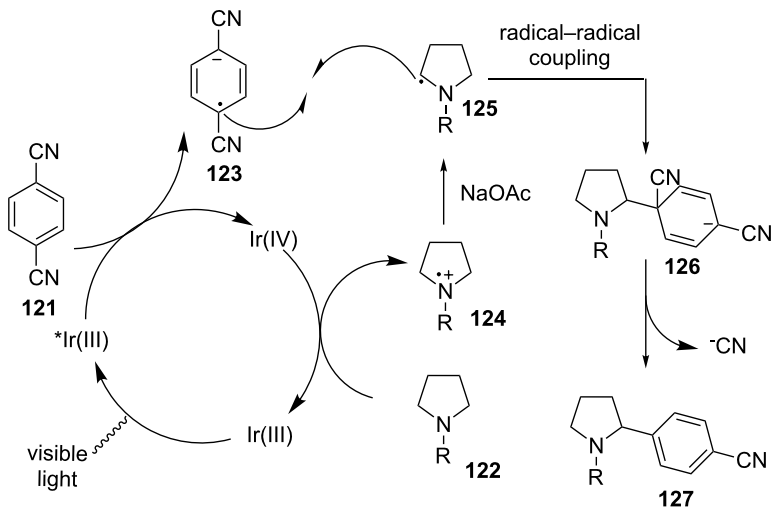

Scheme 28: Plausible mechanism for α-arylation of amines.

visible light (Scheme 29) [101]. The identity of carbon radicals **130a** and **130b** was established by trapping them with a spin trap and then analyzing using EPR. Additionally, detection of benzaldehyde by HPLC and VPC provided further evidence for their formation. In contrast, no products from the amine half (e.g., **131** and **132**) were detected.

Li and Wang recently applied this cleavage reaction to 1,2-diamines, simultaneously generating two classes of synthetically useful intermediates, iminium ions (e.g., **133**, Scheme 30) and α-amino radicals (e.g., **134**, Scheme 30) [102]. The authors then exploited the synthetic utility of these two classes of intermediates. Irradiation of nitroalkanes, TMEDA, and $Ru(bpy)_3Cl_2$ in 1 atm oxygen afforded the aza-Henry products **135**, presumably by trapping the $Me_2N{=}CH_2$ iminium ion **133** that is formed by cleaving TMEDA (Scheme 30, entry 1). Separately, irradiation of 2-hydroxyethylacrylate (HEA), TMEDA, and $Ru(bpy)_3Cl_2$ in air produced a polymer incorporating a dimethylamino group (**136**, Scheme 30, entry 2). The dimethylamino radical, the other intermediate generated by cleaving TMEDA, most likely induced the polymerization. The chemistries involving the iminium ions and α-amino radicals, generated under visible light photoredox conditions, are often limited by the substrate scope of the amine precursors, since aromatic

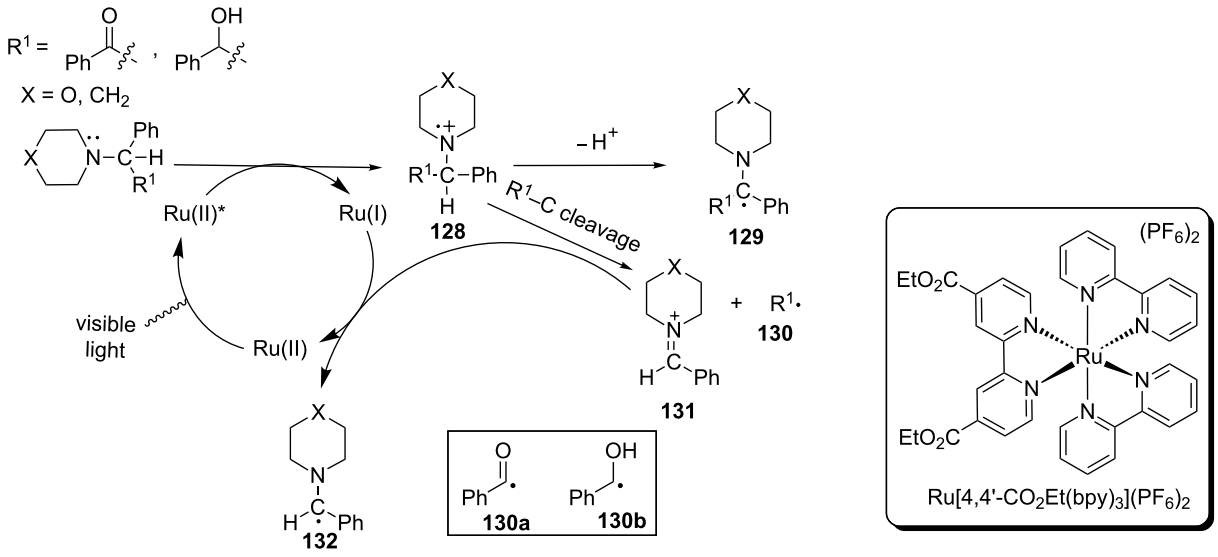

Scheme 29: Photoinduced C–C bond cleavage of tertiary amines.

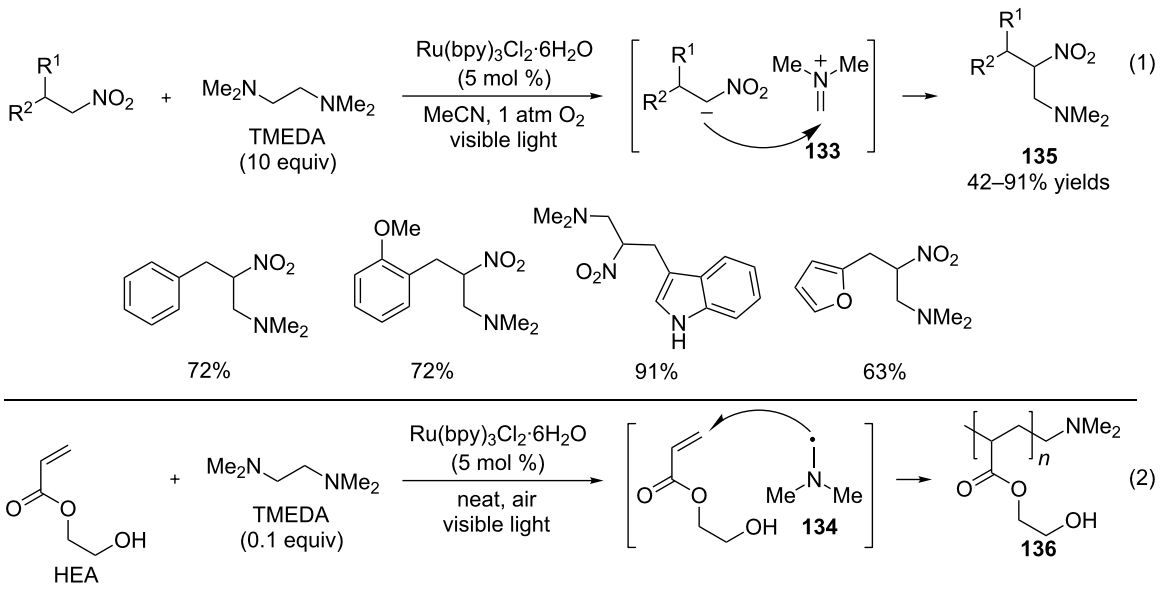

Scheme 30: Photoredox cleavage of C–C bonds of 1,2-diamines.

amines are typically required (vide supra). The cleavage reaction, as demonstrated by Li and Wang's work, has the potential to produce different types of iminium ions and α-amino radicals that are not accessible by oxidizing amines directly.

The reaction is proposed to proceed through the initial oxidation of TMEDA to amine radical cation **137** by the photoexcited state of the Ru(II) complex (Scheme 31). Amine radical cation **137** subsequently induces cleavage of the C–C bond α to the nitrogen atom to form iminium ion **133** and α-amino radical **134** concurrently. By carefully selecting reagents/conditions, either reactive intermediate can selectively participate in the designated reaction. As shown in Li and Wang's work, iminium ion **133** is intercepted by nitroalkane to afford the aza-Henry product **135** while α-amino radical **134** is used to initialize radical polymerization of HEA.

Because of ring strain, cyclopropanes are prone to ring opening via cleavage of one of the three C–C bonds. The resulting reactive intermediates have been shown to participate in a number of synthetic/mechanistic applications [103,104]. One of these applications is a radical clock, which is centered on the cyclopropylcarbonyl to homoallyl radical rearrangement [105]. A homologous rearrangement based on the amine radical cation of *N*-cyclopropylanilines permits cleavage of the C–C bond α to the nitrogen atom but generating a γ-carbon radical iminium ion (distonic ion) [106]. We have applied $Ru(bpz)_3(PF_6)_2$-catalyzed photooxidation of *N*-cyclopropylanilines to induce this

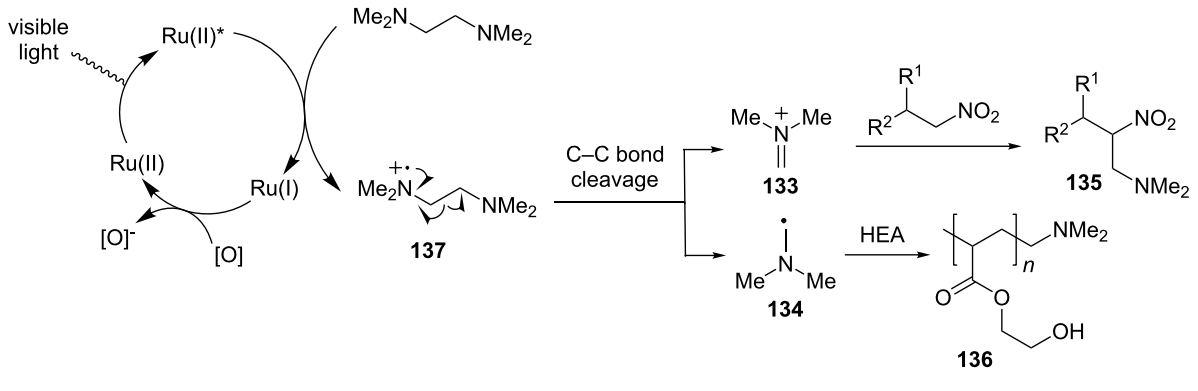

Scheme 31: Proposed mechanism photoredox cleavage of C–C bonds.

rearrangement reaction. The resulting distonic ion was then intercepted by alkenes to produce [3 + 2] annulation products (Scheme 32) [107]. An aryl group on the amine was required for the reaction. Both mono- and bicyclic cyclopropylanilines were viable substrates to provide the annulation products in good to excellent yields. The former gave little to poor diastereoselectivity whereas the later produced modest diastereoselectivity. The reaction has 100% atom economy. It is also overall redox-neutral and thus does not require an external oxidant.

We believe that the annulation reaction proceeds first via reductive quenching of the photoexcited state of Ru(II) by cyclopropylaniline **147** to generate amine radical cation **148** and Ru(I) (Scheme 33). Amine radical cation **148** then triggers the ring opening to release the ring strain while producing a distonic ion **149** with a primary radical. Distonic ion **149** is added via a Giese-type radical addition to an alkene, yielding a more stable distonic ion **151** with a secondary radical. Intramolecular addition of the secondary radical to the iminium ion furnishes a new amine radical cation **152**. Finally, amine radical cation **152** is reduced by Ru(I) to provide the annulation product **153** and regenerate Ru(II), thus completing the catalytic cycle.

Our group also realized cleavage of N–N bonds by irradiation of aromatic hydrazines or hydrazides in the presence of $Ru(bpz)_3(PF_6)_2$ and air (Scheme 34) [108]. A 13 W compact fluorescent light was sufficient as the light source. *N*,*N*-disubstituted hydrazines and hydrazides were suitable substrates provided that at least one of the two substituents on the nitrogen atom was an aryl group. Electron-richer hydrazines were found to be more reactive than hydrazides. This is consistent with our expectation that, similar to amines, hydrazines and hydrazides act as an electron donor to reductively quench the photoexcited Ru(II) complex. The photoexcited state of $Ru(bpz)_3$ ($E_{1/2}{}^{*II/I}$ = 1.45 V vs SCE) is more oxidizing than that of $Ru(bpy)_3$ ($E_{1/2}{}^{*II/I}$ = 0.77 V vs SCE). However, the two catalysts showed a divergent pattern of reactivity in the reaction. $Ru(bpy)_3$ was the more active catalyst for hydrazines, whereas $Ru(bpz)_3$ was more active for hydrazides. The use of MeOH in addition to CH_3CN significantly shortened the reaction time for less reactive hydrazides, but showed little effect for hydrazines. We believe that the cleavage reaction is initialized via the oxidation

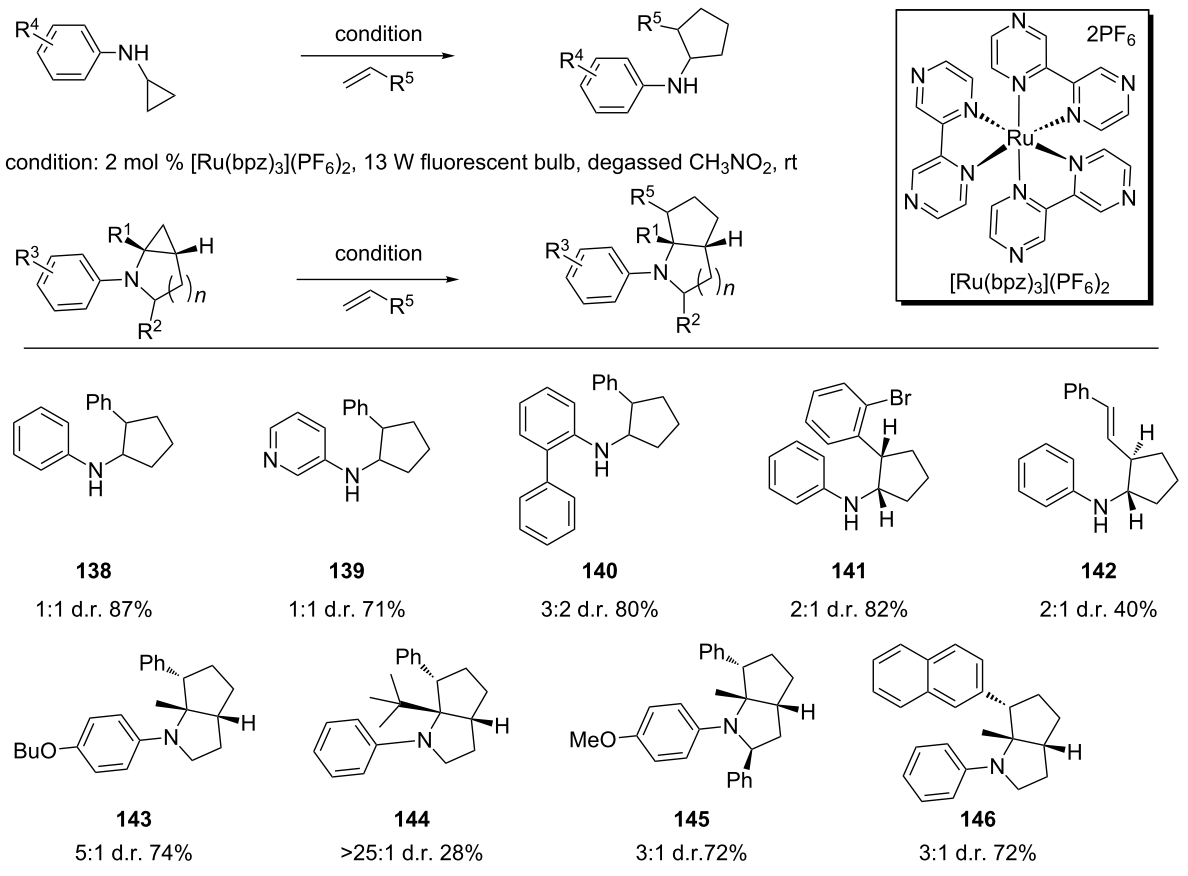

Scheme 32: Intermolecular [3 + 2] annulation of cyclopropylamines with olefins.

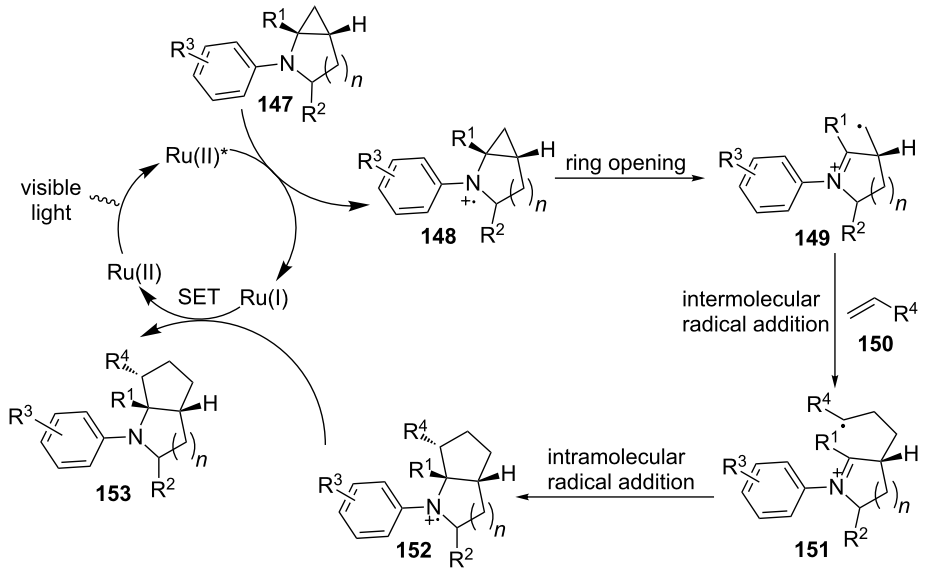

Scheme 33: Proposed mechanism for intermolecular [3 + 2] annulation.

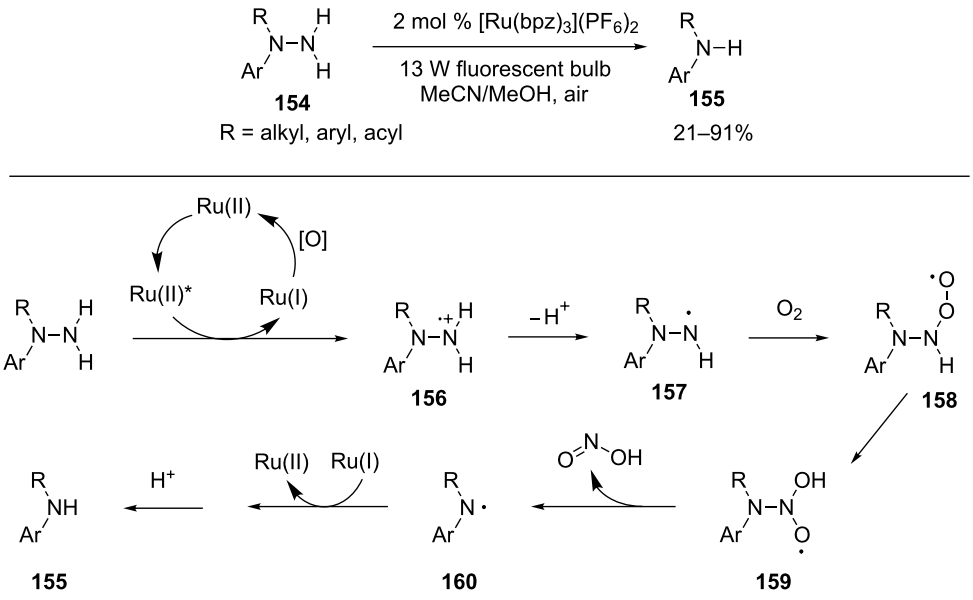

Scheme 34: Photoinduced clevage of N–N bonds of aromatic hydrazines and hydrazides.

of hydrazines or hydrazides to a amine radical cation **156** by the photoexcited Ru(II) complex. Deprotonation of the amine radical cation **156** produces a neutral nitrogen radical **157** that reacts with oxygen to furnish the radical **158**. The radical **158** then rearranges to a new oxygen-based radical **159**, which undergoes a cleavage reaction to yield nitrous acid and a secondary amine radical **160**. Finally, one-electron reduction of the amine radical by Ru(I), followed by protonation provides a secondary amine **155**.

Conclusion

Visible light photoredox catalysis provides a unique way to activate small molecules such as amines. The dual nature of the photocatalyst's photoexcited state as both oxidant and reductant allows accepting or donating one electron strictly dependent upon the small molecules encountered. Amines typically act as an electron donor to reductively quench the photoexcited state while they are oxidized to the corresponding amine radical cations. The resulting nitrogen radical cations are highly useful

reactive intermediates that are capable of initializing multiple downstream pathways leading to diverse synthetic intermediates such as electrophilic iminium ions, nucleophilic α-amino radicals, and distonic ions possessing both an iminium ion and a carbon radical. Interception of these intermediates allows a variety of synthetic transformations to produce a diverse array of amines. Moreover, visible light photoredox catalysis has been merged with other types of catalysis, including enamine catalysis, *N*-heterocyclic carbene (NHC) catalysis, or copper acetylide formation. This dual catalysis approach has significantly expanded the type of bonds that can be formed, particularly bonds formed asymmetrically. In summary, the utility of amine radical cations formed via photooxidation of the amines has been amply demonstrated in a number of synthetic methods. With the organic community's increasing interest in visible light photoredox catalysis, new and innovative applications of this reactive intermediate will continue to develop.

References

1. Chow, Y. L.; Danen, W. C.; Nelson, S. F.; Rosenblatt, D. H. *Chem. Rev.* **1978,** *78,* 243–274. doi:10.1021/cr60313a003
2. Stella, L. *Angew. Chem., Int. Ed. Engl.* **1983,** *22,* 337–350. doi:10.1002/anie.198303373
3. Bauld, N. L. *Tetrahedron* **1989,** *45,* 5307–5363. doi:10.1016/S0040-4020(01)89486-2
4. Schmittel, M.; Burghart, A. *Angew. Chem., Int. Ed. Engl.* **1997,** *36,* 2550–2589. doi:10.1002/anie.199725501
5. Fallis, A. G.; Brinza, I. M. *Tetrahedron* **1997,** *53,* 17543–17594. doi:10.1016/S0040-4020(97)10060-6
6. Moeller, K. D. *Tetrahedron* **2000,** *56,* 9527–9554. doi:10.1016/S0040-4020(00)00840-1
7. Hoffmann, N. *Pure Appl. Chem.* **2007,** *79,* 1949–1958. doi:10.1351/pac200779111949
8. Stella, L. Nitrogen-centered radicals. In *Radicals in Organic Synthesis;* Renaud, P.; Sibi, M. P., Eds.; Wiley-VCH: Weinheim, Germany, 2001; Vol. 2, pp 407–426. doi:10.1002/9783527618293.ch45
9. Chiba, T.; Takata, Y. *J. Org. Chem.* **1977,** *42,* 2973–2977. doi:10.1021/jo00438a005
10. Shono, T.; Matsumura, Y.; Tsubata, K. *J. Am. Chem. Soc.* **1981,** *103,* 1172–1176. doi:10.1021/ja00395a029
11. Baslé, O.; Borduas, N.; Dubois, P.; Chapuzet, J. M.; Chan, T.-H.; Lessard, J.; Li, C.-J. *Chem.–Eur. J.* **2010,** *16,* 8162–8166. doi:10.1002/chem.201000240
12. Tsang, A. S.-K.; Todd, M. H. *Tetrahedron Lett.* **2009,** *50,* 1199–1202. doi:10.1016/j.tetlet.2008.12.101
13. Richter, T.; Mancheño, O. G. *Eur. J. Org. Chem.* **2010,** 4460–4467. doi:10.1002/ejoc.201000548
14. Shu, X.-Z.; Xia, X.-F.; Yang, Y.-F.; Ji, K.-G.; Liu, X.-Y.; Liang, Y.-M. *J. Org. Chem.* **2009,** *74,* 7464–7469. doi:10.1021/jo901583r
15. Murahashi, S.-I.; Zhang, D. *Chem. Soc. Rev.* **2008,** *37,* 1490–1501. doi:10.1039/b706709g
16. Li, C.-J. *Acc. Chem. Res.* **2009,** *42,* 335–344. doi:10.1021/ar800164n
17. Boess, E.; Schmitz, C.; Klussmann, M. *J. Am. Chem. Soc.* **2012,** *134,* 5317–5325. doi:10.1021/ja211697s
18. Ratnikov, M. O.; Doyle, M. P. *J. Am. Chem. Soc.* **2013,** *135,* 1549–1557. doi:10.1021/ja3113559
19. Cho, D. W.; Yoon, U. C.; Mariano, P. S. *Acc. Chem. Res.* **2011,** *44,* 204–215. doi:10.1021/ar100125j
20. Pandey, G.; Gadre, S. R. *ARKIVOC* **2003,** 45–54. doi:10.3998/ark.5550190.0004.306
21. Hoshikawa, T.; Yoshioka, S.; Kamijo, S.; Inoue, M. *Synthesis* **2013,** *45,* 874–887. doi:10.1055/s-0032-1318325
22. Shi, L.; Xia, W. *Chem. Soc. Rev.* **2012,** *41,* 7687–7697. doi:10.1039/c2cs35203f
23. Maity, S.; Zheng, N. *Synlett* **2012,** *23,* 1851–1856. doi:10.1055/s-0032-1316592
24. Campagana, S.; Puntoriero, F.; Nastasi, F.; Bergamini, G.; Balzani, V. *Top. Curr. Chem.* **2007,** *280,* 117–214. doi:10.1007/128_2007_133
25. Juris, A.; Balzani, V.; Barigelletti, F.; Campagna, S.; Belser, P.; von Zelewsky, A. *Coord. Chem. Rev.* **1988,** *84,* 85–277. doi:10.1016/0010-8545(88)80032-8
26. Kalyanasundaram, K. *Coord. Chem. Rev.* **1982,** *46,* 159–244. doi:10.1016/0010-8545(82)85003-0
27. Lowry, M. S.; Bernhard, S. *Chem.–Eur. J.* **2006,** *12,* 7970–7977. doi:10.1002/chem.200600618
28. Flamigni, L.; Barbieri, A.; Sabatini, C.; Ventura, B.; Barigelletti, F. *Top. Curr. Chem.* **2007,** *281,* 143–203. doi:10.1007/128_2007_131
29. Hedstrand, D. M.; Kruizinga, W. H.; Kellogg, R. M. *Tetrahedron Lett.* **1978,** *19,* 1255–1258. doi:10.1016/S0040-4039(01)94515-0
30. Neumann, M.; Füldner, S.; König, B.; Zeitler, K. *Angew. Chem., Int. Ed.* **2011,** *50,* 951–954. doi:10.1002/anie.201002992
31. Meyer, T. J. *Acc. Chem. Res.* **1989,** *22,* 163–170. doi:10.1021/ar00161a001
32. Bard, A. J.; Fox, M. A. *Acc. Chem. Res.* **1995,** *28,* 141–145. doi:10.1021/ar00051a007
33. Lehn, J. M.; Ziessel, R. *Proc. Natl. Acad. Sci. U. S. A.* **1982,** *79,* 701–704. doi:10.1073/pnas.79.2.701
34. Willner, I.; Maidan, R.; Mandler, D.; Duerr, H.; Doerr, G.; Zengerle, K. *J. Am. Chem. Soc.* **1987,** *109,* 6080–6086. doi:10.1021/ja00254a029
35. Prier, C. K.; Rankic, D. A.; MacMillan, D. W. C. *Chem. Rev.* **2013,** *113,* 5322–5363. doi:10.1021/cr300503r
36. Yoon, T. P.; Ischay, M. A.; Du, J. *Nat. Chem.* **2010,** *2,* 527–532. doi:10.1038/nchem.687
37. Tucker, J. W.; Stephenson, C. R. J. *J. Org. Chem.* **2012,** *77,* 1617–1622. doi:10.1021/jo202538x
38. Xuan, J.; Xiao, W.-J. *Angew. Chem., Int. Ed.* **2012,** *51,* 6828–6838. doi:10.1002/anie.201200223
39. Telpý, F. *Collect. Czech. Chem. Commun.* **2011,** *76,* 859–917. doi:10.1135/cccc2011078
40. Narayanam, J. M. R.; Stephenson, C. R. J. *Chem. Soc. Rev.* **2011,** *40,* 102–113. doi:10.1039/b913880n
41. Zeitler, K. *Angew. Chem., Int. Ed.* **2009,** *48,* 9785–9789. doi:10.1002/anie.200904056
42. Xi, Y.; Yi, H.; Lei, A. *Org. Biomol. Chem.* **2013,** *11,* 2387–2403. doi:10.1039/c3ob40137e
43. Gould, I. R.; Ege, D.; Moser, J. E.; Farid, S. *J. Am. Chem. Soc.* **1990,** *112,* 4290–4301. doi:10.1021/ja00167a027
44. Kellett, M. A.; Whitten, D. G.; Gould, I. R.; Bergmark, W. R. *J. Am. Chem. Soc.* **1991,** *113,* 358–359. doi:10.1021/ja00001a052
45. DeLaive, P. J.; Lee, J. T.; Springtschnik, H. W.; Abruña, H.; Meyer, T. J.; Whitten, D. G. *J. Am. Chem. Soc.* **1977,** *99,* 7094–7097. doi:10.1021/ja00463a070
46. DeLaive, P. J.; Foreman, T. K.; Giannotti, C.; Whitten, D. G. *J. Am. Chem. Soc.* **1980,** *102,* 5627–5631. doi:10.1021/ja00537a037

47. Mashraqui, S. H.; Kellog, R. M. *Tetrahedron Lett.* **1985,** *26,* 1453–1456. doi:10.1016/S0040-4039(00)99069-5
48. Fukuzumi, S.; Mochizuki, S.; Tanaka, T. *J. Phys. Chem.* **1990,** *94,* 722–726. doi:10.1021/j100365a039
49. Willner, I.; Tsfania, T.; Eichen, Y. *J. Org. Chem.* **1990,** *55,* 2656–2662. doi:10.1021/jo00296a023
50. Narayanam, J. M. R.; Tucker, J. W.; Stephenson, C. R. J. *J. Am. Chem. Soc.* **2009,** *131,* 8756–8757. doi:10.1021/ja9033582
51. Nguyen, J. D.; D'Amato, E. M.; Narayanam, J. M. R.; Stephenson, C. R. J. *Nat. Chem.* **2012,** *4,* 854–859. doi:10.1038/nchem.1452
52. Tucker, J. W.; Nguyen, J. D.; Narayanam, J. M. R.; Krabbe, S. W.; Stephenson, C. R. J. *Chem. Commun.* **2010,** *46,* 4985–4987. doi:10.1039/c0cc00981d
53. Tucker, J. W.; Stephenson, C. R. J. *Org. Lett.* **2011,** *13,* 5468–5471. doi:10.1021/ol202178t
54. Kim, H.; Lee, C. *Angew. Chem., Int. Ed.* **2012,** *51,* 12303–12306. doi:10.1002/anie.201203599
55. Chen, Y.; Kamlet, A. S.; Steinman, J. B.; Liu, D. R. *Nat. Chem.* **2011,** *3,* 146–153. doi:10.1038/nchem.932
56. Nelson, S. F.; Ippoliti, J. T. *J. Am. Chem. Soc.* **1986,** *108,* 4879–4881. doi:10.1021/ja00276a028
57. Lewis, F. D. *Acc. Chem. Res.* **1986,** *19,* 401–405. doi:10.1021/ar00132a004
58. Parker, V. D.; Tilset, M. *J. Am. Chem. Soc.* **1991,** *113,* 8778–8781. doi:10.1021/ja00023a026
59. Dombrowski, G. W.; Dinnocenzo, J. P.; Zielinski, P. A.; Farid, S.; Wosinska, Z. M.; Gould, I. R. *J. Org. Chem.* **2005,** *70,* 3791–3800. doi:10.1021/jo047813g
60. Freeman, D. B.; Furst, L.; Condie, A. G.; Stephenson, C. R. J. *Org. Lett.* **2012,** *14,* 94–97. doi:10.1021/ol202883v
61. Dinnocenzo, J. P.; Banach, T. E. *J. Am. Chem. Soc.* **1989,** *111,* 8646–8653. doi:10.1021/ja00205a014
62. Zhang, X.; Yeh, S.-R.; Hong, S.; Freccero, M.; Albini, A.; Falvey, D. E.; Mariano, P. S. *J. Am. Chem. Soc.* **1994,** *116,* 4211–4220. doi:10.1021/ja00089a010
63. Wayner, D. D. M.; Dannenberg, J. J.; Griller, D. *Chem. Phys. Lett.* **1986,** *131,* 189–191. doi:10.1016/0009-2614(86)80542-5
64. Condie, A. G.; González-Gómez, J. C.; Stephenson, C. R. J. *J. Am. Chem. Soc.* **2010,** *132,* 1464–1465. doi:10.1021/ja909145y
65. Rueping, M.; Vila, C.; Koenigs, R. M.; Poscharny, K.; Fabry, D. C. *Chem. Commun.* **2011,** *47,* 2360–2362. doi:10.1039/c0cc04539j
66. Kohls, P.; Jadhav, D.; Pandey, G.; Reiser, O. *Org. Lett.* **2012,** *14,* 672–675. doi:10.1021/ol202857t
67. Hari, D. P.; König, B. *Org. Lett.* **2011,** *13,* 3852–3855. doi:10.1021/ol201376v
68. Pan, Y.; Kee, C. W.; Chen, L.; Tan, C.-H. *Green Chem.* **2011,** *13,* 2682–2685. doi:10.1039/c1gc15489c
69. Liu, Q.; Li, Y.-N.; Zhang, H.-H.; Chen, B.; Tung, C.-H.; Wu, L.-Z. *Chem.–Eur. J.* **2012,** *18,* 620–627. doi:10.1002/chem.201102299
70. Pan, Y.; Wang, S.; Kee, C. W.; Dubuisson, E.; Yang, Y.; Loh, K. P.; Tan, C.-H. *Green Chem.* **2011,** *13,* 3341–3344. doi:10.1039/c1gc15865a
71. Dreyer, D. R.; Jia, H.-P.; Bielawski, C. W. *Angew. Chem., Int. Ed.* **2010,** *49,* 6813–6816. doi:10.1002/anie.201002160
72. Jia, H.-P.; Dreyer, D. R.; Bielawski, C. W. *Adv. Synth. Catal.* **2011,** *353,* 528–532. doi:10.1002/adsc.201000748
73. Dreyer, D. R.; Jia, H.-P.; Todd, A. D.; Geng, J.; Bielawski, C. W. *Org. Biomol. Chem.* **2011,** *9,* 7292–7295. doi:10.1039/c1ob06102j
74. Todd, A. D.; Bielawski, C. W. *Catal. Sci. Technol.* **2013,** *3,* 135–139. doi:10.1039/c2cy20474f
75. To, W.-P.; Tong, G. S.-M.; Lu, W.; Ma, C.; Liu, J.; Chow, A. L.-F.; Che, C.-M. *Angew. Chem., Int. Ed.* **2012,** *51,* 2654–2657. doi:10.1002/anie.201108080
76. Xue, Q.; Xie, J.; Jin, H.; Cheng, Y.; Zhu, C. *Org. Biomol. Chem.* **2013,** *11,* 1606–1609. doi:10.1039/c3ob27400d
77. Rueping, M.; Koenigs, R. M.; Poscharny, K.; Fabry, D. C.; Leonori, D.; Vila, C. *Chem.–Eur. J.* **2012,** *18,* 5170–5174. doi:10.1002/chem.201200050
78. DiRocco, D. A.; Rovis, T. *J. Am. Chem. Soc.* **2012,** *134,* 8094–8097. doi:10.1021/ja3030164
79. Zou, Y.-Q.; Lu, L.-Q.; Fu, L.; Chang, N.-J.; Rong, J.; Chen, J.-R.; Xiao, W.-J. *Angew. Chem., Int. Ed.* **2011,** *50,* 7171–7175. doi:10.1002/anie.201102306
80. Rueping, M.; Leonori, D.; Poisson, T. *Chem. Commun.* **2011,** *47,* 9615–9617. doi:10.1039/c1cc13660g
81. Xie, J.; Xue, Q.; Jin, H.; Li, H.; Cheng, Y.; Zhu, C. *Chem. Sci.* **2013,** *4,* 1281–1286. doi:10.1039/c2sc22131d
82. Wang, Z.-Q.; Hu, M.; Huang, X.-C.; Gong, L.-B.; Xie, Y.-X.; Li, J.-H. *J. Org. Chem.* **2012,** *77,* 8705–8711. doi:10.1021/jo301691h
83. Zhu, S.; Rueping, M. *Chem. Commun.* **2012,** *48,* 11960–11962. doi:10.1039/c2cc36995h
84. O'Donnell, J. F.; Mann, C. K. *J. Electroanal. Chem.* **1967,** *13,* 157–162. doi:10.1016/0022-0728(67)80108-6
85. Dai, C.; Meschini, F.; Narayanam, J. M. R.; Stephenson, C. R. J. *J. Org. Chem.* **2012,** *77,* 4425–4431. doi:10.1021/jo300162c
86. Xuan, J.; Cheng, Y.; An, J.; Lu, L.-Q.; Zhang, X.-X.; Xiao, W.-J. *Chem. Commun.* **2011,** *47,* 8337–8339. doi:10.1039/c1cc12203g
87. Xuan, J.; Feng, Z.-J.; Duan, S.-W.; Xiao, W.-J. *RSC Adv.* **2012,** *2,* 4065–4068. doi:10.1039/c2ra20403g
88. Mathis, C. L.; Gist, B. M.; Frederickson, C. K.; Midkiff, K. M.; Marvin, C. C. *Tetrahedron Lett.* **2013,** *54,* 2101–2104. doi:10.1016/j.tetlet.2013.02.031
89. Rueping, M.; Zhu, S.; Koenigs, R. M. *Chem. Commun.* **2011,** *47,* 8679–8681. doi:10.1039/c1cc12907d
90. Espelt, L. R.; Wiensch, E. M.; Yoon, T. P. *J. Org. Chem.* **2013,** *78,* 4107–4114. doi:10.1021/jo400428m
91. Miyake, Y.; Nakajima, K.; Nishibayashi, Y. *J. Am. Chem. Soc.* **2012,** *134,* 3338–3341. doi:10.1021/ja211770y
92. Zhu, S.; Das, A.; Bui, L.; Zhou, H.; Curran, D. P.; Rueping, M. *J. Am. Chem. Soc.* **2013,** *135,* 1823–1829. doi:10.1021/ja309580a
93. Miyake, Y.; Nakajima, K.; Nishibayashi, Y. *Chem.–Eur. J.* **2012,** *18,* 16473–16477. doi:10.1002/chem.201203066
94. Minakata, S.; Ohshima, Y.; Takemiya, A.; Ryu, I.; Komatsu, M.; Ohshiro, Y. *Chem. Lett.* **1997,** *26,* 311–312. doi:10.1246/cl.1997.311
95. Kerr, G. H.; Meth-Cohn, O.; Mullock, E. B.; Suschitzky, H. *J. Chem. Soc., Perkin Trans. 1* **1974,** 1614–1619. doi:10.1039/P19740001614
96. Murahashi, S.; Oda, T.; Sugahara, T.; Masui, Y. *J. Org. Chem.* **1990,** *55,* 1744–1749. doi:10.1021/jo00293a014
97. Izumi, T.; Kohei, K.; Murakami, S. *J. Heterocycl. Chem.* **1993,** *30,* 1133–1136. doi:10.1002/jhet.5570300453
98. Eberson, L.; Persson, O.; Svensson, J. O. *Acta Chem. Scand.* **1998,** *52,* 1293–1300. doi:10.3891/acta.chem.scand.52-1293
99. Lowry, M. S.; Goldsmith, J. I.; Slinker, J. D.; Rohl, R.; Pascal, R. A., Jr.; Malliaras, G. G.; Bernhard, S. *Chem. Mater.* **2005,** *17,* 5712–5719. doi:10.1021/cm051312+
100. McNally, A.; Prier, C. K.; MacMillan, D. W. C. *Science* **2011,** *334,* 1114–1117. doi:10.1126/science.1213920

101. Lee, L. Y. C.; Ci, X.; Giannotti, C.; Whitten, D. G. *J. Am. Chem. Soc.* **1986,** *108,* 175–177. doi:10.1021/ja00261a029
102. Cai, S.; Zhao, X.; Wang, X.; Liu, Q.; Li, Z.; Wang, D. Z. *Angew. Chem., Int. Ed.* **2012,** *51,* 8050–8053. doi:10.1002/anie.201202880
103. Carson, C. A.; Kerr, M. A. *Chem. Soc. Rev.* **2009,** *38,* 3051–3060. doi:10.1039/b901245c
104. Yu, M.; Pagenkopf, B. L. *Tetrahedron* **2005,** *61,* 321–347. doi:10.1016/j.tet.2004.10.077
105. Griller, D.; Ingold, K. U. *Acc. Chem. Res.* **1980,** *13,* 317–323. doi:10.1021/ar50153a004
106. Li, X.; Grimm, M. L.; Igarashi, K.; Castagnoli, N., Jr.; Tanko, J. M. *Chem. Commun.* **2007,** 2648–2650. doi:10.1039/b702157g
107. Maity, S.; Zheng, N. *Angew. Chem., Int. Ed.* **2012,** *51,* 9562–9566. doi:10.1002/anie.201205137
108. Zhu, M.; Zheng, N. *Synthesis* **2011,** 2223–2236. doi:10.1055/s-0030-1260082

License and Terms

Beilstein Journal of Organic Chemistry

3-Pyridinols and 5-pyrimidinols: Tailor-made for use in synergistic radical-trapping co-antioxidant systems

Luca Valgimigli[*1], Daniele Bartolomei[1], Riccardo Amorati[1], Evan Haidasz[2], Jason J. Hanthorn[2], Susheel J. Nara[2], Johan Brinkhorst[2] and Derek A. Pratt[*2]

Full Research Paper

Open Access

Address:
[1]Department of Chemistry "G. Ciamician", University of Bologna, Via S. Giacomo 11, I-40126 Bologna, Italy and [2]Department of Chemistry, University of Ottawa, 10 Marie Curie Pvt., Ottawa, Ontario, Canada K1N 6N5

Email:
Luca Valgimigli[*] - luca.valgimigli@unibo.it; Derek A. Pratt[*] - dpratt@uottawa.ca

* Corresponding author

Keywords:
antioxidants; autoxidation; free radical; phenols; 3-pyridinols; 5-pyrimidinols

Beilstein J. Org. Chem. **2013,** *9,* 2781–2792.
doi:10.3762/bjoc.9.313

Received: 08 October 2013
Accepted: 25 November 2013
Published: 04 December 2013

This article is part of the Thematic Series "Organic free radical chemistry".

Guest Editor: C. Stephenson

Abstract

The incorporation of nitrogen atoms into the aromatic ring of phenolic compounds has enabled the development of some of the most potent radical-trapping antioxidants ever reported. These compounds, 3-pyridinols and 5-pyrimidinols, have stronger O–H bonds than equivalently substituted phenols, but possess similar reactivities toward autoxidation chain-carrying peroxyl radicals. These attributes suggest that 3-pyridinols and 5-pyrimidinols will be particularly effectiveco-antioxidants when used in combination with more common, but less reactive, phenolic antioxidants such as 2,6-di-*tert*-butyl-4-methylphenol (BHT), which we demonstrate herein. The antioxidants function in a synergistic manner to inhibit autoxidation; taking advantage of the higher reactivity of the 3-pyridinols/5-pyrimidinols to trap peroxyl radicals and using the less reactive phenols to regenerate them from their corresponding aryloxyl radicals. The present investigations were carried out in chlorobenzene and acetonitrile in order to provide some insight into the medium dependence of the synergism and the results, considered with some from our earlier work, prompt a revision of the H-bonding basicity value of acetonitrile to β_2^H of 0.39. Overall, the thermodynamic and kinetic data presented here enable the design of co-antioxidant systems comprising lower loadings of the more expensive 3-pyridinol/5-pyrimidinol antioxidants and higher loadings of the less expensive phenolic antioxidants, but which are equally efficacious as the 3-pyridinol/5-pyrimidinol antioxidants alone at higher loadings.

Introduction

Radical-trapping (chain-breaking) antioxidants are arguably the most important class of compounds used to protect organic materials from oxidative degradation from autoxidation (Scheme 1) [1,2]. Phenolic compounds are almost universally used for this purpose – for industrial/commercial applications as well as in nature – since they possess inherently high reactivities to chain-carrying peroxyl radicals ($ROO^{\bullet}$) and are readily manipulated to adjust their physical properties for use under specific conditions. The mechanism of the reaction involves the formal transfer of an H-atom from the phenol (ArOH) to a peroxyl radical $ROO^{\bullet}$ (reaction 1 in Scheme 2).

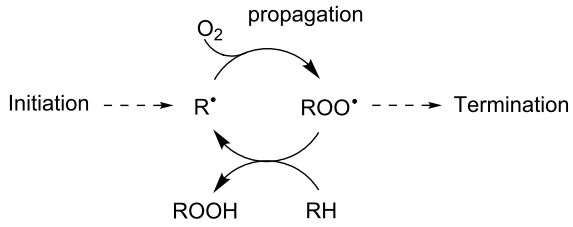

Scheme 1: Autoxidation of an organic substrate RH.

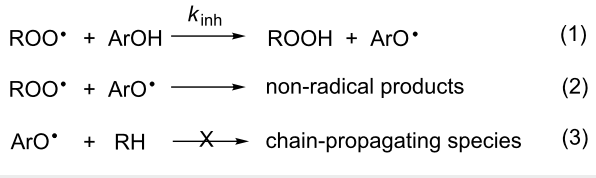

Scheme 2: Inhibition of autoxidation by radical-trapping antioxidants (e.g. ArOH).

In general, the resultant phenoxyl radical ($ArO^{\bullet}$) is sufficiently unreactive toward the substrate (RH) that it reacts with a second peroxyl radical (reaction 2 in Scheme 2), thereby breaking two oxidative chains per molecule of antioxidant – a ratio commonly referred to as the stoichiometric factor (n). However, under some circumstances (e.g. when diffusion of the antioxidant is impeded and it has limited opportunity to encounter other radical species), it is possible for the antioxidant-derived phenoxyl radical to propagate the chain reaction (reaction 3 in Scheme 2). The most relevant example of this is so-called 'tocopherol mediated peroxidation' (TMP), which occurs when α-tocopherol (the most biologically active form of vitamin E) is left alone to protect the lipid core of low-density lipoproteins (LDL). LDL is the particle responsible for the distribution of cholesterol in blood plasma and whose oxidation has been linked to the development of cardiovascular disease. Under these conditions, α-tocopherol is not an effective radical-trapping antioxidant [3,4].

For this (and other) reason(s), radical-trapping antioxidants are rarely used alone – be it in nature or industrial/commercial applications. Instead, organic substrates are generally protected from oxidation by the addition of a combination of antioxidants (or co-antioxidants) that function in a synergistic fashion, i.e. they inhibit autoxidation more effectively together than would be expected from the simple additive contributions of their individual antioxidant activities. The interplay of α-tocopherol and ascorbate (vitamin C) in preventing the oxidation of LDL lipids is perhaps the best-known example of such synergism, since the regeneration of α-tocopherol by reduction of the α-tocopheroxyl radical by ascorbate prevents TMP, and effectively turns a water-soluble reducing equivalent into a lipid-soluble one [5-7].

In recent years, some of us have worked to understand the kinetic and thermodynamic basis for synergism among radical-trapping antioxidants in homogeneous solution, which is summarized in Scheme 3 [8,9]. When two (or more) antioxidants are present in a system, the principal antioxidant (AH) is identified as that which reacts most rapidly with peroxyl radicals than the other(s), the so-called co-antioxidant(s) (co-AH), i.e. $k_{inh}' > k_{inh}''$ in reaction 4 and reaction 5 (Scheme 3), respectively. As a result of its greater reactivity, AH must be consumed before co-AH. However, if the equilibrium in reaction 6 (Scheme 3) is favourable, co-AH can regenerate AH for further reaction with $ROO^{\bullet}$. Of course, this is only true if equilibration is faster than consumption of the AH-derived radical by reaction with a second peroxyl radical, i.e. $k_r[\text{co-AH}] > k_7[ROO^{\bullet}]$ for reaction 6 and reaction 7 (Scheme 3), respectively. However, this is a condition that is generally easily met since $[ROO^{\bullet}]_{ss}$ in the presence of AH/co-AH must be very low and k_r for phenol/phenoxyl couples is normally $\geq 10^4$ $M^{-1}s^{-1}$ [8,9].

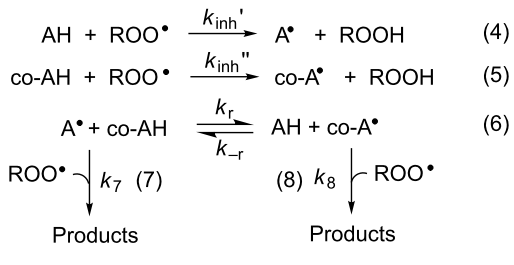

Scheme 3: Relevant reactions in co-antioxidant systems.

Based on this model, in order for synergism to occur among equilibrating phenolic antioxidants it is necessary that the principal antioxidant has both a higher reactivity with peroxyl radicals (k_{inh}) and a higher O–H bond dissociation enthalpy (BDE),

as compared to the co-antioxidant. Unfortunately, this is a very demanding requirement since k_{inh} and the O–H BDE are inversely correlated according to well-established Evans–Polanyi relationships [2,10].

Over the years, our research groups have developed novel air-stable and highly reactive radical-trapping chain-breaking antioxidants based on either 3-pyridinol (**1**) or 5-pyrimidinol (**2**) core structures (Figure 1) [11-17]. Compared to equivalently-substituted phenols, these compounds have been shown to possess stronger O–H bonds (e.g. +1.4 kcal/mol for **1** and +2.5 kcal/mol for **2** relative to **3**) while maintaining similar or higher reactivity toward peroxyl radicals [11,13]. As is the case for phenols, 3-pyridinols and 5-pyrimidinols can be substituted with electron-donating groups to weaken their O–H bonds and increase their rates of reaction with peroxyl radicals in a predictable fashion [11]. Based on these facts, we surmised that 3-pyridinols and 5-pyrimidinols would be ideal principal antioxidants in synergistic co-antioxidant systems with phenols. Herein we describe the rational design and kinetic characterization of such systems based on the combination of suitably substituted 3-pyridinols and 5-pyrimidinols (**4**–**9**) with conventional phenolic antioxidants (**10**–**12**).

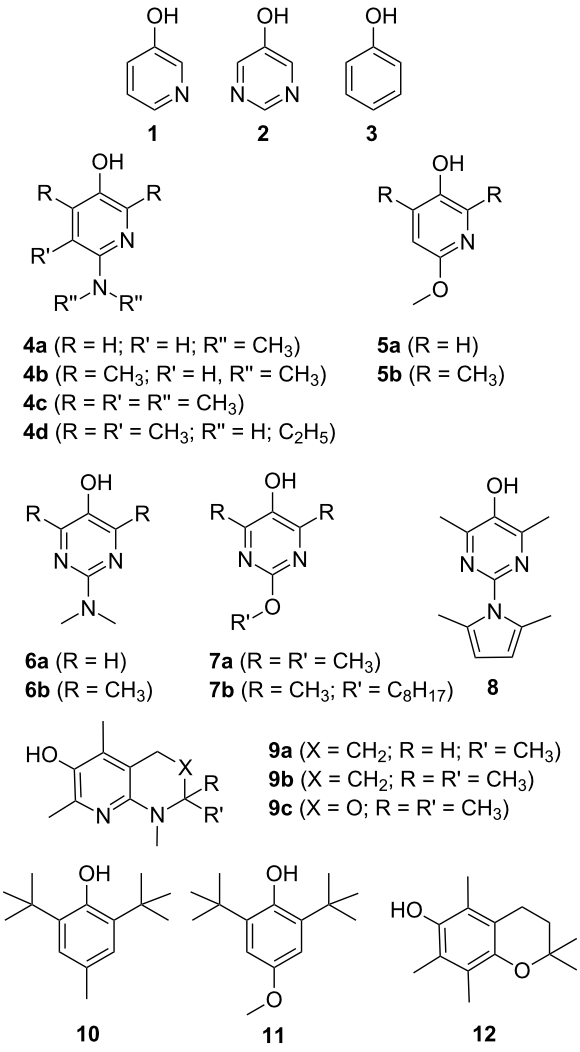

Figure 1: Relevant structures **1**–**12**.

Results and Discussion

Synthesis. The preparation of compounds **4a**, **4b** and **5**–**8** involved installation of the aryl alcohol moiety as the final step via a Cu-catalyzed benzyloxylation/hydrogenolysis sequence on the corresponding pyri(mi)dyl halides, whereas the preparation of **4c**, **4d** and **9** followed a route starting from pyridoxamine, wherein the aryl alcohol is present throughout the sequence. Details are provided in the Experimental section and/or the cited references.

Reactivity with peroxyl radicals. To set up a rational framework for the design of co-antioxidant systems, the rate constants for the reactions of various pyridinols and pyrimidinols with peroxyl radicals (k_{inh}) were measured by the well-established inhibited autoxidation of styrene (or cumene) in chlorobenzene at 303 K. These measurements also included experiments with three well-established phenolic antioxidants: 2,6-di-*tert*-butyl-4-methylphenol (BHT, **10**), 2,6-di-*tert*-butyl-4-methoxyphenol (DBHA, **11**), a hindered analogue of the widely employed BHA, and 2,2,5,7,8-pentamethylchroman-6-ol (PMHC, **12**), a synthetic analogue of α-tocopherol lacking its phytyl sidechain. While some of these rate constants have been reported in the literature, we felt it necessary to determine them all under the exact same conditions in order to be able to predict and/or rationalize observations made when the antioxidants are used in combinations. The results are given in Table 1. It must be pointed out that where previous data have been obtained under comparable conditions, our data are in excellent agreement – with k_{inh} values usually within a factor of two. As a result, the reactivity trends parallel those that have been observed before: the bicyclic naphthyridinol compounds **9a**–**c** generally possess the highest reactivities, followed by the aminopyridinols **4** and aminopyrimidinols **6**, and finally the alkoxypyridinols **5** and alkoxypyrimidinols **7**. A previously unstudied compound – the 2,4-dimethylpyrrole-substituted pyrimidinol **8** – was the least reactive pyri(mi)dinol we studied, with a rate constant almost 200 fold lower than that of the analogous dimethylamino-substituted pyrimidinol **6b** ($k_{inh} = 4.4 \times 10^4$ versus 7.4×10^6 $M^{-1}s^{-1}$, respectively). Clearly, the 2,4-dimethylpyrrole substituent is not as electron-donating as a dimethylamino substituent (the O–H bond in **8** is 6.6 kcal/mol stronger than that in **6b**, vide infra). These results provide an explanation for the significant differences in the radical scavenging activities of pyridinols bearing these substituents in recently reported cell-based assays [18].

Table 1: Rate constants for the reactions of **4–12** with peroxyl radicals (k_{inh}) at 303 K obtained from AIBN-initiated inhibited autoxidations of styrene (50% v/v) in either chlorobenzene (PhCl) or acetonitrile (CH_3CN). O–H Bond dissociation enthalpies calculated using CBS-QB3 are given along with available experimental data where possible.

	k_{inh} (PhCl) /$M^{-1}s^{-1}$	*n*	k_{inh} (CH_3CN) /$M^{-1}s^{-1}$	*n*	k_{inh} (PhCl)/k_{inh} (CH_3CN)	$BDE_{OH}^{calc(exp)}$[a] /kcal/mol
4a	$(3.6 \pm 0.6) \times 10^6$ [b]	1.9	$(5.4 \pm 0.2) \times 10^5$	2.0	7	77.9
4b	$(1.4 \pm 0.6) \times 10^7$ [c]	1.9	$(3.0 \pm 0.3) \times 10^6$	2.0	5	74.8 (75.9)
4c	$(2.0 \pm 1.0) \times 10^6$ [d]	2.1	$(3.1 \pm 0.6) \times 10^5$	2.0	6	78.0
4d	$(8.5 \pm 2.8) \times 10^6$ [d]	1.9	$(3.0 \pm 0.4) \times 10^6$	2.0	3	74.5
5a	$(7.3 \pm 0.4) \times 10^4$	2.2[e]	$(4.1 \pm 0.3) \times 10^4$	1.9[e]	18	82.4
5b	$(4.4 \pm 0.7) \times 10^5$ [c]	2.1	$(3.8 \pm 0.9) \times 10^4$	1.9[e]	12	78.9
6a	$(2.0 \pm 0.6) \times 10^6$ [b]	2.1	$(3.0 \pm 0.7) \times 10^5$	1.9	7	78.3
6b	$(7.4 \pm 0.6) \times 10^6$	2.1	$(1.0 \pm 0.3) \times 10^6$	1.8	7	75.6 (77.1)
7a	$(3.1 \pm 0.4) \times 10^5$	2.0	$(1.1 \pm 0.6) \times 10^4$ [f]	2.1[e]	28	80.9 (81.4)
7b	$(3.7 \pm 0.3) \times 10^5$	2.0	$(1.4 \pm 0.5) \times 10^4$	2.0[e]	26	80.9[g]
8	$(4.4 \pm 1.0) \times 10^4$	2.0[e]	$(1.3 \pm 0.5) \times 10^3$	n.d.	34	81.8
9a	$(5.5 \pm 3.1) \times 10^7$ [h]	1.3	$(9.2 \pm 1.9) \times 10^6$	1.7	6	74.9 (75.2[i])
9b	$(7.8 \pm 0.8) \times 10^7$ [h]	1.5	$(1.3 \pm 0.3) \times 10^7$	1.7	6	75.0 (75.2[i])
9c	$(1.5 \pm 0.2) \times 10^7$ [j]	2.0	$(2.9 \pm 1.4) \times 10^6$	2.0	5	75.4
10	$(1.1 \pm 0.2) \times 10^4$ [k]	2.0[e]	n.d.	n.d.	-	78.7 (79.9[l])
11	$(1.1 \pm 0.2) \times 10^5$ [k]	2.0	$(2.5 \pm 1.0) \times 10^4$ [f]	n.d.	4	75.5 (77.2[l])
12	$(3.2 \pm 0.5) \times 10^6$ [k]	2 [l]	$(6.5 \pm 0.8) \times 10^5$ [f]	2[m]	5	77.7 (77.1[l])

[a]Experimental values (in benzene) obtained by REqEPR at 298 K are from [12,13] and have been corrected for the revised O–H BDE of phenol [19]. [b]Values for **4a** and **6a** were previously determined as 4.8×10^6 $M^{-1}s^{-1}$ and 1.1×10^6 $M^{-1}s^{-1}$ at 303 K from the inhibited oxidation of styrene in PhCl and as 1.1×10^7 $M^{-1}s^{-1}$ and 6.5×10^6 $M^{-1}s^{-1}$ at 310 K in benzene by radical clock [16]. [c]Values of 1.6×10^7 $M^{-1}s^{-1}$ and 2.9×10^5 $M^{-1}s^{-1}$ were previously reported for **4b** and **5b** from inhibited styrene oxidation in PhCl at 303 K [14]. [d]Values for **4c** and **4d** of 3.3×10^6 $M^{-1}s^{-1}$ and 8.7×10^6 $M^{-1}s^{-1}$ measured by inhibited autoxidation of styrene in PhCl and of 1.6×10^6 $M^{-1}s^{-1}$ and 1.4×10^7 $M^{-1}s^{-1}$ in benzene at 310 K by radical clock [17]. [e]Determined from the inhibited autoxidation of cumene at 303 K. [f]Values of 7.9×10^2 $M^{-1}s^{-1}$, 2.2×10^4 $M^{-1}s^{-1}$ and 6.8×10^5 $M^{-1}s^{-1}$were previously measured for **7a**, **11**, **12** from the autoxidation of styrene in acetonitrile at 303 K [20]. [g]Assumed the same as **7a**. [h]Values of 6.1×10^7 $M^{-1}s^{-1}$ and 5.2×10^7 $M^{-1}s^{-1}$ for **9a** and **9b** in benzene at 310 K were obtained by radical clock [15]. [i]Measured for the analogue of **9a/b** with R = R' = H. [j]The value of 3.1×10^7 $M^{-1}s^{-1}$ in benzene at 310 K was obtained by radical clock [15] for an analogue of **9c**. [k]Values of 1.4×10^4 $M^{-1}s^{-1}$, 1.1×10^5 $M^{-1}s^{-1}$ and 3.8×10^6 $M^{-1}s^{-1}$ were previously determined for **10**, **11** and **12** in the inhibited autoxidation of styrene in PhCl at 303 K [21]. [l]From [22]. [m]Used as reference value.

To provide further insight into the relative reactivities of these compounds we also carried out measurements of k_{inh} in acetonitrile as a representative polar solvent. We felt this was necessary since there is essentially no data available in the literature for the reactivity of the vast majority of these compounds in any media other than chlorobenzene (or benzene) and we wanted to examine the solvent-dependence of any synergism we observed (vide infra). The results demonstrate a significant kinetic solvent effect, which was most pronounced for the least reactive compounds. For example, k_{inh} for the methoxy-substituted pyridinol **5a** dropped by a factor of 18 on going from chlorobenzene to acetonitrile, while the reactivity of the more reactive *N*,*N*-dimethylamino-substituted pyridinol **4a** dropped only a factor of 7. Likewise, while k_{inh} for the 2,4-dimethyl-6-methoxy-3-pyridinol (**5b**) dropped 12-fold with the change in solvent, the reactivity of the equivalently-substituted, but less reactive, pyrimidinol **7a** dropped 28-fold.

Ingold has clearly demonstrated that formal H-atom transfer reactions of the type X–H + $Y^{\bullet} \rightarrow X^{\bullet}$ + H–Y, where X is an electronegative atom, can experience a large kinetic solvent effect (KSE). In fact, these reactions are slowed down in hydrogen-bond accepting (HBA) solvents as a result of H-bond formation between X–H and the solvent since the H-bonded complex is essentially unreactive to the abstracting radical; hence only the "free" fraction of X–H in solution can react [23-26]. This KSE (illustrated in Scheme 4) is known to have major impact on the performance of phenolic antioxidants [2,10,27,28].

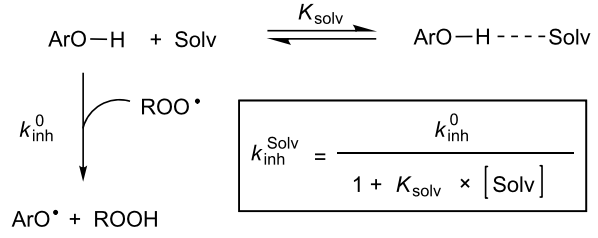

Scheme 4: Model for kinetic solvent effects on the radical-trapping activity of phenolic antioxidants.

Since the formation of the H-bonded complex is driven by both the HBA ability of the solvent and the hydrogen-bond donating (HBD) ability of the H-atom donor, the KSEs evident in the data above reflect the H-bond acidity of the various radical-trapping antioxidants we have studied. On quantitative grounds, an empirical relationship between K_{solv} and the HBD ability of the compound is provided by Abraham's equation (Equation 1), where α_2^H and β_2^H are empirical solvatochromic parameters (range: 0 to 1) quantifying the HBD and HBA ability of the two interacting partners (e.g. the phenol and the solvent), respectively, in the formation of a 1:1 H-bonded complex [29,30].

$$\log\left(K_{solv}/M^{-1}\right) = 7.354 \times \alpha_2^H \beta_2^H - 1.094 \quad (1)$$

An α_2^H value of 0.37 [24] has been reported for α-tocopherol (expectedly identical to PMHC, **12**), while they have been estimated as 0.50 and 0.55 for compounds **4a** and **6a** respectively [2,10], consistent with the larger KSEs on the reactions of the latter (ca. 7) relative to the former (ca. 5).

FTIR measurements. To put the HBD ability of the pyridinols and pyrimidinols on solid quantitative ground, we performed independent (non-kinetic) measurements of K_{solv} for three representative compounds (**5b**, **6b** and **7b**) in three reference solvents of different HBA ability [30]: acetonitrile (β_2^H = 0.44), ethyl acetate (β_2^H = 0.45), and dimethyl sulfoxide (β_2^H = 0.78) using IR spectroscopy [25]. Representative results are shown in Figure 2.

Addition of a HBA solvent to solutions of the pyri(mi)dinols in non-H-bonding CCl_4 resulted in the progressive decrease of the IR signal corresponding to the "free" O–H stretch (~3610 cm^{-1}), accompanied by the growth of a broad intense band at lower frequency attributed to the O–H stretch of the H-bonded species (Figure 2a). By fitting the data corresponding to the integrated IR signal for the free O–H versus the concentration of the HBA co-solvent to the expression in Equation 2 as illustrated in Figure 2b, the values of K_{solv} collected in Table 2 could be obtained.

$$[ArOH]_{free} = \frac{[ArOH]_{tot}}{1 + K_{solv} \times [Solv]} \quad (2)$$

It should be noted that, for any of the compounds that were investigated, there is good agreement between the α_2^H values obtained by Equation 1 from equilibrium constants in ethyl acetate and DMSO, while the value measured for acetonitrile is consistently lower. Indeed, for each of these compounds, K_{solv} measured for acetonitrile is lower than that for ethyl acetate despite the fact that the two solvents are attributed essentially the same HBA ability by Abraham's β_2^H scale (0.44 versus 0.45). A similar trend is observed in available literature kinetic data; the rate constants for formal H-atom transfer from a variety of phenols to a variety of radicals (e.g. alkyl, alkoxyl, peroxyl and DPPH) is consistently higher in acetonitrile than in ethyl acetate [23-28] strongly suggesting that the β_2^H value for acetonitrile needs revision. As a result, we suggest averaging the α_2^H values determined for **5b**, **6b** and **7b** in EtOAc and DMSO, resulting in 0.55, 0.53 and 0.65, respectively. Such values are in line with other phenol-type antioxidants [2,10]. The same values can then be used as inputs in Equation 1 to obtain an average β_2^H of 0.39 for acetonitrile. This value is in

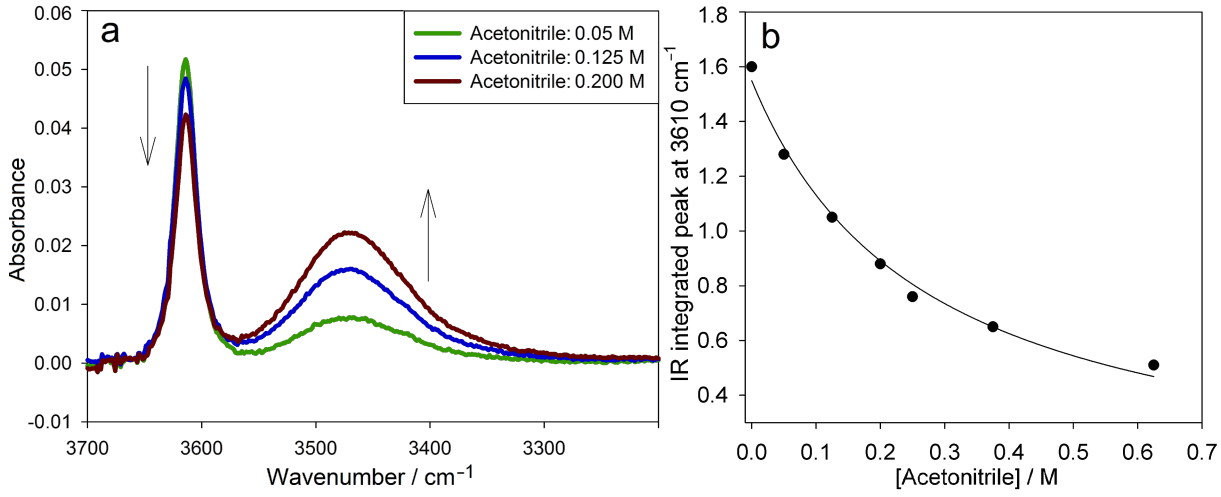

Figure 2: The O–H stretching region of representative FTIR spectra of compound **6b** (10 mM) in CCl_4 containing increasing amounts of acetonitrile as co-solvent (a) and corresponding plot of the integrated signal at 3610 cm^{-1} versus the concentration of acetonitrile, fit to Equation 2 (b).

accord with that obtained from kinetic measurements: for instance, using the reaction of α-tocopherol with *tert*-butoxyl radicals as model, it was shown that acetonitrile has the same HBA ability as water [31], which is attributed a reliable $\beta_2^H = 0.38$ [29,30]. As such, we recommend a value of β_2^H of 0.39 for acetonitrile.

Table 2: FTIR measured equilibrium constants at 298 K for H-bonding of solvents with selected antioxidants (K_{solv}) and corresponding α_2^H values calculated by Equation 1.

	Solvent	K_{solv}/M^{-1}	α_2^H	KSE[a]
	CH_3CN	3.1 ± 0.2	0.49	
5b	EtOAc	5.5 ± 0.3	0.55	
	DMSO	116.1 ± 11.2	0.55	
		average[b]	0.55	12
	CH_3CN	3.0 ± 0.3	0.49	
6b	EtOAc	4.7 ± 0.5	0.53	
	DMSO	95.0 ± 5.9	0.53	
		average[b]	0.53	7
	CH_3CN	6.9 ± 1.8	0.60	
7b	EtOAc	14.1 ± 0.9	0.68	
	DMSO	285.0 ± 9.6	0.62	
		average[2]	0.65	26

[a]KSE = kinetic solvent effect, taken from data in Table 1. [b]Average of the data in EtOAc and DMSO only, see text.

Computational thermodynamics. The rational design of synergistic co-antioxidant mixtures requires knowledge of not only the kinetics of the reactions of the antioxidants with peroxyl radicals, but also the relative stabilities of the antioxidant-derived radicals, since synergism relies on the position of the equilibrium of reaction 6 (Scheme 3) [8,9], which is related to the difference in the O–H BDEs of the equilibrating antioxidants as in Equation 3.

$$\log(K_r) = -1/(2.303 \times RT) \times [\mathrm{BDE(CoAH)} - \mathrm{BDE(AH)}] \quad (3)$$

In order to complete the necessary framework of kinetic and thermodynamic data, we computed the O–H BDEs of compounds **4**–**12** using quantum chemical methods. The calculations were carried out at the CBS-QB3 level of theory [32], since this approach has been shown to provide highly accurate O–H BDEs in phenols and related compounds [19,33-35]. The results of these calculations are given in Table 1 alongside the limited experimental data obtained using the radical equilibration EPR (REqEPR) technique [12,13,22]. The calculated BDEs are in very good agreement with the experimental values, with systematic deviations between 0.2 and 1.7 kcal/mol and, most importantly, they allow insight into the position of equilibrium (reaction 6, Scheme 3) unfettered by differing experimental conditions.

Co-antioxidant systems. Given the foregoing kinetic and thermodynamic data, we next set out to design and test representative co-antioxidant mixtures. For simplicity we investigated only binary AH/co-AH mixtures. The baseline strategy consisted of selecting a pyridinol or a pyrimidinol as principal antioxidant (AH) capable of providing maximum radical-trapping kinetics to the mixture (higher k_{inh}), but at the same time a sufficiently high O–H BDE to be regenerated by the co-antioxidant, co-AH (vide supra), which was selected among the conventional phenols **10**–**12**.

The autoxidation of an organic substrate (e.g. styrene) thermally initiated at a constant rate, R_i, by an azo-initiator will consume oxygen at a constant rate in the absence of an inhibitor. In the presence of a very effective antioxidant such as **4a** ($k_{inh} = 3.6 \times 10^6$ $M^{-1}s^{-1}$, see Table 1) a plot of oxygen uptake versus time shows a clear inhibition period of length τ_0 that depends on the concentration of AH and the stoichiometric factor ($n \sim 2$ for all tested antioxidants, see Table 1). During the inhibited period (cf. Figure 3), i.e. until AH has been consumed, the rate of oxygen consumption is almost completely suppressed, after which it resumes at the uninhibited rate. Figure 3 also shows that an equivalent amount of a modest antioxidant such as **11** ($k_{inh} = 1.1 \times 10^5$ $M^{-1}s^{-1}$, see Table 1) does not produce a neat inhibition of the autoxidation under the same conditions, but instead simply retards oxygen uptake, since the propagation of autoxidation can compete effectively with inhibition. However, when equimolar amounts of **4a** and **11** are present, a clear inhibited period is observed – as was the case for **4a** alone, but its duration is twice what it was in the absence of the equivalent of **11**. This result implies that **11** can regenerate **4a** from its corresponding aryloxyl radical. This reaction is driven by the fact that **4a** has an O–H bond which is 2.4 kcal/mol stronger (77.9 kcal/mol) than the O–H bond in **11** (75.5 kcal/mol). The addition of another equivalent of **11** extends the inhibited period to three times that of **4a** alone, clearly demonstrating that it is effectively used as the sacrificial reductant during the inhibited period.

The duration of the inhibited period (τ) is related to the concentration ratio of the principal antioxidant and co-antioxidant by a proportionality constant α (Equation 4), which represents the efficiency with which AH is regenerated by co-AH, which can be written in terms of the rate constants of the relevant competing reactions in Scheme 3 as in Equation 5; thus, its value may lie between 0 (no regeneration of AH by co-AH) and 1 (complete regeneration of AH by co-AH).

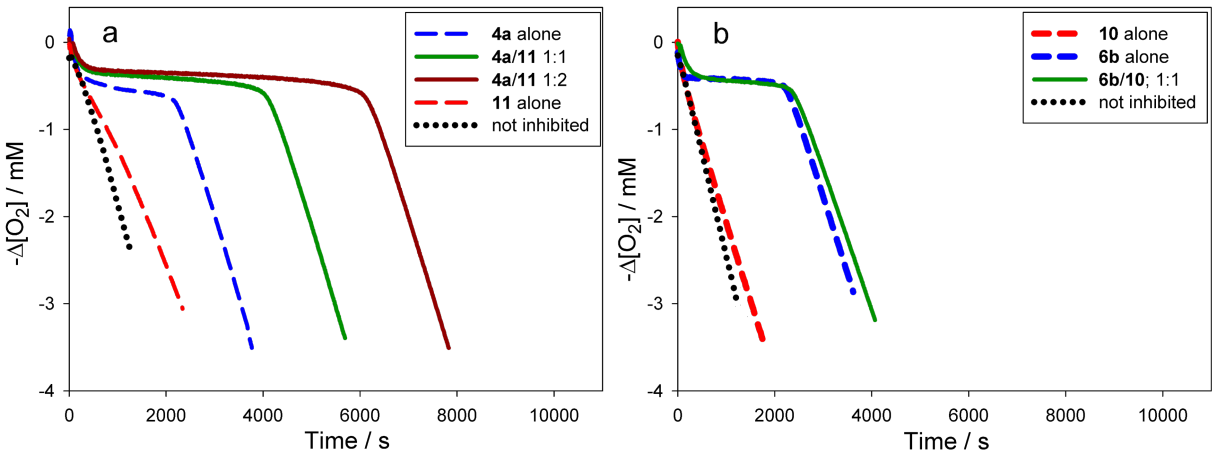

Figure 3: Oxygen-uptake plots recorded during the AIBN initiated autoxidation of styrene in chlorobenzene (50% v/v) at 303 K in the absence or presence of: (a) **4a** (6.2×10^{-6} M), **11** (6.2×10^{-6} M) or a mixture of **4a** (6.2×10^{-6} M) with either one or two equivalents of **11**; (b) **6b** (6.2×10^{-6} M), **10** (6.2×10^{-6} M) or a mixture of **6b** (6.2×10^{-6} M) and one equivalent of **10**.

$$\tau = \tau_0 + \tau_0 \alpha \frac{[\text{co-AH}]}{[\text{AH}]} \quad (4)$$

$$\alpha = K_r \frac{k_8}{k_7} \quad (5)$$

In other words, α is a measure of synergism in the co-antioxidant system. Since the ratio k_8/k_7 (see Scheme 3) for phenolic antioxidants is normally ~1 [8], the efficiency of regeneration depends almost entirely on K_r. Moreover, since H-atom transfer between phenols usually proceeds with a negligible change in entropy, α depends largely on the difference in the O–H BDEs of the two co-antioxidants (Equation 3). If $K_r << 1$, regeneration will be inefficient and no synergism will be observed; under those circumstances the co-antioxidants will simply behave in an additive fashion, as illustrated in Figure 3b for the combination of **6b** (BDE = 75.6 kcal/mol) and **10** (BDE = 78.7 kcal/mol).

Although, in principle, synergism can occur with any AH/co-AH ratio (e.g. Figure 4a), the efficiency often changes to some extent as a function of such ratio, as well as with the actual experimental conditions. For simplicity, all co-antioxidant mixtures were investigated under comparable settings in the low μM range with AH/co-AH ratios of 1:1 and 1:2. As can be seen from Table 3, several of the antioxidant mixtures investigated showed good synergism in chlorobenzene (α > 0.5); particu-

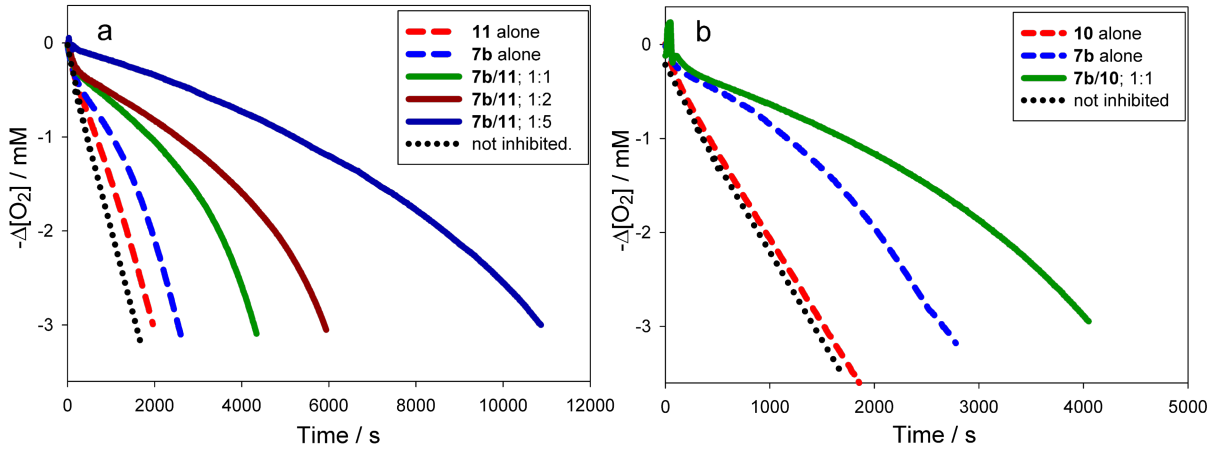

Figure 4: Oxygen-uptake plots recorded during the AIBN initiated autoxidation of styrene in chlorobenzene (50% v/v) at 303 K in the presence of compound **7b** and/or **11** (either 6.1×10^{-6} M) (a) and corresponding plots using compound **10** as co-antioxidant (b).

larly the couples **4a**/**11**, **6a**/**11**, **6a**/**12**, **6b**/**11**, **6b**/**12**, **7a**/**11**, **7a**/**10** (similar to **7b**/**11**, **7b**/**10**), **9c**/**12**. From our results we can conclude that, in general, ΔBDE needs to be > −1 kcal/mol to expect synergism based on the equilibrium of reaction 6. Not surprisingly, regeneration was more efficient when a pyrimidinol was used as the principal antioxidant due to the higher O–H BDEs of the pyrimidinols relative to equivalently substituted pyridinols. On the other hand, it should be noted that the efficiency α is not the only relevant parameter in determining the overall efficacy of a co-antioxidant mixture, since the apparent k_{inh} of the mixture will be identical to that of the most reactive antioxidant in the mixture [8]. For instance, the mixture **4a**/**11** (Figure 3a) is a significantly better antioxidant system than mixtures of **7b**/**11** (Figure 4a) and **7b**/**10** (Figure 4b), despite all systems having α = 1.

Table 3: Regeneration efficiency (α) of a principal antioxidant (AH) by a co-antioxidant (co-AH) in the inhibited autoxidation of styrene in chlorobenzene or acetonitrile (50% v/v) at 303 K.[a]

AH	co-AH	ΔBDE (AH-CoAH)	α (PhCl)	α (CH_3CN)
4a	**11**	+2.4	1.0 ± 0.1	0.5 ± 0.1
4c	**11**	+2.5	~0.1	~0
4d	**11**	−1.0	~0.1	~0.1
	10	−4.2	~0	~0
6a	**11**	+2.8	1.0 ± 0.1	0.8 ± 0.1
	12	+0.6	0.8 ± 0.2	0.4 ± 0.2
	10	−0.4	0.5 ± 0.1	~0
6b	**11**	+0.1	0.7 ± 0.1	0.5 ± 0.1
	10	−2.1	~0	~0
7a	**11**	+4.4	0.9 ± 0.1	n.d.[b]
	10	+2.2	0.9 ± 0.1	0.3 ± 0.1
7b	**11**	+4.4	1.0 ± 0.1	0.7 ± 0.2
	10	+2.2	1.0 ± 0.1	n.d.[b]
9c	**12**	−2.3	0.6 ± 0.2	0.5 ± 0.1

[a]Values are averaged on at least three independent experiments with AH/co-AH ratios of 1:1 and 1:2, in the concentration range 2–10 μM both for AH and co-AH. [b]n.d. = not determined.

Since synergistic activity requires a favourable ΔBDE (vide supra), it seems reasonable to expect that the values of α should correlate with ΔBDE. Such a correlation is shown in Figure 5, in which there appears to be a clear sigmoidal relationship between α and ΔBDE. The correlation is sigmoidal since below ΔBDE values of ca. −1 kcal/mol little to no regeneration is observed, whereas above ca. 1 kcal/mol, regeneration is essentially quantitative.

There are two data points that do not lie on the correlation: the combinations of **4c** with **11**, and **9c** with **12**. The latter has

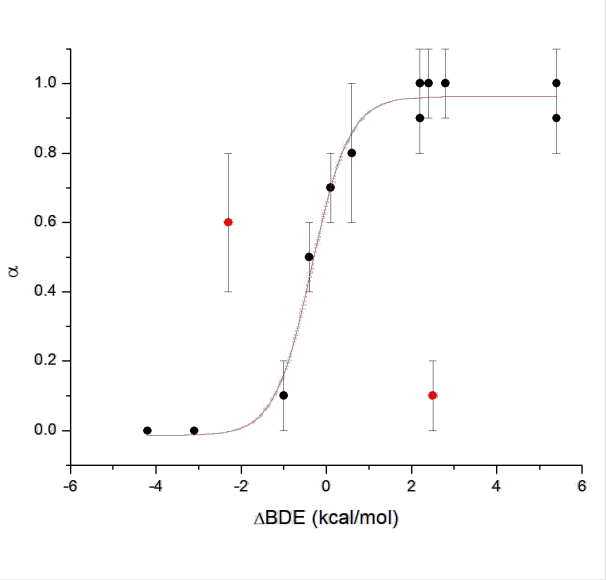

Figure 5: Regeneration efficiencies (α) observed in autoxidations of styrene in chlorobenzene (50% v/v) at 303 K inhibited by co-antioxidant mixtures as a function of the difference in the O–H BDEs of the principal (AH) and co-antioxidant (Co-AH) [ΔBDE = BDE(AH) – BDE(Co-AH)]. The data highlighted in red correspond to the combinations of **9c**/**12** and **4c**/**11**.

ΔBDE = −2.3 kcal/mol, implying that **9c** should not be regenerated by **12**. However, because the phenolic co-antioxidant used in this case (**12**) is a very reactive antioxidant itself (k_{inh} = 3.2 × 10^6 $M^{-1}s^{-1}$ compared to 1.5 × 10^7 $M^{-1}s^{-1}$ for **9c**) it also gives a pronounced inhibited period under the reaction condition (see Supporting Information File 1 for oxygen uptake plots). As such, the additive contributions of **9c** and **12** give the appearance of synergism where only additivity exists. It should also be pointed out that although the simple additive contributions of the highly reactive antioxidants should give α = 1, a value of only ca. 0.6 is observed. This is likely due to the consumption of some **12** by autoxidation at higher concentrations of **9c** due to the longer inhibition period, which is known to lead to lower stoichiometric factors for highly similar compounds (i.e. **9a**, **9b**) [17]. This leaves the **4c**/**11** data point as the only real outlier; since it has ΔBDE = +2.5 kcal/mol, the much more reactive **4c** should be regenerated by the less reactive **11**. This result is puzzling in light of the fact that the structurally similar pyridinol **4a**, which has an essentially identical O–H BDE, is fully regenerated by **11**. The only structural feature which distinguishes **4c** from the other pyridinols and pyrimidinols in Table 3 (and Figure 5) that have positive ΔBDE values (and therefore α ~ 1) is in the conformation of the substituent at the 4-position relative to the reactive hydroxyl moiety. Due to steric interactions between the adjacent ring methyl, the dimethylamino substituent in **4c** is rotated out of the plane of the aromatic ring [17]. On the basis of theoretical calculations, H-atom transfer between phenol and the phenoxyl radical is

believed to be a proton-coupled electron transfer reaction, occurring via an approximately planar transition state wherein the unpaired electron is delocalized across both phenyl rings [36]. As such, it is difficult to envision how the conformation of the dimethylamino substituent in **4c** may slow the analogous reaction between the radical derived from **4c** and **11** relative to the other reaction couples. However, it should be pointed out that theoretical calculations on the phenol/phenoxyl H-atom transfer reaction do not include substituents in the ortho positions relative to the phenolic oxygen, which may change the transition state structure substantially.

Regardless of whether the foregoing rationalization is in fact correct, the lower than expected regeneration efficiency observed for the combination of **4c** and **11** underscores the fact that the actual value of α depends not only on the equilibrium in reaction 6 (Scheme 3) – and hence the ΔBDE – but also on the absolute rates of the other reactions depicted in Scheme 3 [8]. In this connection, it is important to note that the values of α we measured were generally lower in acetonitrile than in chlorobenzene despite the fact that ΔBDE is expected to increase on going from chlorobenzene to acetonitrile due to the stronger H-bonding of the pyridinols and pyrimidinols ($\alpha_2^H \sim 0.5$–0.7) to acetonitrile (vide supra) as compared to the sterically hindered phenols such as **10** and **11** ($\alpha_2^H \sim 0.2$) [37]. The drop in α can only be explained by considering Scheme 3 in more detail. For regeneration of the principal antioxidant AH (the pyridinol/pyrimidinol) to occur, it is necessary that equilibrium of reaction 6 is faster than reaction 7 (Scheme 3), i.e. $k_7 \times [ROO^\bullet]_{SS} < k_r \times [\text{co-AH}]$. In the presence of a good antioxidant AH (rapidly trapping peroxyl radicals by reaction 4 (Scheme 3)) this condition is easily met [8]. However, if the reactivity of AH is hampered by H-bonding to the solvent, the steady state concentration of peroxyl radicals may grow sufficiently to react competitively with co-AH, thereby decreasing the efficiency of regeneration [38].

Conclusion

Herein we have provided the kinetic and thermodynamic rationale for the design of synergistic co-antioxidant systems employing highly reactive 3-pyridinol or 5-pyrimidinol antioxidants in combination with less reactive, but much less expensive, phenolic antioxidants. In several cases, the approach has shown to equal the performance of the best co-antioxidant systems designed by nature, such as the tocopherol/ascorbate system [5] or the tocopherol/catechol system [8]. In general, the most effective individual antioxidants, e.g. the bicyclic pyridinols (**9a–c**), pyridinols (**4b**) and pyrimidinols (**6d**) are not good partners for co-antioxidant systems because their O–H BDEs (74.8–75.6 kcal/mol) are too low. Instead, the slightly less reactive pyridinols and pyrimidinols (e.g. **4a**, **6a**, **7a**/**7b**), which have much stronger O–H bonds (>78 kcal/mol), are the ideal candidates to be used with abundant, persistent phenols such as BHT (**11**). We anticipate that this work will prompt the use of antioxidant mixtures based on 3-pyridinol and 5-pyrimidinol antioxidants, in order to take advantage of the greater reactivities of these compounds, but to minimize the cost of doing so by making use of the inexpensive phenolic antioxidants typically used in industrial/commercial applications to regenerate them in situ.

Experimental

Materials. Solvents were of the highest grade commercially available (Fluka/Aldrich) and were used as received. 2,2,5,7,8-Pentamethyl-6-chromanol (PMHC, **12**, 97%) was commercially available (Aldrich) and used without further purification. Commercial 2,6-di-*tert*-butyl-4-methylphenol (BHT, **10**, 98%) and 2,6-di-*tert*-butyl-4-methoxyphenol (DBHA, **11**, 97%) were re-crystallized from hexane. Commercially available 2,2'-azodiisobutyronitrile (AIBN ≥98%) was recrystallized from hexane and stored at −20 °C. Cumene (98%) and styrene (≥99%) were distilled under reduced pressure and percolated twice through silica and alumina prior to use. All solutions were prepared fresh immediately prior to use.

Synthesis. Compounds **4a**, **4b**, **6a** and **6b** were prepared as described in [39]. Compounds **4c** and **4d** were prepared as described in [17]. Compound **5b** was prepared as in [14]. Compound **7a** was prepared as in [13]. Compounds **9a** and **9b** were prepared as in [15], whereas compound **9c** was prepared as in [40].

3-Hydroxy-6-methoxypyridine (5a). A solution of 3-benzyloxy-6-methoxypyridine [39] in MeOH was treated with 10% Pd/C and the resulting black suspension was stirred at room temperature under an atmosphere of H_2 (1 atm) overnight. The catalyst was removed by filtration through a pad of celite and the filtrate was concentrated under reduced pressure. The crude residue obtained was subjected to flash chromatography on silica gel (eluent: ethyl acetate/hexanes) and the product isolated in quantitative yield. ^{1}H NMR ($CDCl_3$) δ 9.32 (br s, 1H, exchanges with D_2O), 7.75 (s, 1H), 7.25 (d, J = 8.6 Hz, 1H), 6.56 (d, 8.6 Hz, 1H), 3.84 (s, 3H); ^{13}C NMR ($CDCl_3$) δ 54.2, 111.0, 128.7, 132.3, 148.2, 158.3; HRMS (EI^+) m/z: calcd for $C_6H_7NO_2$, 125.0477; found, 125.0484.

5-Hydroxy-2-octyloxy-4,6-dimethylpyrimidine (7b). *O*-Octylisouronium trifluoromethanesulfonate (5.1 g, 15.8 mmol) was dissolved in dry DMF (30 mL), and 3-acetoxy-2,4-pentanedione (2.5 g, 15.8 mmol) was added along with sodium acetate (1.14 g, 15.8 mmol), and the mixture stirred for 24 hours at 70 °C. Water (200 mL) was then added, the pH

adjusted to ~5, and the organics extracted with EtOAc (3 × 100 mL). The organic layers were combined, dried over $MgSO_4$ and concentrated under reduced pressure. The product was then recrystallized from CH_3CN to yield 35% **7b**. ^{1}H NMR ($CDCl_3$) δ 4.15 (t, J = 6.6 Hz, 2H), 2.32 (s, 6H), 1.63 (m, 2H), 1.32 (br m, 2H), 1.17 (m, 8H), 0.78 (t, 6.5 Hz); ^{13}C NMR ($CDCl_3$) δ 14.1, 18.8, 22.6, 26.0, 29.0, 29.2, 29.3, 31.8, 67.4, 142.5, 156.4, 158.3; HRMS (EI^+) *m/z*: calcd for $C_{14}H_{24}N_2O_2$, 252.1838; found, 252.1836.

5-Hydroxy-2-(2,5-dimethyl-1*H*-pyrrol-1-yl)-4,6-dimethylpyrimidine (8). A solution of 5-benzyloxy-2-(2,5-dimethyl-1*H*-pyrrol-1-yl)-4,6-dimethylpyrimidine [41] in MeOH was treated with 10% Pd/C and the resulting black suspension was stirred at room temperature under an atmosphere of H_2 (1 atm) overnight. The catalyst was removed by filtration through a pad of celite and the filtrate was concentrated under reduced pressure. The crude residue obtained was subjected to flash chromatography on silica gel (eluent: ethyl acetate/hexanes) and the product isolated in quantitative yield. ^{1}H NMR ($CDCl_3$) δ 2.15 (s, 6H), 2.43 (s, 6H), 5.71 (s, 2H); ^{13}C NMR ($CDCl_3$) δ 13.2, 18.4, 107.4, 128.6, 145.7, 149.3, 155.3; HRMS (EI^+) *m/z*: calcd for $C_{12}H_{15}N_3O$, 217.1215; found, 217.1217.

Autoxidation studies. The chain-breaking antioxidant activity of the title compounds was evaluated by monitoring the course of thermally initiated inhibited autoxidations of either styrene or cumene (RH) in chlorobenzene or acetonitrile. The autoxidation experiments were performed in a oxygen-uptake apparatus already described elsewhere [42-44]. In a typical experiment, an air-saturated mixture of styrene or cumene in acetonitrile or chlorobenzene (50% v/v) containing AIBN (1–5 × 10^{-2} M) was equilibrated with the reference solution containing also an excess of PMHC (1 × 10^{-2} M) in the same solvent at 30 °C. After equilibration, a concentrated solution of the antioxidant (final concentration 1–10 × 10^{-6} M) was injected into both the sample flasks, and the oxygen consumption of the sample was measured. From the rate of oxygen consumption during the inhibited period (R_{inh}), k_{inh} values were obtained by using Equation 6 [44], where R_0 is the rate of oxygen consumption in the absence of antioxidants, R_i is the initiation rate (in the range 2–10 × 10^{-9} Ms^{-1}), $2k_t$ is the bimolecular termination rate constant of styrylperoxyl or cumylperoxyl radicals (4.2 × 10^7 and 4.6 ×10^4 $M^{-1}s^{-1}$ respectively) [21,43] and n is the stoichiometric coefficient of the antioxidant. The n coefficient was determined experimentally from the length of the inhibited period (τ) by Equation 7.

$$\frac{R_0}{R_{inh}} - \frac{R_{inh}}{R_0} = \frac{nk_{inh}[AH]}{\sqrt{2k_tR_i}} \quad (6)$$

$$n = \frac{R_i\tau}{[AH]} \quad (7)$$

A similar procedure was employed to investigate the kinetics of the antioxidant mixtures. The efficiency, α, was determined from the oxygen uptake plots by the extension of the inhibition period according to Equation 4. In cases where no clear inhibition period was observed, α was obtained by fitting the experimental traces with numerical simulations based on Scheme 3 using Gepasi 3.0 software, as previously described [45].

FTIR spectroscopy. Spectra were recorded at 298 K in a Nicolet Protegé 460 FTIR spectrometer under nitrogen atmosphere using a sealed KBr cell with optical path of 0.5 mm. Solutions of the test compound (10 mM) in CCl_4 and in CCl_4/HBA-solvent mixtures were analyzed in absorbance mode and the blank spectrum of the corresponding solvent mixture was subtracted. The signal in the "free" O–H stretching region at ca. 3610 cm^{-1} was manually integrated after manual baseline correction and plotted versus the concentration of the HBA solvent and fit to Equation 2 [25]. In the case of compound **6b**, similar analysis was repeated using IR peak height in place of peak area and essentially indistinguishable results were obtained. In order to confirm the absence of self-association of the test compounds and to calibrate the spectrometer response, linear regression plots (Absorbance versus [ArOH]) in CCl_4 were preliminarily recorded in the range 1–10 mM. Deviation from linearity was observed only in the case of **7b**, allowing the determination of its self-association equilibrium constant as K_{self} = 121 ± 10 M^{-1}. Therefore, its H-bonding to the solvent was analyzed as described above using Equation 8 (see Supporting Information File 1 for further details).

$$[Solv] = \frac{[ArOH]_{tot}}{[ArOH]_{free}K_{solv}} - \frac{2K_{self}[ArOH]_{free}}{K_{solv}} - \frac{1}{K_{solv}} \quad (8)$$

Supporting Information

Supporting Information File 1

Additional experimental details, oxygen-uptake plots and FTIR spectra, as well as cartesian coordinates for calculated structures.
[http://www.beilstein-journals.org/bjoc/content/supplementary/1860-5397-9-313-S1.pdf]

Acknowledgments

This work was supported by grants from the Italian MIUR (PRIN 2010-2011 2010PFLRJR (PROxi project)) and the Natural Sciences and Engineering Research Council (NSERC)

of Canada to L.V. and D.A.P., respectively. D.A.P. also acknowledges the support of the Canada Research Chairs program. The computational efforts in this work were made possible by generous access to the High Performance Computing Virtual Laboratory, a supercomputing facility funded by the Government of Ontario, the Canada Foundation for Innovation and NSERC Canada.

References

1. Ingold, K. U. *Chem. Rev.* **1961,** *61,* 563–589. doi:10.1021/cr60214a002
2. Valgimigli, L.; Pratt, D. A. In *Encyclopedia of Radicals in Chemistry, Biology and Materials;* Chatgilialoglu, C.; Studer, A., Eds.; John Wiley & Sons, Ltd: Chichester, U.K., 2012; p 1623.
3. Bowry, V. W.; Stocker, R. *J. Am. Chem. Soc.* **1993,** *115,* 6029–6044. doi:10.1021/ja00067a019
4. Bowry, V. W.; Ingold, K. U. *Acc. Chem. Res.* **1999,** *32,* 27–34. doi:10.1021/ar950059o
5. Niki, E.; Saito, T.; Kawakami, A.; Kamiya, Y. *J. Biol. Chem.* **1984,** *259,* 4177–4182.
6. Doba, T.; Burton, G. W.; Ingold, K. U. *Biochim. Biophys. Acta* **1985,** *835,* 298–303. doi:10.1016/0005-2760(85)90285-1
7. Niki, E.; Kawakami, A.; Yamamoto, Y.; Kamiya, Y. *Bull. Chem. Soc. Jpn.* **1985,** *58,* 1971–1975. doi:10.1246/bcsj.58.1971
8. Amorati, R.; Ferroni, F.; Lucarini, M.; Pedulli, G. F.; Valgimigli, L. *J. Org. Chem.* **2002,** *67,* 9295–9303. doi:10.1021/jo026501f
9. Amorati, R.; Ferroni, F.; Pedulli, G. F.; Valgimigli, L. *J. Org. Chem.* **2003,** *68,* 9654–9658. doi:10.1021/jo0351825
10. Amorati, R.; Valgimigli, L. *Org. Biomol. Chem.* **2012,** *10,* 4147–4158. doi:10.1039/c2ob25174d
11. Pratt, D. A.; DiLabio, G. A.; Brigati, G.; Pedulli, G. F.; Valgimigli, L. *J. Am. Chem. Soc.* **2001,** *123,* 4625–4626. doi:10.1021/ja005679l
12. Wijtmans, M.; Pratt, D. A.; Valgimigli, L.; DiLabio, G. A.; Pedulli, G. F.; Porter, N. A. *Angew. Chem., Int. Ed.* **2003,** *42,* 4370–4373. doi:10.1002/anie.200351881
13. Valgimigli, L.; Brigati, G.; Pedulli, G. F.; DiLabio, G. A.; Mastragostino, M.; Arbizzani, C.; Pratt, D. A. *Chem.–Eur. J.* **2003,** *9,* 4997–5010. doi:10.1002/chem.200304960
14. Wijtmans, M.; Pratt, D. A.; Brinkhorst, J.; Serwa, R.; Valgimigli, L.; Pedulli, G. F.; Porter, N. A. *J. Org. Chem.* **2004,** *69,* 9215–9223. doi:10.1021/jo048842u
15. Nam, T.-g.; Rector, C. L.; Kim, H.-y.; Sonnen, A. F.-P.; Meyer, R.; Nau, W. M.; Atkinson, J.; Rintoul, J.; Pratt, D. A.; Porter, N. A. *J. Am. Chem. Soc.* **2007,** *129,* 10211–10219. doi:10.1021/ja072371m
16. Nam, T.-g.; Nara, S. J.; Zagol-Ikapitte, I.; Cooper, T.; Valgimigli, L.; Oates, J. A.; Porter, N. A.; Boutard, O.; Pratt, D. A. *Org. Biomol. Chem.* **2009,** *7,* 5103–5112. doi:10.1039/b912528k
17. Serwa, R.; Nam, T.-g.; Valgimigli, L.; Culbertson, S.; Rector, C. L.; Jeong, B.-S.; Pratt, D. A.; Porter, N. A. *Chem.–Eur. J.* **2010,** *16,* 14106–14114. doi:10.1002/chem.201001382
18. Arce, P. M.; Goldschmidt, R.; Khdour, O. M.; Madathil, M. M.; Jaruvangsanti, J.; Dey, S.; Fash, D. M.; Armstrong, J. S.; Hecht, S. M. *Bioorg. Med. Chem.* **2012,** *20,* 5188–5201. doi:10.1016/j.bmc.2012.07.005
19. Mulder, P.; Korth, H.-G.; Pratt, D. A.; DiLabio, G. A.; Valgimigli, L.; Pedulli, G. F.; Ingold, K. U. *J. Phys. Chem. A* **2005,** *109,* 2647–2655. doi:10.1021/jp047148f
20. Valgimigli, L.; Amorati, R.; Petrucci, S.; Pedulli, G. F.; Hu, D.; Hanthorn, J. J.; Pratt, D. A. *Angew. Chem., Int. Ed.* **2009,** *48,* 8348–8351. doi:10.1002/anie.200903360
21. Burton, G. W.; Doba, T.; Gabe, E. J.; Hughes, L.; Lee, F. L.; Prasad, L.; Ingold, K. U. *J. Am. Chem. Soc.* **1985,** *107,* 7053–7065. doi:10.1021/ja00310a049
22. Lucarini, M.; Pedrielli, P.; Pedulli, G. F.; Cabiddu, S.; Fattuoni, C. *J. Org. Chem.* **1996,** *61,* 9259–9263. doi:10.1021/jo961039i
23. Litwinienko, G.; Ingold, K. U. *Acc. Chem. Res.* **2007,** *40,* 222–230. doi:10.1021/ar0682029
24. Snelgrove, D. W.; Lusztyk, J.; Banks, J. T.; Mulder, P.; Ingold, K. U. *J. Am. Chem. Soc.* **2001,** *123,* 469–477. doi:10.1021/ja002301e
25. Franchi, P.; Lucarini, M.; Pedulli, G. F.; Valgimigli, L.; Lunelli, B. *J. Am. Chem. Soc.* **1999,** *121,* 507–514. doi:10.1021/ja982405d
26. Valgimigli, L.; Banks, J. T.; Ingold, K. U.; Lusztyk, J. *J. Am. Chem. Soc.* **1995,** *117,* 9966–9971. doi:10.1021/ja00145a005
27. Barclay, L. R. C.; Edwards, C. E.; Vinqvist, M. R. *J. Am. Chem. Soc.* **1999,** *121,* 6226–6231. doi:10.1021/ja990878u
28. Valgimigli, L.; Banks, J. T.; Lusztyk, J.; Ingold, K. U. *J. Org. Chem.* **1999,** *64,* 3381–3383. doi:10.1021/jo982360z
29. Abraham, M. H.; Grellier, P. L.; Prior, D. V.; Taft, R. W.; Morris, J. J.; Taylor, P. J.; Laurence, C.; Berthelot, M.; Doherty, R. M.; Kamlet, M. J.; Abboud, J. L. M.; Sraidi, K.; Guiheneuf, G. *J. Am. Chem. Soc.* **1988,** *110,* 8534–8536. doi:10.1021/ja00233a034
30. Abraham, M. H.; Grellier, P. L.; Prior, D. V.; Morris, J. J.; Taylor, P. J. *J. Chem. Soc., Perkin Trans. 2* **1990,** 521–529. doi:10.1039/p29900000521
31. Valgimigli, L.; Ingold, K. U.; Lusztyk, J. *J. Am. Chem. Soc.* **1996,** *118,* 3545–3549. doi:10.1021/ja954030r
32. Montgomery, J. A., Jr.; Ochterski, J. W.; Petersson, G. A. *J. Chem. Phys.* **1994,** *101,* 5900. doi:10.1063/1.467306
33. Amorati, R.; Pedulli, G. F.; Pratt, D. A.; Valgimigli, L. *Chem. Commun.* **2010,** *46,* 5139–5141. doi:10.1039/c0cc00547a
34. Foti, M. C.; Amorati, R.; Pedulli, G. F.; Daquino, C.; Pratt, D. A.; Ingold, K. U. *J. Org. Chem.* **2010,** *75,* 4434–4440. doi:10.1021/jo100491a
35. Hanthorn, J. J.; Valgimigli, L.; Pratt, D. A. *J. Am. Chem. Soc.* **2012,** *134,* 8306–8309. doi:10.1021/ja300086z
36. Mayer, J. M.; Hrovat, D. A.; Thomas, J. L.; Borden, W. T. *J. Am. Chem. Soc.* **2002,** *124,* 11142–11147. doi:10.1021/ja012732c
37. Warren, J. J.; Mayer, J. M. *Proc. Natl. Acad. Sci. U. S. A.* **2010,** *107,* 5282–5287. doi:10.1073/pnas.0910347107
38. As a proof of concept, numerical modelling was carried out for the autoxidation of 4.3 M styrene in PhCl or ACN, initiated at 303 K by AIBN 0.05 M (R_i = 6 ×10^{-9} Ms^{-1}) and inhibited by a mixture of **4a** (5 μM) and **11** (10 μM) using Gepasi 3.0 software. Assuming that k_r is 5 × 10^4 M^{-1}s^{-1} in PhCl and k_7 = 1 × 10^8 M^{-1}s^{-1}, the ratio k_r × [CoAH]/k_7 × [ROO$^•$]$_{SS}$ is calculated as 31.3 in PhCl and 1.2 in CH_3CN. The corresponding calculated α values are 1.0 and 0.46 (see Supporting Information File 1 for full details) in excellent agreement with experiments.
39. Nara, S. J.; Jha, M.; Brinkhorst, J.; Zemanek, T. J.; Pratt, D. A. *J. Org. Chem.* **2008,** *73,* 9326–9333. doi:10.1021/jo801501e
40. Nam, T.-g.; Ku, J.-M.; Rector, C. L.; Choi, H.; Porter, N. A.; Jeong, B.-S. *Org. Biomol. Chem.* **2011,** *9,* 8475–8482. doi:10.1039/c1ob05144j
41. Nara, S. J.; Valgimigli, L.; Pedulli, G. F.; Pratt, D. A. *J. Am. Chem. Soc.* **2010,** *132,* 863–872. doi:10.1021/ja907921w
42. Lucarini, M.; Pedulli, G. F.; Valgimigli, L.; Amorati, R.; Minisci, F. *J. Org. Chem.* **2001,** *66,* 5456–5462. doi:10.1021/jo015653s

43. Enes, R. F.; Tomé, A. C.; Cavaleiro, J. A. S.; Amorati, R.; Fumo, M. G.; Pedulli, G. F.; Valgimigli, L. *Chem.–Eur. J.* **2006,** *12,* 4646–4653. doi:10.1002/chem.200501495
44. Amorati, R.; Pedulli, G. F.; Valgimigli, L. *Org. Biomol. Chem.* **2011,** *9,* 3792–3800. doi:10.1039/c1ob05334e
45. Valgimigli, L.; Amorati, R.; Fumo, M. G.; DiLabio, G. A.; Pedulli, G. F.; Ingold, K. U.; Pratt, D. A. *J. Org. Chem.* **2008,** *73,* 1830–1841. doi:10.1021/jo7024543

License and Terms